Introduction to Aerodynamics

edX Course: MIT.16101

semester="2015_Fall"

David Darmofal, Mark Drela, Alejandra Uranga[1]

March 14, 2016

[1]©2016. All rights reserved. This document may not be distributed without permission from David Darmofal.

Contents

1 Overview **17**

1.1 Overview . . . 17

1.1.1 Objectives, pre-requisites, and modules . . . 17

1.1.2 Measurable outcomes . . . 17

1.1.3 Contents of a module . . . 18

1.1.4 Precision for numerical answers . . . 18

1.1.5 Learning strategy . . . 18

1.1.6 Syllabus . . . 18

1.1.7 Grading . . . 19

1.1.8 Discussion forum guidelines . . . 19

1.2 Spring 2016 Unified Suggested Reading and Problems . . . 21

1.2.1 Overview . . . 21

1.2.2 Week 1 . . . 21

1.2.3 Week 2 . . . 21

1.2.4 Week 3 . . . 21

1.2.5 Week 4 . . . 21

1.2.6 Week 5 . . . 21

1.2.7 Week 6 . . . 21

2 Aircraft Performance **23**

2.1 Overview . . . 23

2.1.1 Measurable outcomes . . . 23

2.1.2 Pre-requisite material . . . 24

2.2 Forces on an Aircraft . . . 25

2.2.1 Types of forces . . . 25

2.2.2 Force and velocity for an aircraft (PROBLEM) . . . 26

2.2.3 Aerodynamic forces . . . 27

2.2.4 Aerodynamic force, pressure, and viscous stresses . . . 28

2.3 Wing and Airfoil Geometry . . . 30

2.3.1 Wing geometric parameters . . . 30
2.3.2 Airfoil thickness and camber . . . 30
2.3.3 NACA 4-digit airfoils . . . 32
2.4 Non-dimensional Parameters and Dynamic Similarity . . . 34
2.4.1 Lift and drag coefficient definition . . . 34
2.4.2 Lift coefficient comparison for general aviation and commercial transport aircraft (PROBLEM) . . . 36
2.4.3 Drag comparison for a cylinder and fairing (PROBLEM) . . . 37
2.4.4 Introduction to dynamic similarity . . . 38
2.4.5 Mach number . . . 38
2.4.6 Reynolds number . . . 40
2.4.7 Mach and Reynolds number comparison for general aviation and commercial transport aircraft (PROBLEM) . . . 42
2.4.8 Pressure coefficient . . . 43
2.4.9 Skin friction coefficient . . . 43
2.4.10 Dynamic similarity: summary . . . 44
2.4.11 Dynamic similarity for wind tunnel testing of a general aviation aircraft at cruise (PROBLEM) . . . 45
2.4.12 A Glimpse into experimental fluid dynamics . . . 46
2.5 Aerodynamic Performance . . . 47
2.5.1 Aerodynamic performance plots . . . 47
2.5.2 Minimum take-off speed (PROBLEM) . . . 50
2.5.3 Drag decomposition . . . 51
2.5.4 Wetted area estimation of friction and form drag . . . 53
2.5.5 Parabolic drag model . . . 54
2.6 Cruise Analysis . . . 55
2.6.1 Range . . . 55
2.6.2 Range estimate for a large commercial transport (PROBLEM) . . . 58
2.6.3 Assumptions in Breguet range analysis . . . 59
2.7 Sample Problems . . . 60
2.7.1 Lift and drag for a flat plate in supersonic flow (PROBLEM) . . . 61
2.7.2 Aerodynamic performance at different cruise altitudes (PROBLEM) . . . 62
2.7.3 Sensitivity of payload to efficiency (PROBLEM) . . . 64
2.7.4 Rate of climb (PROBLEM) . . . 65
2.7.5 Maximum lift-to-drag ratio for parabolic drag (PROBLEM) . . . 66
2.8 Homework Problems . . . 67
2.8.1 Cryogenic wind tunnel tests of an aircraft model (PROBLEM) . . . 68
2.8.2 Impact of a winglet on a transport aircraft (PROBLEM) . . . 69
2.8.3 Minimum power flight with parabolic drag model (PROBLEM) . . . 70

3 Control Volume Analysis of Mass and Momentum Conservation **71**
3.1 Overview . . . 71
3.1.1 Measurable outcomes . . . 71
3.1.2 Pre-requisite material . . . 71
3.2 Continuum Model of a Fluid . . . 72
3.2.1 Continuum versus molecular description of a fluid . . . 72
3.2.2 Solids versus fluids . . . 72
3.2.3 Density . . . 73
3.2.4 Pressure . . . 74
3.2.5 Velocity . . . 74
3.2.6 More on the molecular view of pressure and frictional forces on a body . . . 75
3.2.7 Velocity of a fluid element (PROBLEM) . . . 77
3.2.8 Steady and unsteady flows . . . 78
3.2.9 Fluid element in steady flow (PROBLEM) . . . 79
3.2.10 Pathlines and streamlines . . . 80
3.3 Introduction to Control Volume Analysis . . . 81
3.3.1 Control volume definition . . . 81
3.3.2 Conservation of mass and momentum . . . 81
3.3.3 Release of pressurized air (PROBLEM) . . . 83
3.3.4 Water flow around a spoon (PROBLEM) . . . 84
3.4 Conservation of Mass . . . 85
3.4.1 Rate of change of mass inside a control volume . . . 85
3.4.2 Mass flow leaving a control volume . . . 85
3.4.3 Conservation of mass in integral form . . . 86
3.4.4 Application to channel flow (mass conservation) . . . 86
3.4.5 Release of pressurized air (mass conservation) (PROBLEM) . . . 88
3.5 Conservation of Momentum . . . 89
3.5.1 Rate of change of momentum inside a control volume . . . 89
3.5.2 Momentum flow leaving a control volume . . . 89
3.5.3 Release of pressurized air (momentum flow) (PROBLEM) . . . 90
3.5.4 Forces acting on a control volume . . . 91
3.5.5 Release of pressurized air (forces) (PROBLEM) . . . 93
3.5.6 When are viscous contributions negligible? . . . 94
3.5.7 Conservation of momentum in integral form . . . 94
3.5.8 Release of pressurized air (momentum conservation) (PROBLEM) . . . 95
3.5.9 Application to channel flow (momentum conservation) . . . 96
3.6 Sample Problems . . . 97
3.6.1 Lift generation and flow turning (PROBLEM) . . . 98
3.6.2 Drag and the wake (PROBLEM) . . . 100

4 Conservation of Energy and Quasi-1D Flow **101**

4.1 Overview . . . 101

4.1.1 Measurable outcomes . . . 101

4.1.2 Pre-requisite material . . . 102

4.2 Introduction to Compressible Flows . . . 103

4.2.1 Definition and implications . . . 103

4.2.2 Ideal gas equation of state . . . 104

4.2.3 Internal energy of a gas . . . 104

4.2.4 Enthalpy, specific heats, and perfect gas relationships . . . 106

4.2.5 Comparing air and battery energy (PROBLEM) . . . 108

4.3 Conservation of Energy . . . 109

4.3.1 Introduction to conservation of energy . . . 109

4.3.2 Work . . . 109

4.3.3 Heat . . . 110

4.3.4 Conservation of energy in integral form . . . 110

4.3.5 Total enthalpy along a streamline . . . 111

4.4 Adiabatic and Isentropic Flows . . . 112

4.4.1 Entropy and isentropic relationships . . . 112

4.4.2 Speed of sound . . . 112

4.4.3 Stagnation properties . . . 113

4.4.4 Isentropic variations with local Mach number (PROBLEM) . . . 115

4.4.5 Adiabatic and isentropic flow assumptions . . . 117

4.4.6 Density variations in a low Mach number flow around an airfoil (PROBLEM) . . . 118

4.4.7 Stagnation pressure for incompressible flow and Bernoulli's equation . . . 119

4.5 Quasi-1D Flow . . . 121

4.5.1 Assumptions . . . 121

4.5.2 Incompressible quasi-1D flow . . . 121

4.5.3 Compressible quasi-1D flow . . . 122

4.6 Sample Problems . . . 126

4.6.1 Total enthalpy in an adiabatic flow (PROBLEM) . . . 127

4.6.2 Incompressible nozzle flow (PROBLEM) . . . 128

4.6.3 Subsonic nozzle flow (PROBLEM) . . . 129

4.6.4 Supersonic nozzle flow (PROBLEM) . . . 130

5 Shock Expansion Theory **131**

5.1 Overview . . . 131

5.1.1 Measurable outcomes . . . 131

5.1.2 Pre-requisite material . . . 131

5.2 Introduction . . . 132
5.2.1 Examples . . . 132
5.2.2 Introduction to shock waves . . . 132
5.2.3 Traffic blockage analogy . . . 133
5.2.4 Assumptions for shock and expansion wave analysis . . . 134
5.3 Normal shock waves . . . 135
5.3.1 Isentropic relations . . . 135
5.3.2 Shock reference frame . . . 135
5.3.3 Mach jump relation . . . 136
5.3.4 Static jump relation . . . 137
5.3.5 Shock wave from explosion (PROBLEM) . . . 139
5.3.6 Shock losses . . . 140
5.3.7 Total quantities across a shock (PROBLEM) . . . 141
5.3.8 Summary . . . 142
5.3.9 Supersonic-flow pitot tube (PROBLEM) . . . 143
5.4 Convergent-divergent ducts . . . 145
5.4.1 Introduction to convergent-divergent ducts . . . 145
5.4.2 Purely convergent or divergent ducts (PROBLEM) . . . 146
5.4.3 Subsonic flow and choking . . . 147
5.4.4 Choked flow . . . 148
5.4.5 Choked flow with normal shock . . . 149
5.4.6 Convergent section of choked duct (PROBLEM) . . . 151
5.4.7 Supersonic-exit flows . . . 152
5.4.8 Determination of choked nozzle flows . . . 154
5.4.9 Summary of convergent-divergent duct flows . . . 155
5.4.10 Throat Mach number and area ratio (PROBLEM) . . . 157
5.4.11 Back pressure changes (PROBLEM) . . . 158
5.5 Oblique shocks . . . 160
5.5.1 Mach waves . . . 160
5.5.2 Oblique analysis . . . 160
5.5.3 Equivalence between normal and oblique shocks . . . 162
5.5.4 Mach number jump . . . 162
5.5.5 Wave angle relation . . . 163
5.5.6 Static jumps . . . 164
5.5.7 Summary of oblique shocks . . . 164
5.5.8 Supersonic flow past an upward ramp (PROBLEM) . . . 167
5.6 Expansion waves . . . 169

5.6.1 Oblique shocks and expansion waves . . . 169
5.6.2 Wave flow relations . . . 169
5.6.3 Prandtl-Meyer function . . . 170
5.6.4 Supersonic flow past a downward ramp (PROBLEM) . . . 173
5.7 Sample problems . . . 175
5.7.1 Supersonic engine inlets (PROBLEM) . . . 176
5.7.2 Flat plate in supersonic flow (PROBLEM) . . . 179

6 Differential Forms of Compressible Flow Equations 181
6.1 Overview . . . 181
6.1.1 Measurable outcomes . . . 181
6.1.2 Pre-requisite material . . . 181
6.2 Kinematics of a Fluid Element . . . 182
6.2.1 Kinematics of a fluid element . . . 182
6.2.2 Rotation and vorticity . . . 183
6.2.3 Rotationality in duct flow (PROBLEM) . . . 185
6.2.4 Rotationality for circular streamlines (PROBLEM) . . . 186
6.2.5 Normal strain . . . 187
6.2.6 Calculate normal strain (PROBLEM) . . . 188
6.2.7 Shear strain and strain rate tensor . . . 189
6.2.8 Strain rate for a fluid element in corner flow (PROBLEM) . . . 190
6.2.9 Strain rate for another fluid element in corner flow (PROBLEM) . . . 191
6.2.10 Divergence . . . 192
6.3 Differential Forms of Governing Equations . . . 194
6.3.1 Conservation of mass (the continuity equation) . . . 194
6.3.2 Acoustic measurements (PROBLEM) . . . 195
6.3.3 Conservation of momentum . . . 196
6.3.4 Conservation of momentum in duct flow (PROBLEM) . . . 197
6.3.5 Conservation of energy . . . 198
6.3.6 Substantial derivative . . . 198
6.3.7 Substantial derivative for channel flow (PROBLEM) . . . 200
6.3.8 More on substantial derivative (PROBLEM) . . . 201
6.3.9 A last embedded question on substantial derivative (PROBLEM) . . . 202
6.3.10 Convective forms of the governing equations . . . 203
6.4 Sample Problems . . . 204
6.4.1 Power law (PROBLEM) . . . 205
6.4.2 Circular flow: point (free) vortex (PROBLEM) . . . 206
6.4.3 Pressure over a wing (PROBLEM) . . . 207

6.4.4 Couette flow (PROBLEM) . . . 208
6.5 Homework Problems . . . 209
6.5.1 Flow over a flat plate (PROBLEM) . . . 210
6.5.2 Circular flow: solid-body rotation (PROBLEM) . . . 212
6.5.3 Analyzing the motion of a fluid element (PROBLEM) . . . 214

7 Streamline Curvature and the Generation of Lift 217
7.1 Overview . . . 217
7.1.1 Measurable outcomes . . . 217
7.1.2 Pre-requisite material . . . 217
7.2 Fundamentals of Streamline Curvature . . . 218
7.2.1 Streamline curvature . . . 218
7.2.2 Pressure behavior for bump flow (PROBLEM) . . . 220
7.3 Streamline Curvature and Airfoil Lift Generation . . . 221
7.3.1 Introduction . . . 221
7.3.2 Impact of camber . . . 221
7.3.3 Impact of thickness . . . 223
7.3.4 Leading-edge behavior: stagnation points and suction peaks . . . 224
7.3.5 Leading-edge behavior (PROBLEM) . . . 227
7.4 Sample Problems . . . 229
7.4.1 Pressure behavior in a nozzle and exhaust jet (PROBLEM) . . . 230
7.4.2 Streamline curvature application to a reflexed airfoil (PROBLEM) . . . 231
7.5 Homework Problems . . . 232
7.5.1 Matching airfoils and pressure distributions (PROBLEM) . . . 233
7.5.2 Determining pressure behavior around an airfoil at angle of attack (PROBLEM) 234

8 Fundamentals of Incompressible Potential Flows 235
8.1 Overview . . . 235
8.1.1 Measurable outcomes . . . 235
8.1.2 Pre-requisite material . . . 236
8.2 Justification of Irrotational Flow . . . 237
8.2.1 Incompressible flow equations . . . 237
8.2.2 Vorticity equation . . . 238
8.2.3 Vorticity in incompressible, inviscid flow (PROBLEM) . . . 239
8.2.4 Bernoulli equation . . . 240
8.2.5 Pressure coefficient and Bernoulli's equation . . . 240
8.2.6 Velocity and pressure coefficient relationship for incompressible flow over an airfoil (PROBLEM) . . . 241

8.2.7 The fallacy of the equal transit time theory of lift generation . . . 242
8.2.8 Transit times on a NACA 4502 (PROBLEM) . . . 243
8.3 Potential Flow Modeling . . . 244
8.3.1 Governing equations and the velocity potential . . . 244
8.3.2 Properties of a potential velocity field (PROBLEM) . . . 246
8.3.3 Boundary conditions . . . 247
8.3.4 Equipotential lines and flow tangency (PROBLEM) . . . 248
8.3.5 Potential for corner flow (PROBLEM) . . . 249
8.3.6 Modeling approach . . . 250
8.3.7 Linear superposition in potential flow (PROBLEM) . . . 252
8.4 Two-dimensional Nonlifting Flows . . . 253
8.4.1 Introduction to nonlifting flows . . . 253
8.4.2 Cylindrical coordinate system . . . 253
8.4.3 Source . . . 254
8.4.4 Calculating mass flow rate for a source (PROBLEM) . . . 256
8.4.5 Flow over a Rankine oval . . . 258
8.4.6 A new potential flow (PROBLEM) . . . 261
8.4.7 Doublet . . . 262
8.4.8 Flow over a nonlifting cylinder . . . 263
8.5 Two-dimensional Lifting Flows . . . 266
8.5.1 Point vortex . . . 266
8.5.2 Lifting flow over a rotating cylinder . . . 267
8.5.3 Farfield velocity behavior of lifting and nonlifting flows (PROBLEM) . . . 271
8.5.4 Circulation . . . 272
8.5.5 Kutta-Joukowsky Theorem . . . 272
8.5.6 d'Alembert's Paradox . . . 272
8.6 Sample Problems . . . 273
8.6.1 Drag in incompressible potential flow (PROBLEM) . . . 274
8.7 Homework Problems . . . 276
8.7.1 Modeling the flow over a ridge (PROBLEM) . . . 277
8.7.2 Behavior of nonlifting flow over a cylinder (PROBLEM) . . . 278
8.7.3 Lift and drag in 2D flow with application to an airfoil (PROBLEM) . . . 279

9 Incompressible Potential Flow Aerodynamic Models 281
9.1 Overview . . . 281
9.1.1 Measurable outcomes . . . 281
9.1.2 Pre-requisite material . . . 281
9.2 Airfoil Flows . . . 282

9.2.1 Lifting airfoils and the Kutta condition . . . 282
9.2.2 Properties of two-dimensional steady, inviscid, incompressible flows (PROBLEM) 284
9.2.3 Lift coefficient for a flat plate . . . 285
9.3 Vortex panel methods . . . 286
9.3.1 Introduction to vortex panel methods . . . 286
9.3.2 Vortex sheet model . . . 286
9.3.3 Linear-varying vortex panel model . . . 288
9.3.4 Circulation for linear-varying vortex panel method (PROBLEM) . . . 290
9.3.5 Influence coefficients and linear system . . . 291
9.3.6 Sample vortex panel solutions on a NACA 4412 . . . 291
9.3.7 Lift coefficient behavior for a NACA 3510 using a vortex panel method (PROBLEM) . . . 294
9.4 Thin Airfoil Theory . . . 295
9.4.1 Thin airfoil potential flow model . . . 295
9.4.2 Fundamental equation of thin airfoil theory . . . 297
9.4.3 Symmetric airfoils . . . 298
9.4.4 Pressure differences . . . 299
9.4.5 Cambered airfoils . . . 301
9.4.6 Pitching moment behavior . . . 303
9.5 Sample Problems . . . 305
9.5.1 Vortex panel method for two airfoils (PROBLEM) . . . 306
9.5.2 Parabolic air airfoil (PROBLEM) . . . 307
9.5.3 Quantifying impact of leading and trailing edge flaps (PROBLEM) . . . 308
9.6 Homework Problems . . . 309
9.6.1 Lift coefficient from a vortex panel method (PROBLEM) . . . 310
9.6.2 NACA 34XX aerodynamic performance (PROBLEM) . . . 311
9.6.3 Pressure distributions and moment coefficients (PROBLEM) . . . 312
9.6.4 Airfoil design using thin airfoil theory (PROBLEM) . . . 314

10 Midterm Exam **315**

10.1 Instructions . . . 315
10.1.1 Instructions . . . 315
10.2 Midterm Exam Problems . . . 316
10.2.1 Midterm Problem One (PROBLEM) . . . 317
10.2.2 Midterm Problem Two (PROBLEM) . . . 318
10.2.3 Midterm Problem Three (PROBLEM) . . . 319
10.2.4 Midterm Problem Four (PROBLEM) . . . 321

11 Three-dimensional Incompressible Potential Flow Aerodynamic Models 323
11.1 Overview . . . 323
11.1.1 Measurable outcomes . . . 323
11.1.2 Pre-requisite material . . . 324
11.2 Three-dimensional Nonlifting Flows . . . 325
11.2.1 Spherical coordinate system . . . 325
11.2.2 Source in 3D flow . . . 326
11.2.3 Doublet in 3D flow . . . 327
11.2.4 Nonlifting flow over a sphere . . . 327
11.2.5 Farfield velocity behavior of nonlifting flows in 3D (PROBLEM) . . . 329
11.3 Introduction to Flow over Wings . . . 330
11.3.1 Rectangular wings . . . 330
11.3.2 Trailing vortex images . . . 330
11.3.3 General unswept wings . . . 331
11.3.4 Impact of geometric twist on sectional lift coefficient (PROBLEM) . . . 335
11.4 Lifting Line Models of Unswept Wings . . . 336
11.4.1 Vortex filaments . . . 336
11.4.2 Lifting line model . . . 337
11.4.3 Trefftz plane flow of lifting line model . . . 338
11.4.4 Trefftz plane results for lift and drag . . . 341
11.4.5 Downwash and induced angle of attack . . . 343
11.4.6 Elliptic lift distribution results . . . 346
11.4.7 Downwash for an elliptic lift distribution (PROBLEM) . . . 349
11.4.8 Impact of velocity on downwash and induced drag (PROBLEM) . . . 350
11.4.9 General distribution of lift . . . 351
11.4.10 Calculation of lift, induced drag, and span efficiency . . . 352
11.4.11 Connecting circulation to wing geometry . . . 353
11.4.12 Assumptions of the lifting line model . . . 354
11.4.13 True and false for lifting line theory (PROBLEM) . . . 355
11.5 Sample Problems . . . 356
11.5.1 Elliptic planform wings (PROBLEM) . . . 357
11.5.2 Achieving elliptic lift on a rectangular wing (PROBLEM) . . . 358
11.5.3 Approximate solutions to lifting line for a tapered wing (PROBLEM) . . . 359
11.5.4 Horseshoe vortex model with application to ground effect (PROBLEM) . . . 360
11.5.5 Wing tip vortex flows (PROBLEM) . . . 364
11.6 Homework Problems . . . 366
11.6.1 Aerodynamic trends for wings using lifting line (PROBLEM) . . . 367

11.6.2 Modeling the impact of formation flight (PROBLEM) . . . 372
11.6.3 Designing a wing for an RC aircraft (PROBLEM) . . . 374
11.6.4 Bending moment and wing performance (PROBLEM) . . . 376

12 Two-dimensional Inviscid Compressible Aerodynamic Models 379
12.1 Overview . . . 379
12.1.1 Measurable outcomes . . . 379
12.1.2 Pre-requisite material . . . 379
12.2 Linearized Compressible Potential Equation . . . 380
12.2.1 Assumptions and governing equations for full potential equation . . . 380
12.2.2 Perturbation potential . . . 381
12.2.3 Derivation of linearized compressible potential equation . . . 382
12.2.4 Pressure coefficient for linearized compressible potential flow . . . 383
12.3 Subsonic Linearized Potential Flow . . . 384
12.3.1 Prandtl-Glauert transformation . . . 384
12.3.2 Prandtl-Glauert correction . . . 385
12.3.3 Coefficient of lift versus angle of attack using Prandtl-Glauert correction (PROBLEM) . . . 387
12.3.4 Coefficient of lift versus Mach number using Prandtl-Glauert correction (PROBLEM) . . . 388
12.3.5 Coefficient of drag versus Mach number using Prandtl-Glauert correction (PROBLEM) . . . 389
12.4 Transonic Flow . . . 390
12.4.1 Basic behavior of transonic flow . . . 390
12.4.2 Behavior of lift, drag, and moments in transonic flow . . . 391
12.4.3 Critical Mach number . . . 392
12.4.4 Estimation of critical Mach number for a cylinder (PROBLEM) . . . 400
12.5 Supersonic Linearized Potential Flow . . . 401
12.5.1 Mach wave solutions . . . 401
12.5.2 Flow over a flat plate - revisited . . . 402
12.5.3 Sonic boom (PROBLEM) . . . 403
12.5.4 Flow over an airfoil . . . 404
12.5.5 Minimum wave drag supersonic airfoil design (PROBLEM) . . . 406
12.6 Sample Problems . . . 407
12.6.1 Comparison of linearized supersonic and shock-expansion theory (PROBLEM) 408
12.6.2 Supersonic flow in a duct (PROBLEM) . . . 409
12.7 Homework Problems . . . 410
12.7.1 Impact of thickness on critical Mach number (PROBLEM) . . . 411

12.7.2 Impact of increased Mach number on lift in subsonic flow at constant altitude (PROBLEM) . . . 414
12.7.3 Diamond airfoil performance (PROBLEM) . . . 415
12.7.4 Interacting supersonic airfoils (PROBLEM) . . . 416

13 Incompressible Laminar Boundary Layers 419
13.1 Overview . . . 419
13.1.1 Measurable outcomes . . . 419
13.1.2 Pre-requisite material . . . 420
13.2 The Navier-Stokes Equations . . . 421
13.2.1 Stress tensor . . . 421
13.2.2 Stress acting on flow in channel (PROBLEM) . . . 423
13.2.3 Stress-strain rate relationship . . . 424
13.2.4 Viscous stress and net viscous force for Couette and Poiseuille flow (PROBLEM) 425
13.2.5 Navier-Stokes equations for incompressible flow . . . 426
13.2.6 Solution of two-dimensional Poisseuille flow . . . 427
13.3 Laminar Boundary Layers . . . 428
13.3.1 Introduction to boundary layers . . . 428
13.3.2 Order-of-magnitude scaling analysis: Introduction . . . 428
13.3.3 Order-of-magnitude scaling analysis: Conservation of mass . . . 431
13.3.4 Order-of-magnitude scaling analysis: Conservation of x-momentum . . . 431
13.3.5 Boundary layer thickness dependence on chord length (PROBLEM) . . . 433
13.3.6 Order-of-magnitude scaling analysis: Conservation of y-momentum . . . 434
13.3.7 Boundary layer equations . . . 434
13.3.8 Forces on a fluid element in a boundary layer (PROBLEM) . . . 436
13.3.9 Blasius flat plate boundary layer solution . . . 437
13.3.10 Dependence of laminar flow drag on planform orientation (PROBLEM) . . . 440
13.3.11 Dependence of laminar flow drag on velocity (PROBLEM) . . . 441
13.4 Form Drag and Separation . . . 442
13.4.1 Displacement thickness and effective body . . . 442
13.4.2 Form drag . . . 443
13.4.3 Skin friction behavior in separation (PROBLEM) . . . 447
13.4.4 Separation . . . 448
13.5 Sample Problems . . . 451
13.5.1 Pipe flow (PROBLEM) . . . 452
13.5.2 Shock thickness order-of-magnitude scaling analysis (PROBLEM) . . . 453
13.6 Homework Problems . . . 454
13.6.1 Method of assumed profiles with application to stagnation point boundary layers (PROBLEM) . . . 455

13.6.2 Airfoil drag and skin friction comparisons (PROBLEM) . . . 457
13.6.3 Low Drag Foils, Inc. (PROBLEM) . . . 458

14 Boundary Layer Transition and Turbulence 461

14.1 Overview . . . 461
14.1.1 Measurable outcomes . . . 461
14.1.2 Pre-requisite material . . . 461
14.2 Boundary Layer Transition . . . 462
14.2.1 Introduction to flow instability . . . 462
14.2.2 Types of boundary layer transition . . . 463
14.2.3 Spatial stability of the Blasius flat plate boundary layer . . . 464
14.2.4 Critical condition for boundary layer instability on a sailplane (PROBLEM) . . . 466
14.2.5 Transition prediction . . . 467
14.2.6 Improved flow quality in wind tunnel (PROBLEM) . . . 470
14.3 Turbulent boundary layers . . . 471
14.3.1 Introduction to turbulence . . . 471
14.3.2 Comparison of laminar and turbulent velocity profiles (PROBLEM) . . . 472
14.3.3 Turbulent flat plate flow . . . 473
14.3.4 Dependence of skin friction drag on planform orientation including transition (PROBLEM) . . . 476
14.3.5 Turbulence and separation . . . 477
14.4 Sample Problems . . . 481
14.4.1 Wind tunnel testing for transitional airfoil flows (PROBLEM) . . . 482
14.4.2 Drag versus Reynolds number behavior for thick and thin airfoils (PROBLEM) 483
14.5 Homework Problems . . . 492
14.5.1 Comparison of transitional flow over NACA 0008 and 0016 airfoils (PROBLEM) 493
14.5.2 Airfoil flow classification (PROBLEM) . . . 495
14.5.3 Another airfoil flow classification (PROBLEM) . . . 501
14.5.4 Drag estimation and breakdown for an airplane (PROBLEM) . . . 507

15 Final Exam 509

15.1 Instructions . . . 509
15.1.1 Instructions . . . 509
15.2 Final Exam Problems . . . 510
15.2.1 Final Problem One (PROBLEM) . . . 511
15.2.2 Final Problem Two (PROBLEM) . . . 512
15.2.3 Final Problem Three (PROBLEM) . . . 513
15.2.4 Final Problem Four (PROBLEM) . . . 515

Module 1

Overview

1.1 Overview

1.1.1 Objectives, pre-requisites, and modules

MITx 16.101x is a course about aerodynamics, i.e. the study of the flow of air about a body. In our case, the body will be an airplane, but much of the aerodynamics in this course is relevant to a wide variety of applications from sailboats to automobiles to birds. On campus, the material in 16.101x is covered in Unified Engineering and 16.100. These on-campus courses go beyond the on-line version to include laboratories and projects which provide not only additional content but also hands-on experiences using the content in physical situations and design.

This on-line material requires knowledge of basic physics, vector calculus, and differential equations, at a level common to first-year university subjects. These are serious pre-requisites, and if you do not have this background, you should not be taking this course.

The 16.101x material is organized into a set of modules. Each module covers a core set of topics related to aerodynamics. Topics covered are relevant to the aerodynamic performance of wings and bodies in subsonic, transonic, and supersonic regimes. Specifically, we address basics of aircraft performance; control volume analysis; quasi-one-dimensional compressible flows; shock and expansion waves; subsonic potential flows, including source/vortex panel methods; viscous flows, including laminar and turbulent boundary layers; aerodynamics of airfoils and wings, including thin airfoil theory, lifting line theory, and panel method/interacting boundary layer methods; and supersonic airfoil theory.

1.1.2 Measurable outcomes

Each module begins with a set of outcomes that you should be able to demonstrate upon successfully completing that module. For example,

1.1. A student successfully completing this course will have had fun learning about aerodynamics.

The outcomes are stated in a manner that they can (hopefully) be measured. The entire set of content is designed to help you achieve these outcomes. Further, the various assessment problems and exams are designed to address one or more of these outcomes. Throughout the content, as you consider your progress on learning a particular module, you should always review these measurable outcomes and ask yourself:

1.1.3 Contents of a module

Each module is composed of:

- a set of readings which include some short lecture videos emphasize key ideas. Throughout the readings are embedded questions that are intended to help check your understanding of the material in the readings and videos. Each embedded question also has a corresponding solution video.
- sample problems that are similar to homework problems. A solution video is provided for each sample problem, and is always available for you to view. Some of the sample problems do not have answers to be entered, other sample problems have actual answers you can enter and check.
- homework problems that require you to enter answers. Again, a solution video is provided for each problem.

All parts of the content (i.e. the individual parts of the reading, the embedded questions, the sample problems, and the homework problems) are labeled with the measurable outcomes that are addressed by that part.

1.1.4 Precision for numerical answers

For most problems requiring numerical answers, we will expect three digits of precision meaning that you should provide answers in the form X.YZeP (or equivalent) where X.YZ are the three digit of precision and P is the base 10 exponent using standard scientific notation. If we do not explicitly mention the required precision for a numerical answer, please provide three digits.

Further, we suggest that even though you only need to report three digits of precision, you should maintain the full precision possible on your calculator, software, etc. So, in a multi-part problem, even though you only report three digits of precision in some part, always maintain that high precision answer as you continue to work through the rest of the problem. This is how we have determined the "correct" answer.

1.1.5 Learning strategy

1.1

You could work your way through all of the readings and then work the sample problems, and finally the homework problems. However, you may find it more effective to try the relevant sample problems and/or homework problems just after finishing a portion of the reading. You can use the measurable outcome tags (above) to identify these relationships. (They appear at the top of all content, just underneath the title; hover your mouse over the tag to see the complete description.) Either approach is fine: use whatever way you think is most effective for your learning!

1.1.6 Syllabus

When 16.101x has been offered on-line, the course has been divided into two parts, with a mid-term and final exam. For the Fall 2015 version of 16.101x, the specific release and due dates for the modules were as follows:

Part One

	Name	Release Date	Due Date
1	Overview	28-Sep-2015	Nothing due
2	Aircraft Performance	28-Sep-2015	09-Nov-2015
6	Differential Forms	28-Sep-2015	09-Nov-2015
7	Streamline Curvature	28-Sep-2015	09-Nov-2015
8	Incompressible Potential Flow	05-Oct-2015	09-Nov-2015
9	2D Incompressible Potential Flow Models	05-Oct-2015	09-Nov-2015
	Mid-term Exam	16-Nov-2015	23-Nov-2015

Part Two

10	3D Incompressible Potential Flow Models	23-Nov-2015	04-Jan-2016
11	2D Inviscid Compressible Flow Models	23-Nov-2015	04-Jan-2016
12	Incompressible Laminar Boundary Layers	23-Nov-2015	04-Jan-2016
13	Boundary Layer Transition & Turbulence	23-Nov-2015	04-Jan-2016
	Final Exam	11-Jan-2016	18-Jan-2016

Background

3	Conservation of Mass & Momentum (optional)	28-Sep-2015	Nothing due
4	Conservation of Energy (optional)	28-Sep-2015	Nothing due
5	Shock Expansion Theory (optional)	28-Sep-2015	Nothing due

Now with the course left in an open format, there are not any due dates but the above syllabus gives you a sense of the pacing of the on-line course.

1.1.7 Grading

The grading for 16.101x in the Fall 2015 offering was composed of the following parts and percentages:

5%	Embedded Questions Part One
10%	Homework Problems Part One
35%	Mid-term Exam
5%	Embedded Questions Part Two
10%	Homework Problems Part Two
35%	Final Exam

A certificate for passing 16.101x will be awarded grades of 70% or higher. You can further track your individual proficiency through the letter grades, though please note that these letter grades will not appear on your certificate. The minimum grades for each letter are: A = 90%, B = 80%, C = 70%.

1.1.8 Discussion forum guidelines

The discussion forum can be a very valuable resource for you to get help as well as for you to help others. We hope it contributes to a sense of community and serves as a useful resource for your learning. Here are some guidelines to observe on the forums.

- Search before asking: The forum will be hard to use if there are multiple threads on the same issue and the best discussions happen when several people participate in a single thread. So

before asking a question, use the search feature by clicking on the magnifying glass at the top right of the list of postings.

- Every page of the on-line content includes a discussion thread at the bottom of the page. This is **by far** our prefered method for you to ask questions about material. This has the significant advantage that questions/discussions directly on the material of that page will appear on that page. These discussion threads will also automatically appear in the main discussion forum as well.

- Be polite: We have learners from all around the world and with different backgrounds. Something that is easy for you may be challenging for someone else. Let's build an encouraging community.

- Encourage useful posts by recognizing them: This applies to both questions and responses. Click on the green plus button at the top right of the box for either a post or a response. In this way, useful posts can be found more easily.

- Be specific and concise: Try to compose a title which is descriptive and provide as much information as possible without being overly long. In the question text, describe what aspect you do not understand and what you have already tried doing.

- Write clearly: We know that English is a second language for many of you but correct grammar will help others to respond. Avoid ALL CAPS, abbrv of wrds (abbreviating words), and excessive punctuation!!!!

1.2 Spring 2016 Unified Suggested Reading and Problems

1.2.1 Overview

The following are suggested weekly readings and problems for the Spring 2016 semester of Unified Engineering (MIT on-campus course 16.003/4).

1.2.2 Week 1

- Read Sections: 2.3, 6.2.1-6.2.6, 6.2.10, 6.3.1-6.3.4, 6.3.6-6.3.10
- Problems: 6.2.3, 6.2.4, 6.2.6, 6.3.2, 6.3.4, 6.3.8, 6.3.7, 6.3.9, 6.4.3, 6.5.3. In the following problems, the parts asking about the shear strains are not covered in Unified. You can do those parts of the problems, but they are not required for Unified: 6.4.1, 6.4.2, 6.4.4, 6.5.1, 6.5.2.

1.2.3 Week 2

Read and do all of the embedded questions, sample problems, and homework problems in Module 7 Streamline Curvature and the Generation of Lift.

1.2.4 Week 3

- Read Sections: 2.2, 2.4, 2.5, 11.3
- Problems: 2.4.2, 2.4.3, 2.4.7, 2.4.11, 2.5.2, 2.7.2, 2.7.4, 2.7.5, 2.8.1, 2.8.3, 11.3.4

1.2.5 Week 4

- Read Sections: 8.2-8.4
- Problems: 8.2.3, 8.2.6, 8.2.8, 8.3.2, 8.3.4, 8.3.5, 8.3.7, 8.4.4, 8.4.6, 8.7.1, 8.7.2, 10.2.1, 10.2.3

1.2.6 Week 5

- Read Sections: 8.5, 9.2
- Problems: 8.5.3, 8.6.1, 8.7.3, 9.2.2

1.2.7 Week 6

At this point, we just have a little new reading and related problems to suggest. These are given below. In addition, in preparation for the Fluids exam, we strongly recommend that you re-read and work through all of the material assigned in the previous weeks. As well, re-visiting the homework problems and solutions in the problem sets would be very useful. As an incentive for doing all of the reading and problems in the on-line material as well as re-visiting the problem set problems, I will promise you that at least 25% of the Fluids exam will be exactly taken (i.e. word-for-word) from the problems in the on-line material and the Fluids questions in the problem sets.

- Read Section: 11.4.1

- Problems: 11.5.4, 11.6.2

Module 2

Aircraft Performance

2.1 Overview

2.1.1 Measurable outcomes

The objectives of this module are to introduce key ideas in the aerodynamic analysis of an aircraft and to demonstrate how aerodynamics impacts the overall performance of an aircraft. For aircraft performance, our focus will be on estimating the range of an aircraft in cruise. The focus on cruise range is motivated by the fact the fuel consumption for the flight of transport aircraft is dominated by cruise, with take-off and landing playing a generally smaller role.

Specifically, students successfully completing this module will be able to:

2.1. (a) Define the gravitational, propulsive, and aerodynamic forces that act on an airplane, and (b) Relate the motion of an aircraft (i.e. its acceleration) to these forces.

2.2. (a) Define lift and drag, and (b) Relate the lift and drag to the pressure and frictional stresses acting on an aircraft surface.

2.3. Define common wing parameters including the aspect ratio, taper ratio, and sweep angle.

2.4. Define the chord, camber distribution, and thickness distribution of an airfoil.

2.5. (a) Define the lift and drag coefficients, (b) Utilize the lift and drag coefficients in the aerodynamic analysis of an aircraft, (c) describe the decomposition of the drag into induced, wave, form, and friction drag, and (d) Employ a parabolic drag model to analyze the aerodynamic performance of an aircraft.

2.6. (a) Explain the relationship between the CL-alpha curve and drag polar, and (b) Utilize CL-alpha curves and drag polars to analyze the aerodynamic performance of an aircraft.

2.7. Define and explain the physical significance of the Mach number, the Reynolds number, and the angle of attack.

2.8. Define the pressure coefficient.

2.9. Define the skin friction coefficient.

2.10. (a) Explain the concept of dynamic similarity, (b) Explain its importance in wind tunnel and scale-model testing, and (c) Determine conditions under which flows are dynamically similar.

2.11. (a) Derive the Breguet range equation, (b) Explain how the aerodynamic, propulsive, and structural performance impact the range of an aircraft using the Breguet range equation, and (c) Apply the Breguet range equation to estimate the range of an aircraft.

2.1.2 Pre-requisite material

The material in this module requires some basic algebra, trigonometry, and physics (classical mechanics).

2.2 Forces on an Aircraft

2.2.1 Types of forces

2.1

The forces acting on an aircraft can be separated into:

Gravitational: The gravitational force is the aircraft's weight, including all of its contents (i.e. fuel, payload, passengers, etc.). We will generally denote it **W**.

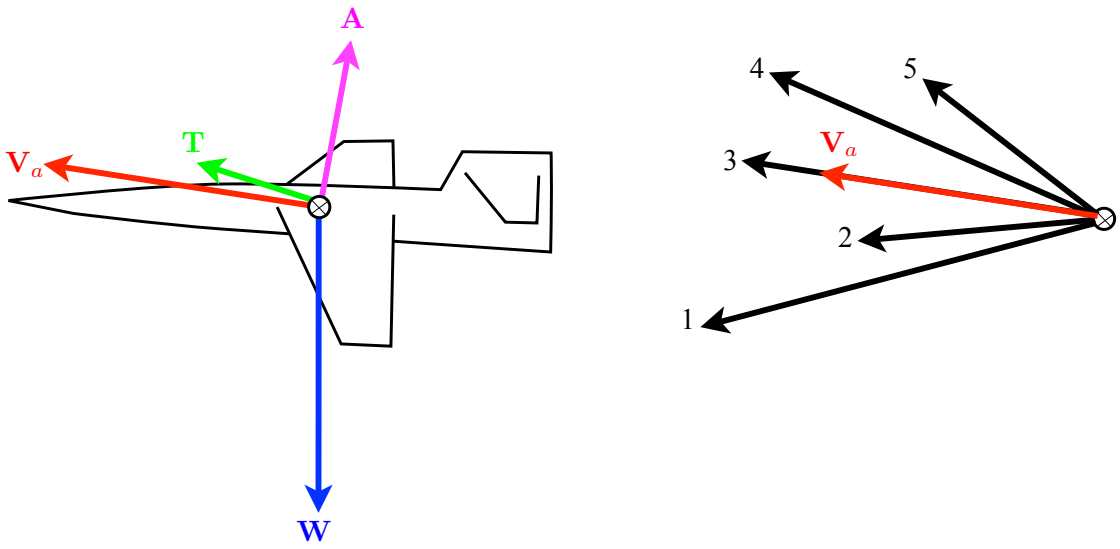
Propulsive: The propulsive force, referred to as the thrust, is the force acting on the aircraft generated by the aircraft's propulsion system. We will generally denote it **T**.

Aerodynamic: The aerodynamic force is defined as the force generated by the air acting on the surface of the aircraft. We will generally denote it **A**.

In reality, the propulsive and aerodynamic forces are often not easy to separate since the propulsive system and rest of the aircraft interact. For example, the thrust generated by a propellor, even placed at the nose of an aircraft, is different depending on the shape of the aircraft. Similarly, the aerodynamic forces generated by an aircraft are impacted by the presence of the propulsive systems. So, while we will use this separation of propulsive and aerodynamic forces, it is important to recognize the thrust generated by the propulsive system depends on the aircraft and the aerodynamic force acting on the aircraft depends on the propulsive system. The entire system is coupled.

edXproblem: 2.2.2 Force and velocity for an aircraft

2.1



As shown in the above figure, the center of mass of an aircraft is moving with velocity $\mathbf{V}_a$. At that instant, the weight of the aircraft is **W**, the thrust is **T**, and the aerodynamic force is **A**. Which of the black arrows shown could be the velocity a short time later? Note the red arrow is the original velocity.

edXsolution

Video Link

2.2.3 Aerodynamic forces

2.2 2.7

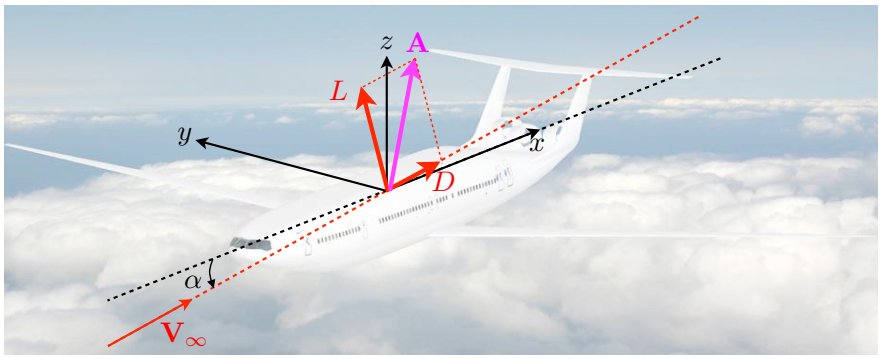


Figure 2.1: Aerodynamic forces for symmetric body without sideslip (the yaw force, Y is assumed zero and not shown).

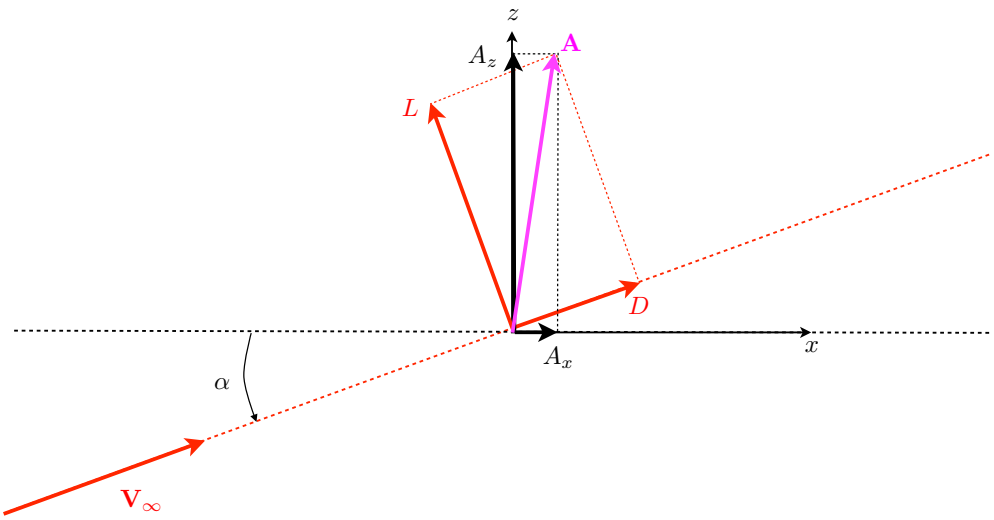


Figure 2.2: Lift and drag forces viewed in x-z plane.

In aerodynamics, the flow about an aircraft is often analyzed using a coordinate system attached to the aircraft, i.e. in the aircraft's frame of reference, often referred to as the geometry or body axes. Suppose in some inertial frame of reference, the velocity of the aircraft is $\mathbf{V}_a$ and the velocity of the wind far ahead of the aircraft is $\mathbf{V}_w$. In the aircraft's frame of reference, the velocity of the wind far upstream of the aircraft is $\mathbf{V}_\infty = \mathbf{V}_w - \mathbf{V}_a$ where $\mathbf{V}_\infty$ is commonly referred to as the freestream velocity and defines the freestream direction. Pilots and people studying the motion of an aircraft often refer to this as the relative wind velocity since it is the wind velocity relative to the aircraft's velocity.

Figure 2.1 shows an aircraft in this frame of reference. The $y = 0$ plane is usually a plane of symmetry for the aircraft with the y-axis pointing outward from the fuselage towards the right wing tip. The distance, b, between the wing tips is called the span and the y-axis is often referred to as the spanwise direction. The x-axis lies along the length of the fuselage and points towards the tail, thus defining what is often referred to as the longitudinal direction. Finally, the z-axis points upwards in such a way that the xyz coordinate system is a right-handed frame.

We will assume that the airplane is symmetric about the $y = 0$ plane. We will also assume that the freestream has no sideslip (i.e. no component in the y-direction). The angle of attack,

α, is defined as the angle between the freestream and the $z = 0$ plane. It is important to note that the specific location of the $z = 0$ plane is arbitrary. In many cases, the $z = 0$ plane is chosen to be parallel to an important geometric feature of the aircraft (e.g. the floor of the passenger compartment) and can be chosen to pass through the center of gravity of the aircraft (not including passengers, cargo, and fuel).

As shown in Figure 2.1, the aerodynamic force is often decomposed into:

Drag: The drag, D, is the component of the aerodynamic force acting in the freestream direction.

Lift: The lift, L, is the component of the aerodynamic force acting normal to the freestream direction. In three-dimensional flows, the normal direction is not unique. However, the situation we will typically focus on is an aircraft that is symmetric such that the left and right sides of the aircraft (though control surfaces such as ailerons can break this symmetry) are the same, and the freestream velocity vector is in this plane of symmetry. In this case, the lift is the defined as the force normal to the freestream in the plane of symmetry as shown in Figure 2.1.

Side: The side force, Y, (also referred to as the yaw force) is the component of the aerodynamic force perpendicular to both the drag and lift directions: it acts along the span-wise direction. For the discussions in this course, the side force will almost always be zero (and has not been shown in Figure 2.1).

For clarity, the lift and drag forces are shown in the x-z plane in Figure 2.2. Also shown are the x and z components of the aerodynamic force whose magnitudes are related to the lift and drag magnitudes by

$$A_x = D\cos\alpha - L\sin\alpha \tag{2.1}$$
$$A_z = D\sin\alpha + L\cos\alpha \tag{2.2}$$

or equivalently

$$D = A_x\cos\alpha + A_z\sin\alpha \tag{2.3}$$
$$L = -A_x\sin\alpha + A_z\cos\alpha\ . \tag{2.4}$$

In other words, (D, L) are related to (A_x, A_z) by a rotation of angle α around the y-axis.

2.2.4 Aerodynamic force, pressure, and viscous stresses

2.2

The aerodynamic force acting on a body is a result of the pressure and friction acting on the surface of the body. The pressure and friction are actually a force per unit area, i.e. a stress. At the molecular level, these stresses are caused by the interaction of the air molecules with the surface.

The pressure stress at a point on the surface acts along the normal direction inward towards the surface and is related to the change in the normal component of momentum of the air molecules when they impact the surface. Consider a location on the surface of the body which has an outward pointing normal (unit length) as shown in Figure 2.3. If the pressure at this location is p, then the pressure force acting on the infinitesimal area $\mathrm{d}S$ is defined as,

$$-p\hat{\mathbf{n}}\,\mathrm{d}S \equiv \text{pressure force acting on surface element } \mathrm{d}S\ . \tag{2.5}$$

Additional information about pressure can be found in Section 3.2.4.

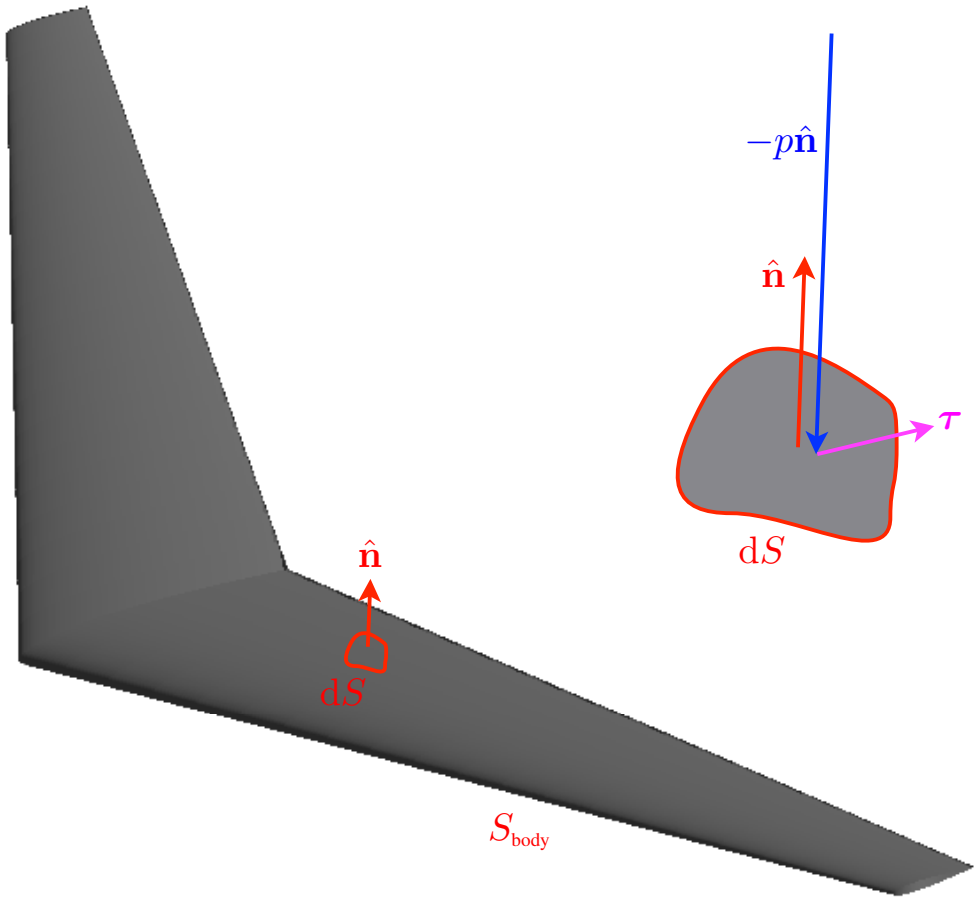


Figure 2.3: Pressure stress $-p\hat{\mathbf{n}}$ and viscous stress $\boldsymbol{\tau}$ acting on an infinitesimal surface element of area $\mathrm{d}S$ and outward normal $\hat{\mathbf{n}}$ (right figure) taken from a wing with total surface S_{body} (left figure).

The frictional stress is related to the viscosity of the air and therefore more generally is referred to as the viscous stress. Near the body, the viscous stress is largely oriented tangential to the surface, however, a normal component of the viscous stress can exist for unsteady, compressible flows (though even in that case, the normal component of the viscous stress is typically much smaller than the tangential component). To remain general, we will define a viscous stress vector, $\boldsymbol{\tau}$ (with arbitrary direction) such that the viscous force acting on $\mathrm{d}S$ is,

$$\boldsymbol{\tau}\,\mathrm{d}S \equiv \text{viscous force acting on } \mathrm{d}S\ . \tag{2.6}$$

The entire aerodynamic force acting on a body can be found by integrating the pressure and viscous stresses over the surface of the body, namely

$$\mathbf{A} = \iint_{S_{\text{body}}} (-p\hat{\mathbf{n}} + \boldsymbol{\tau})\,\mathrm{d}S. \tag{2.7}$$

In the following video, we apply this result to show how the differences in pressure between the upper and lower surfaces of a wing result in a z-component of the aerodynamic force, and discuss how this force is related to the lift.

Video Link

2.3 Wing and Airfoil Geometry

2.3.1 Wing geometric parameters

2.3

In Figure 2.4, the planforms of three typical wings are shown with some common geometric parameters highlighted. The wing-span b is the length of the wing along the y axis. The root chord is labeled c_r and the tip chord is labeled c_t. The leading-edge sweep angle is Λ. Though not highlighted in the figure, S_{planform} is the planform area of a wing when projected to the xy plane.

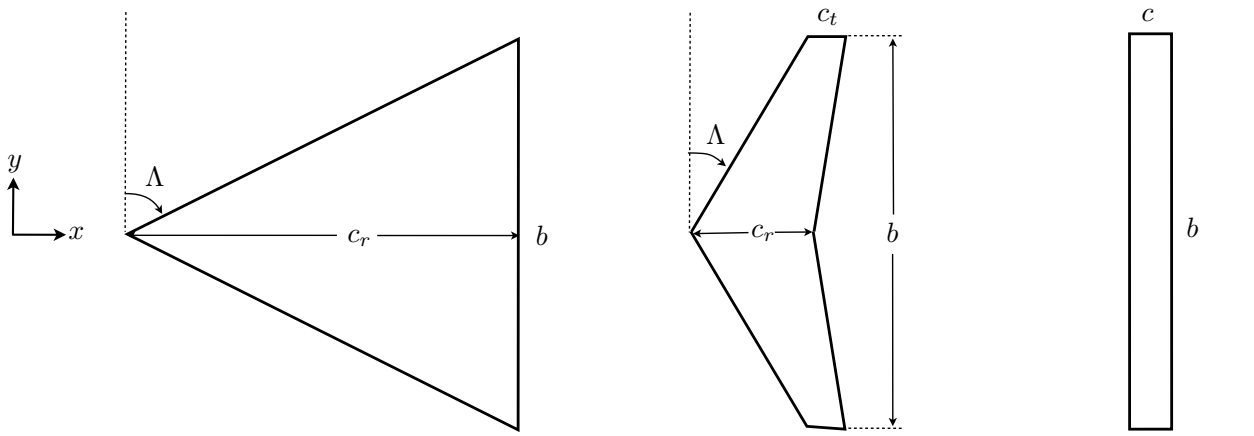


Figure 2.4: Planform views of three typical wings demonstrating different aspect ratios (AR), wing taper ratio (λ), and leading-edge sweep angle (Λ).

A geometric parameter that has a significant impact on aerodynamic performance is the aspect ratio AR which is defined as,

$$AR = \text{aspect ratio} \equiv \frac{b^2}{S_{\text{ref}}} \tag{2.8}$$

where S_{ref} is a reference area related to the geometry. As we will discuss in Section 2.4.1, the wing planform area is often chosen as this reference area, $S_{\text{ref}} = S_{\text{planform}}$.

Figure 2.4 shows wings with three different aspect ratios (choosing $S_{\text{ref}} = S_{\text{planform}}$): a delta wing with $AR = 2$; a swept, tapered wing with $AR = 5$; and a rectangular wing with $AR = 10$. As can be seen from the figure, as the aspect ratio of the wing increases, the span becomes longer relative to the chordwise lengths.

Another geometric parameter is the taper ratio defined as,

$$\lambda = \text{taper ratio} \equiv \frac{c_t}{c_r} \tag{2.9}$$

For the delta wing, $c_t = 0$ giving $\lambda = 0$, while for the rectangular (i.e. untapered, unswept) wing, $c = c_t = c_r$ giving $\lambda = 1$. The $AR = 5$ wing has a taper ratio of $\lambda = 1/3$.

2.3.2 Airfoil thickness and camber

2.4

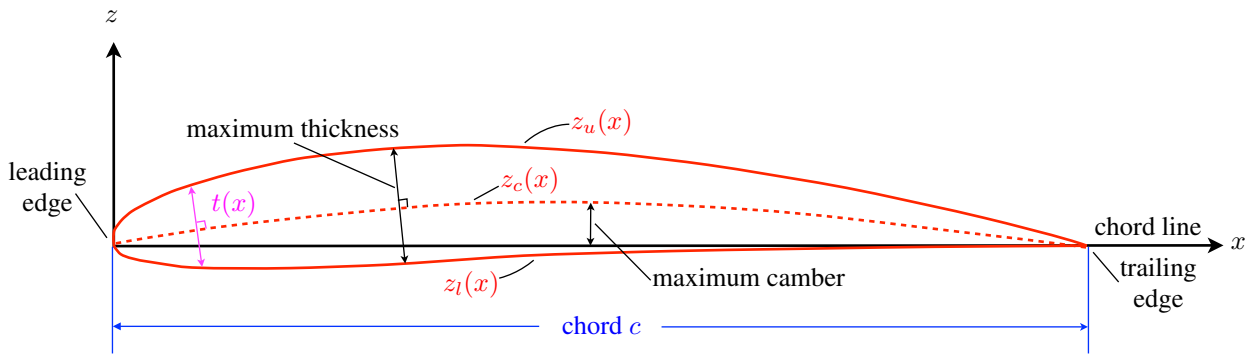


Figure 2.5: Airfoil geometry definition

The cross-section of the wing at a span location produces an airfoil. The common terminology associated with the geometry of airfoils is shown in Figure 2.5. Specifically, we define,

chord line: the chord line is a straight line connecting the leading and trailing edge of the airfoil. In a body-aligned coordinate system, the x-axis is chosen to lie along the chord line.

mean camber line: $z_c(x)$ is the mean camber line and is defined as the curve which is midway between the upper and lower surface measured normal to the mean camber line. The maximum camber is the maximum value of $z_c(x)$.

thickness distribution: $t(x)$ is the thickness distribution and is defined as the distance between the upper and lower surface measured normal to the mean camber line. The maximum thickness is the maximum value of $t(x)$.

Defining the angle of the mean camber line as θ_c such that,

$$\tan\theta_c = \frac{\mathrm{d}z_c}{\mathrm{d}x} \tag{2.10}$$

then the coordinates of points on the upper surface are,

$$x_u = x - \frac{t}{2}\sin\theta_c \tag{2.11}$$

$$z_u = z_c + \frac{t}{2}\cos\theta_c \tag{2.12}$$

and on the lower surface are,

$$x_l = x + \frac{t}{2}\sin\theta_c \tag{2.13}$$

$$z_l = z_c - \frac{t}{2}\cos\theta_c \tag{2.14}$$

We now introduce two other common terms by which airfoils are referred:

uncambered/symmetric airfoil: an airfoil with zero camber, i.e. $z_c(x) = 0$, is known as an uncambered or symmetric airfoil. Both terms are used interchangeably since an uncambered airfoil has an upper and lower surface which is symmetric about the z-axis, i.e. $z_l(x) = -z_u(x)$.

cambered airfoil: a cambered airfoil is one for which $z_c(x) \neq 0$ (at least for some portion of the chord).

2.3.3 NACA 4-digit airfoils

2.4

The NACA 4-digit series of airfoils are used throughout aerodynamics. These airfoils were developed by the National Advisory Committee for Aeronautics (NACA) which was a forerunner to NASA. The four digits of the airfoil are denoted as $MPTT$, e.g. for the NACA 4510 $M = 4$, $P = 5$, $TT = 10$.

The last two digits TT give the maximum thickness of the airfoil as a percent of the chord, specifically,

$$t_{\max} = \frac{TT}{100}c \tag{2.15}$$

The thickness distribution of this series of airfoils is given by,

$$t = t_{\max}\left[2.969\sqrt{\frac{x}{c}} - 1.260\left(\frac{x}{c}\right) - 3.516\left(\frac{x}{c}\right)^2 + 2.843\left(\frac{x}{c}\right)^3 - 1.015\left(\frac{x}{c}\right)^4\right] \tag{2.16}$$

It can be shown that the maximum thickness for these 4-digit airfoils occurs at $x/c = 0.3$. Also, the radius of curvature at the leading edge,

$$\frac{r_{\text{LE}}}{c} = 1.102\left(\frac{t_{\max}}{c}\right)^2 \tag{2.17}$$

Also, note that the thickness for these airfoils is actually non-zero at $x/c = 1$. Occasionally, the thickness definition is modified so that the thickness at the trailing edge is exactly zero. A common approach is to change the last coefficient from -1.015 to -1.036 which has neglible effects on the thickness distribution except in the immediate neighborhood of the trailing edge.

The M and P values are related to the mean camber line. Specifically, M gives the maximum camber as a percent of the chord,

$$z_{c\max} = \frac{M}{100}c \tag{2.18}$$

P gives the location of the maximum camber as a tenth of the chord. In other words, $z_{c\max} = z_c(x_{c\max})$ where

$$x_{c\max} = \frac{P}{10}c \tag{2.19}$$

Defining $m = M/100$ and $p = P/10$, then the formula for the mean camber line for the 4-digit series airfoils is given by,

$$\frac{z_c}{c} = \begin{cases} \frac{m}{p^2}\frac{x}{c}\left(2p - \frac{x}{c}\right), & \text{for } 0 \le \frac{x}{c} \le p \\ \\ \frac{m}{(1-p)^2}\left[1 - 2p + 2p\frac{x}{c} - \left(\frac{x}{c}\right)^2\right], & \text{for } p \le \frac{x}{c} \le 1 \end{cases} \tag{2.20}$$

For example, the NACA 4510 airfoil has a maximum thickness which is 10% of the chord, a maximum camber which is 4% of the chord, and the location of maximum camber is at 50% of the chord. Figure 2.6 shows the NACA 0012 and 4412 airfoils. The NACA 0012 is a symmetric airfoil (in fact, all NACA 00TT airfoils are symmetric), while the NACA 4412 is a cambered airfoil.



Figure 2.6: Symmetric 12% thick airfoil (NACA 0012) on left and cambered 12% thick airfoil (NACA 4412) on right

2.4 Non-dimensional Parameters and Dynamic Similarity

2.4.1 Lift and drag coefficient definition

2.5

Common aerodynamic practice is to work with non-dimensional forms of the lift and drag, called the lift and drag coefficients. The lift and drag coefficients are defined as,

$$C_L \equiv \frac{L}{\frac{1}{2}\rho_\infty V_\infty^2 S_{\text{ref}}} \tag{2.21}$$

$$C_D \equiv \frac{D}{\frac{1}{2}\rho_\infty V_\infty^2 S_{\text{ref}}} \tag{2.22}$$

where ρ_∞ is the density of the air (or more generally fluid) upstream of the body and S_{ref} is a reference area that for aircraft is often defined as the planform area of the aircraft's wing.

The choice of non-dimensionalization of the lift and drag is not unique. For example, instead of using the freestream velocity in the non-dimensionalization, the freestream speed of sound (a_∞) could be used to produce the following non-dimensionalizations,

$$\frac{L}{\frac{1}{2}\rho_\infty a_\infty^2 S_{\text{ref}}}, \quad \frac{D}{\frac{1}{2}\rho_\infty a_\infty^2 S_{\text{ref}}}. \tag{2.23}$$

Or, instead of using a reference area such as the planform area, the wingspan of the aircraft (b) could be used to produce the following non-dimensionalizations,

$$\frac{L}{\frac{1}{2}\rho_\infty V_\infty^2 b^2}, \quad \frac{D}{\frac{1}{2}\rho_\infty V_\infty^2 b^2}. \tag{2.24}$$

A key advantage for using $\rho_\infty V_\infty^2 S_{\text{ref}}$ (as opposed to those given above) is that the lift tends to scale with $\rho_\infty V_\infty^2 S_{\text{ref}}$. While we will learn more about this as we further study aerodynamics, the first hints of this scaling can be seen in the video in Section 2.2.4. In that video, we saw that the lift on a wing is approximately given by,

$$L \approx \overline{p_l - p_u} \times S_{\text{planform}} \tag{2.25}$$

Since the lift on an airplane is mostly generated by the wing (with smaller contributions from the fuselage), then choosing $S_{\text{ref}} = S_{\text{planform}}$ will tend to capture the dependence of lift on geometry for an aircraft. Also, the average pressure difference $\overline{p_l - p_u}$ tends to scale with $\rho_\infty V_\infty^2$ (again, we will learn more about this latter). Thus, this normalization of the lift tends to capture much of the parametric dependence of the lift on the freestream flow conditions and the size of the body. As a result, for a wide-range of aerodynamic applications, from small general aviation aircraft to large transport aircraft, the lift coefficient tends to have similar magnitudes, even though the actual lift will vary by orders of magnitude.

While aerodynamic flows are three-dimensional, significant insight can be gained by considering the behavior of flows in two dimensions, i.e. the flow over an airfoil. For airfoils, the lift and drag are actually the lift and drag per unit length. We will label these forces per unit length as L' and D'. The lift and drag coefficients for airfoils are defined as,

$$c_l \equiv \frac{L'}{\frac{1}{2}\rho_\infty V_\infty^2 c} \tag{2.26}$$

$$c_d \equiv \frac{D'}{\frac{1}{2}\rho_\infty V_\infty^2 c} \tag{2.27}$$

where c is the airfoil's chord length (its length along the x-body axis, i.e. viewed from the z-direction). In principle, other lengths could be used (for example, the maximum thickness of the airfoil). However, since the lift tends to scale with the airfoil chord (analogous to the scaling of lift with the planform area of a wing), the chord is chosen exclusively for aerodynamic applications.

edXproblem: 2.4.2 Lift coefficient comparison for general aviation and commercial transport aircraft

2.5

Determine the lift coefficient at cruise for (1) a propellor-driven general aviation airplane and (2) a large commercial transport airplane with turbofan engines given the following characteristics:

		General aviation	Commercial transport
Total weight	W	2,400 lb	550,000 lb
Wing area	S_{ref}	180 ft^2	4,600 ft^2
Cruise velocity	V_∞	140 mph	560 mph
Cruise flight altitude		12,000 ft	35,000 ft
Density at cruise altitude	ρ_∞	1.6×10^{-3} slug/ft^3	7.3×10^{-4} slug/ft^3

Note that the total weight includes aircraft, passengers, cargo, and fuel. The air density is taken to correspond to the density at the flight altitude of each airplane in the standard atmosphere.

What is the lift coefficient for the general aviation airplane? Provide your answer with two digits of precision (of the form X.YeP).

What is the lift coefficient for the commercial transport airplane? Provide your answer with two digits of precision (of the form X.YeP).

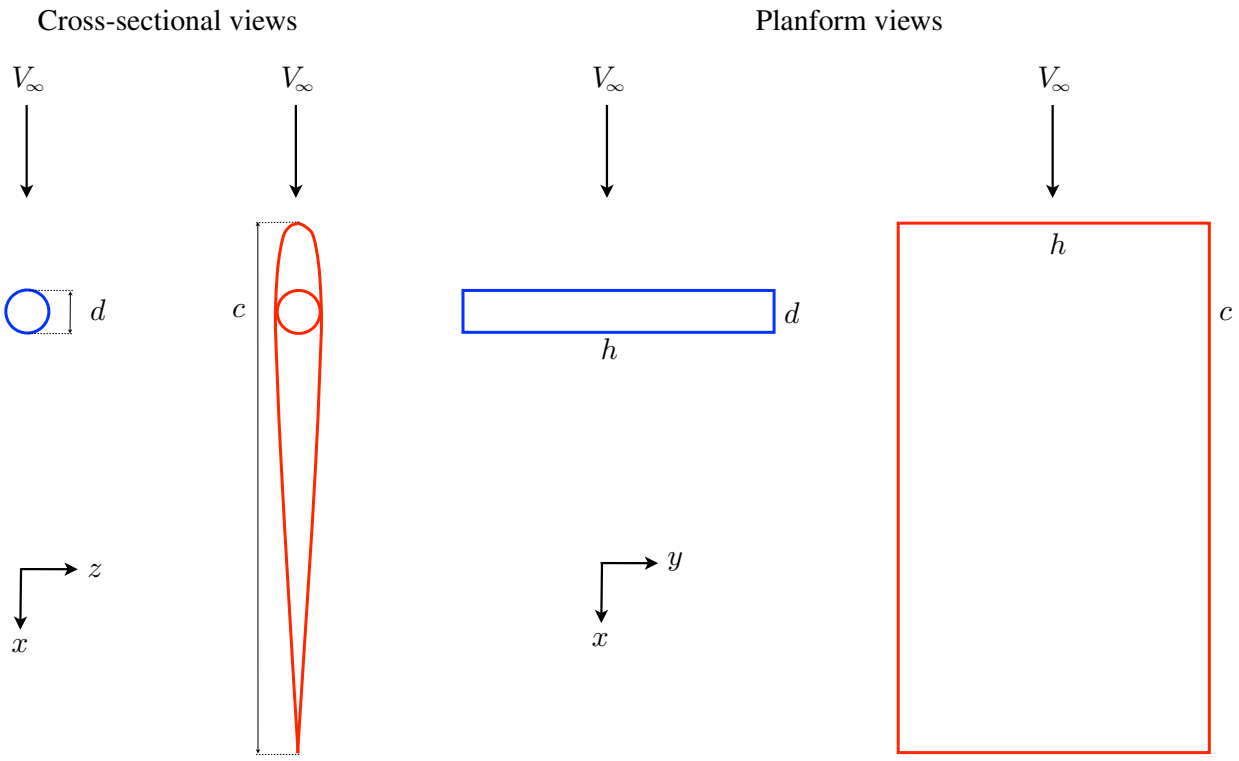
edXsolution

Video Link

edXproblem: 2.4.3 Drag comparison for a cylinder and fairing

2.5

The drag on a cylinder is quite high especially compared to a streamlined-shape such as an airfoil. For situations in which minimizing drag is important, airfoils can be used as fairings to surround a cylinder (or other high drag shape) and reduce the drag. Consider the cylinder (in blue) and fairing (in red) shown in the figure.



For the flow velocity of interest, the drag coefficient for the cylinder is $C_{D\text{cyl}} \approx 1$ using the streamwise projected area for the reference area, i.e. $S_{\text{cyl}} = dh$.

Similarly, consider a fairing with chord $c = 10d$. For the flow velocity of interest, the drag coefficient for the fairing is $C_{D\text{fair}} \approx 0.01$ using the planform area for the reference area, i.e. $S_{\text{fair}} = ch$.

What is $D_{\text{cyl}}/D_{\text{fair}}$, i.e. the ratio of the drag on the cylinder to the drag on the fairing?

edXsolution

Video Link

2.4.4 Introduction to dynamic similarity

2.5 2.7 2.10

One of the important reasons for using the lift and drag coefficients arises in wind tunnel testing, or more generally experimental testing of a scaled model of an aircraft. For example, suppose we have a model in the wind tunnel that is a $1/50^{\text{th}}$-scale version of the actual aircraft, meaning that the length dimensions of the model are $1/50$ the length dimensions of the actual aircraft.

The key question in this scaled testing is: how is the flow around the scaled model of an aircraft related to the flow around the full-scale aircraft? Or, more specifically, how is the lift and drag acting on the scaled model of an aircraft related to the lift and drag acting on the full-scale aircraft?

While almost certainly the actual lift and drag are not equal between the scale and full-scale aircraft, the intent of this type of scale testing is that the lift and drag coefficients will be equal. However, this equality of the lift and drag coefficients only occurs under certain conditions and the basic concept at work is called *dynamic similarity.*

The following video describes the concept of dynamic similarity.

Video Link

2.4.5 Mach number

2.7

As discussed in the video on dynamic similarity in Section 2.4.4, the Mach number is an important non-dimensional parameter determining the behavior of the flow. The Mach number of the freestream flow is defined as,

$$M_\infty \equiv \frac{V_\infty}{a_\infty} \tag{2.28}$$

where a_∞ the speed of sound in the freestream.

The Mach number is an indication of the importance of compressibility (we will discuss this later in the course). Compressibility generally refers to how much the density changes due to changes in pressure. For low freestream Mach numbers, the density of the flow does not usually change significantly due to pressure variations. A low freestream Mach number is typically taken as $M_\infty < 0.3$. In this case, we can often simplify our analysis by assuming that the density of the flow is constant everywhere (e.g. equal to the freestream value). In terms of dynamic similarity, this also implies that matching the Mach number is less important for low Mach number flows. For higher Mach numbers, the effects of compressibility are generally significant and density variations must be accounted for. Therefore, matching the Mach number will be important when applying dynamic similarity to higher Mach number flows.

Flows are frequently categorized as subsonic, transonic, and supersonic. Some of the main features of these flow regimes are shown in Figure 2.7. As we now describe, these regimes have somewhat fuzzy boundaries.

The subsonic regime is one in which the local flow velocity everywhere remains below the local speed of sound. We can define the local Mach number, M, as the ratio of the local velocity and local speed of sound, and a subsonic flow would be one in which the local Mach number is below one everywhere. Since flows that generate lift will typically accelerate the flow, there will be regions in the flow where the local Mach number is larger than the freestream Mach number. For now, the main point is that whether or not a flow is subsonic is not entirely determined by the freestream Mach number being less than one.

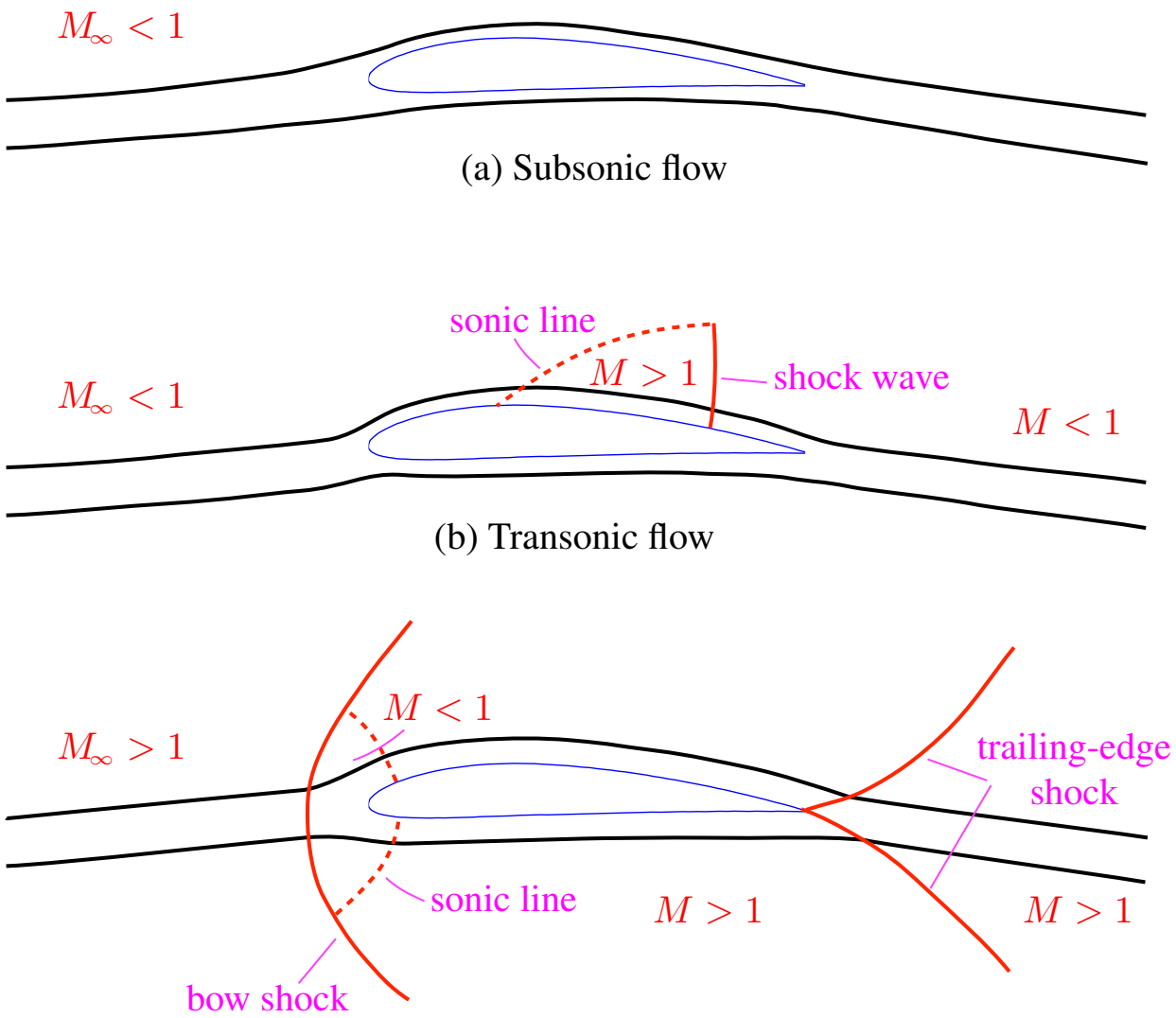


Figure 2.7: Subsonic, transonic, and supersonic flow over an airfoil.

Transonic flows are defined as flows with the Mach number close to unity. A distinguishing feature of transonic flow is that regions in the flow exist where the local Mach number is subsonic and other regions in the flow exist where the local Mach number is supersonic. The dividing line between these regions is known as the sonic line, since on this line the local Mach number $M = 1$. Large modern commercial transports all fly in the transonic regime, with $M_\infty \approx 0.8$. Transonic flows almost always have shock waves which are a rapid deceleration of the flow from supersonic to subsonic conditions. The thickness of the shock wave is so small in most aerospace applications that the deceleration is essentially a discontinuous jump from supersonic to subsonic conditions giving rise to significant viscous stresses and drag. We will learn more about shock waves later in the course.

The term supersonic indicates $M_\infty > 1$ and the local Mach number is almost everywhere supersonic as well. Supersonic flows have shock waves which occur in front of the body and are often called bow shocks in this case. As can be seen from the figure, upstream of the bow shock, the streamlines are straight as the flow is not affected by the body in this region. Downstream of the bow shock, most supersonic flows have some region near the body in which the flow is subsonic,

so technically most flows could be categorized as transonic. However, when the regions of subsonic flow are small, the character of the flow will be dominated by the supersonic regions and the entire flow is categorized as supersonic.

2.4.6 Reynolds number

2.7

As discussed in the video on dynamic similarity in Section 2.4.4, the Reynolds number is another important non-dimensional parameter determining the behavior of the flow. The Reynolds number of the freestream flow is defined as,

$$Re_\infty \equiv \frac{\rho_\infty V_\infty l_{\text{ref}}}{\mu_\infty} \tag{2.29}$$

where l_{ref} is the reference length scale chosen for the problem, and μ_∞ is the freestream dynamic viscosity. Note that another commonly used measure of the viscosity is the kinematic viscosity which is defined as $\nu = \mu/\rho$. Thus, the Reynolds number can also be written as $Re_\infty = V_\infty l_{\text{ref}}/\nu_\infty$.

The Reynolds number is an indication of the importance of viscous effects. Since the Reynolds number is inversely proportional to the viscosity, a larger value of the Reynolds number indicates that viscous effects will play a smaller role in determining the behavior of the flow.

The viscosity of air and water is quite small when expressed in common units, as shown in the following table.

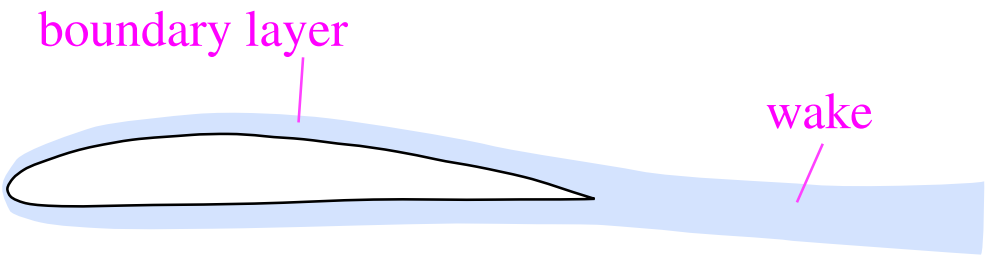
	Air @ STP	Water @ 15°C
μ	1.78×10^{-5} kg/m-s	1.15×10^{-3} kg/m-s
ν	1.45×10^{-5} m^2/s	1.15×10^{-6} m^2/s

From the small values of ν in the table above, it is clear that typical aerodynamic and hydrodynamic flows will have very large Reynolds numbers. This can be seen in the following table, which gives the Reynolds numbers based on the chord length of common winged objects.

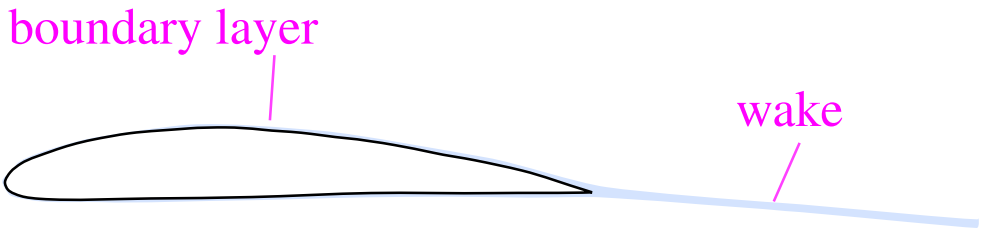
Object	Re_∞
Butterfly	5×10^3
Pigeon	5×10^4
RC glider	1×10^5
Sailplane	1×10^6
Business jet	1×10^7
Boeing 777	5×10^7

The Reynolds number is large even for insects, which means that the flow can be assumed to be inviscid (i.e. $\mu = 0$ and $\boldsymbol{\tau} = 0$) almost everywhere. The only place where the viscous shear is significant is in *boundary layers* which form adjacent to solid surfaces and become a *wake* trailing downstream, as shown in Figure 2.8.

In the boundary layer, the velocity is retarded by the frictional (i.e. viscous) stresses at the wall. Thus, the boundary layer and the wake are regions with lower velocity compared to the freestream. The larger the Reynolds number is, the thinner the boundary layers are relative to the size of the body, and the more the flow behaves as though it was inviscid.



$$Re_\infty = 1 \times 10^4$$
$$c_d \approx 0.035$$



$$Re_\infty = 1 \times 10^6$$
$$c_d \approx 0.0045$$

Figure 2.8: Boundary layer and wake dependence on Reynolds number.

edXproblem: 2.4.7 Mach and Reynolds number comparison for general aviation and commercial transport aircraft

2.7

Continuing with the analysis of the airplanes from Problem 2.4.2, determine the Mach number and Reynolds number at cruise using the following additional information:

		General aviation	Commercial transport
Wing area	S_{ref}	180 ft^2	4,600 ft^2
Mean chord	$\bar{c}$	5 ft	23 ft
Cruise velocity	V_∞	140 mph	560 mph
Cruise flight altitude		12,000 ft	35,000 ft
Density	ρ_∞	1.6×10^{-3} slug/ft^3	7.3×10^{-4} slug/ft^3
Dynamic viscosity	μ_∞	3.5×10^{-7} slug/ft-sec	3.0×10^{-7} slug/ft-sec
Speed of sound	a_∞	1.1×10^3 ft/sec	9.7×10^2 ft/sec

What is the Mach number for the general aviation airplane? Provide your answer with two digits of precision (of the form X.YeP).

What is the Mach number for the commerical transport airplane? Provide your answer with two digits of precision (of the form X.YeP).

Choosing $l_{\text{ref}} = \bar{c}$, what is the Reynolds number for the general aviation airplane? Provide your answer with two digits of precision (of the form X.YeP).

Choosing $l_{\text{ref}} = \bar{c}$, what is the Reynolds number for the commercial transport airplane? Provide your answer with two digits of precision (of the form X.YeP).

edXsolution

Video Link

2.4.8 Pressure coefficient

2.8

In aerodynamics, the pressure is often reported in a non-dimensional form as the pressure coefficient,

$$C_p \equiv \frac{p - p_\infty}{q_\infty} \tag{2.30}$$

$$q_\infty \equiv \frac{1}{2}\rho_\infty V_\infty^2 = \text{ freestream dynamic pressure} \tag{2.31}$$

Note that the freestream dynamic pressure, here given the symbol q_∞, was also used as part of the non-dimensionalization of the lift and drag that produced the lift and drag coefficients. For example, $C_L = L/(q_\infty S_{\text{ref}})$.

With this definition of the pressure coefficient, $C_p < 0$ when the pressure is lower than the freestream pressure, and $C_p > 0$ when the pressure is higher than the freestream pressure.

The C_p distribution around a NACA 4510 airfoil assuming incompressible potential flow at $\alpha = 0°$ is shown in Figure 2.9. Note that the C_p axis of the plot has negative values at the top. This flipped C_p axis is commonly used in aerodynamics since airfoils that generate lift will have lower pressures on the upper surface (on average) than the pressure on the lower surface. Further, the pressures on the upper surface tend to be below p_∞ and hence $C_p < 0$ over much of the upper surface of a lifting airfoil.

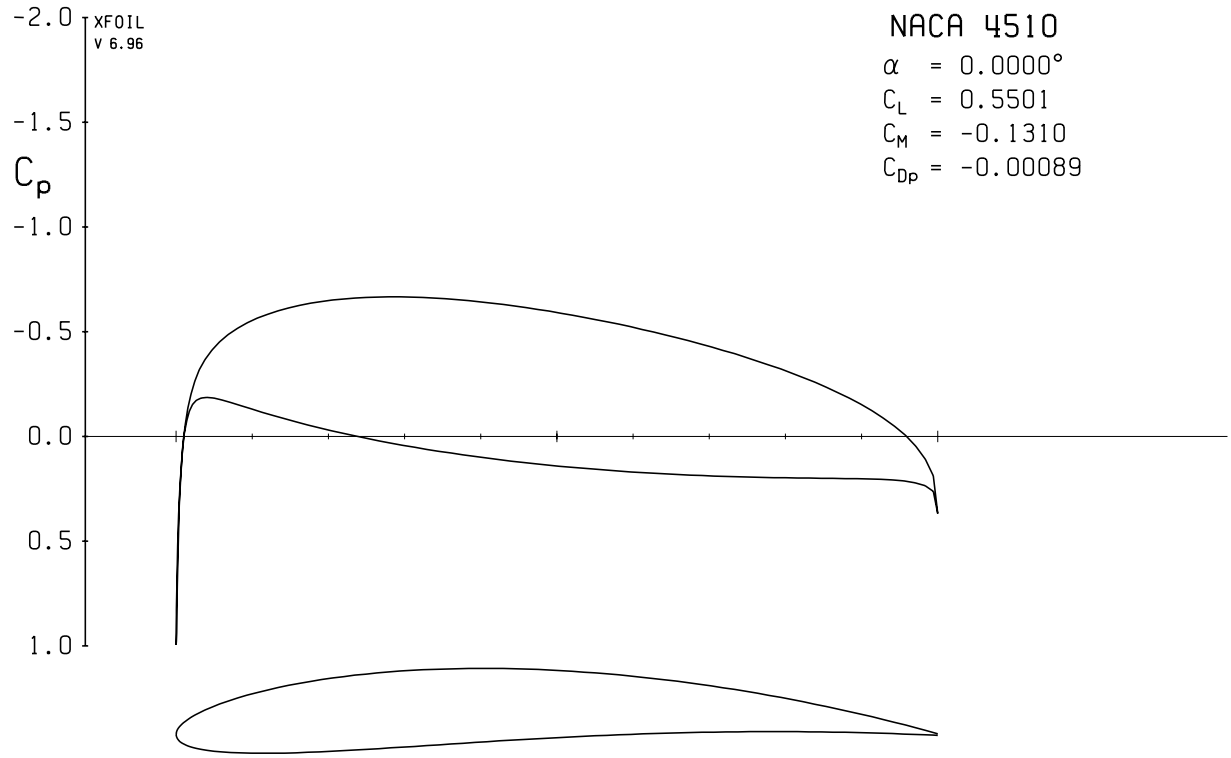


Figure 2.9: C_p distribution for NACA 4510 at $\alpha = 0°$ for incompressibe potential flow.

Finally, returning to the concept of dynamic similarity, when two flows are dynamically similar, then the pressure coefficients are also the same. That is, $C_p(x/c, y/c, z/c)$ are the same.

2.4.9 Skin friction coefficient

2.9

Analogous to the pressure, the skin friction is also often reported in a non-dimensional form as the skin friction coefficient,

$$C_f \equiv \frac{\tau_{wall}}{q_\infty} \tag{2.32}$$

where τ_{wall} is the viscous stress acting along the wall.

2.4.10 Dynamic similarity: summary

2.5 2.7 2.10

In this section, we summarize what we've learned about dynamic similarity in Sections 2.4.4, 2.4.5 and 2.4.6. This is such a critical concept throughout all aspects of aerodynamics, including experimental, theoretical, and computational analysis, that it is worth repeating the major conclusions:

- For a given geometric shape, the lift coefficient, drag coefficient, etc. as well as the flow states in non-dimensional form (e.g. ρ/ρ_∞) are generally functions of the Mach number, Reynolds number, and angle of attack. Other effects may be important, but these are the dominant parameters for a wide range of aerodynamics. Thus, for a given geometry, we will consider C_L and C_D to be functions,

$$C_L = C_L\left(M_\infty, Re_\infty, \alpha\right) \tag{2.33}$$
$$C_D = C_D\left(M_\infty, Re_\infty, \alpha\right) \tag{2.34}$$

- For scale-testing such as occurs in wind tunnel testing, the lift coefficient, drag coefficient, etc. as well as the flow states in non-dimensional form (e.g. C_p, ρ/ρ_∞, etc.), will be equal to the full-scale values if the Mach number, Reynolds number, and angle of attack (as well as any other important non-dimensional parameter) are matched. Specifically, dynamic similarity states that,

$$C_{L\,\text{full}} = C_{L\,\text{scale}} \quad \text{and} \quad C_{D\,\text{full}} = C_{D\,\text{scale}} \tag{2.35}$$

$$\text{if } M_{\infty\,\text{full}} = M_{\infty\,\text{scale}}, \quad Re_{\infty\,\text{full}} = Re_{\infty\,\text{scale}}, \quad \alpha_{\text{full}} = \alpha_{\text{scale}}. \tag{2.36}$$

  This is a direct consequence of Equations (2.33) and (2.34).

edXproblem: 2.4.11 Dynamic similarity for wind tunnel testing of a general aviation aircraft at cruise

2.7 2.10

The Wright Brothers Wind Tunnel at MIT is being considered for wind tunnel testing of the cruise condition of the general aviation aircraft described in Problems 2.4.2 and 2.4.7. The flow in the test section of this wind tunnel has essentially atmospheric conditions (except for its velocity). Since the Wright Brothers Tunnel is at sea level, the test section conditions are $\rho_\infty = 2.4 \times 10^{-3}$ slug/ft^3, $a_\infty = 1.1 \times 10^3$ ft/sec, and $\mu_\infty = 3.7 \times 10^{-7}$ slug/ft-sec. The maximum velocity that can be achieved in the test section is about 200 mph.

What is the maximum Mach number that can be achieved in the Wright Brothers Wind Tunnel? Provide your answer with two digits of precision (of the form X.YeP).

Since the Mach number of the full-scale aircraft and the maximum Mach number in the tunnel are both fairly low, we will assume that the impact of not matching the Mach number for this problem is small. The question then remains whether or not dynamic similarity can be achieved for the Reynolds number.

The Wright Brothers Wind Tunnel has an oval test section which is 10 feet wide and 7 feet tall. The span of the general aviation aircraft is 36 feet. Suppose that the wind tunnel model of the aircraft is designed with a 9 foot span to ensure that the effect of the wind tunnel walls is not too significant.

What is the maximum Reynolds number that can be achieved in the Wright Brothers Wind Tunnel using a 9-foot span scaled model of the general aviation aircraft? Provide your answer with two digits of precision (of the form X.YeP).

Is it possible to achieve dynamic similarity for the Reynolds number using the Wright Brothers Wind Tunnel for general aviation aircraft at cruise?

edXsolution

Video Link

2.4.12 A Glimpse into experimental fluid dynamics

2.7 | 2.10 | 7.1

While we do not have time to cover wind tunnel testing in depth, we thought you might enjoy learning a little more. These videos will give you a glimpse into the world of experimental fluids by describing some of the considerations that go into defining a wind tunnel test. We use as an illustration a test performed in MIT's Wright Brothers Wind Tunnel on a recently designed aircraft configuration.

Note: these videos were created during the Fall 2013 offering of 16.101x, in response to questions from students.

Part 1/2

Video Link

Part 2/2

Video Link

2.5 Aerodynamic Performance

2.5.1 Aerodynamic performance plots

2.6

The variation of the lift and drag coefficient with respect to angle of attack for a typical aircraft (or for a typical airfoil in a two-dimensional problem) is shown in Figure 2.10. For lower values of angle of attack, the lift coefficient depends nearly linearly on the angle of attack (that is, the C_L-α curve is nearly straight). As the angle of attack increases, the lift eventually achieves a maximum value and is referred to as $C_{L\max}$. This maximum lift is often referred to as the stall condition for aircraft. The value of $C_{L\max}$ is a key parameter in the aerodynamic design of an aircraft as it directly impacts the take-off and landing performance of the aircraft (see e.g. Problem 2.5.2).

Also shown on the C_L plot is the angle at which the lift is zero, $\alpha_{L=0}$. This angle is often used in describing the low angle of attack performance since given this value and the slope a_0 a reasonable approximation to C_L-α dependence is

$$C_L \approx a_0(\alpha - \alpha_{L=0}). \tag{2.37}$$

Finally, as the angle of attack decreases beyond $\alpha_{L=0}$, lift also achieves a minimum value. This negative incidence stall is less critical for aircraft, however, it does play a critical role in the performance of blades in axial-flow turbomachinery (setting one limit on the operability of these type of turbomachinery).

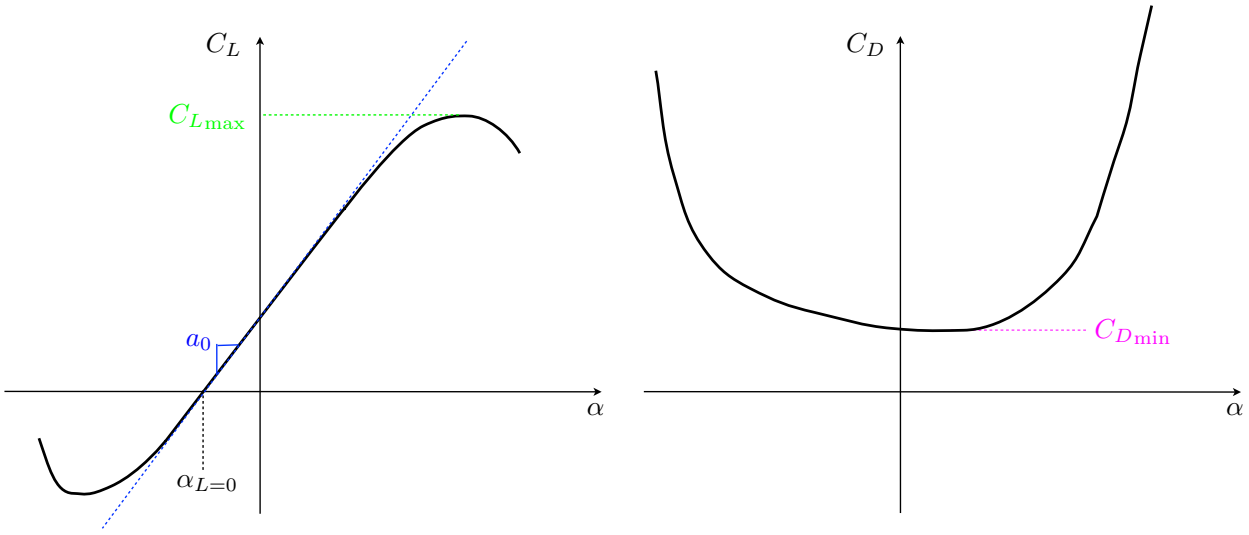


Figure 2.10: Typical lift and drag coefficient variation with respect to angle of attack for an aircraft

C_D is shown to have a minimum value $C_{D\min}$ which will typically occur in the region around which the lift is linear with respect to angle of attack. As the angle of attack increases, C_D also increases with rapid increases often occuring as $C_{L\max}$ is approached. Similar behavior also occurs for the negative incidence stall.

A useful method of plotting the drag coefficient variation is not with respect to angle of attack but rather plotting $C_D(\alpha)$ and $C_L(\alpha)$ along the x and y axis, respectively. This type of plot is commonly referred to as the drag polar and emphasizes the direct relation between lift and drag. It is indeed often more important to know how much drag one needs to "pay" to generate a given lift (or equivalently to lift a given weight).

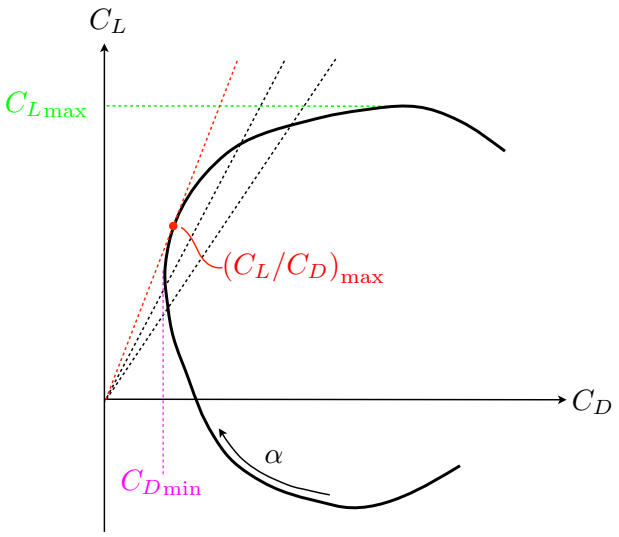


Figure 2.11: Typical drag polar for an aircraft

A typical drag polar is shown in Figure 2.11. In this single plot, the minimum drag and maximum lift coefficients can be easily identified. Also, shown in the plot is the location (the red dot) on the drag polar where C_L/C_D is maximum. Note that constant C_L/C_D occurs along lines passing through $C_D = C_L = 0$ and having constant slope. A few of these lines are shown in the plot. The maximum C_L/C_D line (the red line) must be tangent to the drag polar at its intersection (if not, C_L/C_D could be increased by a small change in the position along the polar).

To help gain further understanding of the magnitude and behavior of c_l and c_d, we consider two airfoils specifically the NACA 0012 and the NACA 4412 previously shown in Figure 2.6. The variation of c_l versus α is shown in Figure 2.12 for these airfoils at two different Reynolds numbers, $Re_\infty = 10^6$ and 10^7. Since the NACA 0012 is symmetric, the lift coefficients at α and $-\alpha$ have the same magnitude (but opposite sign) and $\alpha_{L=0} = 0$. Note that the slope in the linear region is not dependent on Reynolds number, and that $a_0 \approx 0.11$ per degree, or equivalently, 6.3 per radian. The same lift slope is observed for the NACA 4412, but in this case the camber of the airfoil causes $\alpha_{L=0} \approx -4°$, making the lift coefficient higher for a given angle of attack compared to the NACA 0012. Finally, we note that the maximum c_l is dependent on the Reynolds number, with higher $c_{l\max}$ occurring for higher Re_∞. During the course of this subject, we will discuss these various behaviors in detail.

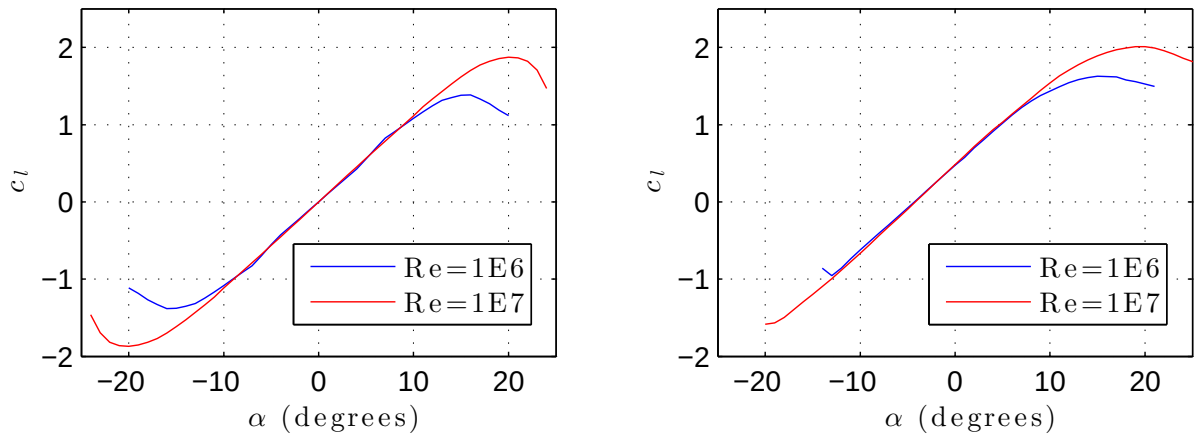


Figure 2.12: c_l versus α for NACA 0012 on left and NACA 4412 on right at $Re_\infty = 10^6$ and 10^7

The drag polars for these airfoils at the two Reynolds numbers are shown in Figure 2.13. Note that the drag coefficient is multiplied by 10^4, which is a frequently used scaling for the drag coefficient. In fact, a c_d increment of 10^{-4} is known as a *count* of drag and is commonly used to report drag coefficients in aerodynamics. Increasing the Reynolds number lowers the drag coefficient at these high Reynolds numbers. The minimum drag for the symmetric airfoil occurs at $c_l = 0$. However, for the cambered airfoil, the minimum drag occurs at $c_l \approx 0.5$. Thus, the maximum lift-to-drag ratio is larger and occurs for a higher c_l for the cambered airfoil. It is this result that leads to almost all aircraft with subsonic and transonic flight speeds to have cambered airfoils.

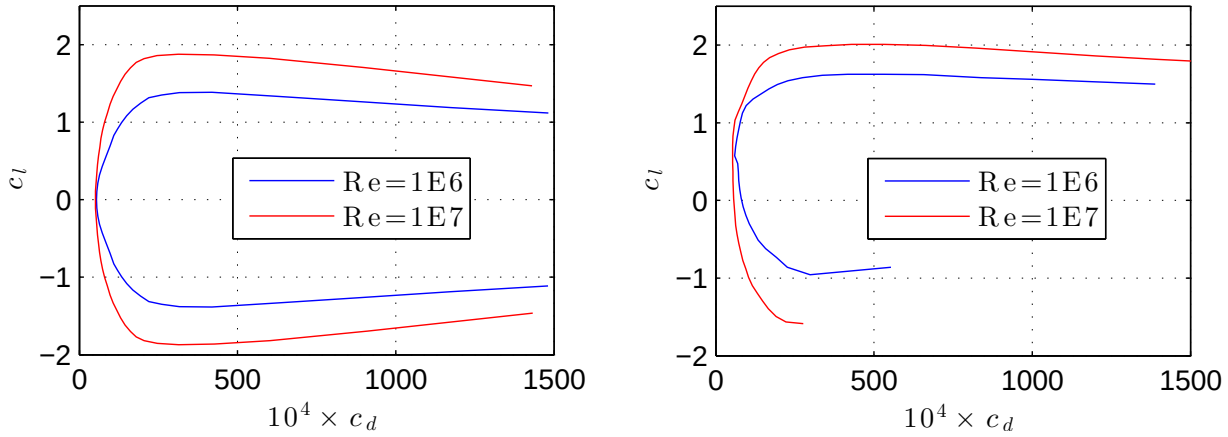
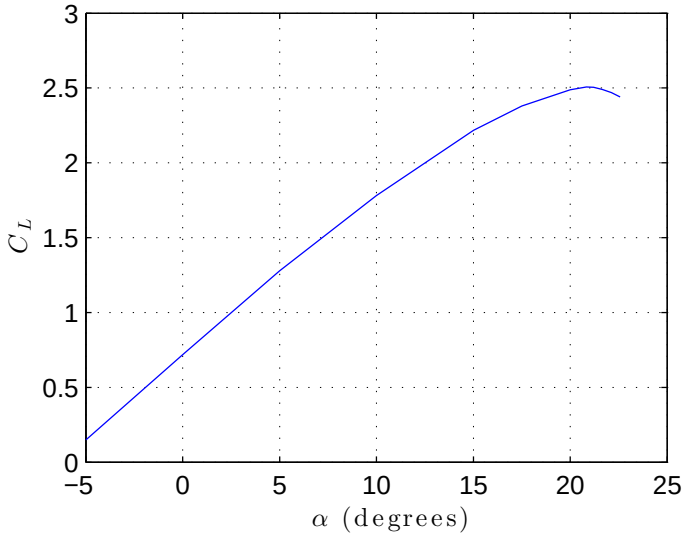


Figure 2.13: Drag polar for NACA 0012 on left and NACA 4412 on right at $Re_\infty = 10^6$ and 10^7

edXproblem: 2.5.2 Minimum take-off speed

2.5 2.6



The figure above shows the lift curve for an aircraft with its flaps deployed in a take-off configuration. Assume that take-off is near sea level (the density is provided below) and that the aircraft has the following characteristics:

		Commercial transport
Take-off weight	W	650,000 lb
Wing area	S_{ref}	4,600 ft^2
Density at take-off	ρ_∞	2.4×10^{-3} slug/ft^3

What is the minimum take-off speed (i.e. the smallest speed at which the aircraft generates enough lift to take-off)? Give your answer in miles per hour (to the nearest miles per hour).

Now consider take-off of this aircraft at an elevation of 5000 ft. Will the minimum take-off speed at this elevation be larger or smaller than the minimum take-off speed at sea level?

edXsolution

Video Link

2.5.3 Drag decomposition

2.5

In this section, we will assume that the coordinate system has been aligned with the freestream flow such that $\mathbf{V}_\infty = V_\infty \hat{\mathbf{i}}$. Using the total aerodynamic force (given in Equation 2.7), the drag is then,

$$D = \mathbf{A} \cdot \hat{\mathbf{i}} = \iint_{S_{\text{body}}} (-p\hat{\mathbf{n}} + \boldsymbol{\tau}) \cdot \hat{\mathbf{i}} \, \mathrm{d}S. \tag{2.38}$$

Thus, the pressure and the viscous stresses can create a drag force which we will denote as D_{pressure} and D_{friction},

$$D_{\text{pressure}} = -\iint_{S_{\text{body}}} p\hat{\mathbf{n}} \cdot \hat{\mathbf{i}} \, \mathrm{d}S, \tag{2.39}$$

$$D_{\text{friction}} = \iint_{S_{\text{body}}} \boldsymbol{\tau} \cdot \hat{\mathbf{i}} \, \mathrm{d}S, \tag{2.40}$$

The pressure drag is often decomposed further into three fundamentally different sources, specifically,

- *Induced drag*, D_{induced}, is due to the presence of the vortex wake that exists behind a body that is generating lift. Induced drag is discussed in detail in Module 11.
- *Wave drag*, D_{wave}, is due to the presence of shock waves. Wave drag is discussed in detail in Module 12, in particular Section 12.4.
- *Form drag*, D_{form}, is due to viscous effects which impact the pressure distribution (compared to a purely inviscid flow) through the creation of boundary layers and, potentially, the separation of the boundary layers from the surface. Boundary layer behavior is discussed in detail in Modules 13 and 14, and form drag is discussed in particular in Section 13.4.

Thus, we can think of the pressure drag as being the sum of,

$$D_{\text{pressure}} = D_{\text{induced}} + D_{\text{wave}} + D_{\text{form}} \tag{2.41}$$

In practice, the estimation of these three drag sources can rarely be done in a manner that would precisely add up to the pressure drag integral. Thus, the equality should probably be thought of as an approximation.

Combining this pressure drag decomposition with the friction drag gives a decomposition of total drag as,

$$D = D_{\text{induced}} + D_{\text{wave}} + D_{\text{form}} + D_{\text{friction}} \tag{2.42}$$

Finally, since the form drag and friction drag are both a result of the effects of viscosity on the flow field, they are often combined into a single drag contribution known as the *profile drag*:

$$D_{\text{profile}} = D_{\text{form}} + D_{\text{friction}} \tag{2.43}$$

The drag sources in this decomposition have corresponding drag coefficients for which we will

use the following notation:

$$C_{Di} \equiv \frac{D_{\text{induced}}}{q_\infty S_{\text{ref}}} \tag{2.44}$$

$$C_{Dw} \equiv \frac{D_{\text{wave}}}{q_\infty S_{\text{ref}}} \tag{2.45}$$

$$C_{D\text{form}} \equiv \frac{D_{\text{form}}}{q_\infty S_{\text{ref}}} \tag{2.46}$$

$$C_{D\text{f}} \equiv \frac{D_{\text{friction}}}{q_\infty S_{\text{ref}}} \tag{2.47}$$

$$C_{Dp} \equiv \frac{D_{\text{profile}}}{q_\infty S_{\text{ref}}} \tag{2.48}$$

Two-dimensional versions of these coefficients exist as well, except for the induced drag which is a strictly three-dimensional phenomenon (i.e. induced drag is zero in a two-dimensional flow). The two-dimensional drag coefficients are defined as,

$$c_{dw} \equiv \frac{D_{\text{wave}}}{q_\infty l_{\text{ref}}} \tag{2.49}$$

$$c_{d\text{form}} \equiv \frac{D_{\text{form}}}{q_\infty l_{\text{ref}}} \tag{2.50}$$

$$c_{d\text{f}} \equiv \frac{D_{\text{friction}}}{q_\infty l_{\text{ref}}} \tag{2.51}$$

$$c_{dp} \equiv \frac{D_{\text{profile}}}{q_\infty l_{\text{ref}}} \tag{2.52}$$

As is derived in Section 11.4, the induced drag coefficient can be shown to be equal to,

$$C_{Di} = \frac{C_L^2}{\pi e AR}. \tag{2.53}$$

The positive parameter e is called the Oswald span efficiency factor and cannot exceed unity. Its value is linked to how lift is distributed along the wing span. While the span efficiency factor may appear to be a constant (for a given geometry), in fact the span efficiency typically varies with the amount of lift generated. As well, the span efficiency factor is dependent upon the aspect ratio for general wing shapes. Thus, in general $e = e(C_L, AR)$. While this is true, for a well-designed wing, e can be made to approach values of nearly 1. As a result, the main geometric dependence for the induced drag coefficient is through the aspect ratio.

Unlike the induced drag, the wave drag does not have a simple form which captures the main dependencies. However, the wave drag is a function of the Mach number (since for low enough Mach number shock waves will not appear and thus the wave drag will be zero) and also the lift coefficient (since for higher lift coefficients the flow will accelerate more, producing higher local Mach numbers, and the greater likelihood for shock waves). Thus, in addition to geometry, the wave drag coefficient is a strong function of M_∞ and C_L, that is $C_{Dw} \approx C_{Dw}(M_\infty, C_L)$. The approximation is because other dependencies certainly do exist, including for example the Reynolds number. But, the dominant dependencies are M_∞, C_L, and (obviously) the geometry.

The friction drag coefficient is predominantly a function of the Reynolds number and to a much lesser extent the Mach number and lift coefficient, in addition to the shape. Thus, to good approximation, we can think of $C_{D\text{f}} = C_{D\text{f}}(Re_\infty)$. One common approach to estimate the friction drag is given in Section 2.5.4.

The form drag is perhaps the most difficult source of drag to estimate, especially as the boundary layers near separation and/or separate. The form drag is dependent strongly on the lift coefficient and to a lesser extent the Reynolds number and Mach number (again, the shape is always an important factor). Thus, $C_{D\text{form}} = C_{D\text{form}}(C_L, Re_\infty, M_\infty)$. A common approach to estimate the form drag is given in Section 2.5.4.

2.5.4 Wetted area estimation of friction and form drag

2.5 2.9 14.3

The friction drag is often estimated using a so-called wetted area approach. Since aerodynamic bodies tend to be thin compared to their streamwise lengths, then the surface tangents over most of the body will be nearly aligned with the streamwise direction (for small angles of attack). Thus, the friction drag can be well-approximated as,

$$D_{\text{friction}} = \iint_{S_{\text{body}}} \boldsymbol{\tau} \cdot \hat{\mathbf{i}} \, \mathrm{d}S \tag{2.54}$$

$$\approx \iint_{S_{\text{body}}} \tau_{\text{wall}} \, \mathrm{d}S \tag{2.55}$$

$$= q_\infty \iint_{S_{\text{body}}} C_{\text{f}} \, \mathrm{d}S \tag{2.56}$$

Since the skin friction coefficient depends on the Reynolds number (see for example Section 14.3.3), a common approach is to break the body into separate parts with a different representative Reynolds number for each part,

$$D_{\text{friction}} \approx q_\infty \sum_i \iint_{S_i} C_{\text{f}} \, \mathrm{d}S \tag{2.57}$$

where S_i is the wetted surface area for the i-th part of the body and the wetted surface area for the entire body would then be $S_{\text{body}} = \sum_i S_i$. The term wetted surface area is defined as the surface area of an object which is exposed to the air (or more generally fluid). For each part of the body, we define an average skin friction coefficient as,

$$\overline{C_{\text{f}}}_i \equiv \frac{1}{S_i} \int_{S_i} C_{\text{f}} \, \mathrm{d}S \tag{2.58}$$

Then, the estimated friction drag is,

$$D_{\text{friction}} \approx q_\infty \sum_i \overline{C_{\text{f}}}_i S_i \tag{2.59}$$

Since most aerodynamic shapes are thin, the main error in this approach will be in determining a reasonable value for $\overline{C_{\text{f}}}_i$ for each part of the body. Finally, the estimated friction drag coefficient using this approach is,

$$C_{D\text{f}} \approx \sum_i \overline{C_{\text{f}}}_i \frac{S_i}{S_{\text{ref}}} \tag{2.60}$$

A common approach to estimate the form drag is to modify the wetted area estimates for the skin friction with a so-called form factor so that the resulting estimate is for both the friction and form drag (in other words, it is the profile drag),

$$D_{\text{profile}} = D_{\text{form}} + D_{\text{friction}} \approx q_\infty \sum_i K_i \overline{C_{\text{f}}}_i S_i \tag{2.61}$$

where K_i are the form factors. In fact, since the skin friction coefficient estimates are usually taken directly from flat plate data, the form factors are used to not only include an estimate of the form drag but also to adjust the skin friction data (to account for non-zero thickness which increases the surface velocity and therefore the skin friction). Sincd both of these effects increase the profile drag from the flat plate case, then $K_i > 1$. The form factors will be a function of the geometry (and the lift) and various references can be found giving approaches to estimate form factors for different shapes.

While the skin friction drag can be reasonably estimated with the this wetted area approach, especially for early design decisions where trends are more important than absolute precision, the form drag estimate based on form factors is much less reliable unless data (from experiments and/or computational simulations) exists from similar situations. Thus, caution should be utilized when applying these profile drag estimates especially if boundary layer separation is a concern (e.g. for high lift).

2.5.5 Parabolic drag model

2.5

For the three-dimensional flow about a body that generates lift, a simple model for the dependence of drag on lift is the so-called parabolic drag model given by

$$C_D = C_{D0} + \frac{C_L^2}{\pi e AR} \tag{2.62}$$

The C_{D0} term is typically referred to as the drag coefficient at zero lift and is due to profile drag and, at higher Mach numbers, wave drag. Since the form drag and wave drag increase with the lift being generated by a vehicle, this simple model will underpredict the increase in C_D with C_L. However, when applied to situations with low to moderate C_L, then the model is quite useful for understanding basic trends and helping to guide aerodynamic design decisions.

2.6 Cruise Analysis

2.6.1 Range

2.11

The range of an aircraft is the distance the aircraft can fly on a specific amount of fuel. In this section, our objectives are to understand how factors such as the weight of the aircraft, the amount of fuel, the drag, and the propulsive efficiency influence an aircraft's range, and to learn how to estimate the range.

In our estimate, we will not directly consider the fuel used during the take-off and landing portions of a flight. We will only focus on the cruise range. Except for very short flights (an hour or less), most of the fuel is burned during the cruise section of the flight: for a typical commercial airliner in transcontinental flight, the fuel consumed during cruise represents around 90% of the total trip fuel. We will assume that an aircraft in cruise has constant speed (relative to the wind) of V_∞ and is flying level (not gaining altitude). This is commonly refered to as *s*teady, level flight. Placing the freestream along the x-axis, and with gravity acting in the $-z$ direction, the forces acting on the aircraft are as shown in Figure 2.14.

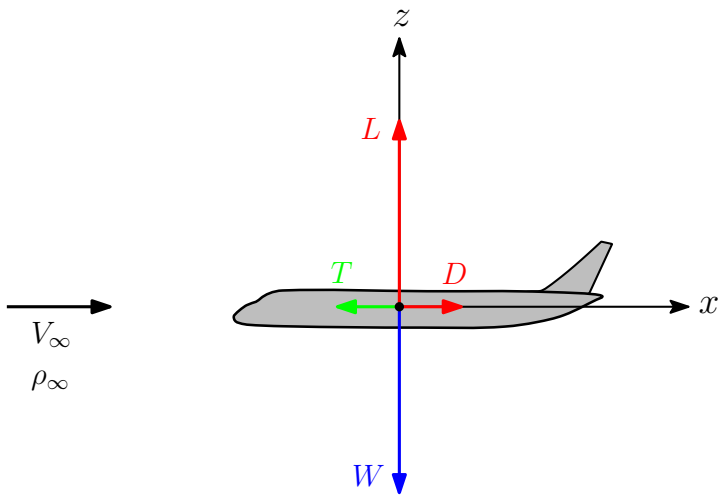


Figure 2.14: An aircraft in steady level flight

Under the assumption that the aircraft has constant velocity during cruise, the acceleration is zero and therefore the sum of the forces must be zero. Thus for steady, level flight we have,

$$L = W \tag{2.63}$$

$$T = D \tag{2.64}$$

For most aircraft in cruise, the weight is a function of time because fuel is being consumed (and the products of the combustion process are then emitted into the atmosphere). Thus, in steady level flight where $L = W$, the lift must also be a function of time. Further, the amount of drag is also dependent on the amount of lift produced, as discussed in previous sections, and since $T = D$ in steady flight, then the thrust also is a function of time. Summarizing, in steady, level flight when fuel is consumed, then the weight, lift, drag, and thrust are all functions of time though they satisfy Equations (2.63) and (2.64).

To determine the cruise range, we will require the rate at which fuel is used during cruise. We

start with the definition of the overall efficiency of a propulsive system,

$$\eta_o \equiv \frac{\text{Propulsive power produced by the propulsive system}}{\text{Power supplied to the propulsive system}} \tag{2.65}$$

The propulsive power produced in steady level flight is TV_∞ (thrust force times distance per unit time gives the rate of thrust work). For a given fuel, we define the heat release during combustion to be Q_R per unit mass of the fuel. Then, the power supplied to the propulsive system is $\dot{m}_f Q_R$ where $\dot{m}_f$ is the fuel mass flow rate. Thus, the overall efficiency of the propulsive system is,

$$\eta_o = \frac{TV_\infty}{\dot{m}_f Q_R} \tag{2.66}$$

For large commercial transport with modern turbofans, the overall efficiencies are around 0.3-0.4. For aircraft using turbojets, the overall efficiencies will tend to be lower than turbofans. While for propellor-driven aircraft, the overall efficiencies will tend to be higher.

The overall efficiency can then be re-arranged to determine the rate at which the total weight of the aircraft (i.e. including the fuel) is changing,

$$\frac{\mathrm{d}W}{\mathrm{d}t} = -g\dot{m}_f \tag{2.67}$$

namely,

$$\frac{\mathrm{d}W}{\mathrm{d}t} = -\frac{gTV_\infty}{\eta_o Q_R} \,. \tag{2.68}$$

Now since $T = D$ and $W/L = 1$ in steady level flight, substituting $T = WD/L$ gives

$$\frac{\mathrm{d}W}{\mathrm{d}t} = -\frac{g}{\eta_o\, Q_R\, L/D} W V_\infty \tag{2.69}$$

Multiplying this equation by $\mathrm{d}t/W$ produces

$$\frac{\mathrm{d}W}{W} = -\frac{g}{\eta_o\, Q_R\, L/D}\, V_\infty \mathrm{d}t \,. \tag{2.70}$$

Finally, we note that $\mathrm{dR} = V_\infty \mathrm{d}t$ is the infinitesimal distance traveled during $\mathrm{d}t$, or infinitesimal change in range, so that

$$-\frac{\mathrm{d}W}{W} = \frac{g}{\eta_o\, Q_R\, L/D}\, \mathrm{dR} \tag{2.71}$$

or equivalently

$$\mathrm{dR} = -\frac{\mathrm{d}W}{W}\, \frac{\eta_o\, Q_R\, L/D}{g} \tag{2.72}$$

The $-\mathrm{d}W/W$ is the fractional change in the weight of the aircraft (the minus sign means that the quantity is positive when the weight decreases). Thus, Equation (2.66) shows that for a given amount of fuel burn $-\mathrm{d}W/W$, the distance traveled will increase if η_o, Q_R or L/D increase. We see here that the range depends on both the aerodynamic and propulsive system performance: the range directly depends on the efficiency of the propulsive system η_o and on the aerodynamic efficiency of the aircraft L/D (airframe efficiency). Also in Equation (2.72) is the impact of the structural design of the aircraft. If an aircraft can be made lighter then W will be smaller. Thus, for the same amount of fuel burn $\mathrm{d}W/W$ will be larger and the range will be larger (all else being equal). In one equation, we see how aerodynamic, propulsive, and structural design impact the overall performance of an aircraft.

If we further make the assumption that η_o and L/D are constant, we can integrate Equation (2.72) to produce the Breguet range equation,

$$\mathrm{R} = \eta_o \frac{L}{D} \frac{Q_R}{g} \ln\left(\frac{W_{\text{initial}}}{W_{\text{final}}}\right) \tag{2.73}$$

which can be used to estimate the range of an aircraft for given estimates of η_o and L/D. The weight ratio can be re-arranged to highlight the fuel weight used,

$$\frac{W_{\text{initial}}}{W_{\text{final}}} = \frac{W_{\text{final}} + W_{\text{fuel}}}{W_{\text{final}}} = 1 + \frac{W_{\text{fuel}}}{W_{\text{final}}}. \tag{2.74}$$

The final weight W_{final} represents the weight of the aircraft structure + crew + passengers + cargo + reserve fuel (i.e. an aircraft lands with a small amount of fuel remaining kept in reserve for safety), while W_{fuel} is the weight of the usable fuel (i.e. not reserved).

The assumption of constant η_o and L/D are not quite accurate. In fact, the overall efficiency will change somewhat over the course of the flight due to the changing amoung of thrust required during the flight. Similarly, L/D will change since the amount of lift and drag change throughout the flight and usually not in proportion to another. However, viewing η_o and L/D as representing average values throughout the cruise, the Breguet range equation produces good estimates of an aircraft's range. Alternatively, the cruise of the aircraft can be broken into segments, each with different η_o and L/D, and then the range for each segment can be summed to obtain the range for the entire cruise.

edXproblem: 2.6.2 Range estimate for a large commercial transport

2.5 2.11

Consider a commercial transport aircraft with the following characteristics:

W_{initial}	400,000 kg
W_{fuel}	175,000 kg
η_o	0.32
L/D	17
Q_R	42 MJ/kg
g	9.81 m/sec^2

Note that we have given the weights W_{initial} and W_{fuel} in kilograms, which is actually a unit of mass. This is fairly common usage when giving weights in metric units, that is weights are often given as mass. To find the weight, we need to multiply the given masses by gravity. So, in reality, $W_{\text{initial}} = 3,924,000$ N and $W_{\text{fuel}} = 1,716,750$ N. However, for the Breguet range equation, we only use the ratio of weights which would be the same as the ratio of masses, that is $W_{\text{initial}}/W_{\text{final}} = m_{\text{initial}}/m_{\text{final}}$. But, be extra careful, because if you actually were to calculate the lift, or the lift coefficient, the weight needs to be in units of force (i.e. Newtons in metric)!

Estimate the range (during cruise portion of flight) for this aircraft. Please use kilometers and provide an answer that has three digits of precision (of the form X.YZeP).

edXsolution

Video Link

2.6.3 Assumptions in Breguet range analysis

2.11 2.5 2.6

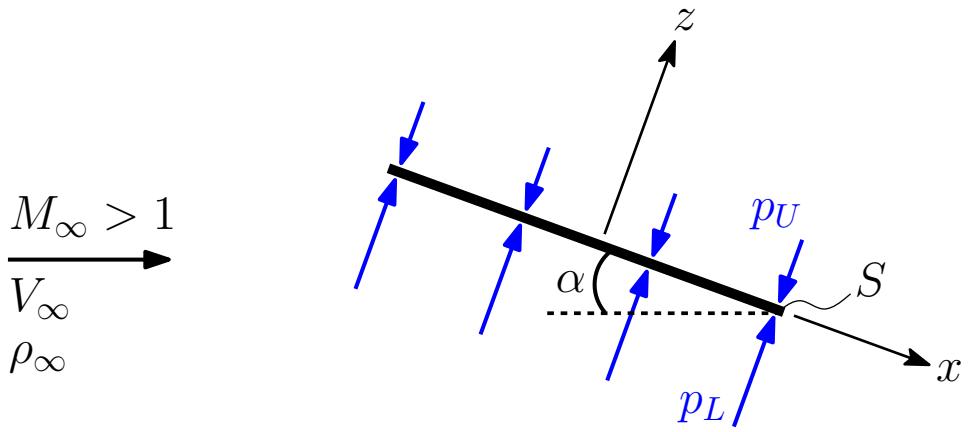
The assumptions used to derive the Breguet range equation (Equation 2.73) in practice do not strongly hold during the cruise portion of a flight. The specific manner in which the assumptions are violated in actual cruise will depend on the manner in which the aircraft is flown. In the following video, we consider the scenario in which L/D and flight speed are held fixed and show that this requires a change in altitude. The change in altitude is then quantified for the large commercial transport in Problem 2.6.2. It is shown that the altitude gain in this scenario will be small compared to the range.

Video Link

2.7 Sample Problems

edXproblem: 2.7.1 Lift and drag for a flat plate in supersonic flow

2.2 2.5



Consider a flat plate in a supersonic flow at an angle of attack α as shown in the figure above, and assume the flow is inviscid. We will learn later in the course that the resulting flow is such that the pressure is uniform on both the upper surface and lower surface of the plate, but of a different magnitude: the pressure on the upper surface, p_U, is lower than the pressure on the lower surface, p_L.

Denote the pressure difference as

$$\Delta p = p_L - p_U > 0 \tag{2.75}$$

and the plate surface area by S. Furthermore, use a small angle approximation for α, that is

$$\cos\alpha \approx 1 \quad , \quad \sin\alpha \approx \alpha \ . \tag{2.76}$$

where α has units of radians.

How does C_L depend on Δp? Answer by giving the power of the dependence, that is the value of m where $C_L \propto \Delta p^m$. Note that $\Delta p^0 = 1$, so $m = 0$ indicates no dependence.

How does C_D depend on Δp? Again, answer by giving the power of the dependence m of the dependence $C_D \propto \Delta p^m$.

We'll learn in the future that, for small values of α, the pressure difference is proportional to α for small α.

What then is the dependence of C_L on α?

What about the dependence of C_D on α?

edXsolution

Video Link

edXproblem: 2.7.2 Aerodynamic performance at different cruise altitudes

2.5

Consider again the commercial transport aircraft of Problem 2.4.2, in uniform level flight (cruise). It has the following characteristics:

$$\text{Cruise total weight:} \quad W = 550,000 \text{ lb} \tag{2.77}$$

$$\text{Wing area:} \quad S = 4,600 \text{ ft}^2 \tag{2.78}$$

$$\text{Aspect ratio:} \quad AR = 9 \tag{2.79}$$

We will compare its flight characteristics between cruise at an altitude of 35,000 ft and cruise at 12,000 ft. The following table gives the air density, ρ_∞, and speed of sound, a_∞, at these two altitudes. Note that, as you'll soon learn, the speed of sound varies with temperature and hence with altitude.

Altitude	Density ρ_∞	Speed of sound a_∞
12,000 ft	1.6×10^{-3} slug/ft^3	1069 ft/s
35,000 ft	7.3×10^{-4} slug/ft^3	973 ft/s

The operating cost of a commercial airliner is linked to the flight time (crew time, plane turn-around for given route) and passengers want to reach their destinations quickly. Thus, it is best to fly as fast as possible. On the other hand, for reasons we will discuss when we study the effects of compressibility and Mach number, the drag coefficient sharply rises as the speed of sound is approched. Therefore, commercial airlines usually cruise at around Mach 0.85, that is at a speed which is equal to 0.85 times the speed of sound at the flight altitude.

So let's assume that our aircraft flies at Mach 0.85, that is

$$V_\infty = 0.85\, a_\infty \ . \tag{2.80}$$

where a_∞ is the speed of sound at the corresponding altitude as given in the table above.

Further, utilize the parabolic drag model, assuming that at both altitudes

$$C_{D_0} = 0.05 \quad , \quad e = 0.8 \ . \tag{2.81}$$

What is the value of C_L when flying at 12,000 ft? Provide your answer with two digits of precision (of the form X.YeP).

What is the value of C_L when flying at 35,000 ft? Provide your answer with two digits of precision (of the form X.YeP).

What is the value of C_D in terms of counts of drag when flying at 12,000 ft? (Round your answer to the nearest drag count e.g. a C_D of 0.00523 would be entered as 52).

What is the value of C_D in terms of counts of drag when flying at 35,000 ft? (Round your answer to the nearest drag count e.g. a C_D of 0.00523 would be entered as 52).

What is L/D when flying at 12,000 ft? Provide your answer with three digits of precision (of the form X.YZeP).

What is L/D when flying at 35,000 ft? Provide your answer with three digits of precision (of the form X.YZeP).

How much thrust is required to fly at 12,000 ft? Give your answer in lb with three digits of precision (of the form X.YZeP).

How much thrust is required to fly at 35,000 ft? Give your answer in lb with three digits of precision (of the form X.YZeP).

How much power is required to fly at 12,000 ft? Give your answer lb·ft/s with three digits of precision (of the form X.YZeP).

How much power is required to fly at 35,000 ft? Give your answer lb·ft/s with three digits of precision (of the form X.YZeP).

edXsolution

Video Link

edXproblem: 2.7.3 Sensitivity of payload to efficiency

2.11

Consider the commercial transport aircraft in Problem 2.6.2. This aircraft has $\eta_o L/D = 5.44$. Suppose that $\eta_o L/D$ is 1% lower than that given, such that $\eta_o L/D = (0.99)(5.44)$. This might happen for example if the design predictions were in error by 1%. Or, as the engine is used, its efficiency tends to decrease overtime due to wear.

One way to estimate the magnitude of this impact is to determine the required decrease in initial weight (keeping the same amount of fuel) in order to maintain the same cruise range at this decreased value of $\eta_o L/D$. For a commercial transport aircraft, this decrease in initial weight would mean fewer passengers could fly at this cruise range.

Assume that the average weight for a passenger (including baggage) is 100 kg. For $\eta_o L/D = (0.99)(5.44)$, how many fewer passengers can fly while still maintaining the original cruise range? Note: round your answer upward since it is not possible to take a fraction of a passenger! Also, if you round any intermediate steps, be careful not to lose too much precision or your answer is likely to be incorrect.

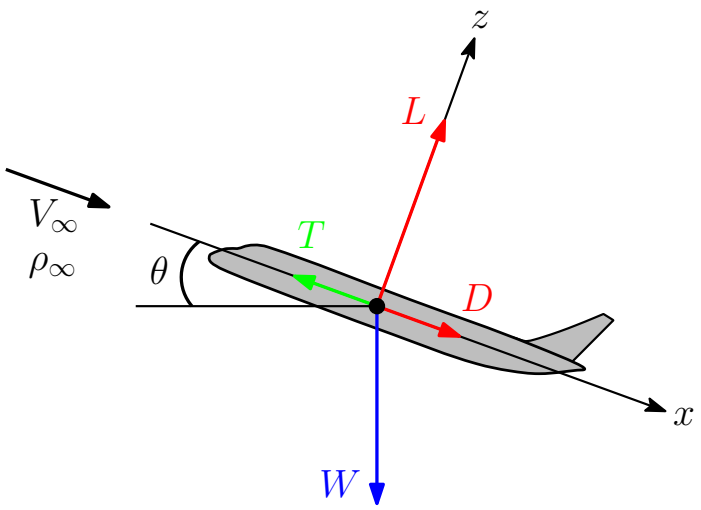
edXsolution

Video Link

edXproblem: 2.7.4 Rate of climb

2.1 2.2

Consider an aircraft climbing at constant velocity (V_∞ is constant) and at an angle θ with respect to the horizontal direction, as shown in the figure below. The vertical velocity of the aircraft, $\dot{h}$, is known as the *rate of climb*.



Derive an expression for the rate of climb in terms of only the following quantities: D, W, T, and V_∞.

edXsolution

Video Link

edXproblem: 2.7.5 Maximum lift-to-drag ratio for parabolic drag

2.5

In this problem, consider the parabolic drag model given in Equation (2.62). Assume that e and C_{D0} do not depend on C_L.

What is the value of C_L at which the lift-to-drag ratio (C_L/C_D) is maximized? Your answer will (at most) be a function of e, AR, and C_{D0}.

At the maximum lift-to-drag ratio, how does the induced drag compare to the drag at zero lift?

What is the maximum value of C_L/C_D? Your answer will (at most) be a function of e, AR, and C_{D0}.

edXsolution

Video Link

2.8 Homework Problems

edXproblem: 2.8.1 Cryogenic wind tunnel tests of an aircraft model

2.7 | 2.10 | 2.5 | 4.2 | 4.5

Consider a small aircraft flying at an altitude with the following characteristics

$$V_{\text{full}} = 10.0 \text{ m/s} \tag{2.82}$$
$$\rho_{\text{full}} = 0.500 \text{ kg/m}^3 \tag{2.83}$$
$$T_{\text{full}} = 233 \text{ K} \tag{2.84}$$

Assume air behaves like a calorically perfect, ideal gas with gas constant $R = 287$ J/kg·K and ratio of specific heats $\gamma = 1.4$.

Further assume that the dependence of air viscosity on temperaure is such that

$$\frac{\mu_1}{\mu_2} = \sqrt{\frac{T_1}{T_2}} \tag{2.85}$$

where $\mu_1 = \mu(T_1)$ and $\mu_2 = \mu(T_2)$ are the viscosities of air at temperatures T_1 and T_2.

For all questions in this problem, please report your answers with three significant digits of precision equivalent to the form X.YZeP.

Compute the pressure (use units of Pascals) in the freestream for the full-scale aircraft p_{full}.

Compute the aircraft's Mach number M_{full}.

A group wants to perform wind tunnel tests on a 1/5-scale model of the aircraft, that is the lengths of the model and full-scale aircraft are related by,

$$l_{\text{model}} = \frac{1}{5} l_{\text{full}} \tag{2.86}$$

They are considering using a cryogenic tunnel for these tests which has a pressure in the test section of

$$p_{\text{model}} = 1 \times 10^5 \text{Pa} \tag{2.87}$$

The air temperature in the cryogenic tunnel can be adjusted by cooling the air in the tunnel.

At which conditions should the wind tunnel tests be performed in order to ensure the flow represents the full size problem? Specifically, determine the following quantities:

Air density ρ_{model} in kg/m^3:

Air temperature T_{model} in K:

Tunnel velocity V_{model} in m/s:

The drag measured on the model at the cruise angle of attack is 100 N. What is the drag (in N) for the full-scale aircraft at the cruise angle of attack?

edXsolution

Video Link

edXproblem: 2.8.2 Impact of a winglet on a transport aircraft

2.11

Winglets can be used to increase L/D while keeping the overall wing span fixed. An airport will be limit and/or charge higher landing fees depending on the wing span of an aircraft. However, while winglets can have aerodynamic advantages, frequently they will add additional weight to the aircraft due to not only the weight of the winglet but also structural modifications that might be needed to support the new load. In this problem, we will quantify the potential impact of a winglet on overall performance.

Consider a commercial transport aircraft without winglets that has the following characteristics:

W_{initial}	225,000 kg	η_o	0.34	L/D	16
W_{fuel}	105,000 kg	Q_R	42 MJ/kg	g	9.81 m/sec^2

Estimate the aircraft range in kilometers (expending all of the fuel accounted for in W_{fuel}).

A winglet has been designed that would reduce the drag by 5%. Assuming that the winglet did not increase the weight of the aircraft (obviously very optimistic), how many kilograms of fuel would be required to achieve the same range as the original aircraft (i.e. the range determined in the previous part)? Assume that W_{fuel} is set to exactly the amount needed to achieve the same range, so at the end of flight $W_{\text{fuel}} = 0$.

Suppose the cost of jet fuel (in U.S. dollars) is \$0.75 per liter (L) and the density of jet fuel is 0.81 kg/L. Assume that the aircraft makes a (one-way) trip at the above range once each day. How much money in U.S. dollars is saved for a 365-day year with the addition of this winglet?

Again consider a winglet that reduces the drag by 5%. But this time determine the maximum increase in weight (due to adding the winglet) that would still allow a 1% reduction in the fuel required to achieve the same range as above. Please express this additional weight increase in kilograms.

In this scenario, how much money would be saved for a 365-day year? Please use U.S. dollars and provide an answer that has three digits of precision (of the form X.YZeP).

edXsolution

Video Link

edXproblem: 2.8.3 Minimum power flight with parabolic drag model

2.1 2.5

In this problem, you will investigate the conditions required to achieve minimum power for a given aircraft in steady level flight. Specifically, consider an aircraft with known values of W (aircraft weight) and S_{plan} and a flight condition with a known density ρ_∞.

- The propulsive power needed to overcome the drag at a flight speed of V_∞ is $P = DV_\infty$. Derive a relationship for P that has the following form,

$$P = f(W, S_{\text{plan}}, \rho_\infty) C_D^{a_1} C_L^{a_2} \tag{2.88}$$

  What is the numerical value of a_1?

  What is the numerical value of a_2?

  What is the function $f(W, S_{\text{plan}}, \rho_\infty)$? When entering this function, use W (make sure to use uppercase) to denote W, S (make sure to use uppercase) for S_{plan}, and r for ρ_∞.

- Next, using the parabolic drag model, $C_D = C_{D0} + C_L^2/(\pi AR e)$, assuming that C_{D0}, AR, and e are known for the given aircraft. The C_L that will minimize the propulsive power will be a function of C_{D0}, AR, and e. Enter the expression for the C_L that minimizes the propulsive power using CD0 to denote C_{D0}, AR for AR, and e for e.

- At the mininum power C_L for the parabolic drag model, what is the ratio (D_i/D) of the induced drag (D_i) to the total drag (D)? Note that $D_i/D = C_{Di}/C_D$.

- Consider now an autonomous aircraft with the following parameters:

  $S_{\text{plan}} = 0.3\,\text{m}^2$, $W = 3.5\,\text{N}$, $\rho_\infty = 1.225\,\text{kg/m}^3$, $AR = 10$, $e = 0.95$, $C_{D0} = 0.02$

  At the minimum power condition:

  Determine C_L:

  Determine C_D:

  Determine the flight speed V_∞ providing an answer in units of m/sec:

  Determine the required thrust providing an answer in units of Newtons:

  Determine the required power providing an answer in units of Watts:

edXsolution

Video Link

Module 3

Control Volume Analysis of Mass and Momentum Conservation

3.1 Overview

3.1.1 Measurable outcomes

In this module, we introduce the fundamental concept of control volume analysis in which we analyze the behavior of a fluid or gas as it evolves inside a fixed region in space, i.e. a control volume. In particular, we will consider how the mass and momentum of the flow can change in a control volume. Then, we apply this control volume statement of the conservation of mass and momentum to a variety of problems with an emphasis on aerospace applications.

Specifically, students successfully completing this module will be able to:

3.1. Describe a continuum model for a fluid and utilize the Knudsen number to support the use of a continuum model for typical atmospheric vehicles.

3.2. Define the density, pressure, and velocity of a flow and utilize a field representation of these (and other) fluid states to describe their variation in space and time. Define the difference between a steady and unsteady flow.

3.3. Define pathlines and streamlines and describe their relationship for unsteady and steady flow.

3.4. Describe an Eulerian and Lagrangian control volume. State the conservation of mass and momentum for an Eulerian control volume.

3.5. Explain the physical meaning of the terms of the integral form of mass conservation.

3.6. Apply the integral form of mass conservation to typical problems in aerospace engineering.

3.7. Explain the physical meaning of the terms of the integral form of momentum conservation.

3.8. Apply the integral form of momentum conservation to typical problems in aerospace engineering.

3.1.2 Pre-requisite material

The material in this module requires vector calculus and Measurable Outcome 2.2.

3.2 Continuum Model of a Fluid

3.2.1 Continuum versus molecular description of a fluid

3.1

We use the term fluid for both liquids and gases. Liquids and gases are made up of molecules. Is this discrete nature of the fluid important for us? In a liquid, molecules are in contact as they slide past each other, and overall act like a uniform fluid material at macroscopic scales.

In a gas, the molecules are not in immediate contact. So we must look at the *mean free path*, which is the distance the average molecule travels before colliding with another. Some known data for the air at different altitudes:

Altitude in km	Mean free path in m
0 (sea level)	10^{-7}
20 (U2 flight)	10^{-6}
50 (balloons)	10^{-5}
150 (low orbit)	1

Thus, the mean free path is vastly smaller than the typical dimension of any atmospheric vehicle. So even though the aerodynamic force on a wing is due to the impingement of discrete molecules, we can assume the air is a continuum for the purpose of computing this force. In contrast, computing the slight air drag on an orbiting satellite requires treating the air as discrete isolated particles since the mean free path and the size of satellite are similar. Even in the atmosphere, if the device has very small dimensions, for example if we are interested in a nanoscale device, we may have to consider the discrete nature of air.

As this discussion indicates, it is not the mean free path alone which is important to consider, but rather the ratio of the mean free path (l_{mfp}) to the reference length (l_{ref}). This ratio is known as the Knudsen number,

$$\text{Kn} \equiv \frac{l_{\text{mfp}}}{l_{\text{ref}}}. \tag{3.1}$$

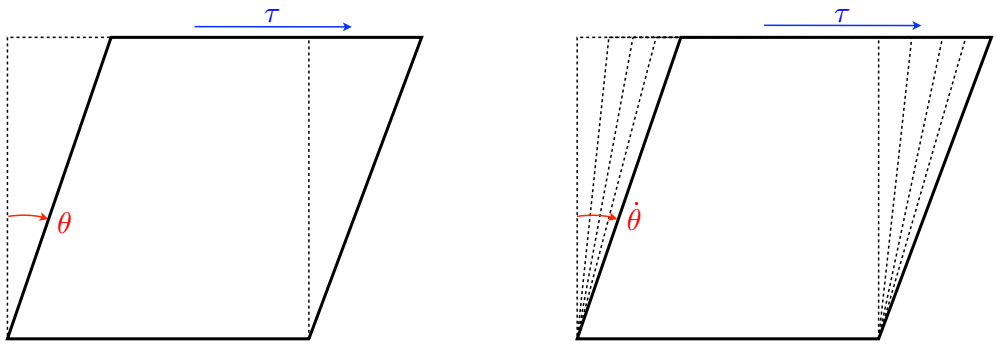
Thus, when the Knudsen number is small, i.e. $\text{Kn} \ll 1$, we do not need to analyze the motion of individual molecules around the vehicle. Instead, we can model the aggregate behavior of the molecules. In particular, instead of modeling each molecule and estimating how each molecule's velocity varies as it interacts with other molecules, we will model the gas as a continuum substance. This approach is called a continuum model and the study of continuum models of substances (solids, liquids, or gasses) is known as continuum mechanics.

The molecular modeling and continuum modeling approaches can be related to each other. This connection can be made by considering the statistical behavior of a population of molecules and determining how the molecular statistics evolve. The study of the statistical behavior of the motion of molecules is known as statistical mechanics. Statistical mechanics can be used to derive the governing equations for a continuum model of a gas. Our approach will be to assume the continuum model is valid and derive governing equations by applying the conservation principles of mass, momentum, and energy to this continuum model. We will however use some understanding of the molecular motion to motivate various assumptions in the derivation of our continuum model.

3.2.2 Solids versus fluids

3.1

Continuum mechanics can be used to model both solids and fluids (with fluids including both liquids and gasses). However, when applying the continuum model to solids and fluids, a key distinction is made with respect to how the solid and fluid responds to the application of a stress. Figure 3.1 shows how an initially square-shaped portion of a solid and fluid responds when a shear stress τ is applied on its upper surface. The solid will deform to a new sheared shape at some angle θ, where θ is commonly refered to as the strain, and will maintain that shape unless the shear stress τ is changed. A fluid will also shear under the action of τ but will do so continually at a strain rate $\dot{\theta}$ and will never achieve a new fixed shape.



(a) Solid (b) Fluid

Figure 3.1: Relation between shear and strain motion in a solid and fluid

The simplest relationships between τ and θ for a solid, or τ and $\dot{\theta}$ for a fluid are linear relationships. For a solid, this linear relationship would be,

$$\tau = G\theta \tag{3.2}$$

where the constant of proportionality G is called the *elastic modulus*, and has the units of force/area. For a fluid, this linear relationship would be,

$$\tau = \mu\dot{\theta}, \tag{3.3}$$

where the constant of proportionality μ is the *dynamic viscosity* (introduced in Sections 2.4.4 and 2.4.6), and has the units of force×time/area.

3.2.3 Density

3.2

The fluid density ρ is defined as the mass/volume of the fluid for an infinitesimally small volume $\delta\mathcal{V}$,

$$\rho \equiv \lim_{\delta\mathcal{V}\to 0} \frac{\delta m}{\delta\mathcal{V}} \tag{3.4}$$

The density can vary in space and possibly also time, so we write the density as the function $\rho(x, y, z, t)$. A scalar quantity such as the density that varies in space and time is a called time-varying scalar field.

The density can also be defined from a molecular view. In the molecular case, we would consider a small volume (though large enough to contain many molecules) at one instant in time and count the number of molecules of the volume at that instant. The density would then be the number of molecules multiplied by molecular mass of a single molecule, and finally divided by the volume.

3.2.4 Pressure

3.2

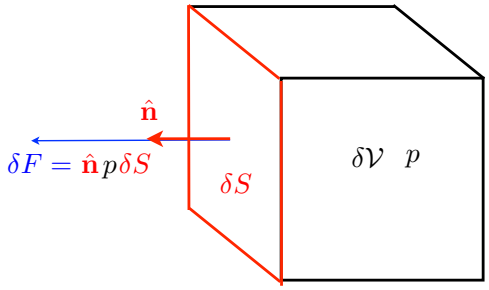


Figure 3.2: A cube-shaped infinitesimal volume with pressure p and volume $\delta\mathcal{V}$. The volume exerts an infinitesimal force δF on neighboring matter through the face δS in the outward normal direction $\hat{\mathbf{n}}$.

The pressure p is defined as the magnitude of the normal force/area that an infinitesimal volume of fluid exerts on neighboring fluid (or on the neighboring material if at the surface of a body). Specifically, consider an infinitesimal volume of fluid $\delta\mathcal{V}$ and an infinitesimal region, δS, of the surface of the volume. Let the outward-pointing normal of δS be $\hat{\mathbf{n}}$. For example, Figure 3.2 shows a cube-shaped infinitesimal volume with square face. Then, the infinitesimal volume exerts an infinitesimal force on the neighboring matter (fluid or otherwise) given by,

$$\delta F = \hat{\mathbf{n}}\, p\, \delta S. \tag{3.5}$$

Equivalently, defining δF_n as the infinitesimal force in the direction of $\hat{\mathbf{n}}$, then the pressure is defined as,

$$p \equiv \lim_{\delta S \to 0} \frac{\delta F_n}{\delta S} \tag{3.6}$$

Like the density, the pressure is a time-varying scalar field, that is, $p(x, y, z, t)$.

At the molecular level, the pressure in a gas can be interpreted as the normal force/area exerted when molecules collide (more accurately, the molecules interact and repel each other prior to actually colliding) as they pass between neighboring regions in space through δS.

3.2.5 Velocity

3.2

In our continuum model of a fluid, we can consider the fluid to be composed of infinitesimal volumes that move with the fluid, such that the volumes always contain the same matter. We will refer to these infinitesimal volumes that move with the fluid as *fluid elements*. Figure 3.3 shows the paths of four fluid elements as they move around an airfoil.

The velocity in our continuum model is defined as,

$$\mathbf{V} \text{ at a point } = \text{ velocity of fluid element as it passes that point} \tag{3.7}$$

This velocity is a vector, with three separate components, and will in general vary between different points and different times,

$$\mathbf{V}(x, y, z, t) \;=\; u(x, y, z, t)\, \hat{\mathbf{i}} \;+\; v(x, y, z, t)\, \hat{\mathbf{j}} \;+\; w(x, y, z, t)\, \hat{\mathbf{k}}. \tag{3.8}$$

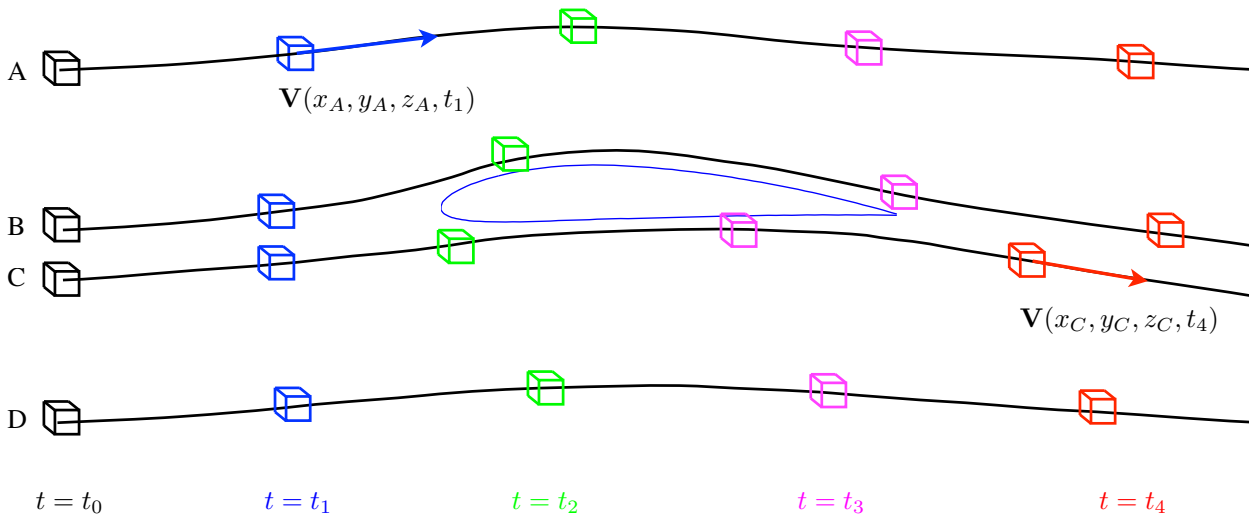


Figure 3.3: Motion of four fluid elements showing their locations at $t = t_0$, t_1, t_2, t_3, and t_4. Velocity vectors shown for fluid element A at t_1 and fluid element C at t_4.

So $\mathbf{V}$ is a time-varying vector field, whose components are three separate time-varying scalar fields u, v, w. We will also use index notation to denote the components of the velocity such that,

$$u_1 = u, \quad u_2 = v, \quad u_3 = w. \tag{3.9}$$

A useful quantity to define is the *speed*, which is the magnitude of the velocity vector.

$$V(x, y, z, t) \;=\; |\mathbf{V}| \;=\; \sqrt{u^2 + v^2 + w^2} \tag{3.10}$$

In general this is a time-varying scalar field. Note that the speed can also be written compactly using index notation as,

$$V = \sqrt{u_i u_i} \tag{3.11}$$

where the repeated index using Einstein's index notation convention expands to a summation over all values of the index, i.e. $u_i u_i = u_1 u_1 + u_2 u_2 + u_3 u_3$.

At the molecular level, the molecules in the vicinity of point (x, y, z) at time t generally do not have the continuum model velocity $\mathbf{V}(x, y, z, t)$. This is because the molecules have random motion associated with the temperature. Thus, the continuum velocity $\mathbf{V}(x, y, z, t)$ represents the average velocity of the molecules around (x, y, z) at time t.

As an example of this random molecular motion, consider the air in a room that does not have a fan, vent, or other source of motion. We observe that the air does not have any velocity, $\mathbf{V} = 0$ everywhere. This is in fact a continuum view of air, which is often how we naturally think about air. In reality, the molecules in the air are moving, and at speed that depends on the temperature in the room. So, unless you are in a room with the temperature being absolute zero, the molecules in the room are moving, even though their average velocity is zero.

3.2.6 More on the molecular view of pressure and frictional forces on a body

2.2 3.1

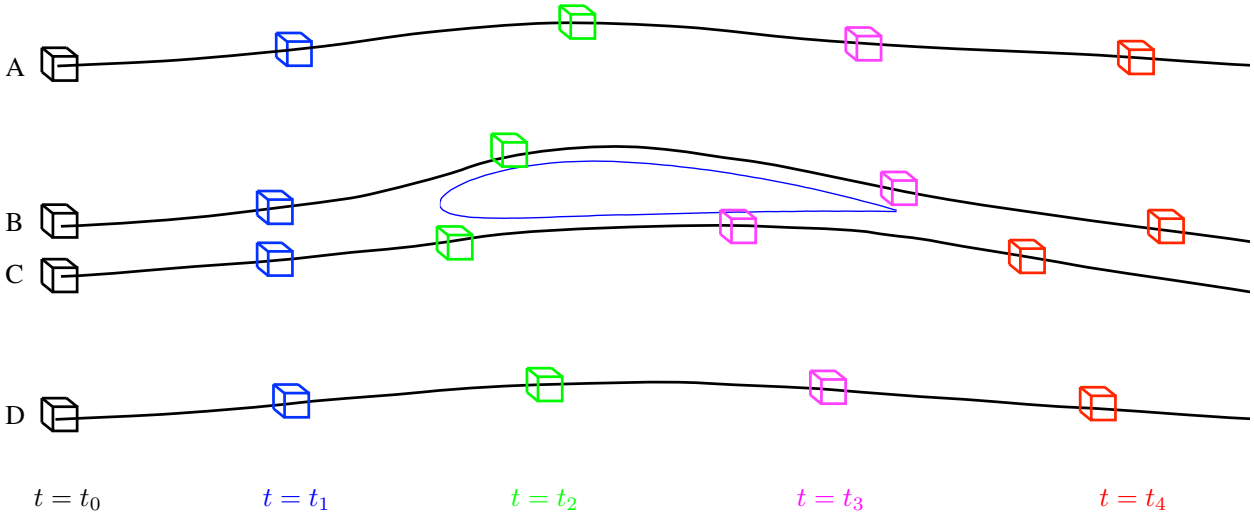
Let's take a brief pause in our development of a continuum model of fluid motion to look a bit more closely at how the "actual" molecular motion gives rise to forces on a body.

Note: this video was created during the Fall 2013 offering of 16.101x, in response to questions from students.

Video Link

edXproblem: 3.2.7 Velocity of a fluid element

3.2



In the figure, assume that the times t_0 through t_4 are all equally spaced, i.e. $t_{j+1} - t_j$ is a constant.

What is the location of the largest speed? Indicate your answer using the following notation: Xjk where X is the fluid element and j and k are the integer the time indices between which the largest speed occurs (note that k must be j+1). For example, D12 is element D between times t_1 and t_2.

What is the location of the smallest speed? (Use the same notation)

edXsolution

Video Link

3.2.8 Steady and unsteady flows

3.2

If the flow is *steady*, then ρ, p, $\mathbf{V}$ (and any other states of the flow) do not change in time for any point, and hence can be given as $\rho(x, y, z)$, $p(x, y, z)$, $\mathbf{V}(x, y, z)$. If the flow is *unsteady*, then these quantities do change in time at some or all points.

edXproblem: 3.2.9 Fluid element in steady flow

3.1 3.2

Consider a fluid element in a steady flow. Which is the best answer with respect to the variation in time of the density and mass of the fluid element?

edXsolution

Video Link

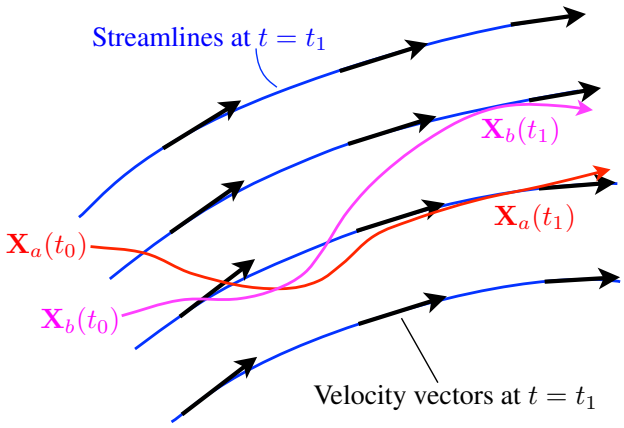


Figure 3.4: Illustration of pathlines and streamlines in an unsteady flow.

3.2.10 Pathlines and streamlines

3.3

As we analyze flows, we often sketch the direction the flow travels. In this section, we make this concept more precise and define pathlines and streamlines.

Pathlines: A pathline is the line along which a fluid element travels. The time rate of change of the position of the fluid element is the velocity,

$$\frac{\mathrm{d}\mathbf{X}}{\mathrm{d}t} = \mathbf{V}(\mathbf{X}, t) \tag{3.12}$$

Then, given an initial position of a fluid element, $\mathbf{X}_0$ at time t_0, the pathline can be found by integrating the velocity field,

$$\mathbf{X}(t) = \mathbf{X}_0 + \int_{t_0}^{t} \mathbf{V}\left(\mathbf{X}, \tau\right) \mathrm{d}\tau \tag{3.13}$$

Streamlines: A streamline is a line which is everywhere tangent to the velocity field at some time. If the velocity field is time dependent (i.e. the flow is unsteady) then the streamlines will be a function of time as well. For a steady flow, the pathlines and streamlines are identical.

Figure 3.4 demonstrates the difference between pathlines and streamlines. The figure shows the pathlines for two fluid elements $\mathbf{X}_a(t)$ and $\mathbf{X}_b(t)$. Also shown are the velocity vectors and streamlines at $t = t_1$. Note that while the pathlines appear to cross each other, in fact the pathlines cannot intersect the same location at the same instant in time. Also note that the pathlines are tangent to the streamlines at $t = t_1$.

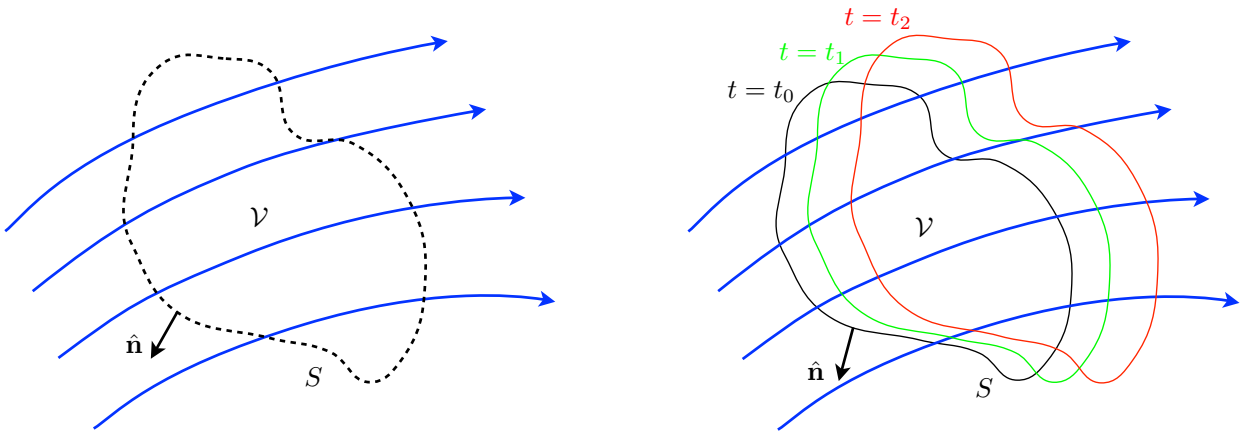
3.3 Introduction to Control Volume Analysis

3.3.1 Control volume definition

3.4

In developing the equations governing aerodynamics, we will invoke the physical laws of conservation of mass, momentum, and energy. However, because we are not dealing with isolated point masses, but rather a continuous deformable medium, we will require new conceptual and mathematical techniques to apply these laws correctly.

One concept is the *control volume*, which is an identified volume of space containing fluid to which we will apply the conservation laws. In principle, the volume could be chosen to move and deform its shape as time evolves. However, in many cases, the control volume is stationary in an appropriately chosen frame of reference. This type of control volume which is fixed in space is frequently refered to as an *Eulerian control volume*. Figure 3.5 shows an Eulerian control volume. In this example, the flow travels freely through the control volume boundaries. In other situations, a portion of the control volume boundary may correspond to a solid surface (e.g. the surface of a wing) through which flow cannot pass.



(a) Eulerian control volume

(b) Lagrangian control volume

Figure 3.5: Examples of an Eulerian control volume and Lagrangian control volume (i.e. control mass). In either case, the volume is denoted $\mathcal{V}$ with its boundary surface denoted S and the outward pointing normal at some location on the surface is $\hat{\mathbf{n}}$.

A closely related concept is the *control mass*, which is an identified mass of the fluid to which the conservation principles are applied. The control mass though will move with the fluid and deform it shape. In fact, a control mass is equivalent a control volume which is defined to follow the fluid. Often, a control mass is refered to as a *Lagrangian control volume*. An example of a Lagrangian control volume (i.e. control mass) is shown in Figure 3.5.

3.3.2 Conservation of mass and momentum

3.4

Before deriving the mathematical statements of the conservation of mass and momentum applied to Eulerian control volumes, we will first state these laws.

Conservation of mass: The conservation of mass requires that mass cannot be created or destroyed. In terms of an Eulerian control volume, mass can enter or leave the control volume at

its boundaries. However, since mass cannot be created or destroyed, this means that the mass in the control volume must change to account for the flow of mass across its boundaries. Specifically, stating the conservation of mass as a rate equation applied to an Eulerian control volume, we could say,

$$\frac{\mathrm{d}}{\mathrm{d}t}\left(\text{mass in } \mathcal{V}\right) = \left(\text{flow of mass into } \mathcal{V}\right). \tag{3.14}$$

However, common convention is to combine the terms and state the conservation of mass as,

$$\frac{\mathrm{d}}{\mathrm{d}t}\left(\text{mass in } \mathcal{V}\right) + \left(\text{flow of mass out of } \mathcal{V}\right) = 0 \tag{3.15}$$

If the two terms on the left were not in balance (i.e. their sum was non-zero), then this would mean that rate of change of mass in the control volume did not equal the flow of mass into the control volume. In other words, mass would have been created (or destroyed). Thus, the sum of the terms on the left-hand side represents the rate at which mass is created within the control volume, and Equation (3.15) states that the rate of mass creation is zero within the control volume.

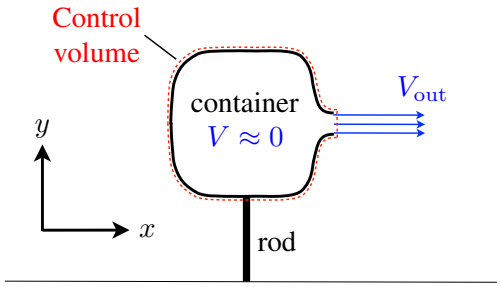
Conservation of momentum: The conservation of momentum states that the rate of change of momentum in a system is equal to the sum of the forces applied to the system. Using the same convention as for the conservation of mass, conservation of momentum applied to an Eulerian control volume gives,

$$\frac{\mathrm{d}}{\mathrm{d}t}\left(\text{momentum in } \mathcal{V}\right) + \left(\text{flow of momentum out of } \mathcal{V}\right) = \sum\left(\text{forces acting on } \mathcal{V}\right) \tag{3.16}$$

As opposed to mass, momentum can be created (or destroyed) in a control volume *if* the sum of the forces on the control volume is non-zero.

edXproblem: 3.3.3 Release of pressurized air

3.6 3.8



A container with pressurized air is being held in place by a rod. The container is emitting air at velocity V_{out} as shown in the figure. Inside the container, the velocity of the air is negligible ($V \approx 0$) which also implies that the momentum in the container is negligible. A control volume that is useful for this problem is also shown in the figure.

The rate of change of mass inside the container is:

The rod is acting on the container with a force that, in the x-direction, is:

edXsolution

Video Link

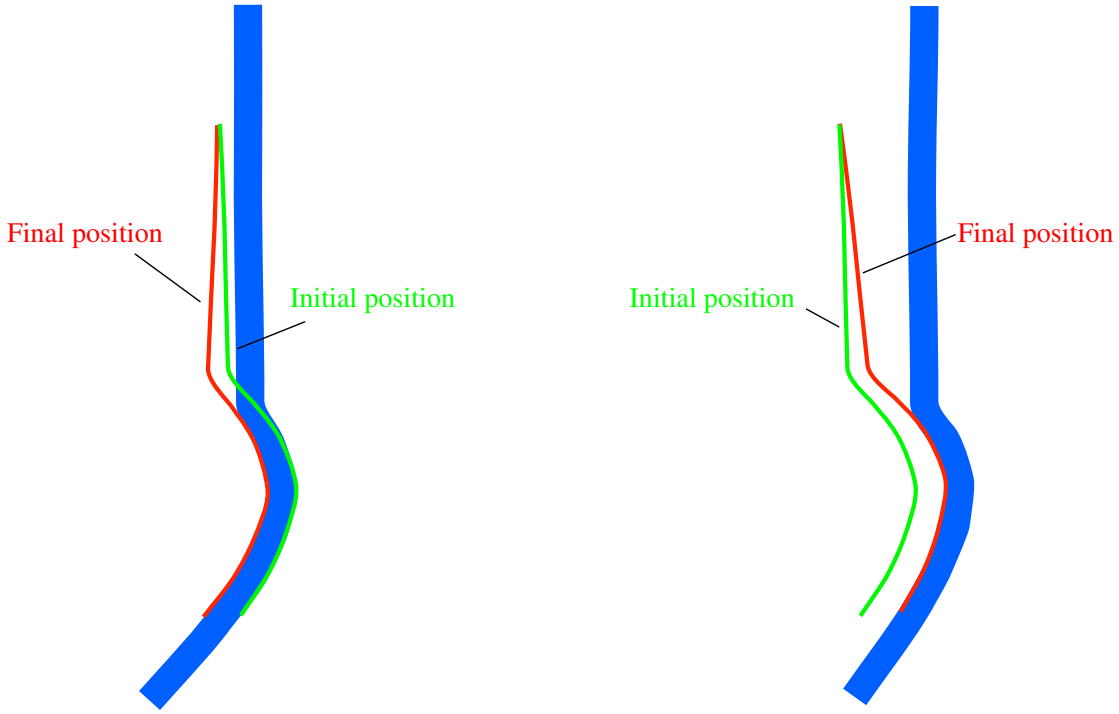
edXproblem: 3.3.4 Water flow around a spoon

3.6 3.8

Now it is time for a little experimental fluid dynamics! In fact, this is an experiment you can do by yourself. All you need is a spoon and a smooth, steady stream of water. To start with, please take a look at the following video which will show you the experimental set-up.

Video Link

I will move the spoon into the stream and the stream will curve around the spoon. As a result, the spoon will rotate into a new steady position. As shown in Figure 3.6, the new position of the spoon will be either (A) to the left from its initial position when it first contacts the water, or (B) to the right from its initial position when it first contacts the water.



(A) Spoon moves to the left (B) Spoon moves to the right

Figure 3.6: What will the new position of the spoon be?

Before doing the experiment yourself, apply the conservation principles to determine the motion of the spoon. What do you predict will be the motion of the spoon?

edXsolution

Here's the solution video:

Video Link

Here's the experiment showing the spoon entering the water:

Video Link

3.4 Conservation of Mass

3.4.1 Rate of change of mass inside a control volume

3.5

In this section, we will express the rate of change of mass inside the control volume mathematically in terms of the fluid states. Since the density is the mass/volume, we may integrate the density throughout the control volume to determine the mass in the control volume,

$$\text{mass in } \mathcal{V} = \iiint_{\mathcal{V}} \rho \, \mathrm{d}\mathcal{V} \tag{3.17}$$

Then, the time rate of change can be found by differentiating with respect to time,

$$\frac{\mathrm{d}}{\mathrm{d}t} (\text{mass in } \mathcal{V}) = \frac{\mathrm{d}}{\mathrm{d}t} \iiint_{\mathcal{V}} \rho \, \mathrm{d}\mathcal{V}. \tag{3.18}$$

For a control volume that is fixed in space, the time derivative can also be brought inside the spatial integral to give,

$$\frac{\mathrm{d}}{\mathrm{d}t} (\text{mass in } \mathcal{V}) = \iiint_{\mathcal{V}} \frac{\partial \rho}{\partial t} \, \mathrm{d}\mathcal{V}. \tag{3.19}$$

3.4.2 Mass flow leaving a control volume

3.5

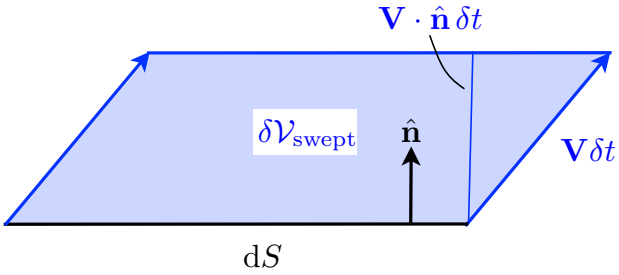


Figure 3.7: Volume of fluid, $\delta \mathcal{V}_{\text{swept}}$, that crosses an infinitesimal surface patch $\mathrm{d}S$ in time δt. (Note: side view shown)

Consider an infinitesimal patch of the surface of the fixed, permeable control volume. As shown in Figure 3.7, the patch has area $\mathrm{d}S$, and normal unit vector $\hat{n}$. The plane of fluid particles which are on the surface at time t will move off the surface at time $t + \delta t$, sweeping out an infinitesimal volume given by,

$$\delta \mathcal{V}_{\text{swept}} \;=\; \mathbf{V} \cdot \hat{\mathbf{n}} \delta t \, \mathrm{d}S, \tag{3.20}$$

where $\mathbf{V} \cdot \hat{\mathbf{n}}$ is the component of the velocity vector normal to the patch.

The mass of fluid in this swept volume can be found by multiplying by the density to give,

$$\delta m_{\text{swept}} \;=\; \rho \, \mathbf{V} \cdot \hat{\mathbf{n}} \delta t \, \mathrm{d}S. \tag{3.21}$$

The total mass that flows out of the entire control volume in time δt can then be found by integrating over the entire surface,

$$\delta m_{\text{swept, total}} \;=\; \delta t \iint_{S} \rho \, \mathbf{V} \cdot \hat{\mathbf{n}} \, \mathrm{d}S \tag{3.22}$$

where δt is taken outside of the integral since it is a constant.

The time rate at which the mass leaves the control volume, called the *mass flow rate* is then

$$\text{mass flow rate} = \lim_{\delta t \to 0} \frac{\delta m_{\text{swept, total}}}{\delta t} = \iint_S \rho \, \mathbf{V} \cdot \hat{\mathbf{n}} \, \mathrm{d}S. \tag{3.23}$$

Another commonly used quantity is the *mass flux* and is defined simply as mass flow per area,

$$\text{mass flux} \equiv \rho \mathbf{V} \cdot \hat{\mathbf{n}} \tag{3.24}$$

At a solid surface, $\mathbf{V} \cdot \hat{\mathbf{n}} = 0$ since the flow cannot enter the solid. So the portion of a control volume boundary at a solid surface does not contribute to the mass flow. This result is frequently used when performing control volume analysis, and is an important consideration when choosing a control volume.

3.4.3 Conservation of mass in integral form

3.5

The conservation of mass for a control volume fixed in space as expressed in Equation (3.15) can be written mathematically using the results in Equations (3.18) and (3.23),

$$\frac{\mathrm{d}}{\mathrm{d}t} \iiint_{\mathcal{V}} \rho \, \mathrm{d}\mathcal{V} + \iint_S \rho \, \mathbf{V} \cdot \hat{\mathbf{n}} \, \mathrm{d}S = 0. \tag{3.25}$$

Or, alternatively, using Equation (3.19),

$$\iiint_{\mathcal{V}} \frac{\partial \rho}{\partial t} \, \mathrm{d}\mathcal{V} + \iint_S \rho \, \mathbf{V} \cdot \hat{\mathbf{n}} \, \mathrm{d}S = 0. \tag{3.26}$$

3.4.4 Application to channel flow (mass conservation)

3.6

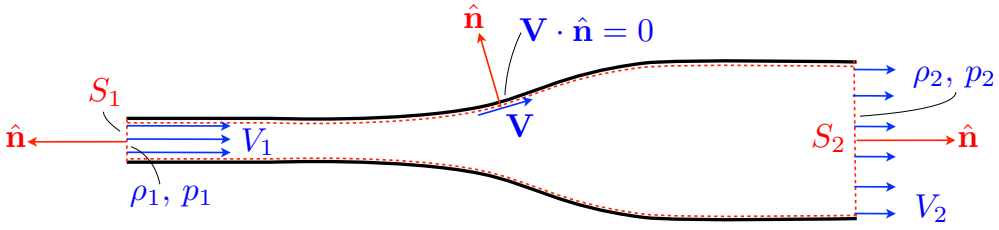


Figure 3.8: Channel control volume and flow conditions

Now, let's apply the integral form of conservation of mass to the channel flow shown in Figure 3.8. The flow is assumed to have uniform velocity, density, and pressure at its inlet (V_1, ρ_1, and p_1) and outlet (V_2, ρ_2, and p_2). Further, we will assume that the flow in the channel is steady. As we will derive in the following video, conservation of mass requires that,

$$\rho_1 V_1 S_1 = \rho_2 V_2 S_2 \tag{3.27}$$

Thus, when there is no unsteadiness, the mass flow leaving the outlet is the same as the mass flow entering the inlet. Further, we can re-arrange this expression to show that the mass flux varies inversely with the area,

$$\frac{\rho_2 V_2}{\rho_1 V_1} = \frac{S_1}{S_2} \tag{3.28}$$

Thus, when the area increases (as drawn in this figure), the mass flux decreases (or vice-versa when the area decreases the mass flux increases). For flows where the density is essentially constant (which would be true for water or for low Mach number air flows), this can be simplified further to,

$$\frac{V_2}{V_1} = \frac{S_1}{S_2} \text{ when } \rho = \text{constant} \tag{3.29}$$

Thus, when the area increases, the velocity decreases (and vice-versa).

Video Link

edXproblem: 3.4.5 Release of pressurized air (mass conservation)

3.6 | 3.2

Suppose that the density and speed of the air emitted from the container in Problem 3.3.3 is $\rho_{\text{out}} = 1.225$ kg/m^3 and $V_{\text{out}} = 10$ m/sec, and the container exit has a diameter of 0.2 m.

What is the rate of change of mass in the container in kg/sec?

Which of the following statements best describes the flow in the container:

edXsolution

Video Link

3.5 Conservation of Momentum

3.5.1 Rate of change of momentum inside a control volume

3.7

In this section, we will express the rate of change of momentum inside the control volume mathematically in terms of the fluid states. This section is an extension of the results in Section 3.4.1. The momentum/volume is given by $\rho\mathbf{V}$, which we may integrate throughout the control volume to determine the momentum in the control volume,

$$\text{momentum in } \mathcal{V} = \iiint_{\mathcal{V}} \rho\mathbf{V}\,\mathrm{d}\mathcal{V} \tag{3.30}$$

Then, the time rate of change can be found by differentiating with respect to time,

$$\frac{\mathrm{d}}{\mathrm{d}t}\left(\text{momentum in } \mathcal{V}\right) = \frac{\mathrm{d}}{\mathrm{d}t}\iiint_{\mathcal{V}} \rho\mathbf{V}\,\mathrm{d}\mathcal{V}. \tag{3.31}$$

For a control volume that is fixed in space, the time derivative can also be brought inside the spatial integral to give,

$$\frac{\mathrm{d}}{\mathrm{d}t}\left(\text{momentum in } \mathcal{V}\right) = \iiint_{\mathcal{V}} \frac{\partial}{\partial t}\left(\rho\mathbf{V}\right)\,\mathrm{d}\mathcal{V}. \tag{3.32}$$

We can also consider a specific component of the momentum, as opposed to the entire momentum vector. For example, the time rate of change for the j-momentum component in the control volume is,

$$\frac{\mathrm{d}}{\mathrm{d}t}\left(j\text{-momentum in } \mathcal{V}\right) = \frac{\mathrm{d}}{\mathrm{d}t}\iiint_{\mathcal{V}} \rho u_j\,\mathrm{d}\mathcal{V} = \iiint_{\mathcal{V}} \frac{\partial}{\partial t}\left(\rho u_j\right)\,\mathrm{d}\mathcal{V}. \tag{3.33}$$

3.5.2 Momentum flow leaving a control volume

3.7

Following the same approach as in Section 3.4.2, the flow of momentum out of the entire control volume

$$\text{momentum flow } = \iint_S \rho\mathbf{V}\,\mathbf{V}\cdot\hat{\mathbf{n}}\,\mathrm{d}S, \tag{3.34}$$

and the momentum flux is,

$$\text{momentum flux} \equiv \rho\mathbf{V}\,\mathbf{V}\cdot\hat{\mathbf{n}} \tag{3.35}$$

Considering only the j-component of momentum gives,

$$j\text{-momentum flow } = \iint_S \rho u_j\,\mathbf{V}\cdot\hat{\mathbf{n}}\,\mathrm{d}S, \tag{3.36}$$

and the j-momentum flux is,

$$j\text{-momentum flux} \equiv \rho u_j\,\mathbf{V}\cdot\hat{\mathbf{n}} \tag{3.37}$$

As with the mass flow, since at a solid surface, $\mathbf{V}\cdot\hat{\mathbf{n}} = 0$ then the portion of a control volume boundary at a solid surface does not contribute to the momentum flow out of the control volume.

edXproblem: 3.5.3 Release of pressurized air (momentum flow)

3.8

Consider again the container in Problem 3.4.5. Recall from that problem that $\rho_{\text{out}} = 1.225$ kg/m^3 and $V_{\text{out}} = 10$ m/sec, and the container exit has a diameter of 0.2 m.

What is the flow of x-momentum out of the container (in units of Newtons)?

edXsolution

Video Link

3.5.4 Forces acting on a control volume

3.7

We will consider two types of forces that act on the control volume:

Body force: a force acting within the volume. In our case, the body force will be gravity.

Surface force: a force acting on the surface of the control volume. In our case, the surface forces arising from the fluid will be due to pressure and viscous stresses. In addition, we will occasionally include surface forces arising from structures that are cut by the control volume surface.

A common difficulty with this distinction of body and surface forces is that, in fact, the pressure and viscous stresses which give rise to the surfaces forces are present inside the volume. However, within the control volume, these forces are balanced between neighboring fluid elements. For example, consider two neighboring fluid elements, element A and element B. The pressure force applied by element A on element B is exactly the opposite of the pressure force applied by element B on element A. Thus, the result is no net force within the volume. However, at the surface of the volume, the pressure produces a non-zero force acting on the fluid that is inside the control volume. The same argument also applies to viscous forces.

The body force due to gravity can be found by integrating the gravitational force/volume over the entire control volume. The gravitational force/volume is given by $\rho\mathbf{g}$ where $\mathbf{g}$ is the gravitational acceleration. Thus, the body force due to gravity acting on the control volume is,

$$\text{gravitational force on } \mathcal{V} = \iiint_{\mathcal{V}} \rho\mathbf{g}\,\mathrm{d}\mathcal{V} \tag{3.38}$$

The pressure and viscous force acting on the surface of a control volume can be determine in the same manner as the pressure and viscous force acting on the surface of the body in Equation (2.7). Thus, the pressure and viscous forces acting on the control volume are,

$$\text{pressure force on } \mathcal{V} = -\iint_S p\,\hat{\mathbf{n}}\,\mathrm{d}S, \tag{3.39}$$

$$\text{viscous force on } \mathcal{V} = \iint_S \boldsymbol{\tau}\,\mathrm{d}S, \tag{3.40}$$

The forces can also be broken into individual components. Doing this give the force in the j-direction as,

$$j\text{-component of gravitational force on } \mathcal{V} = \iiint_{\mathcal{V}} \rho g_j\,\mathrm{d}\mathcal{V} \tag{3.41}$$

$$j\text{-component of pressure force on } \mathcal{V} = -\iint_S p\,\hat{n}_j\,\mathrm{d}S, \tag{3.42}$$

$$j\text{-component of viscous force on } \mathcal{V} = \iint_S \tau_j\,\mathrm{d}S, \tag{3.43}$$

where $g_j = \mathbf{g}\cdot\hat{\mathbf{e}}_j$, $\hat{n}_j = \hat{\mathbf{n}}\cdot\hat{\mathbf{e}}_j$, and $\tau_j = \boldsymbol{\tau}\cdot\hat{\mathbf{e}}_j$ and $\hat{\mathbf{e}}_j$ is the unit vector in the j-coordinate direction.

Occasionally, we are interested in including forces that act on the control volume that do not arise in the fluid. An example of this situation is in Problem 3.3.3 where the support rod is cut by the control volume. To denote this possibility, we will include $\sum \mathbf{F}_{\text{ext}}$ to represent external forces

applied to the control volume. Here, we use the word *external* to represent forces acting on the control volume that are not part of the fluid. When this situation occurs, some region of the control volume must be of non-fluid substance, i.e. there is a region in the control volume that is outside the fluid. Thus, all of the forces which could be included in a control volume analysis are,

$$\iiint_{\mathcal{V}} \rho \mathbf{g} \, \mathrm{d}\mathcal{V} - \iint_{S} p \, \hat{\mathbf{n}} \, \mathrm{d}S + \iint_{S} \boldsymbol{\tau} \, \mathrm{d}S + \sum \mathbf{F}_{\text{ext}} \tag{3.44}$$

When using a control volume that includes not only the fluid but also other materials, if the mass or momentum of the other materials are changing inside the control volume, then that must be accounted for in the application of the conservation law. In the equations we develop, we will assume that the only dynamics occur in the fluid portions of the control volume.

edXproblem: 3.5.5 Release of pressurized air (forces)

3.8

Consider again the container in Problem 3.5.3. Recall from that problem that $\rho_{\text{out}} = 1.225$ kg/m^3 and $V_{\text{out}} = 10$ m/sec, and the container exit has a diameter of 0.2 m.

Further, assume that the air pressure outside of the container (including in the jet emitting from the container) is everywhere equal to the atmospheric pressure, $p_\infty = 1.01 \times 10^5$ Pascals (Pa). Note that this is a reasonable assumption for a nozzle in which the streamlines enter the atmosphere in parallel, straight lines. If the pressure in the jet were different than p_∞, then the streamlines would curve (inward if the pressure in the jet were less than p_∞ and outward if the pressure in the jet were greater than p_∞). We will investigate this phenomenon later in the semester.

What is the x-component of the pressure force with which the air acts on the control volume (in units of Newtons)?

edXsolution

Video Link

3.5.6 When are viscous contributions negligible?

3.7

An important, often subtle, part of control volume analysis is determining when viscous contributions are negligible on a surface of the control volume. Understanding how to choose a control volume such that viscous contributions have negligible impact on the analysis is critical.

In the following video, we discuss when viscous contributions are negligible. We then apply this to the pressurized air container of Problem 3.5.5.

Video Link

3.5.7 Conservation of momentum in integral form

3.7

The conservation of momentum for a control volume fixed in space as expressed in Equation (3.16) can be written mathematically using the results in Equations (3.31) (3.34), (3.38), (3.39), and (3.40),

$$\frac{\mathrm{d}}{\mathrm{d}t}\iiint_{\mathcal{V}}\rho\mathbf{V}\,\mathrm{d}\mathcal{V}+\iint_{S}\rho\mathbf{V}\,\mathbf{V}\cdot\hat{\mathbf{n}}\,\mathrm{d}S=\iiint_{\mathcal{V}}\rho\mathbf{g}\,\mathrm{d}\mathcal{V}-\iint_{S}p\,\hat{\mathbf{n}}\,\mathrm{d}S+\iint_{S}\boldsymbol{\tau}\,\mathrm{d}S+\sum\mathbf{F}_{\text{ext}}. \tag{3.45}$$

Or, alternatively, using Equation (3.32),

$$\iiint_{\mathcal{V}}\frac{\partial}{\partial t}\left(\rho\mathbf{V}\right)\,\mathrm{d}\mathcal{V}+\iint_{S}\rho\mathbf{V}\,\mathbf{V}\cdot\hat{\mathbf{n}}\,\mathrm{d}S=\iiint_{\mathcal{V}}\rho\mathbf{g}\,\mathrm{d}\mathcal{V}-\iint_{S}p\,\hat{\mathbf{n}}\,\mathrm{d}S+\iint_{S}\boldsymbol{\tau}\,\mathrm{d}S+\sum\mathbf{F}_{\text{ext}}. \tag{3.46}$$

Considering only the j-component of momentum gives,

$$\iiint_{\mathcal{V}}\frac{\partial}{\partial t}\left(\rho u_j\right)\,\mathrm{d}\mathcal{V}+\iint_{S}\rho u_j\,\mathbf{V}\cdot\hat{\mathbf{n}}\,\mathrm{d}S=\iiint_{\mathcal{V}}\rho g_j\,\mathrm{d}\mathcal{V}-\iint_{S}p\,\hat{n}_j\,\mathrm{d}S+\iint_{S}\tau_j\,\mathrm{d}S+\sum F_{\text{ext}j}. \tag{3.47}$$

For many aerodynamics applications, the gravitational forces are very small compared to pressure and viscous forces. Thus, unless we specifically mention to include gravitational forces, we will employ the following forms of the momentum conservation equation,

$$\iiint_{\mathcal{V}}\frac{\partial}{\partial t}\left(\rho\mathbf{V}\right)\,\mathrm{d}\mathcal{V}+\iint_{S}\rho\mathbf{V}\,\mathbf{V}\cdot\hat{\mathbf{n}}\,\mathrm{d}S=-\iint_{S}p\,\hat{\mathbf{n}}\,\mathrm{d}S+\iint_{S}\boldsymbol{\tau}\,\mathrm{d}S+\sum\mathbf{F}_{\text{ext}}. \tag{3.48}$$

or, considering only the j-component of momentum,

$$\iiint_{\mathcal{V}}\frac{\partial}{\partial t}\left(\rho u_j\right)\,\mathrm{d}\mathcal{V}+\iint_{S}\rho u_j\,\mathbf{V}\cdot\hat{\mathbf{n}}\,\mathrm{d}S=-\iint_{S}p\,\hat{n}_j\,\mathrm{d}S+\iint_{S}\tau_j\,\mathrm{d}S+\sum F_{\text{ext}j}. \tag{3.49}$$

edXproblem: 3.5.8 Release of pressurized air (momentum conservation)

3.8

Consider again the container in Problem 3.5.5. Recall from that problem that $\rho_{\text{out}} = 1.225$ kg/m^3 and $V_{\text{out}} = 10$ m/sec, and the container exit has a diameter of 0.2 m. Also, the air pressure outside of the container is everywhere equal to the atmospheric pressure, $p_\infty = 1.01 \times 10^5$ Pascals (Pa).

What is the x-component of the force that the rod acts with upon the container (in units of Newtons)?

edXsolution

Video Link

3.5.9 Application to channel flow (momentum conservation)

3.8

Now, let's apply the integral form of conservation of momentum to the channel flow shown in Figure 3.8. Previously, in Section 3.4.4, we applied the integral form of the conservation of mass. As before, the flow is assumed to have uniform velocity and density at its inlet (V_1 and ρ_1) and outlet (V_2 and ρ_2). Further, the flow in the channel is assumed to be steady.

As is described in the following video, applying the x-momentum equations gives,

$$\dot{m}\,(V_2 - V_1) = p_1 S_1 - p_2 S_2 + \iint_{S_{\text{wall}}} p\,\mathrm{d}S_x + \iint_{S_{\text{wall}}} \boldsymbol{\tau} \cdot \hat{\mathbf{i}}\,\mathrm{d}S, \tag{3.50}$$

where $\dot{m} = \rho_1 V_1 S_1 = \rho_2 V_2 S_2$ is the mass flow in the channel.

The video discusses an alternative control volume which does not include the boundary layers, and therefore viscous forces are negligible in this alternative control volume. Using this alternative control volume, we show that if the boundary layers in the channel are small (compared to the diameter of the channel), then the viscous forces can be neglected. The resulting inviscid application of the conservation of x-momentum produces,

$$\dot{m}\,(V_2 - V_1) = p_1 S_1 - p_2 S_2 + \iint_{S_{\text{wall}}} p\,\mathrm{d}S_x. \tag{3.51}$$

Video Link

3.6 Sample Problems

edXproblem: 3.6.1 Lift generation and flow turning

2.2 3.8

In this example problem, we will apply conservation of y-momentum to relate the lift generated by an airplane (or other body) to the turning of the flow. We will use the control volume shown in Figure 3.9.

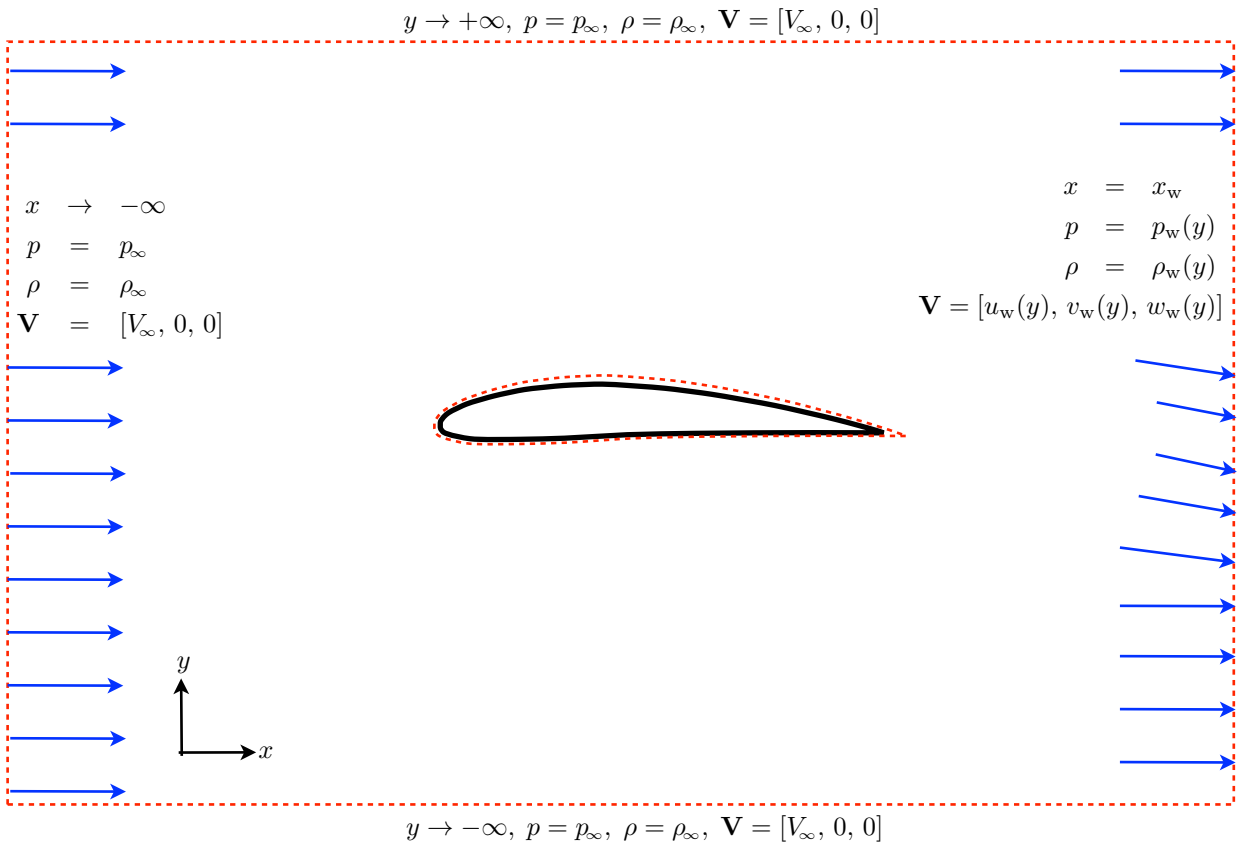


Figure 3.9: Control volume for sample problems.

The lift can be related to an integral of the flow properties in the downstream wake boundary of the form,

$$L = \iint_{S_w} \text{integrand}\, \mathrm{d}S. \tag{3.52}$$

Determine the integrand required to calculate the lift.

edXsolution

The key result we will derive in the video below is,

$$L = -\iint_{S_w} \rho_w v_w u_w \, \mathrm{d}S. \tag{3.53}$$

This result shows clearly that by turning the flow downward (so that in the wake $v_w \leq 0$), a positive lift force is generated. Thus, we can think of lift generation as the process of an aircraft turning a flow downward (in an efficient manner of course)!

As we will see later in the class (specifically, see Section 8.5.5), in two-dimensional flows we actually need to account for the fact that the flow upstream of the lifting body is infinitessimaly

perturbed from the freestream. Thus, the two-dimensional result for the lift using the control volume for this problem would give,

$$L' = \iint_{S_\mathrm{u}} \rho_\mathrm{u} v_\mathrm{u} u_\mathrm{u} \, \mathrm{d}S - \iint_{S_\mathrm{w}} \rho_\mathrm{w} v_\mathrm{w} u_\mathrm{w} \, \mathrm{d}S. \tag{3.54}$$

where S_u is the control volume boundary far upstream of the lifting body, and ρ_u, u_u and v_u are the density and velocity components on that boundary. In other words, we need to account for the fact the $v_\mathrm{u} \neq 0$ in two-dimensional flows.

Video Link

edXproblem: 3.6.2 Drag and the wake

2.2 3.8

In this example problem, we will now apply conservation of x-momentum to relate the drag generated by an airplane (or other body) to the flow properties in the wake. Again, we will use the control volume shown in Figure 3.9.

The drag can be related to an integral on the downstream wake boundary of the form,

$$D = \iint_{S_\mathrm{w}} \text{integrand}\, \mathrm{d}S. \tag{3.55}$$

Determine the integrand required to calculate the drag.

edXsolution

The key result we will derive in the video below is,

$$D = \iint_{S_\mathrm{w}} (p_\infty - p_\mathrm{w})\, \mathrm{d}S + \iint_{S_\mathrm{w}} \rho_\mathrm{w} u_\mathrm{w} (V_\infty - u_\mathrm{w})\, \mathrm{d}S. \tag{3.56}$$

This result shows clearly that drag will appear in the wake as some combination of pressure deficit (such that $p_\mathrm{w} < p_\infty$), and velocity deficits in the wake (such that $u_\mathrm{w} < V_\infty$)

Video Link

Module 4

Conservation of Energy and Quasi-1D Flow

4.1 Overview

4.1.1 Measurable outcomes

In this module, we consider the conservation of energy as the third of our conservation laws in addition to mass and momentum conservation. Again, we use control volume analysis. We also introduce the adiabatic and isentropic process as a useful model of many compressible aerodynamic flows. Finally, the adiabatic and isentropic flow approximation is combined with a quasi-one-dimensional assumption to derive a useful model for flow through variable area passages, e.g. a converging-diverging nozzle.

Specifically, students successfully completing this module will be able to:

4.1. Describe the differences between constant density, incompressible, and compressible flows.

4.2. Relate the pressure, density, and temperature using the ideal gas law. State the definitions of the specific internal energy and specific enthalpy and relate these to the temperature and specific heats for a calorically perfect gas.

4.3. Explain the physical meaning of the terms of the integral form of energy conservation.

4.4. Apply the integral form of energy conservation to typical problems in aerospace engineering.

4.5. Define the speed of sound for a general compressible flow, derive its relationship to changes in pressure and density, and state its dependence on temperature for an ideal gas.

4.6. Define stagnation enthalpy, temperature, pressure, density, etc. and state their relationship to enthalpy, temperature, pressure, density, etc. and the Mach number for a perfect gas. Derive Bernoulli's equation from the low Mach number limit of the stagnation pressure relationship.

4.7. Define the assumptions of an adiabatic and isentropic flow and appropriately apply these to calculate variations in flow properties.

4.8. Derive and apply an isentropic, adiabatic quasi-one-dimensional flow model.

4.1.2 Pre-requisite material

The material in this module requires vector calculus and all of the measurable outcomes from Module 3.

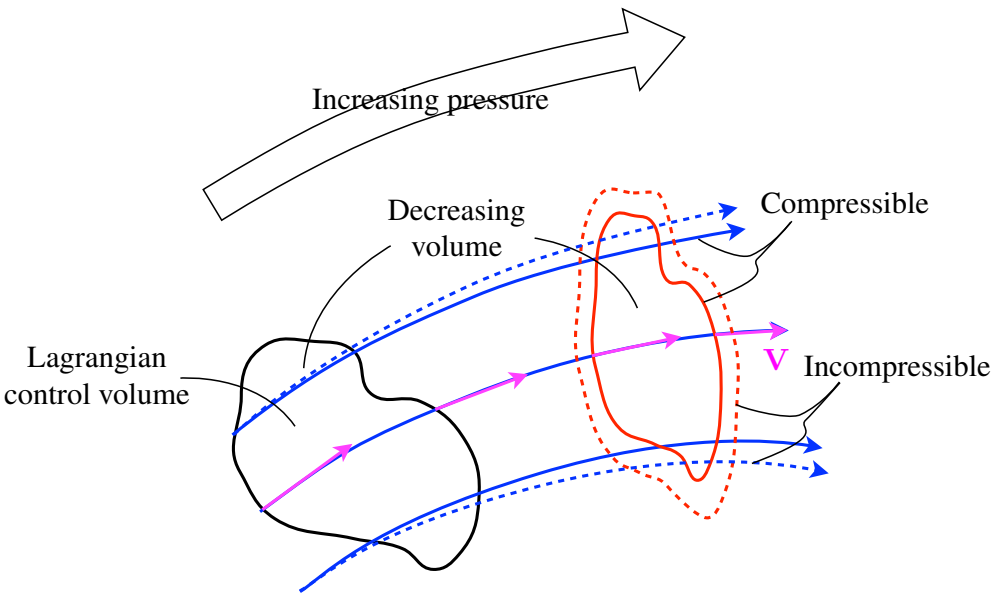


Figure 4.1: Lagrangian control volume in compressible and incompressible flow

4.2 Introduction to Compressible Flows

4.2.1 Definition and implications

4.1

A *compressible substance* is one for which the volume changes when the pressure acting on the material changes. This is equivalent to saying that the density of a substance changes with the pressure. Our main interest is air, and air is compressible. Water (and other liquids more generally) are less compressible than air (and other gases more generally). Thus, for the same changes in pressure, the density of air will change more than the density of water.

A *compressible flow* is a flow in which the fluid density ρ changes with variations in the pressure. Or, somewhat redundantly, a compressible flow is one for which the fluid is compressible! While air flows are technically compressible, for many important applications, the changes in density due to pressure variations are small. In these situations, we can assume the flow is an *incompressible flow*. While we will discuss this more throughout this module (and later in the course), density variations tend to be small when the local flow Mach number remains below 0.3 or so. Conversely, for flows with local Mach numbers above 0.3 or so, compressibility must be accounted for. The effects become especially large when the Mach number approaches and exceeds unity.

Figure 4.1 shows the behavior of a moving Lagrangian Control Volume (CV) which by definition surrounds a fixed mass of fluid m. In incompressible flow the density ρ does not change, so the CV's volume $\mathcal{V} = m/\rho$ must remain constant, though its shape can change. In the compressible flow case, the CV is squeezed or expanded in response to pressure changes, with ρ changing in inverse proportion to $\mathcal{V}$. Since the CV follows the streamlines, changes in the CV's volume must be accompanied by changes in the streamlines as well. Compared to incompressible flows, this will mean that the streamlines contract or expand more in compressible flows.

While pressure variations do not change the density of an incompressible substance, an incompressible substance can be heated to produce a density change. Thus, a difference exists between a *constant density flow* (in which the density of the fluid is assumed constant) and an *incompressible flow* (in which the density of the fluid changes due to temperature variations but not pressure

variations). For air flows, heating and cooling through convecting air over a cold or hot surface are common scenarios in which the air flow is often well-approximated as incompressible, though not constant density. While these flows often have quite low Mach numbers, the density variations of the air can be non-negligible because of the heat transfer.

4.2.2 Ideal gas equation of state

4.2

An *ideal gas* is one whose individual molecules interact only via direct collisions, with no other intermolecular forces present. For such an ideal gas, the properties p, ρ, and the temperature T are related by the following *equation of state*,

$$p = \rho R T \tag{4.1}$$

where R is the specific gas constant which for air, $R = 287$ J/kg-K. In general, the temperature is a time-varying scalar field since p and ρ are also generally time-varying scalar fields.

The appearance of the temperature in the equation of state means that thermodynamics will need to be addressed. So in addition to the conservation of mass and momentum, we will now also need to consider the conservation of energy.

4.2.3 Internal energy of a gas

4.2

The law of conservation of energy involves the concept of *internal energy* of a system; that is, all of the energy inside the system. In our case, the system is the fluid in the control volume and the internal energy is the sum of the energies of all the molecules in the control volume. In thermodynamics, the energy is divided into kinetic energy (associated with the motion of the molecules including velocities, rotations, and vibrations) and potential energy (associated with the static rest energy, chemical bond energy, etc). While we can track all of these energies, in many fluid mechanics applications, only some of these energies change. For example, unless chemical reactions are occurring, the chemical bond energy will not be altered. So, if a type of energy is known not to change in the flow, then that energy does not need to be explicitly tracked since it will automatically be conserved.

In this course, we will only consider the kinetic energy of the molecules. First, consider only the kinetic energy due to the translational motion of the molecules (not include rotational and vibrational motions). In a small region, we can decompose the velocity of any given molecule into the average velocity of the molecules in that region and a random contribution as shown in Figure 4.2. The average molecular velocity is the equivalent of our continuum flow velocity as defined in Section 3.2.5. So, the velocity of molecule i is then,

$$\mathbf{v}_i = \mathbf{V} + \mathbf{c}_i. \tag{4.2}$$

Then, we can sum the kinetic energy (due to translation) over all molecules to find the total kinetic energy (due to translation) of the region. Specifically, let $\mathcal{M}$ be the molecular mass (i.e. the mass

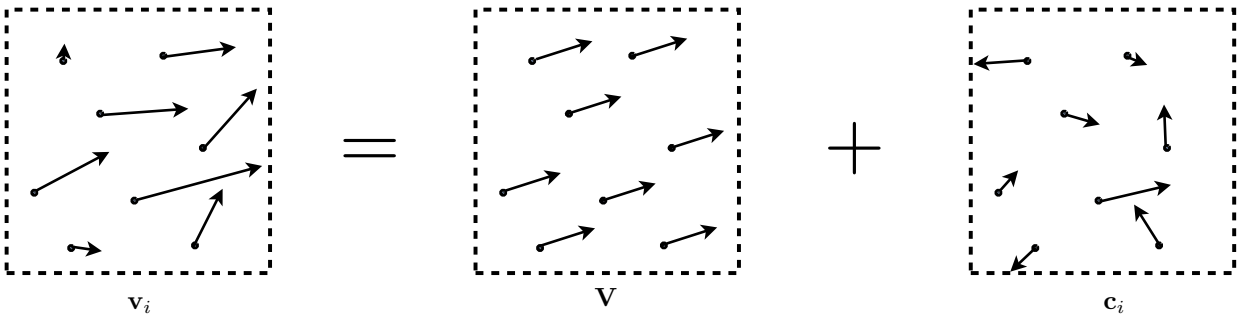


Figure 4.2: Decomposition of molecular velocity $\mathbf{v}_i$ into mean ($\mathbf{V}$) and random ($\mathbf{c}_i$) motion.

of a single molecule), then

$$\text{Translational energy in region} = \sum_i \frac{1}{2}\mathcal{M}\,\mathbf{v}_i \cdot \mathbf{v}_i \tag{4.3}$$

$$= \frac{1}{2}\mathcal{M}\sum_i (\mathbf{V}\cdot\mathbf{V} + 2\mathbf{V}\cdot\mathbf{c}_i + \mathbf{c}_i\cdot\mathbf{c}_i) \tag{4.4}$$

$$= \frac{1}{2}N\mathcal{M}\left(V^2 + \overline{c^2}\right) + \mathcal{M}\mathbf{V}\cdot\sum_i \mathbf{c}_i \tag{4.5}$$

where N is the number of molecules in the region and $\overline{c^2}$ is the mean of the square of the random velocity in the region,

$$\overline{c^2} \equiv \frac{1}{N}\sum_i \mathbf{c}_i\cdot\mathbf{c}_i. \tag{4.6}$$

Since $\mathbf{c}_i$ is the variation of the velocity about the mean velocity, then $\sum_i \mathbf{c}_i = \sum_i(\mathbf{v}_i - \mathbf{V}) = 0$. Thus, the total translational energy of the molecules in the region is,

$$\text{Translational energy in region} = \frac{1}{2}N\mathcal{M}\left(V^2 + \overline{c^2}\right) \tag{4.7}$$

Dividing by the volume of the region, $N\mathcal{M}/\mathcal{V}$ is the density so that,

$$\text{Translational energy in region/Volume} = \frac{1}{2}\rho\left(V^2 + \overline{c^2}\right). \tag{4.8}$$

Returning to our continuum fluid model, we define the *specific total energy*, e_0, as the energy per unit mass of the fluid. As with our other flow quantities, this is a time-varying scalar field, $e_0(x, y, z, t)$. We then define e_0 as,

$$e_0 \equiv e + \frac{1}{2}V^2 \tag{4.9}$$

where e is known as the specific internal energy. Multiplying Equation (4.9) by the density (producing the total energy per unit volume for our continuum flow model) and comparing to Equation (4.8) shows that e accounts for energy due to the random molecular motions. Generally, e will include not only the energy due to random transitional motion (i.e. $\frac{1}{2}\overline{c^2}$) but also energy due to molecular rotations and vibrations. We will discuss in the Section 4.2.4 how we model e for air.

With this definition of the specific total energy, the energy inside a control volume is then,

$$E = \iiint_{\mathcal{V}} \rho\, e_0 \,\mathrm{d}\mathcal{V}. \tag{4.10}$$

4.2.4 Enthalpy, specific heats, and perfect gas relationships

4.2

Enthalpy

In addition to the specific internal energy e, a related and often-used quantity is the *specific enthalpy*, denoted by h, and related to the other variables by

$$h \equiv e + p/\rho \tag{4.11}$$

Note that the units of e and h are (velocity)^2, or m^2/s^2 in SI units.

Analogous to the specific total energy, we also define the *specific total enthalpy* as,

$$h_0 \equiv h + \frac{1}{2}V^2 = e + \frac{p}{\rho} + \frac{1}{2}V^2 = e_0 + \frac{p}{\rho}. \tag{4.12}$$

As we will show in the derivation of the conservation of energy in Section 4.3.4, the enthalpy incorporates the pressure work term, and, of key importance in aerodynamics, the total enthalpy is often a constant in many parts of a flow (see Section 4.3.5).

Thermodynamic equilibrium

We will assume that the gas (i.e. air) is in thermodynamic equilibrium. Thermodynamic equilibrium requires the system (i.e. the gas) to be in balance such that there are no unbalanced forces (mechanical equilibrium), no temperature differences (thermal equilibrium), and no chemical reactions (chemical equilibrium).

Thermodynamic equilibrium is not strictly achieved by many fluid flows that are undergoing an unsteady motion (since unsteady flows are frequently driven by a lack of balanced forces or temperatures, or chemical reactions occurring). Thermodynamic equilibrium is still a good approximation for a gas if molecular collisions occur much more rapidly than any processes that are causing change in the gas. Since air at conditions of interest to us can have on the order of 10^{10} collisions per second, thermodynamic equilibrium is often a reasonable approximation.

When a gas is in thermodynamic equilibrium, any thermodynamic property can be determined from two other thermodynamic properties. This means for example that we can think of e as a function $e(T, p)$ or $e(T, \rho)$ or $e(p, \rho)$ or any other pair of properties.

Specific heats

Two very useful quantities are the *specific heats at constant volume* and *constant pressure* which are defined as,

$$c_v \equiv \left.\frac{\partial e}{\partial T}\right|_v, \tag{4.13}$$

$$c_p \equiv \left.\frac{\partial h}{\partial T}\right|_p. \tag{4.14}$$

v is called the specific volume and is defined as $v = 1/\rho$. Hence, c_v is the derivative of e with respect to T holding the specific volume fixed. Similarly, c_p is the derivative of h with respect to T holding the pressure fixed. While the specific heats have been defined mathematically as the partial derivatives, they have a physical meaning which is hinted at by the *specific heat* term. Consider a system at some uniform state. The amount of heat addition required to raise the temperature of the state when the volume of the system is held fixed can be shown to be $c_v \Delta T$ (per unit mass, hence *specific*). Similarly, the heat addition required to raise the temperature of the system if the pressure is held fixed can be shown to be $c_p \Delta T$ (per unit mass again).

Thermally perfect gas

For a *thermally perfect gas*, the internal energy is assumed to be only a function of temperature, $e = e(T)$. This implies from Equations (4.11) and (4.1) that the enthalpy is also only a function of temperature, $h = h(T)$. Further, since

$$h - e = p/\rho = RT, \tag{4.15}$$

we can differentiate this with respect to T to produce,

$$\frac{\mathrm{d}h}{\mathrm{d}T} - \frac{\mathrm{d}e}{\mathrm{d}T} = R. \tag{4.16}$$

Therefore, we see that for a thermally perfect gas,

$$c_p - c_v = R \tag{4.17}$$

Defining the *ratio of specific heats*, $\gamma \equiv c_p/c_v$, we can with a bit of algebra write

$$c_v = \frac{1}{\gamma - 1} R \tag{4.18}$$

$$c_p = \frac{\gamma}{\gamma - 1} R \tag{4.19}$$

so that c_v and c_p can be replaced with the equivalent variables γ and R.

Calorically perfect gas

Restricting our gas model further to a *calorically perfect gas*, then c_v and c_p are assumed to be constant. This is an excellent model for air at moderate temperatures (say from -50° to 1000° C) and we will use it through this course. For air, $\gamma = 1.4$ is a good approximation (even at 1000° C this is within about 6% of the actual value of 1.321). Also, it is handy to remember,

$$\gamma = 1.4, \quad \frac{1}{\gamma - 1} = 2.5, \quad \frac{\gamma}{\gamma - 1} = 3.5 \tag{4.20}$$

such that $c_v = 717.5$ J/kg-K and $c_p = 1005$ J/kg-K.

For a calorically perfect gas, e and h have the simple linear relationships with T,

$$e = c_v T \tag{4.21}$$

$$h = c_p T \tag{4.22}$$

edXproblem: 4.2.5 Comparing air and battery energy

4.2

We often teach aerodynamics in Room 33-419 on the MIT campus. This room has a floor area of approximately 90 square meters and the ceiling is about 3 meters high. A typical 9-volt battery holds about 19 kiloJoules (kJ) of energy. Approximately how many 9-volt batteries are equivalent to the amount of internal energy of the air in Room 33-419? Note: you only need to account only for the internal energy due to the motion of the air molecules (i.e. no bonding energy, etc.)

edXsolution

Video Link

4.3 Conservation of Energy

4.3.1 Introduction to conservation of energy

4.3

The first law of thermodynamics, which we will refer to as the conservation of energy, applied to our Eulerian control volume is,

$$\frac{\mathrm{d}}{\mathrm{d}t}\,(\text{energy in } \mathcal{V}) + (\text{flow of energy out of } \mathcal{V}) = (\text{rate of work done on } \mathcal{V}) + (\text{rate of heat added to } \mathcal{V}) \tag{4.23}$$

The first two terms are analogous to the terms in the conservation of mass and momentum. For energy, these terms take the mathematical form,

$$\frac{\mathrm{d}}{\mathrm{d}t}\,(\text{energy in } \mathcal{V}) = \frac{\mathrm{d}}{\mathrm{d}t}\iiint_{\mathcal{V}} \rho e_0 \,\mathrm{d}\mathcal{V} = \iiint_{\mathcal{V}} \frac{\partial}{\partial t}\left(\rho e_0\right) \mathrm{d}\mathcal{V}. \tag{4.24}$$

$$\text{energy flow } = \iint_S \rho e_0 \,\mathbf{V}\cdot\hat{\mathbf{n}}\,\mathrm{d}S. \tag{4.25}$$

4.3.2 Work

4.3

Work is done on a system as a result of a force being applied in the direction of motion. As we have expressed the conservation of energy as a rate equation, we are interested in the rate at which work is done on the system (i.e. our control volume). Thus, the rate of work done on the control volume can be generically written as $\mathbf{F}\cdot\mathbf{V}$ where $\mathbf{F}$ is the force applied to a portion of the control volume that is moving with velocity $\mathbf{V}$. The forces we have considered in our fluid dynamics control volume analysis are the pressure, viscous, and external force as given in Equation (3.44). Thus, there are four work terms (note: technically we should say rate of work terms, but we will simply refer to these as work terms with the understanding that they are rates). Specifically, the gravitational work is,

$$\text{gravitational work} = \iiint_{\mathcal{V}} \rho\,\mathbf{g}\cdot\mathbf{V}\,\mathrm{d}\mathcal{V}. \tag{4.26}$$

The pressure work (also commonly refered to as the flow work) is,

$$\text{pressure work} = -\iint_S p\,\hat{\mathbf{n}}\cdot\mathbf{V}\,\mathrm{d}S. \tag{4.27}$$

The viscous work is,

$$\text{viscous work} = \iint_S \tau\cdot\mathbf{V}\,\mathrm{d}S. \tag{4.28}$$

And, the work due to an external force is,

$$\text{external work} = \sum\left(\mathbf{F}_{\text{ext}}\cdot\mathbf{V}_{\text{ext}}\right) \tag{4.29}$$

where $\mathbf{V}_{\text{ext}}$ is the velocity of the location where the external force is applied.

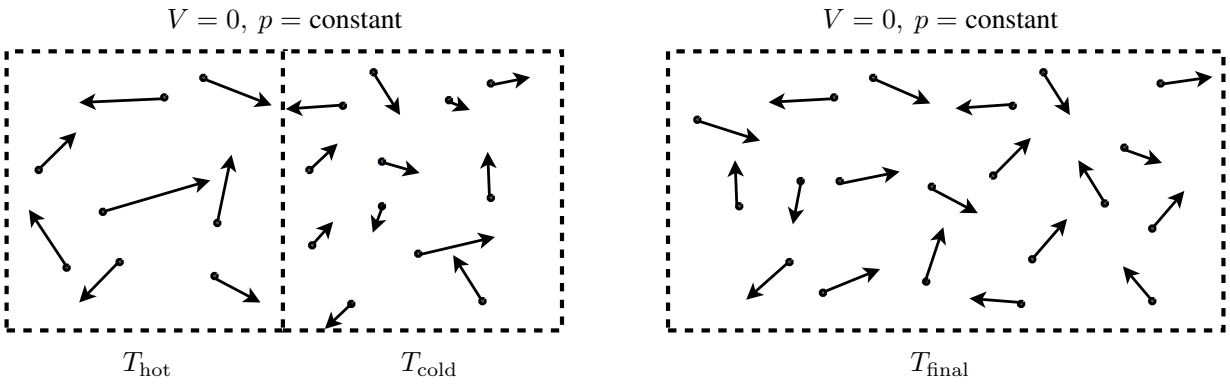


Figure 4.3: Molecular motion in regions with an initial temperature difference. Even without any bulk motion, energy will be exchanged between these regions such that the temperatures will eventually equalize.

4.3.3 Heat

4.3

Energy can also be transferred to a system even without work i.e. without the application of a force during bulk motion. This energy exchange occurs due to molecular interactions in regions of the flow where the temperature varies in space, as depicted in Figure 4.3. We will discuss how this heat transfer is modeled later in the semester. For now, we define the heat flux vector, $\dot{\mathbf{q}}$ as a vector indicating the direction and rate of energy exchange per unit area, such that the rate of energy exchange due to heat transfer through the surface of the control volume can be found as,

$$\text{rate of heat added to } \mathcal{V} = -\iint_S \dot{\mathbf{q}} \cdot \hat{\mathbf{n}}\, \mathrm{d}S. \tag{4.30}$$

Note that the negative sign is because the normal is outward pointing, thus $\dot{\mathbf{q}} \cdot \hat{\mathbf{n}}$ is the heat flux out of the control volume.

4.3.4 Conservation of energy in integral form

4.3

The conservation of energy for a control volume fixed in space as expressed in Equation (4.23) can be written mathematically using the results in Equations (4.24), (4.25), (4.26), (4.27), (4.28), (4.29) and (4.30), as

$$\iiint_{\mathcal{V}} \frac{\partial}{\partial t}(\rho e_0)\, \mathrm{d}\mathcal{V} + \iint_S \rho e_0\, \mathbf{V} \cdot \hat{\mathbf{n}}\, \mathrm{d}S = \iiint_{\mathcal{V}} \rho\, \mathbf{g} \cdot \mathbf{V}\, \mathrm{d}\mathcal{V} - \iint_S p\, \hat{\mathbf{n}} \cdot \mathbf{V}\, \mathrm{d}S + \iint_S \boldsymbol{\tau} \cdot \mathbf{V}\, \mathrm{d}S \tag{4.31}$$

$$+ \sum (\mathbf{F}_{\text{ext}} \cdot \mathbf{V}_{\text{ext}}) - \iint_S \dot{\mathbf{q}} \cdot \hat{\mathbf{n}}\, \mathrm{d}S. \tag{4.32}$$

When applying conservation of energy, here are a few important observations:

- On a stationary solid wall boundary, the velocity normal to the wall is zero, i.e. $\mathbf{V} \cdot \hat{\mathbf{n}} = 0$. Thus, the pressure work term is zero. Further, when viscous effects are included, the flow velocity must match the wall velocity, which for a stationary wall means the $\mathbf{V} = 0$. That is, not only is the normal component but all components of the flow velocity are zero at a wall assuming viscous effects are included. Thus, the viscous work term will also be zero at a stationary wall.

- As with the conservation of momentum, the effects of gravity in the conservation of energy will generally be negligible for aerodynamic applications.
- Similar to viscous effects in the momentum equation (see the discussion in Section 3.5.6), heat transfer will generally be small throughout the flow except where boundary layers are present. Further, for many aerodynamic applications, even the flow at a solid wall can be assumed to be adiabatic, meaning that $\dot{\mathbf{q}} \cdot \hat{\mathbf{n}} \approx 0$.
- Often the pressure work term is incorporated into the energy flow term using the specific total enthalpy (h_0) such that the conservation of energy becomes,

$$\iiint_{\mathcal{V}} \frac{\partial}{\partial t}(\rho e_0)\, \mathrm{d}\mathcal{V} + \iint_S \rho h_0\, \mathbf{V} \cdot \hat{\mathbf{n}}\, \mathrm{d}S = \iiint_{\mathcal{V}} \rho\, \mathbf{g} \cdot \mathbf{V}\, \mathrm{d}\mathcal{V} + \iint_S \boldsymbol{\tau} \cdot \mathbf{V}\, \mathrm{d}S \tag{4.33}$$

$$+ \sum (\mathbf{F}_{\text{ext}} \cdot \mathbf{V}_{\text{ext}}) - \iint_S \dot{\mathbf{q}} \cdot \hat{\mathbf{n}}\, \mathrm{d}S. \tag{4.34}$$

4.3.5 Total enthalpy along a streamline

4.4

In the video, we apply the conservation of energy to a control volume surrounding a streamline of a steady flow. We show the important result that the total enthalpy is constant,

$$h_0 = \text{constant in a steady flow} \tag{4.35}$$

along a streamline where the viscous work and heat transfer are negligible.

Another important conclusion on the behavior of total enthalpy is also demonstrated in Sample Problem 4.6.1. In that problem, we move away from a single streamline to consider the entire flow around an airfoil. Please make sure to study the analysis here and in that problem carefully.

Video Link

4.4 Adiabatic and Isentropic Flows

4.4.1 Entropy and isentropic relationships

4.7

Entropy is another thermodynamic state property. The entropy is a measure of heat addition and irreversibilities (in our case, viscous effects). Entropy is increased by both of these effects. The Gibbs relation can be used to relate an infinitesimal change in entropy, $\mathrm{d}s$, to changes in other thermodynamic properties, specifically,

$$T\mathrm{d}s \equiv \mathrm{d}e + p\,\mathrm{d}(1/\rho) = \mathrm{d}h - (1/\rho)\mathrm{d}p. \tag{4.36}$$

The second form in terms of the enthalpy change can be derived from the first using the definition of the enthalpy.

For a thermally perfect gas, the changes in e and h can be expressed in terms of changes in temperature to give (upon dividing through by $c_v T$ to clean-up the result a little),

$$\mathrm{d}s/c_v \equiv \frac{\mathrm{d}T}{T} - (\gamma-1)\frac{\mathrm{d}\rho}{\rho} = \gamma\frac{\mathrm{d}T}{T} - (\gamma-1)\frac{\mathrm{d}p}{p}. \tag{4.37}$$

An isentropic process is one in which the entropy does not change, i.e. $\mathrm{d}s = 0$. Using Equation (4.37) we can determine how the changes in the temperature and density are related for such an isentropic process,

$$\frac{\mathrm{d}T}{T} = (\gamma-1)\frac{\mathrm{d}\rho}{\rho} \tag{4.38}$$

This result can alternatively be written as,

$$\left.\frac{\partial T}{\partial \rho}\right|_s = (\gamma-1)\frac{T}{\rho} \tag{4.39}$$

which indicates the partial derivative is taken with the entropy fixed (i.e. isentropic).

Similar results can also be found for other states and are summarized here,

$$\frac{\mathrm{d}T}{T} = (\gamma-1)\frac{\mathrm{d}\rho}{\rho} = \frac{\gamma-1}{\gamma}\frac{\mathrm{d}p}{p} \text{ for an isentropic process.} \tag{4.40}$$

Or, alternatively written as partial derivatives,

$$\left.\frac{\partial T}{\partial \rho}\right|_s = (\gamma-1)\frac{T}{\rho}, \quad \left.\frac{\partial T}{\partial p}\right|_s = \frac{\gamma-1}{\gamma}\frac{T}{p}, \quad \left.\frac{\partial p}{\partial \rho}\right|_s = \gamma\frac{p}{\rho}. \tag{4.41}$$

For a calorically perfect gas, since γ is constant, we may integrate Equation (4.40) to produce,

$$\frac{T_2}{T_1} = \left(\frac{\rho_2}{\rho_1}\right)^{\gamma-1} = \left(\frac{p_2}{p_1}\right)^{(\gamma-1)/\gamma} \text{ for an isentropic process between 1 and 2.} \tag{4.42}$$

4.4.2 Speed of sound

4.5

Sound waves are weak pressure perturbations. The speed, a, at which they propagate is determined by isentropic relationships and can be shown to be,

$$a^2 = \left.\frac{\partial p}{\partial \rho}\right|_s . \tag{4.43}$$

From Equation (4.41), the speed of sound for a thermally perfect gas is,

$$a = \sqrt{\frac{\gamma p}{\rho}} = \sqrt{\gamma R T} \tag{4.44}$$

4.4.3 Stagnation properties

4.6 4.7

In Section 4.4.5, we will discuss the analysis of isentropic flows. In this section, we introduce the concept of a stagnation property which is very useful for the analysis of flows, independent of whether or not the flows are isentropic.

Suppose at some time and location, the flow state has properties p, ρ, $\mathbf{V}$, T, e, h, etc. We then define a stagnation state and stagnation properties as follows:

Stagnation state: the state which would occur when a given flow state is adiabatically and isentropically decelerated to zero velocity.

Adiabatic process: A process is one in which no heat is added (or removed) from the system.

Adiabatic and isentropic process: an adiabatic and isentropic must be reversible, meaning that it is possible for the process to be run in reverse and return to its original state. For a process to be reversible, frictional (i.e. viscous) forces must be zero throughout the system (not just at the system boundary).

Stagnation properties: the properties of the stagnation state which we will denote as p_{stag}, ρ_{stag}, etc. (note that $\mathbf{V}_{\text{stag}} = 0$ of course!)

Stagnation enthalpy: For an adiabatic and isentropic process, the total enthalpy does not change. We have seen an example of this in the analysis of the flow along a streamline in Section 4.3.5. Specifically, since an adiabatic and isentropic process means no heat transfer and viscous effects occur, then the total enthalpy along a streamline will not change. Thus, adiabatic and isentropic deceleration of the flow to stagnation conditions does not change the total enthalpy, i.e.

$$h_{0\text{stag}} = h_0 \tag{4.45}$$

The definition of the total enthalpy gives,

$$h_{0\text{stag}} = h_{\text{stag}} + \frac{1}{2} V_{\text{stag}}^2 \tag{4.46}$$

However, since $V_{\text{stag}} = 0$, then the total enthalpy at stagnation conditions is simply the enthalpy at stagnation conditions, i.e.

$$h_{0\text{stag}} = h_{\text{stag}} \tag{4.47}$$

Combining this result with Equation (4.45) gives that

$$h_{\text{stag}} = h_0 \tag{4.48}$$

We conclude that the stagnation enthalpy of a state is equal to the total enthalpy of that state.

Stagnation temperature: The temperature at the stagnation state can be determined from Equation (4.48) for a calorically perfect gas using $h = c_p T$ to give:

$$\begin{aligned} h_{\text{stag}} &= h_0 && (4.49)\\ &= h + \frac{1}{2}V^2 && (4.50)\\ c_p T_{\text{stag}} &= c_p T + \frac{1}{2}V^2 && (4.51)\\ \Rightarrow T_{\text{stag}} &= T + \frac{1}{2}\frac{V^2}{c_p} && (4.52) \end{aligned}$$

With a little additional manipulation, the stagnation temperature and static temperature (i.e. T) can related by the Mach number,

$$\begin{aligned} T_{\text{stag}} &= T\left(1 + \frac{1}{2}\frac{V^2}{c_p T}\right) && (4.53)\\ &= T\left(1 + \frac{\gamma - 1}{2}\frac{V^2}{\gamma R T}\right) && (4.54)\\ &= T\left(1 + \frac{\gamma - 1}{2}\frac{V^2}{a^2}\right) && (4.55)\\ \Rightarrow T_{\text{stag}} &= T\left(1 + \frac{\gamma - 1}{2}M^2\right) && (4.56) \end{aligned}$$

Stagnation pressure: The stagnation pressure p_{stag} can be related to the static pressure p from the isentropic relationships in Equation (4.42). This is possible because our imagined deceleration is isentropic. Thus,

$$\begin{aligned} p_{\text{stag}} &= p\left(\frac{T_{\text{stag}}}{T}\right)^{\frac{\gamma}{\gamma-1}} && (4.57)\\ \Rightarrow p_{\text{stag}} &= p\left(1 + \frac{\gamma - 1}{2}M^2\right)^{\frac{\gamma}{\gamma-1}} && (4.58) \end{aligned}$$

Stagnation density: The stagnation density ρ_{stag} can be related to the (static) density ρ again using the isentropic relationships in Equation (4.42),

$$\rho_{\text{stag}} = \rho\left(1 + \frac{\gamma - 1}{2}M^2\right)^{\frac{1}{\gamma-1}} \quad (4.59)$$

Stagnation speed of sound: One last stagnation quantity which is frequently useful is the stagnation speed of sound, a_{stag} which can be found by multiplying Equation (4.52) or Equation (4.56) by γR resulting in,

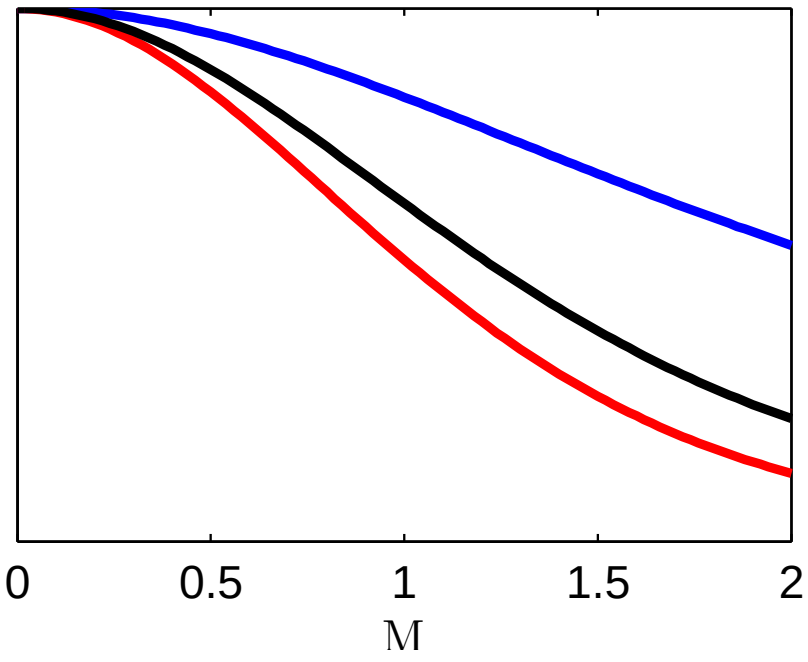
$$\begin{aligned} a^2_{\text{stag}} &= a^2 + \frac{\gamma - 1}{2}V^2 && (4.60)\\ a^2_{\text{stag}} &= a^2\left(1 + \frac{\gamma - 1}{2}M^2\right) && (4.61) \end{aligned}$$

Total versus stagnation properties: For aerodynamic applications, since the total enthalpy and stagnation enthalpy are the same, the terms total and stagnation are used interchangeably. Similarly, we will use the stagnation and total subscripts interchangeably. For example, p_0 and p_{stag} will refer to the same quantity. However, for applications where other forms of energy are included, then the total quantities will be generally different from the stagnation quantities.

edXproblem: 4.4.4 Isentropic variations with local Mach number

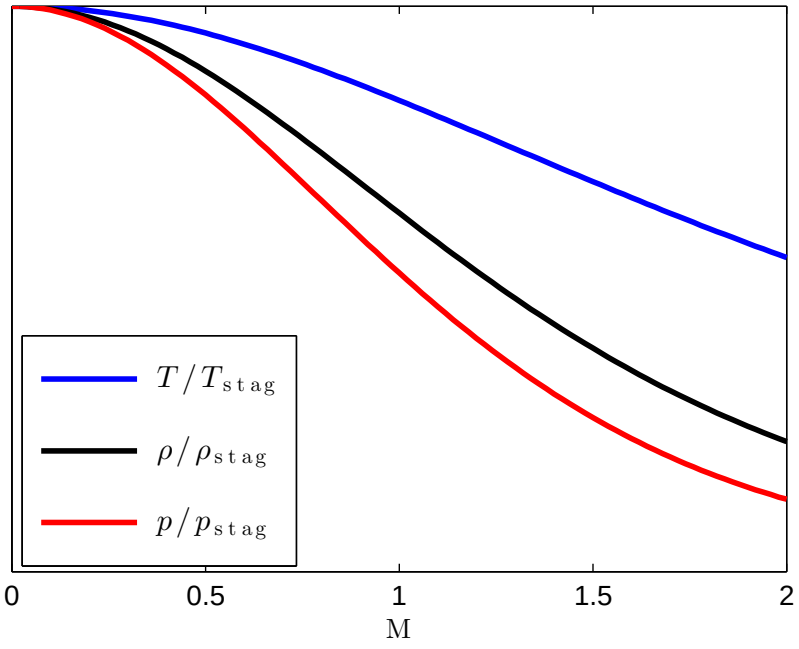
4.6

Identify which lines in the plot correspond to T/T_{stag}, p/p_{stag}, and ρ/ρ_{stag}.



edXsolution

The following figure shows the correctly-labeled legend.



The solution is explained in this video:

Video Link

4.4.5 Adiabatic and isentropic flow assumptions

4.6 4.7

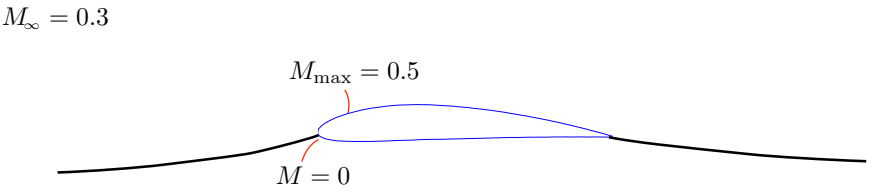
Since many regions in aerodynamic flows have negligible heating and viscous effects, the entropy of a fluid element does not change throughout much of the flow. The main locations where entropy changes occur are in boundary layers, wakes, and shock waves. Also, the main regions where heat transfer is significant is near a solid surface. Thus, if these regions are small, aerodynamic flows can often be modeled as adiabatic and isentropic.

Some care is needed though in assuming an adiabatic and isentropic flow depending on what is being estimated. For example, when estimating the amount of heat transfer that occurs from the air to the body, assuming an adiabatic flow would not be appropriate (that is pretty obvious I suppose). A little more subtly, when estimating the drag, assuming an isentropic flow is not appropriate since this requires viscous effects to be neglected (hence no drag due to friction will be estimated).

In steady aerodynamic applications , since far upstream of the body the flow tends to be uniform (i.e. $\mathbf{V}_\infty$, p_∞, T_∞, etc. are constant), then the upstream stagnation quantities will also be the uniform (and equal to p_{stag_∞}, T_{stag_∞}, etc.). Thus, assuming an adiabatic, isentropic steady flow coupled with a uniform freestream condition implies that the stagnation properties are constant everywhere in the flow. If the upstream flow were non-uniform, then the stagnation properties would generally vary from streamline-to-streamline, though they would be constant along streamlines (in an adiabatic and isentropic steady flow).

edXproblem: 4.4.6 Density variations in a low Mach number flow around an airfoil

4.4



Consider the steady air flow around an airfoil in which the freestream Mach number is $M_\infty = 0.3$ and $\gamma = 1.4$. Assume the flow can be approximated as adiabatic and isentropic. Suppose the highest local Mach number of the flow is $M = 0.5$. The lowest local Mach number will be zero, since the flow will come to rest on the airfoil (even in the isentropic flow where viscous effects are neglected, there is a stagnation point on the body, in the vicinity of the leading-edge of the airfoil).

What is the ratio of the maximum density in the flow relative to the freestream density (this will be a number greater than one)? Use two decimal points so that your answer has the form X.YZ.

What is the ratio of minimum density in the flow relative to the freestream density (this will be a number less than one)? Use two decimal points so that your answer has the form X.YZ.

edXsolution

Video Link

4.4.7 Stagnation pressure for incompressible flow and Bernoulli's equation

4.6 4.7

As was demonstrated in Problem 4.4.6, the variation of density in a low Mach number flow can be very small. Thus, for low Mach number flows, we will often assume the flow is incompressible.

In the low Mach number limit, the stagnation pressure also takes on a simplified form. To see this, we derive an approximate form of p_{stag} for low M^2 taking a Taylor series in terms of M^2:

$$p_{\text{stag}} = p\left(1+\frac{\gamma-1}{2}M^2\right)^{\gamma/(\gamma-1)} \tag{4.62}$$

$$p_{\text{stag}} \approx p + p\frac{\gamma}{2}M^2 + O(M^4) \tag{4.63}$$

Since $\gamma p M^2 = \rho a^2 M^2 = \rho V^2$, then Equation (4.63) becomes,

$$p_{\text{stag}} \approx p + \frac{1}{2}\rho V^2 \tag{4.64}$$

Thus, the incompressible definition of the stagnation pressure is recovered in the limit as $M^2 \to 0$.

For an adiabatic and isentropic, incompressible (i.e. low Mach number) flow, then we have that,

$$p_{\text{stag}} \equiv p + \frac{1}{2}\rho V^2 = \text{constant along a streamline in incompressible flow} \tag{4.65}$$

This is the well-known Bernoulli equation (later in the course, we will derive the Bernoulli equation in a different manner). As in the compressible case, when the flow originates from a uniform upstream condition, then $p + \frac{1}{2}\rho V^2$ is constant everywhere, specifically, we then have that

$$p + \frac{1}{2}\rho V^2 = p_\infty + \frac{1}{2}\rho V_\infty^2 \tag{4.66}$$

Recall also the definition of the pressure coefficient is C_p (see Equation 2.30),

$$C_p \equiv \frac{p - p_\infty}{\frac{1}{2}\rho_\infty V_\infty^2} \tag{4.67}$$

When Bernoulli's equation can be applied back to the freestream conditions as done in Equation (4.66), then the pressure coefficient is related to the velocity by,

$$C_p = 1 - \left(\frac{V}{V_\infty}\right)^2 \tag{4.68}$$

In this form, we see that at a stagnation condition (where $V = 0$) then $C_p = 1$. We also note that when $V = V_\infty$, then $C_p = 0$.

A comment on incompressible flow and the $M \to 0$ limit: We have argued that $M \to 0$ can often be approximated as an incompressible flow. A common temptation is to think that since $M \to 0$ then $V \to 0$. In other words, the flow is not moving (which would not make for much of a flow)! However, $V \to 0$ is not a requirement of $M \to 0$. An alternative interpretation is to think of the speed of sound as being very large compared to the flow velocity. Using the definition of the speed of sound in Equation (4.43), an infinitesimal change in density caused by a infinitesimal change in pressure is:

$$\mathrm{d}\rho = \frac{1}{a^2}\mathrm{d}p \text{ (assuming an isentropic perturbation)} \tag{4.69}$$

Thus, a nearly-incompressible substance will have a large speed of sound. Further, the Mach number can be thought of as a non-dimensional measure of the compressibility of the flow.

As an example, consider that the speed of sound of water at room temperature is about 1500 m/s. By comparison, air has a speed of sound at room temperature of about 350 m/s. Thus, sound waves travel about 4× faster in water than air. Water is much less compressible than air. Further, the flow velocities of interest in water (i.e. in hydrodynamic applications) are usually much smaller than the flow velocities in aerodynamic applications. Thus, the Mach number for hydrodynamics will generally be significantly smaller than most aerodynamic applications, and hydrodynamic applications can be assumed to be incompressible to good approximation.

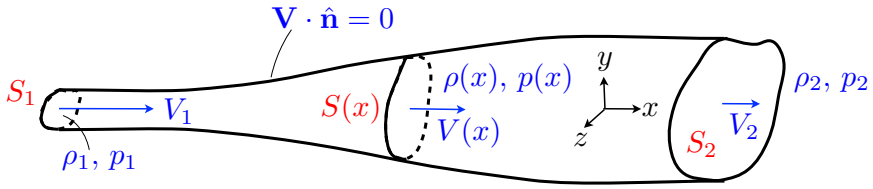


Figure 4.4: Quasi-1D flow model

4.5 Quasi-1D Flow

4.5.1 Assumptions

4.8

In this section, we utilize the conservation equations and the adiabatic, isentropic relationships to develop the quasi-one-dimensional (quasi-1D) flow model which is depicted in Figure 4.4. The assumptions of the quasi-1D model we will develop in this module are:

- Steady
- Adiabatic
- Isentropic
- Flow properties only depends on x, i.e. $\rho(x)$, $p(x)$, $V(x)$, ...
- The velocity components are negligible in the y and z direction, i.e. $|v|, |w| \ll |u|$.

Note that the last two assumptions require that the geometry varies gradually in the x direction.

This quasi-1D flow model has a variety of applications and provides a powerful yet simple method to qualitatively and often quantitatively estimate the flow behavior. In Section 4.5.2, the incompressible model is developed. Then, the compressible model is developed in Section 4.5.3.

4.5.2 Incompressible quasi-1D flow

4.8

The conservation of mass for incompressible quasi-1D flow was derived in Section 3.4.4 and given by Equation (3.29), which we write in the following manner,

$$VS = \text{constant}. \tag{4.70}$$

The Bernoulli equation can then be applied since we have assumed adiabatic, isentropic, and incompressible flow. Thus we have,

$$p + \frac{1}{2}\rho V^2 = \text{constant}. \tag{4.71}$$

If the cross-sectional area increases, then the velocity decreases (applying conservation of mass) and the pressure increases (applying Bernoulli). And, the opposite trends occur if the area decreases.

While these trends of flow properties with respect to area changes are clear to see for incompressible flow, the corresponding results for compressible flow are more involved. The approach

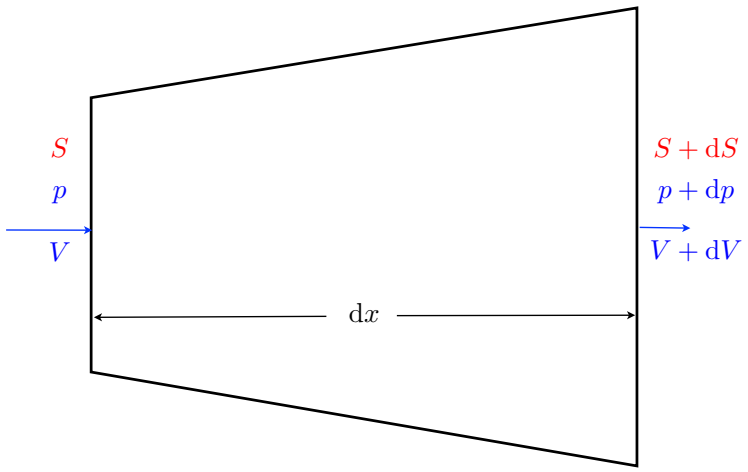


Figure 4.5: Infinitesimal control volume for quasi-1D flow

used in compressible flow is to consider infinitesimal changes that occur between x and $x + \mathrm{d}x$. We will apply that analysis here to demonstrate the approach in the simpler incompressible case.

Consider the infinitesimal control volume shown in Figure 4.5. At x and $x + \mathrm{d}x$, we assume that the area, velocity, and pressure are S, V, p and $S + \mathrm{d}S$, $V + \mathrm{d}V$, $p + \mathrm{d}p$, respectively. Then conservation of mass gives,

$$(S + \mathrm{d}S)(V + \mathrm{d}V) = SV \tag{4.72}$$

$$SV + S\mathrm{d}V + V\mathrm{d}S + \mathrm{d}S\,\mathrm{d}V = SV \tag{4.73}$$

$$S\mathrm{d}V + V\mathrm{d}S + \mathrm{d}S\,\mathrm{d}V = 0 \tag{4.74}$$

$$S\mathrm{d}V + V\mathrm{d}S = 0 \tag{4.75}$$

$$\Rightarrow \frac{\mathrm{d}V}{V} + \frac{\mathrm{d}S}{S} = 0 \tag{4.76}$$

Note that the fourth step uses the result that the quadratic infinitesimal term $(\mathrm{d}S\,\mathrm{d}V)$ will be small compared to terms which are linear with respect to $\mathrm{d}S$ or $\mathrm{d}V$. Thus, Equation (4.76) illustrates the previous conclusion that increasing the area (i.e. $\mathrm{d}S > 0$) causes the velocity to decrease (i.e. $\mathrm{d}V < 0$).

An alternative derivation of this result is to differentiate Equation (4.70) directly, i.e.,

$$\mathrm{d}\,(VS = \text{constant}) \Rightarrow S\mathrm{d}V + V\mathrm{d}S = 0. \tag{4.77}$$

Similarly, differentiating the Bernoulli equation gives,

$$\mathrm{d}p + \rho V\mathrm{d}V = 0 \tag{4.78}$$

$$\Rightarrow \frac{\mathrm{d}p}{\rho V^2} + \frac{\mathrm{d}V}{V} = 0 \tag{4.79}$$

Thus, when $\mathrm{d}V < 0$ then $\mathrm{d}p > 0$.

4.5.3 Compressible quasi-1D flow

4.8

For the compressible flow case, the conservation of mass is,

$$\rho VS = \text{constant}, \tag{4.80}$$

As demonstrated for the incompressible flow in Section 4.5.2, we will perform the differential change analysis. For conservation of mass, we find that,

$$\frac{\mathrm{d}\rho}{\rho} + \frac{\mathrm{d}V}{V} + \frac{\mathrm{d}S}{S} = 0. \tag{4.81}$$

Next, we will directly consider the momentum equation. We can utilize the result derived for the inviscid channel flow in Section 3.5.9. Specifically, applying Equation (3.51) to the infinitesimal control volume in Figure 4.5 gives

$$\rho V S \mathrm{d}V = pS - (p + \mathrm{d}p)(S + \mathrm{d}S) + p\,\mathrm{d}S. \tag{4.82}$$

Note that the last term is the approximation of the integral $\int p\,\mathrm{d}S_x$ retaining only the terms that are linear in the infinitesimal changes. The right-hand side can be manipulated to give,

$$\rho V S \mathrm{d}V = -S\,\mathrm{d}p. \tag{4.83}$$

where again only the linear terms are retained. Thus we see that the pressure and velocity changes are related by,

$$\mathrm{d}p + \rho V \mathrm{d}V = 0. \tag{4.84}$$

For an incompressible flow, this produces the Bernoulli's equation result. For the compressible flow case, the result is not Bernoulli's equation since ρ is not constant. Still, Equation (4.84) can be combined with Equation (4.81) to provide significant insight into quasi-one-dimensional compressible flow.

Since we have assumed the flow is isentropic, changes in pressure and density can be related through the speed of sound, i.e. $\mathrm{d}p = a^2 \mathrm{d}\rho$. Substituting this into Equation (4.84) gives,

$$\frac{\mathrm{d}\rho}{\rho} = -M^2 \frac{\mathrm{d}V}{V} \tag{4.85}$$

This shows that for low Mach number flows, the fractional change in density will be small compared to the fractional change in velocity. For Mach numbers above one (i.e. supersonic flow), the fractional changes in density are larger than the fractional changes in velocity. Thus, we have a further illustration for why the Mach number can be considered as a non-dimensional measure of the compressibility of a flow.

Then, substituting Equation (4.85) into Equation (4.81) gives,

$$\frac{\mathrm{d}V}{V} = \frac{-1}{1 - M^2} \frac{\mathrm{d}S}{S} \tag{4.86}$$

This key result shows that for subsonic flow, the velocity decreases ($\mathrm{d}V < 0$) for increases in area ($\mathrm{d}S > 0$). Thus, subsonic compressible flow behaves qualitatively like the incompressible case (in fact the limit of $M \to 0$ produces the incompressible result). However, for supersonic flow the area-velocity relationship is the opposite: increases in area cause increases in the velocity!

Finally, what happens at $M = 1$? At a location where $M = 1$, $\mathrm{d}V$ would be infinite unless the cross-sectional area is not changing, i.e. $\mathrm{d}S = 0$. This suggests that the only place where $M = 1$ can occur is a minimum of the area variation. Note that $M = 1$ cannot occur at a maximum of the area (even though $\mathrm{d}S = 0$). To see this, note that upstream of the area maximum, $\mathrm{d}S > 0$. Though not shown here (because the derivation is a bit tedious), changes in velocity have the same sign as changes in Mach number. Thus, if the flow were subsonic upstream of the area maximum, $\mathrm{d}M < 0$. Similarly, if the flow were supersonic in this region, then $\mathrm{d}M > 0$. In either case, $M = 1$ cannot occur at the maximum of the area.

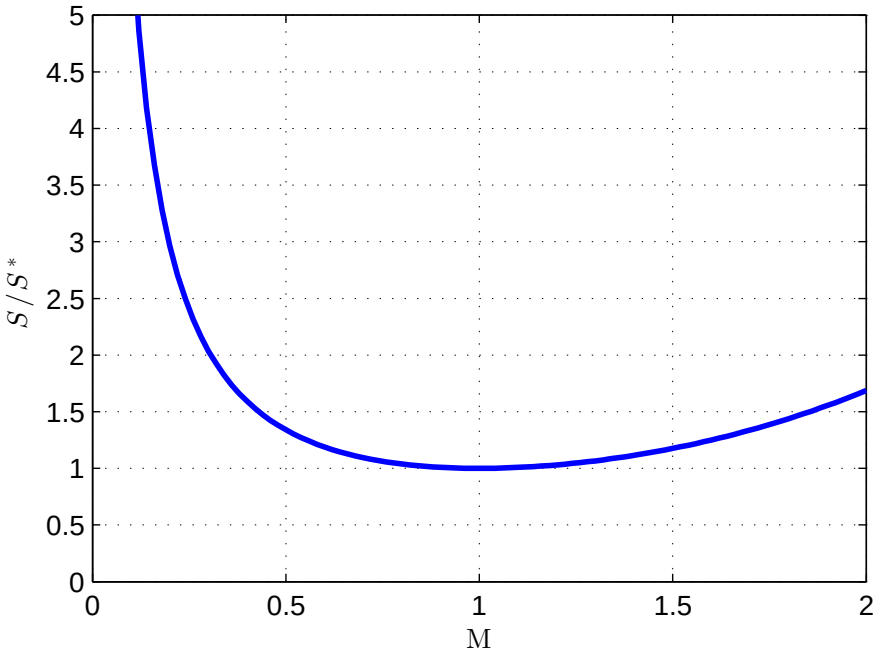


Figure 4.6: S/S^* versus M for $\gamma = 1.4$

This is a key result which we summarize: $M = 1$ *can only occur at a throat (i.e. a minimum in the area) for a steady, adiabatic, isentropic flow.* Note however that the inverse statement is not required, that is, the flow at a throat does not have to be $M = 1$.

The last step of this analysis will be to algebraically relate the variation in the Mach number and area to facilitate quantitative analysis of quasi-one-dimensional compressible flows. The common way to do this is to non-dimensionalize the various flow properties by the values at $M = 1$. Define ρ^*, V^*, a^*, etc. to be the values of these quantities when $M = 1$. Also, to reduce clutter, we will refer to the stagnation quantities as ρ_0 and a_0.

Applying conservation of mass, gives,

$$\rho V S = \rho^* V^* S^* \tag{4.87}$$

Note that $V^* = a^*$ since $M = 1$ by definition of these quantities. Therefore,

$$\frac{S}{S^*} = \frac{\rho^*}{\rho}\frac{a^*}{V} = \frac{\rho^*}{\rho_0}\frac{\rho_0}{\rho}\frac{a^*}{a_0}\frac{a_0}{a}\frac{a}{V} \tag{4.88}$$

Note that,

$$\frac{\rho^*}{\rho_0} = \left(\frac{\gamma+1}{2}\right)^{-\frac{1}{\gamma-1}}, \quad \frac{a^*}{a_0} = \left(\frac{\gamma+1}{2}\right)^{-\frac{1}{2}} \tag{4.89}$$

. Using this and the previous ρ/ρ_0 and a/a_0 relationships produces,

$$\frac{S}{S^*} = \frac{1}{M}\left[\frac{2}{\gamma+1}\left(1+\frac{\gamma-1}{2}M^2\right)\right]^{\frac{\gamma+1}{2(\gamma-1)}} \tag{4.90}$$

Thus, we have a function which relates the area to the Mach number. $S/S^*(M)$ is plotted in Figure 4.6.

We highlight a few key points about this relationship:

- The minimum area does occur at $M = 1$.
- When analyzing a particular flow, the actual area does not have to equal S^*. It is just a convenient manner to non-dimensionalize the results.
- The typical approach for solving a problem is to determine e.g. the Mach number at some location in the flow based on some combination of mass flow and boundary pressures. From this, one can determine S^* based on the Mach number and S at the location. With this, the rest of the flow can be determined from the ratio of S/S^* at any other location.
- For any $S/S^* > 1$, there is a subsonic and supersonic Mach number possible. Thus, which Mach number actually occurs will depend on other factors in the problem being analyzed (e.g. upstream and downstream pressures).
- If a flow was desired to be accelerated from subsonic Mach number to a supersonic Mach number, the area would first have to contract accelerating the flow to $M = 1$ at the throat. Then, the area would increase causing the Mach number to increase further **if** the downstream pressure is sufficiently low to cause further acceleration beyond the throat. Thus, the shape needed to accelerate a flow to supersonic conditions would be a converging-diverging nozzle.
- Another possibility is that a shock wave can occur in the flow. We will discuss this possibility later in the course.

4.6 Sample Problems

edXproblem: 4.6.1 Total enthalpy in an adiabatic flow

4.4

In this example problem, we will now apply conservation of energy to the flow around an airplane (or other body). Again, we will use the control volume shown in Figure 3.9. Assume that the airplane body is adiabatic, i.e. $\dot{\mathbf{q}} \cdot \hat{\mathbf{n}} = 0$ on the body.

Determine the value of the following integral by applying the conservation of energy to the control volume:

$$\iint_{S_\mathrm{w}} \rho_\mathrm{w} u_\mathrm{w} \left(h_{0\mathrm{w}} - h_{0\infty}\right) \mathrm{d}S = ? \tag{4.91}$$

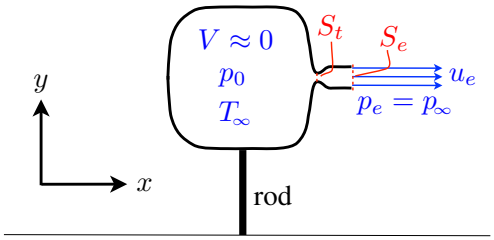
edXsolution

The key result we will derive in the video below is,

$$\iint_{S_\mathrm{w}} \rho_\mathrm{w} u_\mathrm{w} \left(h_{0\mathrm{w}} - h_{0\infty}\right) \mathrm{d}S = 0. \tag{4.92}$$

Thus, even though h_0 may vary from $h_{0\infty}$ due to viscous effects, for an adiabatic flow, the net flux of h_0 does not change. This can be interpreted as saying that the mass-averaged total enthalpy is constant for a steady, adiabatic flow (even though viscous effects are present).

Video Link



edXproblem: 4.6.2 Incompressible nozzle flow

4.7 4.8

Consider the rocket (in the figure) which is being held in place by the rod (i.e. the test stand). Test stands are used in this manner to estimate the thrust a rocket can generate by measuring the force with which the test stand must provide to keep the rocket stationary.

The air in the rocket has been compressed to a pressure p_0. The temperature of the air in the rocket is the atmospheric temperature T_∞. As described in Problem 3.5.5, assuming the streamlines enter the atmosphere from the nozzle in parallel lines implies that the pressure in the exhaust jet must be equal to p_∞. We will consider this motion in more detail later in the course.

Assume an incompressible, adiabatic, and isentropic flow. You may also assume a steady flow (which requires that the flow rate is small so that the impact of the unsteadiness due to the change in mass is small).

Specifically, determine the mass flow $\dot{m}$ and the force of the rod F_{rod}. How does the throat area S_t impact $\dot{m}$ and F_{rod} for incompressible flow?

edXsolution

Video Link

edXproblem: 4.6.3 Subsonic nozzle flow

4.7 4.8

Consider again the rocket from Problem 4.6.2. In this problem, we will consider compressibility effects but limited to subsonic flow ($M \leq 1$ everywhere). As before, assume an adiabatic, isentropic, and steady flow.

Determine the mass flow $\dot{m}$ and the force of the rod F_{rod}. How does the throat area S_t impact $\dot{m}$ and F_{rod} for subsonic compressible flow?

edXsolution

Video Link

edXproblem: 4.6.4 Supersonic nozzle flow

4.7 4.8

Consider again the rocket from Problems 4.6.2 and 4.6.3. In this problem, we will consider the supersonic exit flow case. As before, assume an adiabatic, isentropic, and steady flow.

Determine the mass flow $\dot{m}$ and the force of the rod F_{rod}. How does the throat area S_t impact $\dot{m}$ and F_{rod} for supersonic compressible flow?

edXsolution

Video Link

Module 5

Shock Expansion Theory

5.1 Overview

5.1.1 Measurable outcomes

This modules covers the fundamentals of shock-expansion theory relevant to aerodynamics applications. It includes shock waves (normal and oblique) and expansion waves in external flows, as well as the application to convergent-divergent ducts.

Specifically, students successfully completing this module will be able to:

5.1. Determine the jump in flow properties across steady normal and oblique shocks.

5.2. Determine changes in flow properties through an expansion fan.

5.3. Analyze the supersonic flow around simple 2D shapes using shock-expansion theory including determination of qualitative streamline shapes, flow properties, and forces.

5.4. Analyze steady compressible flows in converging-diverging ducts applying quasi-one-dimensional flow modeling including flows with shocks.

5.5. Explain how an inviscid flow with shocks produces drag.

5.1.2 Pre-requisite material

The material in this module requires prior knowledge of calculus and thermodynamics. You will also need a good understanding of the content and measurable outcomes from Module 4, from which we use a number of formulas.

5.2 Introduction

5.2.1 Examples

5.1 5.2

A *shock wave* appears in many types of supersonic flows. Some examples are shown in Figure 5.1 below. Any blunt-nosed body in a supersonic flow will develop a curved *bow shock*, which is normal to the flow locally just ahead of the body. Another common example is a supersonic nozzle flow, which is typically found in a jet or rocket engine. A normal shock can appear in the diverging part of the nozzle under certain conditions which will be discussed extensively in this module. The supersonic flow past a simple 2D shape, such as the diamond airfoil shown in the figure, can generate shock waves as well as expansion fans.

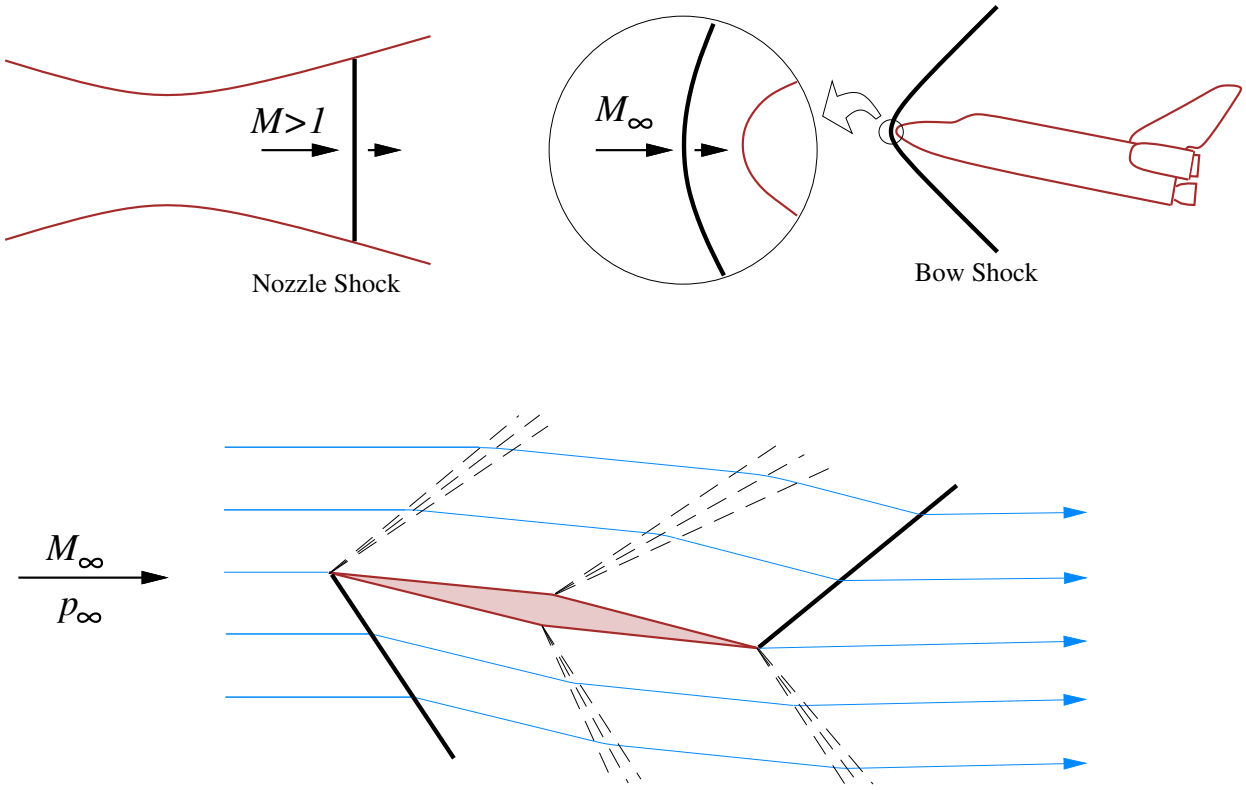


Figure 5.1: Examples of shock and expansion waves: flow in a nozzle (top left), flow around the nose of a space shuttle (top right), and shock-expansion wave pattern around a supersonic diamond airfoil (bottom).

5.2.2 Introduction to shock waves

5.1

Compressibility of a fluid allows the existence of *waves*, which are variations in the flow properties that propagate at some speed. A common example of a wave is sound. Ordinary sound consists of very small variations which move at the speed of sound a. A *shock wave* results in a finite variation in flow quantities and moves at a larger speed $V_s > a$. Figure 5.2 illustrates the difference in these two types of waves. The shock wave has a flow velocity behind it equal to the piston speed V_p, but

the shock itself advances into the still air at a much higher speed $V_s > a$. The air properties ρ, p, and h all increase past the shock.

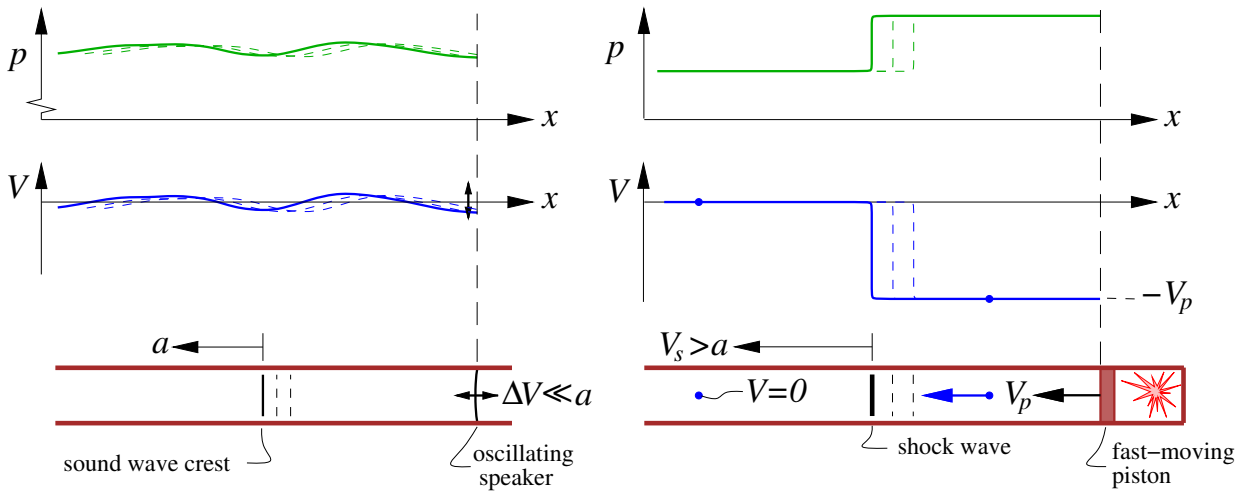


Figure 5.2: Differences between a sound wave (left) and a shock wave (right).

Examine now the piston shock flow in the frame of the shock by shifting all the velocities by $+V_s$ as illustrated in Figure 5.3: imagine that you are riding on the shock. In this frame the flow is steady and is therefore the most convenient frame for analyzing the shock. The quantities ρ, p, and h are static flow properties and are of course unchanged by this frame change.

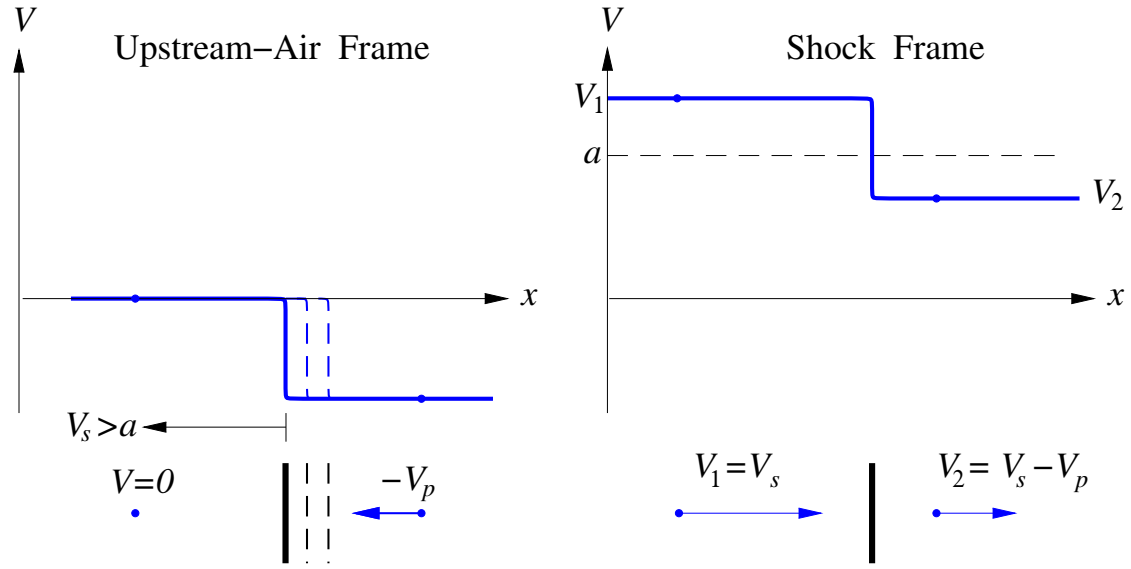


Figure 5.3: To change from the stationary reference frame (left) and the shock reference frame (right), shift all velocities by the shock speed V_s.

5.2.3 Traffic blockage analogy

5.1

An intuitive understanding of a shock wave is perhaps best obtained by looking at the situation in the downstream-air frame. The shock now propagates against the oncoming upstream flow. This situation is closely analogous to how a traffic blockage propagates backward against the oncoming

traffic, and is illustrated in Figure 5.4. As a car encounters a stop light, it halts and sends a signal (shock) to the car behind it to also stop, which in turn stops and signals to the next car to stop, and so on. As the shock propagates rearward, a larger and larger number of cars are stopped at the light.

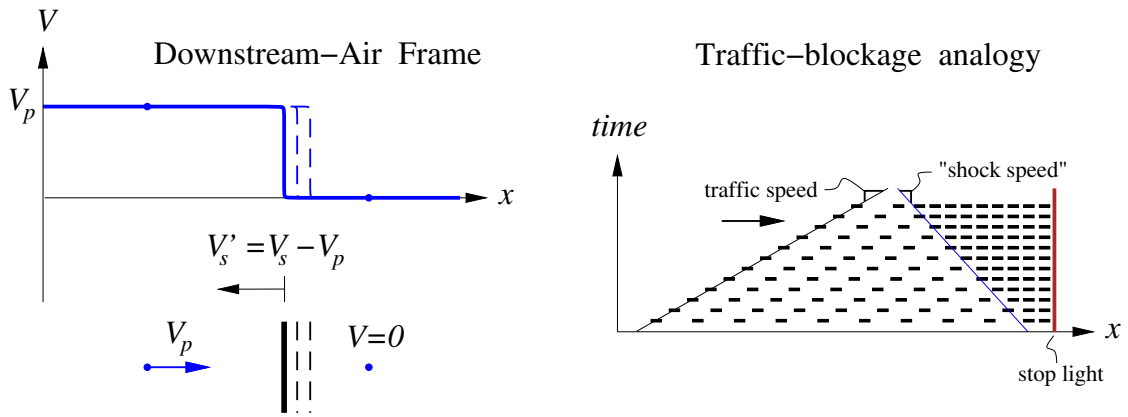


Figure 5.4: Shock as observed from the downstream-air frame (left) and traffic blockage analogy (right).

5.2.4 Assumptions for shock and expansion wave analysis

5.4 5.1 5.2 5.3

There is no heat addition across a shock (no heat source), so the flow is adiabatic. However, a shock is typically very thin (of the order of 10^{-6} m or so at sea level) but with very large gradients in flow properties: viscous forces across a shock are therefore important, and the flow is irreversible.

In the study of shock waves and expansion waves of this module, we will analyze the flow in the reference frame of the wave and make the following assumptions:

- The flow is steady: $\partial/\partial t \equiv 0$
- The flow is adiabatic
- All body forces (*e.g.* gravitational force) are negligible
- The fluid behaves like an ideal gas
- The fluid can be treated as a calorically perfect gas

It is generally convenient in this analysis to use specific enthalpy, h, as one of the flow properties which together with either density or pressure uniquely define the thermodynamic state of the fluid. However, enthalpy is not something that can be measured and it is also useful to analyze the temperature. As was seen in section 4.2.4, for a *callorically perfect gas* these two flow properties are related through the specific heat at constant pressure: $h = c_p T$. We will thus be able to use enthalpy and temperature interchangeably.

5.3 Normal shock waves

5.3.1 Isentropic relations

5.1

While seeking a relation between the quantities upstream of the shock and the quantities downstream of the shock, it is useful to define all quantities as a function of the local Mach number. For this, we make use of the so-called *isentropic relations*, which relate stagnation (or total) quantities to their static counterparts and were derived in section 4.4.3. For convenience, let's recall equations (4.59), (4.58), (4.56):

$$\frac{\rho_0}{\rho} = (1+\frac{\gamma-1}{2}M^2)^{\frac{1}{\gamma-1}} \tag{5.1}$$

$$\frac{p_0}{p} = (1+\frac{\gamma-1}{2}M^2)^{\frac{\gamma}{\gamma-1}} \tag{5.2}$$

$$\frac{T_0}{T} = 1+\frac{\gamma-1}{2}M^2 \tag{5.3}$$

$$\tag{5.4}$$

in which we use the subscript 0 to denote stagnation (or total) quantities.

Note that under the calorically perfect gas assumption, enthalpy and temperature are proportional, and hence

$$\frac{h_0}{h} = \frac{T_0}{T} = 1+\frac{\gamma-1}{2}M^2 \ . \tag{5.5}$$

These are known as the *isentropic relations* since when a flow with properties ρ, p, T is brought to a stop (stagnates) through an isentropic process, the result is the stagnation state with properties ρ_0, p_0, T_0.

Derivation

These isentropic relations were derived in section 4.4.3, but you are encouraged to derive them yourself at this point. Recall that the isentropic relation for enthalpy (and temperature) can be obtained by using the definition of stagnation enthalpy together with an expression for the speed of sound for an ideal gas. The relations for pressure and density then follow from Gibbs relation

$$T\,ds = de + pd\left(\frac{1}{\rho}\right) = dh - \frac{1}{\rho}dp \ , \tag{5.6}$$

where s denotes entropy and $ds = 0$ for an isentropic process. The following video shows a detailed derivation.

Video Link

5.3.2 Shock reference frame

5.1

We can examine the flow in the reference frame of the moving shock wave. In this frame, the shock is stationary and we can define a control volume that straddles the shock, as shown in Figure 5.5. We denote by a subscript 1 the flow properties upstream of the shock, and by a subscript 2 the properties downstream of the shock.

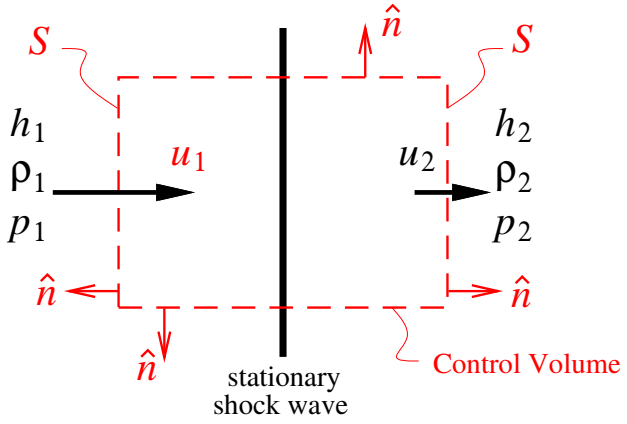


Figure 5.5: Control volume used in the analysis of normal shocks.

The flow in and out of this small control volume is one-dimensional. We can thus simplify the control volume forms of the conservation laws (continuity, x-momentum, energy, equation of state) to

$$\rho_1 u_1 = \rho_2 u_2 \ , \tag{5.7}$$

$$\rho_1 u_1^2 + p_1 = \rho_2 u_2^2 + p_2 \ , \tag{5.8}$$

$$h_1 + \frac{1}{2}u_1^2 = h_2 + \frac{1}{2}u_2^2 \ , \tag{5.9}$$

$$p_2 = \frac{\gamma - 1}{\gamma}\rho_2 h_2 \ . \tag{5.10}$$

These are known as the *Rankine-Hugoniot shock equations.*

In a typical shock flow analysis, the quantities upstream of the shock are known (u_1, ρ_1, p_1, h_1), and the goal is to determine the downstream quantities. Having four equations and four unknowns, the downstream condition is uniquely determined by the upstream flow. We will now derive equations for the ratios of downstream to upstream quanties as functions of Mach number only.

5.3.3 Mach jump relation

5.1

One can manipulate the Rankine-Hugoniot shock equations (5.7)–(5.10) to get an expression for M_2 as a function of M_1 only, which reads

$$M_2^2 = \frac{1 + \frac{\gamma-1}{2}M_1^2}{\gamma M_1^2 - \frac{\gamma-1}{2}} \ . \tag{5.11}$$

A plot of M_2 versus M_1 is shown in Figure 5.6 below for $\gamma = 1.4$. The function is not shown for $M_1 < 1$, since this would correspond to an "expansion shock" which is physically impossible based on irreversibility considerations.

Note that M_2 is a decreasing function of M_1. Therefore the higher the upstream Mach number M_1, the lower the downstream Mach number M_2. The limit $M_1 \to 1^+$, $M_2 \to 1^-$ corresponds to an infinitesimal shock: a sound wave.

Derivation

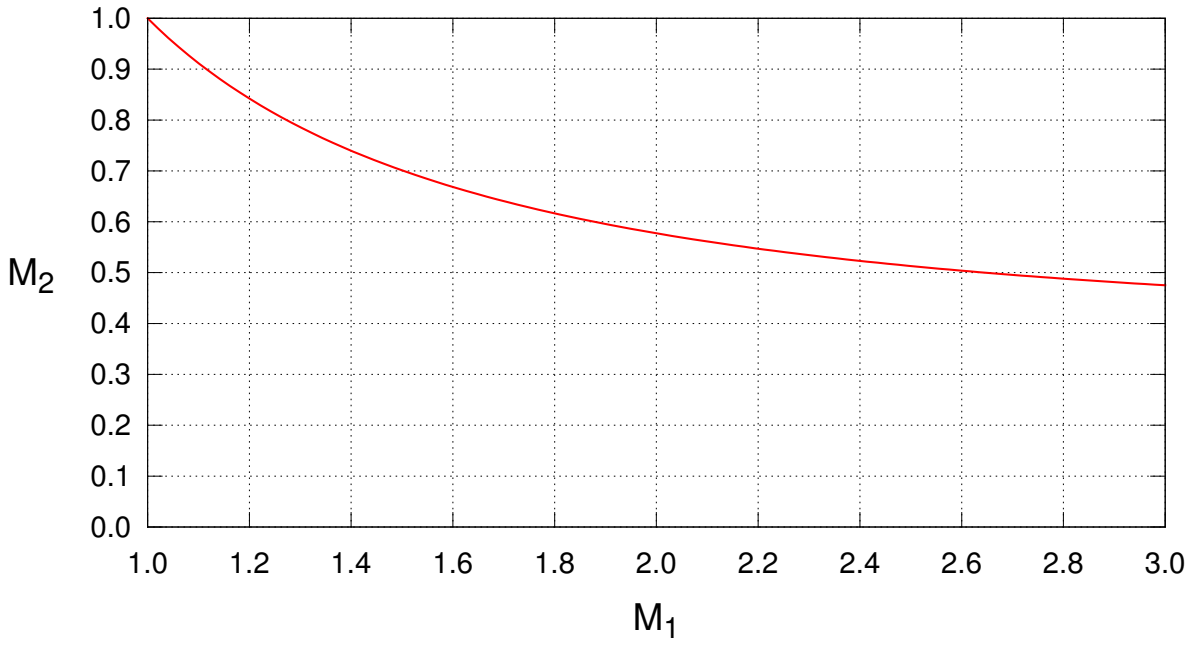


Figure 5.6: Plot of downstream Mach number M_2 as a function of upstream Mach number M_1 across a normal shock.

The steps taken to derive equation (5.11) are as follows: divide the x-momentum by the continuity equation and use the equation of state to write an equation for u_1, u_2, h_1, h_2; use the energy equation to convert this into an equation with u_1, u_2, and h_0; use the definition of the speed of sound to replace h_0 by a and M, and simplify to get an expression with only M_1 and M_2; isolate M_2 and simplify to obtain equation (5.11).

Again, you are encouraged to derive this equation yourself (as something you would like to do once). A detailed derivation is given in the following video.

Video Link

5.3.4 Static jump relation

5.1

Using again equations (5.7)– (5.10), we can derive expressions for the jumps in the static flow variables and through (5.11) write them as functions of M_1 only. The ratios of downstream-to-upstream static quantities are given by

$$\frac{\rho_2}{\rho_1} = \frac{(\gamma+1)M_1^2}{2 + (\gamma-1)M_1^2}, \tag{5.12}$$

$$\frac{p_2}{p_1} = 1 + \frac{2\gamma}{\gamma+1}\left(M_1^2 - 1\right), \tag{5.13}$$

$$\frac{T_2}{T_1} = \frac{h_2}{h_1} = \frac{p_2}{p_1}\frac{\rho_1}{\rho_2} = \left[1 + \frac{2\gamma}{\gamma+1}\left(M_1^2 - 1\right)\right]\frac{2 + (\gamma-1)M_1^2}{(\gamma+1)M_1^2}. \tag{5.14}$$

These three static quantity ratios are plotted versus M_1 in Figure 5.7.

A few important points to note:

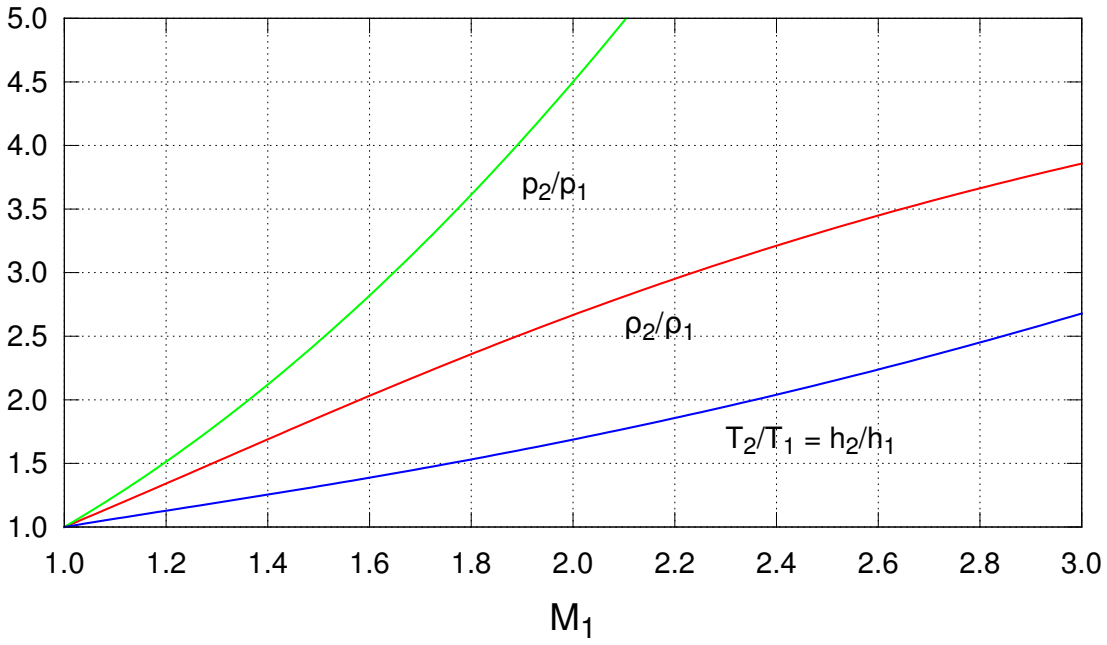


Figure 5.7: Plot of static jump relations: ratios of downstream-to-upstream static flow properties across a normal shock versus upstream Mach number M_1.

- All of the static quantities (pressure, density, temperature, enthalpy) increase across a shock since all the ratios are larger than unity.
- The higher the upstream Mach number M_1, the higher the ratios: stronger shocks induce larger flow changes.

Derivation

The jump relation for density can be derived by starting from the continuity equation and re-using some of the steps in the derivation of the Mach number relation. The relation for the pressure jump is then obtained by using the one for density. These derivations are complex, but as always you are encouraged to try on your own. You can then watch the following video which goes through the derivations.

Video Link

edXproblem: 5.3.5 Shock wave from explosion

5.1

A rocket motor explodes during a ground test, sending a spherical shock wave traveling away from the explosion into still ambient air which has the following conditions:

$$T = 300\,\mathrm{K} \quad , \quad p = 100 \times 10^3\,\mathrm{Pa}\ . \tag{5.15}$$

When the shock reaches an observer some distance away from the explosion point, the observer feels a sudden increase in the ambient static pressure of

$$\Delta p = 50 \times 10^3\,\mathrm{Pa}\ . \tag{5.16}$$

The shock can be approximated as normal (since the spherical shock has a large radius compared to the observer size). Assume air behaves like an ideal gas with $\gamma = 1.4$ and $R = 287\,\mathrm{J/kg \cdot K}$.

Note: This sounds traumatic, but you feel the same pressure rise when diving down 17 feet underwater.

1) What is the Mach number of the flow into the shock, in the shock's frame? Provide your answer with two digits of precision (of the form X.YeP).

2) What is the air pressure behind the shock in Pascals? Provide your answer with three digits of precision (of the form X.YZeP).

3) What is the air temperature (in degrees K) behind the shock? Provide your answer with three digits of precision (of the form X.YZeP).

4) What is the velocity of the shock relative to the observer in m/s? Provide your answer with three digits of precision (of the form X.YZeP).

5) What is the air velocity in m/s felt by the observer after the shock passes? Provide your answer with three digits of precision (of the form X.YZeP).

What is its direction?

edXsolution

Video Link

5.3.6 Shock losses

5.1

The quantity $1 - p_{0_2}/p_{0_1}$ is a measure of the losses across a shock. From the isentropic relations, we have

$$1 - \frac{p_{0_2}}{p_{0_1}} = 1 - \frac{p_2}{p_1}\left(\frac{1 + \frac{\gamma-1}{2}M_2^2}{1 + \frac{\gamma-1}{2}M_1^2}\right)^{\gamma/(\gamma-1)} \tag{5.17}$$

where both p_2/p_1 and M_2 are functions of the upstream Mach number M_1, as derived previously. The above quantity can thus be written as a function of M_1 only, and is plotted in Figure 5.8

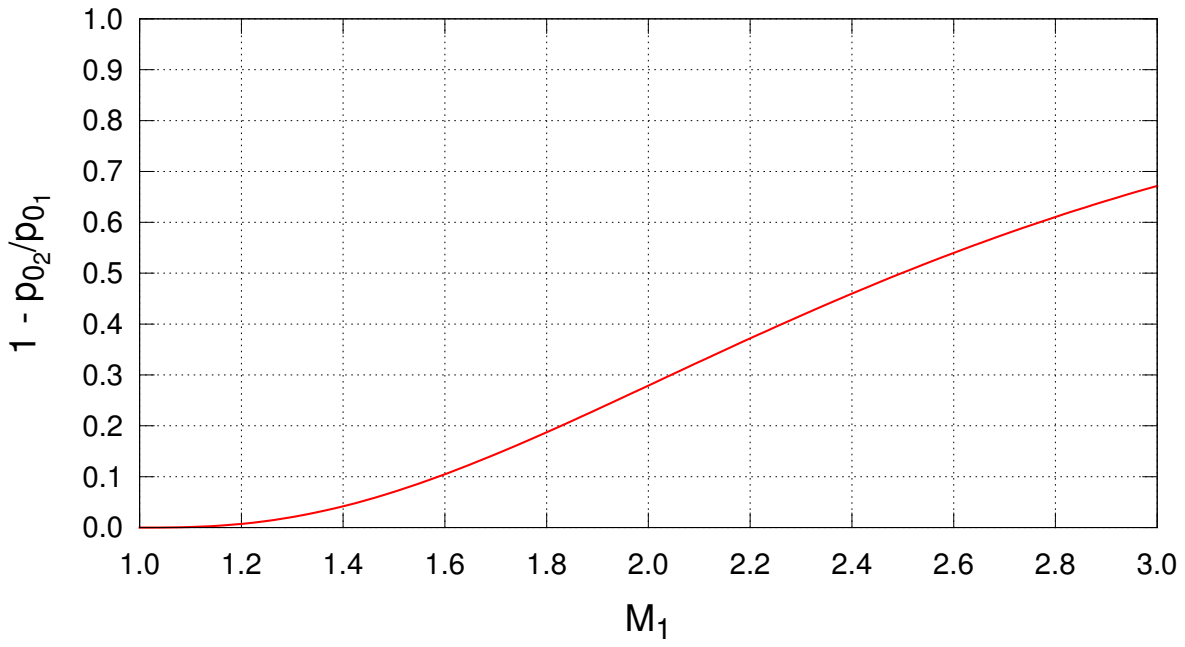


Figure 5.8: Measure of losses across a shock: $1 - p_{0_2}/p_{0_1}$ plotted as a function of upstream Mach number M_1.

The fractional shock total pressure loss $1 - p_{0_2}/p_{0_1}$ is small for M_1 close to unity, but increases rapidly for higher Mach numbers. Minimizing this loss is of great practical importance, since it cuts directly into the performance of supersonic ducts and air-breathing engines.

edXproblem: 5.3.7 Total quantities across a shock

5.1

We derived relations for the ratios of static quantities across a shock which show all static quantities ρ, p, T (or h) increase across a shock. We then showed just now through equation (5.17) that $1 - p_{0_2}/p_{0_1} < 1$, and hence the total pressure decreases.

Select all of the following statements that are true regarding the total density (ρ_0), total temperature (T_0) and total enthalpy (h_0)?

edXsolution

Video Link

5.3.8 Summary

5.1

In practice, it is useful to use shock tables, which list the upstream Mach number and ratios of static quantities, instead of computing these values through the formulas. The first column contains the upstream Mach number M_1, and the subsequent columns give the downstream Mach number M_2 and the ratios ρ_2/ρ_1, p_2/p_1, T_2/T_1. If the desired value of M_1 is not listed, linear interpolation is done between two consecutive table rows.

Similarly, in order to obtain the stagnation quantities, it is customary to use isentropic tables, which list ratios of ρ_0/ρ, p_0/p, T_0/T indexed by the Mach number M in the first column.

A typical normal shock problem is to determine the conditions downstream of a shock given the upstream conditions, specifically M_1, ρ_1, p_1, T_1. The process is as follows:

Step 1: Find the downstream Mach number M_2 by either looking it up on a normal shock table or computing it from equation (5.11).

Step 2: Find the ratios of static quantities ρ_2/ρ_1, p_2/p_1, T_2/T_1, again using a table or the jump relations (5.12)–(5.14).

Step 3: Compute the downstream static conditions given the ratios found in Step 2, *e.g.* $p_2 = (p_2/p_1) \times p_1$.

This is all that is needed to uniquely define the downstream flow. If the stagnation quantities are also of interest, one can proceed with the additional three steps:

Step 4: Find the ratios of stagnation to static quantities in the downstream flow ρ_{0_2}/ρ_2, p_{0_2}/p_2, T_{0_2}/T_2, given that M_2 is known from Step 1 and using isentropic tables or the isentropic relations (5.1)–(5.3).

Step 5: Compute the downstream stagnation conditions by using the ratios from Steps 2 and 4, and given the known upstream conditions, *e.g.* $p_{0_2} = (p_{0_2}/p_2) \times (p_2/p_1) \times p_1$.

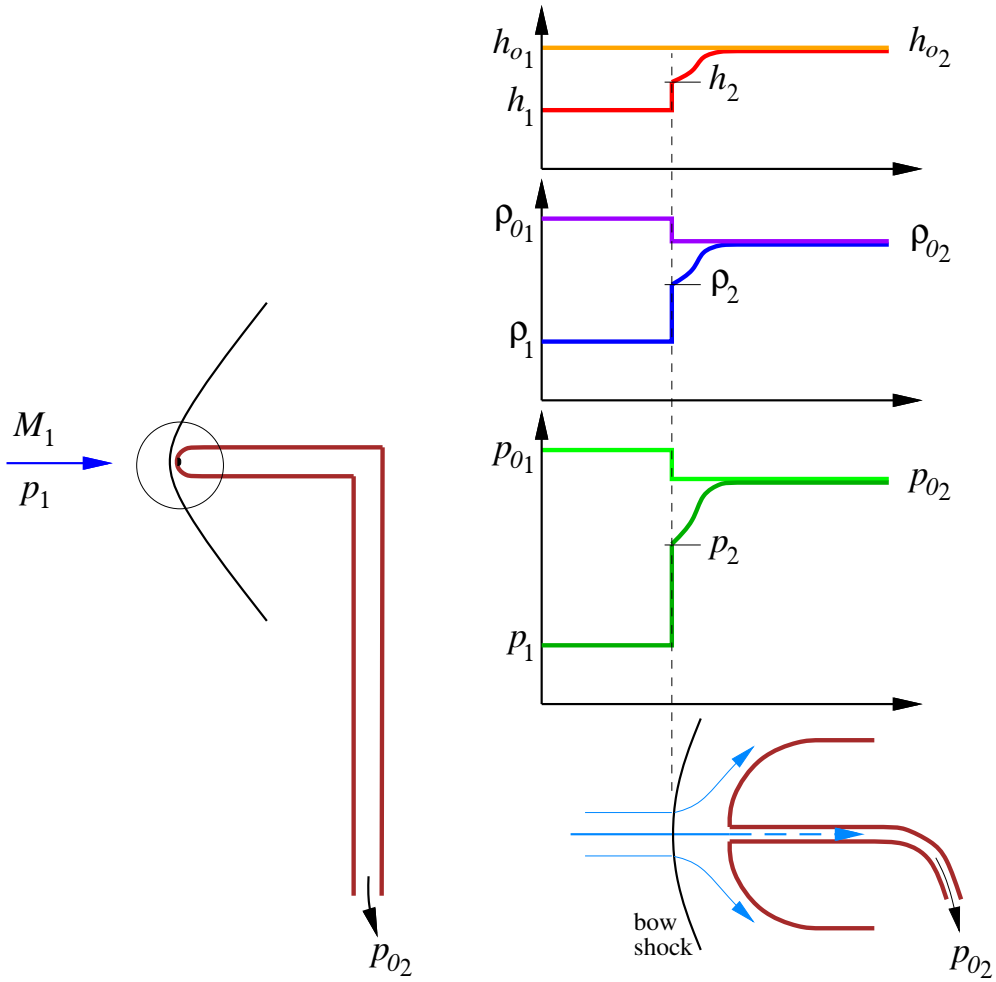
Step 6: Compute the upstream stagnation conditions ρ_{0_1}, p_{0_1}, T_{0_1}, from the known static conditions ρ, p, T, and upstream Mach number M_1 using either an isentropic table or the isentropic relations (5.1)–(5.3).

edXproblem: 5.3.9 Supersonic-flow pitot tube

5.1 5.3

A pitot probe in a supersonic stream will have a *bow shock* ahead of it. This complicates the flow measurement, since the shock causes a drop in the total pressure, from p_{0_1} to p_{0_2}, the latter being what is sensed by the pitot port.

The figure below shows a schematic of the pitot tube and the changes in flow properties past the shock ahead of the tube.



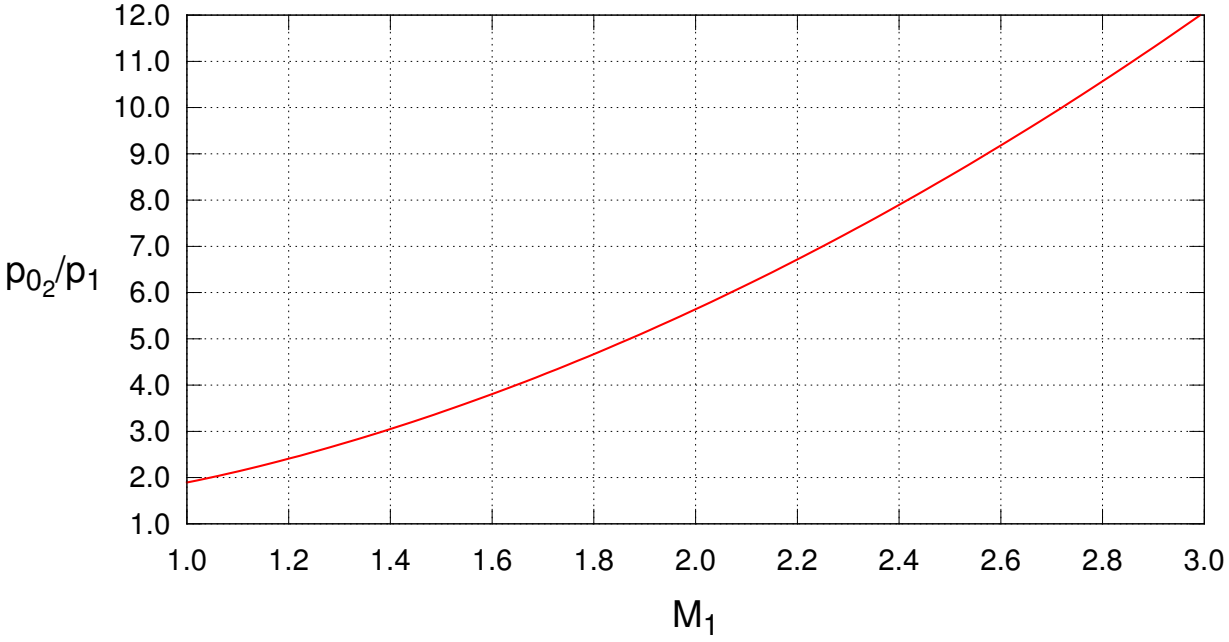
In order for a supersonic pitot tube to be an effective flow-speed measuring device, we need a way to compute the flow (upstream) Mach number M_1 as a function of the total pressure p_{0_2} measured by the pitot tube when placed in supersonic flow. We can write the following

$$\frac{p_{0_2}}{p_1} = \frac{p_{0_2}}{p_2}\frac{p_2}{p_1} \,. \tag{5.18}$$

and treat the bow shock as a normal shock since the tip of the pitot probe is small. The second ratio on the righ-hand-side is now as a function of M_1 from the pressure jump relation (5.13). The first ratio on the right-hand-side can be written in terms of M_1 only by introducing the expression for M_2 as a function of M_1 (5.11) into the isentropic relation (5.2). After some minor manipulation, we obtain the *Rayleigh Pitot tube formula*

$$\frac{p_{0_2}}{p_1} = \left(\frac{(\gamma{+}1)^2 M_1^2}{4\gamma M_1^2 - 2(\gamma{-}1)}\right)^{\gamma/(\gamma-1)} \frac{1-\gamma+2\gamma M_1^2}{\gamma{+}1} \,. \tag{5.19}$$

This is an implicit equation for M_1 as a function of p_{0_2}, if we measure p_1 via other means (*e.g.* static pressure hole somewhere in the upstream flow). Tables with values of p_{0_2}/p_1 and M_1 are generally used to determine the flow Mach number from a pitot tube placed in a supersonic flow, but the plot of p_{0_2}/p_1 versus Mach number shown in the figure below can also be used.



The upstream flow is measured to have a static pressure of $p_1 = 100 \times 10^3$ Pa, and the pitot probe reads $p_{0_2} = 300 \times 10^3$ Pa. Assume air behaves like an ideal gas with $\gamma = 1.4$ and $R = 287\,\mathrm{J/kg \cdot K}$.

1) Using the plot above, determine the Mach number of the flow in which the probe is placed. Provide your answer with two digits of precision (of the form X.YeP).

2) How do the ratios p_{0_2}/p_1 and p_{0_1}/p_1 compare?

3) What is the Mach number behind the shock, M_2? Provide your answer with two digits of precision (of the form X.YeP).

4) Could you treat the flow between the shock and the pitot tube front hole as incompressible?

edXsolution

Video Link

5.4 Convergent-divergent ducts

5.4.1 Introduction to convergent-divergent ducts

5.4

A typical geometry encountered in supersonic flows is a convergent-divergent duct, such as the one shown in Figure 5.9: it's a duct with a changing cross-sectional area which decreases and then increases. The location of smallest area is called the *throat*. Engine nozzles are an example.

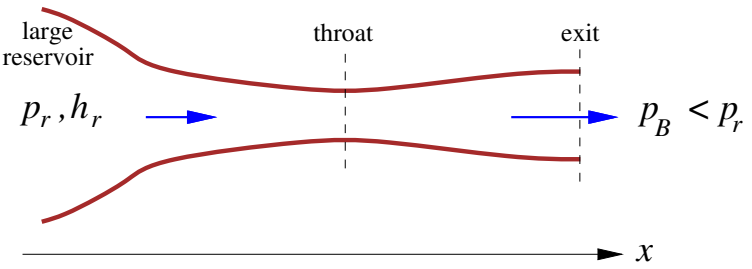


Figure 5.9: Convergent-divergent duct geometry.

At the inlet, the upstream-most end of the duct (left end in the Figure), there is a large reservoir such that flow conditions there are close to stagnation. The reservoir total pressure is p_r and enthalpy is h_r: these two quantities define the state of the flow in the still-air reservoir ($M_r = 0$).

The *exit* is the downstream-most end of the duct (right end in the Figure), where conditions are denoted by the subscript e.

Further downstream of the exit, the static pressure is adjustable and called *back pressure*, p_B. As p_B is gradually reduced from p_r, air flows from the reservoir to the exit with a mass flow $\dot{m}$.

We'll assume that flow changes in the streamwise direction x dominate changes in any other direction: that is, the flow is *quasi-1D*. All flow properties are thus a function of x only.

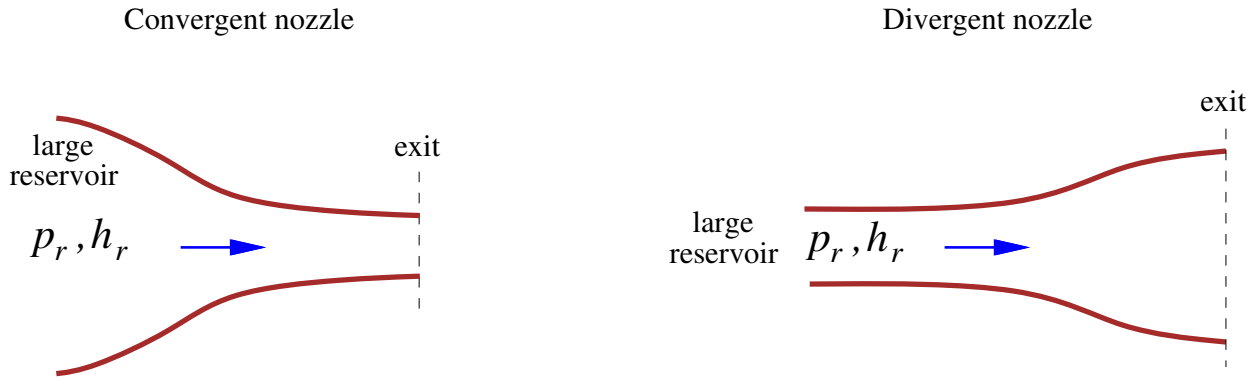
The duct geometry is characterized by the changes in cross-sectional area $S(x)$, and the flow is then uniquely determined by the reservoir conditions and back pressure. We are interested in the flow properties variation along the duct, in particular $M(x)$ and $p(x)$. The same analysis applies whether we are dealing with a 2D channel geometry or a 3D axisymmetric duct.

The present section uses and expands what was covered in Module 4, specifically in the section on quasi-1D flows.

For a given $S(x)$, the flow along the duct can be quite different depending on the ratio p_r/p_B:

- the flow remains subsonic all along: $M(x) < 1$ everywhere;
- the flow is *choked* with $M = 1$ at the throat but $M < 1$ everywhere else;
- there is a normal shock in the divergent part of the duct and $M_e < 1$;
- the flow is supersonic in the divergent part of the duct and $M_e > 1$.

edXproblem: 5.4.2 Purely convergent or divergent ducts



1) Consider a convergent duct, that is one whose cross-sectional area uniformly decreases downstream as shown on the left of the Figure above. Is it possible for the flow to go from subsonic to supersonic in the duct, or vice-versa (supersonic to subsonic)?

2) Consider a divergent duct, that is one whose cross-sectional area uniformly increases downstream as shown on the right of the Figure above. Is it possible for the flow to go from subsonic to supersonic in the duct, or vice-versa (supersonic to subsonic)?

edXsolution

Video Link

5.4.3 Subsonic flow and choking

5.4

Let us first consider the case for which the flow remains subsonic all along the duct. In the absence of shocks, the stagnation conditions are constant all along the duct and equal to the reservoir values:

$$p_0 = p_r \quad , \quad a_0^2 = (\gamma{-}1)h_0 = (\gamma{-}1)h_r \quad , \quad \rho_0 = \frac{\gamma\, p_0}{(\gamma{-}1)h_0} = \frac{\gamma\, p_r}{(\gamma{-}1)h_r} \, . \tag{5.20}$$

If we assume isentropic flow, $\dot{m}$ can be computed with the isentropic relations applied at the exit, using the known exit pressure $p_e = p_B$ and known exit area S_e, namely

$$\dot{m} = \rho_e u_e S_e = \frac{\gamma\, p_0}{\sqrt{(\gamma{-}1)h_0}}\, M_e \left(1 + \frac{\gamma{-}1}{2} M_e^2\right)^{-\frac{\gamma+1}{2(\gamma-1)}} S_e \, , \tag{5.21}$$

where the exit Mach number is given by

$$M_e^2 = \frac{2}{\gamma{-}1}\left[\left(\frac{p_0}{p_e}\right)^{\frac{\gamma-1}{\gamma}} - 1\right] \, . \tag{5.22}$$

As usual, take the time to derive these two relations on your own. Note that $\dot{m}$ is only a function of the reservoir conditions (p_0, h_0), exit area (S_e), and back pressure ($p_e = p_B$).

The observed relation between p_e and $\dot{m}$ is shown on the bottom right of Figure 5.10. As p_e is reduced, $\dot{m}$ will first increase, but at some point it will level off and remain constant even if p_e is reduced all the way to zero (vacuum). When $\dot{m}$ no longer increases with a reduction in p_e, the duct is said to be *choked*.

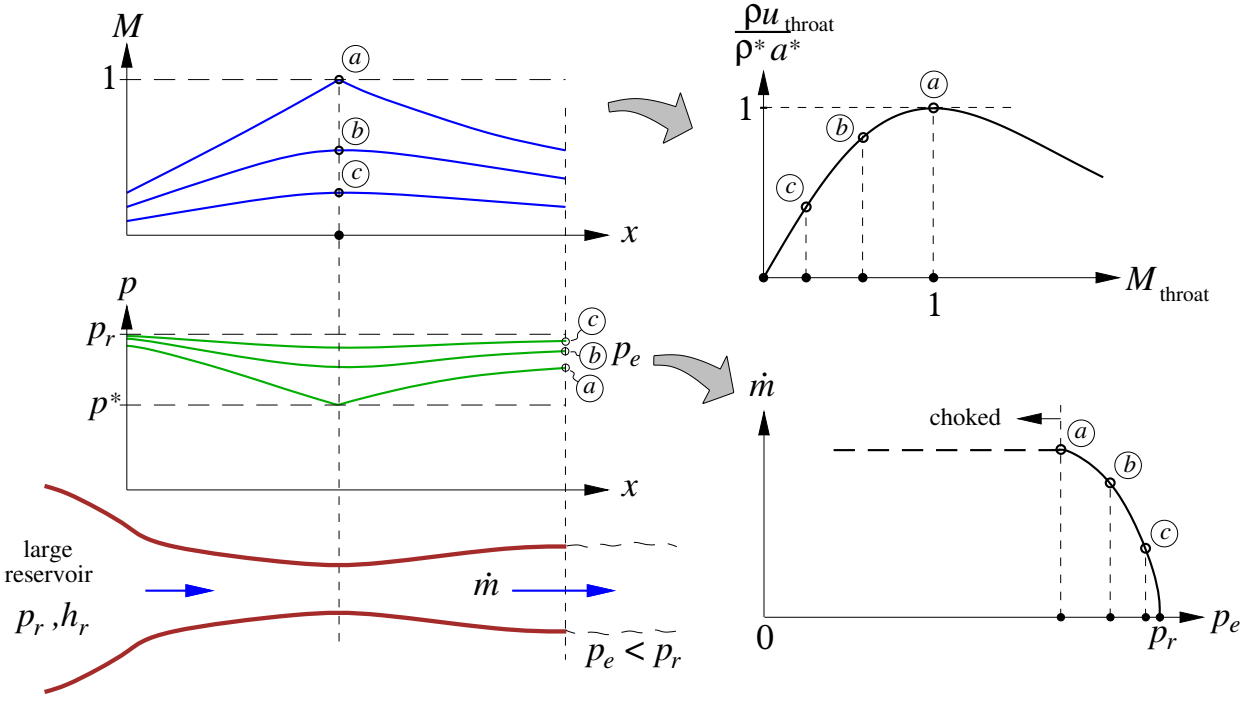


Figure 5.10: Onset of choking in a convergent-divergent duct: for given reservoir conditions, the maximum mass flux is reached once $M_{\text{throat}} = 1$.

If we examine the various flow properties along the duct, it is evident that the onset of choking coincides with the *throat* reaching $M = 1$ locally as illustrated at the top of Figure 5.10.

5.4.4 Choked flow

5.4

When the flow is choked ($M = 1$ at the throat), the mass flow is the maximum it can be, given the reservoir conditions and duct geometry. This corresponds to the mass flux ρu at the throat reaching its maximum possible value $\rho^* a^*$, which is given by

$$\rho^* a^* = \rho_0 a_0 \frac{\rho^*}{\rho_0}\frac{a^*}{a_0} = \frac{\gamma\, p_r}{\sqrt{(\gamma-1)h_r}} \left(1 + \frac{\gamma-1}{2}\right)^{-\frac{\gamma+1}{2(\gamma-1)}} . \tag{5.23}$$

The superscript $*$ is used to denote throat conditions for choked flow: since for choked flow $M_{\text{throat}} = M^* = 1$, then $u^* = a^*$ and the flux is written above as $\rho^* a^*$ instead of $\rho^* u^*$. The pressure $p^* = \rho^* {a^*}^2/\gamma$ is the throat pressure required to reach choking.

From equation (5.23), it is evident that the only way to change the mass flow $\dot{m} = \rho^* a^* S_{\text{throat}}$ of a choked duct is to change the reservoir's total properties p_r and/or h_r.

Recall from Module 4 that the ratio of area to sonic throat area is given by equation (4.90), that is

$$\frac{S}{S^*} = \frac{1}{M}\left[\frac{2}{\gamma+1}\left(1 + \frac{\gamma-1}{2}M^2\right)\right]^{\frac{\gamma+1}{2(\gamma-1)}} . \tag{5.24}$$

This is known as the *area-Mach relation*, which is usually available as a chart or in tabulated form. It uniquely relates the local Mach number M to the area ratio S/S^*, and is used to solve compressible duct flow problems. If the duct geometry $S(x)$ is given, and S^* is defined from the known duct mass flow and stagnation quantities, then $M(x)$ can be determined using the graphical technique shown in Figure 5.11, or using the equivalent numerical tables. Once $M(x)$ is determined, any remaining quantity of interest, such as $p(x)$, $\rho(x)$, $u(x)$, can be computed from the isentropic or adiabatic relations.

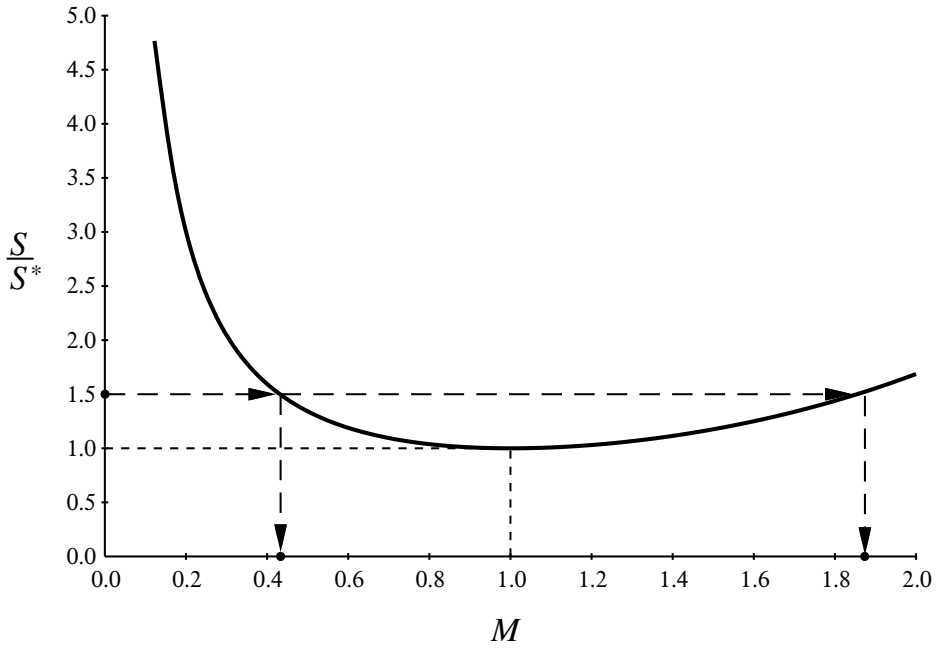


Figure 5.11: Graphical determination of M at any location with area S using a plot of the area-Mach relation.

Note that for any given area $S(x)$, two solutions are possible for a certain mass flow: a subsonic

solution with $M < 1$, and a supersonic solution with $M > 1$. Which solution corresponds to the actual flow depends on whether the flow upstream of that x location is subsonic or supersonic.

5.4.5 Choked flow with normal shock

5.4

When the back pressure is reduced below the level required to reach choking, a new flow pattern emerges, called a *Laval nozzle flow*, with the following important features as illustrated in Figure 5.12:

- The flow upstream of the throat no longer changes with p_e, but remains the same as at the choking-onset condition. This is consistent with the mass flow being fixed.
- The flow past the throat becomes supersonic. The Mach number continues to increase and pressure to decrease as the area increases downstream.
- A *normal shock* forms in the duct, and the flow behind the shock returns to subsonic. The Mach number then decreases and pressure increases towards p_e as the area increases.
- The shock incurs a total pressure loss, so that $p_0 < p_r$ behind the shock all the way to the exit. Both $p(x)$ and $M(x)$ behind the shock are then lower than what they would be with isentropic flow at the onset of choking.

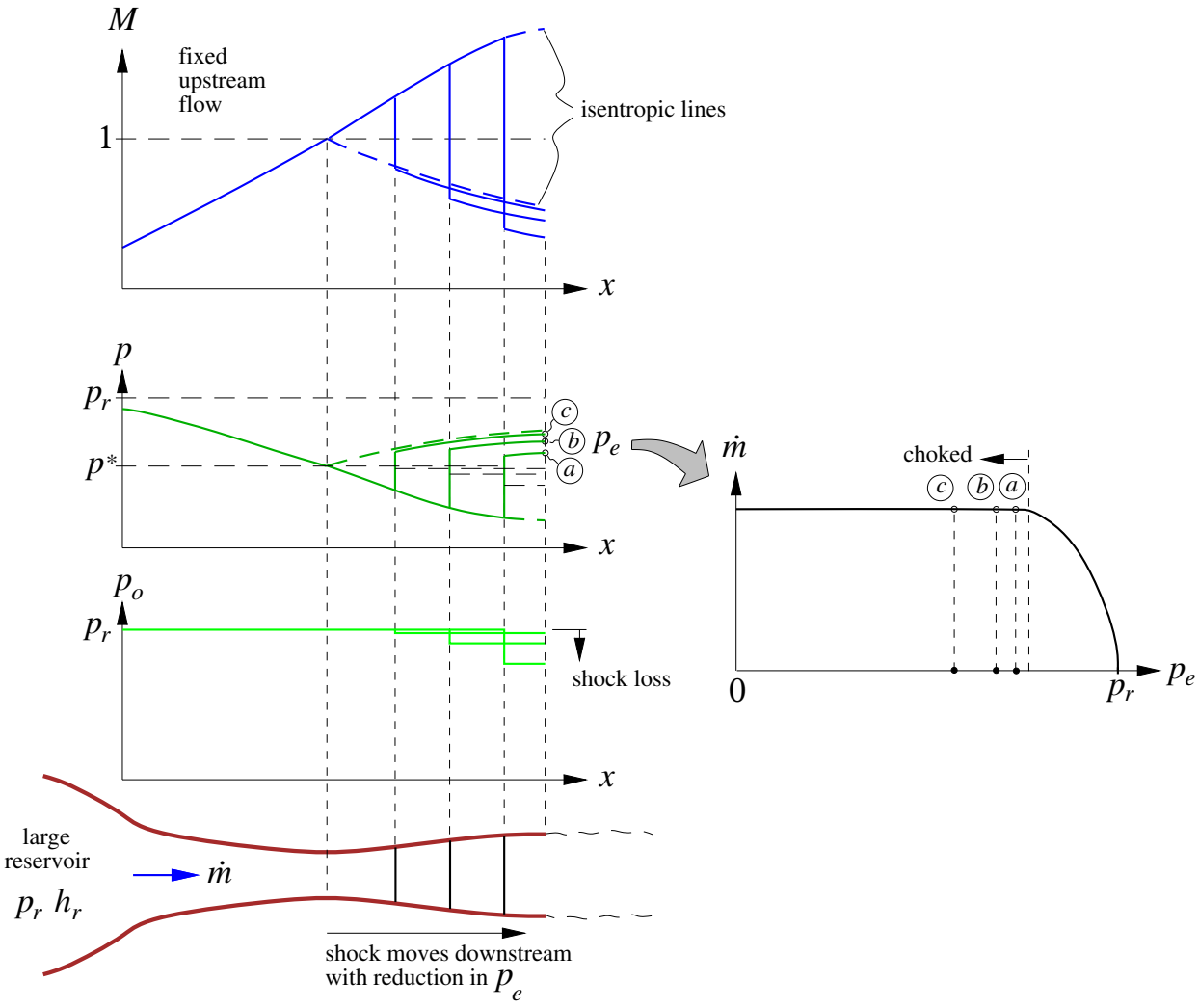


Figure 5.12: Laval nozzle flow: subsonic-supersonic-subsonic flow in a convergent-divergent duct.

edXproblem: 5.4.6 Convergent section of choked duct

In a choked flow through a convergent-divergent duct with given reservoir conditions, how would you change the back pressure in order to change the flow in the convergent section of the duct?

edXsolution

It is impossible to change the flow conditions in the convergent part of a choked convergent-divergent duct (Laval nozzle flow).

Information can *not* travel upstream of the sonic condition at the throat. Once the duct is choked, the flow in the convergent section reamains unchanged by any changes at the exit, in the back pressure. The flow will adapt in the divergent section or even downstream of the exit (*past the throat*) to match the back pressure, but will remain fixed in the convergent section for a set reservoir.

5.4.7 Supersonic-exit flows

5.4

With sufficiently low back pressure, the shock can be moved back to nearly the exit plane. If the back pressure is reduced further, below the sonic pressure p^*, the exit flow becomes supersonic, leading to three possible types of exit flow. In these cases it is necessary to distinguish between the exit pressure p_e of the duct flow, and the back pressure p_B of the surrounding air, since these two pressures will in general no longer be the same.

Over-expanded nozzle flow

When $p_B < p^*$, the exit flow is supersonic but $p_B > p_e$ and the flow must adjust to a higher pressure. This is done through oblique shocks attached to the duct nozzle exit edges as shown in Figure 5.13. The streamline at the edge of the jet behaves much like a solid wall, whose turning angle adjusts itself so that the post-shock pressure is equal to p_B.

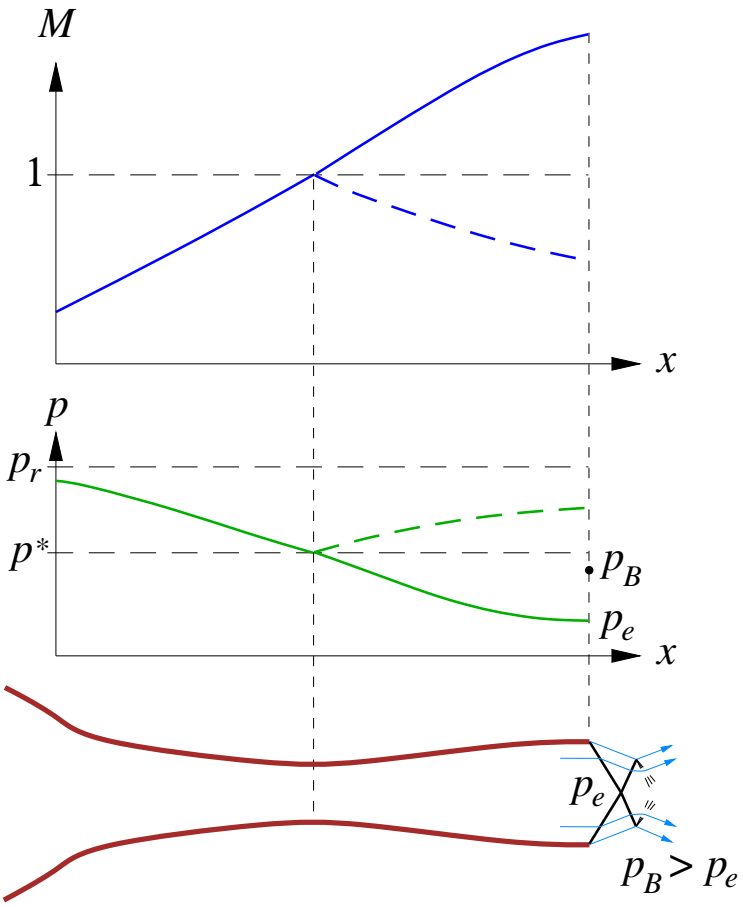


Figure 5.13: Over-expanded nozzle flow: $p_e < p_B < p^*$. The pressure p_e of the exiting flow is too low and goes through a series of shocks until its pressure rises to p_B

Ideally-expanded (matched) nozzle flow

When the back pressure is reduced just so $p_B = p_e$, the duct nozzle flow comes out at the same pressure as the surrounding air, and hence no turning takes place. There are no shocks present and the flow is isentropic throughout as shown in Figure 5.14. When designing a nozzle for *e.g.* rocket engines, this is the ideal condition since it generates a high-speed, high-mass-flow jet with minimum

losses.

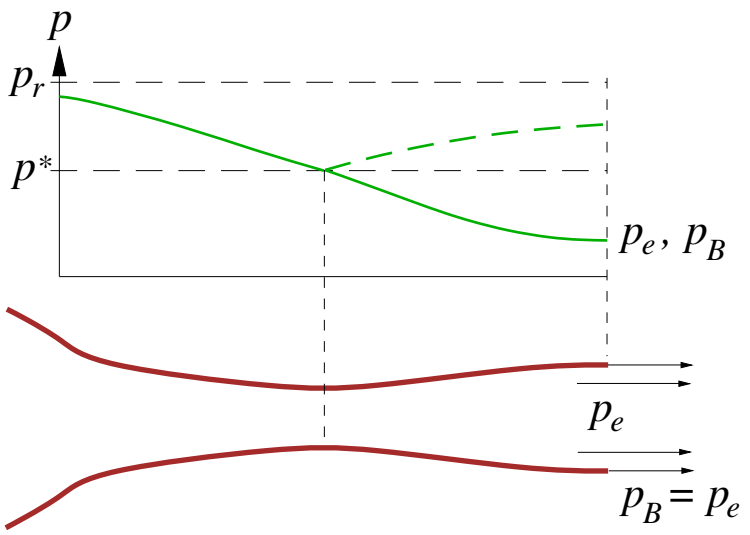


Figure 5.14: Ideally-expanded nozzle flow: $p_B = p_e$. The exiting jet is high-speed, high-mass-flow with minimum losses.

Under-expanded nozzle flow

If the back pressure is reduced below the isentropic exit pressure, $p_B < p_e$. The duct nozzle flow must now expand to reach p_B, which is done through expansion fans attached to the duct nozzle exit edges. This process is shown in Figure 5.15.

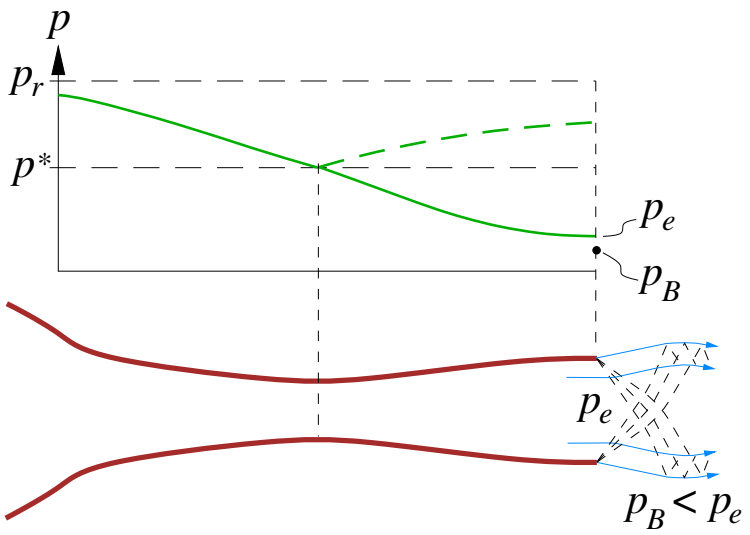


Figure 5.15: Under-expanded nozzle flow: $p_B < p_e$. The pressure p_e of the exiting flow is too high and the flow is expanded through expansion waves until its pressure is reduced to p_B.

Jet shock diamonds

In the under-expanded and over-expanded nozzle flows, each initial (emanating from the nozzle exit edge) oblique shock or expansion fan impinges on the opposite edge of the jet, turning the flow towards (shock) or away (expansion) the centerline. The shock or expansion fan reflects off the edge, and propagates back to the other side, repeating the cycle until the jet dissipates though

mixing. These flow patterns are known as *shock diamonds*, which are often visible in the exhaust of rocket or jet engines.

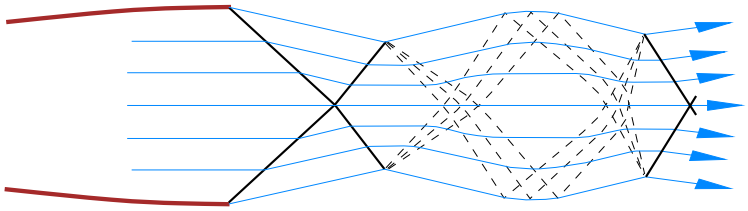


Figure 5.16: Illustration of jet shock diamonds present at the exit of a convergent-divergent duct with over- or under-expanded nozzles.

5.4.8 Determination of choked nozzle flows

5.4

A common flow problem is to determine the exit conditions and losses of a given choked nozzle with prescribed reservoir stagnation conditions p_r, h_r, and prescribed exit pressure p_e.

We first note that the mass flow in this situation is known, and given by combining relation (5.23) with the fact that $S^* = S_t$ for a choked throat to get

$$\dot{m} \;=\; \rho^* a^* S_t \;=\; \frac{\gamma\, p_r}{\sqrt{(\gamma-1)h_r}} \left(1 + \frac{\gamma-1}{2}\right)^{-\frac{\gamma+1}{2(\gamma-1)}} S_t \;. \qquad \text{(choked)} \qquad (5.25)$$

To then determine the exit conditions corresponding to this mass flow, we use the mass flow expression (5.21), but recast it in terms of the (known) exit static pressure rather than the (unknown) exit total pressure. Using the fact that $h_0 = h_r$ for adiabatic flow, we get

$$\dot{m} \;=\; \frac{\gamma p_e}{\sqrt{(\gamma-1)h_r}}\, M_e \left(1 + \frac{\gamma-1}{2} M_e^2\right)^{1/2} S_e \;. \qquad \text{(choked)} \qquad (5.26)$$

Equating (5.25) and (5.26), and squaring the result, gives

$$M_e^2 \left(1 + \frac{\gamma-1}{2} M_e^2\right) \;=\; \left(\frac{p_r}{p_e}\,\frac{S_t}{S_e}\right)^2 \left(1 + \frac{\gamma-1}{2}\right)^{-\frac{\gamma+1}{\gamma-1}} \;. \qquad \text{(choked)} \qquad (5.27)$$

This is a quadratic equation for M_e^2, which can be solved for a specified right-hand-side.

The exit total pressure is then obtained via its definition

$$p_{0_e} \;=\; p_e \left(1 + \frac{\gamma-1}{2} M_e^2\right)^{\frac{\gamma}{\gamma-1}} \;. \qquad (5.28)$$

The overall nozzle total pressure ratio p_{0_e}/p_r is due to the loss across the shock, so that

$$\frac{p_{0_e}}{p_r} \;=\; \left(\frac{p_{o_2}}{p_{o_1}}\right)_{\text{shock}} \;=\; f(M_1) \;, \qquad (5.29)$$

where $f(M_1)$ is the shock total pressure ratio function, also available in tabulated form. This equation therefore implicitly determines M_1 just in front of the shock, which together with the universal flow area function $S/S^* = f(M)$ determines the nozzle area at the shock and hence the location of the shock within the duct.

5.4.9 Summary of convergent-divergent duct flows

5.4

Figure 5.17 gives a graphical summary of the possible cases for the flow in a convergent-divergent duct.

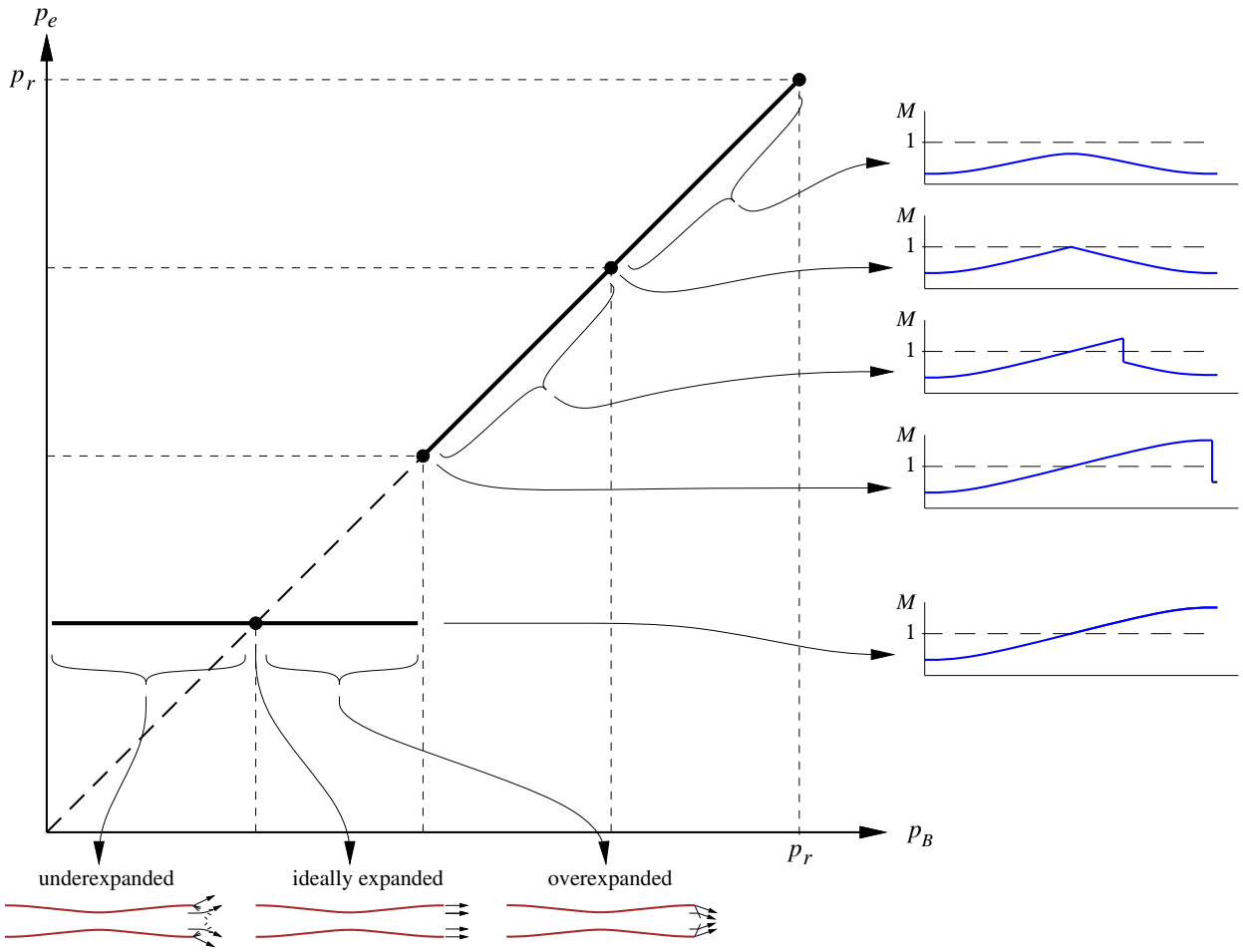


Figure 5.17: Summary of convergent-divergent duct flows.

When working out a problem involving a convergent-divergent duct, the process is usually as follows:

Step 1: Determine whether the duct is choked or not. To do this, assume that the flow is *not* choked, and hence $p_0 = p_r$ everywhere, then

1.1: Determine the Mach number M at a known location from the isentropic relation for $p_0/p = p_r/p$ as a funcion of M (or its equivalent form (5.22).

1.2: Compute S/S^* at this known location from equation (5.24) with the hypothetical value of M just found.

1.3: Compare the ratio S/S^* with S/S_t from the known geometry: if $S_t < S^*$, then the hypothesis was wrong and the duct is choked.

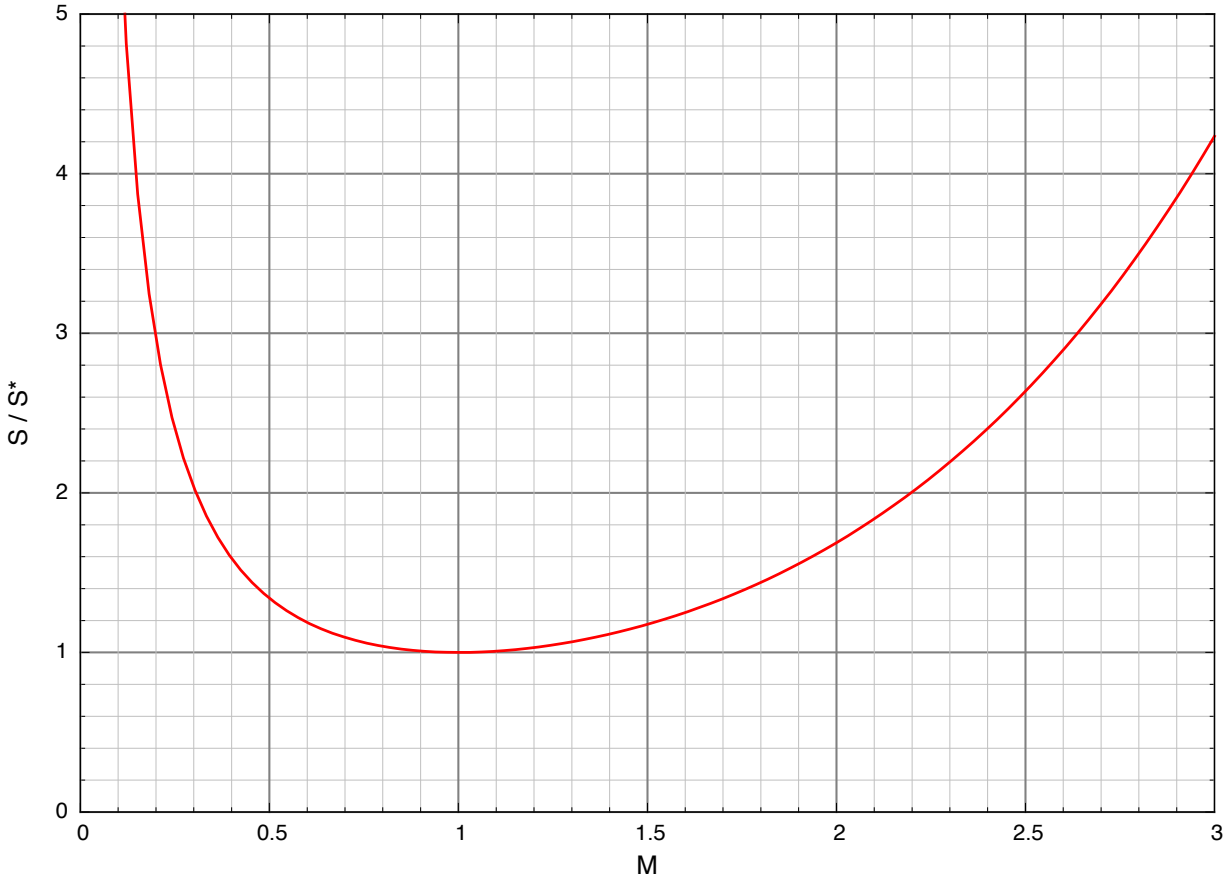
Step 2a: If the flow is indeed not choked, the steps above should give you all that you need.

Step 2b: If the flow is actually choked, then $M_t = 1$ and the throat conditions can be computed from the isentropic flow between the reservoir and the throat ($p_{0_t} = p_r$). The next thing is to determine the exit conditions, again by first assuming that the flow is isentropic (no shock is present) and compare the thus-obtained exit pressure with the back pressure.

edXproblem: 5.4.10 Throat Mach number and area ratio

5.4

Assume the fluid is air and that it behaves like an ideal gas with $\gamma = 1.4$ and $R = 287\,\mathrm{J/kg \cdot K}$. Use the S/S^* versus M chart below for your answers.



1) A convergent-divergent duct has an area ratio $S_e/S_t = 1.5$, and an exit-to-reservoir pressure ratio of $p_e/p_r = 0.95$. Determine the Mach number M_t at the throat. Provide your answer with two digits of precision (of the form X.YeP).

2) A different convergent-divergent duct has an air reservoir at $h_r = 3.0 \times 10^5\,\mathrm{m^2/s^2}$, and $p_r = 4.0 \times 10^5\,\mathrm{Pa}$. It is observed to have $p_e = 1.0 \times 10^5\,\mathrm{Pa}$.

What is S_e/S^* at the exit? Provide your answer with three digits of precision (of the form X.YZeP).

What is the S_e/S_t ratio for this nozzle? Provide your answer with three digits of precision (of the form X.YZeP).

edXsolution

Video Link

edXproblem: 5.4.11 Back pressure changes

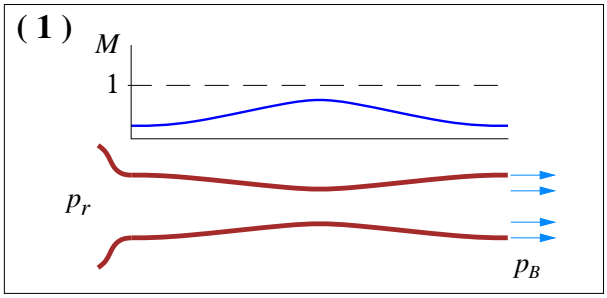
5.4

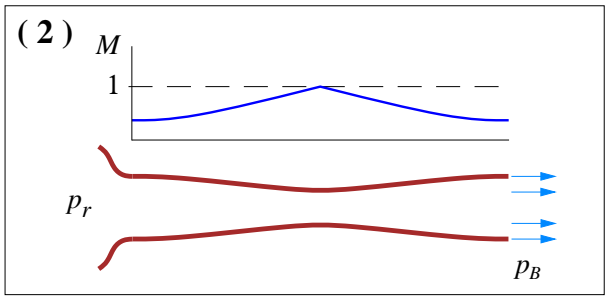
A convergent-divergent duct has $S_e/S_t = 1.53$, and a reservoir pressure of $p_r = 2.0 \times 10^5$ Pa. The fluid is air and behaves like an ideal gas with $\gamma = 1.4$ and $R = 287\,\text{J/kg} \cdot \text{K}$.

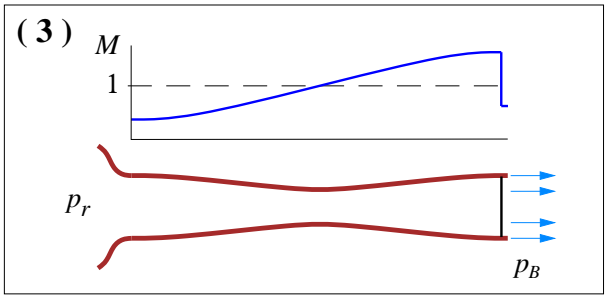
Note: $S/S^* = 1.53$ for $M = 0.424$ and $M = 1.878$.

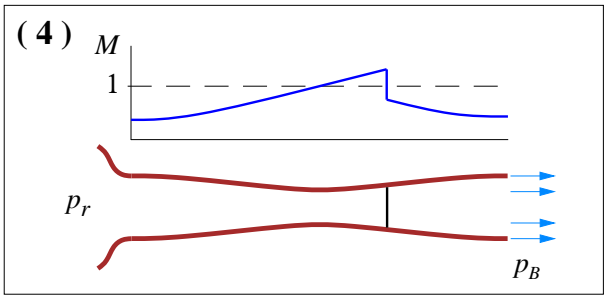
Drag and drop the Mach number evolution schematics to their corresponding pressure ratios of back pressure to reservoir pressure.

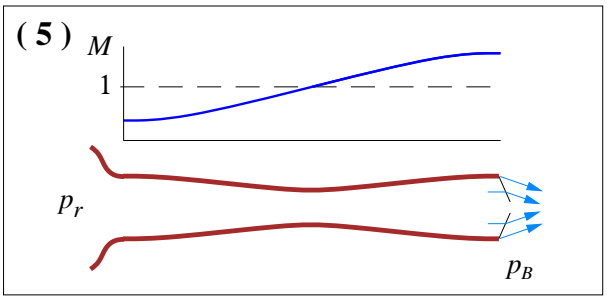
For the following pressure ratios of back pressure to reservoir pressure, select the corresponding Mach number evolution from the schematics below by indicating the appropriate schematic number.

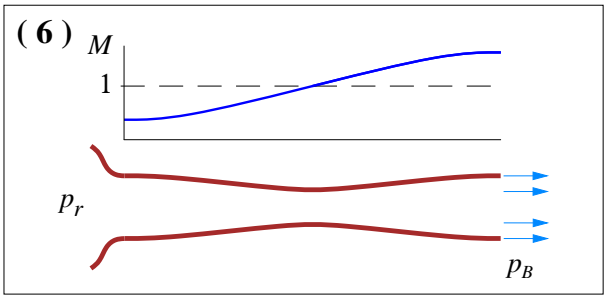


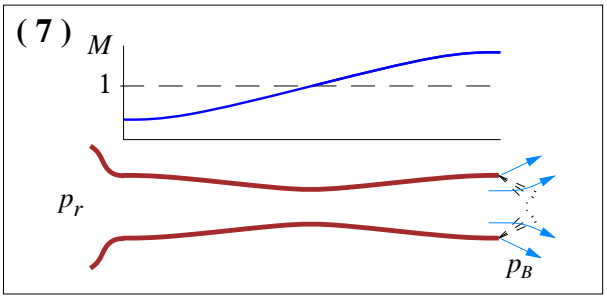












(a) $p_B/p_r = 0.1$

(b) $p_B/p_r = 0.5$

(c) $p_B/p_r = 0.7$

(d) $p_B/p_r = 0.9$

edXsolution

Video Link

5.5 Oblique shocks

5.5.1 Mach waves

5.1

Small disturbances created by a slender body in a supersonic flow will propagate diagonally away as *Mach waves*. These consist of small isentropic variations in V, ρ, p, and h, and are loosely analogous to the water waves sent out by a speedboat. Mach waves appear stationary with respect to the object generating them, but when viewed relative to the still air, they are in fact indistinguishable from sound waves and their normal-direction speed of propagation is equal to a, the speed of sound. This is illustrated in Figure 5.18.

As with normal shocks, it is convenient to analyze problems with oblique shocks from the reference frame of the moving body, where the flow is steady.

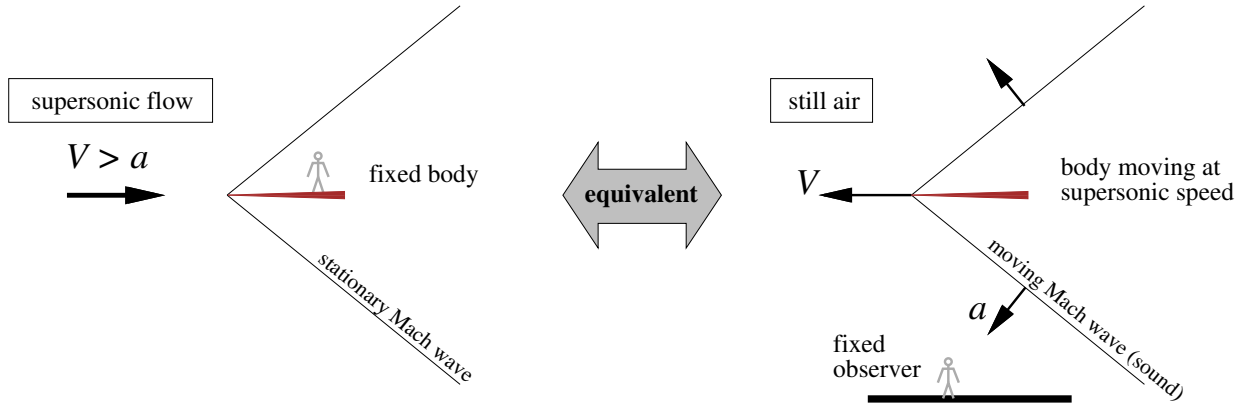


Figure 5.18: Mach waves as seen by an observer moving with the body that generates them (left) and by an observer in a stationary frame (right).

The angle μ of a Mach wave relative to the flow direction is called the *Mach angle*. It can be determined by considering the wave to be the superposition of many pulses emitted by the body, each one producing a disturbance circle (in 2-D) or sphere (in 3-D) which expands at the speed of sound a, as illustrated in Figure 5.19. At some time interval t after the pulse is emitted, the radius of the circle will be at, while the body will travel a distance Vt. The Mach angle is then seen to be

$$\mu \;=\; \arcsin\left(\frac{at}{Vt}\right) \;=\; \arcsin\left(\frac{1}{M}\right) \tag{5.30}$$

which can be defined at any point in the flow. In the subsonic flow case where $M = V/a < 1$ the expanding circles do not coalesce into a wave front, and the Mach angle is not defined.

5.5.2 Oblique analysis

5.1

As for normal shocks, a control volume analysis is applied to the oblique shock flow, using a control volume that straddles the shock as shown in Figure 5.20. The top and bottom boundaries are chosen to lie along streamlines so that only the boundaries parallel to the shock, with area S, have mass flow across them.

Velocity components are taken in the x-z coordinates normal and tangential to the shock, as shown. The tangential z axis is tilted from the upstream flow direction by the *wave angle* β. The

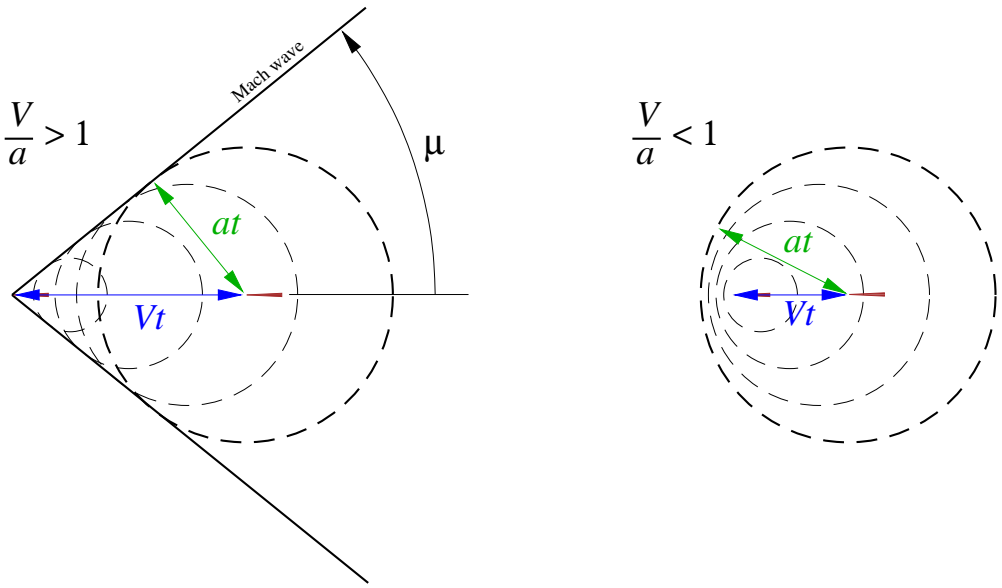


Figure 5.19: Mach wave as superposition of pulses emitted from a body moving at supersonic speeds (left). In the subsonic case (right), no Mach wave forms.

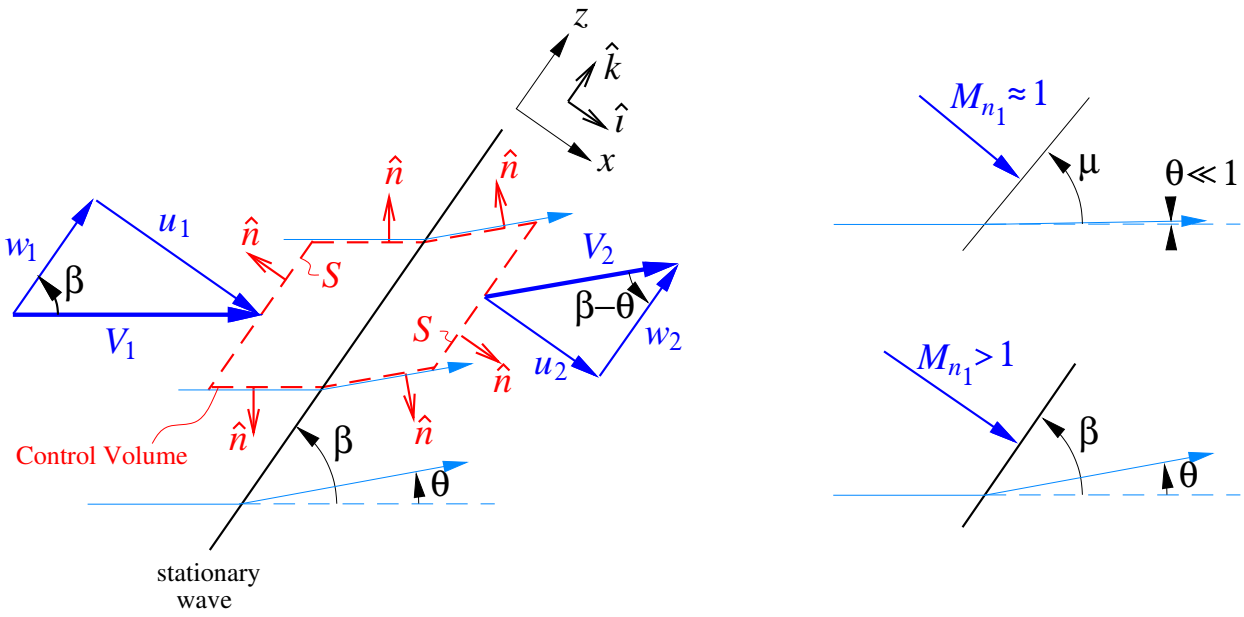


Figure 5.20: Control volume used for the analysis of oblique shocks. The flow velocity is decomposed into normal, u, and tangential components, w. The Mach number also has a normal (denoted by the subscript n) and a tangential (subscript t) components.

upstream flow velocity components in the normal direction, u, and tangential direction, w, are

$$u_1 \;=\; V_1 \sin\beta \quad , \quad w_1 \;=\; V_1 \cos\beta \; . \tag{5.31}$$

If the shock is infinitesimally weak, the wave angle β and Mach angle μ are the same. For a finite-strength shock, $\beta > \mu$.

The integral conservation equations (mass, x-momentum, z-momentum, energy) and the state

equation applied to the control volume read

$$\rho_1 u_1 = \rho_2 u_2 \tag{5.32}$$

$$\rho_1 u_1^2 + p_1 = \rho_2 u_2^2 + p_2 \tag{5.33}$$

$$w_1 = w_2 \tag{5.34}$$

$$h_1 + \frac{1}{2}u_1^2 = h_2 + \frac{1}{2}u_2^2 \tag{5.35}$$

$$p_2 = \frac{\gamma - 1}{\gamma}\rho_2 h_2 \tag{5.36}$$

Simplification of equation (5.34) makes use of (5.32) to eliminate $\rho u S$ from both sides. Simplification of equation (5.35) makes use of (5.32) to eliminate $\rho u S$ and then (5.34) to eliminate w from both sides. Take the time to start from the standard control volume equations and go through these simplifications on your own.

5.5.3 Equivalence between normal and oblique shocks

5.1

It is apparent that equations (5.32), (5.33), (5.35), (5.36) are in fact identical to the normal-shock equations derived earlier. The one additional z-momentum equation (5.34) simply states that the tangential velocity component doesn't change across a shock: $w_1 = w_2$.

This can be physically interpreted if we examine the oblique shock from the viewpoint of an observer moving with the everywhere-constant tangential velocity $w = w_1 = w_2$, as shown in Figure 5.21. The moving observer sees a normal shock with upstream velocity u_1 and downstream velocity u_2. The static fluid properties p, ρ, h, a are of course the same in both frames.

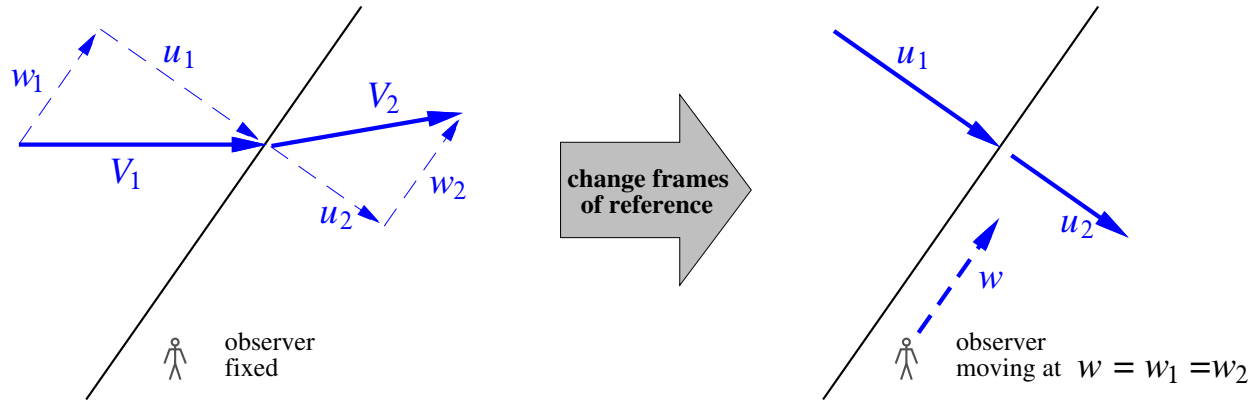


Figure 5.21: Reference frame change used to show that the tangential velocity is constant across a shock.

The effective equivalence between an oblique and a normal shock allows us to re-use the previously derived normal shock jump relations: we only need to construct the necessary transformation from one frame to the other.

5.5.4 Mach number jump

5.1

Define the *normal Mach number components* seen by the moving observer as

$$M_{n_1} \equiv \frac{u_1}{a_1} = \frac{V_1 \sin\beta}{a_1} = M_1 \sin\beta \ , \tag{5.37}$$

$$M_{n_2} \equiv \frac{u_2}{a_2} = \frac{V_2 \sin(\beta-\theta)}{a_2} = M_2 \sin(\beta-\theta) \ . \tag{5.38}$$

These are then related via our previous normal-shock $M_2 = f(M_1)$ relation (5.11), if we make the substitutions $M_1 \mapsto M_{n_1}$ and $M_2 \mapsto M_{n_2}$, to get

$$M_{n_2}^2 = \frac{1 + \frac{\gamma-1}{2} M_{n_1}^2}{\gamma M_{n_1}^2 - \frac{\gamma-1}{2}} \ . \tag{5.39}$$

The fixed-frame M_2 quantity then follows from trigonometry, and is given by

$$M_2 = \frac{M_{n_2}}{\sin(\beta-\theta)} \ . \tag{5.40}$$

5.5.5 Wave angle relation

5.1

We now need to determine the wave angle β. Using the result $w_1 = w_2$, the velocity triangles on the two sides of the shock can be related by

$$\frac{\tan(\beta-\theta)}{\tan\beta} = \frac{u_2}{u_1} = \frac{\rho_1}{\rho_2} = \frac{2 + (\gamma-1)M_1^2 \sin^2\beta}{(\gamma+1)M_1^2 \sin^2\beta} \ . \tag{5.41}$$

Solving this for θ gives

$$\tan\theta = \frac{2}{\tan\beta} \frac{M_1^2 \sin^2\beta - 1}{M_1^2(\gamma + \cos 2\beta) + 2} \ , \tag{5.42}$$

which is an implicit definition of the wave angle as the function $\beta(\theta, M_1)$.

Use of this equation is problematic, since it must be numerically solved to obtain the $\beta(\theta, M_1)$ result. A convenient alternative is to obtain this result graphically, from an *oblique shock chart* such as the one illustrated in Figure 5.22.

The $\beta(\theta, M_1)$ chart reveals a number of important features:

- There is a maximum turning angle $\theta_{\max}$ for any given upstream Mach number M_1. If the wall angle exceeds this, or $\theta > \theta_{\max}$, no oblique shock is possible. Instead, a *detached shock* forms ahead of the concave corner. Such a detached shock is in fact the same as a *bow shock* discussed earlier.

- If $\theta < \theta_{\max}$, two distinct oblique shocks with two different β angles are physically possible. The smaller β case is called a *weak shock*, and is the one most likely to occur in a typical supersonic flow. The larger β case is called a *strong shock*, and it has a subsonic flow behind it. To determine which shock wave actually occurs depends on what is happening further downstream of where the shock emanates from. Generally speaking, the weak shock tends to be observed most frequently, however, when the downstream flow requires significant flow changes (for example because of a body further downstream), then the strong shock can occur.

- The strong-shock case in the limit $\theta \to 0$ and $\beta \to 90°$, in the upper-left corner of the oblique shock chart, corresponds to the normal-shock case.

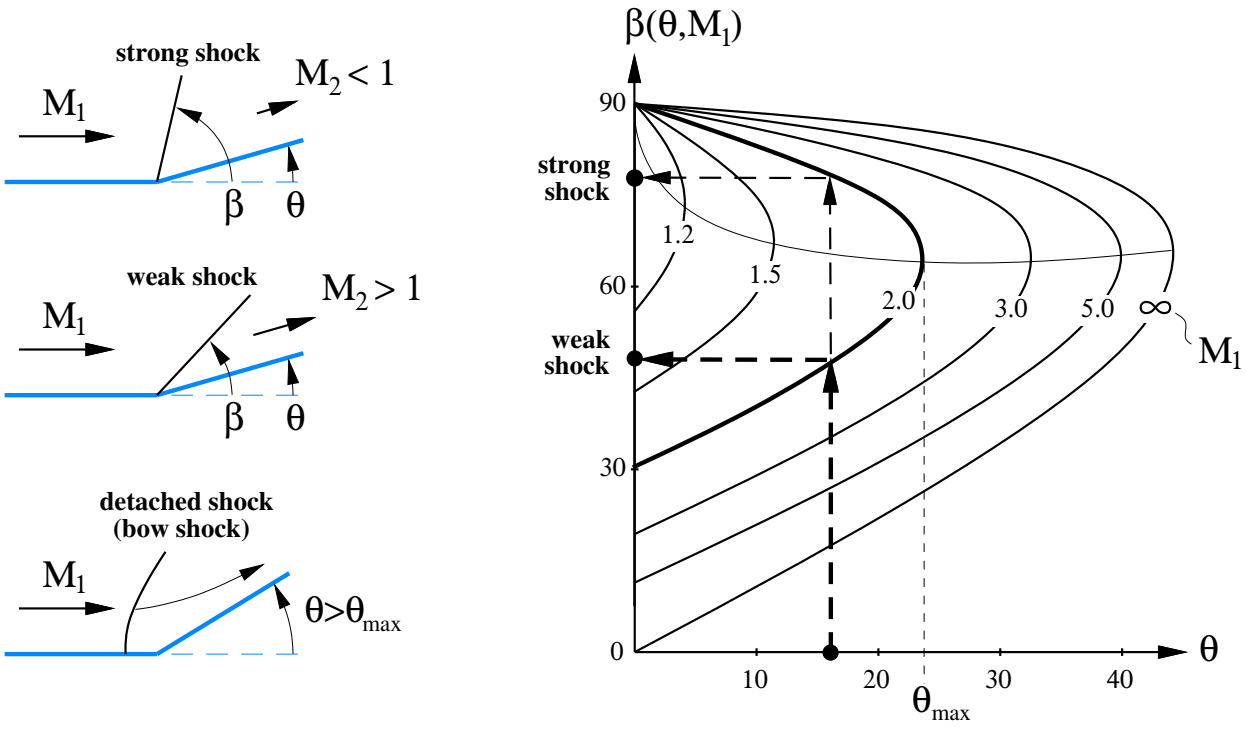


Figure 5.22: Oblique-shock chart: determination of the wave angle β is usually done graphically from $\beta(M_1)$ versus θ lines. Two solutions are possible: a weak shock one and a strong shock one. The latter is unlikely to form over straight-edge walls.

Derivation

The relations (5.41) and (5.42) can be derived using only trigonometry and algebra. Make sure you are able to write them on your own. The following video shows their derivations.

Video Link

5.5.6 Static jumps

5.1

The static flow property ratios are likewise obtained using the previous normal-shock relations (5.12), (5.13), (5.14), and using M_{n_1} as the relevant upstream Mach number, that is

$$\frac{\rho_2}{\rho_1} = \frac{(\gamma+1)M_{n_1}^2}{2 + (\gamma-1)M_{n_1}^2} , \tag{5.43}$$

$$\frac{p_2}{p_1} = 1 + \frac{2\gamma}{\gamma+1}\left(M_{n_1}^2 - 1\right) , \tag{5.44}$$

$$\frac{T_2}{T_1} = \frac{h_2}{h_1} = \frac{p_2}{p_1}\frac{\rho_1}{\rho_2} = \left[1 + \frac{2\gamma}{\gamma+1}\left(M_{n_1}^2 - 1\right)\right]\frac{2 + (\gamma-1)M_{n_1}^2}{(\gamma+1)M_{n_1}^2} . \tag{5.45}$$

5.5.7 Summary of oblique shocks

5.1

Thanks to the equivalence between a normal shock and an oblique shock through a simple

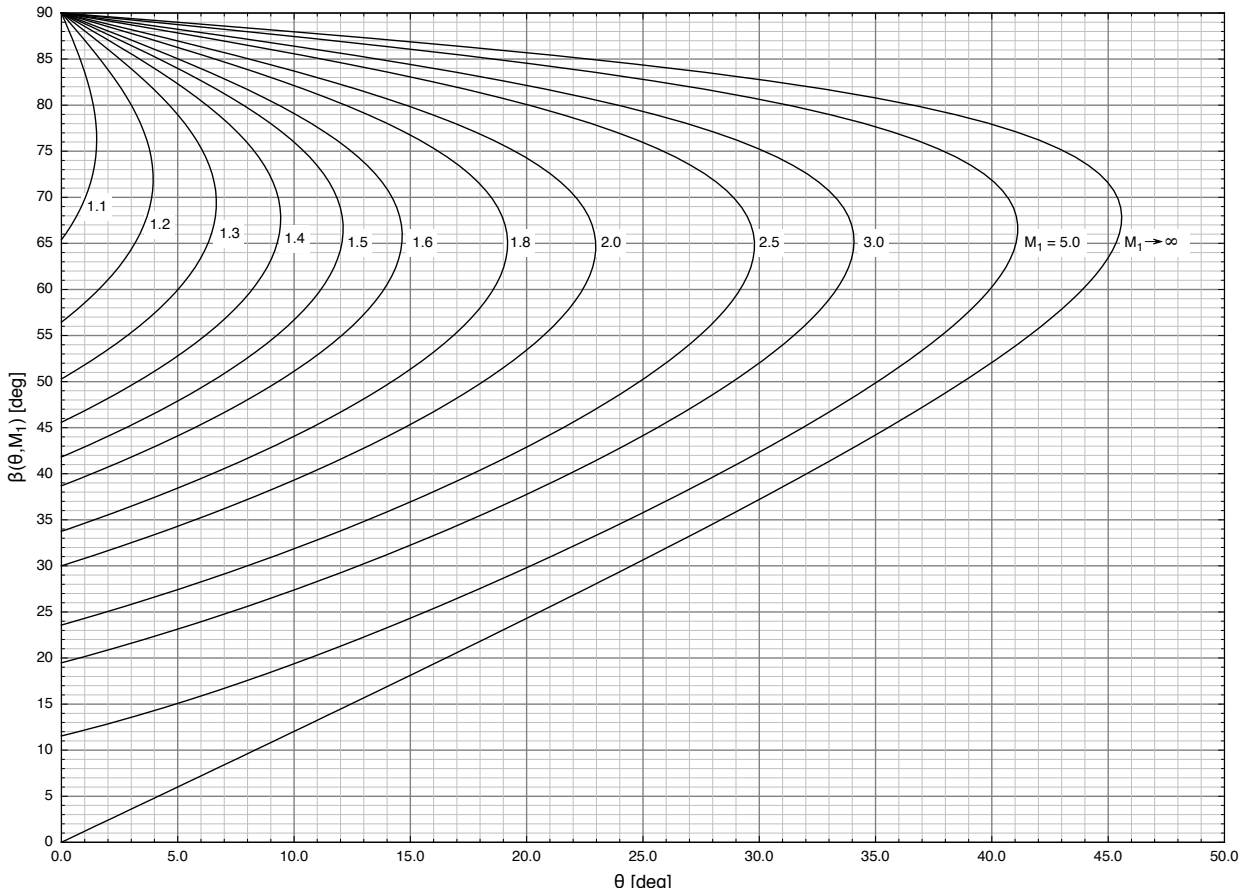


Figure 5.23: Oblique-shock chart: wave angle β versus turning angle θ for various upstream Mach numbers M_1.

reference frame change, the solution of problems with oblique shocks is almost identical to the cases that involve normal shocks.

Solving a typical oblique shock problem thus involves the following steps:

Step 1: Find the wave angle β from the upstream Mach number M_1 and the deflection (body surface) angle θ using equation (5.42) or its chart in Figure 5.22.

Step 2: Find the upstream normal Mach number M_{n_1} from its definition (5.37) and the result of Step 1.

Step 3: Compute the downstream normal Mach number M_{n_2} from its definition (5.38) and the result of Step 2. Compute also the downstream Mach number M_2 from the relation (5.40).

Step 4: Find the ratios of static quantities ρ_2/ρ_1, p_2/p_1, T_2/T_1 using normal shock tables at the M_{n_1} row or the jump relations (5.43)–(5.45) given the result of Step 2.

Step 5: Compute the downstream static conditions given the ratios found in Step 4, *e.g.* $p_2 = (p_2/p_1) \times p_1$.

These steps are all that is needed to uniquely define the downstream flow. As in a normal shock problem, if the stagnation quantities are also of interest, one can proceed with the additional three steps:

Step 6: Find the ratios of stagnation to static quantities in the downstream flow ρ_{0_2}/ρ_2, p_{0_2}/p_2, T_{0_2}/T_2 given that M_2 is know from Step 3, and by using isentropic tables or the isentropic relations (5.1)–(5.3).

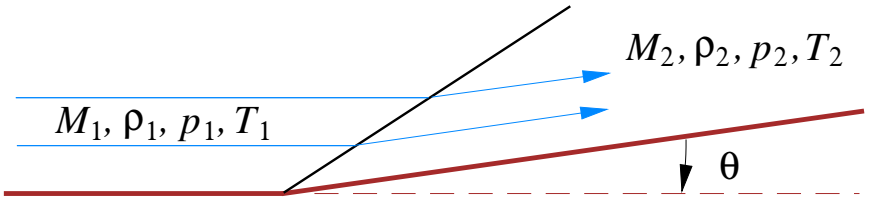
Step 7: Compute the downstream stagnation conditions by using the ratios from Steps 4 and 5, and given the known upstream conditions, *e.g.* $p_{0_2} = (p_{0_2}/p_2) \times (p_2/p_1) \times p_1$.

Step 8: Compute the upstream stagnation conditions ρ_{0_1}, p_{0_1}, T_{0_1} from the known static conditions ρ, p, T, and upstream Mach number M_1 using either an isentropic table or the isentropic relations (5.1)–(5.3).

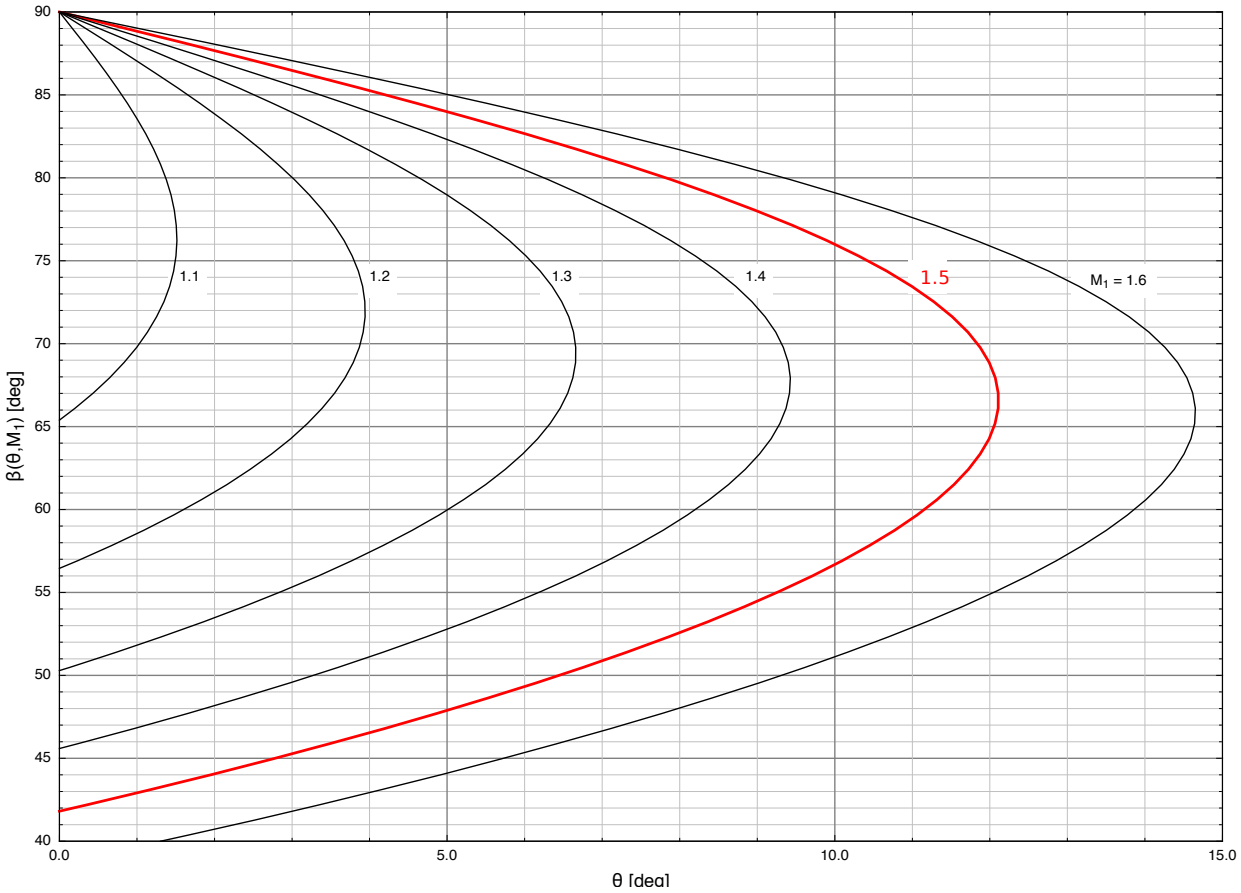
edXproblem: 5.5.8 Supersonic flow past an upward ramp

5.1 5.3

Consider an upward ramp (concave corner) with angle $\theta = 10°$ as shown in the Figure below. The incoming airflow is supersonic with $M_1 = 1.5$, $p_1 = 10^5\,\text{Pa}$, $T_1 = 298\,\text{K}$. Assume air behaves like an ideal gas with $\gamma = 1.4$ and $R = 287\,\text{J/kg}\cdot\text{K}$, and that the shock is weak.



1) Determine the conditions past the shock. Use the $\beta(\theta, M)$ chart below.



Provide the Mach number with three digits of precision (of the form X.YZeP): $M_2 =$

Provide the pressure (in Pascals) with three digits of precision (of the form X.YZeP): $p_2 =$

Provide the temperature with three digits of precision (of the form X.YZeP): $T_2 =$

Provide the density with two digits of precision (of the form X.YeP): $\rho_2 =$

2) What is the total pressure loss $1 - p_{0_2}/p_{0_1}$? Provide your answer with two digits of precision (of the form X.YeP).

edXsolution

Video Link

5.6 Expansion waves

5.6.1 Oblique shocks and expansion waves

5.2

Mach waves can be either compression waves ($p_2 > p_1$) or expansion waves ($p_2 < p_1$), but in either case their strength is by definition very small (*i.e.* $|p_2 - p_1| \ll p_1$). A body of finite thickness, however, will generate oblique waves of finite strength, and now we must distinguish between compression and expansion types.

Figure 5.24 illustrates the simplest body shapes for generating such waves, namely

- a concave corner (ramp up), which generates an *oblique shock* (compression), or
- a convex corner (ramp down), which generates an *expansion fan*.

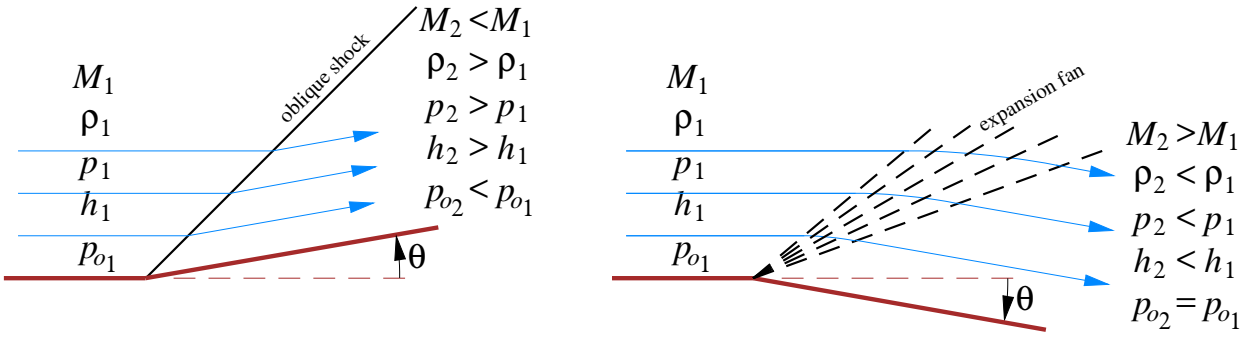


Figure 5.24: Generation of oblique waves by wall corners: a concave corner, or upward ramp, generates compressive an oblique shock (left), while a convex corner, or downward ramp, generates an expansion fan (right).

The flow quantity changes across an oblique shock are in the same direction as across a normal shock, and across an expansion fan they are in the opposite direction. One important difference is that p_0 decreases across the shock, while the fan is isentropic, so that it has no loss of total pressure and hence $p_{0_2} = p_{0_1}$.

The combination of oblique-shock relations and Prandtl-Meyer wave relations (which will be derived next) constitutes *Shock-Expansion Theory*, which can be used to determine the flow properties and forces for simple 2-D shapes in supersonic flow.

5.6.2 Wave flow relations

5.2

An expansion fan, sometimes also called a *Prandtl-Meyer expansion wave*, can be considered as a continuous sequence of infinitesimal Mach expansion waves. To analyze this continuous change, we will now consider the flow angle θ to be a flowfield variable, like M or V.

Across each Mach wave of the fan, the flow direction changes by $d\theta$, while the speed changes by dV. Oblique-shock analysis dictates that only the normal velocity component u can change across any wave, so that dV must be entirely due to the normal-velocity change du.

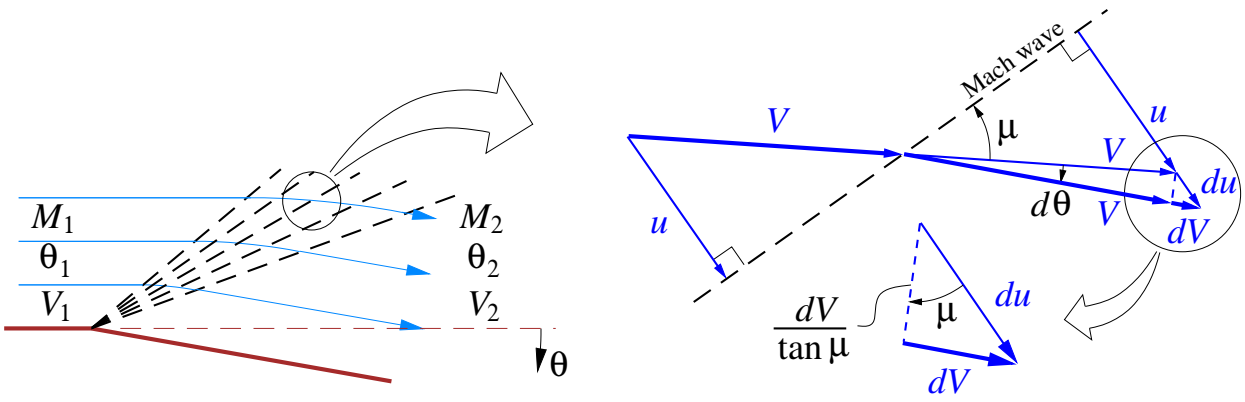


Figure 5.25: Expansion fan illustration (left) and velocity triangles across a single Mach expansion wave (right).

From the u-V and du-dV velocity triangles shown in Figure 5.25, and assuming that the flow angle change $d\theta$ across a single expansion wave is small ($d\theta \ll 1$), it is evident that $d\theta$ and dV are related by

$$d\theta \;=\; \frac{dV}{\tan\mu}\,\frac{1}{V}\;. \tag{5.46}$$

where μ is the Mach angle. Using the fact that $\sin\mu = 1/M$ from (5.30), we have

$$\frac{1}{\tan\mu} \;=\; \frac{\cos\mu}{\sin\mu} \;=\; \frac{\sqrt{1-\sin^2\mu}}{\sin\mu} \;=\; \frac{\sqrt{1-1/M^2}}{1/M} \;=\; \sqrt{M^2-1} \tag{5.47}$$

and so the flow relation above becomes

$$d\theta \;=\; \sqrt{M^2-1}\,\frac{dV}{V} \tag{5.48}$$

This is a differential equation which relates a change $d\theta$ in the flow angle to a change dV in the flow speed throughout the expansion fan.

5.6.3 Prandtl-Meyer function

5.2

The differential equation (5.48) can be integrated if we first express V in terms of M as follows

$$V \;=\; M\,a \;=\; M\,a_0\left(1+\frac{\gamma-1}{2}M^2\right)^{-1/2} \tag{5.49}$$

$$\ln V \;=\; \ln M \;+\; \ln a_0 \;-\; \frac{1}{2}\,\ln\!\left(1+\frac{\gamma-1}{2}M^2\right) \tag{5.50}$$

$$\frac{dV}{V} \;=\; \frac{dM}{M} \;-\; \frac{1}{2}\left(1+\frac{\gamma-1}{2}M^2\right)^{-1}\frac{\gamma-1}{2}\,2M\,dM \tag{5.51}$$

$$\frac{dV}{V} \;=\; \frac{1}{1+\frac{\gamma-1}{2}M^2}\,\frac{dM}{M}\;. \tag{5.52}$$

Equation (5.48) then becomes

$$d\theta \;=\; \frac{\sqrt{M^2-1}}{1+\frac{\gamma-1}{2}M^2}\,\frac{dM}{M}\;. \tag{5.53}$$

Integrating between any two points 1 and 2 through the Prandtl-Meyer wave

$$\int_{\theta_1}^{\theta_2} d\theta \;=\; \int_{M_1}^{M_2} \frac{\sqrt{M^2-1}}{1+\frac{\gamma-1}{2}M^2}\,\frac{dM}{M} \tag{5.54}$$

we get an expression for the change in flow angle between any two points

$$\theta_2 - \theta_1 \;=\; \nu(M_2) \;-\; \nu(M_1) \tag{5.55}$$

$$\text{where} \qquad \nu(M) \;\equiv\; \sqrt{\frac{\gamma+1}{\gamma-1}}\,\arctan\sqrt{\frac{\gamma-1}{\gamma+1}\,(M^2-1)} \;-\; \arctan\sqrt{M^2-1} \tag{5.56}$$

Here, $\nu(M)$ is called the *Prandtl-Meyer function*, and is plotted for $\gamma = 1.4$ in Figure 5.26.

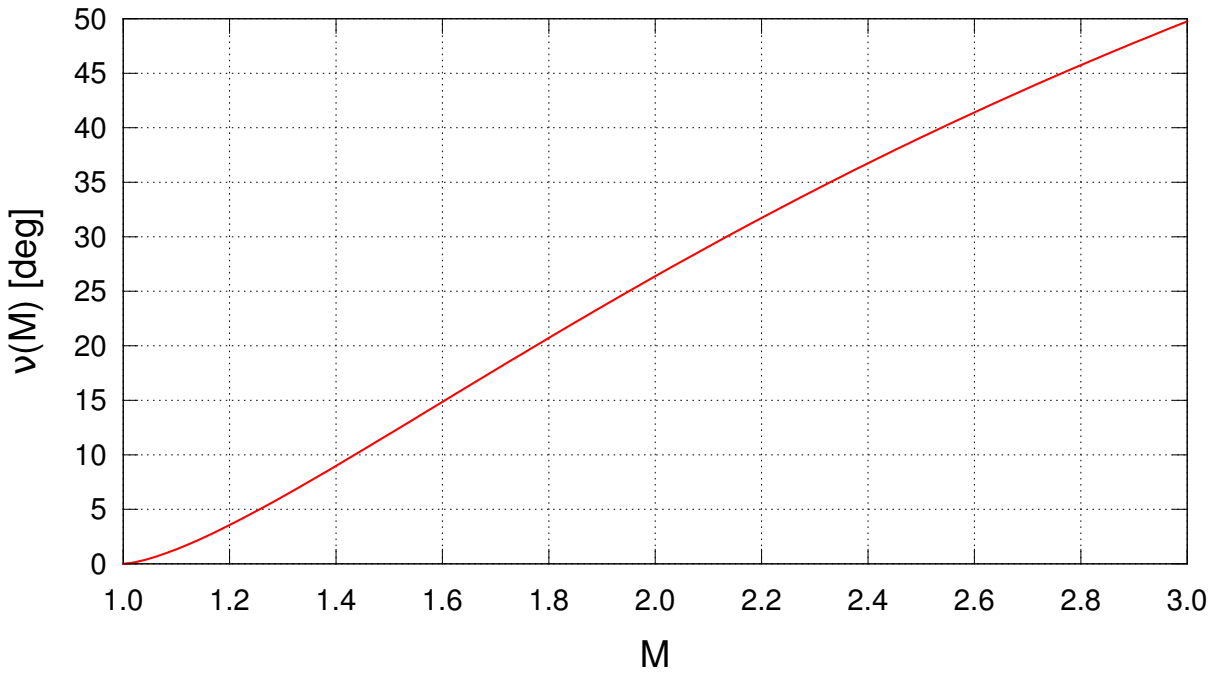


Figure 5.26: Prandtl-Meyer function $\nu(M)$.

Equation (5.55) can be applied to any two points within an expansion fan, but the most common use is to relate the two flow conditions before and after the fan. Reverting back to our previous notation where θ is the total turning of the corner, the relation between θ and the upstream and downstream Mach numbers is

$$\theta \;=\; \nu(M_2) \;-\; \nu(M_1)\;. \tag{5.57}$$

This can be considered an implicit definition of $M_2(M_1, \theta)$, which can be evaluated graphically using the $\nu(M)$ function plot, as illustrated in Figure 5.27 below. The Prandtl-Meyer function and the fact that total pressure is constant across an expansion fan is all that is needed to determine the downstream state.

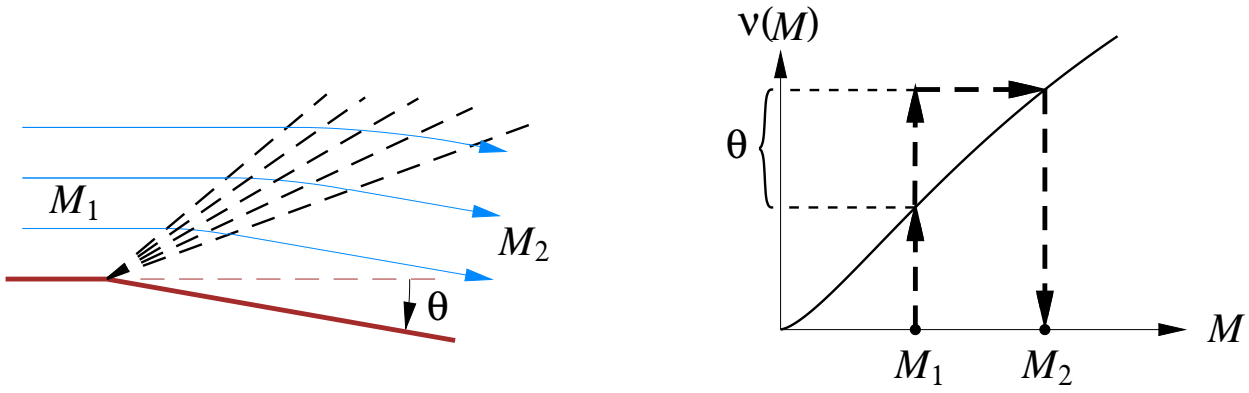
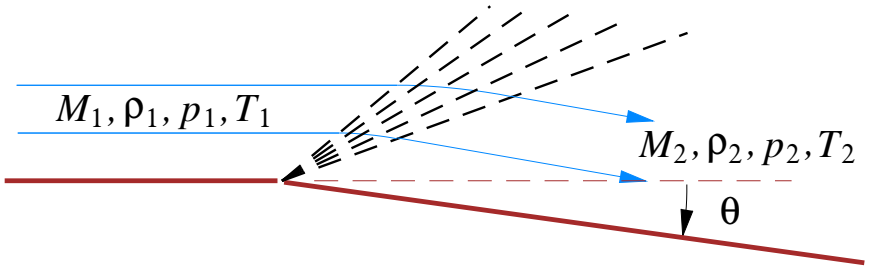


Figure 5.27: Illustration of the use of the Prandtl-Meyer function $\nu(M)$ to evaluate M_2 across an expansion fan given M_1 and θ.

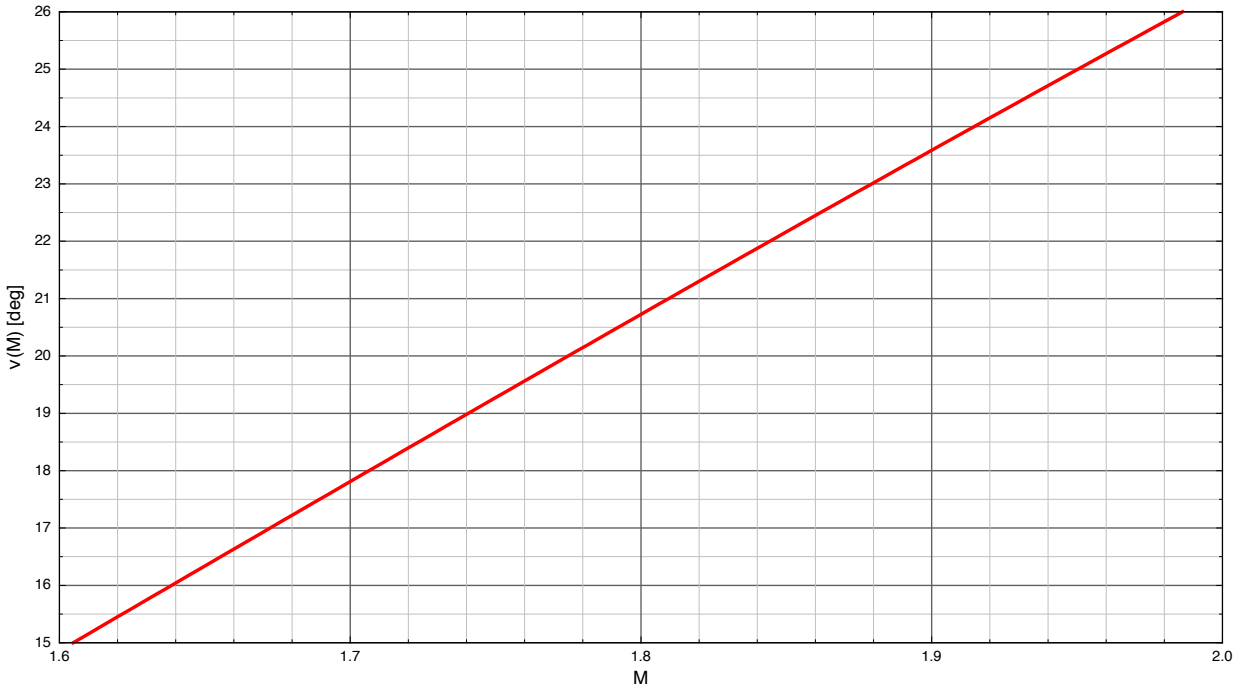
edXproblem: 5.6.4 Supersonic flow past a downward ramp

5.2 5.3

Consider a downward ramp (convex corner) with angle $\theta = 10°$ as shown in the Figure below. The incoming airflow is supersonic with $M_1 = 1.5$, $p_1 = 10^5\,\text{Pa}$, $T_1 = 298\,\text{K}$. Assume air behaves like an ideal gas with $\gamma = 1.4$ and $R = 287\,\text{J/kg}\cdot\text{K}$.



1) Determine the conditions past the expansion fan. Use the Prandtl-Meyer function to compute $\nu(M_1)$ exactly, but its zoomed-in plot below to get M_2 from $\nu(M_2)$.



Provide the Mach number with three digits of precision (of the form X.YZeP): $M_2 =$

Provide the pressure (in Pascals) with three digits of precision (of the form X.YZeP): $p_2 =$

Provide the temperature with three digits of precision (of the form X.YZeP): $T_2 =$

Provide the density with two digits of precision (of the form X.YeP): $\rho_2 =$

2) What is the total pressure loss $1 - p_{0_2}/p_{0_1}$? Provide your answer with two digits of precision (of the form X.YeP).

edXsolution

Video Link

5.7 Sample problems

edXproblem: 5.7.1 Supersonic engine inlets

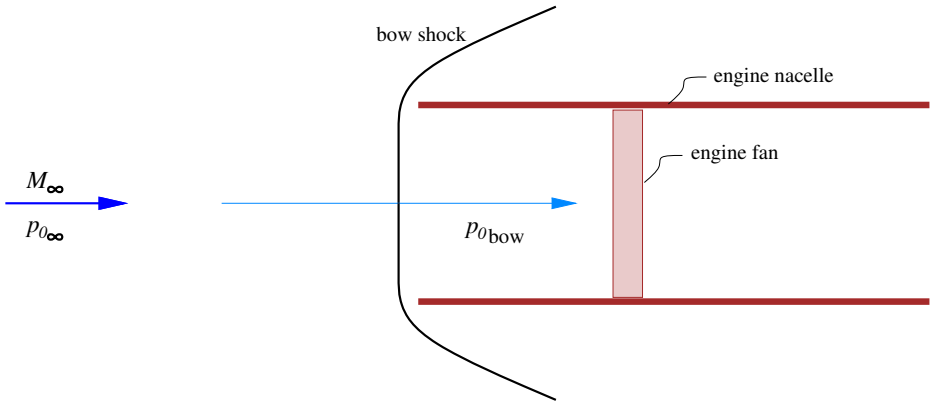
5.3

A key measure of a supersonic engine inlet is the total pressure of the air that it delivers to the engine, typically measured as the "inlet efficiency" $p_{0_{\text{inlet}}}/p_{0_\infty}$. The higher this inlet efficiency, the greater the engine thrust and fuel economy.

In this problem we will compare the efficiency of a simple bow-shock engine inlet with a more sophisticated oblique-shock inlet such as the one found on the Concorde. Both of these are illustrated in the figures below.

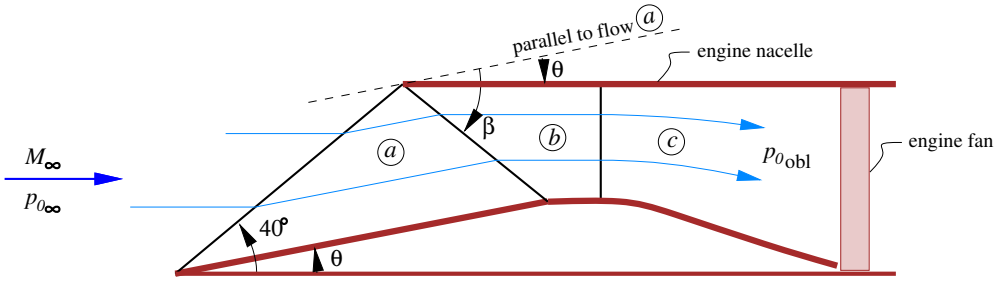
We will assume a flight Mach number of $M_\infty = 2.0$ for both cases, typical of a Concorde in cruise, and only pressure ratios will be considered. Further assume air behaves like an ideal gas with $\gamma = 1.4$ and $R = 287\,\text{J/kg}\cdot\text{K}$.

Simple bow shock inlet

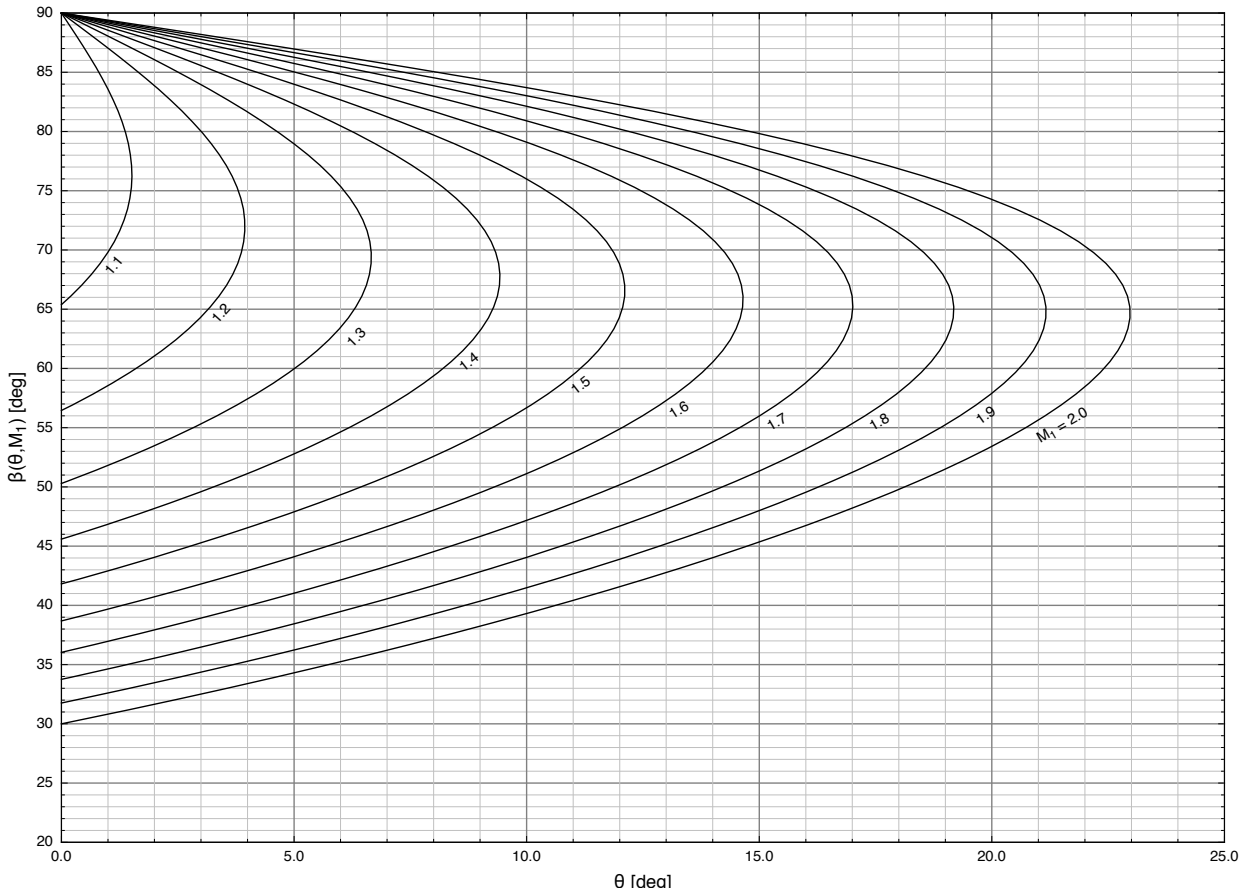


1) For the simple bow shock inlet shown above, determine the total pressure recovery $p_{0_{\text{bow}}}/p_{0_\infty}$ of the air going into the engine. Assume the shock is normal to the freestream and provide your answer with two digits of precision (of the form X.YeP).

Oblique-shock inlet



2) The oblique-shock inlet shown above must have the front oblique shock angled at 40° so that it intersects the tip of the top nacelle wall. Determine the necessary wedge angle θ, and also M_{a} and $p_{0_{\text{a}}}/p_{0_\infty}$ behind the front shock.



Use the $\beta(\theta, M_1)$ chart above, and provide your answer for θ (in degrees) with three digits of precision (of the form X.YZeP). : $\theta =$

Provide the Mach number with two digits of precision (of the form X.YeP): $M_{\rm a} =$

Provide the pressure ratio with two digits of precision (of the form X.YeP): $p_{0_{\rm a}}/p_{0_\infty} =$

3) The second oblique shock is also the result of a simple wedge flow, but which is "upside down" and tilted by the wedge angle θ found previously. Determine the angle β of the second shock. Also determine $M_{\rm b}$ and $p_{0_{\rm b}}/p_{0_\infty}$.

Use again the $\beta(\theta, M_1)$ chart above and provide the wave angle (in degrees) with three digits of precision (of the form X.YZeP): $\beta =$

Provide the Mach number with two digits of precision (of the form X.YeP): $M_{\rm b} =$

Provide the pressure ratio with two digits of precision (of the form X.YeP): $p_{0_{\rm b}}/p_{0_\infty} =$

4) The third shock is a simple normal shock. Determine $M_{\rm c}$ and the total pressure ratio $p_{0_{\rm obl}}/p_{0_\infty} = p_{0_{\rm c}}/p_{0_\infty}$ going into the fan.

Provide the Mach number with two digits of precision (of the form X.YeP): $M_{\rm c} =$

Provide the pressure ratio with two digits of precision (of the form X.YeP): $p_{0_{\text{obl}}}/p_{0_\infty} = p_{0_\text{c}}/p_{0_\infty} =$

Comparison

5) Compare the efficiencies of the bow-shock and oblique-shock inlets, specifically:

- Which of the two inlets is more efficient?

- What is the ratio $p_{0_{\text{bow}}}/p_{0_{\text{obl}}}$ Provide your answer with two digits of precision (of the form X.YeP)?

edXsolution

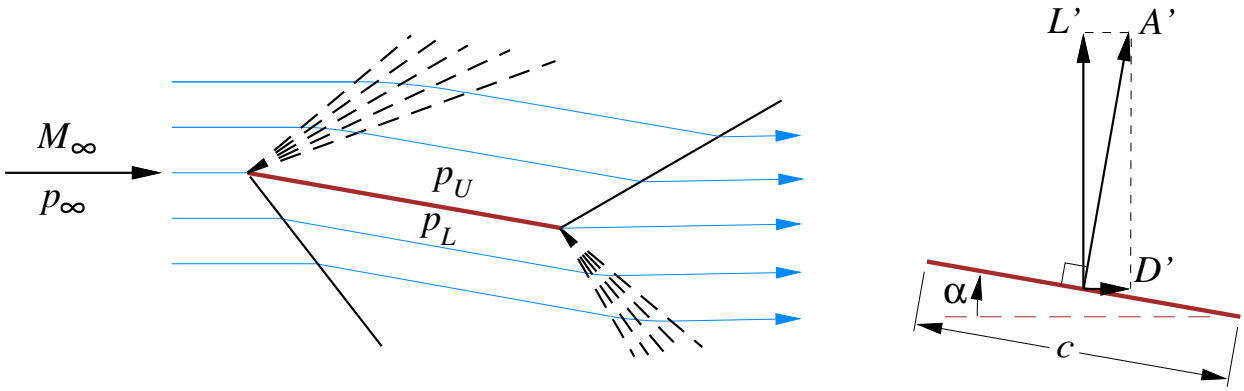
Video Link

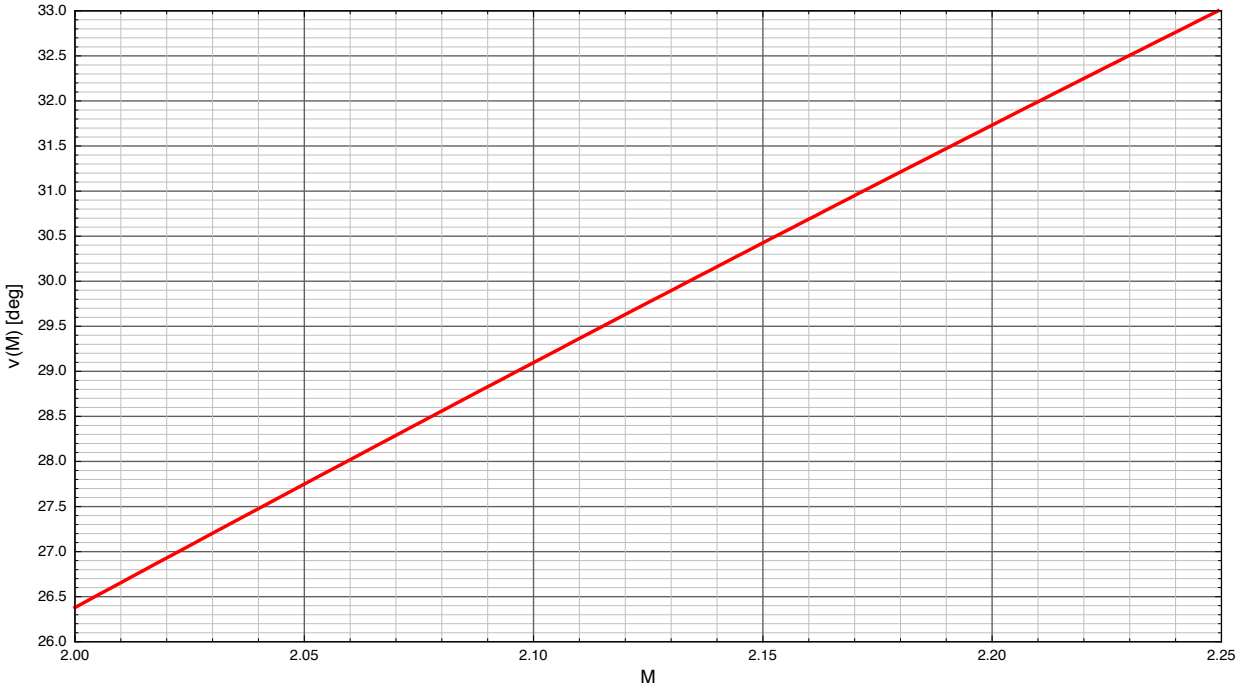
edXproblem: 5.7.2 Flat plate in supersonic flow

5.3 | 5.5

Consider a flat plate placed at an angle of attack of $\alpha = 5°$ in a flow at $M_\infty = 2$ as illustrated below.

Use the $\beta(\theta, M)$ and $\nu(M)$ charts below, and give your answers for Mach number and pressure ratios with three digits of precision (of the form X.YZeP).



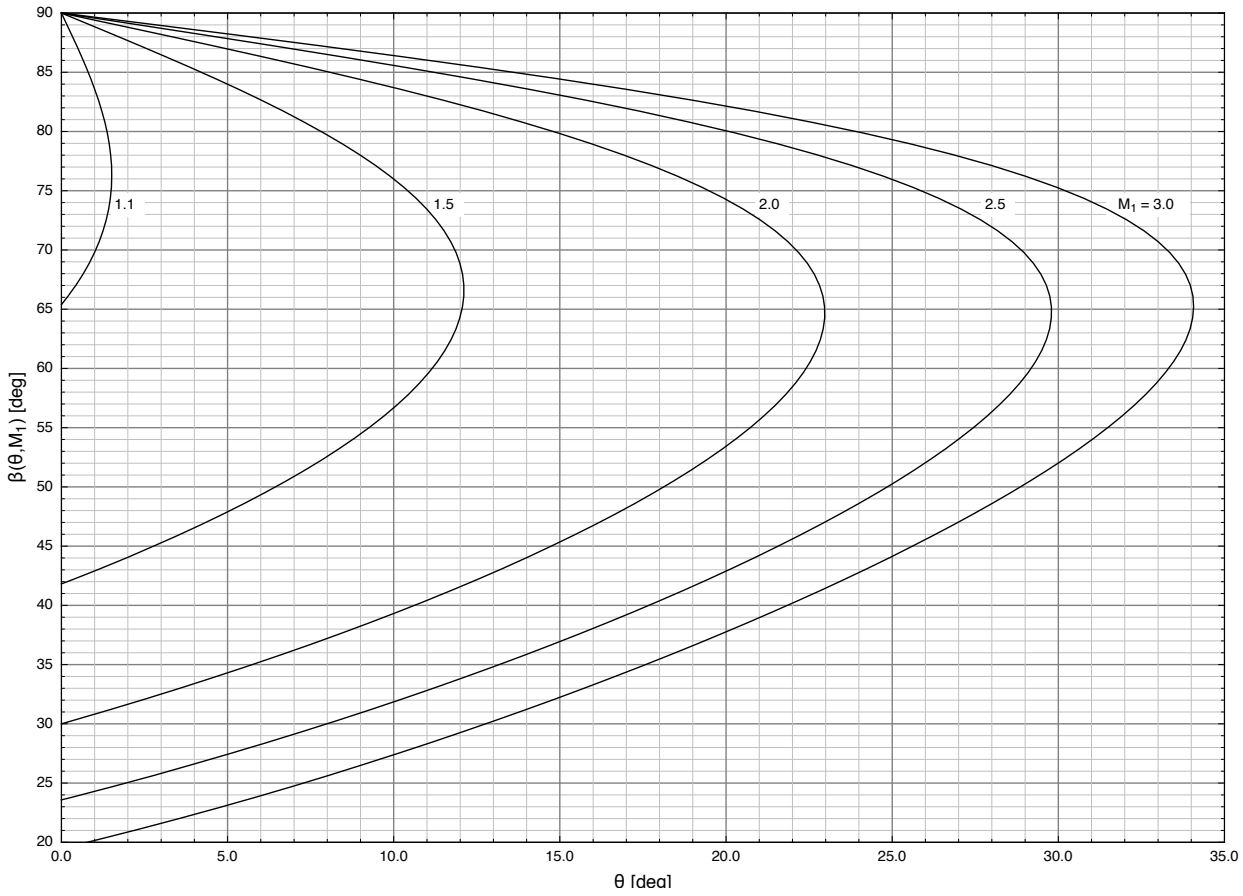


1) Determine the Mach number and ratio of freestream to static pressures on the upper surface.

$M_U =$

$p_U/p_\infty =$

2) Determine the Mach number and ratio of freestream to static pressures on the lower surface. Use the $\beta(\theta, M)$ chart below.



$M_L =$

$p_L/p_\infty =$

3) Determine the lift and drag coefficients of this plate. Hint: $\rho\, V^2 \;=\; \gamma\, p\, M^2$.
Provide the lift coefficient with two digits of precision (of the form X.YeP): $c_\ell =$

Round the drag coefficient to within 10 drag counts (and report your answer in counts): $c_d =$

edXsolution

Video Link

Module 6

Differential Forms of Compressible Flow Equations

6.1 Overview

6.1.1 Measurable outcomes

Control volume analysis is particularly well suited to relating fluid properties at the boundary of a system to important engineering quantities such as the forces generated by a body, the power required by a jet engine, etc. However, additional details can often be determined by considering the behavior of the flow more locally, i.e. at points in the flow as opposed to over an entire region. This local view leads to considering an infinitesimal control volume and deriving governing equations in a differential form that apply at all points in the flow. In this module, our goal is to introduce the fundamentals of this differential view.

Specifically, students successfully completing this module will be able to:

6.1. Explain the motion and deformation of a fluid element using kinematics including the concepts of shear strain, normal strain, vorticity, divergence, and substantial derivative.

6.2. Derive the differential form of the governing equations of a compressible, viscous flow from the integral forms of these equations.

6.3. Relate the terms of the differential form of the governing equations to physical effects considered in the conservation laws by applying the integral form to an infinitesimal fluid element.

6.4. Apply the differential form of the governing equations to describe and quantify the motion, forces acting on, work applied to, and heat addition to a fluid element.

6.1.2 Pre-requisite material

The material in this module requires vector calculus and all of the measurable outcomes from the Conservation of Mass, Momentum, and Energy modules (see Sections 3.1.1 and 4.1.1).

6.2 Kinematics of a Fluid Element

6.2.1 Kinematics of a fluid element

6.1

Prior to deriving the differential form of the conservation equations, we will look at the motion of a fluid element, which is nothing more than an infinitesimal volume of the fluid. As opposed to our previous control volume analysis which was a fixed volume in space, a fluid element is fixed to the fluid (i.e. the fluid element is always the same fluid, though it moves, distorts its shape, varies in its properties, etc). Figure 6.1 shows a fluid element that at $t = 0$ has a square shape and a short time later at $t = \Delta t$ has moved and deformed. The motion of the fluid element, i.e. the kinematics

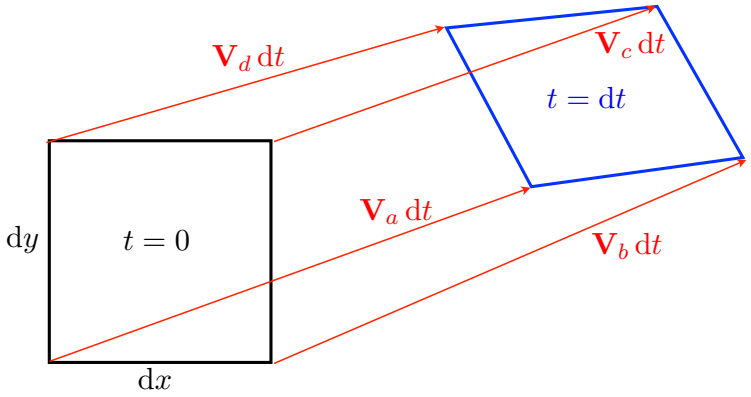


Figure 6.1: Motion of a fluid element from $t = 0$ to an infinitesimal time later $t = \Delta t$.

of the fluid element, over this infinitesimal time can be broken into four distinct types of motion:

Convection: the motion of the center of mass of the fluid element.

Rotation: the angular motion of the fluid element about its center of mass.

Normal strain: the compression or elongation of the fluid element without changing its angles.

Shear strain: skewing the fluid element such that its angles change without compressing or elongating the element.

These different types of motion are shown in Figure 6.2.



(a) Convection (b) Rotation (c) Normal strain (d) Shear strain

Figure 6.2: Four types of pure motion of a fluid element.

Next, we relate the different types of motions to the velocity field. The simplest motion is the convection of the fluid element and is given directly by the velocity, $\mathbf{V}$. We can think of this as the motion of the center of mass of the fluid element. The remaining types of fluid element motion describe the rotation and distortion of the shape of the fluid element.

6.2.2 Rotation and vorticity

6.1

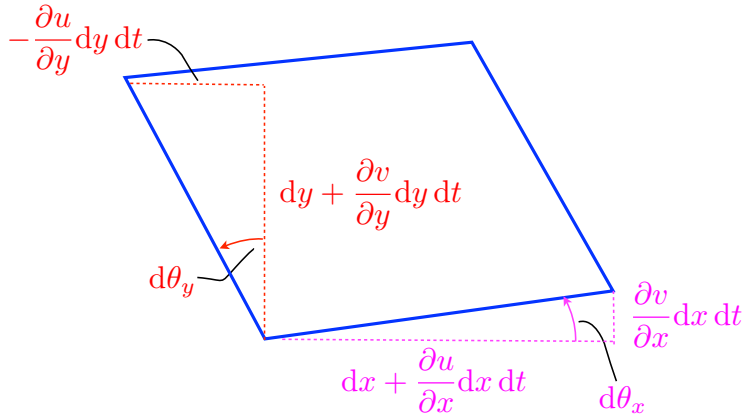


Figure 6.3: Detailed diagram of the fluid element at $t = \Delta t$.

Consider now the rotation of the fluid element shown in Figure 6.3. We define the rotation rate about the z-axis as the average rate of change of the angles θ_x and θ_y,

$$\Omega_z \equiv \frac{1}{2}\left(\frac{\mathrm{d}\theta_x}{\mathrm{d}t} + \frac{\mathrm{d}\theta_y}{\mathrm{d}t}\right) \tag{6.1}$$

From the figure, we can relate $\mathrm{d}\theta_x$ to the velocity field,

$$\tan \mathrm{d}\theta_x = \frac{\frac{\partial v}{\partial x}\mathrm{d}x\,\mathrm{d}t}{\mathrm{d}x + \frac{\partial u}{\partial x}\mathrm{d}x\,\mathrm{d}t} \tag{6.2}$$

$$\mathrm{d}\theta_x = \frac{\partial v}{\partial x}\mathrm{d}t \tag{6.3}$$

where the final result uses the small angle approximation for $\tan \mathrm{d}\theta_x$ and neglects $\partial u/\partial x\,\mathrm{d}x\,\mathrm{d}t$ (which is quadratic with respect to infinitesimal parameters) since it will be small compared to $\mathrm{d}x$ (which is only linear). Thus, we have

$$\frac{\mathrm{d}\theta_x}{\mathrm{d}t} = \frac{\partial v}{\partial x} \tag{6.4}$$

Similarly, the time rate of change of θ_y is,

$$\frac{\mathrm{d}\theta_y}{\mathrm{d}t} = -\frac{\partial u}{\partial y} \tag{6.5}$$

Combining these results gives,

$$\Omega_z = \frac{1}{2}\left(\frac{\partial v}{\partial x} - \frac{\partial u}{\partial y}\right) \tag{6.6}$$

And, similarly, for rotation about the x and y axes,

$$\Omega_x = \frac{1}{2}\left(\frac{\partial w}{\partial y} - \frac{\partial v}{\partial z}\right) \qquad \Omega_y = \frac{1}{2}\left(\frac{\partial u}{\partial z} - \frac{\partial w}{\partial x}\right) \tag{6.7}$$

Mathematically, the rotation rate vector can be seen to be half the curl of the velocity vector,

$$\boldsymbol{\Omega} = \frac{1}{2}\nabla \times \mathbf{V} \tag{6.8}$$

However, in fluid dynamics, it is more common to work with the curl of the velocity vector rather than the rotation rate vector. The curl of the velocity vector is known as the vorticity vector, ω,

$$\omega \equiv \nabla \times \mathbf{V} \tag{6.9}$$

As we will discuss in detail later, many problems of interest in aeronautics have zero vorticity through a significant portion of the flow. This leads to the concept of an *irrotational flow*:

An irrotational flow is one in which the vorticity is zero everywhere.

Otherwise, the flow is known as rotational.

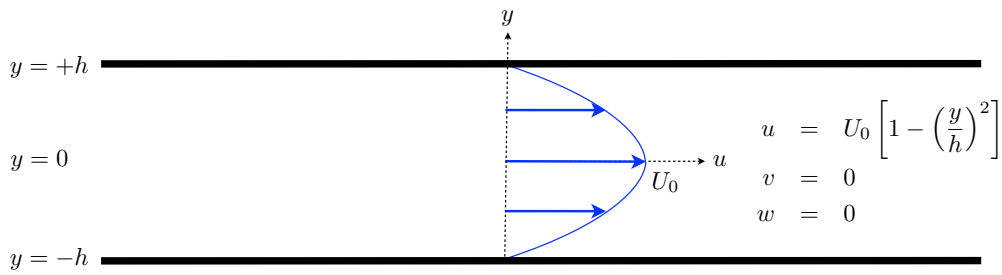
Please watch the following video from the NSF Fluid Mechanics Series. It provides helpful discussion and includes experimental demonstrations of the concept of vorticity.

Video Link

edXproblem: 6.2.3 Rotationality in duct flow

6.1

The low speed flow through a long duct has the velocity field shown below:



Select all of the statements which are true about the rotation of fluid elements:

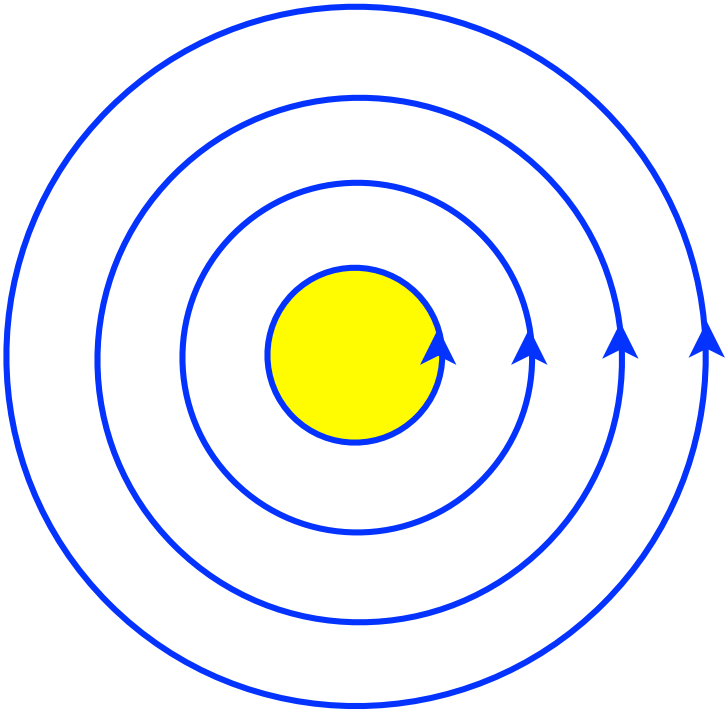
edXsolution

Video Link

edXproblem: 6.2.4 Rotationality for circular streamlines

6.1

Consider the flow about a cylinder having the streamlines given below:



Which is true?

edXsolution

Video Link

6.2.5 Normal strain

6.1

The normal strain rate in a direction is defined as the fractional rate of change of the length of the element face in that direction. For example, the normal strain rate for the face originally along the x-direction is,

$$\epsilon_{xx} \equiv \frac{1}{l_x}\frac{\mathrm{d}l_x}{\mathrm{d}t} \tag{6.10}$$

where l_x is the length of the face. At $t = 0$, $l_x = \mathrm{d}x$. Then, at time $t = \mathrm{d}t$,

$$l_x + \mathrm{d}l_x = \mathrm{d}x + \frac{\partial u}{\partial x}\mathrm{d}x\,\mathrm{d}t \tag{6.11}$$

$$\Rightarrow \mathrm{d}l_x = \frac{\partial u}{\partial x}\mathrm{d}x\,\mathrm{d}t \tag{6.12}$$

$$\tag{6.13}$$

Thus, the normal strain rate in x is,

$$\epsilon_{xx} = \frac{\partial u}{\partial x} \tag{6.14}$$

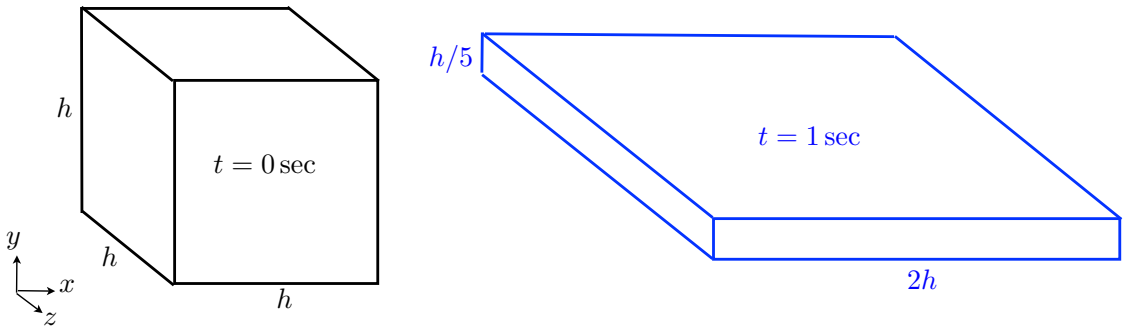
And, similarly, the normal strain rate in y and z is,

$$\epsilon_{yy} = \frac{\partial v}{\partial y} \qquad \epsilon_{zz} = \frac{\partial w}{\partial z} \tag{6.15}$$

edXproblem: 6.2.6 Calculate normal strain

6.1

Consider a fluid element that has an initial cubic shape with length h in the x, y, and z directions. For one second, the element undergoes a constant normal strain rate (constant over time, though not necessarily the same in each direction) such that its length in x is $2h$ and its length in y is $h/5$ as shown in the figure.



What is ϵ_{xx} (in units of sec^{-1})? Please provide your answer with three digits of precision in the form X.YZeP.

What is ϵ_{yy} (in units of sec^{-1})? Please provide your answer with three digits of precision in the form X.YZeP.

What is ϵ_{zz} (in units of sec^{-1}) such that the volume of the fluid element does not change? Please provide your answer with three digits of precision in the form X.YZeP.

edXsolution

Video Link

6.2.7 Shear strain and strain rate tensor

6.1

The shear strain rate for the fluid element shown in Figure 6.3 is defined as the average rate at which the angle between the x and y faces decreases,

$$\epsilon_{xy} \equiv \frac{1}{2}\left(\frac{\mathrm{d}\theta_x}{\mathrm{d}t} - \frac{\mathrm{d}\theta_y}{\mathrm{d}t}\right) \tag{6.16}$$

Then, using Equations (6.4) and (6.5) gives,

$$\epsilon_{xy} = \frac{1}{2}\left(\frac{\partial v}{\partial x} + \frac{\partial u}{\partial y}\right) \tag{6.17}$$

And, similarly,

$$\epsilon_{yz} = \frac{1}{2}\left(\frac{\partial w}{\partial y} + \frac{\partial v}{\partial z}\right) \qquad \epsilon_{xz} = \frac{1}{2}\left(\frac{\partial w}{\partial x} + \frac{\partial u}{\partial z}\right) \tag{6.18}$$

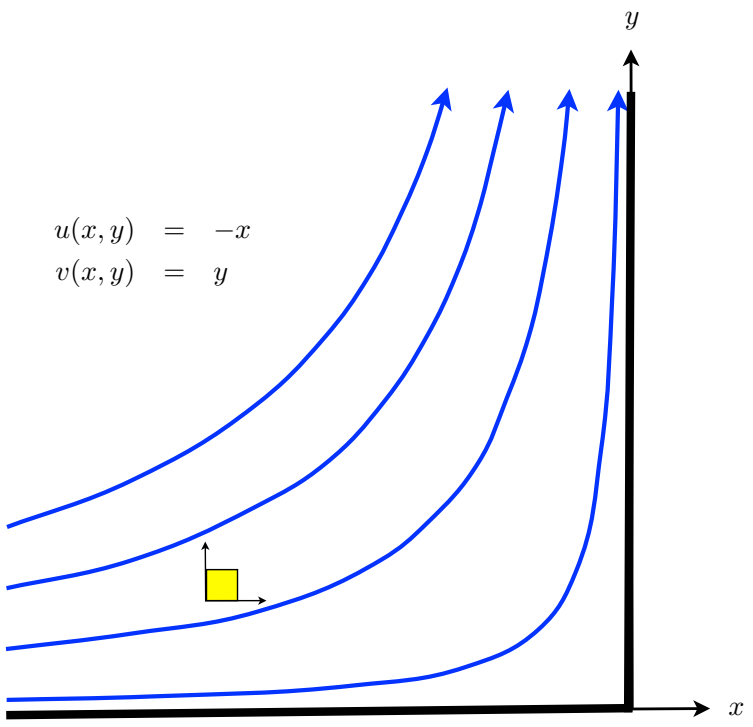
The normal strain rates and the shear strain rates can be combined into a single simple notation,

$$\epsilon_{ij} = \frac{1}{2}\left(\frac{\partial u_i}{\partial x_j} + \frac{\partial u_j}{\partial x_i}\right) \tag{6.19}$$

This notation is often referred to as the strain rate tensor where ϵ_{ij} can be thought of as a matrix of the various strain rates. In particular, the matrix is symmetric as, following from the definition, $\epsilon_{ij} = \epsilon_{ji}$.

edXproblem: 6.2.8 Strain rate for a fluid element in corner flow

6.1



Streamlines for the flow around a 90° corner are shown in the figure above. The velocity field is given by

$$u(x,y) = -x \tag{6.20}$$
$$v(x,y) = y \tag{6.21}$$

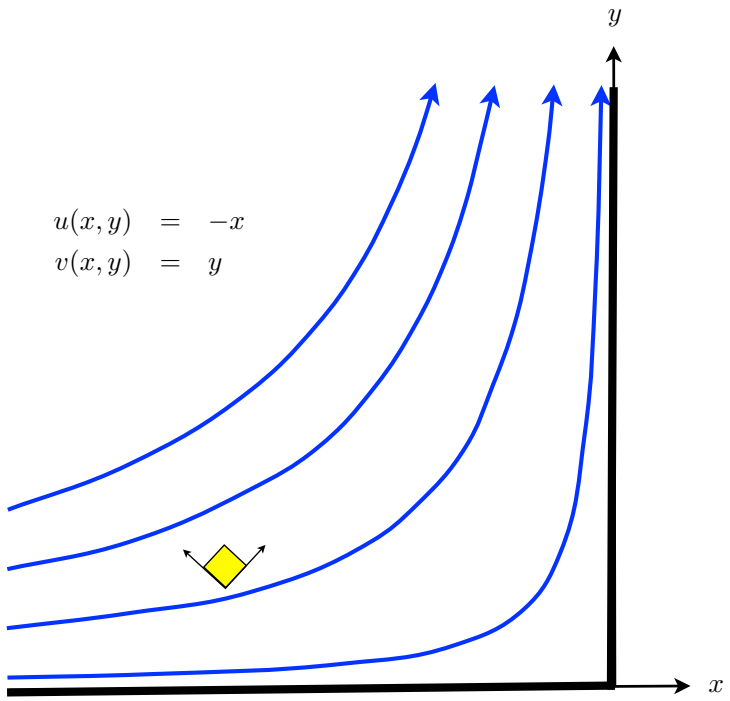
Consider the infinitesimal element shown in the figure. Which of the following answers best describes the deformation and rotation of this fluid element:

edXsolution

Video Link

edXproblem: 6.2.9 Strain rate for another fluid element in corner flow

6.1



Once again, consider the same flow around a 90° corner as in Problem 6.2.8. Recall the velocity field is given by

$$u(x,y) = -x \tag{6.22}$$
$$v(x,y) = y \tag{6.23}$$

Consider the infinitesimal element shown in the figure. The position of this element is oriented at 45° to the x-axis. Which of the following answers best describes the deformation and rotation of this fluid element:

edXsolution

Video Link

6.2.10 Divergence

6.1 6.3

Before we leave this section on kinematics, we will consider one last quantity that relates to the change in shape of a fluid element. Specifically, the divergence of the velocity field, which is written as,

$$\text{divergence of } \mathbf{V} \equiv \nabla \cdot \mathbf{V} = \frac{\partial u_i}{\partial x_i} = \epsilon_{ii} \tag{6.24}$$

In the last two equalities, we have introduced Einstein's index notation which by convention performs a sum over any repeated index. Thus,

$$\frac{\partial u_i}{\partial x_i} = \frac{\partial u_1}{\partial x_1} + \frac{\partial u_2}{\partial x_2} + \frac{\partial u_3}{\partial x_3} \quad \text{and} \quad \epsilon_{ii} = \epsilon_{11} + \epsilon_{22} + \epsilon_{33} \tag{6.25}$$

Further, we will usually associate (x_1, x_2, x_3) with (x, y, z). So, these expressions are also equivalent to,

$$\frac{\partial u_i}{\partial x_i} = \frac{\partial u}{\partial x} + \frac{\partial v}{\partial y} + \frac{\partial w}{\partial z} \quad \text{and} \quad \epsilon_{ii} = \epsilon_{xx} + \epsilon_{yy} + \epsilon_{zz} \tag{6.26}$$

We will now show that the divergence of the velocity field is equal to the fractional rate of change of the volume of a fluid element. Mathematically, this means,

$$\lim_{\delta\mathcal{V}\to 0} \frac{1}{\delta\mathcal{V}} \frac{\mathrm{d}}{\mathrm{d}t} (\delta\mathcal{V}) = \nabla \cdot \mathbf{V} \tag{6.27}$$

where $\delta\mathcal{V}$ is the volume of the (infinitesimal) fluid element.

The proof begins by considering an arbitrary Lagrangian control volume of fluid as shown in Figure 6.4 and calculating its rate of volume change. The analysis is identical to the calculation of

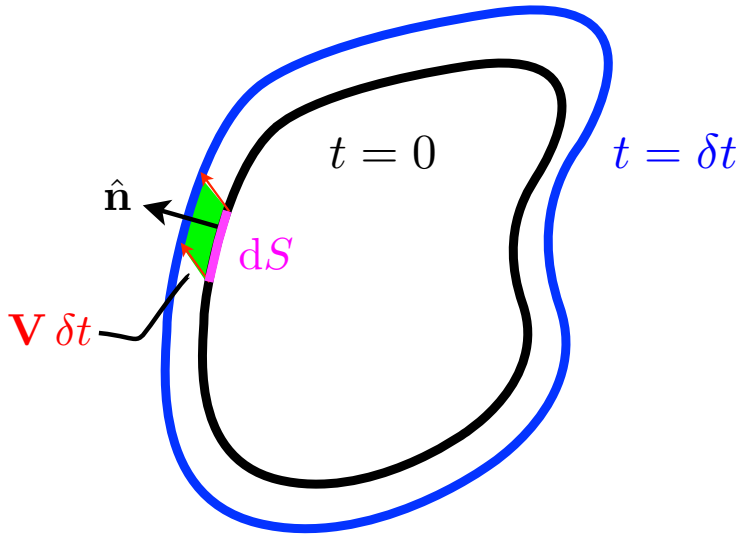


Figure 6.4: Calculating the time rate of change of the volume of a fluid from $t = 0$ to $t = \delta t$. The infinitesimal surface area $\mathrm{d}S$ moves a distance $\mathbf{V}\delta t$ which sweeps out a volume $\mathbf{V} \cdot \hat{\mathbf{n}}\,\mathrm{d}S\,\delta t$.

the volume swept by a fluid moving through a fixed Eulerian control volume, as was described in Section 3.4.2. In the present case of a Lagrangian control volume, the swept volume is the change in volume of the material as it moves. Using Equation (3.20) and integrating around the entire surface, the change in the volume of this fluid is,

$$\mathcal{V}(\delta t) - \mathcal{V}(0) = \delta t \iint_S \mathbf{V} \cdot \hat{\mathbf{n}}\,\mathrm{d}S \tag{6.28}$$

Now, dividing this by δt and taking the limit as $\delta t \to 0$ produces,

$$\frac{\mathrm{d}\mathcal{V}}{\mathrm{d}t} = \iint_S \mathbf{V} \cdot \hat{\mathbf{n}} \, \mathrm{d}S \tag{6.29}$$

Then, we can use the divergence theorem (also called Gauss's theorem) which states that for any continuously differentiable vector field $\mathbf{F}(\mathbf{x})$,

$$\iint_S \mathbf{F} \cdot \hat{\mathbf{n}} \, \mathrm{d}S = \iiint_{\mathcal{V}} \nabla \cdot \mathbf{F} \, \mathrm{d}\mathcal{V}. \tag{6.30}$$

So, in our case, $\mathbf{F} = \mathbf{V}$ giving,

$$\frac{\mathrm{d}\mathcal{V}}{\mathrm{d}t} = \iiint_{\mathcal{V}} \nabla \cdot \mathbf{V} \, \mathrm{d}\mathcal{V} \tag{6.31}$$

Now, applying this result to an infinitesimal fluid element with initial volume $\delta\mathcal{V}$ gives,

$$\lim_{\delta\mathcal{V}\to 0} \frac{1}{\delta\mathcal{V}} \frac{\mathrm{d}}{\mathrm{d}t}(\delta\mathcal{V}) = \lim_{\delta\mathcal{V}\to 0} \frac{1}{\delta\mathcal{V}} \iiint_{\delta\mathcal{V}} \nabla \cdot \mathbf{V} \, \mathrm{d}\mathcal{V} = \nabla \cdot \mathbf{V} \tag{6.32}$$

6.3 Differential Forms of Governing Equations

6.3.1 Conservation of mass (the continuity equation)

6.2 6.3

In this section, we will derive a differential form of the conservation of mass, momentum, and energy equations for a compressible flow.

We will start with the conservation of mass for a fixed, finite control volume as derived in Section 3.4.3. Specifically, recall the conservation of mass as given in Equation (3.26),

$$\iiint_{\mathcal{V}} \frac{\partial \rho}{\partial t} \, \mathrm{d}\mathcal{V} + \iint_{S} \rho \, \mathbf{V} \cdot \hat{\mathbf{n}} \, \mathrm{d}S = 0. \tag{6.33}$$

Then applying the divergence theorem (Equation 6.30) with $\mathbf{F} = \rho \mathbf{V}$, gives

$$\iint_{S} \rho \mathbf{V} \cdot \hat{\mathbf{n}} \, \mathrm{d}S = \iiint_{\mathcal{V}} \nabla \cdot (\rho \mathbf{V}) \, \mathrm{d}\mathcal{V} \tag{6.34}$$

Substituting Equation (6.34) into the conservation of mass gives,

$$\iiint_{\mathcal{V}} \left[\frac{\partial \rho}{\partial t} + \nabla \cdot (\rho \mathbf{V}) \right] \mathrm{d}\mathcal{V} \;\; = \;\; 0 \tag{6.35}$$

Since this equation (i.e. the integral form of conversation of mass) is true for any volume we choose, it follows that the integrand must be zero everywhere. Otherwise, if the integrand were non-zero in some region, we could choose a control volume surrounding this region and the integral would be non-zero (contradicting the requirement that it is zero). Thus, the conservation of mass in the form of a partial differential equation is,

$$\frac{\partial \rho}{\partial t} + \nabla \cdot (\rho \mathbf{V}) = 0 \tag{6.36}$$

or, equivalently using index notation,

$$\frac{\partial \rho}{\partial t} + \frac{\partial}{\partial x_i} (\rho u_i) = 0 \tag{6.37}$$

In the case when the flow is assumed to have constant density, then the conservation of mass reduces to,

$$\nabla \cdot \mathbf{V} = 0 \tag{6.38}$$

or, equivalently using index notation,

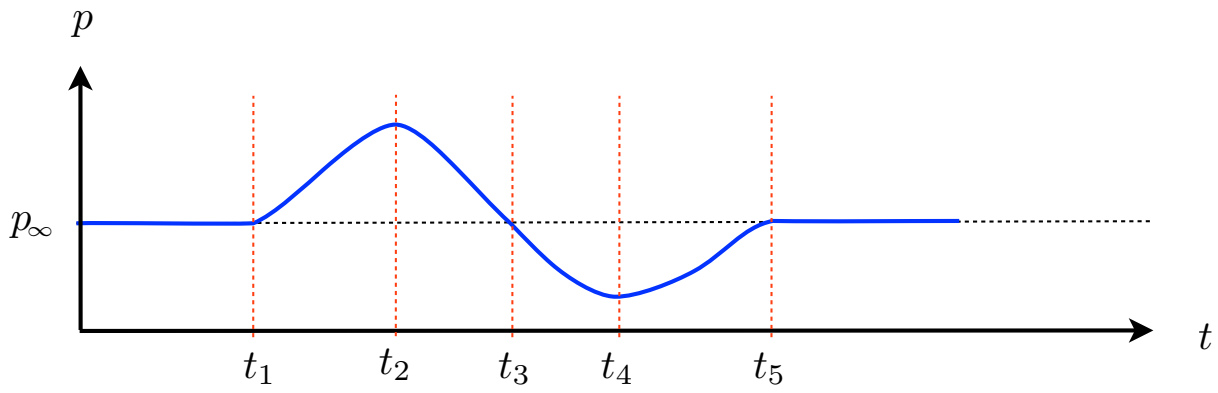
$$\frac{\partial u_i}{\partial x_i} = 0 \tag{6.39}$$

Since $\nabla \cdot \mathbf{V}$ is the fractional rate of change of the volume of a fluid element (as shown in Section 6.2.10), we can interpret the incompressible form of the conservation of mass as requiring that the volume of a fluid element remains constant. This must be true since the mass of a fluid element cannot change, and therefore if the fluid element's density is constant, then its volume must also be constant.

Note that the differential forms of the conservation of mass equation are often referred to as the continuity equation, and we will use the terms interchangeably throughout the course.

In the following video, we look at this result more closely, in particular showing how $\nabla \cdot (\rho \mathbf{V})$ can be interpreted as the flow of mass per unit volume out of an infinitesimal control volume.

Video Link



edXproblem: 6.3.2 Acoustic measurements

6.4 | 4.5 | 4.7

A sensor is being used to measure the time variation of pressure due to sound generation. Without sound generation, the pressure is p_∞. The figure shows the measured pressure variation. The variation in pressure due to the sound is small and can be assumed to be isentropic.

Identify the time ranges during which $\nabla \cdot (\rho \mathbf{V}) < 0$ at the sensor.

edXsolution

Video Link

6.3.3 Conservation of momentum

6.2 6.3

Next, we will derive the differential form of the conservation of momentum equation. Recall from Equation (3.49) that the integral form of conservation of the j-component of momentum is,

$$\iiint_{\mathcal{V}} \frac{\partial}{\partial t}\left(\rho u_j\right)\,\mathrm{d}\mathcal{V} + \iint_S \rho u_j\,\mathbf{V}\cdot\hat{\mathbf{n}}\,\mathrm{d}S = -\iint_S p\,\hat{n}_j\,\mathrm{d}S + \iint_S \tau_j\,\mathrm{d}S. \tag{6.40}$$

External forces have not been included because we are developing equations governing only the fluid. Thus, our control volumes now only contain fluid and no other materials. Following the same approach as for conservation of mass, the left-hand side can be written,

$$\iiint_{\mathcal{V}} \left[\frac{\partial}{\partial t}\left(\rho u_j\right) + \nabla\cdot\left(\rho u_j\mathbf{V}\right)\right]\,\mathrm{d}\mathcal{V} \;=\; -\iint_S p\,\hat{n}_j\;\mathrm{d}S \;+\; \iint_S \tau_j\;\mathrm{d}S \tag{6.41}$$

The pressure surface integral can be written as a volume integral using the divergence theorem, i.e. Equation (6.30), in which $\mathbf{F} = p\hat{\mathbf{e}}_j$, giving,

$$\iint_S p\,\hat{n}_j\;\mathrm{d}S = \iiint_{\mathcal{V}} \frac{\partial p}{\partial x_j}\,\mathrm{d}\mathcal{V} \tag{6.42}$$

We will discuss the viscous stress term in more detail later. For now, we will assume that at any point in the control volume, the net viscous force in the j-direction per unit volume is f_j^τ and satisfies,

$$\iint_S \tau_j\;\mathrm{d}S = \iiint_{\mathcal{V}} f_j^\tau\,\mathrm{d}\mathcal{V} \tag{6.43}$$

Combining Equations (6.41), (6.42), and (6.43) leads to the differential form of the conservation of the $\mathbf{e}_j$-momentum,

$$\frac{\partial}{\partial t}\left(\rho u_j\right) + \nabla\cdot\left(\rho u_j\mathbf{V}\right) = -\frac{\partial p}{\partial x_j} + f_j^\tau \tag{6.44}$$

Or, using index notation, this can be written,

$$\frac{\partial}{\partial t}\left(\rho u_j\right) + \frac{\partial}{\partial x_i}\left(\rho u_j u_i\right) = -\frac{\partial p}{\partial x_j} + f_j^\tau \tag{6.45}$$

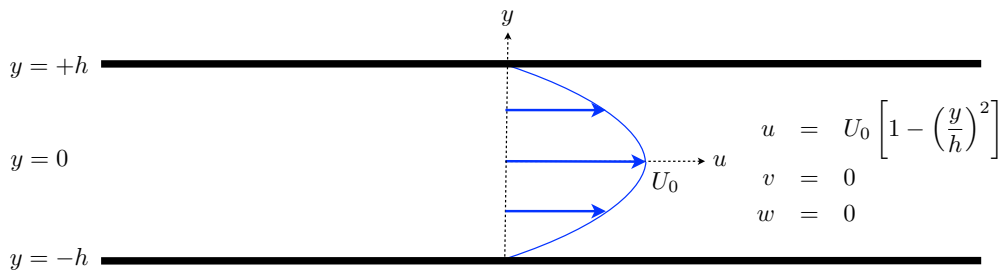
In the following video, we look at the pressure gradient term $-\nabla p$ and show how it is the force per unit volume due to pressure acting on infinitesimal control volume.

Video Link

edXproblem: 6.3.4 Conservation of momentum in duct flow

6.4

The low speed flow through a long duct has the velocity field shown below: The pressure can



be shown to vary linearly with x with no dependence on y, i.e. the pressure field has the following form,

$$p(x) = C_0 + C_1 x \tag{6.46}$$

where C_0 and C_1 are non-zero constants. Because of the low speed, the density can assumed to be constant.

Consider the differential form of the conservation of momentum equation. Which of the following terms are non-zero?

edXsolution

Video Link

6.3.5 Conservation of energy

6.2

Finally, we will derive the differential form of the conservation of energy equation. Recall the integral form of conservation of energy is (neglecting the work due to gravity and external forces) from Equation (4.32) is,

$$\iiint_{\mathcal{V}} \frac{\partial}{\partial t}\left(\rho e_0\right)\,\mathrm{d}\mathcal{V} + \iint_S \rho e_0\,\mathbf{V}\cdot\hat{\mathbf{n}}\,\mathrm{d}S = -\iint_S p\,\hat{\mathbf{n}}\cdot\mathbf{V}\,\mathrm{d}S + \iint_S \boldsymbol{\tau}\cdot\mathbf{V}\,\mathrm{d}S - \iint_S \dot{\mathbf{q}}\cdot\hat{\mathbf{n}}\,\mathrm{d}S. \tag{6.47}$$

We will discuss the viscous work term in more detail later. For now, we will assume that at any point in the control volume, the net (rate of) work of the viscous stresses per unit volume is $\dot{w}^\tau$ and satisfies,

$$\iint_S \boldsymbol{\tau}\cdot\mathbf{V}\;\mathrm{d}S = \iiint_{\mathcal{V}} \dot{w}^\tau\;\mathrm{d}\mathcal{V} \tag{6.48}$$

Following the same derivation as for mass and momentum, we arrive at the differential form of the conservation of energy equation,

$$\frac{\partial}{\partial t}\left(\rho e_0\right) + \nabla\cdot\left(\rho e_0\mathbf{V}\right) = -\nabla\cdot\left(p\mathbf{V}\right) + \dot{w}^\tau - \nabla\cdot\dot{\mathbf{q}} \tag{6.49}$$

Or, using index notation, this can be written,

$$\frac{\partial}{\partial t}\left(\rho e_0\right) + \frac{\partial}{\partial x_i}\left(\rho e_0 u_i\right) = -\frac{\partial}{\partial x_i}\left(p u_i\right) + \dot{w}^\tau - \frac{\partial \dot{q}_i}{\partial x_i} \tag{6.50}$$

6.3.6 Substantial derivative

6.1

The so-called convective form of the differential equations can be derived by manipulating the left-hand side terms. Starting with the left-hand side from the conservation of mass,

$$\frac{\partial \rho}{\partial t} + \frac{\partial}{\partial x_i}\left(\rho u_i\right) = \frac{\partial \rho}{\partial t} + u_i\frac{\partial \rho}{\partial x_i} + \rho\frac{\partial u_i}{\partial x_i} \tag{6.51}$$

The first two terms of this relationship (i.e. $\partial\rho/\partial t + u_i\partial\rho/\partial x_i$) are the so-called *substantial*, *material*, *convective* or *total* derivative of the density. All of these terms are used interchangeably. The expression *substantial derivative* is used as these terms represent the time rate of change of a quantity (in this case density) following the substance, i.e. traveling along with the flow. To see this, consider a fluid element with its position as a function of time given by $\mathbf{X}(t)$. The time rate of change of the density of this fluid element is the combination of two terms,

$$\text{Time-rate-of-change of } \rho \text{ following a fluid element} = \frac{\partial \rho}{\partial t} + \frac{\partial \rho}{\partial x_i}\frac{\mathrm{d}X_i}{\mathrm{d}t} \tag{6.52}$$

Note that the time rate of change of the element's position is simply the velocity,

$$\frac{\mathrm{d}X_i}{\mathrm{d}t} = u_i(\mathbf{X}(t), t). \tag{6.53}$$

Thus, the time rate of change of ρ for moving with the fluid is, $\partial\rho/\partial t + u_i\partial\rho/\partial x_i$.

The first term, $\partial\rho/\partial t$, represents the time rate of change of the density at a fixed location in space (as opposed to following along with a fluid). It is the time rate of change we would observe if

we had a probe to measure the density, and we used that probe to measure density (as a function of time) at a fixed location in the flow.

The second term, $u_i \partial\rho/\partial x_i$, represents the time rate of change the density caused by the motion of the fluid element (with velocity components u_i) through a spatially-varying density field (with density variations $\partial\rho/\partial x_i$). Thus, even if the flow were steady (such that $\partial\rho/\partial t = 0$ everywhere), the density of a specific fluid element can vary if the element is moving through a region with spatial variations of density.

The concept of the substantial derivative is so important that it is given its own notation, specifically,

$$\frac{\mathrm{D}}{\mathrm{D}t}(\,) \equiv \frac{\partial}{\partial t}(\,) + u_i \frac{\partial}{\partial x_i}(\,) \tag{6.54}$$

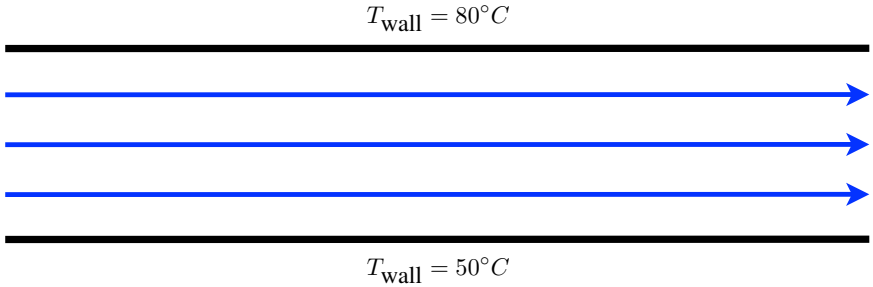
This can also be written using vector notation,

$$\frac{\mathrm{D}}{\mathrm{D}t}(\,) \equiv \frac{\partial}{\partial t}(\,) + \mathbf{V} \cdot \nabla(\,) \tag{6.55}$$

edXproblem: 6.3.7 Substantial derivative for channel flow

6.1

Consider the following flow path and temperatures: The image is a small portion of a much



longer channel (with the rest of the channel and flow conditions being the same as shown here). Further, assume that these flow paths occur after the temperatures on the walls have existed as shown for a long time.

Which of these is most likely true?

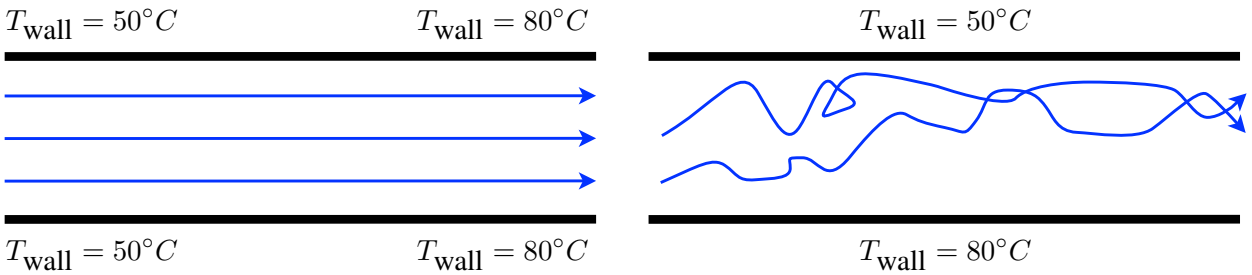
edXsolution

Video Link

edXproblem: 6.3.8 More on substantial derivative

6.1

Consider the following flow paths and temperatures:



(1) (2)

Assume that these flow paths occur after the temperatures on the walls have existed as shown for a long time.

Which of these is most likely true?

edXsolution

Video Link

edXproblem: 6.3.9 A last embedded question on substantial derivative

6.1

A fluid element is moving at a constant velocity of 10 m/sec in the x-direction. At one instant in time, the temperature of the fluid element is T =300 K. At a time 10 seconds later, the temperature of the fluid element is 330 K. Which of the following quantities can you estimate? For those that you can estimate, do so.

1) Can you estimate $\frac{\partial T}{\partial t}$? If yes, entire your estimate (in units of K/sec). If no, enter -999.

2) Can you estimate $\frac{\partial T}{\partial x}$? If yes, entire your estimate (in units of K/m). If no, enter -999.

3) Can you estimate $\frac{\mathrm{D}T}{\mathrm{D}t}$? If yes, entire your estimate (in units of K/sec). If no, enter -999.

edXsolution

Video Link

6.3.10 Convective forms of the governing equations

6.1 6.2 6.3

Using the substantial derivative, the *convective* form of the conservation of mass can be written,

$$\frac{\mathrm{D}\rho}{\mathrm{D}t} = -\rho\frac{\partial u_i}{\partial x_i} \tag{6.56}$$

Or, using vector notation,

$$\frac{\mathrm{D}\rho}{\mathrm{D}t} = -\rho\nabla\cdot\mathbf{V} \tag{6.57}$$

Next, the left-hand side of the conservation of momentum can be expanded as,

$$\frac{\partial}{\partial t}\left(\rho u_j\right) + \frac{\partial}{\partial x_i}\left(\rho u_j u_i\right) = u_j\left[\frac{\partial\rho}{\partial t} + \frac{\partial}{\partial x_i}\left(\rho u_i\right)\right] + \rho\frac{\mathrm{D}u_j}{\mathrm{D}t} = \rho\frac{\mathrm{D}u_j}{\mathrm{D}t}. \tag{6.58}$$

Note the square-bracketed term is zero from conservation of mass. Combining this with Equation (6.45) gives the convective form of the conservation of momentum,

$$\rho\frac{\mathrm{D}u_j}{\mathrm{D}t} = -\frac{\partial p}{\partial x_j} + f_j^{\tau} \tag{6.59}$$

A similar manipulation of the left-hand side of Equation (6.50) gives the convective form of the conservation of energy,

$$\rho\frac{\mathrm{D}e_0}{\mathrm{D}t} = -\frac{\partial}{\partial x_i}\left(pu_i\right) + \dot{w}^{\tau} - \frac{\partial\dot{q}_i}{\partial x_i} \tag{6.60}$$

In the following video, we provide an interpretation of these convective forms of the governing equations. The intent is to build your intuition for what the mathematics of the partial differential equations represents in terms of the motion of a fluid element.

Video Link

6.4 Sample Problems

edXproblem: 6.4.1 Power law

6.1

As you will see towards the end of this course, the velocity field near a stationary wall (i.e. boundary layer flow) can be assumed to only depend on the direction y normal to the wall, and approximated using a power law

$$u = C\,y^a \tag{6.61}$$
$$v = 0 \tag{6.62}$$

where $a = 1/7$ and C is a constant.

1) Derive an expression for the vorticity components.

2) Derive an expression for the rate of strain.

edXsolution

Video Link

edXproblem: 6.4.2 Circular flow: point (free) vortex

6.1

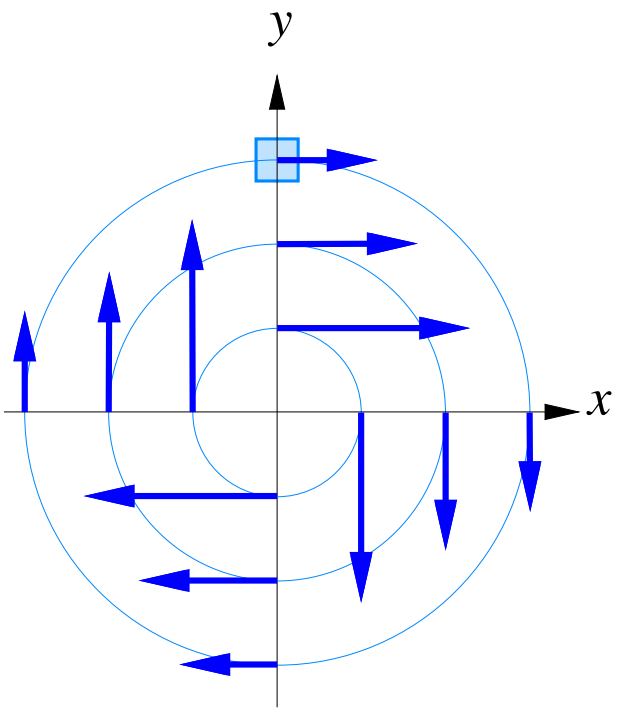
Consider the flow whose velocity field is given by

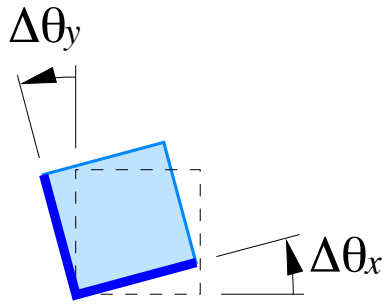
$$u = \frac{y}{x^2+y^2}\ , \tag{6.63}$$

$$v = \frac{-x}{x^2+y^2}\ . \tag{6.64}$$

This is known as a point (or free) vortex, and its streamlines are circles centered at the origin.

As shown in the figure, a small square fluid element is placed at the point $(x, y) = (0, 1)$ at $t = 0$: it moves and distorts with the fluid. Assume that the flow is incompressible.





1) Determine the angles of the two sides $\Delta\theta_x$ and $\Delta\theta_y$ at some small later time $t = \Delta t$, and sketch the shape of the fluid element at that later time.

2) Compute the flow's vorticity field. Is the flow rotational or irrotational?

3) Compute the rate of strain.

4) Compute the substantial derivatives $\mathrm{D}u/\mathrm{D}t$ and $\mathrm{D}v/\mathrm{D}t$

edXsolution

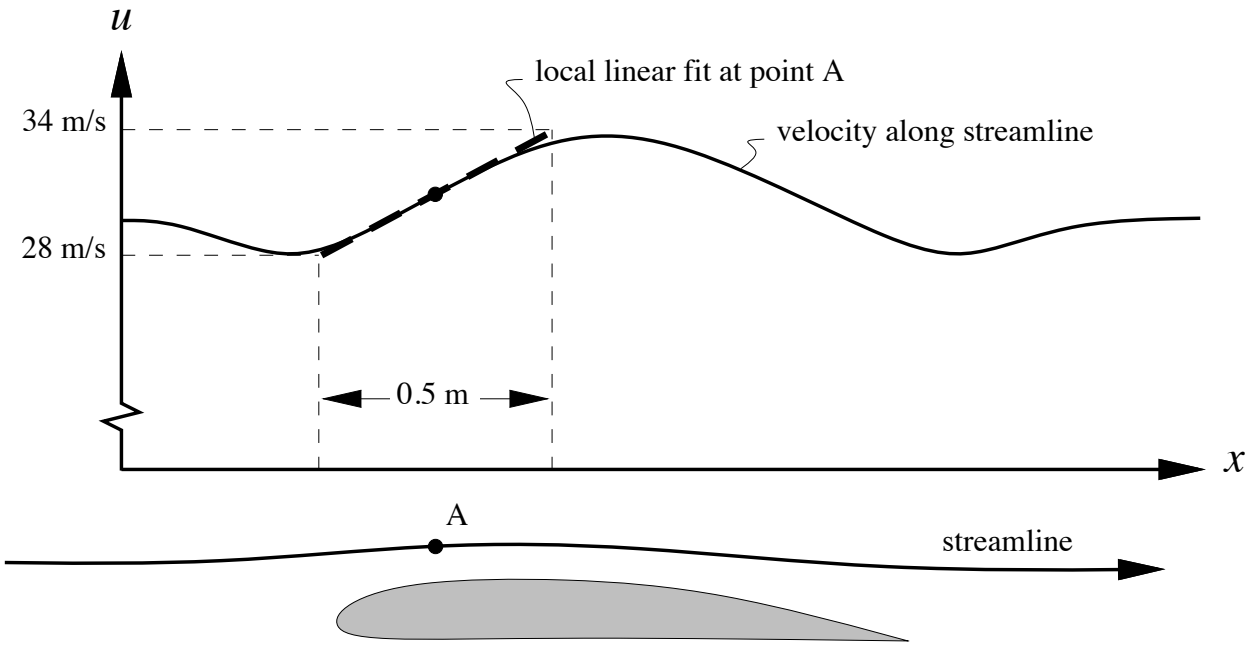
Video Link

edXproblem: 6.4.3 Pressure over a wing

6.1 6.4

A small civil airplane is flying at a steady speed of $V_\infty = 30$ m/s at some altitude where the air density is $\rho_\infty = 1.2$ kg/m^3 and the ambient pressure is $p_\infty = 100,000$ Pa.

The figure below shows the velocity distribution $u(x)$ along a streamline just above the wing, as seen by the pilot. The flow direction is nearly along the x axis, so we will consider only the accelerations and velocities in the x-direction, *i.e.* $v \approx 0$ and $w \approx 0$. To answer the questions below, and to give numerical results, use the local linear approximation to the velocity curve, shown as the heavy dashed line in the figure. Point A is at the midpoint of the 0.5 m interval shown.



1) Determine the acceleration of the fluid at point A.

2) Determine the streamwise pressure gradient $\partial p/\partial x$ at point A using the momentum equation.

3) Determine again the streamwise pressure gradient but this time using Bernoulli's equation.

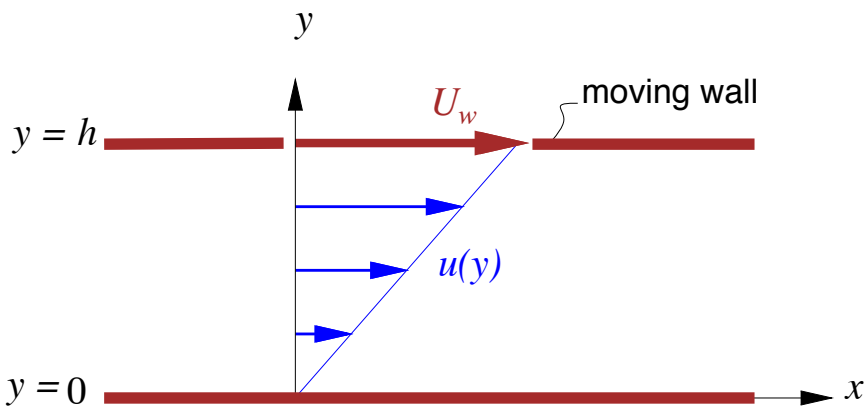
edXsolution

Video Link

edXproblem: 6.4.4 Couette flow

6.1 6.4

Consider the 2D, incompressible, steady flow between parallel walls as illustrated in the figure below: the bottom wall is stationary and the top one is moving at a constant velocity U_w. The pressure is constant.



Assuming the flow is fully developed (*i.e.* independent of x), we can write $\partial/\partial x \equiv 0$. We will also assume that the flow has parallel streamlines so that the y-velocity component is zero. The x-component of the velocity field is then linear and given by

$$u(y) = U_w \frac{y}{h} \tag{6.65}$$

Your answers to the questions below can only depend on x, y, h, U_w. In the answer box, use Uw to denote U_w.

1) Using the x- and y-momentum equations, derive the expression for the viscous term $\mathbf{f}^\tau$.

$f_1^\tau =$

$f_2^\tau =$

2) Write the expression for the vorticity (ω_z).

3) Is the flow rotational or irrotational?

4) Write the expressions for the strain rate components.

$\varepsilon_{xx} =$

$\varepsilon_{yy} =$

$\varepsilon_{xy} =$

edXsolution

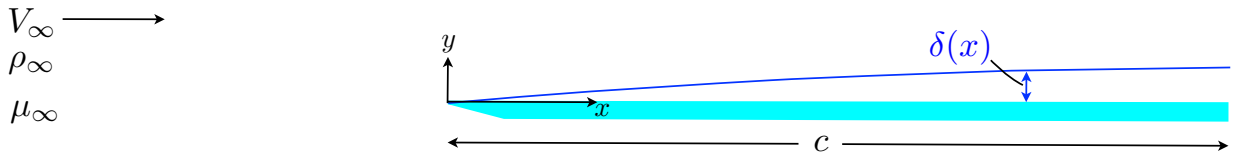
Video Link

6.5 Homework Problems

edXproblem: 6.5.1 Flow over a flat plate

6.1 | 6.4

A flat plate is moving through the atmosphere with velocity V_∞.



The Reynolds number for the flat plate is defined as,

$$Re \equiv \frac{\rho_\infty V_\infty c}{\mu_\infty} \tag{6.66}$$

and for this problem, $Re = 2 \times 10^6$. The Mach number can assumed to be low, i.e. $M_\infty \ll 1$.

An approximate model for the velocity distribution in the boundary layer of a flat plate is

$$u(x,y) = V_\infty \left[2\frac{y}{\delta} - \left(\frac{y}{\delta}\right)^2 \right] \tag{6.67}$$

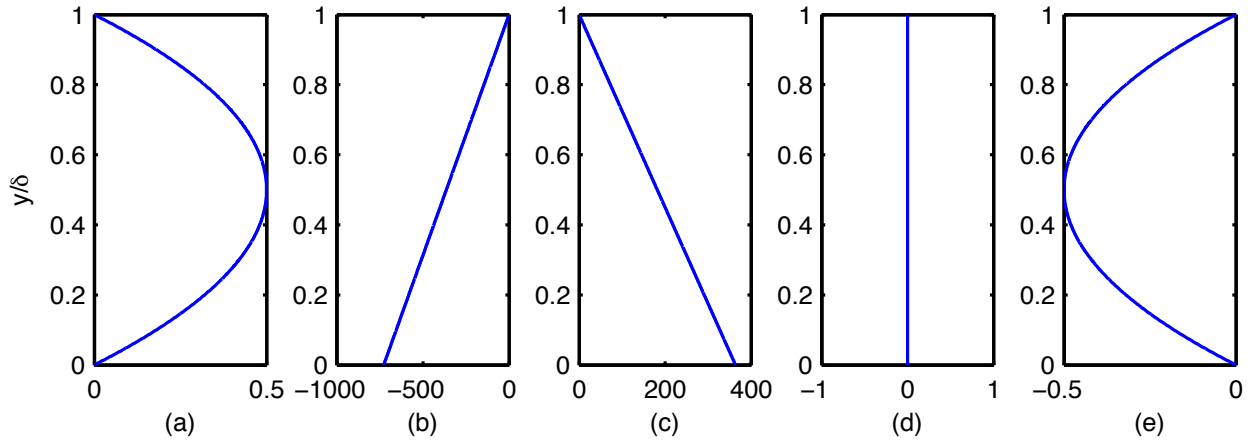
$$v(x,y) = V_\infty \left[\left(\frac{y}{\delta}\right)^2 - \frac{2}{3}\left(\frac{y}{\delta}\right)^3 \right] \frac{\mathrm{d}\delta}{\mathrm{d}x} \tag{6.68}$$

$$\delta(x) = \frac{5.5x}{\sqrt{Re_x}} \tag{6.69}$$

$$Re_x \equiv \frac{\rho_\infty V_\infty x}{\mu_\infty} \tag{6.70}$$

Note: this velocity distribution is valid within the boundary layer from $0 \le y \le \delta(x)$. For $y > \delta(x)$, the velocity returns (approximately) to V_∞.

The plots below show the variation of ϵ_{xx}, ϵ_{xy}, ϵ_{yy}, $\nabla \cdot \mathbf{v}$, and ω_z through the boundary layer (i.e. as a function of y/δ) at the mid-chord ($x/c = 0.5$). Note that each of the quantities has been plotted in a non-dimensional form in which they have been normalized by (i.e. divided by) V_∞/c. Determine which quantity is shown in each figure.



Which figure is $\epsilon_{xx}/(V_\infty/c)$?

Which figure is $\epsilon_{xy}/(V_\infty/c)$?

Which figure is $\epsilon_{yy}/(V_\infty/c)$?

Which figure is $\nabla \cdot \mathbf{v}/(V_\infty/c)$?

Which figure is $\omega_z/(V_\infty/c)$?

edXsolution

Video Link

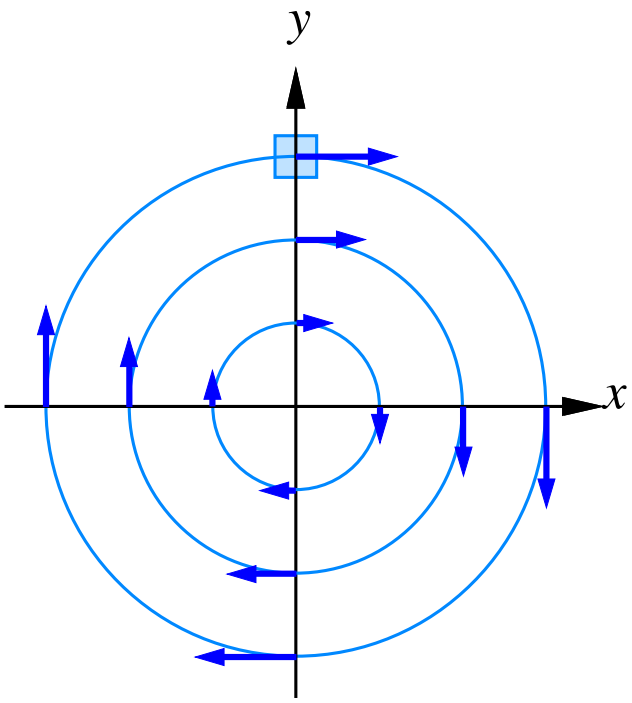
edXproblem: 6.5.2 Circular flow: solid-body rotation

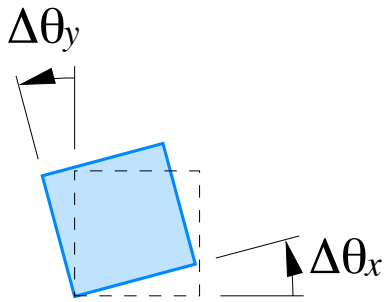
6.1 6.4

Consider a flow whose velocity field is given by

$$u = y, \tag{6.71}$$
$$v = -x \tag{6.72}$$

and illustrated in the figure below. The streamlines are circles centered at the origin, and this flow is an example of a solid-body rotation. Assume that the flow is incompressible.





All of your answers below should use only x, y, Δt, ρ. In the answer boxes, use Dt to denote Δt and rho for ρ.

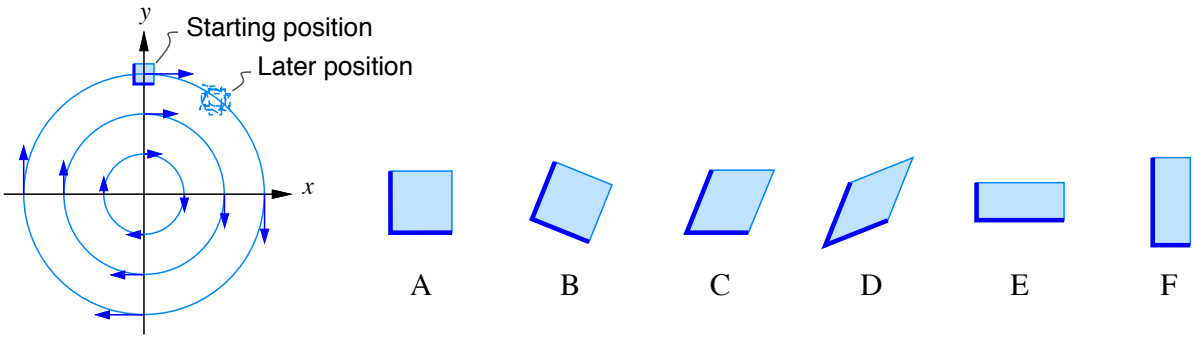
As shown in the figure, consider a small square fluid element at the point $(x, y) = (0, 1)$ at $t = 0$: it moves and distorts with the fluid. In the first part of this problem, we only consider the shape change of the fluid element.

Specifically, determine the angles $\Delta\theta_x$ and $\Delta\theta_y$ of the fluid element at some small later time $t = \Delta t$.

What is $\Delta\theta_x$?

What is $\Delta\theta_y$?

Among the different shapes below, pick the one that shows this fluid element at time Δt.



In all of the remaining parts of this problem, you are to derive the requested quantity for any (x, y) location. In other words, the answers could be expressions with a dependence on x and y.

What is ω_x?

What is ω_y?

What is ω_z?

Is the flow rotational or irrotational?

What is ε_{xx}?

What is ε_{yy}?

What is $\mathrm{D}u/\mathrm{D}t$?

What is $\mathrm{D}v/\mathrm{D}t$?

For this particular flow, $f_i^\tau = 0$. Using the x- and y-momentum equations, find expressions for the components of the pressure gradient ∇p.

What is $\dfrac{\partial p}{\partial x}$?

What is $\dfrac{\partial p}{\partial y}$?

Integrate the pressure gradient components to find an expression for $p(x, y) - p(0, 0)$.

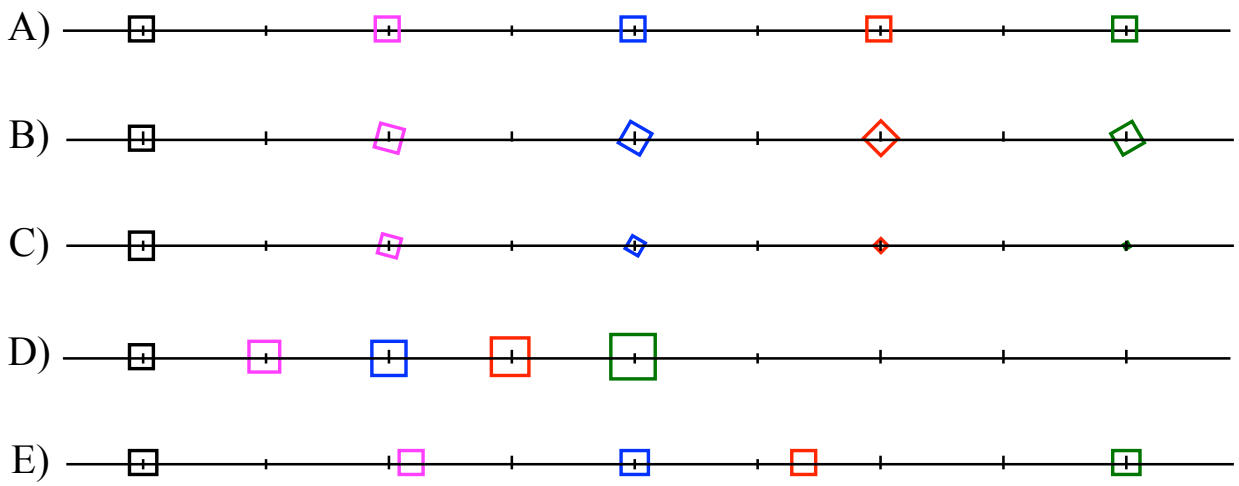
edXsolution

Video Link

edXproblem: 6.5.3 Analyzing the motion of a fluid element

6.1 6.4

The following image shows the position and shape of five *infinitesimal* fluid elements (element A, B, C, D, and E) in two-dimensional flow at equal *infinitesimal* time intervals dt. Note: each element motion is unrelated to the other (i.e. flow A, B, C, D, and E are different from each other). The initial location of the elements at time $t = 0$ is shown in black, the next location at time $t = \mathrm{d}t$ is shown in magenta, and so on with the final time shown being $t = 4\,\mathrm{d}t$ in green. Also, the vertical tick marks on each line are equi-distant (though *infinitesimally*) from each other.



For the following questions, your answer could include more than one of the motions (A, B, C, D, and E). If none of the motions satisfy the condition, you should answer none.

1) For which motions is $\nabla \cdot \vec{V} = 0$ possible?

2) For which motions is $\nabla \times \vec{V} = 0$ possible?

3) For which motions is $\mathrm{D}\vec{V}/\mathrm{D}t = 0$ possible?

4) For each of the motions, determine if the density of the fluid element is constant, increasing, or decreasing during the motion.

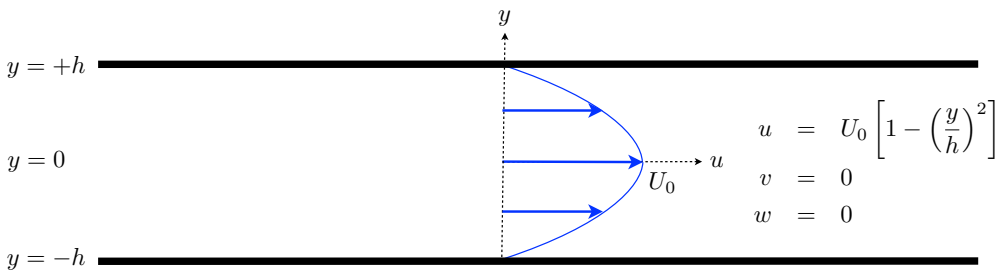
5) For each of the motions, determine if the fluid elements are subjected to a non-zero net force at some time during its motion.

The flow through a long duct has the velocity field shown below:

6) Select all of the statements which are true about this duct flow:

edXsolution

Video Link


y
y = +h
y = 0
y = −h
u
U0
u = U0 [1 − (y/h)^2]
v = 0
w = 0

Module 7

Streamline Curvature and the Generation of Lift

7.1 Overview

7.1.1 Measurable outcomes

This module considers airfoil derives a relationship for steady and inviscid flow between streamline curvature and pressure gradient normal to a streamline. Then, we use this relationship to qualitatively describe the pressure distribution on an airfoil and the generation of lift.

Specifically, students successfully completing this module will be able to:

7.1. Explain the relationship between streamline curvature and pressure, and apply this relationship to determine the qualitative behavior of the pressure in common flows.

7.2. Explain and sketch the pressure distribution on an airfoil based on streamline curvature arguments, with emphasis on the effects of camber and thickness on lift generation and understanding of the flow in the leading edge region.

7.1.2 Pre-requisite material

The material in this module requires the measurable outcomes from Modules 6.

7.2 Fundamentals of Streamline Curvature

7.2.1 Streamline curvature

7.1

A key to understanding aerodynamic flows is the connection between the turning of the flow and the behavior of the pressure. In this section, we will first show how the streamline curvature and the pressure are related in a steady, inviscid flow. Then, we will apply this insight in some common flows. In particular, in Section 7.3, we will use streamline curvature to describe the behavior of the pressure distribution on an airfoil and the generation of lift.

We begin by simplifying the momentum equations in Equation (6.45) to steady, two-dimensional, inviscid flow which gives

$$\rho u_j \frac{\partial u}{\partial x_j} = -\frac{\partial p}{\partial x}, \tag{7.1}$$

$$\rho u_j \frac{\partial v}{\partial x_j} = -\frac{\partial p}{\partial y}. \tag{7.2}$$

Instead of an (x, y) coordinate system, these equations can be written in a stream-aligned coordinated system (r, s). As shown in Figure 7.1, r is the direction normal to the local streamwise direction and s is the local streamwise direction. Natural coordinates are also often refered to as

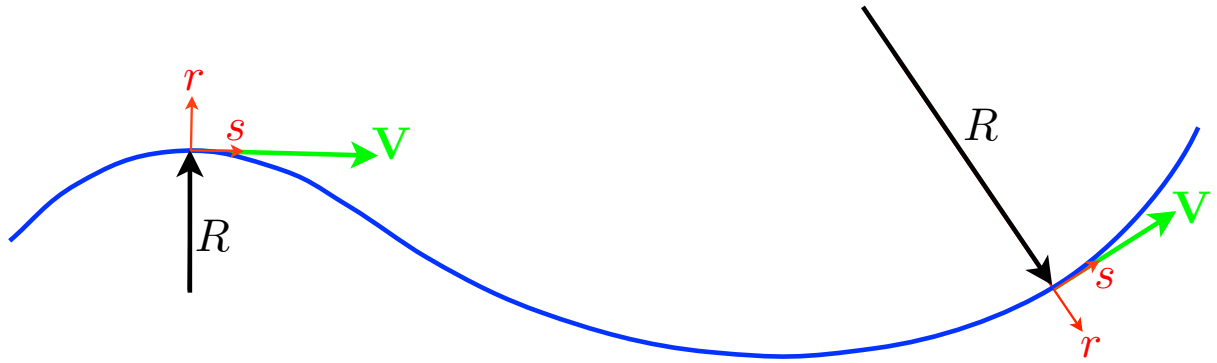


Figure 7.1: Natural coordinate system (r, s). r is the direction normal to the streamwise direction (pointing along the radius of curvature), s is in the streamwise direction (tangent to the velocity vector, $\mathbf{V}$). R is the magnitude of the radius of curvature.

intrinsic coordinates. In this coordinate system, the steady inviscid momentum equations are,

$$\rho V \frac{\partial V}{\partial s} = -\frac{\partial p}{\partial s}, \tag{7.3}$$

$$\rho \frac{V^2}{R} = \frac{\partial p}{\partial r}, \tag{7.4}$$

where $V = |\mathbf{V}|$ is the magnitude of the velocity vector (i.e. the speed).

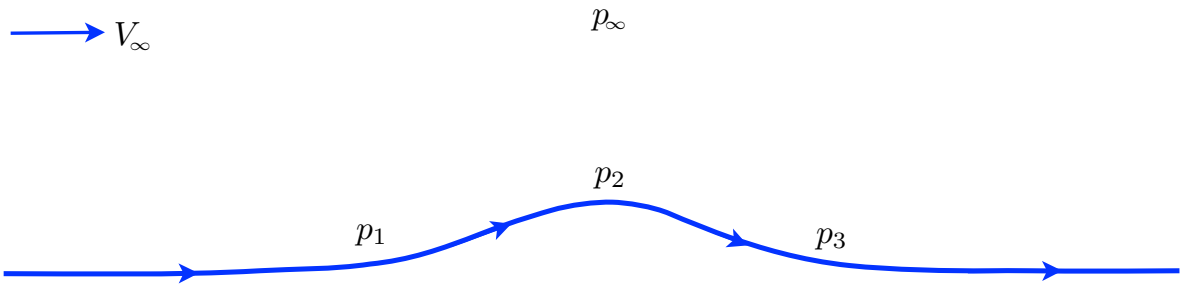
The streamwise momentum equation (Equation 7.3) produces the well-known Bernoulli's equation if the density is constant. However, the key to understanding lift generation is not Bernoulli's equation but rather the normal momentum equation, Equation (7.4). The normal momentum equation is also refered to as the streamline curvature equation.

In the following video, we will look a little more closely at the streamline curvature result and show how it is related to the basic mechanics results for rigid body circular motion.

Video Link

Now, we will apply streamline curvature to qualitatively describe the behavior of the pressure along a curved wall.

Video Link



edXproblem: 7.2.2 Pressure behavior for bump flow

7.1

Consider the flow of the bump shown in the figure. Apply streamline curvature to determine how the pressures p_1, p_2, and p_3 compare to p_∞.

edXsolution

Video Link

7.3 Streamline Curvature and Airfoil Lift Generation

7.3.1 Introduction

7.2

A major objective in this course is an understanding of the generation of lift on wings and lifting bodies. While both pressure and viscous stresses contribute to the forces generated by a body, the lift for most applications of interest is dominated by the resultant forces due to pressure. In this section, we will apply the streamline curvature analysis that we derived in Section 7.2.1 to qualitatively describe how the geometry of an airfoil impacts the pressure distribution and hence the lift generated by an airfoil. Recall that the assumptions in the streamline curvature analysis are inviscid and steady flow.

7.3.2 Impact of camber

7.2

The impact of camber on the pressure distributions can be demonstrated most simply by considering an airfoil with a circular arc camber line and zero thickness as shown in Figure 7.2. Far

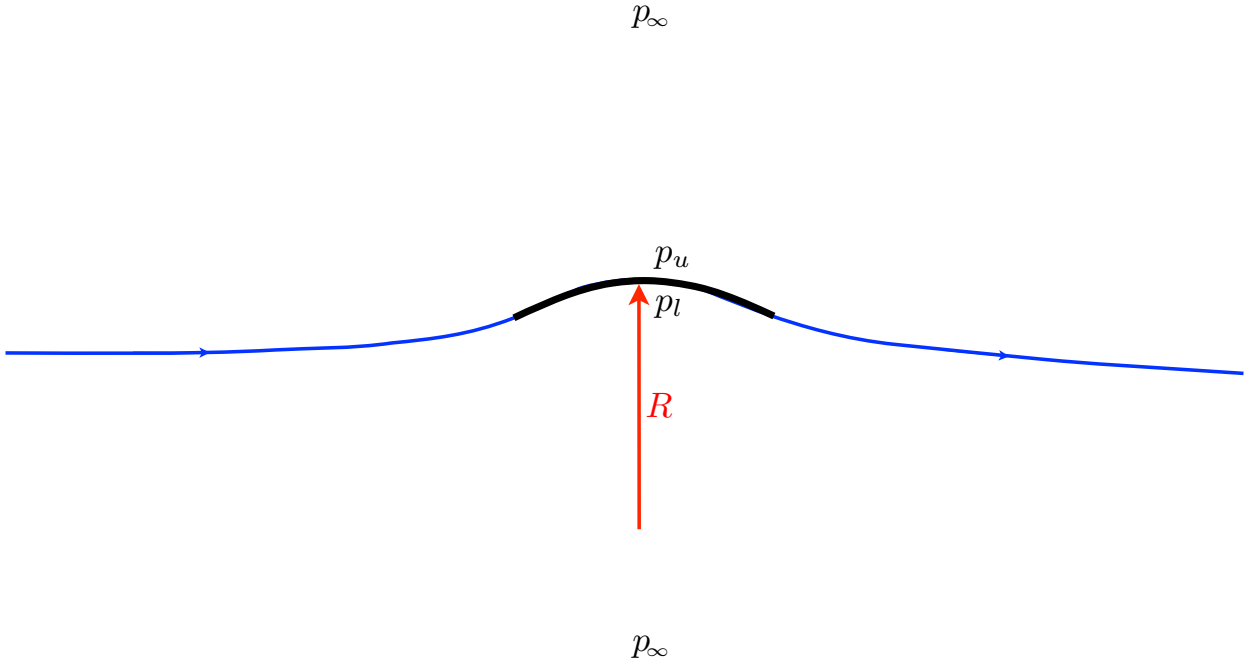


Figure 7.2: Airfoil with a circular arc camber line with radius R and zero thickness. p_u is the upper surface pressure, p_l is the lower surface pressure.

away from the airfoil, the pressure returns to the freestream pressure p_∞.

On the surface of the airfoil (which must be a streamline), we know that $\partial p/\partial r > 0$ from Equation (7.4). Thus, above the airfoil the pressure increases as the distance from the airfoil increases. Since the pressure must eventually return to p_∞, this implies that $p_u < p_\infty$. Summarizing the logic chain,

$$\frac{\partial p}{\partial r} = \rho \frac{V^2}{R} > 0 \Rightarrow p_\infty - p_u > 0 \Rightarrow p_u < p_\infty. \tag{7.5}$$

Similarly, on the lower surface,

$$\frac{\partial p}{\partial r} = \rho \frac{V^2}{R} > 0 \Rightarrow p_l - p_\infty > 0 \Rightarrow p_l > p_\infty. \tag{7.6}$$

Combining these results which are solely based on the curvature of the surface, we see that $p_u < p_\infty < p_l$. Thus, this airfoil will generate lift since the pressure is lower on the upper surface than on the lower surface.

In the following video, we further discuss this example of lift generation for a circular arc airfoil.

Video Link

To illustrate the pressure distribution on a thin airfoil, consider the NACA 4502 airfoil. This airfoil has a maximum thickness which is 2% of the chord length. The maximum camber is 4% of the chord and occurs at $x/c = 0.5$. Note: the NACA 4-digit series airfoils have camber lines which are two parabolic arcs that meet at the maximum camber location. Thus, when the maximum camber is at $x/c = 0.5$, the two parabolic arcs are the actually the same and the radius of curvature will vary smoothly along the camberline. The C_p distribution for the 4502 at a $c_l = 0.5$ is shown in Figure 7.3. Recall that when the pressure is below p_∞, $C_p < 0$ and vice-versa. The C_p distribution for the 4502 shows that the pressures are below p_∞ on the upper surface, and above p_∞ on the lower surface. Furthermore, the decrease in pressure on the upper surface is nearly equal to the increase in pressure on the lower surface which is reasonable since the radius of curvature is essentially the same on both the upper and lower surface.

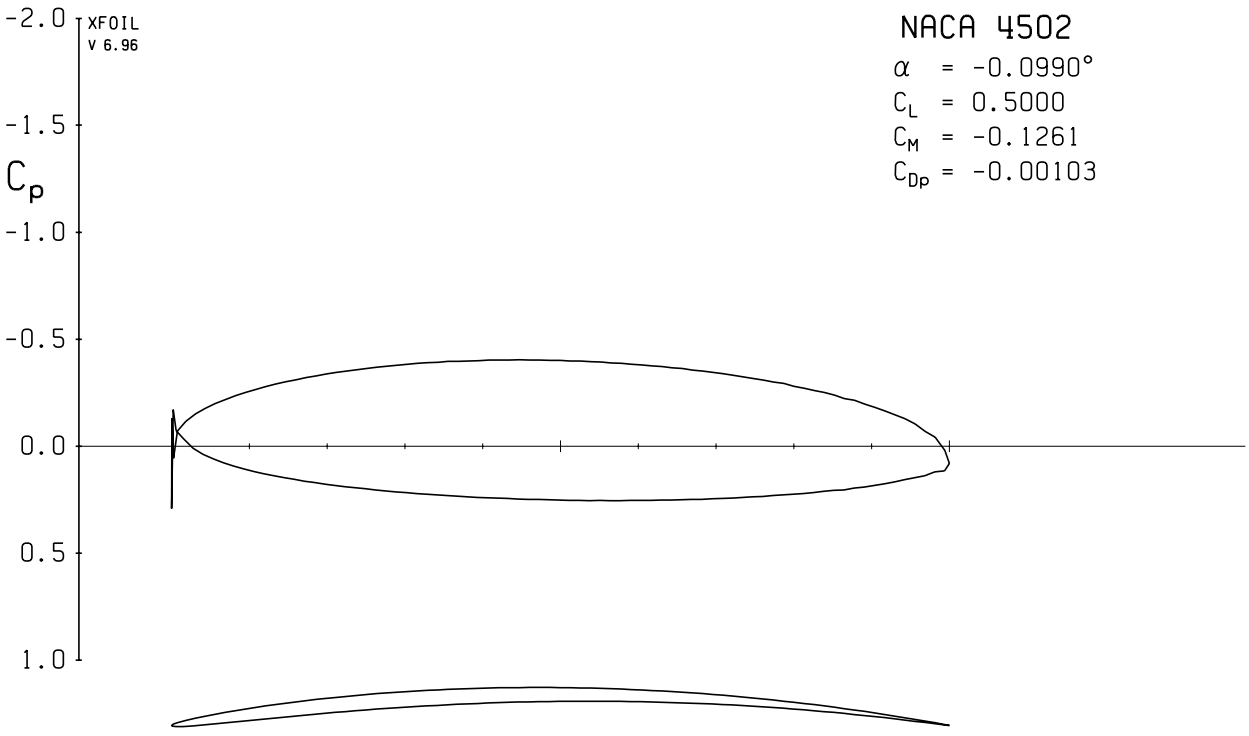


Figure 7.3: C_p distribution for NACA 4502, $c_l = 0.5$.

Note that near the leading edge, the flow will have a stagnation point, $V = 0$. This corresponds to $C_p = 1$ (see Section 4.4.7 for more information). However, in Figure 7.3, the C_p at the leading edge has a maximum value of about $C_p = 0.3$. The reason the stagnation point is not observed is purely numerical; the method used to calculate the potential flow does not have enough resolution in the leading-edge region. If the resolution at the leading edge were increased, or the thickness of

the airfoil were increased, then the leading-edge stagnation point would be better resolved and C_p would approach 1.

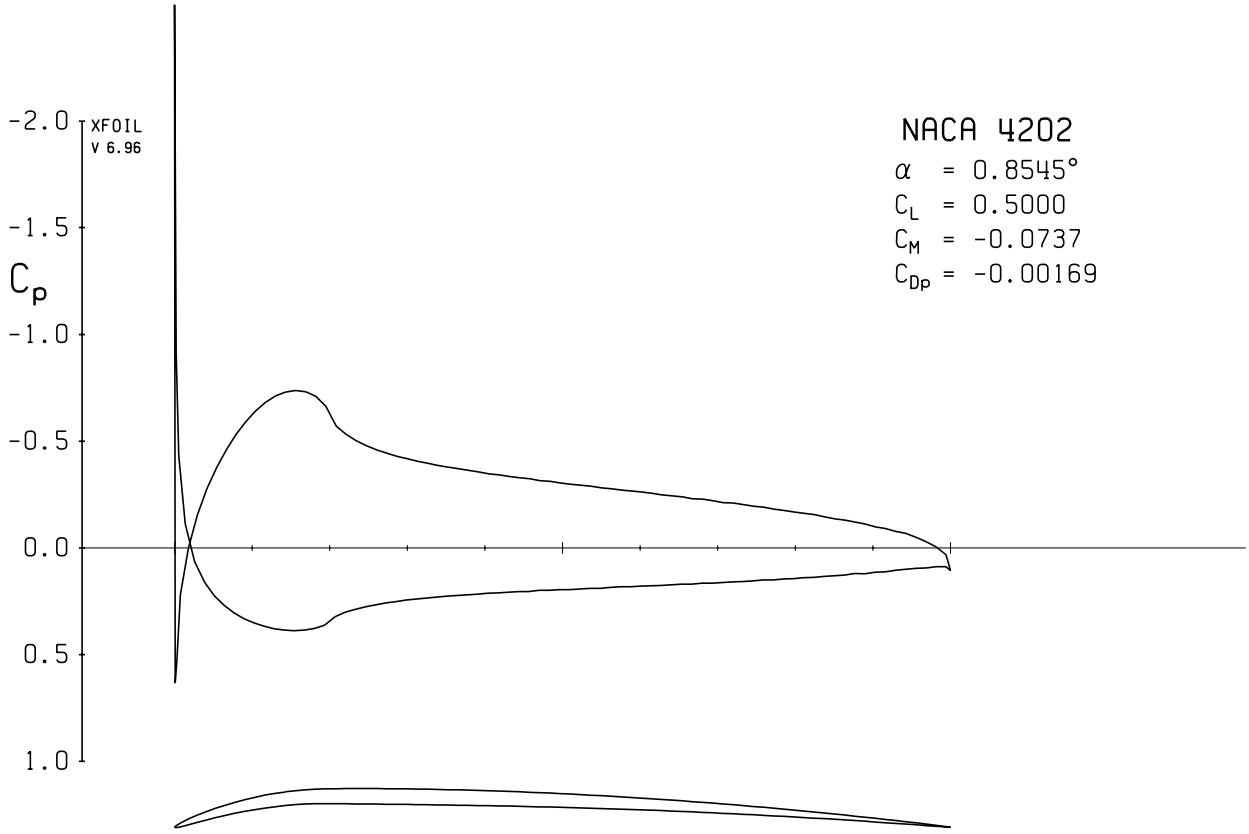


Figure 7.4: C_p distribution for NACA 4202, $c_l = 0.5$.

As another example of the impact of camber on the pressure distribution, Figure 7.4 shows the pressure distribution for a NACA 4202. This airfoil has a camber line with two different parabolic arcs with a jump in the radius of curvature at the maximum camber at $x/c = 0.2$. The radius of curvature is smaller from $x/c < 0.2$, thus the normal pressure gradients are generally expected to be larger in this region than for $x/c > 0.2$. This behavior is clearly observed in the C_p distribution. The magnitude of the C_p's drop abruptly for $x/c > 0.2$.

7.3.3 Impact of thickness

7.2

The impact of thickness can also be explained qualitatively from streamline curvature arguments. Consider a symmetric airfoil with thickness. In this case, the curvature of the upper and lower surfaces are in opposite directions. Thus, the logic chain becomes,

$$\frac{\partial p}{\partial r} = \rho \frac{V^2}{R} > 0 \Rightarrow p_\infty - p_u > 0 \Rightarrow p_u < p_\infty. \tag{7.7}$$

Similarly, on the lower surface,

$$\frac{\partial p}{\partial r} = \rho \frac{V^2}{R} > 0 \Rightarrow p_\infty - p_l > 0 \Rightarrow p_l < p_\infty. \tag{7.8}$$

Thus, for a symmetric airfoil at zero angle of attack, the pressures on the surface are generally expected to be lower than p_∞. As examples of symmetric airfoils, the C_p distributions for NACA

0002 and 0010 airfoils at zero angle of attack are shown in Figure 7.5. The low pressures are observed on both surfaces (note: the flow is symmetric since the geometry is symmetric and $\alpha = 0$, thus the C_p on the upper and lower surfaces are the same). Also, the pressures are lower for the thicker airfoil as would be expected since the radius of curvature is small for the thicker airfoil.

On a cambered airfoil, the trends with thickness are similar to the trends on a symmetric airfoil. Specifically, the addition of thickness will tend to lower the C_p on both sides of the airfoil. Once again, this qualitative behavior can be motivated using streamline curvature arguments. Increasing the thickness on a cambered airfoil will tend to decrease the radius of curvature of the upper surface, and increase the radius of curvature of the lower surface. Thus, we have the following chain of reasoning for how the pressure on the upper surface is affected by increasing thickness,

$$\text{thickness} \uparrow \quad R_u \downarrow \quad \frac{\partial p}{\partial r} = \rho \frac{V^2}{R} \uparrow \quad p_\infty - p_u \uparrow \quad p_u \downarrow . \tag{7.9}$$

Similarly, on the lower surface,

$$\text{thickness} \uparrow \quad R_l \uparrow \quad \frac{\partial p}{\partial r} = \rho \frac{V^2}{R} \downarrow \quad p_l - p_\infty \downarrow \quad p_l \downarrow . \tag{7.10}$$

Since the addition of thickness to a cambered airfoil tends to lower both the upper and lower surface pressure and the lift is an integral of the upper and lower surface pressure difference, the resulting lift will be relatively unaffected by thickness. These trends in C_p and c_l can be observed by comparing the 10% thick cambered airfoils shown in Figure 7.6 to the 2% thick cambered airfoils shown in Figures 7.3 and 7.4. Note: the thicker airfoils were simulated at the same angles of attack for the corresponding thinner airfoils. For these conditions, the 5 times increase in thickness from 2% to 10% changes the lift by less than 10%.

7.3.4 Leading-edge behavior: stagnation points and suction peaks

7.2

Next, we will consider the behavior of the flow at the leading edge. As was noted above, the flow will stagnate near the leading edge which corresponds to $C_p = 1$. In addition to the high pressure at the stagnation point, the pressures in the vicinity of the leading edge can also be very low. For example, the C_p distribution around the NACA 4202 airfoil at $c_l = 0.5$ shows $C_p < -2$ at the leading edge. This very low pressure is referred to as a *leading-edge suction peak* and the behavior can be highly detrimental to the performance of an airfoil potentially resulting in separation of the boundary layer immediately downstream of the suction peak.

The cause of the suction peak can also be explained through the streamline curvature argument. In this case, the radius of curvature at the leading edge is very small. And, as $R \to 0$,

$$\lim_{R \to 0} \frac{\partial p}{\partial r} = \rho \frac{V^2}{R} \to \infty. \tag{7.11}$$

Thus, the pressures at the leading edge will need to be very low if the flow wraps around a leading edge with a small radius of curvature.

In the following video, we look in more detail at the behavior of the flow at a leading edge.

Video Link

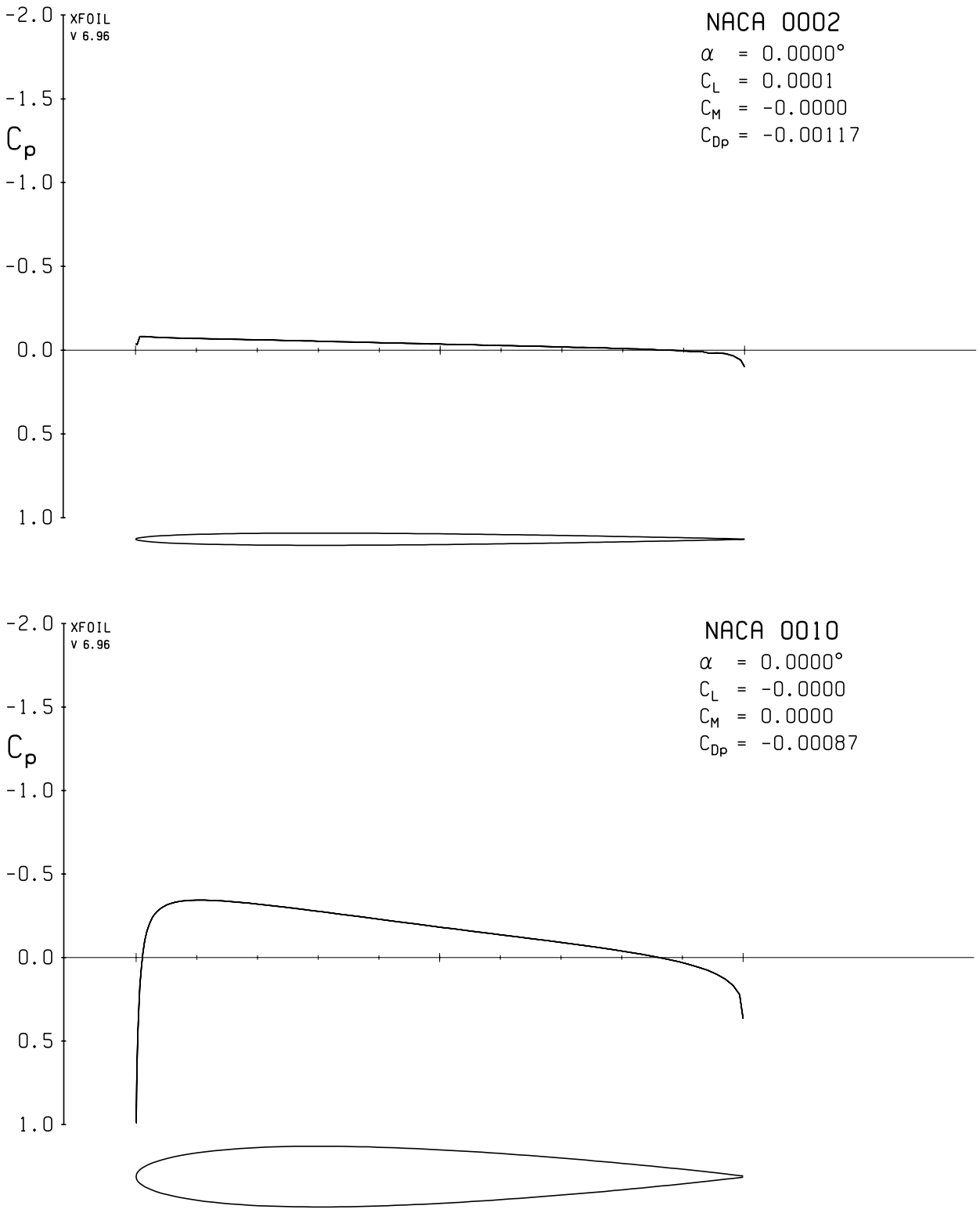


Figure 7.5: C_p distributions for NACA 0002 and 0010, $\alpha = 0°$.

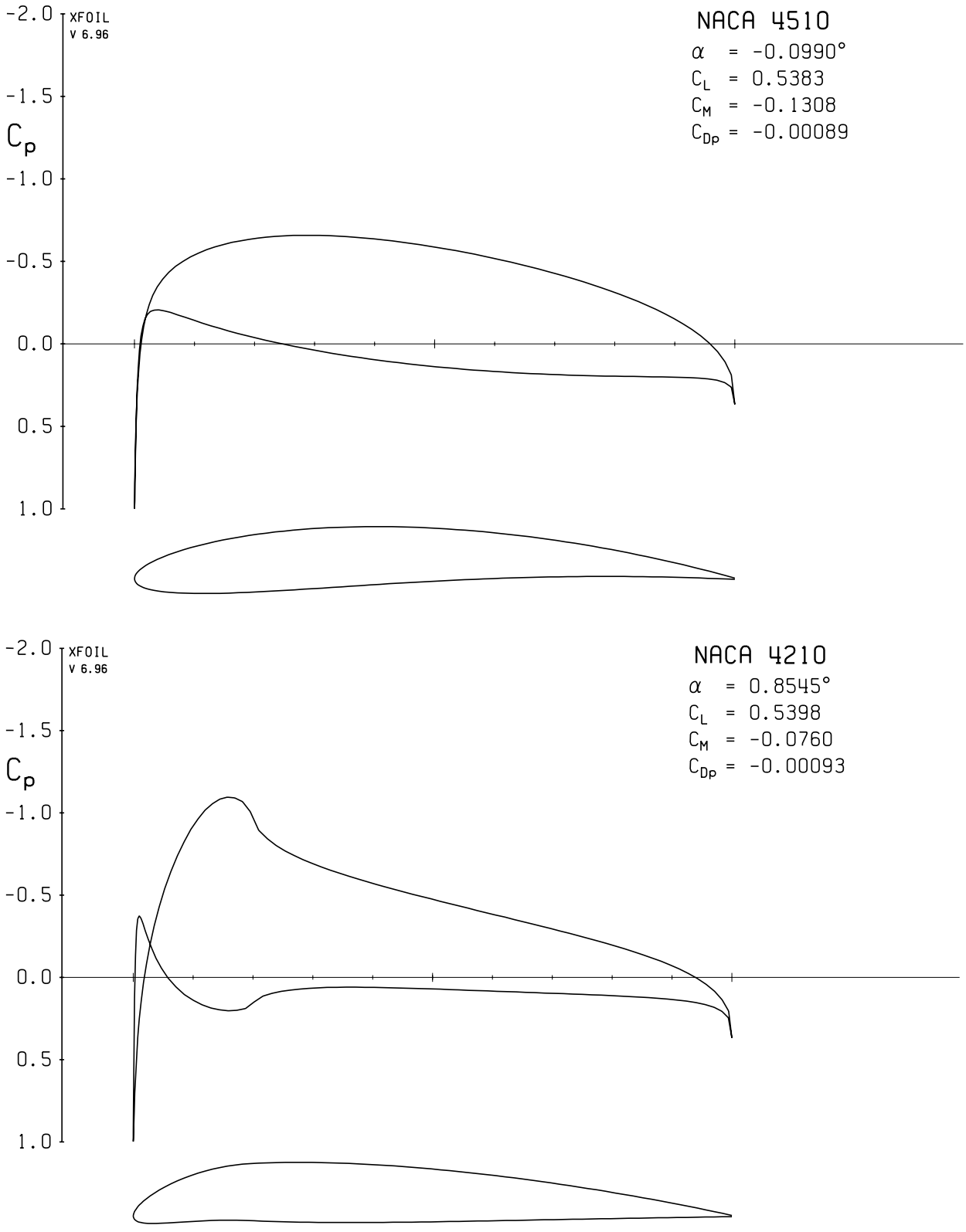


Figure 7.6: C_p distributions for NACA 4510, $\alpha = -0.0990°$ and NACA 4210, $\alpha = 0.8545°$.

edXproblem: 7.3.5 Leading-edge behavior

7.2

Figure 7.7 shows the C_p distributions for the NACA 0002 and NACA 4202 for $c_l = 0.5$.

Is the leading-edge stagnation point on the lower surface or upper surface for the NACA 0002?

Is the leading-edge stagnation point on the lower surface or upper surface for the NACA 4202?

edXsolution

Video Link

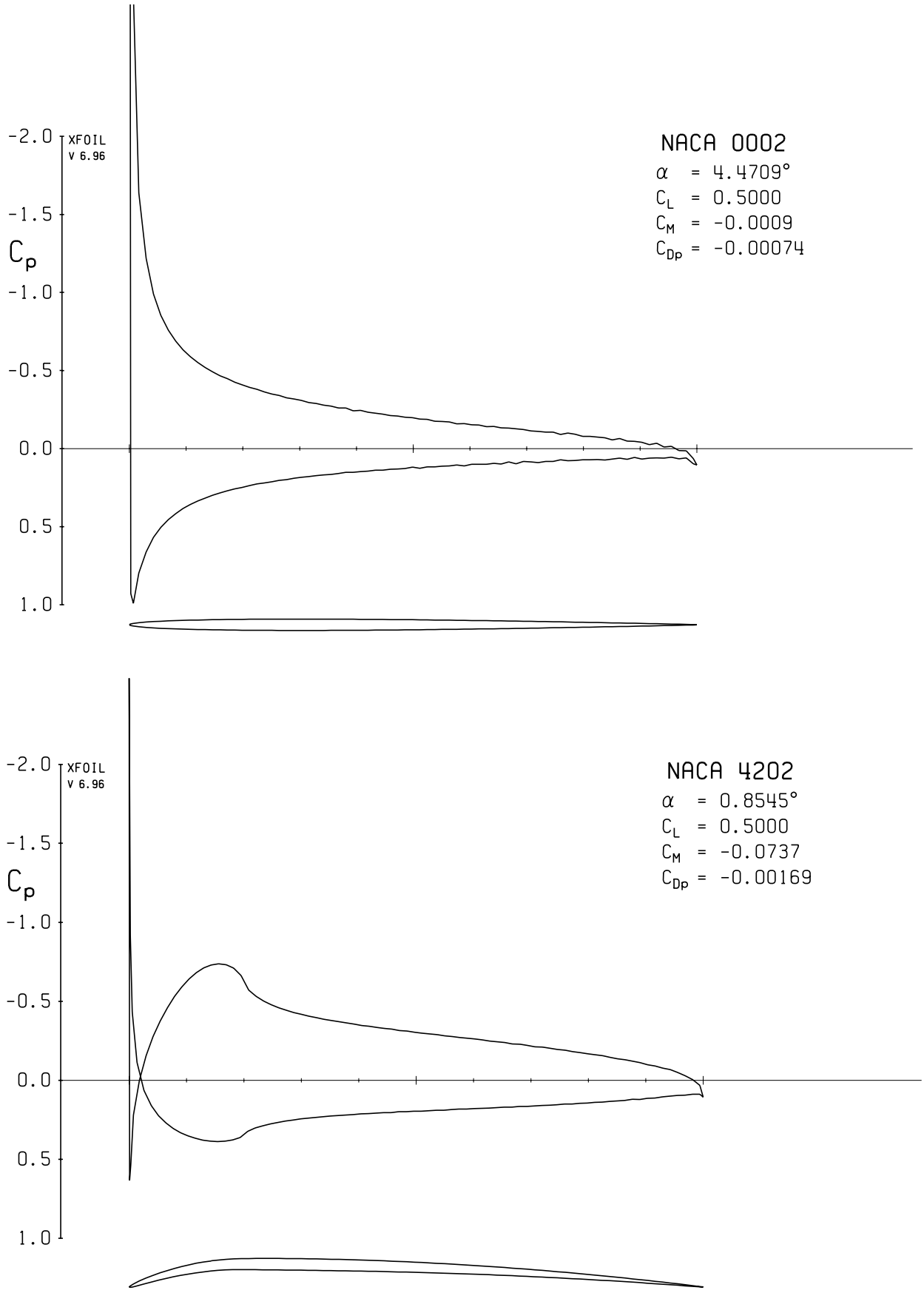
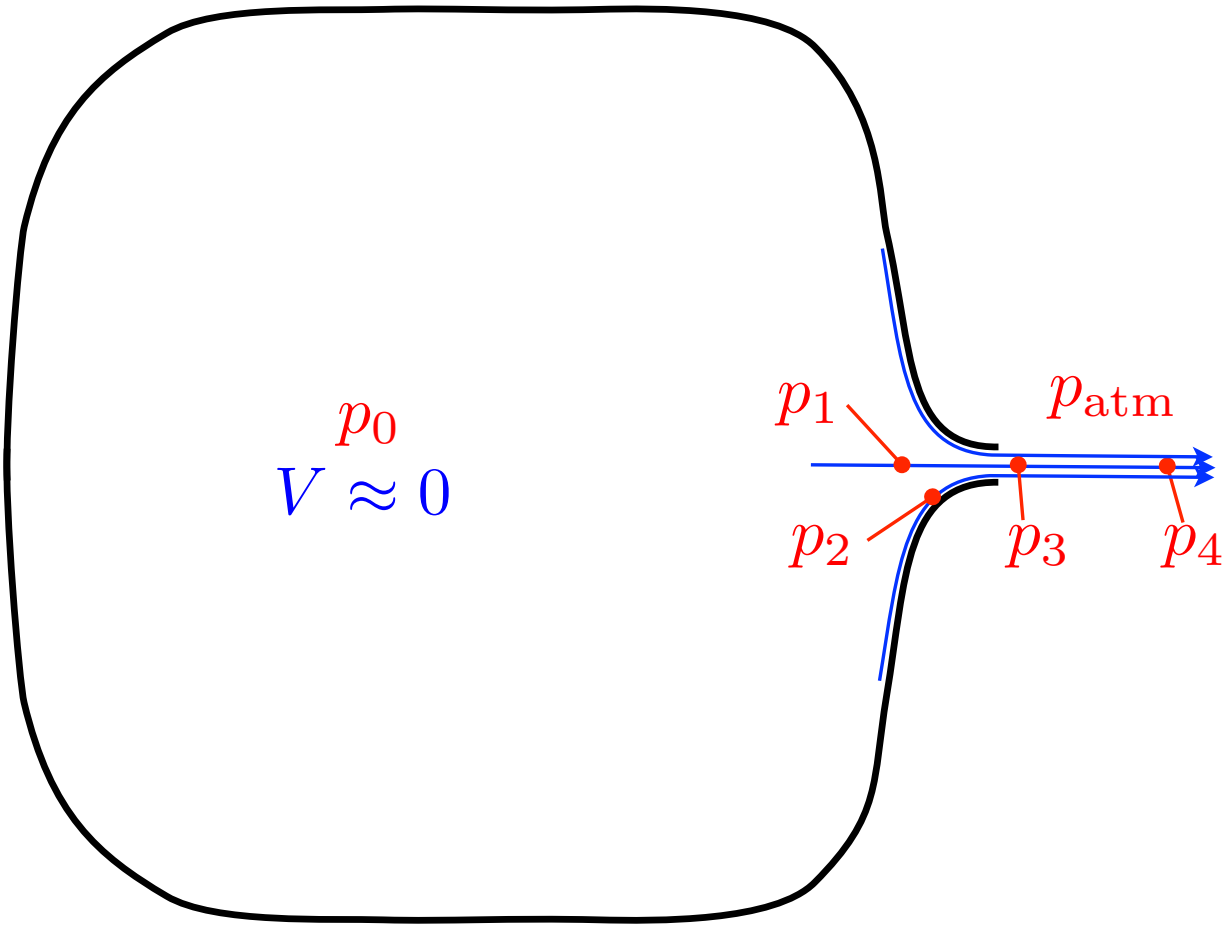


Figure 7.7: NACA 0002 and 4202, $c_l = 0.5$.

7.4 Sample Problems

edXproblem: 7.4.1 Pressure behavior in a nozzle and exhaust jet

8.2 | 7.2



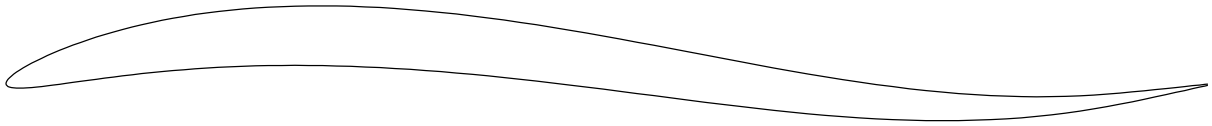
A jet is exitting out of a nozzle with the streamline pattern shown. Assuming the flow can be modeled as incompressible, inviscid, and steady, determine how the pressures p_0, p_1, p_2, p_3, and p_4 compare to the atmospheric pressure p_{atm}. Specifically, determine if p_i is less than, equal to, or greater than p_{atm}, or alternatively if you need more information to make this determination.

edXsolution

Video Link

edXproblem: 7.4.2 Streamline curvature application to a reflexed airfoil

7.2



For the airfoil shown above, carefully sketch the pressure distribution for $c_l = 0.4$ assuming an incompressible potential flow. Also, assume that the airfoil has been designed so that, at this lift coefficient, there is no suction peak at the leading edge.

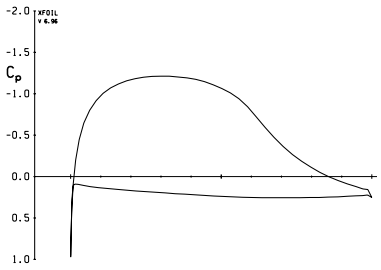
edXsolution

Video Link

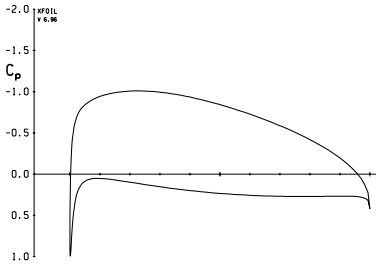
7.5 Homework Problems

edXproblem: 7.5.1 Matching airfoils and pressure distributions

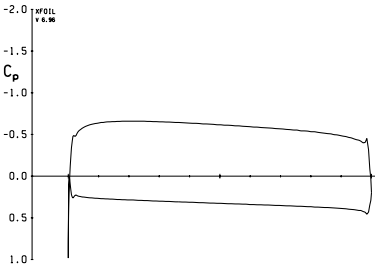
7.2



Distribution 1



Distribution 2



Distribution 3



Airfoil A



Airoil B



Airfoil C

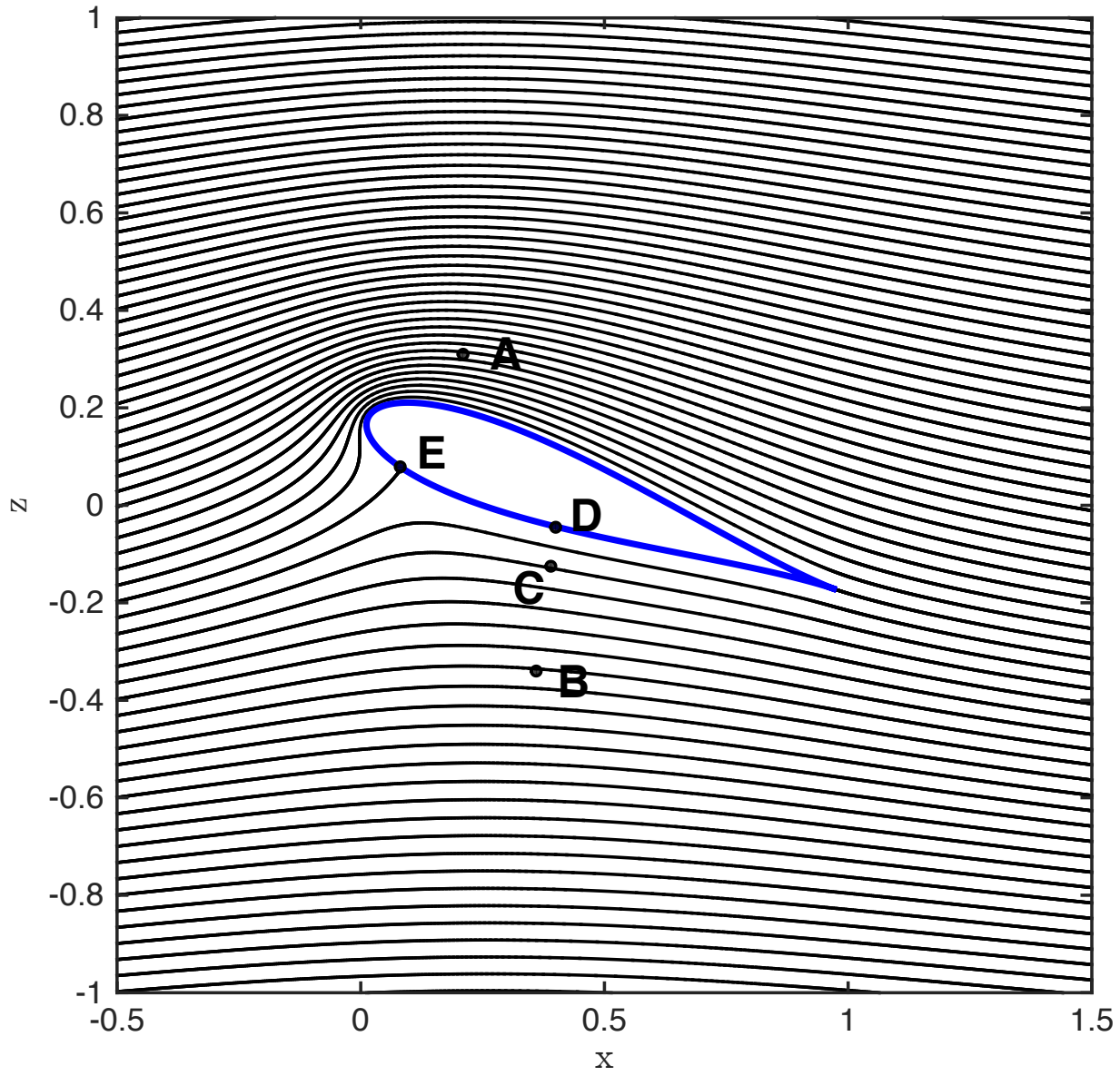
Three airfoil geometries and the pressure distributions for these airfoils are shown for an incompressible, inviscid flow with a lift coefficient of 0.9. Match the airfoil geometries with the pressure distributions. Specifically, select the three options below which are true.

edXsolution

Video Link

edXproblem: 7.5.2 Determining pressure behavior around an airfoil at angle of attack

8.2 | 7.2



The streamlines for the steady, inviscid, and incompressible flow around a symmetric airfoil at an angle of attack are shown in the above figure. The flow in the freestream (far upstream of the airfoil) has uniform velocity $\vec{V} = V_\infty \hat{i}$ and uniform pressure p_∞. The density is ρ.

How do the pressures at the labeled points relate to p_∞:

edXsolution

Video Link

Module 8

Fundamentals of Incompressible Potential Flows

8.1 Overview

8.1.1 Measurable outcomes

In this module, we will begin the study of potential flow modeling in aerodynamics. While the term potential flow is commonly used, the fundamental principle at work is irrotationality. Specifically, many aspects of aerodynamic flows can be modeled as being irrotational. Recall that an irrotational flow is a flow that has zero vorticity. For flows with zero vorticity, there exists a scalar function whose gradient is the velocity, i.e.

$$\mathbf{V} = \nabla\phi \tag{8.1}$$

where $\phi(x, y, z, t)$ is the scalar function and is refered to as the velocity potential. Note also that the curl of $\nabla\phi$ can be shown to be zero (try it out yourself!). Thus, an irrotational flow has a velocity which can be expressed as the gradient of a potential, and, vice-versa, the gradient of a potential gives a velocity which is irrotational.

We begin the module with a discussion of when an incompressible flow can be approximated as irrotational. Then, using the incompressible momentum equations, we will also derive the Bernoulli equation and again consider the assumptions it requires.

Then, our focus will shift to how models of flows can be constructed using potential flow theory. While we will concentrate on two-dimensional flows in this module, the basic modeling approach will be the same for three-dimensional flows. Thus, Section 8.3, which describes the modeling approach, is left general to three-dimensional potential flows. Then, in the remainder of this module, we consider some fundamental two-dimensional potential flows.

Specifically, students successfully completing this module will be able to:

8.1. Describe the behavior of vorticity in an incompressible flow and describe when the use of an irrotational flow model for incompressible aerodynamic applications is justified.

8.2. Derive the Bernoulli equation from the incompressible momentum equations, describe the assumptions required to apply the Bernoulli equation, and apply the Bernoulli equation to solve fluid dynamic problems.

8.3. Apply the Bernoulli equation to relate the pressure coefficient to the local flow speed in incompressible flow.

8.4. State the governing equations and boundary conditions for a potential flow model for the flow around a body.

8.5. Describe how linear superposition of potential flows can be applied to approximate the flow around a body.

8.6. Define the velocity field for a uniform flow, source, doublet, and vortex in two dimensions. Derive the relationship between the strength of a source, mass flow, and the conservation of mass. Derive the relationship between the strength of a vortex, circulation, and irrotationality.

8.7. State the Kutta-Joukowsky Theorem and apply it to determine the lift generated by a body in a two-dimensional incompressible inviscid flow in a uniform freestream.

8.8. State and apply d'Alembert's Paradox that the drag is zero on a body in a two-dimensional incompressible inviscid flow in a uniform freestream.

8.9. Combine a freestream, doublet, and point vortex to model the potential flow around a cylinder (lifting and non-lifting). Determine the location of stagnation points as a function of the circulation. Determine the pressure coefficient distribution on the cylinder surface. Determine the lift and drag by integration of the surface pressures.

8.1.2 Pre-requisite material

The material in this module requires the measurable outcomes from Modules 6.

8.2 Justification of Irrotational Flow

8.2.1 Incompressible flow equations

8.1 8.2

The starting point for our development of incompressible potential flow will be the incompressible conservation of mass and momentum equations in differential form, Equations (6.38) and (6.59), respectively. Repeating those equations here for convenience, we have conservation of mass,

$$\nabla \cdot \mathbf{V} = 0 \tag{8.2}$$

and conservation of momentum (using the convective form),

$$\rho \frac{\mathrm{D}u_j}{\mathrm{D}t} = -\frac{\partial p}{\partial x_j} + f_j^\tau \tag{8.3}$$

for $j = 1$, 2, and 3. While Equation (8.2) is only valid for incompressible flows, Equation (8.3) is valid for both compressible and incompressible flows.

Also, the conservation of momentum can be written as a vector equation,

$$\rho \frac{\mathrm{D}\mathbf{V}}{\mathrm{D}t} = -\nabla p + \mathbf{f}^\tau \tag{8.4}$$

In doing this, it is important to note exactly what $\mathrm{D}\mathbf{V}/\mathrm{D}t$ means. Writing this term out,

$$\frac{\mathrm{D}\mathbf{V}}{\mathrm{D}t} = \frac{\partial \mathbf{V}}{\partial t} + (\mathbf{V} \cdot \nabla)\,\mathbf{V} \tag{8.5}$$

$$= \left[\frac{\partial u_1}{\partial t} + \mathbf{V} \cdot \nabla u_1\right] \hat{\mathbf{e}}_1 \tag{8.6}$$

$$+ \left[\frac{\partial u_2}{\partial t} + \mathbf{V} \cdot \nabla u_2\right] \hat{\mathbf{e}}_2 \tag{8.7}$$

$$+ \left[\frac{\partial u_3}{\partial t} + \mathbf{V} \cdot \nabla u_3\right] \hat{\mathbf{e}}_3 \tag{8.8}$$

where $\hat{\mathbf{e}}_i$ is the unit vector in the i-coordinate direction. Also, a very useful form of $(\mathbf{V} \cdot \nabla)\,\mathbf{V}$ can be found from the vector identity,

$$\nabla(\mathbf{a} \cdot \mathbf{b}) = (\mathbf{a} \cdot \nabla)\,\mathbf{b} + (\mathbf{b} \cdot \nabla)\,\mathbf{a} + \mathbf{a} \times (\nabla \times \mathbf{b}) + \mathbf{b} \times (\nabla \times \mathbf{a}) \tag{8.9}$$

where $\mathbf{a}$ and $\mathbf{b}$ are arbitrary vector fields. Setting $\mathbf{a} = \mathbf{b} = \mathbf{V}$ gives,

$$(\mathbf{V} \cdot \nabla)\,\mathbf{V} = \frac{1}{2}\nabla\left(V^2\right) - \mathbf{V} \times \omega \tag{8.10}$$

Thus, Equation (8.4) can be written,

$$\rho\left[\frac{\partial \mathbf{V}}{\partial t} + \frac{1}{2}\nabla\left(V^2\right) - \mathbf{V} \times \omega\right] = -\nabla p + \mathbf{f}^\tau \tag{8.11}$$

8.2.2 Vorticity equation

8.1

To consider when a flow can be approximated as irrotational, we will derive an equation for the evolution of the vorticity. To do this, we take the curl of the momentum equation (as written in Equation 8.11 and assuming constant density),

$$\rho\nabla\times\left[\frac{\partial\mathbf{V}}{\partial t}+\frac{1}{2}\nabla\left(V^2\right)-\mathbf{V}\times\omega\right] = -\nabla\times\nabla p+\nabla\times\mathbf{f}^{\tau} \tag{8.12}$$

$$\rho\left[\frac{\partial\omega}{\partial t}-\nabla\times\mathbf{V}\times\omega\right] = \nabla\times\mathbf{f}^{\tau} \tag{8.13}$$

Then, we can use the following vector identity,

$$\nabla\times(\mathbf{a}\times\mathbf{b})=\mathbf{a}\nabla\cdot\mathbf{b}-\mathbf{b}\nabla\cdot\mathbf{a}+(\mathbf{b}\cdot\nabla)\,\mathbf{a}-(\mathbf{a}\cdot\nabla)\,\mathbf{b} \tag{8.14}$$

Setting $\mathbf{a}=\mathbf{V}$ and $\mathbf{b}=\omega$ and notating that $\nabla\cdot\omega=\mathbf{0}$ from a mathematical identity and $\nabla\cdot\mathbf{V}=0$ because of incompressible flow, then,

$$\nabla\times(\mathbf{V}\times\omega)=(\omega\cdot\nabla)\,\mathbf{V}-(\mathbf{V}\cdot\nabla)\,\omega \tag{8.15}$$

Thus, Equation (8.13) becomes,

$$\rho\frac{\mathrm{D}\omega}{\mathrm{D}t}=\rho\,(\omega\cdot\nabla)\,\mathbf{V}+\nabla\times\mathbf{f}^{\tau} \tag{8.16}$$

Equation (8.16) describes the time rate of change of the vorticity of a fluid element. The following points about the vorticity can be made utilizing this equation:

- The term, $\nabla\times\mathbf{f}^{\tau}$, is the torque caused by viscous stresses acting on the fluid element.
- If a fluid element has zero vorticity at some instant $\omega=\mathbf{0}$, then the only manner in which the vorticity would be created is through viscous effects since $\rho\,(\omega\cdot\nabla)\,\mathbf{V}=0$.
- In a uniform upstream flow, the velocity $\mathbf{V}$ does not vary in space. Since the vorticity is a combination of spatial derivatives of the velocity, then any fluid element originating from the freestream will have vorticity that is initially zero, and following from the previous comment, will remain zero unless it enters a region where viscous effects are important.
- Somewhat more of a detail, but still useful to note is that the $\rho\,(\omega\cdot\nabla)\,\mathbf{V}$ term is zero in two-dimensional flows. For example, consider a flow which is entirely in the $x-y$ plane and for which all z-derivatives are zero. In this case, the only possibly non-zero component of vorticity is in the z-direction, i.e. $\omega_1=\omega_2=0$. Thus, this term simplifies to,

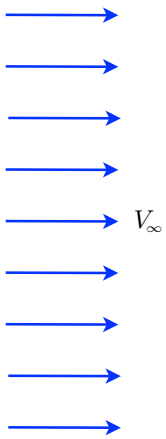
  $$\rho\omega_3\frac{\partial u_i}{\partial x_3}\hat{\mathbf{e}}_i \tag{8.17}$$

  but in this two-dimensional flow $\partial/\partial x_3=0$. Thus, $\rho\,(\omega\cdot\nabla)\,\mathbf{V}=0$ in two-dimensional flow.

The first three points when combined lead to the conclusion that if the boundary layers and wakes are thin, then the flow around a body can be reasonably approximated as irrotational. However, boundary layers, even when thin, are rotational because vorticity is generated at a solid surface in a viscous flow (we have seen that a boundary layer is rotational in Problem 6.4.1). Thus, assuming an entirely irrotational flow will mean that aerodynamic performance that is impacted significantly by the boundary layer behavior (e.g. the drag due to friction) will not be possible to estimate using a purely irrotational model. Still, the irrotational model can be used to estimate the pressure distributions on a body and the forces and moments arising from these surface pressures (assuming boundary layers are thin).

edXproblem: 8.2.3 Vorticity in incompressible, inviscid flow

8.1





Assuming an incompressible, inviscid flow around an airfoil with a uniform freestream as pictured in the figure, which of the following is true?

edXsolution

Video Link

8.2.4 Bernoulli equation

8.2

Assuming the flow is incompressible and steady, the momentum equation as written in Equation (8.11) can be simplified to,

$$\nabla\left(p+\frac{1}{2}\rho V^2\right)=\rho\mathbf{V}\times\omega+\mathbf{f}^{\tau} \tag{8.18}$$

The left-hand side is the gradient of the incompressible form of the total pressure, $p_0 \equiv p+\frac{1}{2}\rho V^2$ (see the discussion in Section 4.4.7) . Thus, we see that the total pressure in incompressible steady flow will not vary (i.e. the gradient is zero) when the flow is irrotational and the viscous effects are neglible. As discussed in Section 8.2.2, for flows with uniform freestream velocity, the vorticity is zero unless the fluid element enters a region (such as boundary layers or wakes) in which viscous effects are important. Thus, the conditions required for total pressure to be constant are the same as required for the flow to be approximated as irrotational, namely, viscous effects must be negligible.

We note that even when the vorticity is non-zero, if viscous effects are negligible then the total pressure along a streamline is constant. To see this, consider the inviscid form of Equation (8.18),

$$\nabla\left(p+\frac{1}{2}\rho V^2\right)=\rho\mathbf{V}\times\omega \tag{8.19}$$

The component of this equation along the streamwise direction can be found by taking the dot product of the equation along the streamwise direction. Since $\mathbf{V}\times\omega$ is perpendicular to $\mathbf{V}$ (and to ω) then the right-hand side is zero along the streamwise direciton. Thus, we have

$$\frac{\partial}{\partial s}\left(p+\frac{1}{2}\rho V^2\right)=0\Rightarrow p+\frac{1}{2}\rho V^2=\text{constant along a streamline} \tag{8.20}$$

in steady, inviscid, incompressible flow. Further, when a steady, inviscid, and incompressible flow has no vorticity (e.g. if the freestream has uniform velocity) then,

$$\nabla\left(p+\frac{1}{2}\rho V^2\right)=0\Rightarrow p+\frac{1}{2}\rho V^2=\text{constant everywhere} \tag{8.21}$$

In particular, for this problem we can evaluate the total pressure in the freestream and we have,

$$p+\frac{1}{2}\rho V^2=p_\infty+\frac{1}{2}\rho V_\infty^2 \tag{8.22}$$

Equations (8.20)-(8.22) are refered to Bernoulli's equation after its originator Daniel Bernoulli who published this classic result in 1738. Commonly, the term $\frac{1}{2}\rho V^2$ is refered to as the *dynamic pressure* while p is the static pressure (or simply the pressure).

8.2.5 Pressure coefficient and Bernoulli's equation

2.8 8.2 8.3

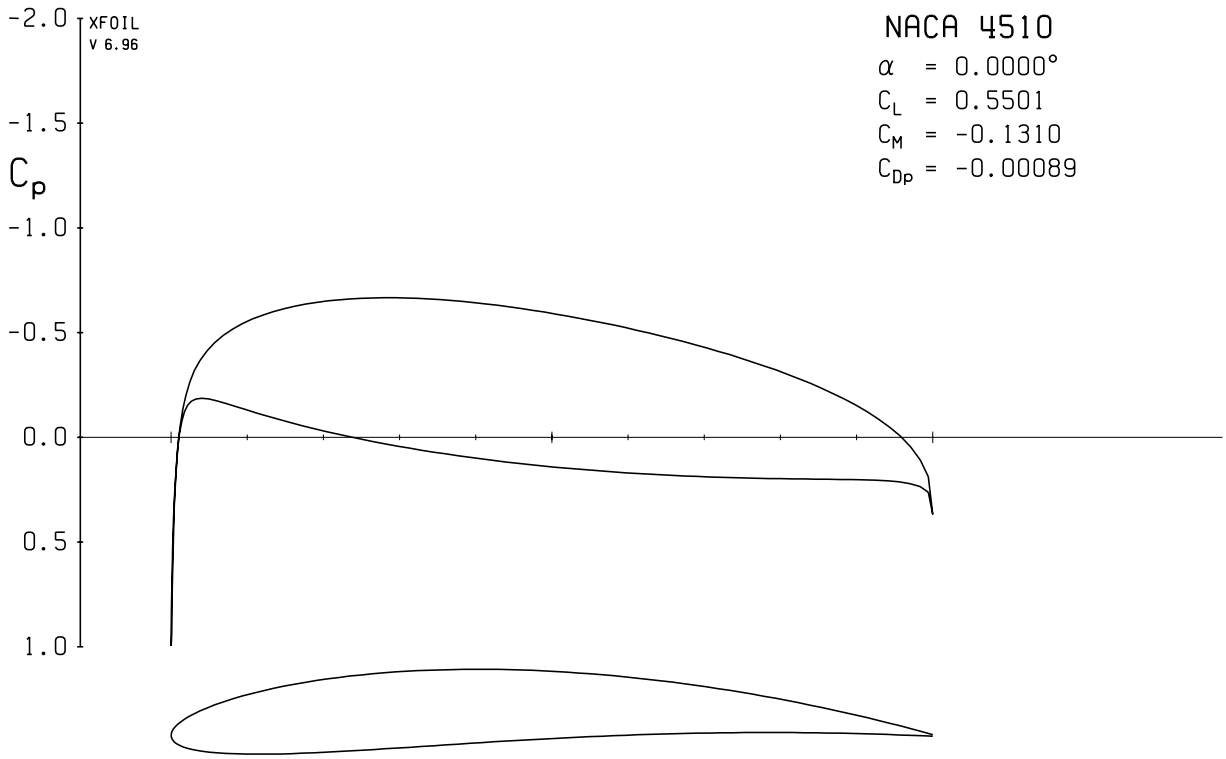
In the situation in which viscous effects are negligible and the freestream velocity and pressure are uniform, then Bernoulli's equation can be used to relate the C_p to the local flow speed, giving,

$$C_p=1-\left(\frac{V}{V_\infty}\right)^2 \tag{8.23}$$

We note that at a stagnation point $C_p=1$ since $V=0$. Refering back to Figure 2.9, we can see the presence of the stagnation point at the leading edge of the airfoil (i.e. $x=0$) where $C_p=1$.

edXproblem: 8.2.6 Velocity and pressure coefficient relationship for incompressible flow over an airfoil

8.2 | 2.8



Consider the C_p distribution for the NACA 4510 at $\alpha = 0°$ in incompressible potential flow as shown in Figure 2.9 and repeated in the figure above.

Estimate V/V_∞ on the upper surface of the airfoil at $x/c = 0.3$ (note that dash marks along the x axis are in increments of 0.1 starting at $x/c = 0$ and ending at $x/c = 1$). Use two decimal points so that your answer has the form X.YZ.

Estimate V/V_∞ on the lower surface of the airfoil at $x/c = 0.8$ Use two decimal points so that your answer has the form X.YZ.

edXsolution

Video Link

8.2.7 The fallacy of the equal transit time theory of lift generation

7.2 2.4

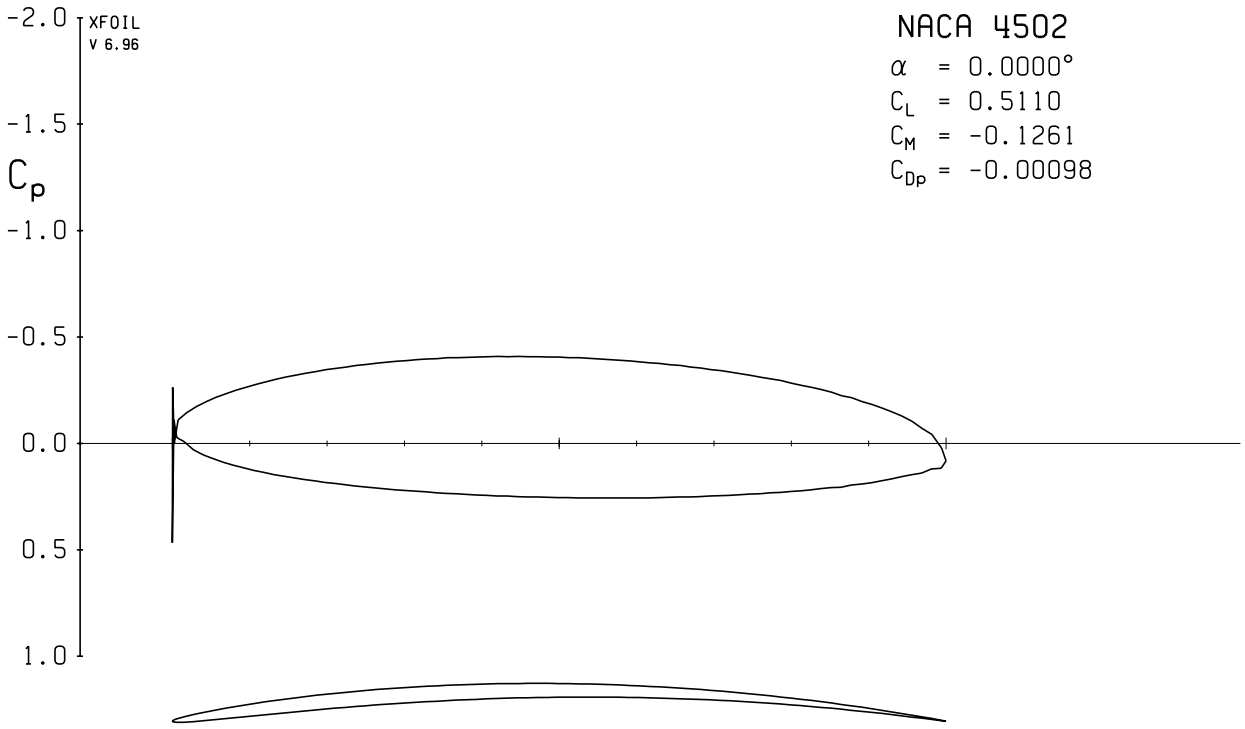
As we have seen in Module 7, the generation of lift can be explained using streamline curvature arguments. A common misconception with respect to the generation of lift is the so-called equal-transit-time theory of lift generation. This theory has the following basic components: (1) the flow that impinges on the leading edge and traverses along the upper surface must reach the trailing edge in the same amount of time as flow that impinges on the leading edge and traverses along the lower surface, i.e. the equal transit time assumption, (2) the upper surface of an airfoil is longer than the lower surface of an airfoil and thus combined with the equal transit time assumption, the velocity on the upper surface must be faster than that on lower surface, and (3) applying Bernoulli's equation demonstrates that the pressure on the lower surface is higher than that on the upper surface because the lower surface air velocity is slower than upper surface air velocity. Hence, lift is generated. This seemingly plausible theory is incorrect in both Step (1) and (2). Step (3) is just Bernoulli's equation and there is nothing wrong with Bernoulli's equation.

The problem with (1) is that there is absolutely no physical principle which requires the flow that travels along the upper surface to traverse the airfoil in the same time as the flow along the lower surface.

The problem with (2) is that even very thin airfoils generate lift. In fact, an airfoil that is infinitesimally thin can generate lift as long as it is curved and/or at an angle of attack. Even for airfoils with typical amounts of thickness (say 5% to 20%), the length of the upper and lower surfaces will be within a few percent of each other.

edXproblem: 8.2.8 Transit times on a NACA 4502

8.2 | 2.4 | 7.2



Consider the NACA 4502 airfoil in incompressible, potential flow at $\alpha = 0°$. The pressure distribution is shown above. The upper surface has a length of $1.007c$ and the lower surface has a length of $1.003c$.

Estimate $T_u V_\infty / c$ where T_u is the transit time of a fluid element from the leading edge to trailing edge on the upper surface. Report your answer rounded to the nearest tenth, i.e., an answer of 1.234 should be entered as 1.2.

Estimate $T_l V_\infty / c$ where T_l is the transit time of a fluid element from the leading edge to trailing edge on the lower surface. Report your answer rounded to the nearest tenth, i.e., an answer of 1.234 should be entered as 1.2.

edXsolution

Video Link

8.3 Potential Flow Modeling

8.3.1 Governing equations and the velocity potential

8.4

In the next two modules, we will assume that the flow around a body can be approximated as,

- Steady: the properties of the flow do not depend on time
- Inviscid: viscous stresses are assumed negligible
- Incompressible: the density is assumed constant
- Uniform freestream flow: the flow properties far upstream of the body are uniform
- Irrotational: the vorticity is zero *essentially everywhere* in the flow

In this section on Potential Flow Modeling, we will remain general to both two-dimensional and three-dimensional as the basic governing equations, boundary conditions, and modeling approach do not change between two- and three-dimensional flows. In the rest of this module and the next, we will solely focus on two-dimensional flows.

As you can see in the list of assumptions, the statement of irrotationality is qualified as the vorticity being zero *essentially everywhere*. This qualification is because we will allow vorticity at boundaries, which are not technically within the flow field, and in the three-dimensional flows we consider in the next module, along infinitely thin lines or sheets. In summary, we will use the term *irrotational* to describe flows that have zero vorticity almost everywhere, and proceed with caution.

The flow variables that we wish to determine are the pressure field $p(x, y, z)$ and the velocity field $\mathbf{V}(x, y, z)$. Far upstream of the body, the uniform conditions will be p_∞ for the pressure and,

$$\mathbf{V}_\infty = V_\infty \cos\alpha\, \hat{\mathbf{i}} + V_\infty \sin\alpha\, \hat{\mathbf{k}} \tag{8.24}$$

for the velocity vector where α is the angle of attack. We assume density ρ is constant and given.

With the assumptions stated, we can now determine $p(x, y, z)$ and $\mathbf{V}(x, y, z)$ using the statements of conservation of mass and momentum. Recall that the conservation of mass for an incompressible flow is,

$$\nabla \cdot \mathbf{V} = 0 \tag{8.25}$$

Since the flow has zero vorticity (because of our irrotational assumption), this means that the velocity vector field can be written as the gradient of a scalar function. This is a general result from vector calculus, that is a vector field with zero curl can always be written as the gradient of a scalar field. Using this, we can define a scalar field, $\phi(x, y, z)$, as,

$$\mathbf{V} = \nabla\phi \tag{8.26}$$

which we will call the velocity potential, or just the potential for short. Substituting this into Equation (8.25) produces the conservation of mass in terms of the velocity potential,

$$\nabla \cdot (\nabla\phi) = 0 \tag{8.27}$$

$$\nabla^2\phi = 0 \tag{8.28}$$

where this partial differential equation for ϕ is known as Laplace's equation, and ∇^2 is called the Laplacian and is defined as,

$$\nabla^2 \equiv \frac{\partial^2}{\partial x^2} + \frac{\partial^2}{\partial y^2} + \frac{\partial^2}{\partial z^2} \tag{8.29}$$

The conservation of momentum reduces to the Bernoulli equation, as derived in Equation (8.22), and repeated here,

$$p + \frac{1}{2}\rho V^2 = p_\infty + \frac{1}{2}\rho V_\infty^2 \tag{8.30}$$

The basic process for determining $\mathbf{V}$ and p then is

1 Solve Equation (8.28) for ϕ

2 Determine the velocity from Equation (8.26)

3 Find the pressure from Bernoulli's equation, Equation (8.30)

edXproblem: 8.3.2 Properties of a potential velocity field

8.4

Given a function $\phi(x, y, z)$ with first and second derivatives that are finite, and the associated steady velocity field $\mathbf{V} = \nabla\phi$, the velocity field (select all that are true):

edXsolution

Video Link

8.3.3 Boundary conditions

8.4

In order to solve Equation (8.28), boundary conditions are needed on ϕ. The boundaries of concern in our application will be on the surface of the body and far away from the body (in what we will refer to as the farfield). Mathematically, Laplace's equation allows only one boundary condition to be set on ϕ at any point on the boundary of the domain.

At a solid surface, we will require that the flow must be tangent to the surface, that is, the flow cannot enter the surface. Thus, flow tangency on a stationary surface requires that the component of the velocity normal to the surface is zero,

$$\mathbf{V} \cdot \hat{\mathbf{n}} = 0 \tag{8.31}$$

where $\hat{\mathbf{n}}$ is the normal to the surface. Substituting in the potential, the flow tangency boundary condition becomes,

$$\nabla\phi \cdot \hat{\mathbf{n}} = \frac{\partial \phi}{\partial n} = 0 \text{ at a solid surface.} \tag{8.32}$$

In the farfield (as $|\mathbf{x}| \to \infty$), we will assume that the flow velocity in the freestream direction returns to $\mathbf{V}_\infty$,

$$\mathbf{V} \cdot \mathbf{t}_\infty = V_\infty \text{ as } |\mathbf{x}| \to \infty \tag{8.33}$$

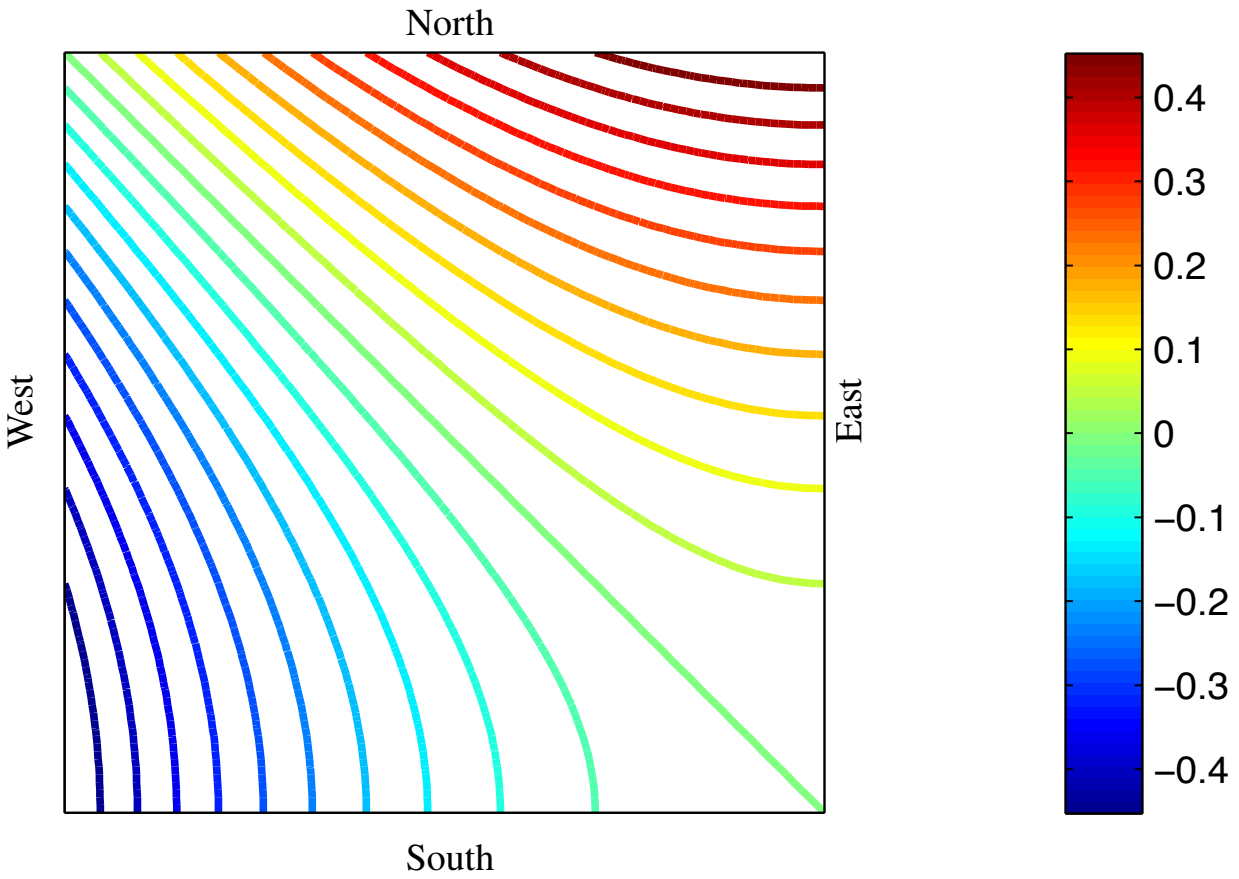
where $\mathbf{t}_\infty \equiv \mathbf{V}_\infty / V_\infty$ is the unit vector in the direction of the freestream. In terms of the potential, this boundary condition is,

$$\nabla\phi \cdot \mathbf{t}_\infty = V_\infty \text{ as } |\mathbf{x}| \to \infty \tag{8.34}$$

This farfield boundary condition permits non-zero velocity perturbations in the plane normal to the freestream direction. However, in two-dimensional steady potential flows on unbounded domains, all components of the velocity perturbations can be shown to approach zero in the farfield (we will see this in the Embedded Question in Section 8.5.3 of the next module). In three-dimensional flows, perturbations can exist normal to the freestream and are an important feature of these flows. Specifically, a physical example of how these velocity perturbations can be non-zero is the vortex wake system downstream of a lifting body in three-dimensional flows (often associated with the wing tip vortex). In this case, the vortical motion far downstream of the body will be swirling about the freestream direction.

edXproblem: 8.3.4 Equipotential lines and flow tangency

8.4



The figure above shows equipotential lines (i.e. lines along which ϕ is constant) for a two-dimensional incompressible potential flow. In this problem, you must use the equipotential lines to determine which boundaries the flow is entering the domain, tangent to the boundary, or exiting the domain.

For each boundary, select the correct answer:

edXsolution

Video Link

edXproblem: 8.3.5 Potential for corner flow

8.4

In Problems 6.2.8 and 6.2.9, we considered a corner flow where the velocity was given by,

$$u = -x \tag{8.35}$$
$$v = y \tag{8.36}$$

This flow is in fact irrotational (you might try to verify this) and therefore the velocity potential exists. Determine the velocity potential for this velocity field. Note that an arbitrary constant can be added to any potential since the velocity would be unaffected by the constant (because the gradient of a constant is zero). To make the potential unique, for this problem set $\phi = 0$ at the origin, $\phi(x = 0, y = 0) = 0$.

Enter the formula for ϕ (hint: it will be a function of x and y).

edXsolution

Video Link

8.3.6 Modeling approach

8.4 8.5

The approach used in potential flow modeling in aerodynamics is based on the principle of linear superposition. Let's consider two different potentials ϕ_1 and ϕ_2 both of which satisfy the conservation of mass (i.e. Laplace's equation),

$$\nabla^2\phi_1 = 0 \tag{8.37}$$
$$\nabla^2\phi_2 = 0 \tag{8.38}$$

Now, let us add these two potentials together including an arbitrary weighting to each, to define a new potential,

$$\phi_{\text{new}} = c_1\phi_1 + c_2\phi_2 \tag{8.39}$$

where c_1 and c_2 are arbitrary constants. This new potential can be shown to satisfy the conservation of mass as well,

$$\nabla^2\phi_{\text{new}} = \nabla^2\left(c_1\phi_1 + c_2\phi_2\right) \tag{8.40}$$
$$= \nabla^2\left(c_1\phi_1\right) + \nabla^2\left(c_2\phi_2\right) \tag{8.41}$$
$$= c_1\nabla^2\phi_1 + c_2\nabla^2\phi_2 \tag{8.42}$$
$$= 0 \tag{8.43}$$

This generalizes to an arbitrary number of potentials such that if ϕ is defined as,

$$\phi = \sum_{i=1}^{N} c_i\phi_i \tag{8.44}$$

where $\nabla^2\phi_i = 0$ for all i, then $\nabla^2\phi = 0$. This means that the flow field arising from any linear combination of ϕ_i will satisfy conservation of mass.

Let's get a little more specific and introduce our first (and simplest) potential flow. That is, the potential for a uniform velocity of $\mathbf{V}_\infty$. We will label this velocity potential as ϕ_∞,

$$\phi_\infty \equiv xV_\infty\cos\alpha + zV_\infty\sin\alpha \tag{8.45}$$

Then, taking the gradient of ϕ_∞, the velocity of this potential is,

$$\mathbf{V} = \nabla\phi_\infty = V_\infty\cos\alpha\hat{\mathbf{i}} + V_\infty\sin\alpha\hat{\mathbf{k}} \tag{8.46}$$

Thus, ϕ_∞ represents a uniform flow at an angle α and speed V_∞.

Now, we consider the following linear combination of potentials,

$$\phi = \phi_\infty + \sum_{i=1}^{N} c_i\phi_i \tag{8.47}$$

And, as before we assume that $\nabla^2\phi_i = 0$. Further, we assume that the ϕ_i also satisfy,

$$\nabla\phi_i\cdot\mathbf{t}_\infty = 0 \text{ as } |\mathbf{x}| \to \infty \tag{8.48}$$

In other words, the ϕ_i do not perturb the farfield velocity along the freestream direction. If we can find such ϕ_i, then the ϕ defined by Equation (8.47) will satisfy the farfield boundary condition (given by Equation 8.34) for any values of c_i (you might try to do this proof yourself!). This means that

the c_i values can then be freely chosen to satisfy the flow tangency condition at the solid boundaries for the body of interest.

These ϕ_i are the building blocks for approximating our aerodynamic flows. The key then to this modeling approach is to find the ϕ_i which satisfy Laplace's equation and the farfield boundary condition in Equation (8.48). We consider this in the next section for two-dimensional flows and along the way encounter some classic potential flows.

edXproblem: 8.3.7 Linear superposition in potential flow

8.4 8.5

In this question, we will consider two incompressible potential flows ϕ_A and ϕ_B that have the same uniform freestream pressure p_∞ and velocity vector $\mathbf{V}_\infty$. Specifically, the potentials have the following form,

$$\phi_A = \phi_\infty + \phi_a \tag{8.49}$$
$$\phi_B = \phi_\infty + \phi_b \tag{8.50}$$

where ϕ_∞ is given by Equation (8.45), ϕ_A and ϕ_B satisfy Laplace's equation, and ϕ_a and ϕ_b satisfy the farfield condition given by Equation (8.48). Also, since these are incompressible potential flows with uniform freestream conditions, Bernoulli's equation holds between any two points of the flow.

Now, define a third incompressible potential flow ϕ_C again having the same uniform freestream conditions where

$$\phi_C = \phi_\infty + \phi_a + \phi_b \tag{8.51}$$

Which of the following statements are true (check all that apply):

edXsolution

Video Link

8.4 Two-dimensional Nonlifting Flows

8.4.1 Introduction to nonlifting flows

8.4

In this section, we will consider potential flows in which the lift is zero. Then, in the next section, we introduce the additional concepts required to model lifting flows.

8.4.2 Cylindrical coordinate system

8.4

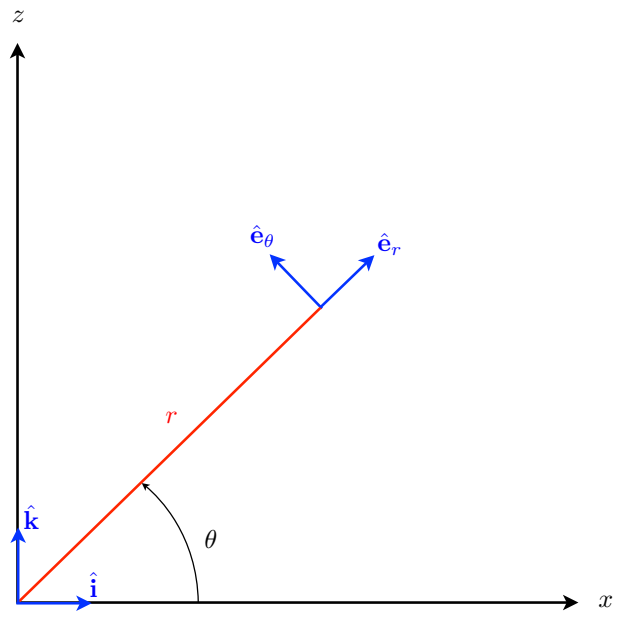


Figure 8.1: Two-dimensional cylindrical coordinate system

Many of the basic potential flows we will use as the building blocks of our aerodynamic models are easier to represent and analyze in cylindrical coordinates. As the two-dimensional coordinate system for our main application to airfoils is in the (x, z) plane (refer to Figure 2.5), we define the cylindrical coordinate system as shown in Figure 8.1. This gives the following relationship between (x, z) and (r, θ)

$$x = r\cos\theta \tag{8.52}$$
$$z = r\sin\theta \tag{8.53}$$

The unit vectors in the r and θ direction are,

$$\hat{\mathbf{e}}_r = \cos\theta\hat{\mathbf{i}} + \sin\theta\hat{\mathbf{k}} \tag{8.54}$$
$$\hat{\mathbf{e}}_\theta = -\sin\theta\hat{\mathbf{i}} + \cos\theta\hat{\mathbf{k}} \tag{8.55}$$

The radial and θ velocity components are related to u and w by,

$$u_r = u\cos\theta + w\sin\theta \tag{8.56}$$
$$u_\theta = -u\sin\theta + w\cos\theta \tag{8.57}$$

The gradient operator in cylindrical coordinates can be applied to ϕ to find u_r and u_θ,

$$u_r = \frac{\partial \phi}{\partial r} \tag{8.58}$$

$$u_\theta = \frac{1}{r}\frac{\partial \phi}{\partial \theta} \tag{8.59}$$

The divergence and curl of the velocity vector in cylindrical coordinates are,

$$\nabla \cdot \mathbf{V} = \frac{1}{r}\frac{\partial}{\partial r}\left(r u_r\right) + \frac{1}{r}\frac{\partial u_\theta}{\partial \theta} \tag{8.60}$$

$$\nabla \times \mathbf{V} = \left[\frac{1}{r}\frac{\partial u_r}{\partial \theta} - \frac{1}{r}\frac{\partial}{\partial r}\left(r u_\theta\right)\right]\hat{\mathbf{j}} \tag{8.61}$$

Finally, we note that Laplace's equation for ϕ in cylindrical coordinates is,

$$\nabla^2 \phi = \frac{1}{r}\frac{\partial}{\partial r}\left(r\frac{\partial \phi}{\partial r}\right) + \frac{1}{r^2}\frac{\partial^2 \phi}{\partial \theta^2} = 0 \tag{8.62}$$

8.4.3 Source

8.6

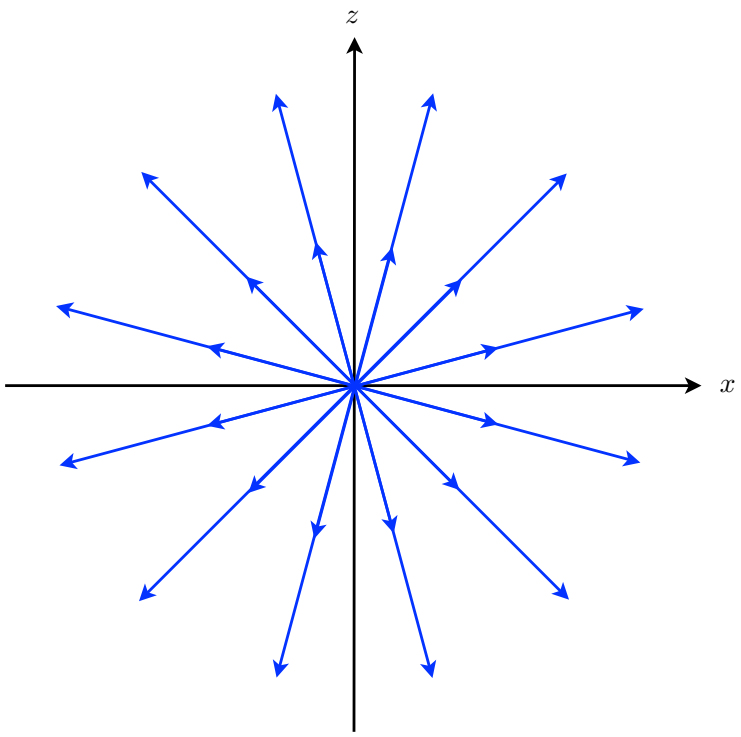


Figure 8.2: Streamlines for a point source

The first of our building blocks in two-dimensional potential flows is called a source and has the following potential and velocity field,

$$\phi = \frac{\Lambda}{2\pi}\ln r \tag{8.63}$$

$$u_r = \frac{\Lambda}{2\pi r} \tag{8.64}$$

$$u_\theta = 0 \tag{8.65}$$

where Λ is a scaling constant called the *source strength*. Note that the units of Λ are $(\text{length})^2/\text{time}$. As shown in Figure 8.2, the streamlines for the point source emit from the origin and are purely radial (since $u_\theta = 0$). Clearly, this means that the source emits mass at its origin. When $\Lambda < 0$, then the flow is drawn into the origin and in this case can be refered to as a *sink*.

The fact that a source produces mass would appear to be a violation of the conservation of mass. In the following video, we will explore this issue and a few others as we consider the source flow in more detail.

Video Link

Summarizing the main results of this video, we see that:

- A source emits mass at a rate of $\rho\Lambda$ per unit span.
- A source satisfies the conservation of mass except at its origin. That is $\nabla \cdot \mathbf{V} = 0$ everywhere in the flow expect at its origin. And, at the origin, $\nabla \cdot \mathbf{V}$ is infinite.

In some situations, it is useful to have the potential and velocity for a source in (x, z) coordinates. For completeness, we include those expressions here.

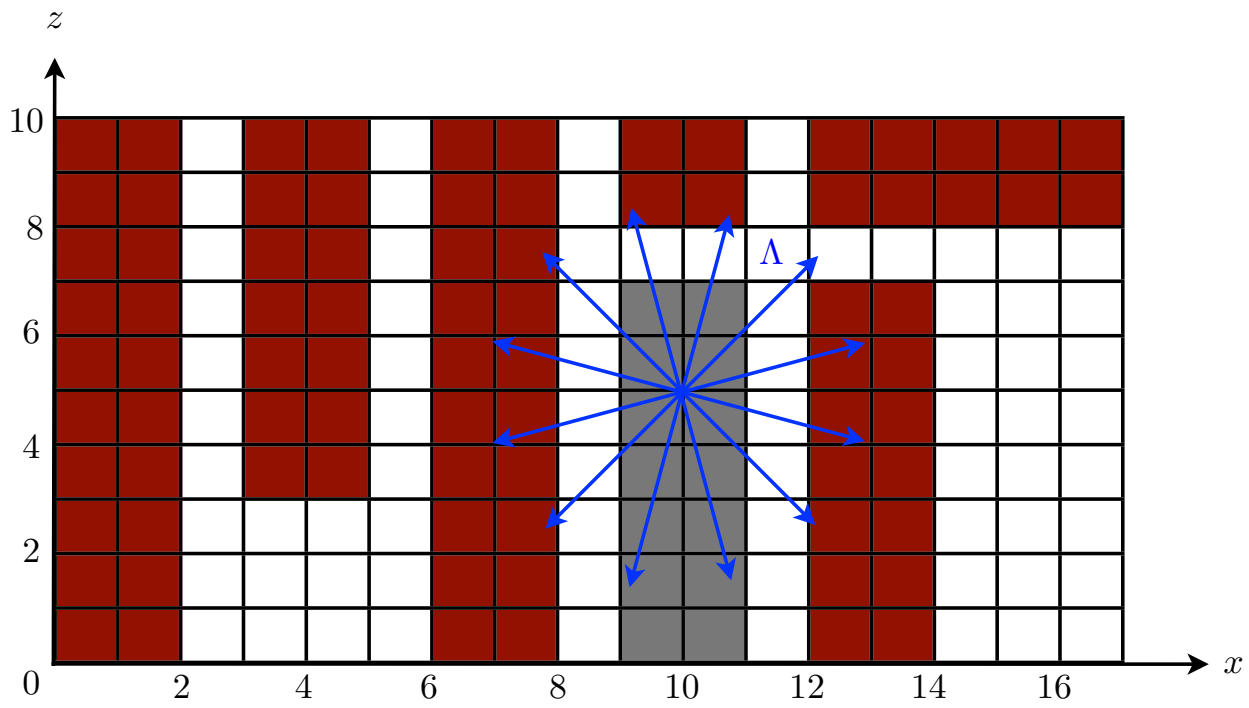
$$\phi = \frac{\Lambda}{2\pi} \ln \sqrt{x^2 + z^2} \tag{8.66}$$

$$u = \frac{\Lambda}{2\pi} \frac{x}{x^2 + z^2} \tag{8.67}$$

$$w = \frac{\Lambda}{2\pi} \frac{z}{x^2 + z^2} \tag{8.68}$$

edXproblem: 8.4.4 Calculating mass flow rate for a source

8.6



Consider the flow created by a source with strength $\Lambda = 11$ smoot^2/s as shown in the above figure. Note that a *smoot* is a unit of length occasionally used at MIT and the coordinate system in the figure is in smoots. (If you want to know more about smoots, do an Internet search). The fluid has a density of 7 kg/smoot^3. Determine the net mass flow rate (per span) out of the surfaces of the rectangular control volumes shown in the figure (in other words, determine $\int \rho \mathbf{V} \cdot \hat{\mathbf{n}} \, \mathrm{d}S$ for each control volume, where $\hat{\mathbf{n}}$ is an outward point normal). Provide your answers in units of kg/smoot-s and use two significant digits.

What is the net mass flow rate out of the control volume with corners at $(0, 0)$ and $(2, 10)$?

What is the net mass flow rate out of the control volume with corners at $(3, 3)$ and $(5, 10)$?

What is the net mass flow rate out of the control volume with corners at $(6, 0)$ and $(8, 10)$?

What is the net mass flow rate out of the control volume with corners at $(9, 0)$ and $(11, 7)$?

What is the net mass flow rate out of the control volume with corners at $(9, 8)$ and $(11, 10)$?

What is the net mass flow rate out of the control volume with corners at $(12, 0)$ and $(14, 7)$?

What is the net mass flow rate out of the control volume with corners at $(12, 8)$ and $(17, 10)$?

edXsolution

Video Link

8.4.5 Flow over a Rankine oval

8.5 8.6

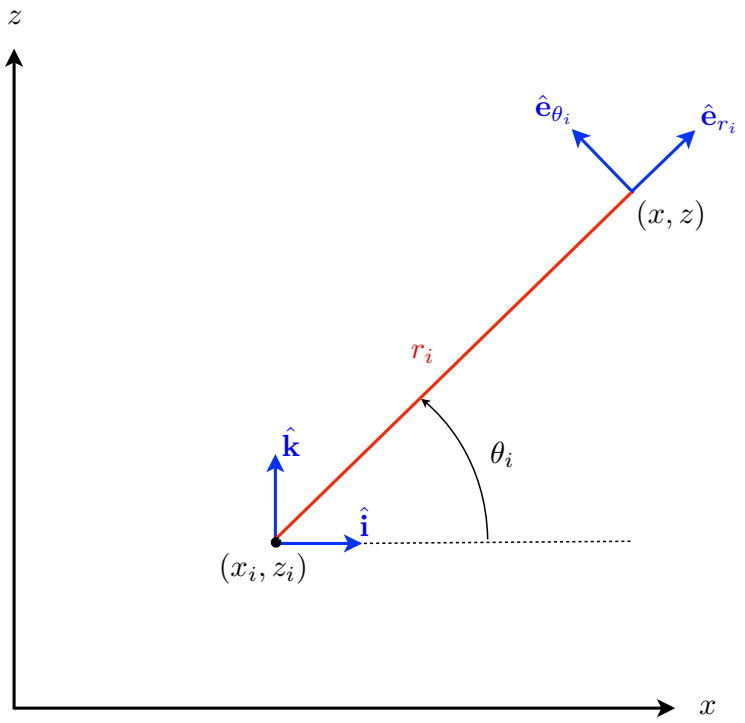


Figure 8.3: Two-dimensional cylindrical coordinate system about a point (x_i, z_i).

In this section, we describe the potential flow over a shape known as the Rankine oval. It will be our first potential flow in which we combine multiple potentials. In this case, we will combine a freestream at zero angle of attack with two sources. A source with positive strength Λ will be located at $(-l, 0)$ and a source with negative strength $-\Lambda$ (in others words, this is a sink) will be located at $(l, 0)$. To do this, we will need to translate the source potentials from the origin as they are given in Equations (8.63)-(8.65), to $(\pm l, 0)$. We define the coordinate system about a point (x_i, z_i) as shown in Figure 8.3, where

$$r_i = \sqrt{(x - x_i)^2 + (z - z_i)^2} \tag{8.69}$$

$$\theta_i = \arctan \frac{z - z_i}{x - x_i} \tag{8.70}$$

Using this coordinate system, a source of strength Λ_i located at point (x_i, z_i) has the following potential and velocity,

$$\phi = \frac{\Lambda_i}{2\pi} \ln r_i \tag{8.71}$$

$$u_{r_i} = \frac{\Lambda_i}{2\pi r_i} \tag{8.72}$$

$$u_{\theta_i} = 0 \tag{8.73}$$

To emphasize, these radial and circumferential velocity components are in the $\hat{\mathbf{e}}_{r_i}$ and $\hat{\mathbf{e}}_{\theta_i}$ directions, not the radial and circumferential directions about the origin (in otherwords, not about $\hat{\mathbf{e}}_r$ and $\hat{\mathbf{e}}_\theta$).

The x and z velocity component expressions for these translated sources are,

$$\phi = \frac{\Lambda_i}{2\pi} \ln \sqrt{(x-x_i)^2 + (z-z_i)^2} \tag{8.74}$$

$$u = \frac{\Lambda_i}{2\pi} \frac{x-x_i}{(x-x_i)^2 + (z-z_i)^2} \tag{8.75}$$

$$w = \frac{\Lambda_i}{2\pi} \frac{z-z_i}{(x-x_i)^2 + (z-z_i)^2} \tag{8.76}$$

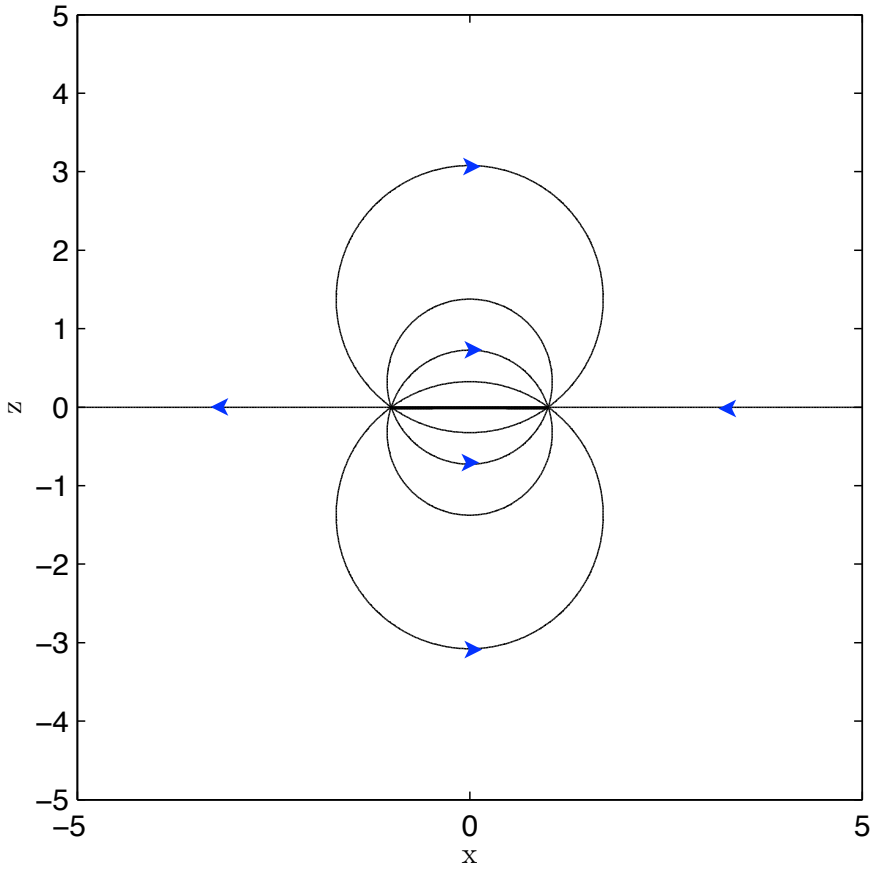


Figure 8.4: Streamlines for sources of strength $\Lambda = \mp 4$ located at $(\pm 1, 0)$.

Let's consider first the flow due to just the two sources. We will consider the specific case in which $\Lambda/(V_\infty l) = 4$. Non-dimensionalizing the velocities by V_∞ and the spatial coordinates by l, we will place the sources at $x = \pm 1$ (and $z = 0$) with strengths of ∓ 4. Figure 8.4 shows the flow induced only by the two sources. We can see that the flow is emitted from the source at $x = -1$ and is drawn into the source (which is acting as a sink) at $x = 1$.

Then, adding the freestream velocity produces the flow about a Rankine oval as shown in Figure 8.5. In the following video, we discuss this Rankine flow in more detail.

Video Link

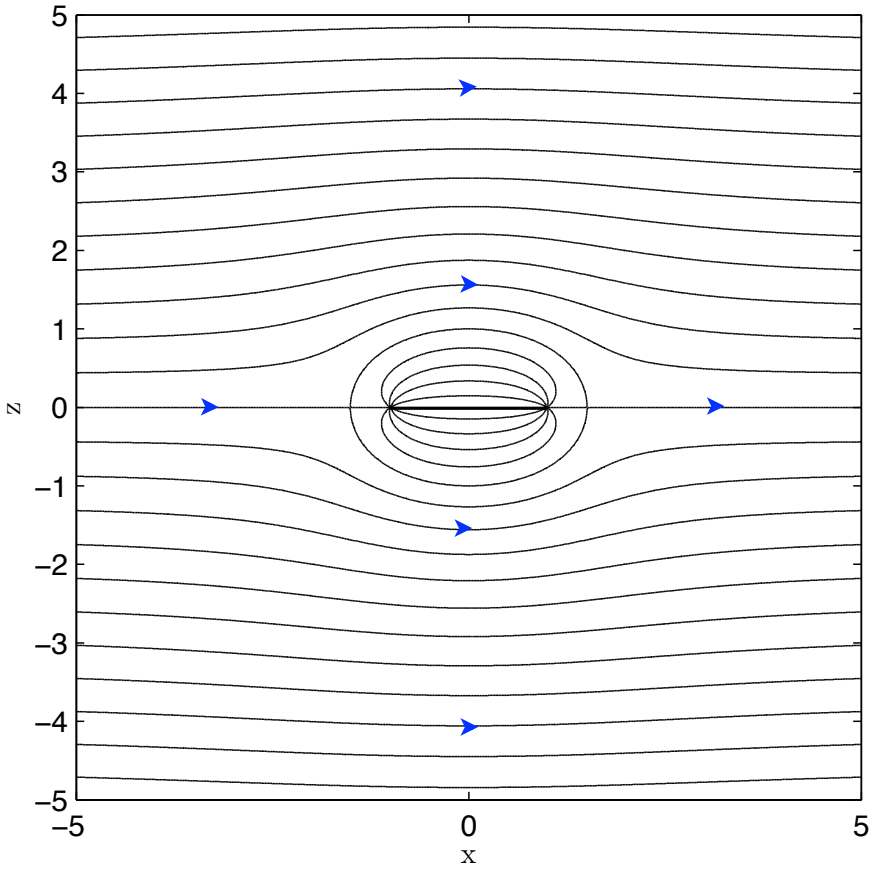


Figure 8.5: Streamlines for Rankine oval produced by a freestream flow and sources of strength $\Lambda = \mp 4$ located at $(\pm 1, 0)$.

edXproblem: 8.4.6 A new potential flow

8.4 8.6

Suppose we have a potential, $\phi(x, y, z)$ which satisfies the conservation of mass (Laplaces equation),

$$\nabla^2 \phi = 0 \tag{8.77}$$

A new potential ϕ_{new} can be defined that satisfies conservation of mass by setting ϕ_{new} equal to the x, y, or z derivative of ϕ. For example, suppose $\phi_{\text{new}} = \partial\phi/\partial x$. Applying the Laplacian to ϕ_{new} gives

$$\begin{aligned}
\nabla^2 \phi_{\text{new}} &= \left(\frac{\partial^2}{\partial x^2} + \frac{\partial^2}{\partial y^2} + \frac{\partial^2}{\partial z^2}\right) \phi_{\text{new}} && (8.78)\\
&= \left(\frac{\partial^2}{\partial x^2} + \frac{\partial^2}{\partial y^2} + \frac{\partial^2}{\partial z^2}\right) \left(\frac{\partial \phi}{\partial x}\right) && (8.79)\\
&= \frac{\partial}{\partial x}\left[\left(\frac{\partial^2}{\partial x^2} + \frac{\partial^2}{\partial y^2} + \frac{\partial^2}{\partial z^2}\right) \phi\right] && (8.80)\\
&= \frac{\partial}{\partial x}\left[\nabla^2 \phi\right] && (8.81)\\
&= \frac{\partial}{\partial x}\left[0\right] && (8.82)\\
&= 0 && (8.83)
\end{aligned}$$

In this embedded question, consider defining a new potential which is the x-derivative of a source,

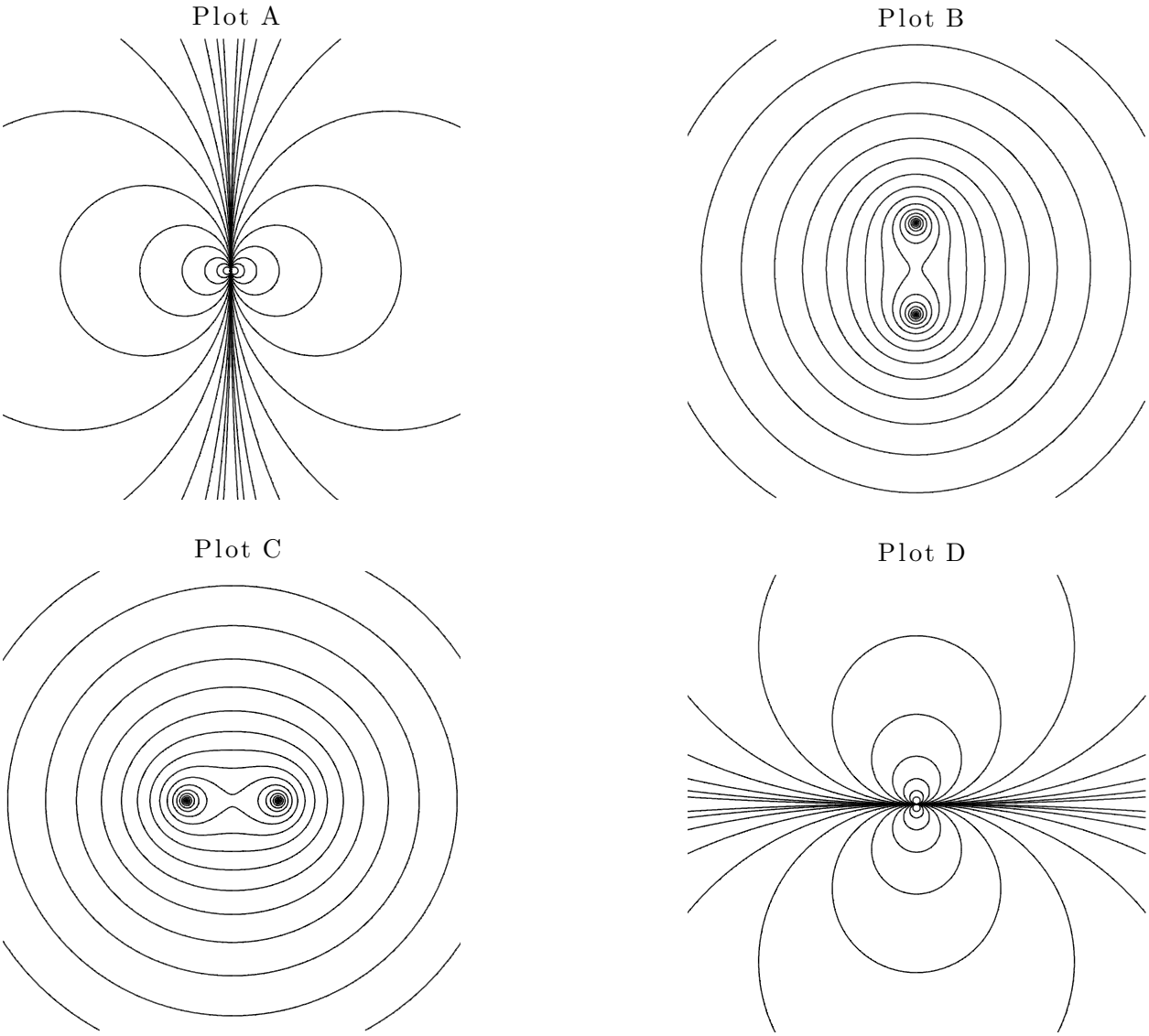
$$\phi_{\text{new}} = \frac{\Lambda_{\text{new}}}{2\pi} \frac{\partial}{\partial x} (\ln r) \tag{8.84}$$

where Λ_{new} will be the strength of this new potential.

The above graphs are possible streamline patterns, plotted in a square box centered on the origin. The streamlines of the flow corresponding to ϕ_{new} (assuming non-zero Λ_{new}) are:

edXsolution

Video Link



8.4.7 Doublet

8.5 8.6

Another building block potential flow is the doublet which has the following potential and velocities,

$$\phi = \frac{\kappa}{2\pi}\frac{\cos\theta}{r} = \frac{\kappa}{2\pi}\frac{x}{x^2+z^2} \tag{8.85}$$

$$u_r = -\frac{\kappa}{2\pi}\frac{\cos\theta}{r^2} \tag{8.86}$$

$$u_\theta = -\frac{\kappa}{2\pi}\frac{\sin\theta}{r^2} \tag{8.87}$$

$$u = \frac{\kappa}{2\pi}\frac{z^2-x^2}{(x^2+z^2)^2} \tag{8.88}$$

$$w = \frac{\kappa}{2\pi}\frac{-2xz}{(x^2+z^2)^2} \tag{8.89}$$

A common way that the doublet flow can be derived is by combining two sources at $(\pm l, 0)$ with strengths $\mp\Lambda$ (which is identical to the source-sink combination in the Rankine oval flow from

Section 8.4.5), and taking the limit as $l \to 0$ while holding $\kappa \equiv 2\Lambda l =$ constant. The potential for this flow is,

$$\phi = \lim_{l \to 0} \frac{\kappa}{4\pi l} \left[\ln \sqrt{(x+l)^2 + z^2} - \ln \sqrt{(x-l)^2 + z^2} \right] \tag{8.90}$$

Then, note that,

$$\lim_{l \to 0} \frac{1}{2l} \left[\ln \sqrt{(x+l)^2 + z^2} - \ln \sqrt{(x-l)^2 + z^2} \right] = \frac{\partial}{\partial x} \left(\ln \sqrt{x^2 + z^2} \right) = \frac{x}{x^2 + z^2} \tag{8.91}$$

Substituting this into Equation (8.90) gives the final result,

$$\phi = \frac{\kappa}{2\pi} \frac{x}{x^2 + z^2} = \frac{\kappa}{2\pi} \frac{\cos\theta}{r} \tag{8.92}$$

The streamlines of the doublet flow are shown in Figure 8.6. We also recommend returning to Embedded Question 8.4.6 to see the relationship between the doublet flow and ϕ_{new} studied in that problem.

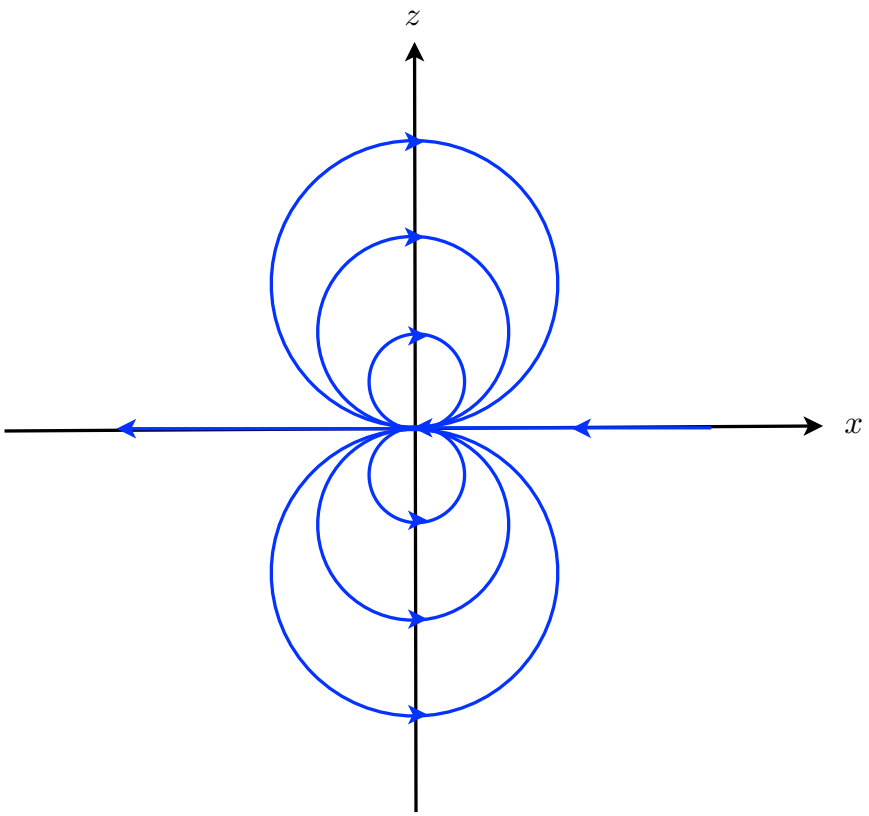


Figure 8.6: Streamlines for a doublet

8.4.8 Flow over a nonlifting cylinder

8.4 8.5 8.6 8.9

By combining a freestream (in the x-direction) with a doublet, the potential flow over a cylinder can be determined. First, we begin by determining the relationship between the doublet strength (κ), the freestream velocity (V_∞), and the radius of the cylinder (R). The potential and velocity for

this flow are,

$$\phi = V_\infty r\cos\theta + \frac{\kappa}{2\pi}\frac{\cos\theta}{r} \tag{8.93}$$

$$u_r = V_\infty \cos\theta - \frac{\kappa}{2\pi}\frac{\cos\theta}{r^2} \tag{8.94}$$

$$u_\theta = -V_\infty \sin\theta - \frac{\kappa}{2\pi}\frac{\sin\theta}{r^2} \tag{8.95}$$

On the surface of the cylinder, flow tangency requires $u_r(R,\theta) = 0$. Evaluating u_r at $r = R$ and enforcing $u_r = 0$ gives the doublet strength in terms of V_∞ and R,

$$u_r(R,\theta) = V_\infty \cos\theta - \frac{\kappa}{2\pi}\frac{\cos\theta}{R^2} = 0 \Rightarrow \kappa = 2\pi R^2 V_\infty \tag{8.96}$$

Thus, the potential and velocity for the flow around a cylinder of radius R in a freestream of velocity V_∞ are,

$$\phi = V_\infty R\cos\theta\left(\frac{r}{R} + \frac{R}{r}\right) \tag{8.97}$$

$$u_r = V_\infty \cos\theta\left(1 - \frac{R^2}{r^2}\right) \tag{8.98}$$

$$u_\theta = -V_\infty \sin\theta\left(1 + \frac{R^2}{r^2}\right) \tag{8.99}$$

The streamlines for this potential flow are shown in Figure 8.7.

On the surface of the cylinder where $r = R$, the velocity components and velocity magnitude are,

$$u_r = 0 \tag{8.100}$$

$$u_\theta = -2V_\infty \sin\theta \tag{8.101}$$

$$V = 2V_\infty |\sin\theta| \tag{8.102}$$

The pressure on the surface can then be determined using Bernoulli's equation,

$$p(R,\theta) = p_\infty + \frac{1}{2}\rho V_\infty^2 - \frac{1}{2}\rho V^2 \tag{8.103}$$

$$= p_\infty + \frac{1}{2}\rho V_\infty^2\left(1 - 4\sin^2\theta\right) \tag{8.104}$$

The corresponding pressure coefficient on the surface is,

$$C_p(R,\theta) = \frac{p(R,\theta) - p_\infty}{\frac{1}{2}\rho V_\infty^2} = 1 - 4\sin^2\theta \tag{8.105}$$

A plot of the surface velocity and pressure are shown in Figure 8.8. The velocity begins and ends at stagnation points and reaches a maximum speed which is $2V_\infty$ at the apex of the cylinder. The C_p has the corresponding behavior with $C_p = 1$ at the high pressure stagnation points and $C_p = -3$ at the low pressure apex.

We can see from the symmetry of the flow field that the lift and drag for this potential flow will be zero. For the lift, the flow is symmetric so that the pressure on the upper surface at some x is equal to the pressure on the lower surface at the same x. Thus, the net pressure force in the z direction will be zero as the upper and lower surface contributions will be equal magnitude but opposite directions. For the drag, the flow is also symmetric about the z axis (in otherwords, the pressure at x and $-x$ are the same). Thus, due to this front-to-back symmetry, the net pressure force in the x direction (which is the drag) will also be zero. We will derive these results in detail once we include the possibility of lift (by allowing for the cylinder to rotate) in the next module.

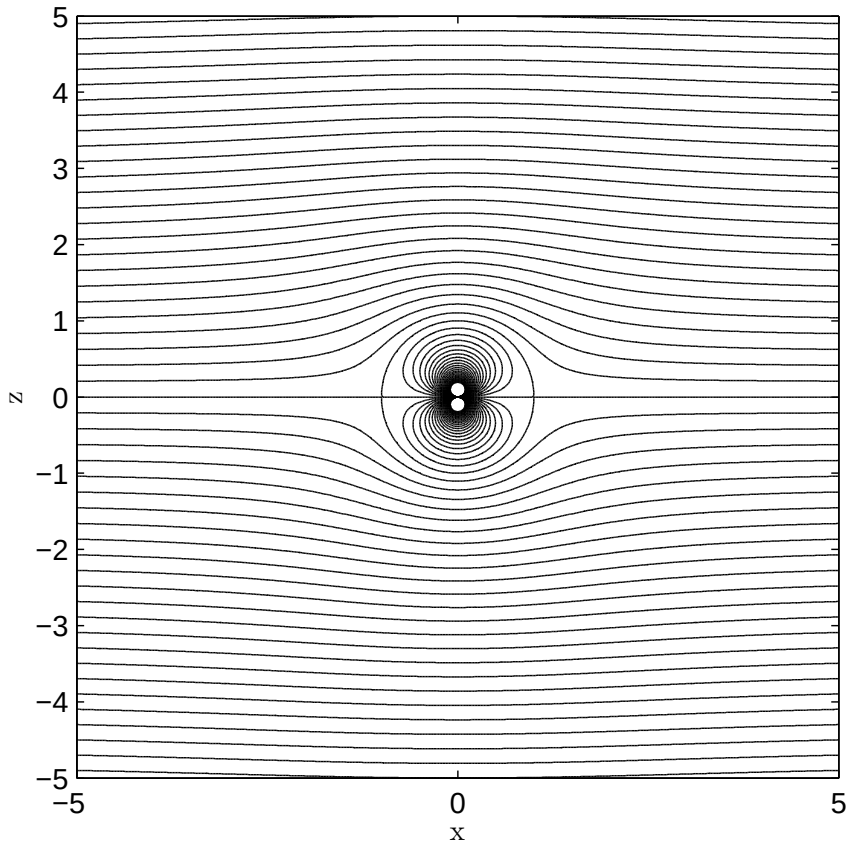


Figure 8.7: Streamlines for nonlifting flow over a cylinder

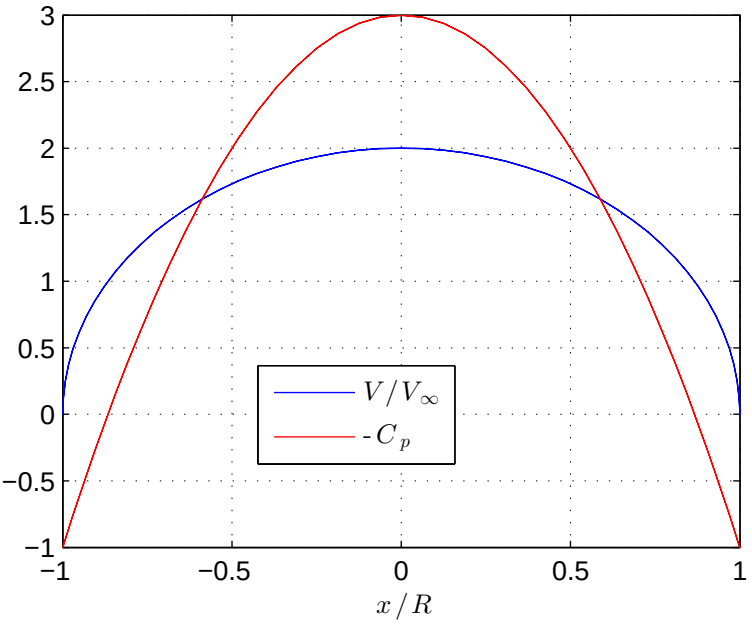


Figure 8.8: Surface V/V_∞ and C_p on a nonlifting cylinder.

8.5 Two-dimensional Lifting Flows

8.5.1 Point vortex

8.6

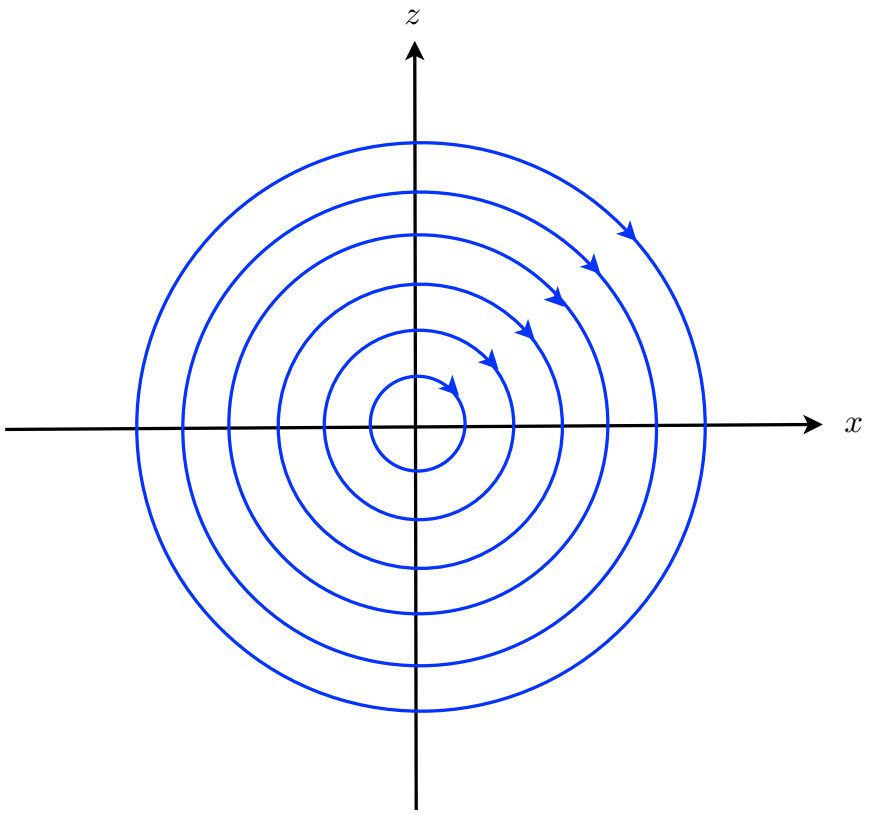


Figure 8.9: Streamlines for a point vortex

The last of our building block two-dimensional potential flows is called a point vortex and has the following potential and velocity field,

$$\phi = -\frac{\Gamma}{2\pi}\theta \tag{8.106}$$

$$u_r = 0 \tag{8.107}$$

$$u_\theta = -\frac{\Gamma}{2\pi r} \tag{8.108}$$

where Γ is a scaling constant called the *circulation* of the vortex. Note that the units of Γ are (length)^2/time. As shown in Figure 8.9, the streamlines of the point vortex are circles about the origin. The velocity becomes infinite as $r \to 0$.

The point vortex has zero vorticity everywhere except at its center where the vorticity is infinite. This is analogous to how $\nabla \cdot \mathbf{V}$ is infinite at the center of a point source, though everywhere else is equal to zero. The infinite vorticity at the origin of the point vortex can be derived using Stokes theorem. Stokes theorem applied to a two-dimensional velocity field (in the (x, z) plane) states that,

$$\oint_C \mathbf{V} \cdot \mathrm{d}\mathbf{l} = -\iint_S (\nabla \times \mathbf{V}) \cdot \hat{\mathbf{j}}\, \mathrm{d}S \tag{8.109}$$

where C is a contour surrounding an area S and the direction of integration around C is taken so

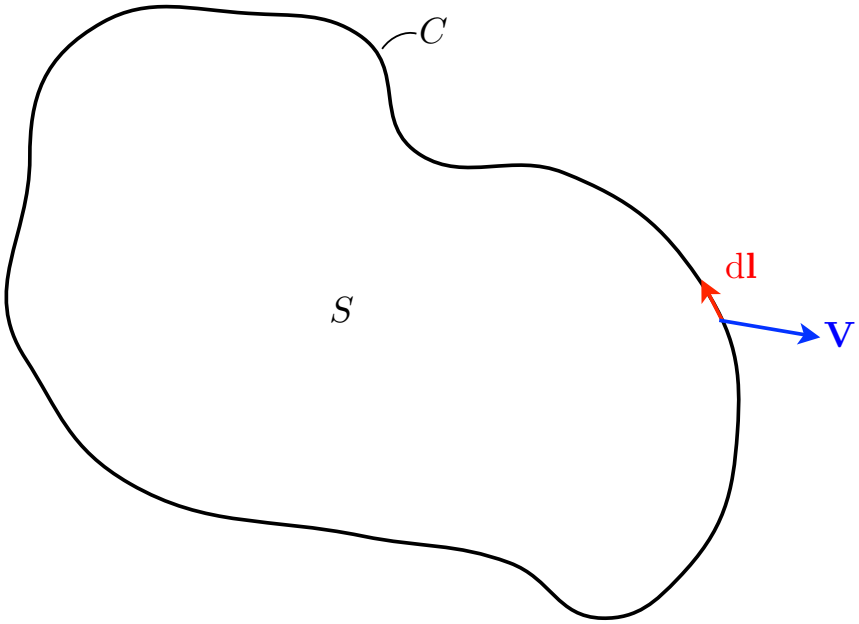


Figure 8.10: Contour integration used in applying Stokes Theorem

that the area is to the left of $d\mathbf{l}$ (see Figure 8.10). In the following video, we apply Stokes Theorem to a point vortex to show that

- $\oint_C \mathbf{V} \cdot d\mathbf{l} = -\Gamma$ for any contour surrounding the origin and $\oint_C \mathbf{V} \cdot d\mathbf{l} = 0$ for any contour that does not surround the origin.
- the vorticity is infinite at the origin.

Video Link

8.5.2 Lifting flow over a rotating cylinder

8.4 | 8.5 | 8.6 | 8.9 | 8.7 | 8.8

Since the vortical flow does not perturb the radial velocity, we may add a point vortex to the nonlifting cylinder flow and the flow will still be tangent to the cylinder. The resulting flow will produce lift. We can think of this flow as being a model for the flow around a spinning cylinder. The potential and velocity for the lifting cylinder flow is,

$$\phi = V_\infty R \cos\theta \left(\frac{r}{R} + \frac{R}{r}\right) - \frac{\Gamma}{2\pi}\theta \tag{8.110}$$

$$u_r = V_\infty \cos\theta \left(1 - \frac{R^2}{r^2}\right) \tag{8.111}$$

$$u_\theta = -V_\infty \sin\theta \left(1 + \frac{R^2}{r^2}\right) - \frac{\Gamma}{2\pi r} \tag{8.112}$$

The streamlines for the flow with $\Gamma/(2\pi V_\infty R) = \frac{1}{2}$ and 1 are shown in Figures 8.11 and 8.12, respectively.

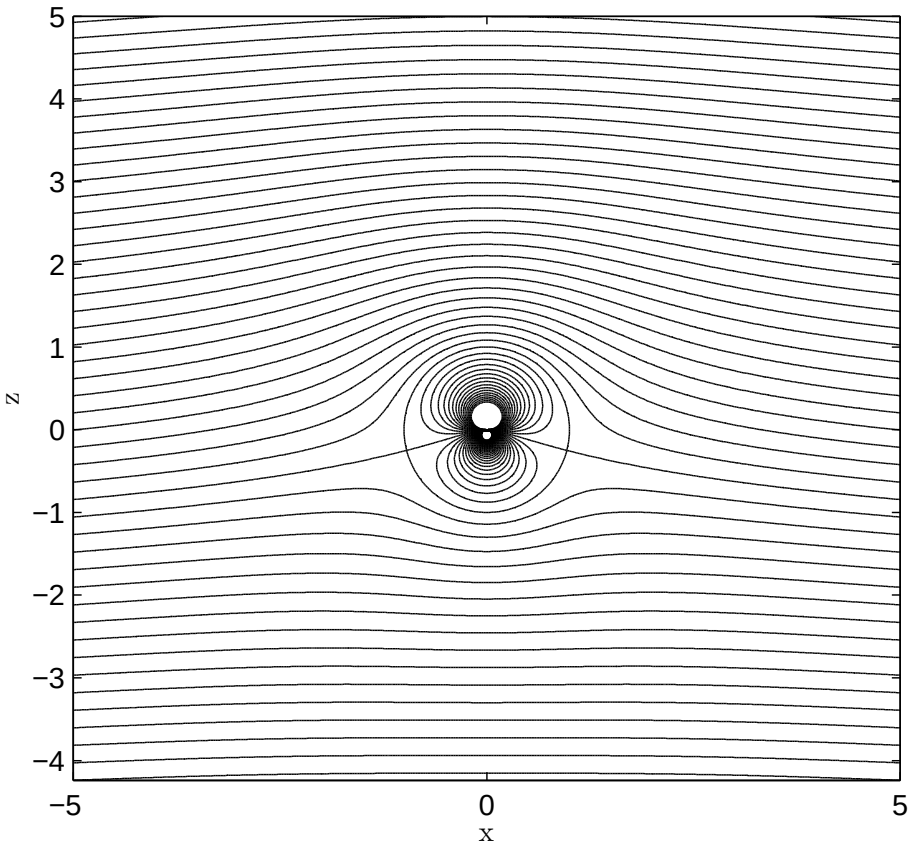


Figure 8.11: Streamlines for lifting cylinder flow for $\Gamma/(2\pi V_\infty R) = \frac{1}{2}$.

On the surface of the cylinder, the velocity components and velocity magnitude are,

$$u_r = 0 \tag{8.113}$$

$$u_\theta = -2V_\infty \sin\theta - \frac{\Gamma}{2\pi R} \tag{8.114}$$

$$V = \left| 2V_\infty \sin\theta + \frac{\Gamma}{2\pi R} \right| \tag{8.115}$$

$$\tag{8.116}$$

From this, we can determine the location of the stagnation points by determining the angles θ_{stag} at which $V = 0$, specifically,

$$2V_\infty \sin\theta_{\text{stag}} + \frac{\Gamma}{2\pi R} = 0 \tag{8.117}$$

$$\sin\theta_{\text{stag}} = -\frac{\Gamma}{4\pi V_\infty R} \tag{8.118}$$

Thus, there will be two stagnation points on the surface as long as $|\Gamma/(4\pi V_\infty R)| < 1$. For higher values, the stagnation point occurs off of the surface in the middle of the flow. We also note that $\sin\theta_{\text{stag}} = z_{\text{stag}}/R$ is the z location of the stagnation points. For the $\Gamma/(2\pi V_\infty R) = \frac{1}{2}$ case shown in Figure 8.11, the stagnation points are located at,

$$\frac{z_{\text{stag}}}{R} = -\frac{1}{4} \quad \text{or, equivalently} \quad \theta_{\text{stag}} = 194.5^\circ \text{ and } 345.5^\circ \tag{8.119}$$

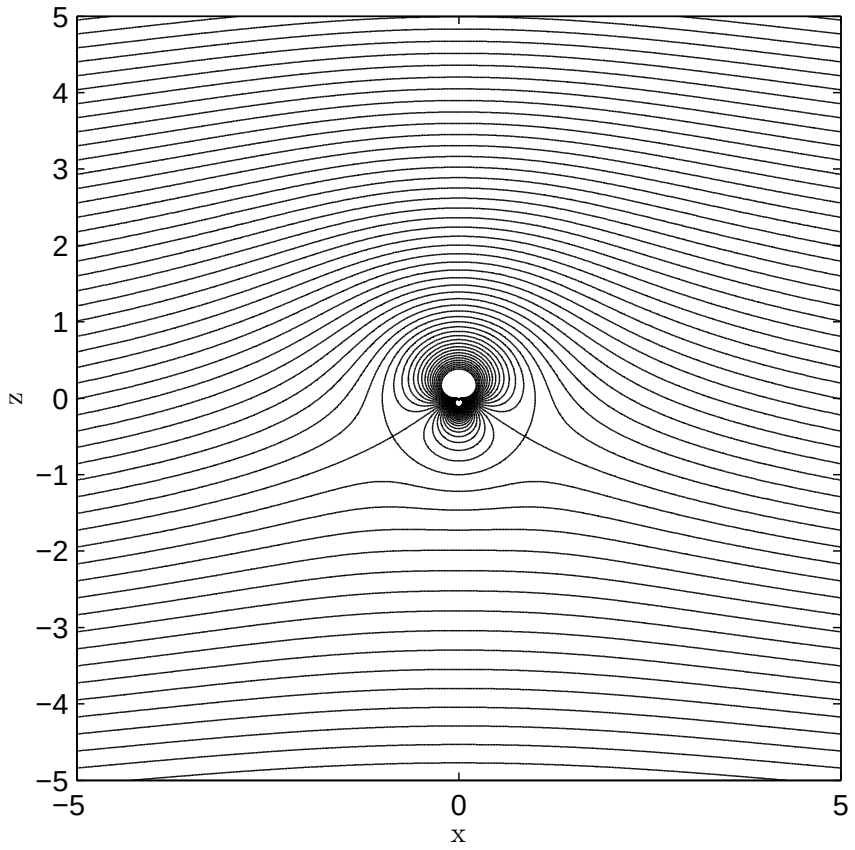


Figure 8.12: Streamlines for lifting cylinder flow for $\Gamma/(2\pi V_\infty R) = 1$.

For the $\Gamma/(2\pi V_\infty R) = 1$ case shown in Figure 8.12, the stagnation points are located at,

$$\frac{z_{\text{stag}}}{R} = -\frac{1}{2} \quad \text{or, equivalently} \quad \theta_{\text{stag}} = 210^\circ \text{ and } 330^\circ \tag{8.120}$$

The corresponding pressure coefficient on the surface is,

$$C_p(R,\theta) = \frac{p(R,\theta) - p_\infty}{\frac{1}{2}\rho V_\infty^2} = 1 - 4\sin^2\theta - \left(\frac{\Gamma}{2\pi V_\infty R}\right)^2 - \left(\frac{2\Gamma}{\pi V_\infty R}\right)\sin\theta. \tag{8.121}$$

In Figure 8.13, V and C_p on the cylinder surface are shown for $\Gamma/(2\pi V_\infty R) = 1$. The difference between the lower surface and upper surface C_p means that lift will be generated (since the pressures on the lower surface are higher than the pressures on the upper surface).

In the following video, we integrate the pressures around the surface of the cylinder to determine the lift and drag. The results of this analysis show that,

$$L' = \rho V_\infty \Gamma \quad \text{(Kutta-Joukowsky Theorem)} \tag{8.122}$$

$$D' = 0 \quad \text{(d'Alembert's Paradox)} \tag{8.123}$$

Thus, we see that the lift is directly related to the circulation and the drag is always zero on the cylinder for any values of Γ. In fact, both of these results are more general and apply to any shape in two-dimensional incompressible potential flows. The result that $L' = \rho V_\infty \Gamma$ is known as the Kutta-Joukowsky Theorem and we generalize it to other shapes in Sections 8.5.4 and 8.5.5. The result that $D' = 0$ is often referred to as d'Alembert's paradox and we discuss it further in Section 8.5.6.

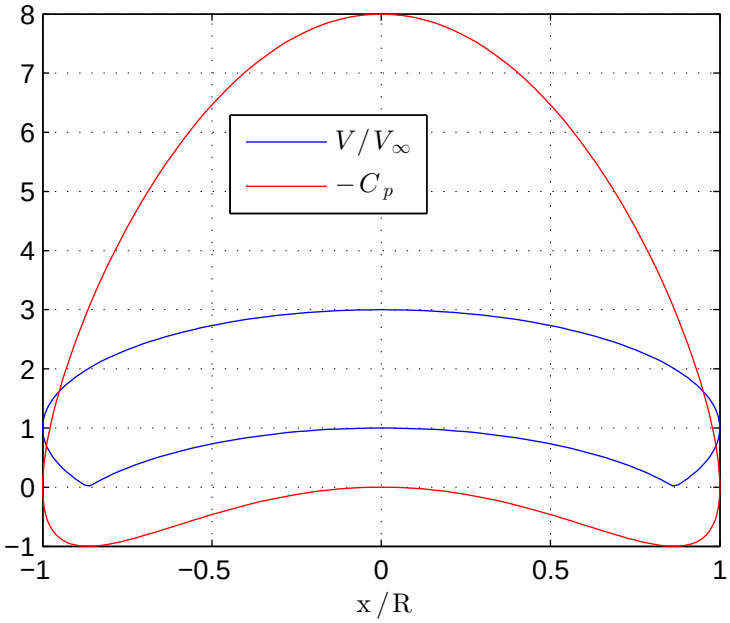


Figure 8.13: Surface V/V_∞ and C_p on a lifting cylinder for $\Gamma/(2\pi V_\infty R) = 1$.

Video Link

edXproblem: 8.5.3 Farfield velocity behavior of lifting and nonlifting flows

8.6 8.9

Using the diameter $(2R)$ as the reference length, the lift coefficient for the cylinder is defined as

$$c_l \equiv \frac{L'}{q_\infty (2R)} \tag{8.124}$$

Consider the flow around a cylinder with $c_l = 0$. Consider the flow speed V at $(x, z) = (0, 100R)$ and at $(0, 1000R)$. What is the ratio of:

$$\frac{(V - V_\infty)_{(x,z)=(0,1000R)}}{(V - V_\infty)_{(x,z)=(0,100R)}}? \tag{8.125}$$

Enter your answer with two significant digits of accuracy (X.YeP). For example, 1.2e3.

Consider the flow around a cylinder with $c_l = 1$. What is the ratio of:

$$\frac{(V - V_\infty)_{(x,z)=(0,1000R)}}{(V - V_\infty)_{(x,z)=(0,100R)}} \tag{8.126}$$

Enter your answer with two significant digits of accuracy (X.YeP). For example, 1.2e3.

edXsolution

Video Link

8.5.4 Circulation

8.6

As we have seen for the lifting flow on a cylinder, the strength of the point vortex Γ is called the circulation of the vortex and is directly related to the lift. The circulation is a more general concept than just the strength of the point vortex. The general definition of the circulation is,

$$\Gamma \equiv -\oint_C \mathbf{V} \cdot d\mathbf{l} \tag{8.127}$$

Suppose we have a point vortex with strength Γ_i. As we have seen in Section 8.5.1, $-\oint_C \mathbf{V} \cdot d\mathbf{l} = \Gamma_i$ for any contour containing the point vortex. Hence, the strength of the point vortex is equal to the circulation for a contour containing the vortex, i.e., $\Gamma \equiv -\oint_C \mathbf{V} \cdot d\mathbf{l} = \Gamma_i$.

8.5.5 Kutta-Joukowsky Theorem

8.7

For an incompressible steady two-dimensional potential flow with a uniform freestream, the lift on a body can be related to the circulation on a contour surrounding the body using the Kutta-Joukowsky Theorem,

$$\text{Kutta-Joukowsky Theorem: } L' = \rho V_\infty \Gamma \tag{8.128}$$

where Γ is the circulation defined by Equation (8.127) for a contour C surrounding the body. This result is true for any shape.

In the following video, we derive the Kutta-Joukowsky Theorem.

Video Link

8.5.6 d'Alembert's Paradox

8.8

For an incompressible steady two-dimensional potential flow with a uniform freestream, the drag on a body is zero:

$$\text{d'Alembert's Paradox: } D' = 0 \tag{8.129}$$

As with the Kutta-Joukowsky Theorem, this result is true for any shape. The proof of this result was derived in Homework Problem 8.6.1. This proof relied on the fact that the perturbation of the velocity (from $\mathbf{V}_\infty$) decays as x_w^{-1} downstream of the body. While we will not prove this rigorously in this course (though it can be proven), we observe that all of the fundamental solutions in two-dimensional flow decay at least as fast as x_w^{-1}. Specifically, the velocity for a source and vortex are proportional to r^{-1}. The velocity for the doublet is proportional to r^{-2}. The result is that the wake contributions to the drag integral will all be zero in two-dimensional incompressible flow.

8.6 Sample Problems

edXproblem: 8.6.1 Drag in incompressible potential flow

3.8 | 8.2 | 3.6

In Sample Problem 3.6.2, we found that the drag for a steady three-dimensional flow around a body in a uniform freestream was related to the wake properties by,

$$D = \iint_{S_w} (p_\infty - p_w)\, \mathrm{d}S + \iint_{S_w} \rho_w u_w (V_\infty - u_w)\, \mathrm{d}S. \tag{8.130}$$

Now, in this homework problem, we will further assume that the flow is inviscid and incompressible. Define the perturbation of the velocity components from the freestream as $\tilde{u}$, $\tilde{v}$, and $\tilde{w}$ such that the velocity components at any point are,

$$u(x,y,z) = \tilde{u}(x,y,z) + V_\infty \tag{8.131}$$
$$v(x,y,z) = \tilde{v}(x,y,z) \tag{8.132}$$
$$w(x,y,z) = \tilde{w}(x,y,z) \tag{8.133}$$

Show that the drag in this steady, inviscid, incompressible flow has the following form,

$$D = \rho_\infty \iint_{S_w} (c_1 \tilde{u}_w^{a_1} + c_2 \tilde{v}_w^{a_2} + c_3 \tilde{w}_w^{a_3})\, \mathrm{d}S \tag{8.134}$$

where a_1, a_2, and a_3, and c_1, c_2, and c_3 are constants. Specifically, determine that value of these constants.

1) What is the value of a_1?

2) What is the value of c_1?

3) What is the value of a_2?

4) What is the value of c_2?

5) What is the value of a_3?

6) What is the value of c_3?

Consider a two-dimensional (incompressible, steady, inviscid) flow in the (x,y) coordinate plane (so $w = 0$ and there is no variation with z).

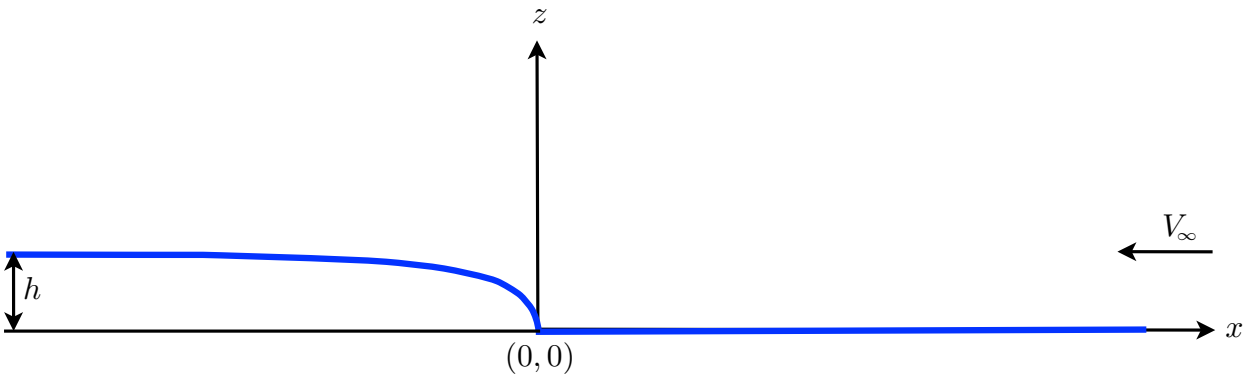
WARNING: sorry about using (x,y) for this two-dimensional flow when the coordinate system for the airfoil we have just chosen to be (x,z) in this module (see Figure 2.5). I should have used (x,z) but did not get the chance to make this self-consistent. Unfortunately, aerodynamic analysis of airfoils is often performed in (x,y), and I will unintentionally flip between (x,y) and (x,z) because of this. Interestingly (or maybe a better word would be frustratingly), even though the airfoil coordinate system is often chosen as (x,y), the spanwise coordinate is also often chosen as y (by the same author!) So, it is important to be a bit flexible and be prepared for y to be sometimes used for the two-dimensional airfoil coordinate, or sometimes the spanwise coordinate.

7) For this two-dimensional (x, y) flow, it is possible to show that $\tilde{u}$ and $\tilde{v}$ are proportional to x_w^{-1} where x_w is the distance along the x-axis from the airfoil to S_w. (We will show this in the next module). Which of the following options are possible for the value of drag (i.e. select all options that are possible)?

edXsolution

Video Link

8.7 Homework Problems



edXproblem: 8.7.1 Modeling the flow over a ridge

8.6

As shown in the figure, a glider is flying in the vicinity of a ridge, using the upward wind velocity caused by the ridge to remain aloft for a longer time. Specifically, in the following problem, you are to model the flow over the ridge by combining a point source and a freestream. The windspeed, V_∞, far away from the ridge is 15 m/s. The height of the ridge, h, is 400 m. The x-location x_s and strength Λ of the point source that generates the flow over the ridge is shown in the figure. Assume the source is located on the x-axis (i.e. $z_s = 0$). Using the coordinate system shown in the figure in which the foot of the ridge is at $(x, z) = (0, 0)$, answer the following questions.

1) What is Λ? Enter your answer in units of m^2/s with three digits of precision in the form X.YZeP.

2) What is x_s? Enter your answer in units of meters with three digits of precision in the form X.YZeP.

The glider pilot would prefer to fly in where the vertical velocity $w \geq 1m/s$. It can be shown that the region in the flow that meets this condition is a circle with radius r_{up} and centered at $(x_{\text{up}}, z_{\text{up}})$. Note that the circle will overlap with the ridge.

3) What is r_{up}? Enter your answer in units of meters with three digits of precision in the form X.YZeP.

4) What is x_{up}? Enter your answer in units of meters with three digits of precision in the form X.YZeP.

5) What is z_{up}? Enter your answer in units of meters with three digits of precision in the form X.YZeP.

edXsolution

Video Link

edXproblem: 8.7.2 Behavior of nonlifting flow over a cylinder

8.6 8.9

Throughout this problem, we will consider the incompressible potential nonlifting flow around the cylinder.

1) What is the pressure coefficient at $(x, z) = (-2R, 0)$? Enter your answer with two digits of precision in the form X.YeP.

2) What is the pressure coefficient at $(x, z) = (2R, 0)$? Enter your answer with two digits of precision in the form X.YeP.

3) What is the pressure coefficient at $(x, z) = (0, 2R)$? Enter your answer with two digits of precision in the form X.YeP.

4) What is the pressure coefficient at $(x, z) = (0, -2R)$? Enter your answer with two digits of precision in the form X.YeP.

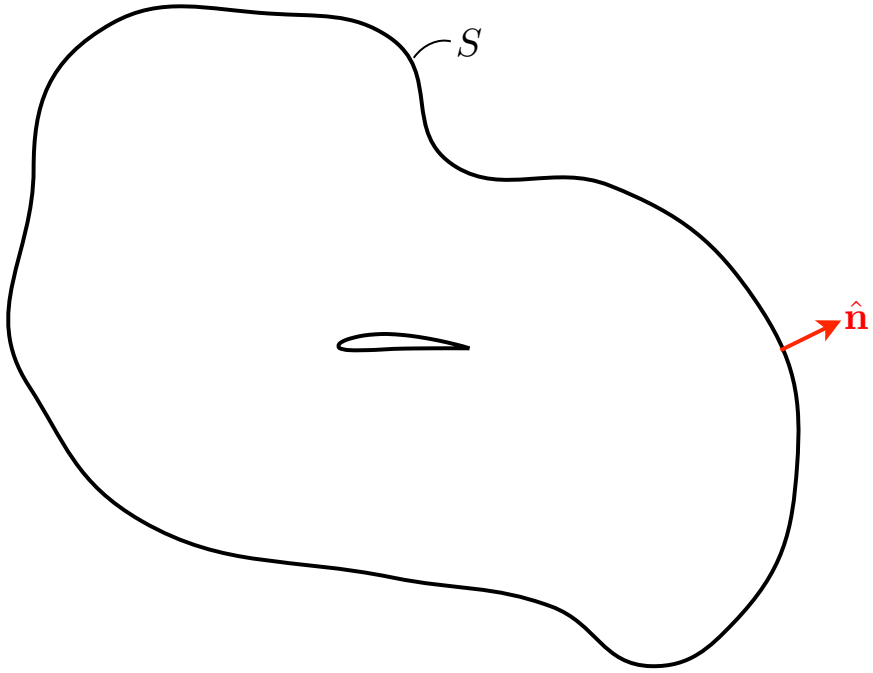
5) Determine the mass flow (per unit depth since this is a two-dimensional problem) between the apex of the cylinder at $(x, z) = (0, R)$ and a point a distance H above it at $(x, z) = (0, R + H)$. Enter your formula using the following symbols: d = ρ, V = V_∞, H = H, R = R.

6) For a streamline that starts far upstream at $(x, z) = (-\infty, R)$, what is the value of H/R for the streamline as it passes over the apex? Enter your answer with two digits of precision in the form X.YeP.

edXsolution

Video Link

edXproblem: 8.7.3 Lift and drag in 2D flow with application to an airfoil



1) Consider an inviscid, steady, two-dimensional flow around an airfoil here the freestream velocity is in the x-direction. The drag and lift on the airfoil can be related to the following integrals on an arbitrary surface S that surrounds the airfoil:

$$D' = \int_S \left(A_p \, p \, \hat{n} \cdot \hat{i} + A_u \, \rho u \vec{V} \cdot \hat{n} + A_w \, \rho w \vec{V} \cdot \hat{n} \right) \, \mathrm{d}S \tag{8.135}$$

$$L' = \int_S \left(B_p \, p \, \hat{n} \cdot \hat{k} + B_u \, \rho u \vec{V} \cdot \hat{n} + B_w \, \rho w \vec{V} \cdot \hat{n} \right) \, \mathrm{d}S \tag{8.136}$$

where A_p, A_u, A_w, B_p, B_u, and B_w are constants. Apply the integral conservation of momentum to determine the values of these six constants. Note that the normal $\hat{\mathbf{n}}$ is is a unit normal to S and points outward (i.e. away from the airfoil).

Enter the value of A_p:

Enter the value of A_u:

Enter the value of A_w:

Enter the value of B_p:

Enter the value of B_u:

Enter the value of B_w:

Let the airfoil be positioned near the origin at $(x, z) = (0, 0)$. Assuming the flow is incompressible, inviscid, and steady, the velocity distribution far away from the airfoil is given by,

$$\vec{V} = V_\infty \hat{i} - K\frac{V_\infty c}{2\pi r}\hat{e}_\theta \tag{8.137}$$

where $r = \sqrt{x^2 + z^2}$, c is the airfoil chord, K is a constant, and $\hat{e}_\theta$ is the unit vector in the θ direction. In the remainder of the questions for this problem, you are asked to enter formulas which should be expressed in terms of x, z, c, K, V_∞, and ρ. When entering the formulas, use x for x, z for z, c for c, K for K, V for V_∞ and d for ρ.

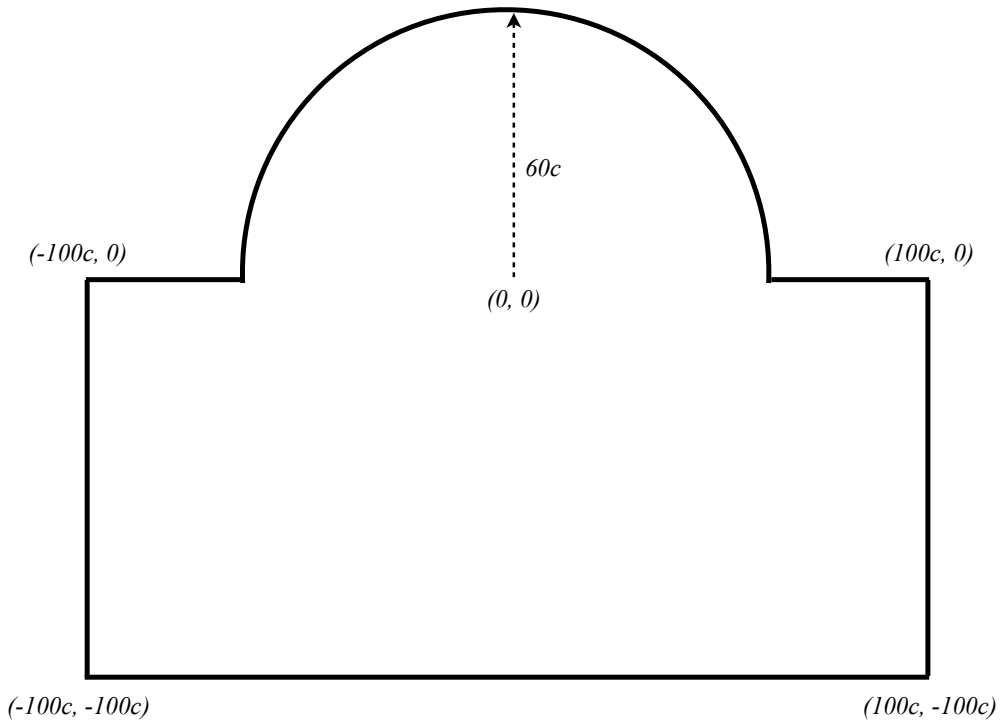
2) For this velocity field, determine $\nabla \cdot \vec{V}$ (for any point (x, z) except the origin):

3) For this velocity field, determine $\nabla \times \vec{V}$ (for any point (x, z) except the origin):

Now consider a surface S as shown in the figure below (note that the airfoil is not shown, but is still located at the origin). For the velocity in Equation (8.137):

4) Determine the airfoil's drag coefficient:

5) Determine the airfoil's lift coefficient:



edXsolution

Video Link

Module 9

Incompressible Potential Flow Aerodynamic Models

9.1 Overview

9.1.1 Measurable outcomes

In this Module, we specifically develop models for the potential flow around airfoils. These models are quite powerful allowing quantiative estimates of the lift and pressure distribution over airfoils.

Specifically, students successfully completing this module will be able to:

9.1. Describe how the potential flow around a body has infinitely many solutions, each with a different circulation. State and apply the Kutta condition to determine the specific potential flow that represents the physically-observed behavior of the flow at a sharp trailing edge.

9.2. Describe a vortex sheet including how it is a linear combination of infinitesimal-strength point vortices and how the lift generated by the vortex sheet is related to the integral of its circulation distribution.

9.3. Describe a linear-varying vortex panel method including (1) the number and meaning of the unknowns representing the vortex distribution, (2) the imposition of the flow tangency boundary condition, (3) the imposition of the Kutta condition, (4) the structure and meaning of the influence coefficient matrix, and (5) the calculation of the lift from the vortex panel solution.

9.4. (1) Describe the assumptions of thin airfoil theory and (2) apply thin airfoil theory to estimate the forces and moments on airfoils in two-dimensional incompressible flow.

9.5. Describe the basic trends of lift and drag with respect to geometry and angle of attack observed in applying two-dimensional potential flow analysis of airfoils and, in particular, how these trends differ from actually-observed (viscous) flows.

9.1.2 Pre-requisite material

The material in this module requires the measurable outcomes from Module 9.

9.2 Airfoil Flows

9.2.1 Lifting airfoils and the Kutta condition

9.1

For any body, there are actually infinitely many potential flow solutions that satisfy the boundary conditions. The appearance of an infinite number of solutions is demonstrated in the cylinder flows in Section 8.5.2. Any value of circulation still produces a valid solution for the flow around the cylinder.

For the case of an airfoil, infinitely many solutions also exist and again depend on the circulation. Figures 9.1, 9.2, and 9.3 show the potential flow over an airfoil with three different circulation values. The question is which of the infinitely many flows best corresponds to the flow observed in reality?

The key feature to determine this is the behavior of the flow at the trailing edge. For $\Gamma/(V_\infty c) = 0$, the flow wraps around the trailing edge from the lower surface to the upper surface. For $\Gamma/(V_\infty c) = 0.9$, the flow leaves smoothly from the trailing edge. For $\Gamma/(V_\infty c) = 1.8$, the flow wraps around the trailing edge from the upper surface to the lower surface. However, flow wrapping around a sharp edge would require the pressure to be infinitely low due to the vanishing radius of curvature. Through Bernoulli this implies the velocity is infinitely high. Thus, in the actual physical flow (not the potential flow model), the flow at a sharp trailing edge leaves smoothly without wrapping around such is observed for the $\Gamma/(V_\infty c) = 0.9$ flow.

This observation gives rise to the *Kutta condition*: the potential flow that leaves smoothly off a sharp trailing edge is an appropriate model for the actual flow observed in nature. Thus, the Kutta condition can be used to pick the physically-realistic potential flow out of the infinitely many that exist for a given body. In the airfoil examples above, enforcing the Kutta condition would result in the $\Gamma/(V_\infty c) = 0.9$ flow being chosen.

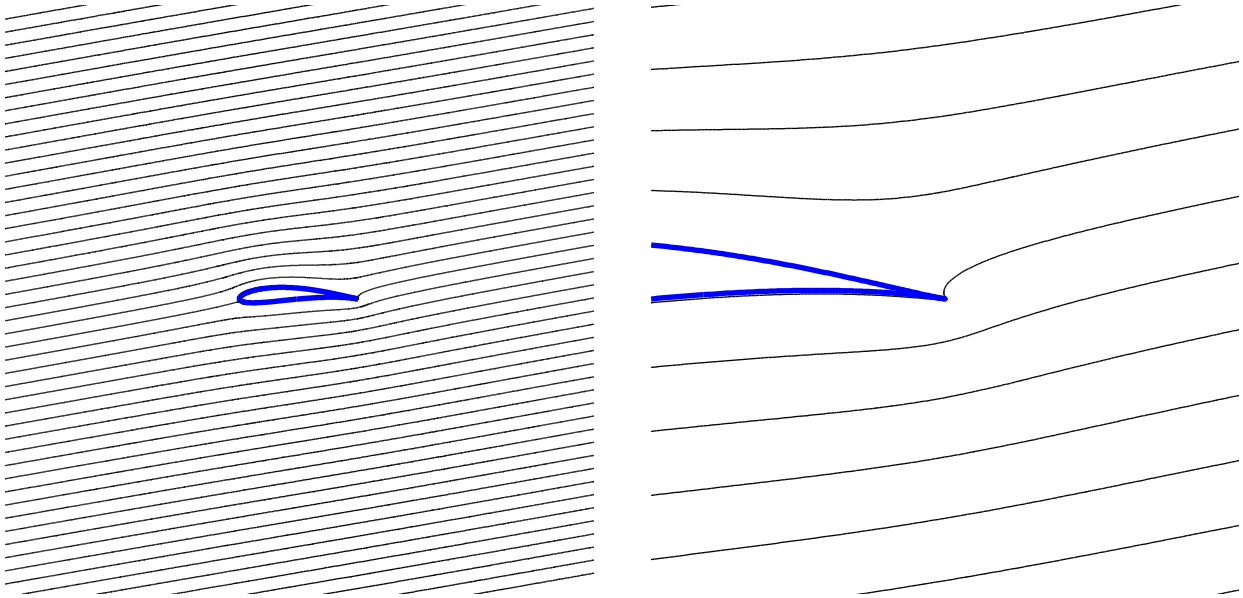


Figure 9.1: $\frac{\Gamma}{V_\infty c} = 0$ flow over airfoil

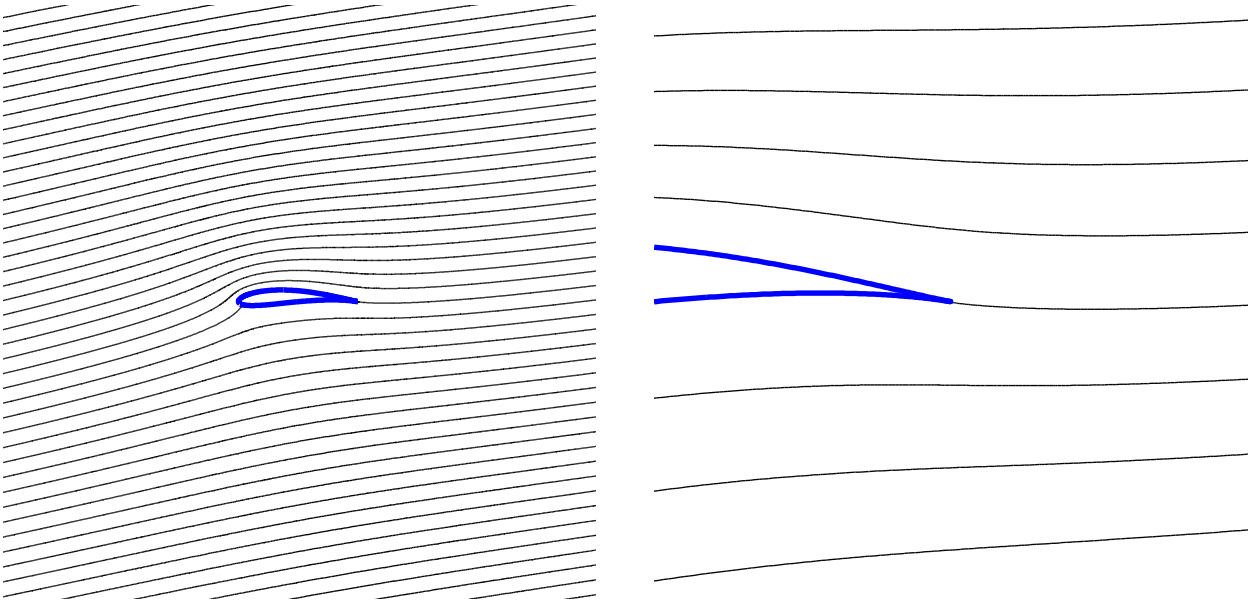


Figure 9.2: $\frac{\Gamma}{V_\infty c} = 0.9$ flow over airfoil

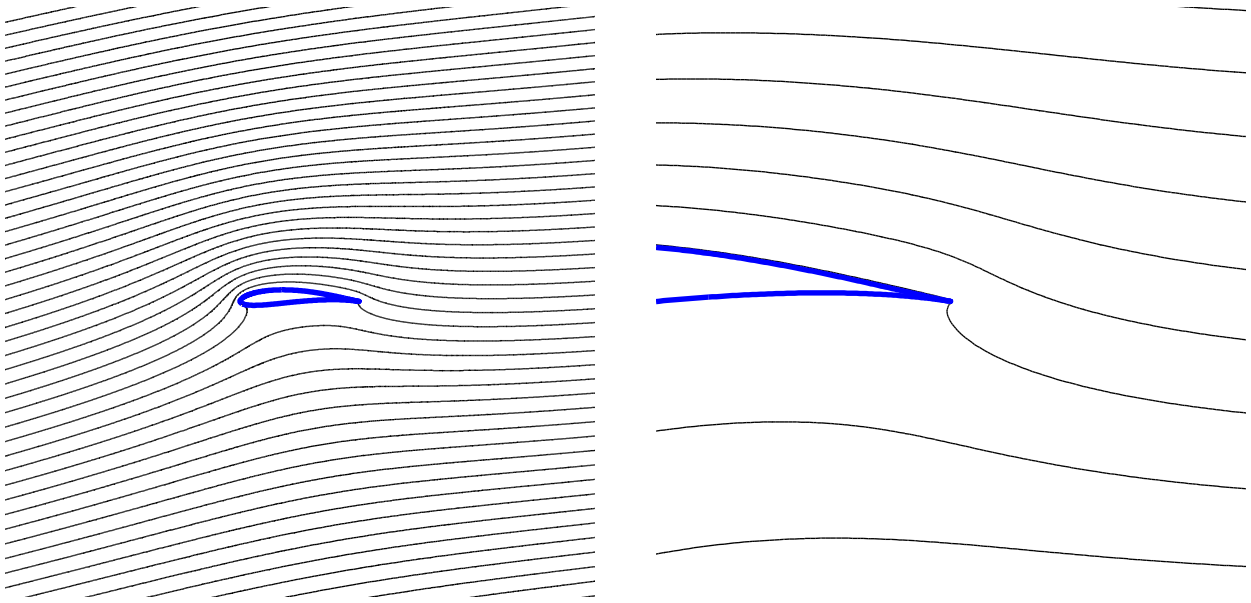


Figure 9.3: $\frac{\Gamma}{V_\infty c} = 1.8$ flow over airfoil

edXproblem: 9.2.2 Properties of two-dimensional steady, inviscid, incompressible flows: 1 Point

8.1 | 8.4 | 8.7 | 8.8

Consider the two-dimensional steady, inviscid, incompressible flow about a body. Assume that far upstream, the flow is uniform with velocity magnitude V_∞, angle of attack α, static pressure p_∞, and density ρ. Assume that the body is generating lift $L' > 0$.

Select all that are true:

edXsolution

Video Link

9.2.3 Lift coefficient for a flat plate

8.1 | 9.1 | 8.8 | 8.7 | 9.5

The exact solution of the potential flow around airfoils requires conformal mapping techniques. In practice, conformal mapping techniques are difficult to extend to arbitrary geometries, as a result, numerical methods known as panel methods are used to model potential flows around general airfoil shapes. However, the variation of the lift for a flat plate is a result is useful to understand, and in particular, for comparison to approximate methods.

Specifically, the circulation that satisfies the Kutta condition for a flat plate of chord c is,

$$\Gamma = \pi V_\infty c \sin\alpha \tag{9.1}$$

Thus, the lift generated (using the Kutta-Joukowsky Theorem) is,

$$L' = \rho V_\infty \Gamma = \pi \rho V_\infty^2 c \sin\alpha \tag{9.2}$$

The lift coefficient is

$$c_l = 2\pi \sin\alpha \tag{9.3}$$

For small angles of attack the lift slope is

$$\frac{\mathrm{d}c_l}{\mathrm{d}\alpha} \approx 2\pi \tag{9.4}$$

and the lift coefficient can then be approximated as,

$$c_l \approx 2\pi\alpha \tag{9.5}$$

Note: α is in radians.

A very important point is that this potential flow result suggests that c_l will continue to rise until $\alpha = 90°$. In the actual flow observed in nature, this will not happen since the boundary layer will separate at the leading edge at very low angles of attack for a flat plate. The neglect of boundary layer behavior places a limit to the applicability of potential flow models. While potential flow models will continue to predict increasing lift as the angle of attack increases (until the angle of attack approaches 90°), the actual viscous flows will stall at much lower angles. Specifically, as the boundary layer thickens and, in particular, when the boundary layer separates, potential flow models will no longer provide an accurate description of the flow.

And, finally, do not forget that the drag for this two-dimensional potential flow is zero according to d'Alembert's Paradox. So, $D' = 0$ and $c_d = 0$. Again, this is not true and is a reflection that viscous effects have not been included.

9.3 Vortex panel methods

9.3.1 Introduction to vortex panel methods

8.4 8.5 8.6 8.7 8.8 9.1 9.3

Thus far, our potential flow modeling has been for relatively simple geometric shapes. Now, we turn our attention to developing a potential flow modeling approach that can be applied to airfoils of any shape. The approach is founded upon the same ideas of applying linear superposition of basic building block solutions to Laplaces equation (i.e. conservation of mass), satisfying flow tangency on the body surface, utilizing the Kutta condition to select a potential flow that is physically-realistic at sharp trailing edges, and then using Bernoulli's equation and the Kutta-Joukowsky Theorem to determine the pressure distribution and the lift. So, while the mathematics will get a bit more involved, please keep in mind that the basic principles are no different than the simpler flows we have already studied in this module.

9.3.2 Vortex sheet model

8.6 8.5 8.7 9.2

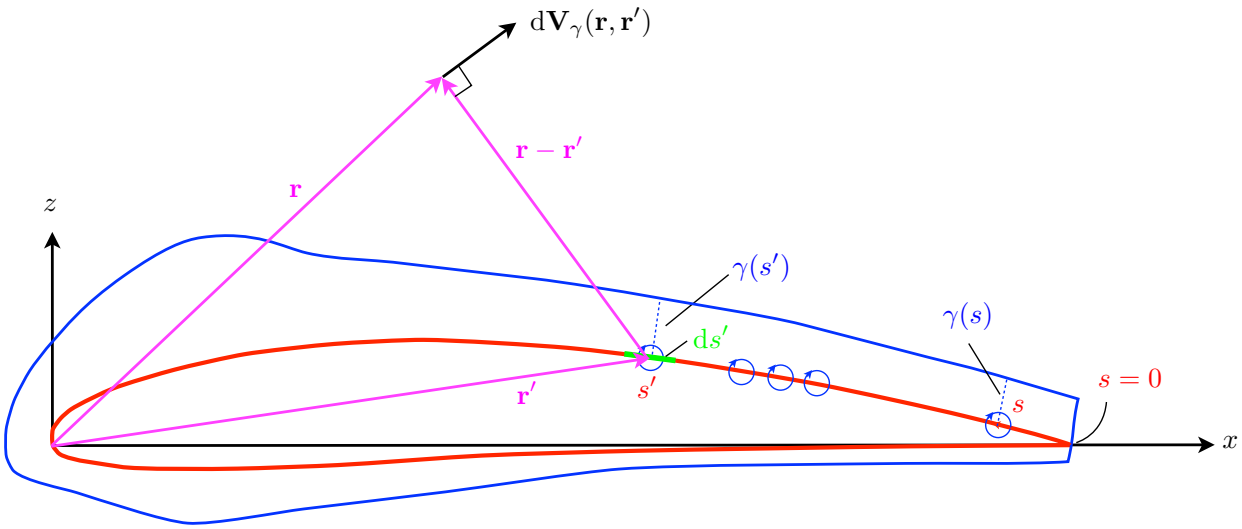


Figure 9.4: Vortex sheet on the surface of an airfoil and the infinitesimal velocity contribution $d\mathbf{V}_\gamma(\mathbf{r},\mathbf{r}')$ at $\mathbf{r}$ induced by the point vortex at $\mathbf{r}'$ with strength $\gamma(s')ds'$.

The basis of the vortex panel model is a vortex sheet placed on the surface of the airfoil as shown in Figure 9.4. A vortex sheet in two-dimensional flows is a curve along which infinitely-many point vortices are placed with the strength of the vortex at s being $\gamma(s)ds$. Thus, $\gamma(s)$ is a circulation per unit length. For a given airfoil geometry and angle of attack, the question is what is $\gamma(s)$ such that the flow is tangent to the airfoil and satisfies the Kutta condition. Then, once $\gamma(s)$ is determined, we can calculate the velocity field, the pressure distribution (using the Bernoulli equation), the lift coefficient (using the Kutta-Joukowsky Theorem), and so on.

The infinitesimal velocity contribution at $\mathbf{r}$ due to the point vortex at $\mathbf{r}'$ is,

$$d\mathbf{V}_\gamma(\mathbf{r},\mathbf{r}') = -\frac{\gamma(s')ds'}{2\pi\,|\mathbf{r}-\mathbf{r}'|}\hat{\mathbf{e}}_{\theta'} \tag{9.6}$$

where $\hat{\mathbf{e}}_{\theta'}$ is the unit vector in the θ-direction from a coordinate system centers at $\mathbf{r}'$. This is equivalent to the velocity field of the point vortex given in Equations (8.107) and (8.108) where

$\Gamma = \gamma(s')\mathrm{d}s'$ and the vortex is located at $\mathbf{r}'$ instead of the origin. At $\mathbf{r}$, the direction of $\hat{\mathbf{e}}_{\theta'}$ is perpendicular to $\mathbf{r} - \mathbf{r}'$ and oriented counter-clockwise, thus,

$$\hat{\mathbf{e}}_{\theta'} = \frac{\mathbf{r} - \mathbf{r}'}{|\mathbf{r} - \mathbf{r}'|} \times \hat{\mathbf{j}} \tag{9.7}$$

Substituting this expression into Equation (9.6) produces,

$$\mathrm{d}\mathbf{V}_\gamma(\mathbf{r}, \mathbf{r}') = \frac{\gamma(s')\mathrm{d}s'}{2\pi} \frac{\hat{\mathbf{j}} \times (\mathbf{r} - \mathbf{r}')}{|\mathbf{r} - \mathbf{r}'|^2} \tag{9.8}$$

The velocity induced at $\mathbf{r}$ by the entire vortex sheet is then an integral around the sheet,

$$\mathbf{V}_\gamma(\mathbf{r}) = \frac{1}{2\pi} \int \gamma(s') \frac{\hat{\mathbf{j}} \times (\mathbf{r} - \mathbf{r}')}{|\mathbf{r} - \mathbf{r}'|^2} \, \mathrm{d}s' \tag{9.9}$$

Recall that the first step in our potential flow modeling approach (see Sections 8.3.1 and 8.3.6) is to construct a potential using linear superposition of basic building block flows that all satisfy conservation of mass (Laplaces equations). The vortex sheet velocity field in Equation (9.9) is a linear combination of (infinitesimal strength) point vortices, and point vortices satisfy conservation of mass. Thus, $\nabla \cdot \mathbf{V}_\gamma = 0$. Also, in using a vortex sheet, we have not expressed the potential of the vortex sheet, rather we have directly written the velocity induced by the sheet. This is just expedient since the analysis we will do focuses on the velocity field (in particular satisfying flow tangency and applying Bernoulli equation to find the pressures).

The entire velocity includes the freestream contribution so that the velocity at any point $\mathbf{r}$ is,

$$\mathbf{V}(\mathbf{r}) = \mathbf{V}_\infty + \mathbf{V}_\gamma(\mathbf{r}) = \mathbf{V}_\infty + \frac{1}{2\pi} \int \gamma(s') \frac{\hat{\mathbf{j}} \times (\mathbf{r} - \mathbf{r}')}{|\mathbf{r} - \mathbf{r}'|^2} \, \mathrm{d}s' \tag{9.10}$$

Flow tangency then requires that $\mathbf{V}(\mathbf{r}) \cdot \hat{\mathbf{n}}(\mathbf{r}) = 0$ for all $\mathbf{r}$ on the airfoil surface,

$$\frac{1}{2\pi} \int \gamma(s') \frac{\left[\hat{\mathbf{j}} \times (\mathbf{r} - \mathbf{r}')\right] \cdot \hat{\mathbf{n}}(\mathbf{r})}{|\mathbf{r} - \mathbf{r}'|^2} \, \mathrm{d}s' = -\mathbf{V}_\infty \cdot \hat{\mathbf{n}}(\mathbf{r}) \tag{9.11}$$

We must also satisfy the Kutta condition at the sharp trailing edge. To do this, we require that the strength of the point vortex at the trailing edge be zero. If this strength were non-zero, then the velocity induced by the point vortex would induce a flow around the trailing edge. The strength per (unit length) of the vortex at the trailing edge is a sum of $\gamma(0)$ and $\gamma(s_{\mathrm{te}})$ where s_{te} is the length of the entire surface of the airfoil (in other words, the length starting at the trailing edge, wrapping around the airfoil, and reaching the trailing edge again). Thus, the Kutta condition requires,

$$\gamma(0) + \gamma(s_{\mathrm{te}}) = 0 \tag{9.12}$$

Once the solution $\gamma(s)$ is determined that satisfies flow tangency (Equation 9.11) and the Kutta condition (Equation 9.12), the lift coefficient can be determined using the Kutta-Joukowsky Theorem result that $L' = \rho V_\infty \Gamma$. Since each portion $\mathrm{d}s$ of the vortex sheet has a vortex with strength $\gamma(s)\mathrm{d}s$, then the total circulation is the integral,

$$\Gamma = \int_{s=0}^{s_{\mathrm{te}}} \gamma(s')\mathrm{d}s' \tag{9.13}$$

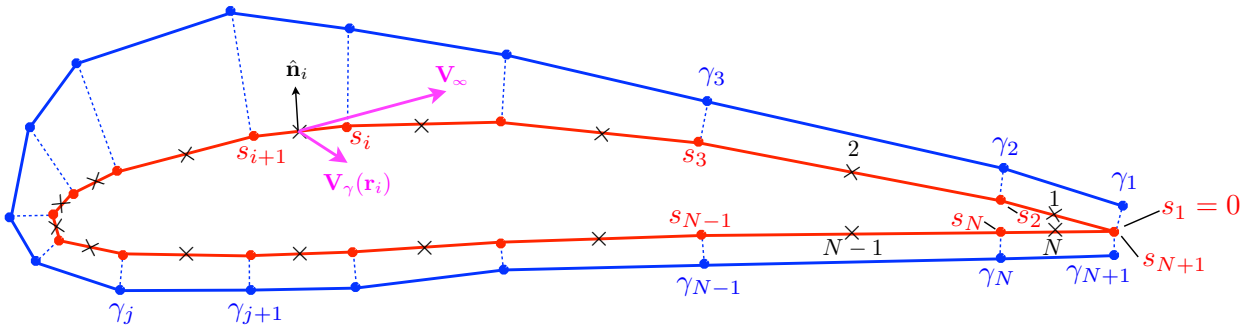


Figure 9.5: Panel representation of airfoil surface with linear-varying vortex sheet on each panel. Control points where flow tangency is enforced are marked by black × and labeled by the panel number.

9.3.3 Linear-varying vortex panel model

9.3

The vortex sheet model presented in Section 9.3.2 requires the solution of Equation (9.11) which is an integral equation for the $\gamma(s)$. This equation generally cannot be solved in closed-form analytically. Instead, we will solve it approximately.

The method we use will replace the geometry of the airfoil (and therefore the vortex sheet) with a set of panels as shown in Figure 9.5. The end points of the panels, which we will refer to as the *panel nodes*, are labeled with the surface distance s_i. Thus, panel i lies in the range $s_i \le s \le s_{i+1}$.

The $\gamma(s)$ distribution is assumed to vary linearly along each panel, such that for panel j,

$$\gamma(s) = \gamma_j + \frac{s - s_j}{s_{j+1} - s_j}\left(\gamma_{j+1} - \gamma_j\right) \tag{9.14}$$

It is this linear variation of $\gamma(s)$ on each panel that gives rise to the term *linear-varying vortex panel*. Note that at the trailing edge the upper and lower surface vortex strength γ_1 and γ_{N+1} have individual values. Thus, the total number of variables to describe $\gamma(s)$ over the entire paneled airfoil is $N+1$. This means that we will need to have $N+1$ equations to determine the $N+1$ values of γ_i.

The $N+1$ equations will be N flow tangency conditions and the Kutta condition. We will enforce flow tangency at the midpoints of each panel, which we will refer to as the *control points*. The control points are marked with × in Figure 9.5. The flow tangency condition in Equation (9.11) applied at the control point of panel i becomes,

$$\sum_{j=1}^{N} \frac{1}{2\pi} \int_{s_j}^{s_{j+1}} \gamma(s') \frac{\left[\hat{\mathbf{j}} \times (\mathbf{r}_i - \mathbf{r}')\right] \cdot \hat{\mathbf{n}}_i}{|\mathbf{r}_i - \mathbf{r}'|^2} \, \mathrm{d}s' = -\mathbf{V}_\infty \cdot \hat{\mathbf{n}}_i \tag{9.15}$$

where $\gamma(s')$ is given in Equation (9.14), specifically,

$$\gamma(s') = \gamma_j + \frac{s' - s_j}{s_{j+1} - s_j}\left(\gamma_{j+1} - \gamma_j\right) \tag{9.16}$$

Also, $\mathbf{r}'$ is a function of s', specifically,

$$\mathbf{r}'(s') = \mathbf{r}_j + \frac{s' - s_j}{s_{j+1} - s_j}\left(\mathbf{r}_{j+1} - \mathbf{r}_j\right) \tag{9.17}$$

The integrals from s_j to s_{j+1}, while complicated, can be performed analytically. We will not cover the result here, but it can be done. The final result will depend linearly on the value of γ_j and γ_{j+1} and we will define the following notation,

$$\frac{1}{2\pi}\int_{s_j}^{s_{j+1}} \gamma(s') \frac{\left[\hat{\mathbf{j}} \times (\mathbf{r}_i - \mathbf{r}')\right] \cdot \hat{\mathbf{n}}_i}{|\mathbf{r}_i - \mathbf{r}'|^2} \, \mathrm{d}s' = K_{i,j}^{(j)} \gamma_j + K_{i,j+1}^{(j)} \gamma_{j+1} \tag{9.18}$$

where $K_{i,j}^{(j)}$ and $K_{i,j+1}^{(j)}$ can be found by integration and will only be functions of the geometry of panel j and the location of control point i. Substituting Equation (9.18) into Equation (9.15) gives,

$$\sum_{j=1}^{N} \left[K_{i,j}^{(j)} \gamma_j + K_{i,j+1}^{(j)} \gamma_{j+1} \right] = -\mathbf{V}_\infty \cdot \hat{\mathbf{n}}_i \tag{9.19}$$

Since flow tangency is enforced at the control point of each panel, this produces N equations; that is, $i = 1$ through N.

In addition to flow tangency, the Kutta condition is also enforced using Equation (9.12), which for this vortex panel representation is,

$$\gamma_1 + \gamma_{N+1} = 0 \tag{9.20}$$

edXproblem: 9.3.4 Circulation for linear-varying vortex panel method: 1 Point

8.5 | 8.6 | 8.7 | 9.3

The circulation for a linear-varying vortex panel method can be written as a sum over each panel of the form,

$$\Gamma = \sum_{j=1}^{N} \Gamma_j \tag{9.21}$$

where Γ_j is the circulation contribution from panel j. Using Equation (9.13), determine the formula for Γ_j as a function of only s_j, s_{j+1}, γ_j, and γ_{j+1}. In the formula response, use the following notation: s_j =s0, s_{j+1} =s1, γ_j =g0, and γ_{j+1} =g1.

edXsolution

Video Link

9.3.5 Influence coefficients and linear system

9.3

The N flow tangency equations (Equation 9.19) and the Kutta condition (Equation 9.20) can be written as a linear system of $N+1$ equations of the form,

$$Kg = b \tag{9.22}$$

where g the length $N+1$ vector of γ_i,

$$g = [\gamma_1, \gamma_2, \ldots, \gamma_N, \gamma_{N+1}] \tag{9.23}$$

K is an $N+1 \times N+1$ matrix, and b is a length $N+1$ vector.

The flow tangency equations are placed in the first N rows of the K matrix, and the Kutta condition is placed in the last row. The system of equations has the following form,

$$\begin{bmatrix} K_{1,1} & K_{1,2} & \ldots & K_{1,N} & K_{1,N+1} \\ K_{2,1} & K_{2,2} & \ldots & K_{2,N} & K_{2,N+1} \\ \vdots & \vdots & \vdots & \vdots & \vdots \\ K_{N-1,1} & K_{N-1,2} & \ldots & K_{N-1,N} & K_{N-1,N+1} \\ K_{N,1} & K_{N,2} & \ldots & K_{N,N} & K_{N,N+1} \\ 1 & 0 & 0 & 0 & 1 \end{bmatrix} \begin{pmatrix} \gamma_1 \\ \gamma_2 \\ \vdots \\ \gamma_{N-1} \\ \gamma_N \\ \gamma_{N+1} \end{pmatrix} = \begin{pmatrix} -\mathbf{V}_\infty \cdot \hat{\mathbf{n}}_1 \\ -\mathbf{V}_\infty \cdot \hat{\mathbf{n}}_2 \\ \vdots \\ -\mathbf{V}_\infty \cdot \hat{\mathbf{n}}_{N-1} \\ -\mathbf{V}_\infty \cdot \hat{\mathbf{n}}_N \\ 0 \end{pmatrix} \tag{9.24}$$

where the entries $K_{i,j}$ for $i \leq N$ are known as the influence coefficients and represent the entire influence of γ_j on the flow tangency condition at control point i. The values of $K_{i,j}$ are,

$$K_{i,j} = \begin{cases} K_{i,1}^{(1)} & \text{if } j = 1 \\ K_{i,j}^{(j-1)} + K_{i,j}^{(j)} & \text{if } 1 < j < N+1 \\ K_{i,N+1}^{(N)} & \text{if } j = N+1 \end{cases} \tag{9.25}$$

9.3.6 Sample vortex panel solutions on a NACA 4412

9.3

To demonstrate the behavior of the linear-varying vortex panel method described in this section, we consider the incompressible potential flow around a NACA 4412 airfoil. First, we consider the effect that the number of panels has on the solution. Figure 9.6 shows the geometry and C_p distributions for $N = 10$ to 320 panels. At $N = 10$ panels, the C_p distribution does not predict the low pressure at the leading edge, but for $N \geq 80$ panels, the minimum C_p is fairly constant at approximately -1.8. Figure 9.7 shows the c_l variation with N. We observe that the asymptotic answer (for large N) is approximately $c_l = 0.986$ and that already bu $N = 40$ panels, c_l is predicted within one percent of that value. The reality is that vortex panel methods require very little computation and so even for $N = 320$ panels run nearly instantaneously on laptops. Typically, the bigger issue is that the panel method by itself does not account for viscous effects and so the accuracy of the answer is limited by the inviscid assumption. Thus, linear-varying vortex panel methods for two-dimensional flows typically will only use 100-200 panels.

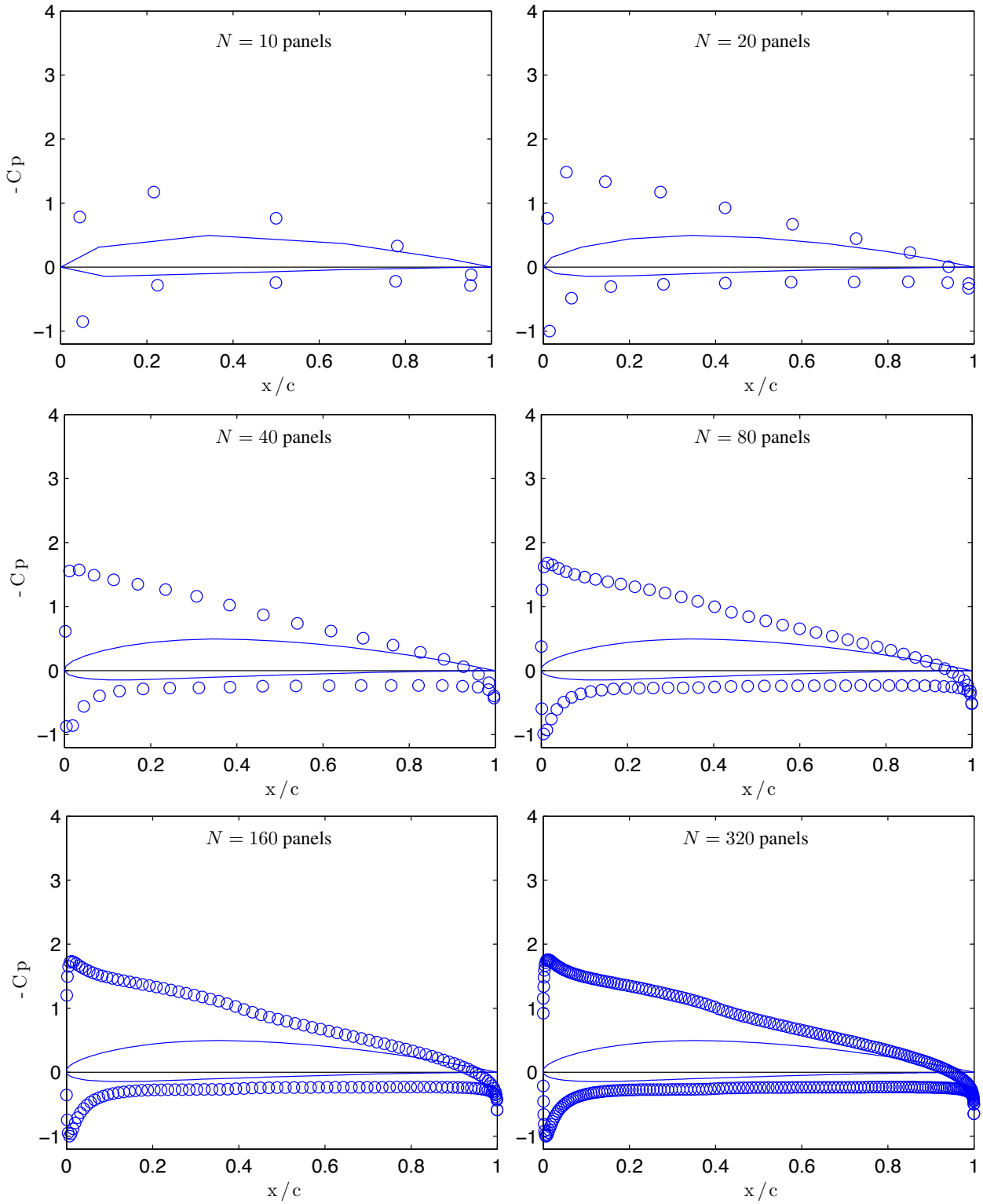


Figure 9.6: NACA 4412 incompressible flow, $\alpha = 5°$. C_p distributions for different numbers of vortex panels.

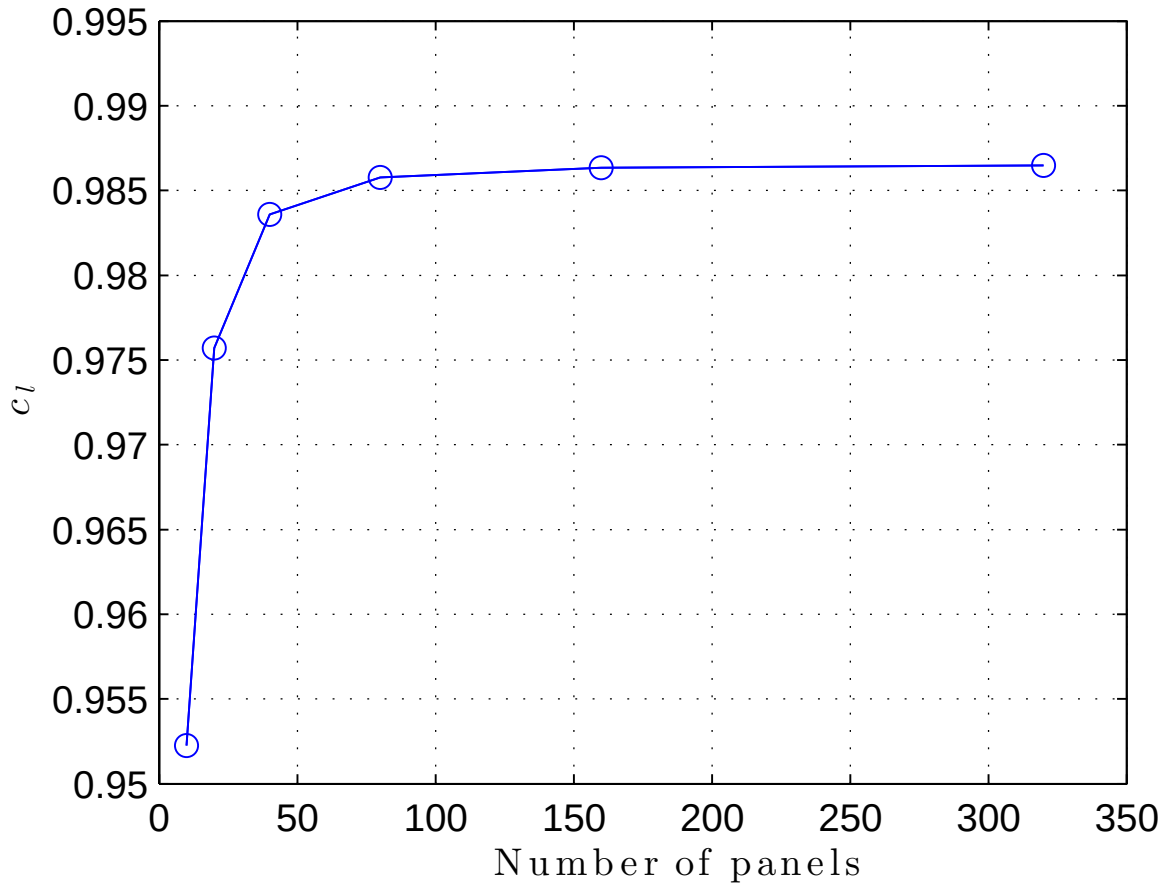
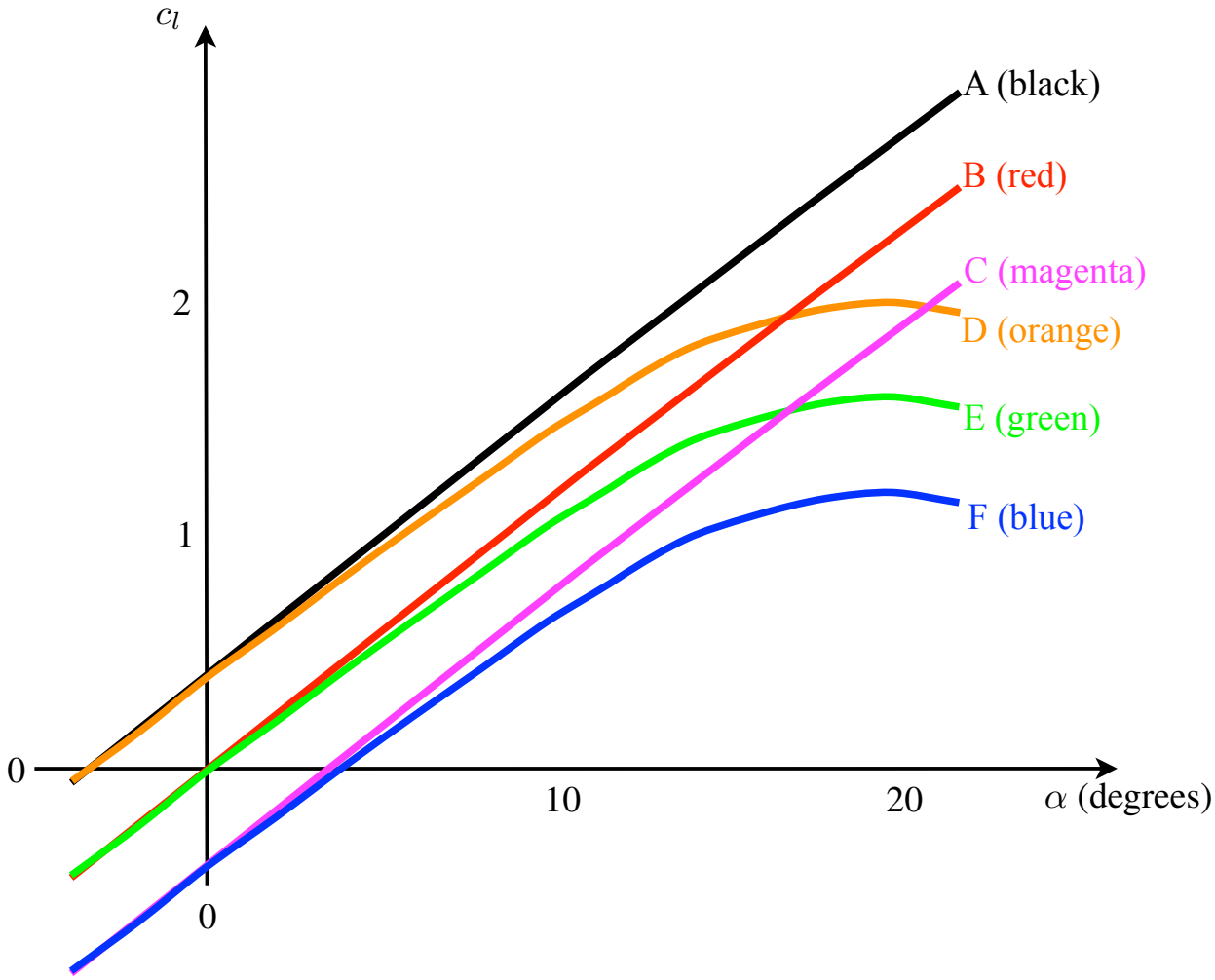


Figure 9.7: NACA 4412 incompressible flow, $\alpha = 5°$. Convergence of c_l with number of vortex panels.

edXproblem: 9.3.7 Lift coefficient behavior for a NACA 3510 using a vortex panel method: 1 Point

2.4 | 9.3 | 9.5



Which of the $c_l(\alpha)$ curves is the lift coefficient of a NACA 3510 airfoil modeled with the vortex panel method described in this module (assume that a large number of panels is used)?

edXsolution

Video Link

9.4 Thin Airfoil Theory

9.4.1 Thin airfoil potential flow model

9.4

Panel methods are a critical tool in modern aerodynamic design. However, the dependence of the aerodynamic performance (C_p distribution, c_l, ...) on geometry and angle of attack can only be determined by trial-and-error (running the panel method for variations in geometry and angle of attack). As a complement to a panel method, we therefore desire to have a theoretical understanding of how geometry and angle of attack influence the aerodynamic performance. In this section, we derive a simplied vortex sheet model which allows analytic solution. This model and the analytic results are known as *thin airfoil theory*.

The assumptions of thin airfoil theory are

- Two-dimensional, steady incompressible potential flow (see Section 8.3.1).
- Small angle of attack: $\alpha \ll 1$ (radians)
- Small thickness: $t_{\max}/c \ll 1$
- Small camber and camber slope: $z_{c\max}/c \ll 1$ and $\frac{\mathrm{d}z_c}{\mathrm{d}x} \ll 1$
- Small velocity perturbations: $|\mathbf{V} - \mathbf{V}_\infty|/V_\infty \ll 1$.

Applying the small angle of attack assumption gives the freestream velocity in simplified form,

$$\mathbf{V}_\infty = V_\infty \cos\alpha \hat{\mathbf{i}} + V_\infty \sin\alpha \hat{\mathbf{k}} \approx V_\infty \hat{\mathbf{i}} + V_\infty \alpha \hat{\mathbf{k}} \tag{9.26}$$

Thin airfoil theory uses the vortex sheet model described in Section 9.3.2 applied to airfoils that have small thickness and camber. Applying the small thickness assumption, we collapse the vortex sheet on the upper and lower surfaces to the mean camber line. As shown in Figure 9.8, the resulting vortex sheet on the camber line has a strength $\gamma(x)$ which is effectively the sum of the upper and lower surface vortex sheet strengths in the original case with finite thickness. The flow tangency condition is applied on the camber line requiring on the upper surface,

$$\mathbf{V}_\gamma(x, z_c^+(x)) \cdot \hat{\mathbf{n}}_c(x) = -\mathbf{V}_\infty \cdot \hat{\mathbf{n}}_c(x) \tag{9.27}$$

and on the lower surface,

$$\mathbf{V}_\gamma(x, z_c^-(x)) \cdot \hat{\mathbf{n}}_c(x) = -\mathbf{V}_\infty \cdot \hat{\mathbf{n}}_c(x) \tag{9.28}$$

where $z_c^+(x)$ and $z_c^-(x)$ are defined as the value of z just above and below the camber line. However, while the velocity jumps across the vortex sheet, it can be shown that this jump is only in the velocity component tangential to the sheet. Specifically, defining the jump in the velocity across the sheet as,

$$\Delta\mathbf{V}_\gamma(x) \equiv \mathbf{V}_\gamma(x, z_c^+(x)) - \mathbf{V}_\gamma(x, z_c^-(x)) \tag{9.29}$$

Then,

$$\Delta\mathbf{V}_\gamma(x) \cdot \hat{\mathbf{n}}_c(x) = 0 \tag{9.30}$$

The tangential velocity jump is directly related to $\gamma(x)$,

$$\Delta\mathbf{V}_\gamma(x) \cdot \hat{\mathbf{t}}_c(x) = \gamma(x) \tag{9.31}$$

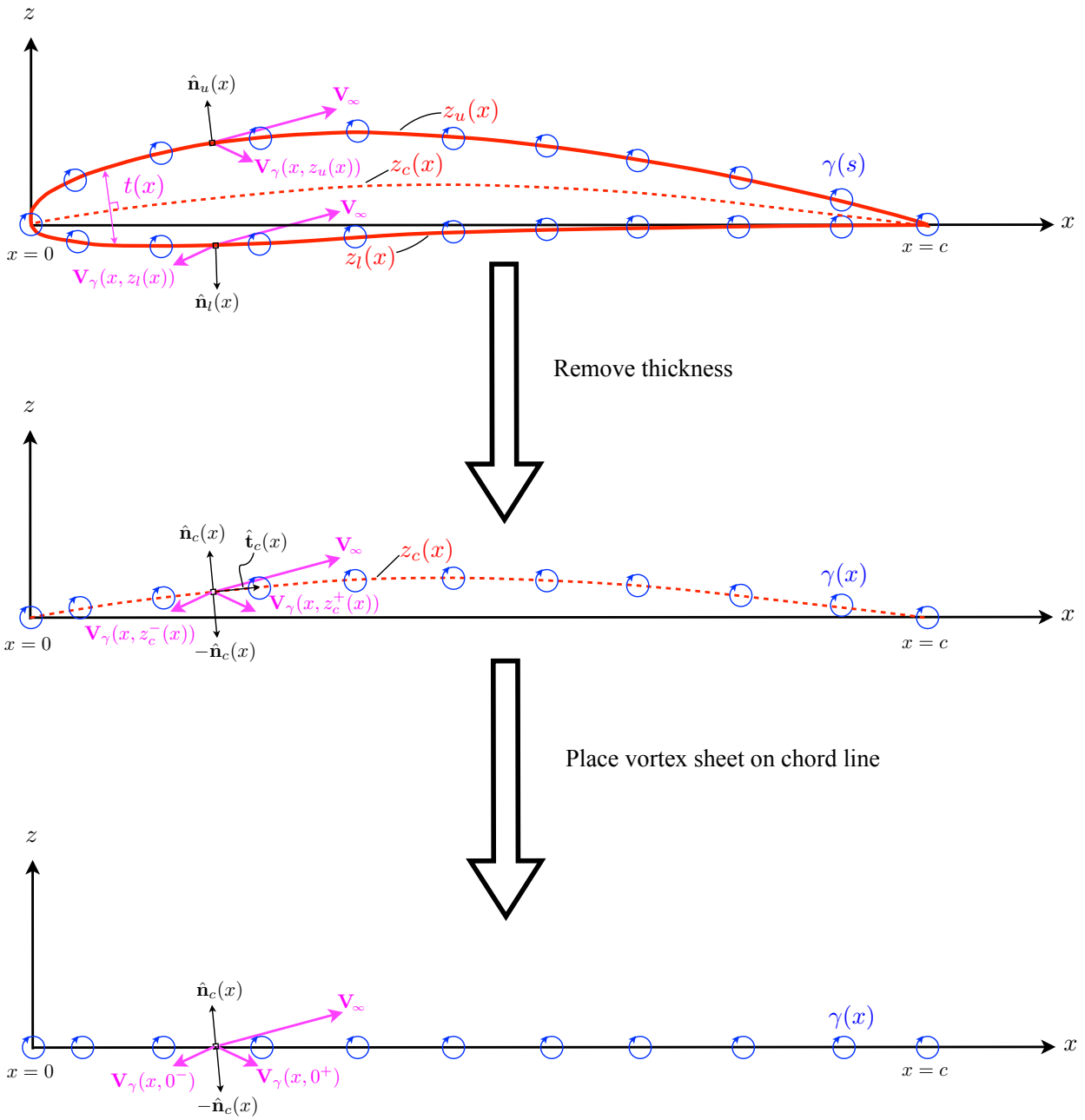


Figure 9.8: Transformation from vortex sheet on airfoil surface to thin airfoil representation with the vortex sheet on the chord line.

where $\hat{\mathbf{t}}_c(x)$ is the tangent unit vector defined as,

$$\hat{\mathbf{t}}_c(x) \equiv \hat{\mathbf{j}} \times \hat{\mathbf{n}}_c(x) \tag{9.32}$$

We note that Equations (9.30) and (9.31) are valid for any vortex sheet.

Since the normal velocity component is the same for both $z_c^{\pm}(x)$ then the flow tangency condition can just be written as,

$$\mathbf{V}_\gamma(x, z_c(x)) \cdot \hat{\mathbf{n}}_c(x) = -\mathbf{V}_\infty \cdot \hat{\mathbf{n}}_c(x) \tag{9.33}$$

Next, we apply the assumption that the camber is small. This allows the vortex sheet to be moved from the camber line to the chord line ($z = 0$). With this approximation, flow tangency is

now,

$$\mathbf{V}_\gamma(x,0)\cdot\hat{\mathbf{n}}_c(x) = -\mathbf{V}_\infty\cdot\hat{\mathbf{n}}_c(x) \tag{9.34}$$

Note that although the camber is small, we still use the slope of the camber line in applying flow tangency. If we had also set the slope to zero, then the normal $\hat{n}_c$ would be in the z direction. In other words, the thin airfoil theory would model every airfoil as if it had no camber.

9.4.2 Fundamental equation of thin airfoil theory

9.4

The flow tangency condition for the thin airfoil model in Equation (9.34) can be simplified. Recall that the expression for the velocity at a point $\mathbf{r}$ induced by a general vortex sheet is given by Equation (9.9),

$$\mathbf{V}_\gamma(\mathbf{r}) = \frac{1}{2\pi}\int \gamma(s')\frac{\hat{\mathbf{j}}\times(\mathbf{r}-\mathbf{r}')}{|\mathbf{r}-\mathbf{r}'|^2}\,\mathrm{d}s' \tag{9.35}$$

For the thin airfoil theory model, the sheet is along the x-axis so $s = x$ (and similarly then the integration variable s' we will set to x'). To apply flow tangency, we need the velocity at $(x,0)$, thus,

$$\mathbf{r} = x\hat{\mathbf{i}} \quad \text{and} \quad \mathbf{r}' = x'\hat{\mathbf{i}} \tag{9.36}$$

Thus, $\mathbf{V}_\gamma$ at $(x,0)$ is,

$$\mathbf{V}_\gamma(x,0) = -\hat{\mathbf{k}}\frac{1}{2\pi}\int_0^c \frac{\gamma(x')}{x-x'}\,\mathrm{d}x' \tag{9.37}$$

Recall from Equation (2.10) that the angle of the camber line is $\tan\theta_c = \mathrm{d}z_c/\mathrm{d}x$. For small camber slope, this can be approximated as,

$$\tan\theta_c \approx \theta_c \approx \frac{\mathrm{d}z_c}{\mathrm{d}x} \tag{9.38}$$

The normal to the camber line is,

$$\hat{\mathbf{n}}_c = -\sin\theta_c\hat{\mathbf{i}} + \cos\theta_c\hat{\mathbf{k}} \approx -\frac{\mathrm{d}z_c}{\mathrm{d}x}\hat{\mathbf{i}} + \hat{\mathbf{k}} \tag{9.39}$$

Substituting Equations (9.37) and (9.39) into the flow tangency condition (Equation 9.34) gives,

$$\frac{1}{2\pi}\int_0^c \frac{\gamma(x')}{x-x'}\,\mathrm{d}x' = V_\infty\left(\alpha - \frac{\mathrm{d}z_c}{\mathrm{d}x}\right) \tag{9.40}$$

which must be satisfied for all x from $0 < x < c$. Equation (9.40) is known as the *fundamental equation of thin airfoil theory*. While it took some manipulations to get to this result, remember that it represents the flow tangency condition $\mathbf{V}\cdot\hat{n} = 0$ for a thin airfoil modeled with a vortex sheet along its chordline. The goal in performing thin airfoil theory analysis is to determine the $\gamma(x)$ that satisfies this equation for the desired camber and angle of attack.

Finally, in addition to satisfying Equation (9.40), the Kutta condition must also be satisfied. For the thin airfoil theory model, this requires,

$$\gamma(c) = 0 \tag{9.41}$$

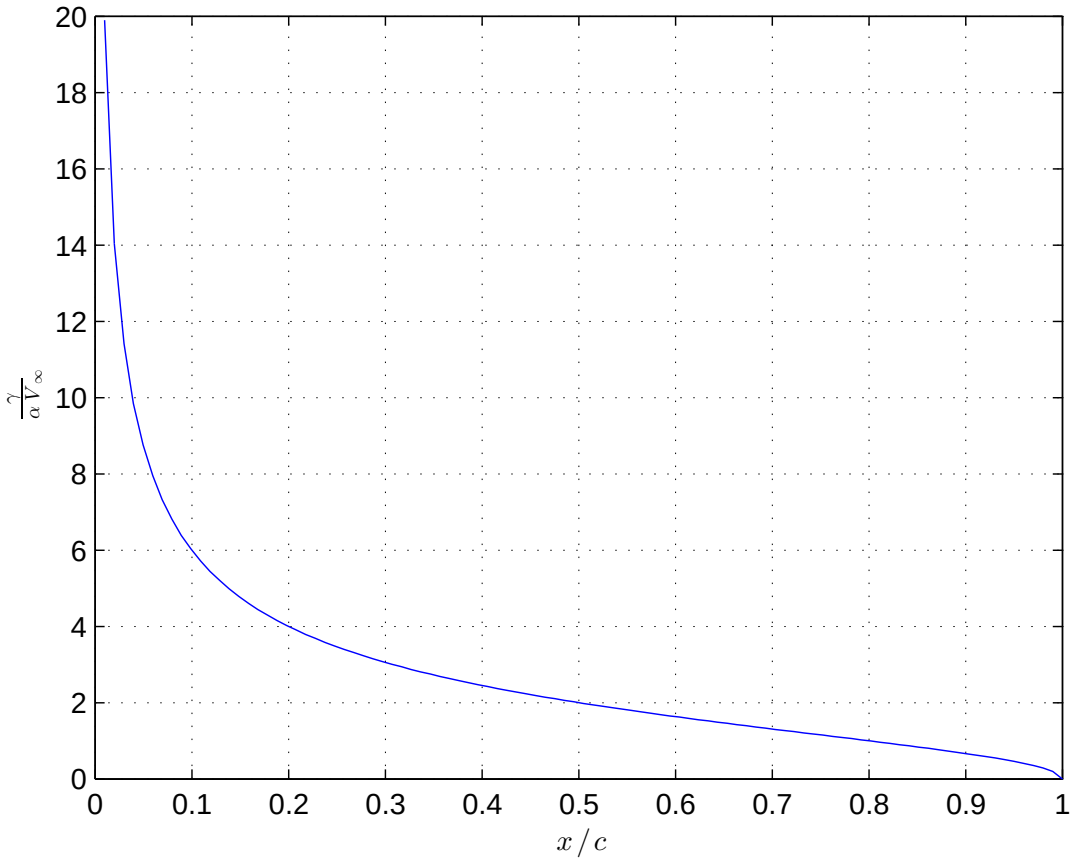


Figure 9.9: $\gamma(x)$ distribution for a symmetric airfoil.

9.4.3 Symmetric airfoils

9.4

For a symmetric airfoil, $z_c = 0$. Thus, the fundamental equation of thin airfoil theory (Equation 9.40) reduces to,

$$\frac{1}{2\pi}\int_0^c \frac{\gamma(x')}{x - x'}\,\mathrm{d}x' = V_\infty \alpha \tag{9.42}$$

The vortex strength distribution which satisfies this equation (and the Kutta condition) is,

$$\gamma(x) = 2\alpha V_\infty \sqrt{\frac{c - x}{x}} \tag{9.43}$$

A plot of this result is shown in Figure 9.9. We see that $\gamma(x)$ is infinite at the leading edge. In the next section, we link the pressure differences to γ and discuss why $\gamma(x)$ is infinite at the leading edge.

The lift can be determined from the Kutta-Joukowsky Theorem by calculating the circulation

$$\Gamma = \int_0^c \gamma(x')\mathrm{d}x' \tag{9.44}$$

This integral of $\gamma(x)$ can be performed through a transformation of variables from x to ξ where, ξ is defined as,

$$x \equiv \frac{c}{2}(1 - \cos\xi) \tag{9.45}$$

Note that $\xi = 0$ is the leading edge and $\xi = \pi$ is the trailing edge. Further, differentiation of this transformation gives,

$$\mathrm{d}x \equiv \frac{c}{2} \sin\xi \, \mathrm{d}\xi \tag{9.46}$$

Substituting this transformation into Equation (9.43) gives,

$$\gamma(\xi) = 2\alpha V_\infty \frac{1 + \cos\xi}{\sin\xi} \tag{9.47}$$

Finally, performing the integration,

$$\begin{aligned} \Gamma &= \frac{c}{2} \int_0^\pi \gamma(\xi') \sin\xi' \, \mathrm{d}\xi' && (9.48) \\ &= \alpha c V_\infty \int_0^\pi (1 + \cos\xi') \mathrm{d}\xi' && (9.49) \\ &= \pi \alpha c V_\infty && (9.50) \end{aligned}$$

Thus,

$$\begin{aligned} L &= \rho V_\infty \Gamma = \pi \alpha \rho V_\infty^2 c && (9.51) \\ c_l &= 2\pi\alpha && (9.52) \end{aligned}$$

The result that $c_l = 2\pi\alpha$ for symmetric airfoils is a classic result in aerodynamics. Figures 9.10 through 9.12 shows comparisons between this thin airfoil theory result, potential flow (using a vortex panel method) and predictions which include viscous effects. Three airfoils are considered: NACA 0006, 0012, and 0021. All results agree most closely for the thinnest airfoil (NACA 0006) with larger discrepancies for increasing thickness. Interesting, the potential flow model predicts larger lift than the thin airfoil theory result, and the thin airfoil theory result is in better agreement with the viscous results. This is a common behavior which is apparently due to the approximations made in thin airfoil theory having similar behavior as the viscous effects (however, there should not be anything more fundamental made of this point; just a coincidence that the two effects have similar behavior). In principle, thin airfoil theory has more approximations than the panel method in terms of solving potential flows.

9.4.4 Pressure differences

9.4

In this section, our goal is to relate $\gamma(x)$ from thin airfoil theory to the pressure distribution. We begin by defining the velocity field in terms of the freestream and perturbations similar to Homework Problem 8.6.1. In thin airfoil theory, we have not aligned the freestream to the x-axis so the result is a little different, specifically,

$$\begin{aligned} u(x,z) &= V_\infty \cos\alpha + \tilde{u}(x,z) && (9.53) \\ w(x,z) &= V_\infty \sin\alpha + \tilde{w}(x,z) && (9.54) \end{aligned}$$

The square of the velocity magnitude is then,

$$\begin{aligned} V^2 &= u^2 + w^2 && (9.55) \\ &= (V_\infty \cos\alpha + \tilde{u})^2 + (V_\infty \sin\alpha + \tilde{w})^2 && (9.56) \\ &= V_\infty^2 + 2V_\infty (\tilde{u}\cos\alpha + \tilde{w}\sin\alpha) + \tilde{u}^2 + \tilde{w}^2 && (9.57) \end{aligned}$$

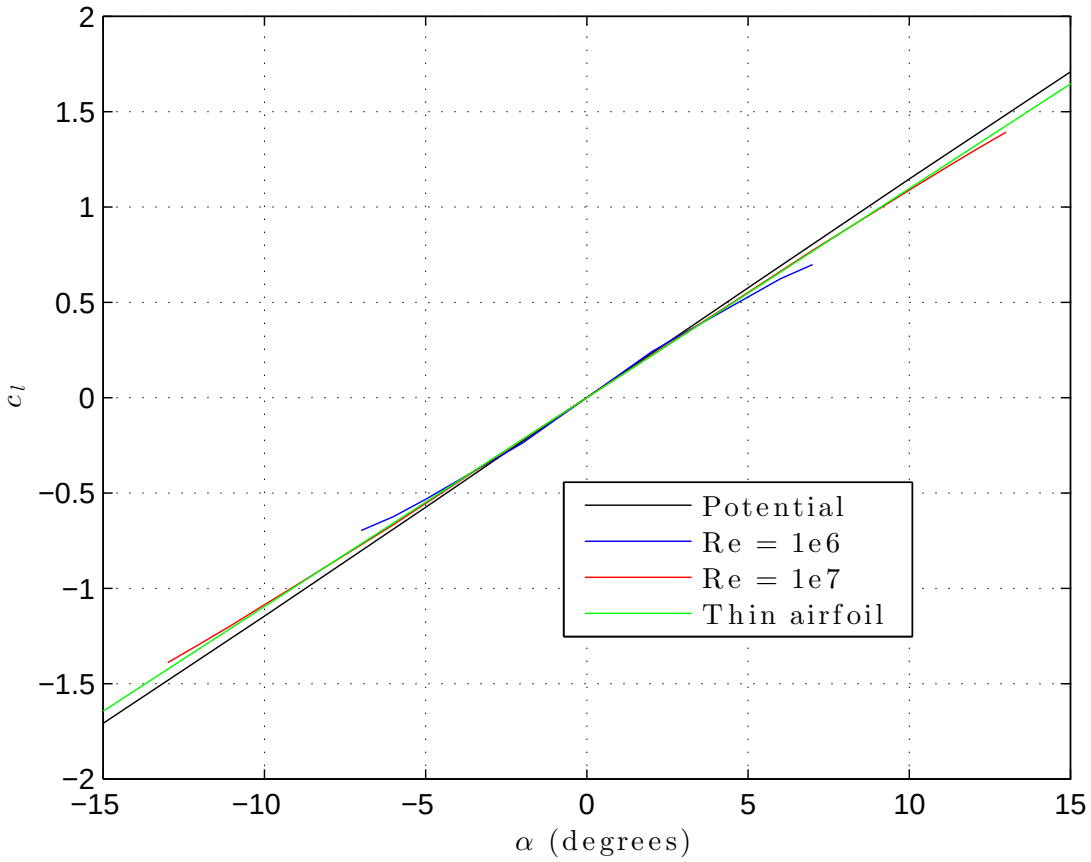


Figure 9.10: Comparison of $c_l(\alpha)$ for NACA 0006 for potential flow, thin airfoil theory, and $Re = 1E6$ and $Re = 1E7$ viscous calculations.

For small angles $\cos\alpha \approx 1$ and $\sin\alpha \approx \alpha$, thus,

$$V^2 = V_\infty^2 + 2V_\infty\left(\tilde{u} + \tilde{w}\alpha\right) + \tilde{u}^2 + \tilde{w}^2 \tag{9.58}$$

Recall using Bernoulli's equation, C_p is,

$$C_p = 1 - \frac{V^2}{V_\infty^2} \tag{9.59}$$

$$\approx -2\frac{\tilde{u}}{V_\infty} - 2\frac{\tilde{w}}{V_\infty}\alpha - \frac{\tilde{u}^2}{V_\infty^2} - \frac{\tilde{w}^2}{V_\infty^2} \tag{9.60}$$

The first term is linear in small quantities (scaling with $\tilde{u}/V_\infty$) while the last three terms are quadratic (scaling with quadratic combinations of $\tilde{u}/V_\infty$, $\tilde{w}/V_\infty$, and α). Thus, under the assumptions of thin airfoil theory, these quadratic terms will be much smaller giving the following approximation for the C_p,

$$C_p \approx -2\frac{\tilde{u}}{V_\infty} \tag{9.61}$$

The jump in the pressure between the upper and lower surface (normalized by the dynamic

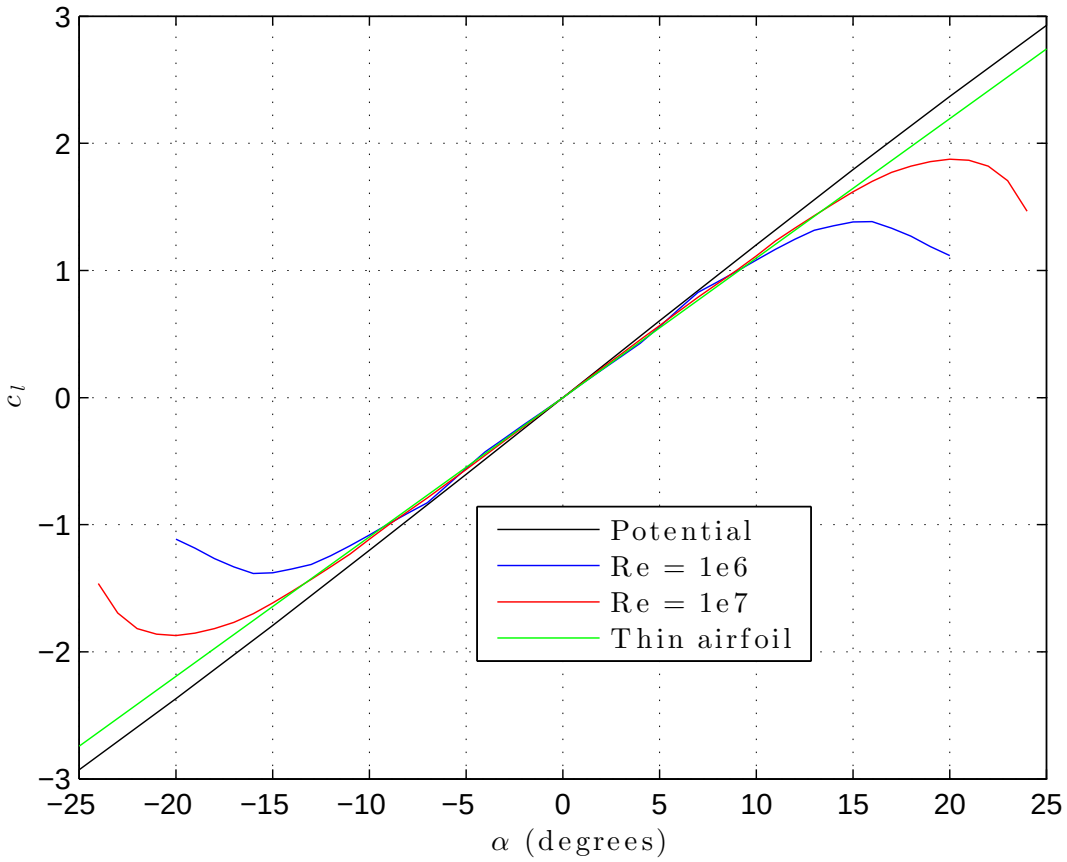


Figure 9.11: Comparison of $c_l(\alpha)$ for NACA 0012 for potential flow, thin airfoil theory, and $Re = 1E6$ and $Re = 1E7$ viscous calculations.

pressure) is,

$$\frac{p_l - p_u}{q_\infty} = \frac{p_l - p_\infty}{q_\infty} - \frac{p_u - p_\infty}{q_\infty} \tag{9.62}$$

$$= C_{p_l} - C_{p_u} \tag{9.63}$$

$$\approx 2\frac{\tilde{u}_u - \tilde{u}_l}{V_\infty} \tag{9.64}$$

For the vortex sheet in thin airfoil theory, Equation (9.31) gives,

$$\tilde{u}_u - \tilde{u}_l = \gamma \tag{9.65}$$

Thus, we arrive at the result that,

$$C_{p_l} - C_{p_u} \approx 2\frac{\gamma}{V_\infty} \tag{9.66}$$

In the following video, we discuss the results of the symmetric airfoil and in particular consider the leading-edge behavior of the pressure differences.

Video Link

9.4.5 Cambered airfoils

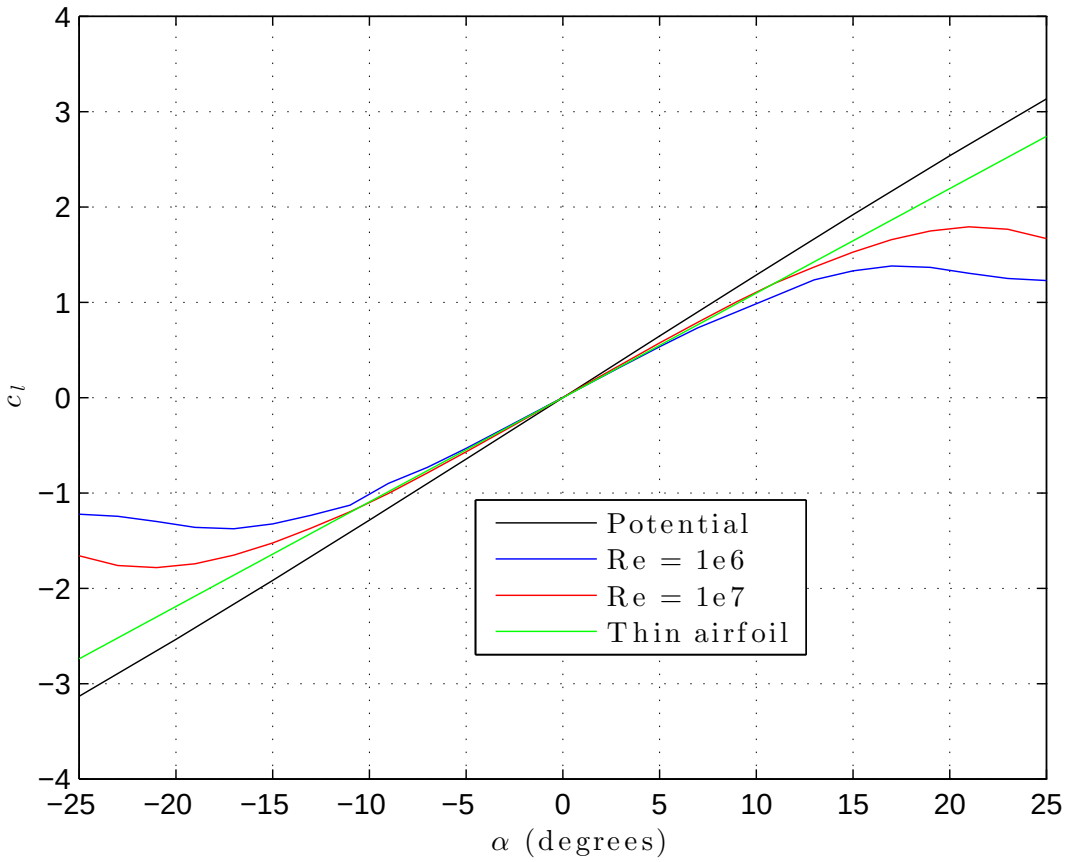


Figure 9.12: Comparison of $c_l(\alpha)$ for NACA 0021 for potential flow, thin airfoil theory, and $Re = 1E6$ and $Re = 1E7$ viscous calculations.

9.4

The analysis of cambered airfoils can be performed by expressing $\gamma(x)$ as a linear combination of the symmetric airfoil solution in Equation (9.43) and a series of additional modes. Specifically, using the ξ transformed coordinate, the general solution for $\gamma(x)$ is of the form,

$$\gamma(\xi) = 2V_\infty \left(A_0 \frac{1+\cos\xi}{\sin\xi} + \sum_{n=1}^{\infty} A_n \sin n\xi \right) \tag{9.67}$$

where all of the A_n are unknown values that determine the circulation distribution. With significant manipulations, the A_n can be related to the camber distribution and α,

$$A_0 = \alpha - \frac{1}{\pi}\int_0^\pi \frac{\mathrm{d}z_c}{\mathrm{d}x}\mathrm{d}\xi' \tag{9.68}$$

$$A_n = \frac{2}{\pi}\int_0^\pi \frac{\mathrm{d}z_c}{\mathrm{d}x}\cos n\xi' \mathrm{d}\xi' \tag{9.69}$$

Thus, the solution process to determine $\gamma(x)$ is reduced to performing the integrals of the camber slope given in Equations (9.68) and (9.69).

The circulation can be determined for this general γ distribution (beginning with Equation 9.48),

$$\Gamma = \frac{c}{2}\int_0^\pi \gamma(\xi')\sin\xi'\,\mathrm{d}\xi' \tag{9.70}$$

$$= cV_\infty\left[A_0\int_0^\pi(1+\cos\xi')\mathrm{d}\xi' + \sum_{n=1}^{\infty}A_n\int_0^\pi \sin n\xi'\sin\xi'\mathrm{d}\xi'\right] \tag{9.71}$$

The first integral is from the symmetric airfoil analysis done previously and has a value of π. The second integral is a result for Fourier integrals and is given by,

$$\int_0^\pi \sin n\xi'\sin\xi'\mathrm{d}\xi' = \begin{cases}\pi/2 & \text{for } n=1\\ 0 & \text{for } n\neq 1\end{cases} \tag{9.72}$$

Thus, for this general distribution we have,

$$\Gamma = cV_\infty\left(\pi A_0 + \frac{\pi}{2}A_1\right) \tag{9.73}$$

Which leads to the lift coefficient being given by,

$$c_l = \pi(2A_0 + A_1) \tag{9.74}$$

Or, equivalently, using Equations (9.68) and (9.69),

$$c_l = 2\pi\left[\alpha + \frac{1}{\pi}\int_0^\pi \frac{\mathrm{d}z_c}{\mathrm{d}x}(\cos\xi' - 1)\mathrm{d}\xi'\right] \tag{9.75}$$

This final form shows clearly that camber does not impact the lift slope which remains 2π, but camber does create an offset in the lift curve. A common way to write this result is,

$$c_l = 2\pi(\alpha - \alpha_{L=0}) \tag{9.76}$$

where the angle of zero lift is given by,

$$\alpha_{L=0} = \frac{1}{\pi}\int_0^\pi \frac{\mathrm{d}z_c}{\mathrm{d}x}(1-\cos\xi')\mathrm{d}\xi' \tag{9.77}$$

9.4.6 Pitching moment behavior

9.4

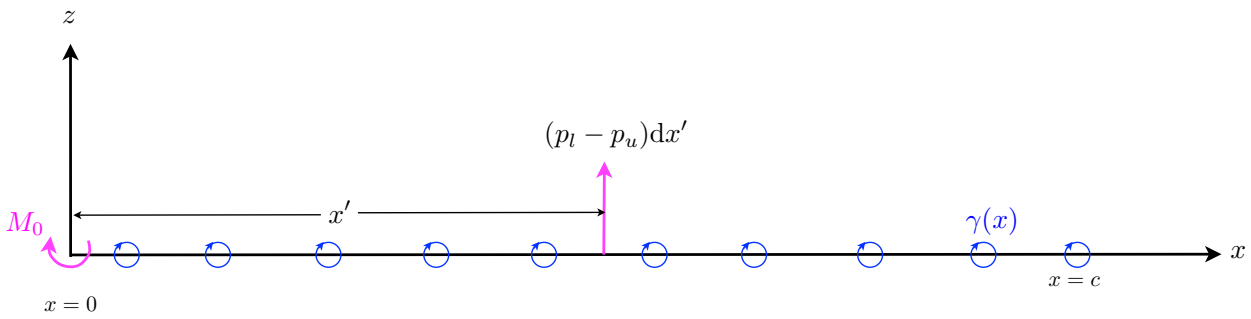


Figure 9.13: Calculation of the pitching moment about the leading edge from thin airfoil theory.

In addition to the lift, the moments created by aerodynamic forces are important and play a critical role in the stability of an aircraft. The pitching moment can be estimated in thin airfoil

theory by integrating across the chord the moment created by the pressure differences as shown in Figure 9.13. The pitching moment is defined as positive when it raises the nose of the airfoil. Thus, the pitching moment about the leading edge is,

$$M_0 = -\int_0^c (p_l - p_u) x' \mathrm{d}x' \tag{9.78}$$

$$= -\rho V_\infty \int_0^c \gamma(x') x' \mathrm{d}x' \tag{9.79}$$

$$= -\frac{1}{2}\rho V_\infty^2 c^2 \int_0^\pi \left(A_0 \frac{1+\cos\xi'}{\sin\xi'} + \sum_{n=1}^{\infty} A_n \sin n\xi' \right) (1-\cos\xi') \sin\xi' \mathrm{d}\xi' \tag{9.80}$$

Performing the integration and normalizing by $q_\infty c^2$ produces the moment coefficient about the leading edge,

$$c_{m\mathrm{le}} = -\frac{\pi}{2}\left(A_0 + A_1 - \frac{A_2}{2} \right) \tag{9.81}$$

This can be written in terms of c_l as,

$$c_{m\mathrm{le}} + \frac{c_l}{4} = \frac{\pi}{4}(A_2 - A_1) \tag{9.82}$$

The left-hand side of this result is the moment coefficient taken about the quarter chord, i.e. $x = c/4$. Thus, another form of the thin airfoil theory moment result is,

$$c_{mc/4} = \frac{\pi}{4}(A_2 - A_1) \tag{9.83}$$

Since A_1 and A_2 do not depend on α, then thin airfoil theory predicts that the moment about $c/4$ does not depend on the angle of attack. The location at which the aerodynamic moment is constant with respect to variations in α is called the *aerodynamic center*.

For symmetric airfoils, since $A_1 = A_2 = 0$, then $c_{mc/4} = 0$. The *center of pressure* is the x-location at which the aerodynamic moments are zero. Thus, for symmetric airfoils, the center of pressure and the aerodynamic center are located at $c/4$. However, for cambered airfoils, the center of pressure will vary with α. Specifically, we can solve for x_{cp} be determing the location at which the moment is zero:

$$c_m(x_{cp}) = 0 \tag{9.84}$$

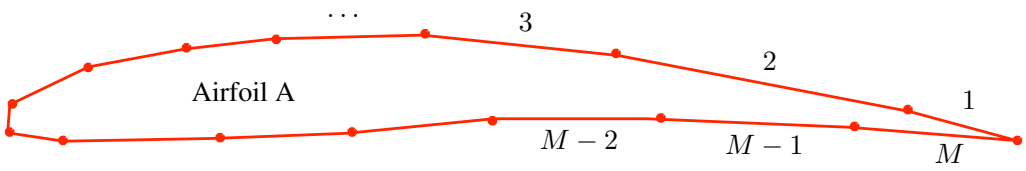
$$= c_{mc/4} + \left(\frac{x_{cp}}{c} - \frac{1}{4} \right) c_l \tag{9.85}$$

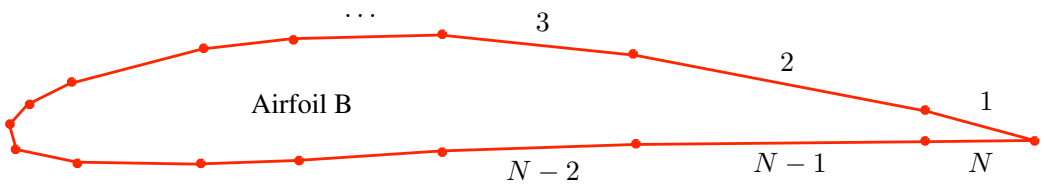
$$\Rightarrow \frac{x_{cp}}{c} = \frac{1}{4} - \frac{c_{mc/4}}{c_l} \tag{9.86}$$

9.5 Sample Problems

edXproblem: 9.5.1 Vortex panel method for two airfoils: 1 Point

9.1 9.3





Consider the application of a linear-varying vortex panel method to model the flow around two airfoils that are near each other as shown in figure. Airfoil A has M panels and Airfoil B has N panels.

- How many unknowns are used to represent the vortex sheet strength distributions and what are these unknowns?
- What equations are used to determine these unknowns?
- Describe the structure of K, g, and b for the system of equations, $Kg = b$, representing this set of unknowns and governing equations.

edXsolution

Video Link

edXproblem: 9.5.2 Parabolic air airfoil: 1 Point

9.4

In this problem, we will use thin airfoil theory to analyze the aerodynamic performance of an airfoil with a parabolic arc camber line given by,

$$z_c(x) = 4z_{c_{\max}} \frac{x}{c}\left(1 - \frac{x}{c}\right) \tag{9.87}$$

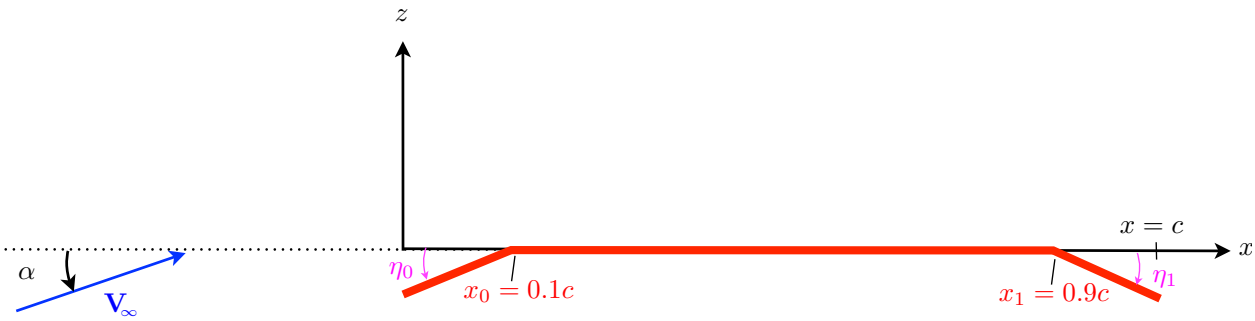
- Determine the value of all of the vortex sheet strength coefficients, A_n for any $n \geq 0$.
- Determine the angle of zero lift $\alpha_{L=0}$. Your answer will be a function of $z_{c_{\max}}/c$.
- What is the angle of attack and $z_{c_{\max}}/c$ needed to produce a lift coefficient $c_l = 0.5$ with no leading-edge suction peak?
- Determine and plot $C_{p_l} - C_{p_u}$ as a function of x/c for the $c_l = 0.5$, no suction peak condition.
- Determine the moment coefficient at the quarter-chord ($c_{mc/4}$) and the center of pressure (x_{cp}/c) for the $c_l = 0.5$, no suction peak condition.

edXsolution

Video Link

edXproblem: 9.5.3 Quantifying impact of leading and trailing edge flaps: 1 Point

9.4



In this problem, we will consider the aerodynamic impact of leading- and trailing-edge flaps on an airfoil using thin airfoil theory. To be specific, consider the camberline shown below with the angle of attack (α) and the flap angles (η_0 and η_1) all measured relative to the x axis. Note that η_0 and η_1 are defined as positive when the flap is deflected downwards.

- Calculate the derivative of the lift coefficient with respect to the leading-edge flap deflection angle, $\partial c_l/\partial \eta_0$.
- Calculate the derivative of the lift coefficient with respect to the trailing-edge flap deflection angle, $\partial c_l/\partial \eta_1$.
- Show that the trailing-edge flap has a significantly greater impact on the lift coefficient than the leading-edge flap.
- The reason for using a leading-edge flap is to decrease the possibility of leading-edge separation by aligning the airfoil's leading-edge camber in the direction of the local flow and thereby reducing the suction peak. Suppose the trailing-edge flap is not deflected ($\eta_1 = 0$). For a general freestream angle of attack α, what leading-edge flap angle is required to eliminate the leading-edge suction peak (according to thin airfoil theory)?
- For $c_l = 0.5$, what are the freestream angle of attack and the leading-edge flap deflection required to produce this lift without a suction peak?

edXsolution

Video Link

9.6 Homework Problems

edXproblem: 9.6.1 Lift coefficient from a vortex panel method

8.8 | 8.7 | 9.1 | 9.3

A linear-varying vortex panel method with 10 panels is used to simulate the flow around a symmetric airfoil at an angle of attack. The values of γ_i/V_∞ and s_i/c are given in the following table. Note, we are using the convention shown in Figure 9.5 where the panel starts at the trailing edge on the upper surface and wraps around the leading edge and back to the trailing edge at the lower surface.

i	s_i/c	γ_i/V_∞
1	0.0000	-0.0943
2	0.0964	0.9720
3	0.3479	1.1602
4	0.6575	1.3648
5	0.9079	1.7366
6	1.0139	1.5473
7	1.1199	-0.6248
8	1.3703	-0.8768
9	1.6798	-0.9150
10	1.9314	-0.8739
11	2.0277	γ_{11}/V_∞

What is the value of γ_{11}/V_∞?

What is the lift coefficient predicted by this panel method (Please provide the answer in the form $X.XX$)?

What is the drag coefficient predicted by this panel method?

Using thin airfoil theory, estimate the angle of attack at which this vortex panel solution was calculated? Provide your answer in degrees, to the nearest tenth of a degree (in other words, your answer should be of the form XX.X).

edXsolution

Video Link

edXproblem: 9.6.2 NACA 34XX aerodynamic performance: 1 Point

9.4

In this problem, you will estimate the aerodynamic performance of the NACA 34XX airfoils using thin airfoil theory.

1) Determine the angle of zero lift ($\alpha_{L=0}$) for these airfoils. Give your answer in degrees with the following precision X.YeP.

2) At what angle of attack is the leading-edge suction peak eliminated? Give your answer in degrees with the following precision X.YeP.

3) What is the lift coefficient at this angle of attack? Give your answer with the following precision X.YZeP.

edXsolution

Video Link

edXproblem: 9.6.3 Pressure distributions and moment coefficients

9.4

The goal of this problem is to understand how the pressure distribution on an airfoil depends on the moment coefficient about $x = c/4$. Specifically, you will design the camberline of three airfoils using thin airfoil theory such that the following design constraints are met:

- The lift coefficient is 0.5.
- There is no suction peak at the leading edge.

Using the constraints, determine A_0, A_1, and A_2 as a function of $c_{m_{c/4}}$. Use CM to represent $c_{m_{c/4}}$ when entering your formulas. DO NOT ENTER SPECIFIC VALES FOR $c_{m_{c/4}}$ but leave it as a variable in your formulas.

1) Enter your formula for A_0:

2) Enter your formula for A_1:

3) Enter your formula for A_2:

Assume the camberline is given by,

$$\frac{z_c}{c} = b_1 \frac{x}{c}\left(1 - \frac{x}{c}\right) + b_2 \frac{x}{c}\left(1 - \frac{x}{c}\right)\left(1 - 2\frac{x}{c}\right) \tag{9.88}$$

where b_1 and b_2 are constants to be determined. The slope of the camber line is equal to,

$$\frac{\mathrm{d}z_c}{\mathrm{d}x} = b_1 \cos\xi + b_2\left(\frac{3}{4}\cos 2\xi + \frac{1}{4}\right) \tag{9.89}$$

Determine α, b_1, and b_2 as a function of $c_{m_{c/4}}$. Use CM to represent $c_{m_{c/4}}$ when entering your formulas. DO NOT ENTER SPECIFIC VALUES FOR $c_{m_{c/4}}$ but leave it as a variable in your formulas.

4) Enter your formula for α (leave your answer in radians, do not include conversion factors to degrees):

5) Enter your formula for b_1:

6) Enter your formula for b_2:

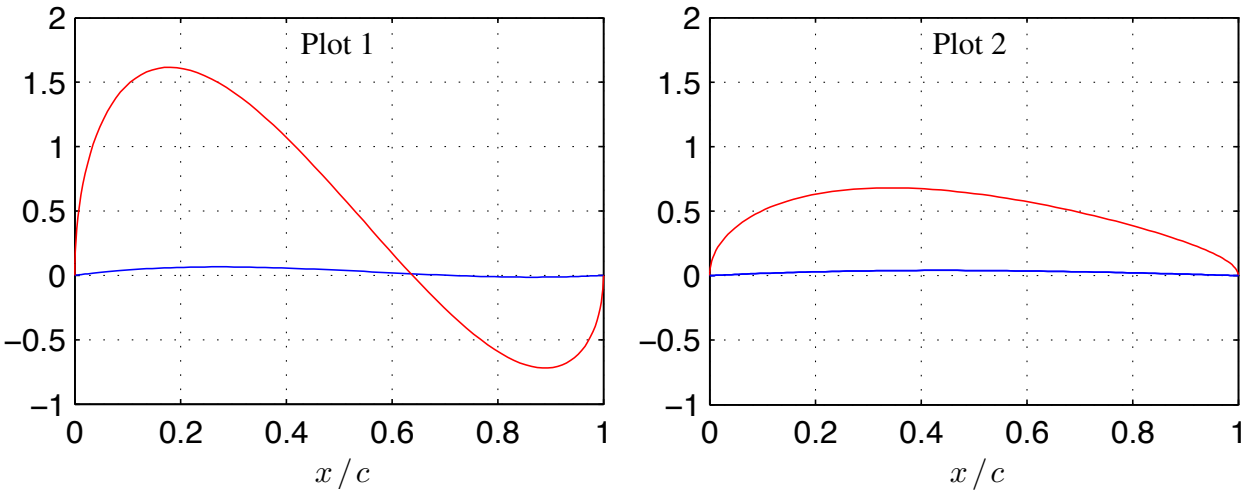
7) Which of the following plots of z_c/c and $C_{p_l} - C_{p_u}$ correspond to $c_{m_{c/4}} = -0.1$:

8) Which of the following plots of z_c/c and $C_{p_l} - C_{p_u}$ correspond to $c_{m_{c/4}} = 0$:

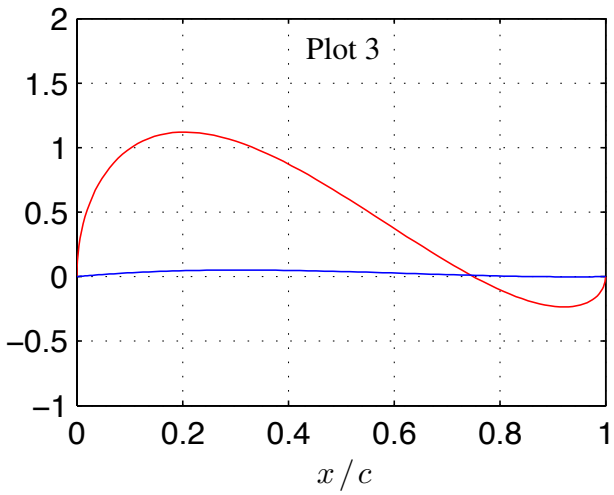
9) Which of the following plots of z_c/c and $C_{p_l} - C_{p_u}$ correspond to $c_{m_{c/4}} = 0.1$:

edXsolution

Video Link


Plot 1
2
1.5
1
0.5
0
−0.5
−1
0
0.2
0.4
0.6
0.8
1
x / c

Plot 2
2
1.5
1
0.5
0
−0.5
−1
0
0.2
0.4
0.6
0.8
1
x / c


Plot 3
2
1.5
1
0.5
0
−0.5
−1
0
0.2
0.4
0.6
0.8
1
x / c

edXproblem: 9.6.4 Airfoil design using thin airfoil theory

9.4

In this problem, apply thin airfoil theory to determine the camber distribution and angle of attack of an airfoil such that it has the following design constraints:

- $c_l = 0.7$
- No leading-edge suction peak
- The center of pressure is $0.05c$ in front of the aerodynamic center.

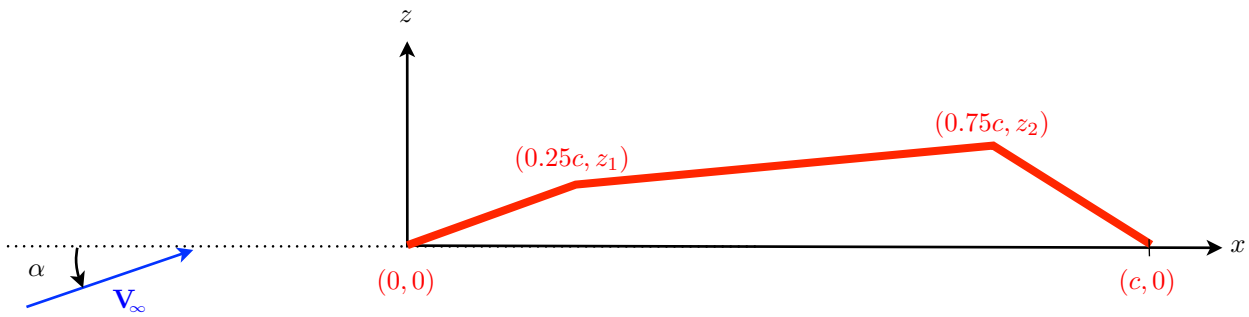
For all questions in this problem, please report your answers with three significant digits of precision equivalent to the form X.YZeP.

1) What is the moment coefficient at $c/4$?

2) What is the A_0 coefficient for the γ distribution given in Equation (9.67)?

3) What is the A_1 coefficient for the γ distribution given in Equation (9.67)?

4) What is the A_2 coefficient for the γ distribution given in Equation (9.67)?



Consider the simple segmented shape for the camberline. Determine the values of z_1/c and z_2/c that satisfy the desired design constraints.

5) What is the value of z_1/c?

6) What is the value of z_2/c?

7) What is the angle of attack at which this airfoil camber distribution satisfies the desired design constraints? Pleae provide your answer in degrees.

edXsolution

Video Link

Module 10

Midterm Exam

10.1 Instructions

10.1.1 Instructions

The following instructions for the Midterm applied to the Fall 2015 offering of 16.101x. We have left these instructions for you to have a sense of what was required when 16.101x was last offered for certification. These instructions no longer apply and you can feel free to discuss all of these problems.

This is a reminder that Midterm exam begins on Monday, November 16nd at 20:00 UTC. You have until Monday, November 23rd at 20:00 UTC to complete the exam. The exam will cover the material from Part 1.

You must complete the exam on your own without help from others. If there is a question of clarification or if you have double checked your work and think there might be a bug in the system, please communicate that in the discussion forum. Please do NOT use the discussion forums to discuss the problems on the exam in any way. Such posts will be immediately deleted.

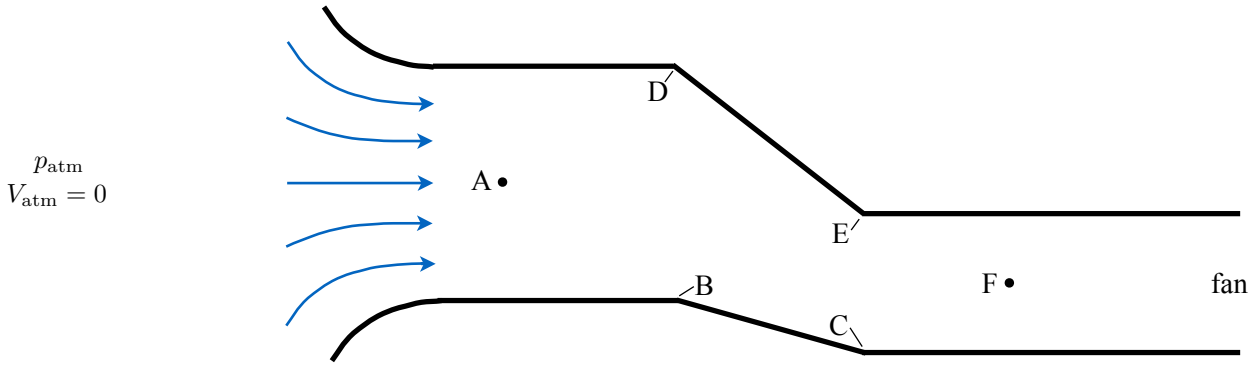
Finally, in terms of the Midterm: **You must complete the exam on your own without help from others.** If there is a question of clarification or if you have double checked your work and think there might be a bug in the system, please communicate that in the discussion forum. Please do NOT use the discussion forum (or any other means) to discuss the problems on the exam in any other way until after the exam deadline has passed. Such posts in our 16.101x forum will be immediately deleted.

Good luck!

10.2 Midterm Exam Problems

edXproblem: 10.2.1 Midterm Problem One: 25 Points

3.6 | 7.1 | 8.1 | 8.2



Flow is drawn into a duct from a still ($V_{\text{atm}} = 0$) atmosphere by a fan as shown in the figure. The flow is steady throughout the duct. The speed of the flow is in general much less than the speed of sound, so you may treat the flow as incompressible. Further, assume that the viscous effects are small so you may treat the flow as inviscid.

Select all of the answers that are true:

edXsolution

Video Link

edXproblem: 10.2.2 Midterm Problem Two: 25 Points

9.4

In this problem, you will use thin airfoil theory to design the shape of an airfoil. The goal is to produce an airfoil which produces a $c_l = 1$ while minimizing the magnitude of the jump in pressure coefficient, $|C_{p_u} - C_{p_l}|$. For all numerical answers in this problem, please provide three digits of precision (X.YZeP).

1) To begin, consider an airfoil which has only two coefficients A_0 and A_1 in its circulation series distribution which may be non-zero with all other coefficient zero, i.e. $A_n = 0$ for $n > 1$. Determine the values of A_0 and A_1 for which the magnitude of the pressure coefficient jump is minimized while achieving $c_l = 1$.

What is the value of A_0?

What is the value of A_1?

What is the maximum magnitude of the pressure coefficient jump $\left|C_{p_u} - C_{p_l}\right|$ on the airfoil?

2) Now, consider an airfoil which has three coefficients A_0, A_1, and A_2 which may be non-zero with all other coefficients zero, i.e. $A_n = 0$ for $n > 2$. Determine the values of A_0, A_1, and A_2 for which the magnitude of the pressure coefficient jump is minimized while achieving $c_l = 1$.

What is the value of A_0?

What is the value of A_1?

What is the value of A_2?

What is the maximum magnitude of the pressure coefficient jump $\left|C_{p_u} - C_{p_l}\right|$ on the airfoil?

3) Finally, consider an airfoil which has three coefficients A_0, A_1, and A_3 which may be non-zero with all other coefficients zero, i.e $A_2 = 0$ and $A_n = 0$ for $n > 3$. Determine the values of A_0, A_1, and A_3 for which the magnitude of the pressure coefficient jump is minimized while achieving $c_l = 1$.

What is the value of A_0?

What is the value of A_1?

What is the value of A_3?

What is the maximum magnitude of the pressure coefficient jump $\left|C_{p_u} - C_{p_l}\right|$ on the airfoil?

edXsolution

Video Link

edXproblem: 10.2.3 Midterm Problem Three: 25 Points

2.5	2.8	6.4	7.2	8.6	8.7

The following problem is a collection of different, relatively short, questions.

1) Consider the two-dimensional flow over an airfoil with chord c generating a lift coefficient c_l. Let the freestream be in the x-direction, $\mathbf{V}_\infty = V_\infty \hat{\mathbf{i}}$. Let the airfoil quarter-chord location be at the origin $(x, z) = (0, 0)$. Estimate the slope of the flow w/u at a point $10c$ in front of the airfoil, i.e. at $(x, z) = (-10c, 0)$. Specifically, for a $c_l = 0.5$, determine w/u at this point. Provide your answer with two digits of precision (X.YeP).

2) Consider a two-dimensional flow with velocity $u = -x$ and $v = y$ (the units of u and v are m/sec and x and y are m). Determine the acceleration vector of a fluid element at the point $(x, y) = (1, 10)$ in units of m/sec^2. Specifically:

What is the x-component of the acceleration vector:

What is the y-component of the acceleration vector:

Assuming an inviscid flow and that the density at point $(1, 10)$ is $\rho = 2\,\text{kg/m}^3$, determine the pressure gradient ∇p (in Pascals/m) at the point. Specifically:

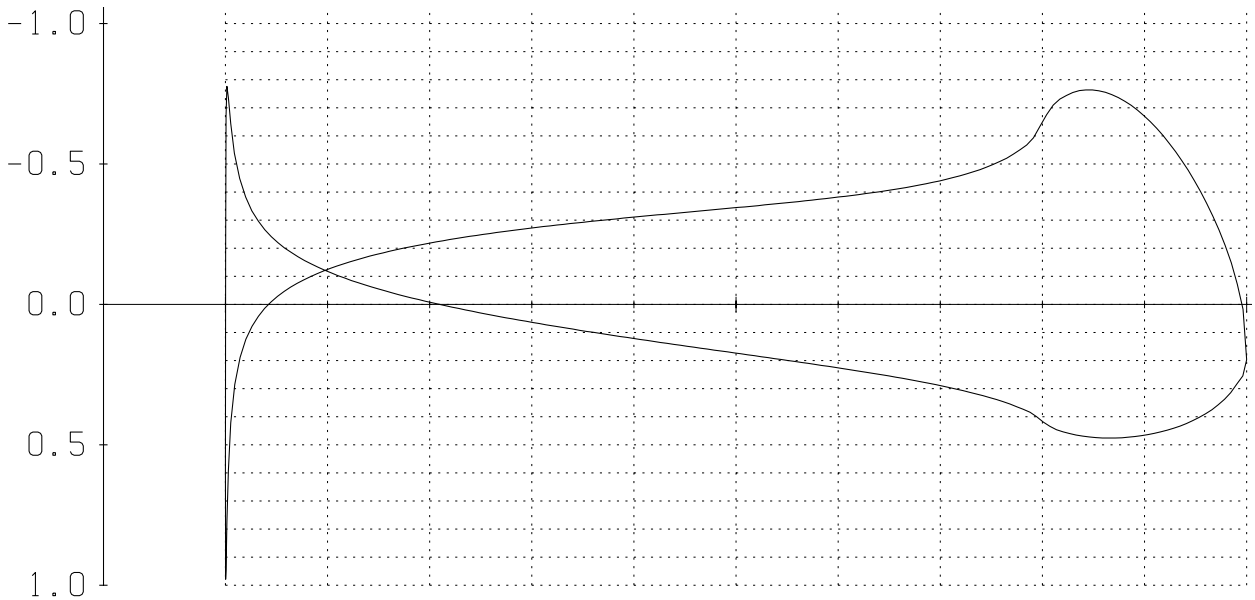
What is the x-component of ∇p:

What is the y-component of ∇p:

3) Consider the C_p distribution for an airfoil shown in the figure (this is the usual plot of C_p versus x/c with a grid overlayed of 0.1×0.1 rectangles). The airfoil is producing a positive lift $c_l > 0$. Estimate the lift coefficient c_l and determine if the leading edge stagnation point is on the upper or lower surface. If the leading edge stagnation point is on the upper surface, enter your estimate of $c_l + 10$. For example, if your estimate of $c_l = 1.2$ and the leading edge stagnation point is on the upper surface, you would enter 11.2. If the leading edge stagnation point is on the lower surface, enter -(your estimate of $c_l + 10$). For example, if your estimate of $c_l = 1.2$ and the leading edge stagnation point is on the lower surface, you would enter -11.2. Provide your answer with three digits of precision XY.Z.

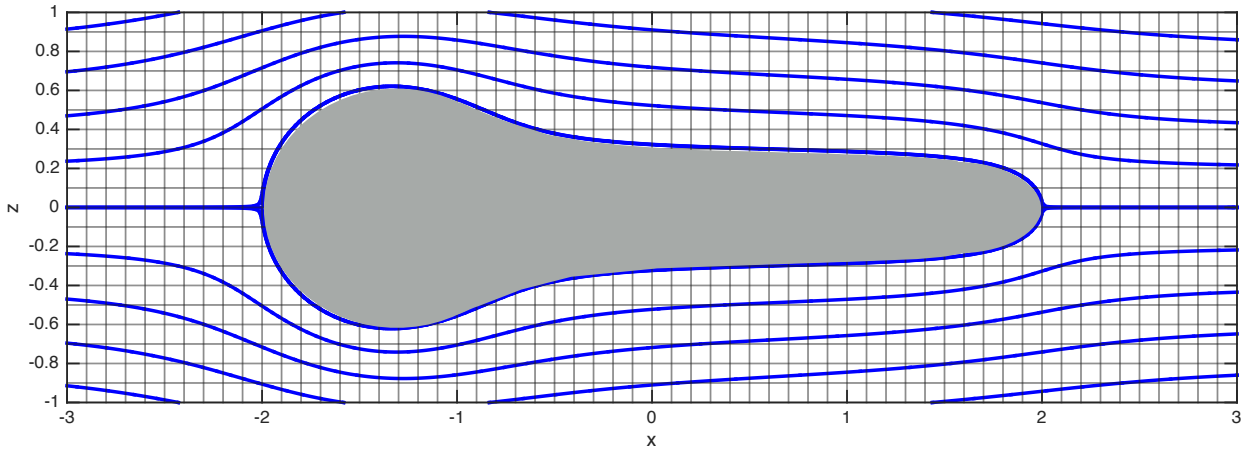
edXsolution

Video Link


-1.0
-0.5
0.0
0.5
1.0

edXproblem: 10.2.4 Midterm Problem Four: 25 Points

8.5 8.6



Streamlines for an incompressible two-dimensional potential flow around a body are shown in the figure. The body starts at $x = -2$ and ends at $x = 2$. The freestream velocity is $\mathbf{V}_\infty = 1\hat{\mathbf{i}}$. The flow can be represented by three point sources on the x-axis combined with the freestream. Let x_a, x_b, and x_c be the locations of the sources, defined so that $x_a < x_b < x_c$. The location of the sources are from the following set of 20 numbers

$$x_a, x_b, x_c \in \{-1.9,\ -1.7,\ -1.5,\ \ldots, 1.5,\ 1.7,\ 1.9\} \tag{10.1}$$

The corresponding source strengths are Λ_a, Λ_b, and Λ_c (these can have any value). Determine the location and strength of the three sources. Hint: once you have determined the correct source locations, the source strengths can be determined quite precisely applying your knowledge of the behavior of the flow and the shape of the body.

Enter x_a:

Enter x_b:

Enter x_c:

Enter Λ_a (Provide your answer with two digits of precision X.YeP):

Enter Λ_b (Provide your answer with two digits of precision X.YeP):

Enter Λ_c (Provide your answer with two digits of precision X.YeP):

edXsolution

This solution was a bit long and was broken into two videos.

Part 1/2:

Video Link

Part 2/2:

Video Link

Module 11

Three-dimensional Incompressible Potential Flow Aerodynamic Models

11.1 Overview

11.1.1 Measurable outcomes

In this module, we develop potential flow models for estimating the aerodynamic performance of three-dimensional bodies, in particular wings. Along the way, we will discover that three-dimensional potential flow around bodies that generate lift have non-zero drag. This lift-related drag is often refered to as *induced drag*.

Specifically, students successfully completing this module will be able to:

11.1. Define the velocity field for a source and doublet in three dimensions. Derive the relationship between the strength of a source, mass flow, and the conservation of mass.

11.2. Combine a freestream and doublet to model the potential flow around a sphere. Determine the pressure coefficient distribution on the sphere surface.

11.3. Utilize the Biot-Savart law to determine the velocity field induced by vortex filament. Show that the flow induced by vortex filament satisfies conservation of mass and is irrotational (except on the filament).

11.4. Describe how the generation of lift on a wing results in a vortical motion behind the wing due to the general motion of the flow from the high pressure lower surface around to the lower pressure upper surface.

11.5. Describe how the sectional lift distribution is a related to the bending moment at the root of a wing. Describe how the sectional lift coefficient behavior is related to the potential for stall.

11.6. Describe how the presence of a vortical wake gives rise to finite velocity perturbations in the Trefftz plane and that these perturbations, which increase the kinetic energy of the flow, must result from work being done on the air by a force acting in the direction of motion of the body (i.e. equal-and-opposite of the drag force which acts on the body). Further, interpret the induced drag in terms of the downwash created by the trailing vortical wake which tilts the effective sectional lift into the freestream direction.

11.7. Explain the lifting line model for a high aspect ratio wing including the assumptions. Describe the key results for the lift and induced drag including the dependence on aspect ratio, the relationship to two-dimensional potential flow, and the optimality of the elliptic lift distribution. Describe how the variation in the lift distribution is related to the vorticity in the trailing wake.

11.8. Apply the lifting line model to estimate the behavior of the flow and the aerodynamic performance of a wing. Apply the lifting line model to design a wing that meets desired aerodynamic performance.

11.1.2 Pre-requisite material

The material in this module requires the measurable outcomes from Modules 9.

11.2 Three-dimensional Nonlifting Flows

11.2.1 Spherical coordinate system

8.4

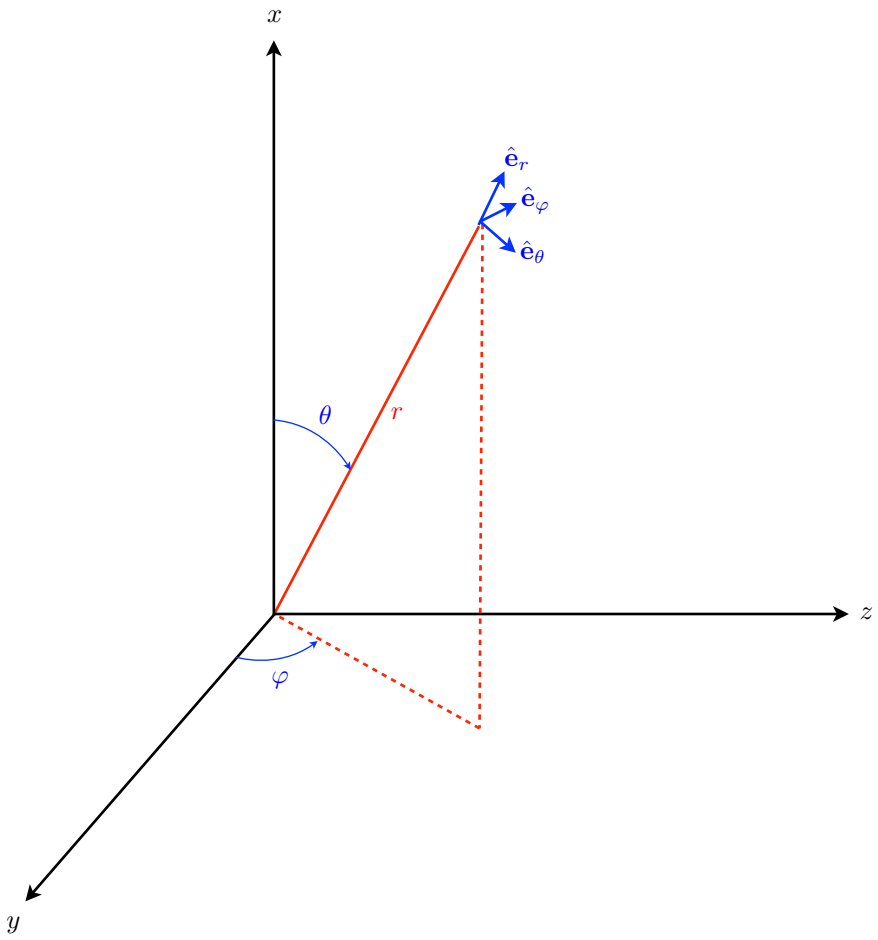


Figure 11.1: Three-dimensional spherical coordinate system

Spherical coordinates can be useful in describing three-dimensional potential flows. Figure 11.1 shows the spherical coordinate system we will use in this course. Specifically, the relationship between (x, y, z) and (r, θ, φ) is,

$$x = r\cos\theta \tag{11.1}$$
$$y = r\sin\theta\cos\varphi \tag{11.2}$$
$$z = r\sin\theta\sin\varphi \tag{11.3}$$

The unit vectors in the r, θ, and φ directions are,

$$\hat{\mathbf{e}}_r = \cos\theta\,\hat{\mathbf{i}} + \sin\theta\cos\varphi\,\hat{\mathbf{j}} + \sin\theta\sin\varphi\,\hat{\mathbf{k}} \tag{11.4}$$
$$\hat{\mathbf{e}}_\theta = -\sin\theta\,\hat{\mathbf{i}} + \cos\theta\cos\varphi\,\hat{\mathbf{j}} + \cos\theta\sin\varphi\,\hat{\mathbf{k}} \tag{11.5}$$
$$\hat{\mathbf{e}}_\varphi = -\sin\varphi\,\hat{\mathbf{j}} + \cos\varphi\,\hat{\mathbf{k}} \tag{11.6}$$

The radial, φ, and θ velocity components are related to u, v and w by,

$$u_r = u\cos\theta + v\sin\theta\cos\varphi + w\sin\theta\sin\varphi \tag{11.7}$$
$$u_\theta = -u\sin\theta + v\cos\theta\cos\varphi + w\cos\theta\sin\varphi \tag{11.8}$$
$$u_\varphi = -v\sin\varphi + w\cos\varphi \tag{11.9}$$

The gradient operator in spherical coordinates can be applied to ϕ to find u_r, u_θ, and u_φ

$$u_r = \frac{\partial\phi}{\partial r} \tag{11.10}$$
$$u_\theta = \frac{1}{r}\frac{\partial\phi}{\partial\theta} \tag{11.11}$$
$$u_\varphi = \frac{1}{r\sin\theta}\frac{\partial\phi}{\partial\varphi} \tag{11.12}$$

The divergence and curl of the velocity vector in spherical coordinates are,

$$\nabla\cdot\mathbf{V} = \frac{1}{r^2}\frac{\partial}{\partial r}\left(r^2u_r\right) + \frac{1}{r\sin\theta}\frac{\partial}{\partial\theta}\left(u_\theta\sin\theta\right) + \frac{1}{r\sin\theta}\frac{\partial u_\varphi}{\partial\varphi} \tag{11.13}$$

$$\nabla\times\mathbf{V} = \frac{1}{r^2\sin\theta}\begin{vmatrix} \hat{\mathbf{e}}_r & r\hat{\mathbf{e}}_\theta & (r\sin\theta)\hat{\mathbf{e}}_\varphi \\ \frac{\partial}{\partial r} & \frac{\partial}{\partial\theta} & \frac{\partial}{\partial\varphi} \\ u_r & ru_\theta & (r\sin\theta)u_\varphi \end{vmatrix} \tag{11.14}$$

Finally, we note that Laplace's equation for ϕ in spherical coordinates is,

$$\nabla^2\phi = \frac{1}{r^2}\frac{\partial}{\partial r}\left(r^2\frac{\partial\phi}{\partial r}\right) + \frac{1}{r^2\sin\theta}\frac{\partial}{\partial\theta}\left(\sin\theta\frac{\partial\phi}{\partial\theta}\right) + \frac{1}{r^2\sin^2\theta}\frac{\partial^2\phi}{\partial\varphi^2} = 0 \tag{11.15}$$

11.2.2 Source in 3D flow

11.1

Similar to the source in two-dimensional flow discussed in Section 8.4.3, a three-dimensional source has only radial velocity. In three dimensions, the potential and velocity components of a source are,

$$\phi = -\frac{\lambda}{4\pi r} \tag{11.16}$$
$$u_r = \frac{\lambda}{4\pi r^2} \tag{11.17}$$
$$u_\theta = 0 \tag{11.18}$$
$$u_\varphi = 0 \tag{11.19}$$

where λ is source strength. Similar to the two-dimensional case, the following results can be proven,

- A 3D source emits mass at a rate of $\rho\lambda$.
- A source satisfies the conservation of mass except at its origin. That is $\nabla\cdot\mathbf{V} = 0$ everywhere in the flow expect at its origin. And, at the origin, $\nabla\cdot\mathbf{V}$ is infinite.

11.2.3 Doublet in 3D flow

8.5 11.1

Analogous to the two-dimensional doublet flow described in Section 8.4.7, a doublet in three-dimensional flow can be defined by combining two sources at $(x, y, z) = (\pm l, 0, 0)$ with strength $\mp\lambda$ and taking the limit $l \to 0$ while holding $\mu \equiv 2\lambda l =$ constant. μ is the strength of the 3D doublet. The potential and velocity components for this flow are,

$$\phi = \frac{\mu}{4\pi}\frac{\cos\theta}{r^2} \tag{11.20}$$

$$u_r = -\frac{\mu}{2\pi}\frac{\cos\theta}{r^3} \tag{11.21}$$

$$u_\theta = -\frac{\mu}{4\pi}\frac{\sin\theta}{r^3} \tag{11.22}$$

$$u_\varphi = 0 \tag{11.23}$$

11.2.4 Nonlifting flow over a sphere

8.4 8.5 11.1 8.8 8.7 11.2

By combining a freestream (in the x-direction) with a doublet, the potential flow over a sphere can be determined. First, we begin by determining the relationship between the doublet strength (μ), the freestream velocity (V_∞), and the radius of the sphere (R). The velocity components for this flow are,

$$u_r = V_\infty \cos\theta - \frac{\mu}{2\pi}\frac{\cos\theta}{r^3} \tag{11.24}$$

$$u_\theta = -V_\infty \sin\theta - \frac{\mu}{4\pi}\frac{\sin\theta}{r^3} \tag{11.25}$$

$$u_\varphi = 0 \tag{11.26}$$

On the surface of the sphere, flow tangency requires $u_r(R, \theta) = 0$. Evaluating u_r at $r = R$ and enforcing $u_r = 0$ gives the doublet strength in terms of V_∞ and R,

$$u_r(R,\theta) = V_\infty \cos\theta - \frac{\mu}{2\pi}\frac{\cos\theta}{R^3} = 0 \Rightarrow \mu = 2\pi R^3 V_\infty \tag{11.27}$$

Thus, the velocity components for the flow around a sphere of radius R in a freestream of velocity V_∞ are,

$$u_r = V_\infty \cos\theta\left(1 - \frac{R^3}{r^3}\right) \tag{11.28}$$

$$u_\theta = -V_\infty \sin\theta\left(1 + \frac{1}{2}\frac{R^3}{r^3}\right) \tag{11.29}$$

$$u_\varphi = 0 \tag{11.30}$$

On the surface of the sphere where $r = R$, the velocity components and velocity magnitude are,

$$u_r = 0 \tag{11.31}$$

$$u_\theta = -\frac{3}{2}V_\infty \sin\theta \tag{11.32}$$

$$u_\varphi = 0 \tag{11.33}$$

$$V = \frac{3}{2}V_\infty |\sin\theta| \tag{11.34}$$

The pressure on the surface can then be determined using Bernoulli's equation,

$$p(R,\theta) = p_\infty + \frac{1}{2}\rho V_\infty^2 - \frac{1}{2}\rho V^2 \tag{11.35}$$

$$= p_\infty + \frac{1}{2}\rho V_\infty^2 \left(1 - \frac{9}{4}\sin^2\theta\right) \tag{11.36}$$

The corresponding pressure coefficient on the surface is,

$$C_p(R,\theta) = \frac{p(R,\theta) - p_\infty}{\frac{1}{2}\rho V_\infty^2} = 1 - \frac{9}{4}\sin^2\theta \tag{11.37}$$

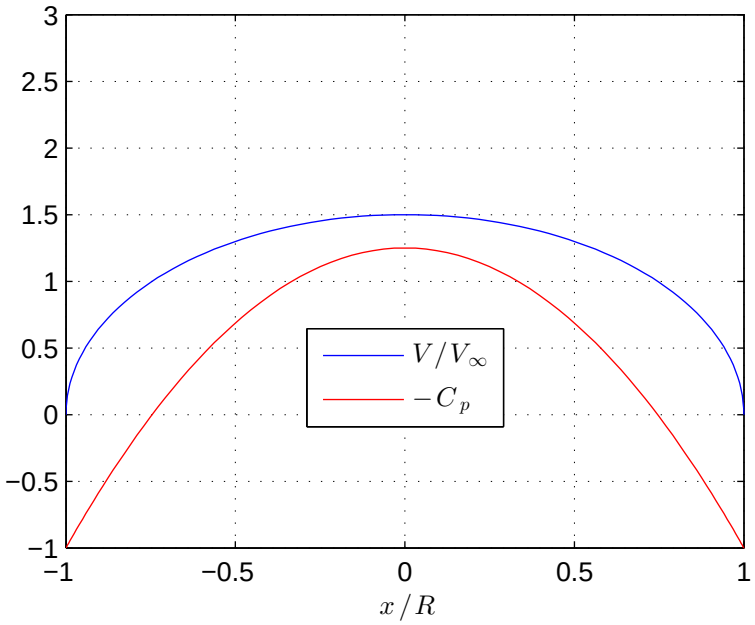


Figure 11.2: Surface V/V_∞ and C_p on a nonlifting sphere.

A plot of the surface velocity and pressure are shown in Figure 11.2. The velocity begins and ends at stagnation points and reaches a maximum speed which is $\frac{3}{2}V_\infty$ at the apex of the sphere. The C_p has the corresponding behavior with $C_p = 1$ at the high pressure stagnation points and $C_p = -\frac{5}{4}$ at the low pressure apex. Recall that the flow around the cylinder achieves a faster velocity of $2V_\infty$ at its apex. This behavior in which the perturbations from the freestream are larger in two-dimensional flows than in three-dimensional flows is common and is often referred to as *three-dimensional relief*. One way to understand this is to consider that the two-dimensional cylinder flow is equivalent to a cylinder with infinite span in the three-dimensional flow. Thus, it is not surprising that the cylinder will perturb the flow more significantly than the sphere which has a finite span.

Finally, analogous to the cylinder flow, the symmetry of the flow field from front-to-back implies that the drag will zero due to equal and opposite pressure force contributions. As well, symmetric from top-to-bottom implies the lift will be zero.

edXproblem: 11.2.5 Farfield velocity behavior of nonlifting flows in 3D

11.1 11.2

In Embedded Question 8.5.3, we investigate the behavior of flow velocity perturbations with respect to the distance from the body. For the nonlifting flow about a cylinder, we found that the velocity perturbations scaled with $1/r^2$ while for lifting flow the velocity perturbations scaled with $1/r$. In this Embedded Question, we now consider the behavior of velocity perturbations in nonlifting three-dimensional flow. In particular, we will consider the potential flow about a sphere, though the scaling result is in fact general for any nonlifting, incompressible flow.

For the nonlifting, incompressible potential flow around a sphere with radius R, consider the flow speed V in the $x = 0$ plane with $r = 100R$ and $r = 1000R$. What is the ratio of:

$$\frac{(V - V_\infty)_{(x,r)=(0,1000R)}}{(V - V_\infty)_{(x,r)=(0,100R)}}? \tag{11.38}$$

Enter your answer with two significant digits of accuracy (X.YeP). For example, 1.2e3.

edXsolution

Video Link

11.3 Introduction to Flow over Wings

11.3.1 Rectangular wings

11.4 11.5

The purpose of this entire section is to provide an introduction to the flow over wings. While we will not develop a model to estimate the aerodynamic performance of wings, we will introduce some key concepts in the behavior of the flow over wings and as well define the generic wing geometry.

To begin this section, we will start relatively simply with a rectangular wing having the same airfoil along the entire span. In this video, we introduce the key idea that the lift is distributed along the span of the wing such that even though the airfoil is identical at all spanwise locations (recall that the spanwise direction is along the y-axis), the lift (per unit span) and lift coefficient will generally vary with y.

Video Link

Summarizing the main points of this video

- For a wing generating lift, the (generally) lower pressures on the upper surface and (generally) higher pressures on the lower surface cause an outward motion of the air towards the wing tips on the lower surface and inward motion towards the wing root on the upper surface. The result is a swirling, vortical motion which will remain downstream of the wing in the form of a vortical wake.
- At the wing tips, the upper and lower surface pressures equalize such that the lift generated by the airfoil at the wing tip is approximately zero, thus $L'(y = \pm b/2) = 0$. Over the rest of the wing, the lift will vary with the spanwise location $L' = L'(y)$.
- As the aspect ratio of the wing increases, the relieving effect of the pressure equalization at the wing tips will have less influence on the flow over the central portion of the wing. Thus, as AR increases, we expect the performance of the wing to approach two-dimensional behavior.
- The total lift generated by the wing is,

$$L = \int_{-b/2}^{b/2} L'(y)\mathrm{d}y \tag{11.39}$$

- Since the lift generated by the airfoil sections varies with spanwise location, the sectional lift coefficient c_l is also a function of y,

$$c_l(y) = \frac{L'(y)}{q_\infty c} \tag{11.40}$$

- If we choose the reference area as the planform area, $S_{\text{ref}} = bc$ then the lift coefficient of the wing is equal to the average sectional lift coefficient, $C_L = \overline{c_l}$ where

$$\overline{c_l} \equiv \frac{1}{b}\int_{-b/2}^{b/2} c_l(y)\,\mathrm{d}y \tag{11.41}$$

11.3.2 Trailing vortex images

11.4

The following is a small collection of images depicting wing tip vortices.



Figure 11.3: Wing tip vortex of an agricultural plane highlighted by a colored smoke rising from the ground. (NASA Langley Research Center. Photo ID: EL-1996-00130. Public domain image).

11.3.3 General unswept wings

11.4 11.5

Now we move away from rectangular wings with constant airfoil sections, to allow more general wing shapes. Specifically, we will consider wings with the following properties:

- The chord distribution can vary with y: $\Rightarrow c = c(y)$
- The quarter-chord location of the airfoils is unswept and level (no dihedral or anhedral). These assumptions can be removed, but in this first look at the flow over wings, we will not consider these effects.
- The wing can have *geometric twist* such that the angle of the local chordline can vary with y: $\Rightarrow \alpha_g = \alpha_g(y)$
- The airfoil sections can vary with span. This is often referred to as *aerodynamic twist*.

The constraint that the quarter-chord line is unswept requires the line to be perpendicular to the freestream direction (the x-axis). The constraint that the quarter-chord line is level requires



Figure 11.4: Wingtip vortices on a C-17 Globemaster III highlighted by smoke from flares. (U.S. Air Force. Author: Tech. Sergeant Russell E. Cooley IV. May 16, 2006. Public domain image).

that it has constant z. We will define our unswept, level wing geometry such that the quarter-chord line lies along the y-axis ($x = z = 0$). The planform view of one such unswept wing with varying chord is shown in Figure 11.6.

The geometric twist angle $\alpha_g(y)$ is defined relative to an arbitrarily chosen reference line. Commonly, this reference line is chosen to be the axis of the fuselage. Thus, the overall angle of attack of an airfoil section is the sum of $\alpha + \alpha_g(y)$, where α is the angle from the freestream direction to the reference line, and $\alpha_g(y)$ is the angle from the reference line to the local chord line. In our analysis, we align the freestream with the x-axis. This is shown in Figure 11.7.

As described in the discussion of rectangular wings (see Section 11.3.1), the sectional lift $L'(y)$ and the sectional lift coefficient $c_l(y)$ are all functions of the spanwise location y. For rectangular wings, since the chord is constant, then $c_l(y)$ and $L'(y)$ have the same variation with y except for the constant scale factor of $q_\infty c$. For a wing with varying chord, this is no longer true and $c_l(y)$ will have a different dependence on y than $L'(y)$. Both the behavior of $L'(y)$ and $c_l(y)$ play an important role in the design of wings. $L'(y)$ is important in determining the bending moments which the wing structure must be designed for. $c_l(y)$ is important in determining the stall behavior of the wing. In the following video, we discuss both of these points.

Video Link

Summarizing the main points of this video



Figure 11.5: Vortex caused by flap illustrating the creation of vortices in locations where lift distribution changes rapidly. (November 28, 2006. Author: Miguel Andrade. Public domain image).

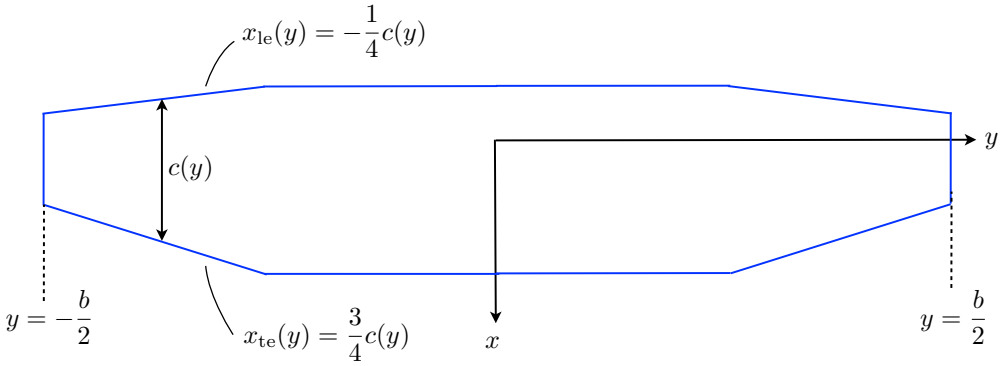


Figure 11.6: Planform view of wing with varying chord and unswept quarter-chord along y-axis

- The bending moment at the root ($y = 0$) of a wing is given by

$$M_{\text{bend}} = \int_0^{b/2} yL'(y)\mathrm{d}y \tag{11.42}$$

- A common non-dimensional measure used to report the lift distribution $L'(y)$ is

$$\frac{L'(y)}{q_\infty c_{\text{ref}}} = \frac{c_l(y)c(y)}{c_{\text{ref}}} \tag{11.43}$$

  where c_{ref} is a reference length (for example, the root chord, the average chord, and so on).

- Since we are using a potential flow model, the model cannot predict stall which is a viscous phenomenon. However, we can use the sectional lift coefficient as an indication of where on the wing stall is more likely. Specifically, regions on a wing where the sectional lift coefficient $c_l(y)$ is high are more likely to stall (assuming the airfoil sections have similar maximum c_l).

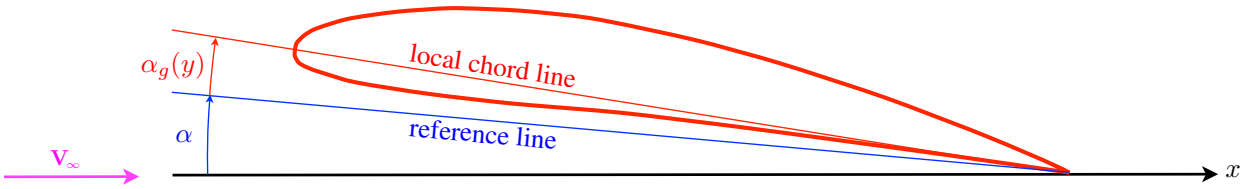


Figure 11.7: Definition of geometric angle of attack $\alpha_g(y)$ for an airfoil section of a wing and the freestream angle of attack α. Both angles are defined relative to a chosen reference line orientation.

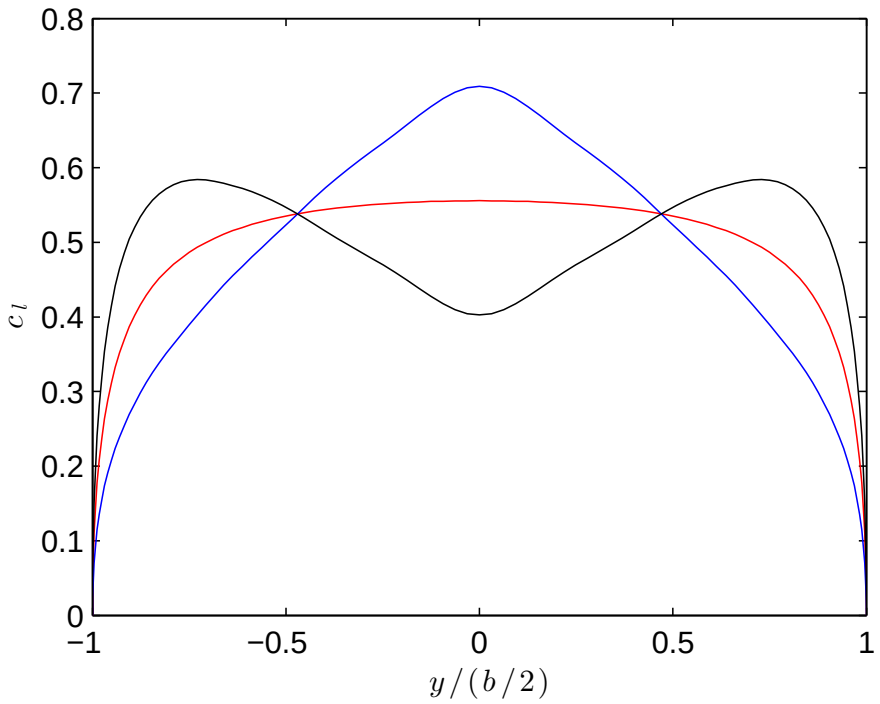
If we have estimates for the $c_{l_{\max}}(y)$, then we can compare the $c_l(y)$ to $c_{l_{\max}}(y)$ to determine where stall is likely.

- When the reference area used in the calculation of C_L is chosen as the planform area of the wing, C_L is equal to the planform-area-weighted average of the sectional lift coefficients $c_l(y)$. As a result, C_L must lie in the range of the $c_l(y)$ on the wing (but will generally not be equal to $\overline{c_l}$ defined in Equation 11.41).

edXproblem: 11.3.4 Impact of geometric twist on sectional lift coefficient

11.5

In this problem, we will consider the impact of geometric twist on the $c_l(y)$ distribution. A wing with *geometric washin* has a geometric angle of attack that is larger at the wing tip ($y = \pm b/2$) than at the wing root ($y = 0$). A wing with *geometric washout* has a geometric angle of attack that is larger at the wing root ($y = 0$) than at the wing tip ($y = \pm b/2$).



The sectional lift coefficient distribution, $c_l(y)$ is shown in the figure for three $AR = 10$ wings producing $C_L = 0.5$. The wings are identical except for the geometric twist. In particular, the wings have a rectangular planform ($c(y) =$ constant), and the airfoil shape does not vary with y (no aerodynamic twist). The three twist distributions are:

- No geometric twist ($\alpha_g(y) = 0$)
- Geometric washout varying linearly with y from $\alpha_g(0) = 5°$ to $\alpha_g(\pm b/2) = 0°$.
- Geometric washin varying linearly with y from $\alpha_g(0) = 0°$ to $\alpha_g(\pm b/2) = 5°$.

Select all of the statements that are correct:

edXsolution

Video Link

11.4 Lifting Line Models of Unswept Wings

11.4.1 Vortex filaments

11.3

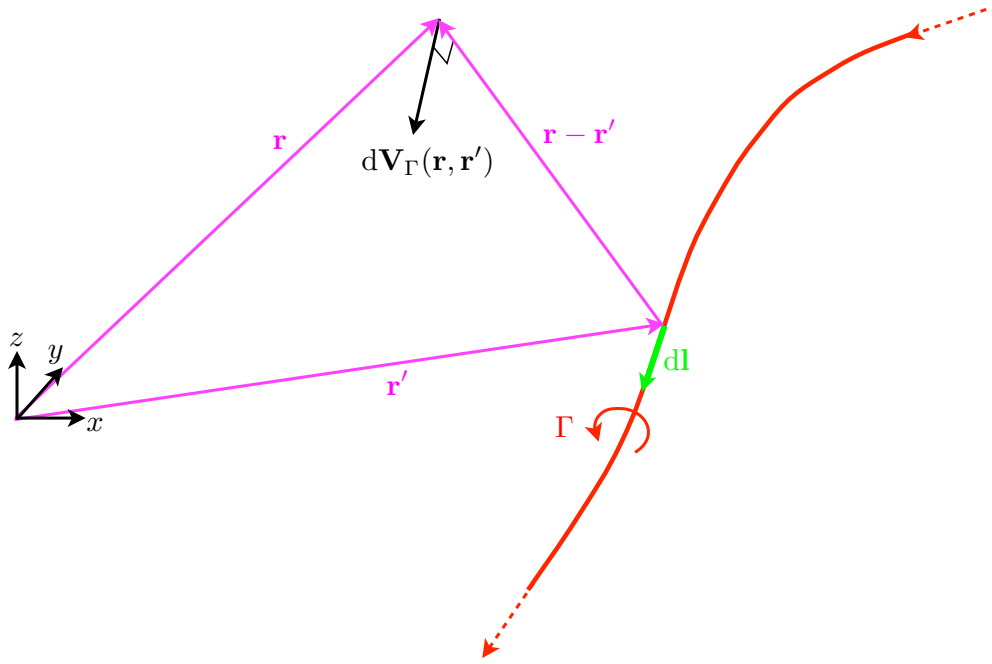


Figure 11.8: Vortex filament with strength Γ inducing a velocity $d\mathbf{V}_\Gamma(\mathbf{r}, \mathbf{r}')$.

The three-dimensional version of a point vortex is a vortex filament. As shown in Figure 11.8, a vortex filament has a strength Γ and the infinitesimal velocity induced by a length $d\mathbf{l}$ of the filament is given by,

$$d\mathbf{V}_\Gamma(\mathbf{r}, \mathbf{r}') = \frac{\Gamma}{4\pi} \frac{d\mathbf{l} \times (\mathbf{r} - \mathbf{r}')}{|\mathbf{r} - \mathbf{r}'|^3} \tag{11.44}$$

By applying Stokes theorem on a surface surrounding a filament, it can be shown that the strength of the filament can never change. In other words, Γ is a constant along the entire filament. Further, this implies that a filament cannot simply end in the fluid, since this is equivalent to the strength Γ changing to zero. Thus, a vortex filament must be infinitely long, or it must form a closed circuit. These results are known as Helmholtz vortex theorems.

The velocity induced by the entire filament can be found by integrating along the length of the filament,

$$\mathbf{V}_\Gamma(\mathbf{r}) = \frac{\Gamma}{4\pi} \int_{\text{filament}} \frac{d\mathbf{l} \times (\mathbf{r} - \mathbf{r}')}{|\mathbf{r} - \mathbf{r}'|^3} \tag{11.45}$$

This integral is equivalent to the calculation of a magnetic field induced by an electric current using the Biot-Savart Law. In our aerodynamic case, a velocity field is induced by the circulation.

As a simple example, in the following video we consider a straight (infinitely long) vortex filament lying along the y-axis. We show that the velocity induced by this vortex filament is equivalent to the point vortex in two-dimensional flow. Thus, we can interpret the two-dimensional point vortex in the (x, z) plane as the flow induced by an infinitely long, straight vortex filament along the y-direction.

Video Link

11.4.2 Lifting line model

11.7

In principle, the potential flow around a three-dimensional lifting body can be modeled by placing vortex filaments (on panels) over the entire body surface similar to the vortex panel method developed for airfoils. We will simplify this approach considerably to arrive at a model that demonstrates the fundamental issues that arise in three-dimensional lifting flows while being significantly easier to analyze theoretically (without the aid of a computer). This simpler model is known as lifting line and was originally developed by Ludwig Prandtl around the time of World War I.

An assumption inherent in the lifting line model is that the wing is high aspect ratio. Lifting line takes this assumption to its extreme and views the wing simply as a line (imagine looking at a high aspect ratio wing from far overhead such that it effectively looks like a line). Then, the flow due to the airfoil sections is represented by a vortex placed along this line. This vortex is often referred to as the *bound vortex*. However, the circulation of the bound vortex must vary with y since the sectional lift varies $L'(y)$. This implies that a single vortex filament cannot be used to represent the bound vortex since a vortex filament must have a constant circulation.

To model the varying circulation $\Gamma(y)$ of the bound vortex, the lifting line approach combines many vortex filaments with a shape known as a horseshoe vortex as shown in Figure 11.9. While the figure only shows four horseshoe vortices for clarity, we will in fact use infinitely many vortices. The horseshoe vortex starts far downstream (at $x \to \infty$) and runs parallel to the x-axis until it reaches the y axis. Then, it turns to the right along the y-axis and, after an infinitesimal distance $\mathrm{d}y$, turns back into the x direction returning infinitely far downstream. The strength of the horseshoe vortex centered at y is $\Gamma(y)$. By combining (infinitely) many of these horseshoe vortices, an arbitrary circulation (and therefore an arbitrary section lift) distribution can be represented.

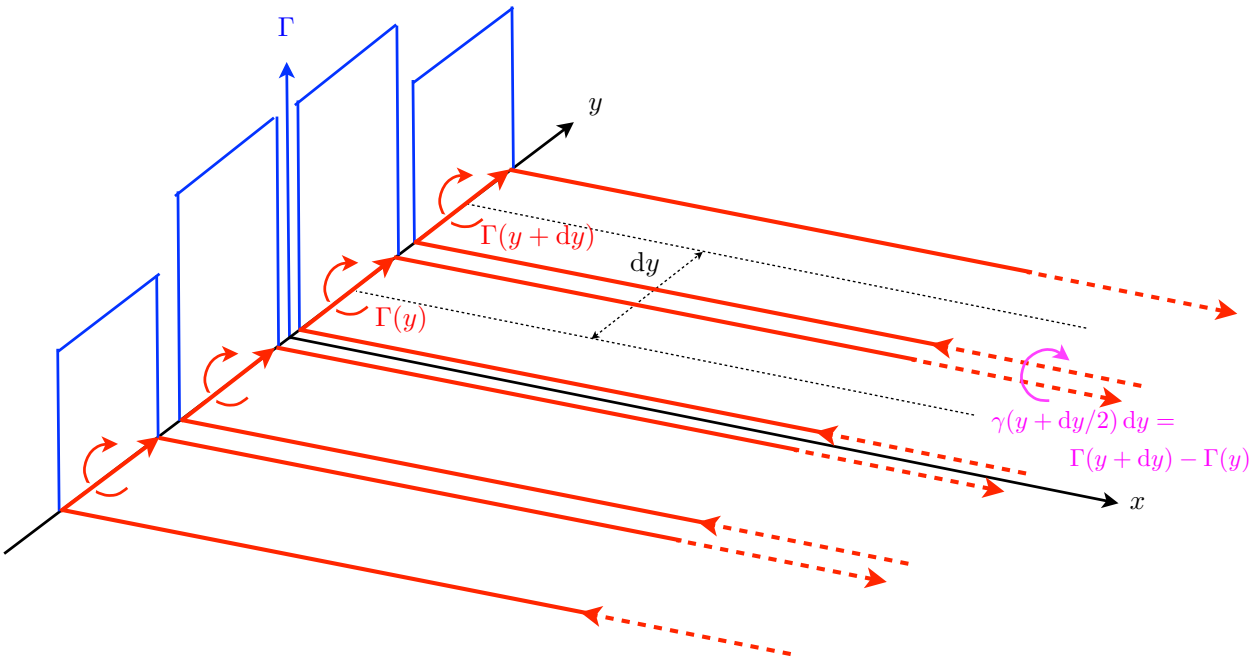


Figure 11.9: Construction of a lifting line from horseshoe vortices

The two neighboring horseshoe vortices at y and $y + \mathrm{d}y$ combine so that the net strength of the filament at $y + \mathrm{d}y/2$, which we label $\gamma(y + \mathrm{d}y/2)\,\mathrm{d}y$, is,

$$\gamma(y + \mathrm{d}y/2)\,\mathrm{d}y = \Gamma(y + \mathrm{d}y) - \Gamma(y) \tag{11.46}$$

Then, taking the limit as $\mathrm{d}y \to 0$,

$$\lim_{\mathrm{d}y\to 0} \gamma(y+\mathrm{d}y/2)\mathrm{d}y = \lim_{\mathrm{d}y\to 0} \Gamma(y+\mathrm{d}y) - \Gamma(y) \tag{11.47}$$

$$\gamma(y)\mathrm{d}y = \frac{\mathrm{d}\Gamma}{\mathrm{d}y}\mathrm{d}y \tag{11.48}$$

In the limit of $\mathrm{d}y \to 0$, the lifting line model as shown in Figure 11.10 is a vortex sheet with a bound vortex of strength $\Gamma(y)$ and the trailing sheet composed of semi-infinite vortex filaments (from $x = 0$ to $x \to \infty$) with strength per length $\gamma(y) = \mathrm{d}\Gamma/\mathrm{d}y$.

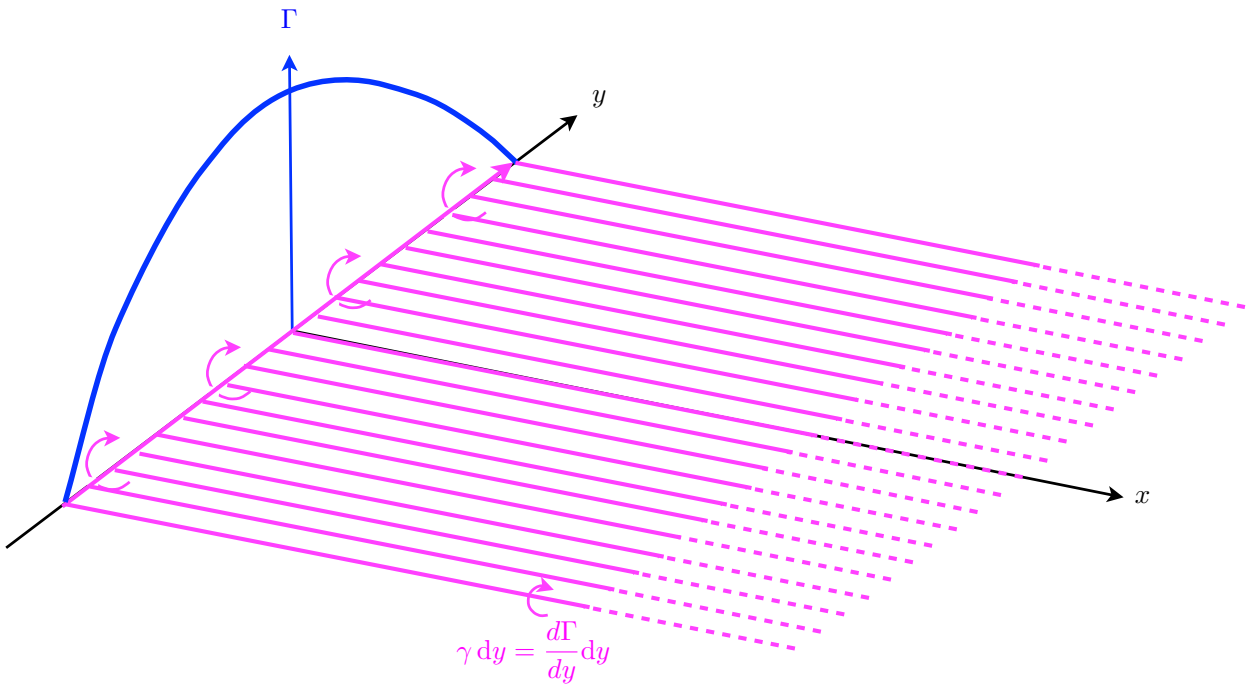


Figure 11.10: Lifting line with trailing vortices of strength $\gamma\,\mathrm{d}y = \frac{\mathrm{d}\Gamma}{\mathrm{d}y}\mathrm{d}y$

The following video is another of the classic videos in the NSF Fluid Mechanics Series. While the entire video is interesting, in particular please watch the following portions of the video:

- From 2:59 through 6:42: the discussion of the generation of circulation as an airfoil accelerates from rest.
- From 7:50 though 11:20: the discussion of the vortex system of a wing

Video Link

11.4.3 Trefftz plane flow of lifting line model

11.7 11.6

Although this lifting line model appears somewhat contrived, in fact the actual flow over a high aspect ratio wing is quite similar to this model. In particular, a wing does have a wake in which the vorticity is concentrated. However, the actual wake is not planar, but instead rolls up into concentrated trailing vortices (see the images in Section 11.3.2). That is, the vorticity in the actual flow convects into concentrated trailing vortices while the vorticity in the lifting line model is in the

planar sheet. This difference in the wake structure leads to an error between the lifting line and the actual flow, however, this error has a relatively small impact on the estimation of the lift-related forces on a high-aspect ratio wing.

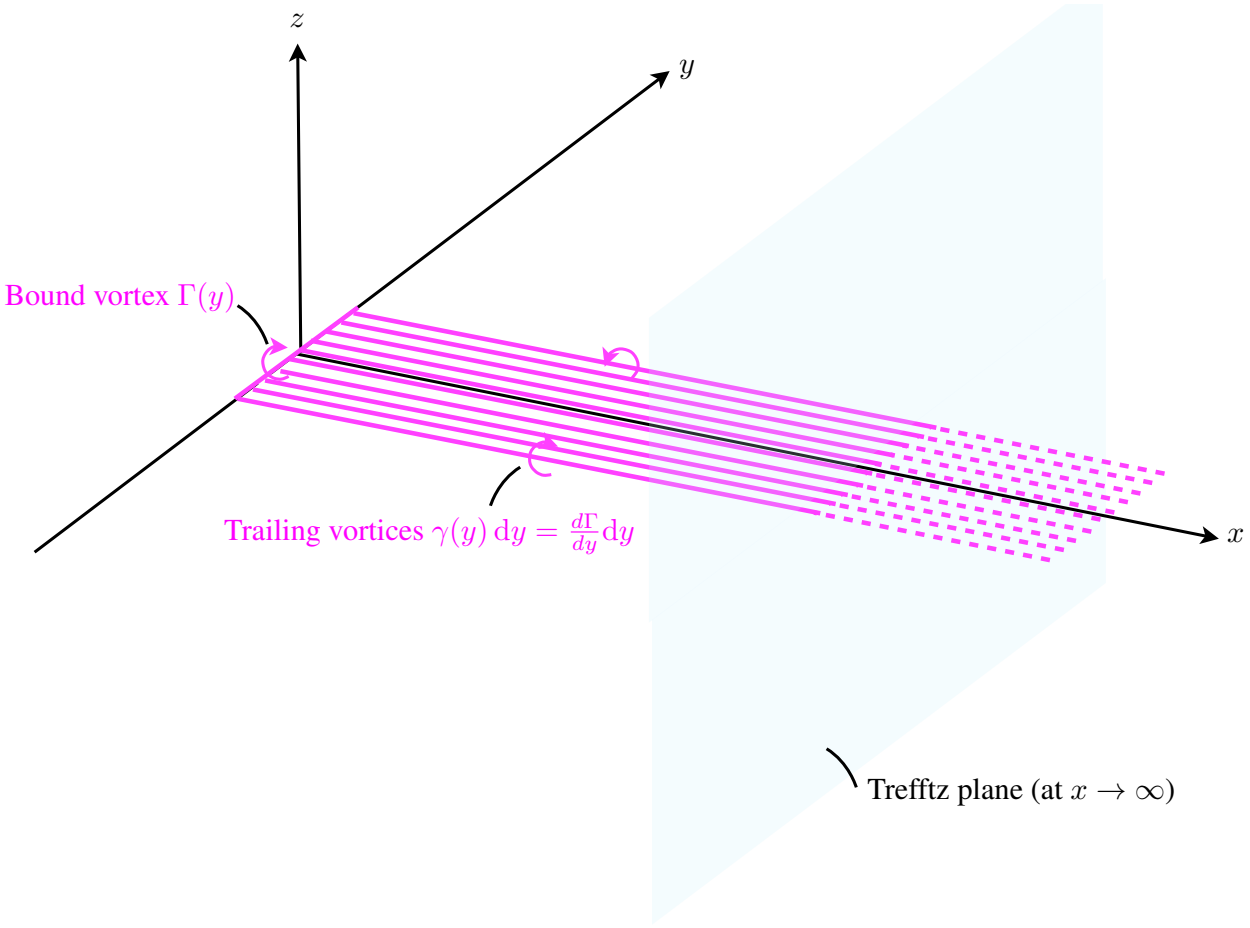


Figure 11.11: Trefftz plane with lifting line model

Some additional insight can be gained by considering the velocity distribution in the plane far downstream of the wing as shown in Figure 11.11. This plane is known as the Trefftz plane. Recall that we have already seen how the lift and drag can be related to the flow in the Trefftz plane (see Sample Problems 3.6.1 and 3.6.2 and Homework Problem 8.6.1). We will return to calculating the lift and drag for the lifting line model shortly, for now, we look at the velocity in the Trefftz plane.

Since the Trefftz plane is infinitely far from the y axis, the lifting line's bound vortex has no contribution to the velocity. Further, since the vortex filaments in the trailing sheet are all parallel to the x-axis, the x-velocity in the Trefftz plane is not perturbed at this location. Thus, in the Trefftz's plane, $u = V_\infty$.

To calculate the y and z components of the velocity, we can apply the Biot-Savart law over the entire wake. In the Trefftz plane, the vortex filaments extend infinitely far upstream and downstream, so the velocity induced by each vortex filament is equivalent to the two-dimensional velocity induced by a point vortex with strength $\gamma(y)\,\mathrm{d}y$ (see Figure 11.12). Thus, the velocity induced by the lifting line in the Trefftz plane can be found by integrating the contributions from the entire sheet of filaments,

$$\mathbf{V}_{\mathrm{w,line}}(y,z) = -\int_{-b/2}^{b/2} \frac{\gamma(y')\mathrm{d}y'}{2\pi r'}\hat{\mathbf{e}}_{\theta'} \tag{11.49}$$

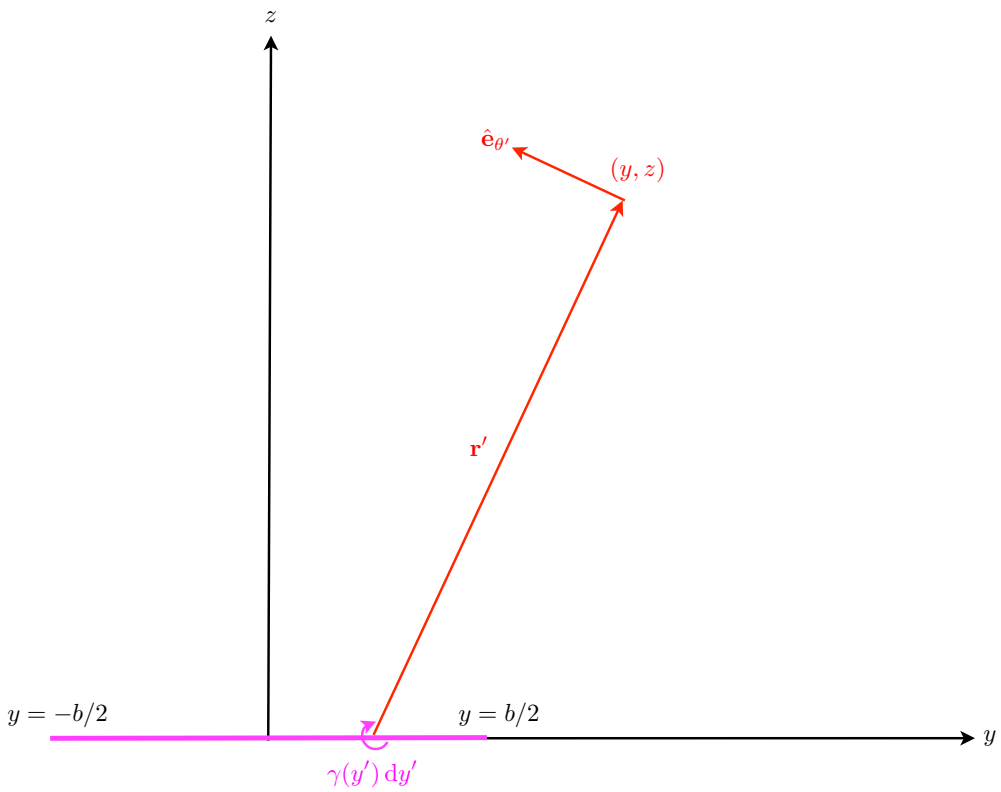


Figure 11.12: Trefftz plane showing trailing vortex sheet from lifting line model and geometry for velocity calculation

We will now consider the Trefftz plane velocity distribution for a couple of representive circulation distributions. We begin with perhaps the most important circulation distribution,

$$\Gamma = \Gamma_0 \sqrt{1 - \left(\frac{y}{b/2}\right)^2} \tag{11.50}$$

where Γ_0 is a parameter that is equal to the circulation at the root ($y = 0$). This is known as the *elliptic distribution* (because the formula is that of an ellipse) and is shown Figure 11.13.

Recall that the strength of the vortex filaments is given by $\gamma(y)\,\mathrm{d}y = \mathrm{d}\Gamma/\mathrm{d}y\,\mathrm{d}y$ and thus the strongest filaments will be where the most rapid variation of Γ is. This occurs at the wing tips for the elliptic lift distribution, and therefore we expect the vortical flow to be most evident at the tips. The velocity vectors in the Trefftz plane for the elliptic distribution are shown in Figure 11.14. The presence of the wing tip vortices can be clearly seen in the velocity vectors.

Next, we consider what the circulation and Trefftz plane flow might look like with a trailing-edge flap deflected. Since the trailing edge flap will increase the local lift, we will increase Γ in the region of the flap. Specifically, as shown in Figure 11.15, we add a rapid increase in the circulation from $0.25 < |y|/(b/2) < 0.5$ to represent what the circulation might be with a trailing edge flap deflected in this region (note: we will discuss how to specifically calculate the impact of geometry including flaps on Γ. So, for now, this is just representative of what Γ might be).

The velocity vectors in the Trefftz plane are shown in Figure 11.16 and zoomed in to the region of the flap in Figure 11.17. At the larger view in Figures 11.14 and 11.16, it is difficult to see much difference. However, the zoomed figure clearly shows the presence of two smaller vortices at approximately $y/(b/2) = 0.25$ and $y/(b/2) = 0.5$. Thus we again observe vortical flow where the sectional lift, and therefore the circulation, vary rapidly with y. You might also refer back to

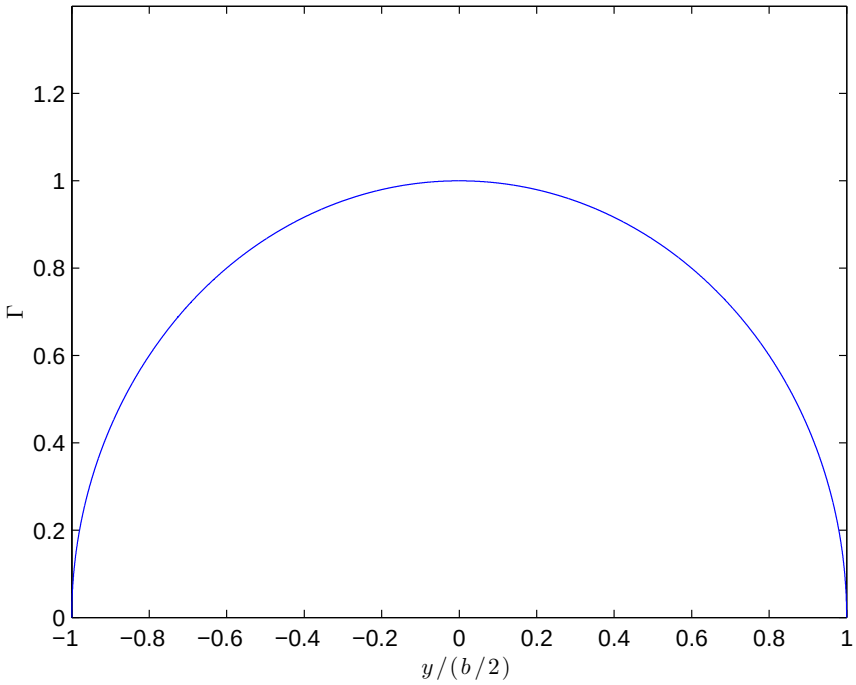


Figure 11.13: Elliptic circulation distribution

the photograph of a flap vortex in Figure 11.5, which shows physical evidence of the existence of a vortex generated at the edges of the flap.

11.4.4 Trefftz plane results for lift and drag

11.7 11.6

In this section, we will relate the lift and drag to the circulation distribution using the Trefftz plane. Specifically, recall the derivation from the problem in Section 3.6.1 relating the farfield flow behavior to the lift. Note that this result was derived with the y-axis being the lift direction. However, the coordinate system we have been using in our discussion of 3D flows uses the z-axis as the lift direction. Thus, switching to the z-axis being the lift direction, the result for the lift is,

$$L = -\iint_{S_\mathrm{w}} \rho_\mathrm{w} w_\mathrm{w} u_\mathrm{w} \, \mathrm{d}S. \tag{11.51}$$

As we are considering incompressible flow, $\rho_\mathrm{w} = \rho$. Also, for the lifting line model, $u_\mathrm{w} = V_\infty$ giving,

$$L = -\rho V_\infty \iint_{S_\mathrm{w}} w_\mathrm{w} \, \mathrm{d}S. \tag{11.52}$$

From this point, the derivation gets a little mathematically intense, but we can eventually find the unsurprising result that for the lifting line model,

$$L = \rho V_\infty \int_{-b/2}^{b/2} \Gamma(y) \mathrm{d}y \tag{11.53}$$

For the drag, we use the result from Homework Problem 8.6.1, which showed that for an inviscid,

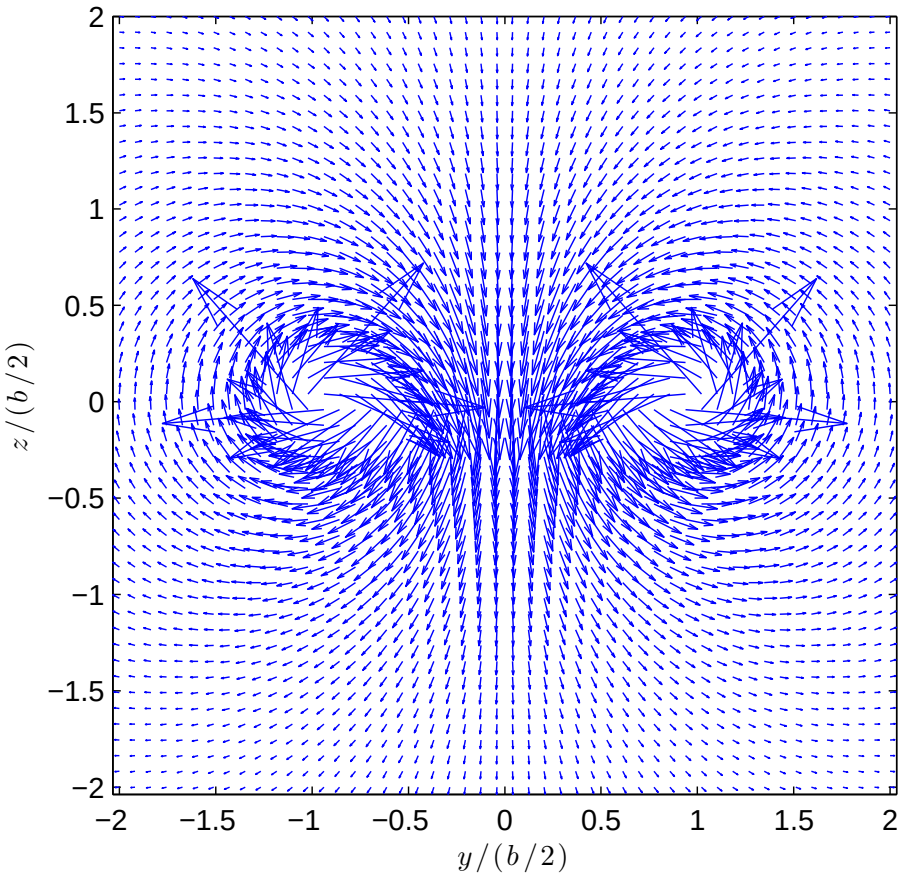


Figure 11.14: Velocity vectors in the Trefftz plane for the elliptic circulation distribution

incompressible flow, the drag is related to the Trefftz plane flow by,

$$D_i = \frac{1}{2}\rho \iint_{S_\mathrm{w}} \left(\tilde{v}_\mathrm{w}^2 + \tilde{w}_\mathrm{w}^2 - \tilde{u}_\mathrm{w}^2\right) \mathrm{d}S \tag{11.54}$$

where D_i is used to indicate that this is the induced drag (the only drag present in an incompressible potential flow). Recall that for the lifting line model $u_w = V_\infty$ thus $\tilde{u}_w = u_w - V_\infty = 0$ in the wake. Further, since the freestream is in the x direction, $\tilde{v} = v$ and $\tilde{w} = w$ giving,

$$D_i = \frac{1}{2}\rho \iint_{S_\mathrm{w}} \left(v_\mathrm{w}^2 + w_\mathrm{w}^2\right) \mathrm{d}S \tag{11.55}$$

Again, the mathematical derivation gets a bit challenging, but it is possible to then express this result in terms of the lifting line circulation,

$$D_i = -\frac{1}{2}\rho \int_{-b/2}^{b/2} w_\mathrm{w}(y,0)\Gamma(y)\mathrm{d}y \tag{11.56}$$

Applying Equation (11.49) gives,

$$w_\mathrm{w}(y,0) = \int_{-b/2}^{b/2} \frac{\gamma(y')\mathrm{d}y'}{2\pi(y'-y)} \tag{11.57}$$

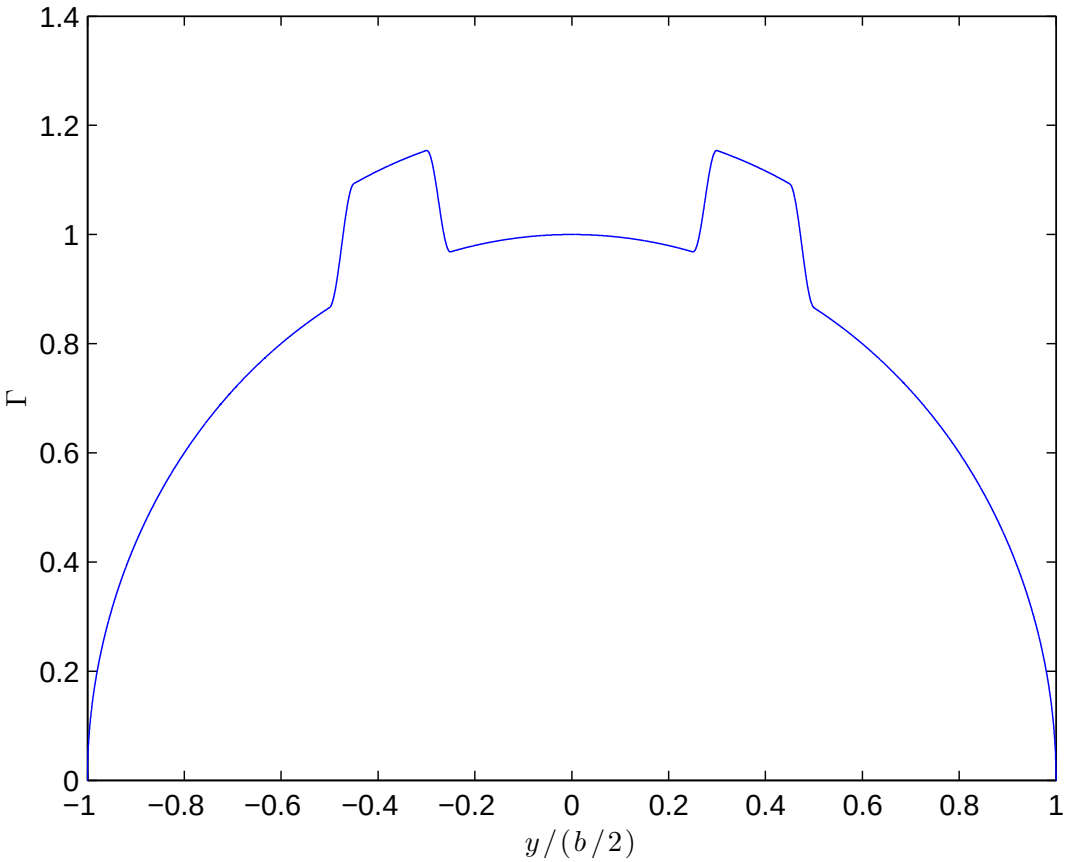


Figure 11.15: Elliptic circulation distribution with a flap deflection from $0.25 < |y|/(b/2) < 0.5$

Before we move on, let's take a short break to notice that the induced drag result in Equation (11.55) is the integral of the kinetic energy due to the velocity components that are perpendicular to the freestream (often referred to as the *crossflow*). Upstream of the wing, the freestream is uniform. However, downstream of the wing the vortical wake induces velocity in the crossflow direction. The result is a change in the kinetic energy of the flow. This change in kinetic energy of the flow as the airplane moves must be a result of work being done on the flow. And, this work is provided by the induced drag. In other words, while the air is acting on the wing with a force to oppose its motion, the wing acts on the air with an equal and opposite force. Since it is opposite the drag, this means the force on the air is in the direction of motion of the wing. Thus, the reaction force to the drag does work on the air. We can state this as a rate, which is to say the rate of work done on the air is $D_i V_\infty$ and the rate of increase of kinetic energy in the air is $V_\infty \int_{S_\mathrm{w}} \frac{1}{2}\rho(\tilde{v}^2+\tilde{w}^2)\mathrm{d}S$. Equating these two expressions gives our earlier result,

$$D_i = \int_{S_\mathrm{w}} \frac{1}{2}\rho(\tilde{v}^2+\tilde{w}^2)\mathrm{d}S \tag{11.58}$$

11.4.5 Downwash and induced angle of attack

11.6

The Trefftz plane results for lift and induced drag in Equations (11.53) and (11.56) can be intrepreted in terms of the behavior of the sectional flow on the wing.

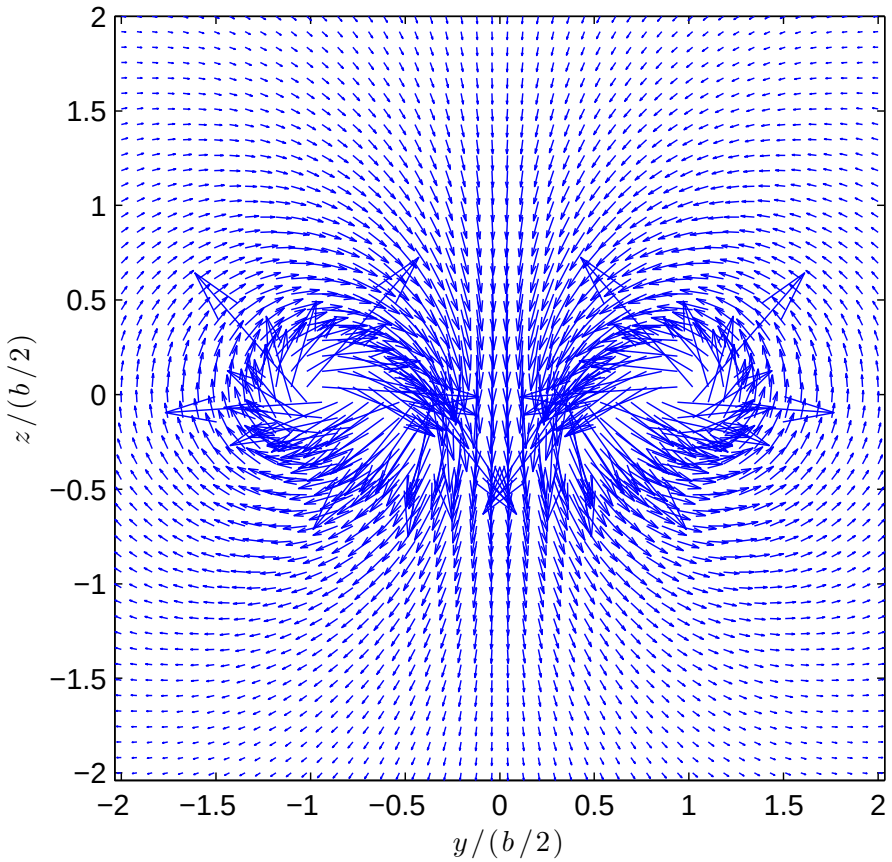


Figure 11.16: Velocity vectors in the Trefftz plane for an elliptic circulation distribution with a trailing edge flap deflection from $0.25 < |y|/(b/2) < 0.5$.

We begin this intrepretation by comparing the velocity induced by the trailing wake at the bound vortex at $(x, y, z) = (0, y, 0)$ and at the corresponding location in the Trefftz plane at $(\infty, y, 0)$. At the bound vortex, the vortex filaments are semi-infinite (extending only downstream to $x \to \infty$). From a position on the Trefftz plane, the filaments extend infinitely in both directions (upstream to the bound vortex which is infinitely far away, and downstream they never end). Thus, the velocity induced by the wake at the bound vortex is exactly half the velocity induced at the corresponding location in the Trefftz plane. In particular, for the z-velocity component which enters Equation (11.56), this implies

$$w(0, y, 0) = \frac{1}{2} w(\infty, y, 0) \tag{11.59}$$

Thus, the induced drag for the lifting-line model can be equivalently written as,

$$D_i = -\rho \int_{-b/2}^{b/2} w_{\mathrm{i}}(y)\Gamma(y)\mathrm{d}y \tag{11.60}$$

where $w_i(y)$ is the velocity induced by the wake along the bound vortex,

$$w_i(y) \equiv w(0, y, 0) \tag{11.61}$$

Over most of the bound vortex, $w_i(y)$ is negative and as a result $-w_i(y)$ is frequently is referred to as the *downwash*. However, $w_i(y)$ can be positive in particular in regions of the wing where the

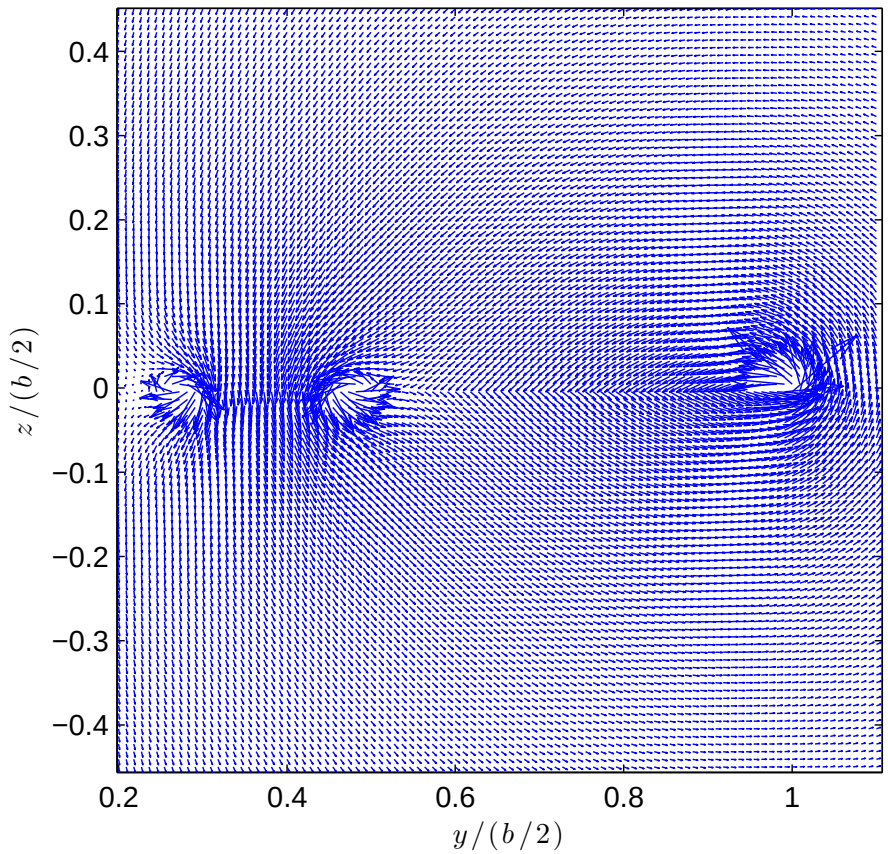


Figure 11.17: Velocity vectors in the Trefftz plane for an elliptic circulation distribution with a trailing edge flap deflection from $0.25 < |y|/(b/2) < 0.5$. This image is zoomed in to highlight the effect of the flap deflection on the Trefftz plane flow.

circulation is increasing rapidly (for example, at the edges of a flap $w_i(y)$ can be upward as can be seen in the Trefftz plane velocity shown in Figure 11.17).

The downwash can be thought of as changing the angle of attack at the bound vortex. As shown in Figure 11.18, the angle of attack of the local section relative to the freestream velocity is $\alpha + \alpha_g(y)$. However, the presence of the downwash creates an effective velocity $\mathbf{V}_{\text{eff}}$ which is at a smaller *effective angle of attack*, α_{eff}, where

$$\alpha_{\text{eff}}(y) = \alpha + \alpha_g(y) - \alpha_i(y) \tag{11.62}$$

and the *induced angle of attack* is,

$$\alpha_i = \tan^{-1}\left(-\frac{w_i}{V_\infty}\right) \approx -\frac{w_i}{V_\infty} \tag{11.63}$$

where the final result assumes $|w_i|/V_\infty \ll 1$.

Next, substituting for w_i into Equation (11.60),

$$D_i = \rho V_\infty \int_{-b/2}^{b/2} \alpha_i(y)\Gamma(y)\mathrm{d}y \tag{11.64}$$

From the Kutta-Joukowski Theorem, we can intrepret $\rho V_\infty \Gamma(y)$ as the sectional lift produced at y. But, since the effective freestream direction is $\mathbf{V}_{\text{eff}}(y)$, then the lift produced by the potential flow

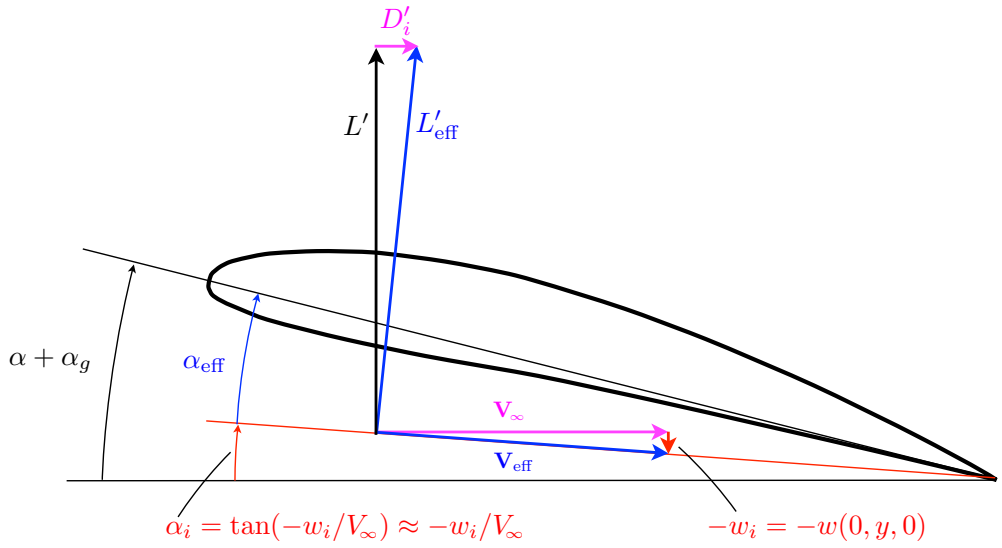


Figure 11.18: Downwash caused by the vortex wake creates an effective velocity $\mathbf{V}_{\text{eff}}$ which is different than the freestream $\mathbf{V}_\infty$. The lift L'_{eff} generated by the airfoil is perpendicular to $\mathbf{V}_{\text{eff}}$ which tilts it slightly into the drag direction producing a sectional contribution to the induced drag D'_i.

around this section would act perpendicular to this effective direction. So, we define this as the effective lift,

$$L'_{\text{eff}}(y) = \rho V_\infty \Gamma(y) \tag{11.65}$$

The final step is to resolve this effective lift into the lift and drag directions relative to the actual freestream velocity $\mathbf{V}_\infty$. The contribution to the sectional lift (defined relative to the actual freestream) is,

$$L' = L'_{\text{eff}} \cos\alpha_i \approx L'_{\text{eff}} \tag{11.66}$$

and the contribution to the sectional induced drag (in the actual freestream direction) is,

$$D'_i = L'_{\text{eff}} \sin\alpha_i \approx L'_{\text{eff}} \alpha_i \tag{11.67}$$

Comparing this result to the integrand in Equation (11.60) shows they are completely consistent. In otherwords, we may interpret the production of induced drag to be the result of downwash at the bound vortex, created by the trailing vortical wake, that tilts the sectional lift into the streamwise direction.

11.4.6 Elliptic lift distribution results

11.7

In this section, we consider the specific case of the elliptic lift distribution as given in Equation (11.50). First, we calculate the total lift by integrating the sectional lift for an elliptic lift distribution,

$$L = \rho V_\infty \Gamma_0 \int_{-b/2}^{b/2} \sqrt{1 - \left(\frac{y}{b/2}\right)^2}\, \mathrm{d}y \tag{11.68}$$

Then, we use the following variable transformation to bring this integral into a well-known form,

$$y = -\frac{b}{2}\cos\beta \tag{11.69}$$

where the spanwise direction varies between $0 \leq \beta \leq \pi$. Thus, the elliptic lift distribution in terms of β is,

$$\begin{aligned} \Gamma &= \Gamma_0 \sqrt{1 - \left(\frac{y}{b/2}\right)^2} && (11.70) \\ &= \Gamma_0 \sqrt{1 - \cos^2 \beta} && (11.71) \\ &= \Gamma_0 \sin \beta && (11.72) \end{aligned}$$

In other words, we are expressing the lift distribution as a function of the new variable β instead of y.

Then, differential changes in y are related to changes in β by,

$$\mathrm{d}y = \frac{b}{2} \sin \beta \, \mathrm{d}\beta \tag{11.73}$$

Substituting Equations (11.69) and (11.73) into the lift integral gives,

$$\begin{aligned} L &= \frac{1}{2} \rho V_\infty b \Gamma_0 \int_0^\pi \sin^2 \beta \, \mathrm{d}\beta && (11.74) \\ \Rightarrow L &= \frac{\pi}{4} \rho V_\infty b \Gamma_0 && (11.75) \end{aligned}$$

where the last step of this derivation uses $\int_0^\pi \sin^2 \beta \, \mathrm{d}\beta = \pi/2$. The lift coefficient then is,

$$C_L = \frac{L}{q_\infty S_{\text{ref}}} = \frac{\pi}{2} \frac{\Gamma_0 b}{V_\infty S_{\text{ref}}} \tag{11.76}$$

The induced drag requires calculation of $w_i(y)$,

$$w_i(y) = \frac{1}{4\pi} \int_{-b/2}^{b/2} \frac{\gamma(y') \mathrm{d}y'}{y' - y} \tag{11.77}$$

First determining $\gamma(y')\mathrm{d}y'$,

$$\gamma \, \mathrm{d}y' = \frac{\mathrm{d}\Gamma}{\mathrm{d}y'} \mathrm{d}y' = \frac{\mathrm{d}\Gamma}{\mathrm{d}\beta'} \mathrm{d}\beta' = \Gamma_0 \cos \beta' \, \mathrm{d}\beta' \tag{11.78}$$

This gives,

$$w_i(\beta) = \frac{\Gamma_0}{2\pi b} \int_0^\pi \frac{\cos \beta' \, \mathrm{d}\beta'}{\cos \beta - \cos \beta'} \tag{11.79}$$

The value of the integral can be shown to be,

$$\int_0^\pi \frac{\cos \beta' \, \mathrm{d}\beta'}{\cos \beta' - \cos \beta} = \pi \tag{11.80}$$

$$\Rightarrow w_i(\beta) = -\frac{\Gamma_0}{2b} \tag{11.81}$$

In others words, the downwash for elliptic lift is constant (i.e. it does not depend on y).

The induced drag can now be determined using Equation (11.60),

$$\begin{aligned} D_i &= -\rho \int_{-b/2}^{b/2} w_{\mathrm{i}}(y) \Gamma(y) \mathrm{d}y && (11.82) \\ \Rightarrow D_i &= \frac{\pi}{8} \rho \Gamma_0^2 && (11.83) \end{aligned}$$

The induced drag coefficient is,

$$C_{Di} \equiv \frac{D_i}{q_\infty S_{\text{ref}}} = \frac{\pi \rho \Gamma_0^2}{8 q_\infty S_{\text{ref}}} \tag{11.84}$$

This can be written in a convenient form in terms of the lift coefficient using Equation (11.76),

$$C_{Di} = \frac{C_L^2}{\pi \mathcal{AR}} \tag{11.85}$$

Comparing this to the more general result given in Equation (2.53), we can see that the span efficiency for an elliptic lift distribution is $e = 1$. Though we have not yet derived the following result, it can be shown (see Section 11.4.10) that the span efficiency for the lifting line model is at most one, i.e. $e \leq 1$. Thus, the elliptic lift distribution produces the lowest amount of induced drag for a given lift and aspect ratio. A very important corollary to this result is that by including three-dimensional effects, even potential flow models will have non-zero drag for bodies which generate lift. That is, drag is an unavoidable consequence of producing lift (even without including viscous effects or shock waves, both of which will further increase the drag).

edXproblem: 11.4.7 Downwash for an elliptic lift distribution

11.8 11.3

Consider a wing that achieves an elliptic lift distribution at its design condition which is at a speed of 60 m/sec. The aspect ratio of the wing is $AR = 10$ and the lift coefficient at this design condition is $C_L = 0.5$. Apply lifting line theory to answer the following questions.

What is the induced drag coefficient C_{Di}? Provide your answer in counts of drag and answer to the nearest count. Recall that a count of drag is $1E-4$. So, if $C_{Di} = 0.01487$ then your answer should be 149.

What is w_i at $y = -b/4$? Provide your answer in m/sec with precision of X.YeP. Be careful to include the correct sign (negative or positive)!

What is w_i at $y = 0$? Provide your answer in m/sec with precision of X.YeP.

What is w_i at $y = b/4$? Provide your answer in m/sec with precision of X.YeP.

What is w_w at $(y, z) = (-b/4, 0)$? Provide your answer in m/sec with precision of X.YeP.

What is w_w at $(y, z) = (0, 0)$? Provide your answer in m/sec with precision of X.YeP.

What is w_w at $(y, z) = (b/4, 0)$? Provide your answer in m/sec with precision of X.YeP.

edXsolution

Video Link

edXproblem: 11.4.8 Impact of velocity on downwash and induced drag

11.8 | 11.3

Suppose the wing in Problem 11.4.7 is flying at 30 m/sec. Assume that the required lift is unchanged from 60 m/sec. Apply lifting line theory to answer the following questions. Assume that the lift distribution is still elliptic at this slower velocity.

What is the ratio of lift coefficients at 30 m/sec and 60 m/sec: $\frac{C_L(30 \text{ m/sec})}{C_L(60 \text{ m/sec})}$?

What is the ratio of lift coefficients at 30 m/sec and 60 m/sec: $\frac{C_L(30 \text{ m/sec})}{C_L(60 \text{ m/sec})}$?

What is the ratio of induced drag coefficients at 30 m/sec and 60 m/sec: $\frac{C_{Di}(30 \text{ m/sec})}{C_{Di}(60 \text{ m/sec})}$?

What is ratio of w_i at 30 m/sec and 60 m/sec: $\frac{w_i(30 \text{ m/sec})}{w_i(60 \text{ m/sec})}$?

What is the ratio of the induced drags at 30 m/sec and 60 m/sec: $\frac{D_i(30 \text{ m/sec})}{D_i(60 \text{ m/sec})}$?

edXsolution

Video Link

11.4.9 General distribution of lift

11.7

In general, the lift on a wing will not have an elliptic distribution. Thus, we need a method for analyzing wings for a general lift distribution. To do this, we will utilize a Fourier series decomposition of the lift distribution. Specifically, in terms of β, we will now utilize a Fourier series representation of the circulation distribution,

$$\Gamma(\beta) = 2bV_\infty \sum_{n=1}^{\infty} B_n \sin n\beta \tag{11.86}$$

A few important points on this Fourier series choice are:

- As described in Section 11.3.1, the lift at the wing tips goes to zero, $L'(\pm b/2) = 0$. Since $L' = \rho V_\infty \Gamma$, then $\Gamma(\pm b/2) = 0$. In terms of β, this means $\Gamma(\beta = 0) = \Gamma(\beta = \pi) = 0$. The choice of a Fourier series using $\sin n\beta$ terms satisfies this requirement.
- The odd terms, B_1, B_3, B_5, ..., are symmetric with respect to the wing root. The even terms, B_2, B_4, B_6, ..., are asymmetric. Plots of $\sin n\beta$ are shown in Figure 11.19.

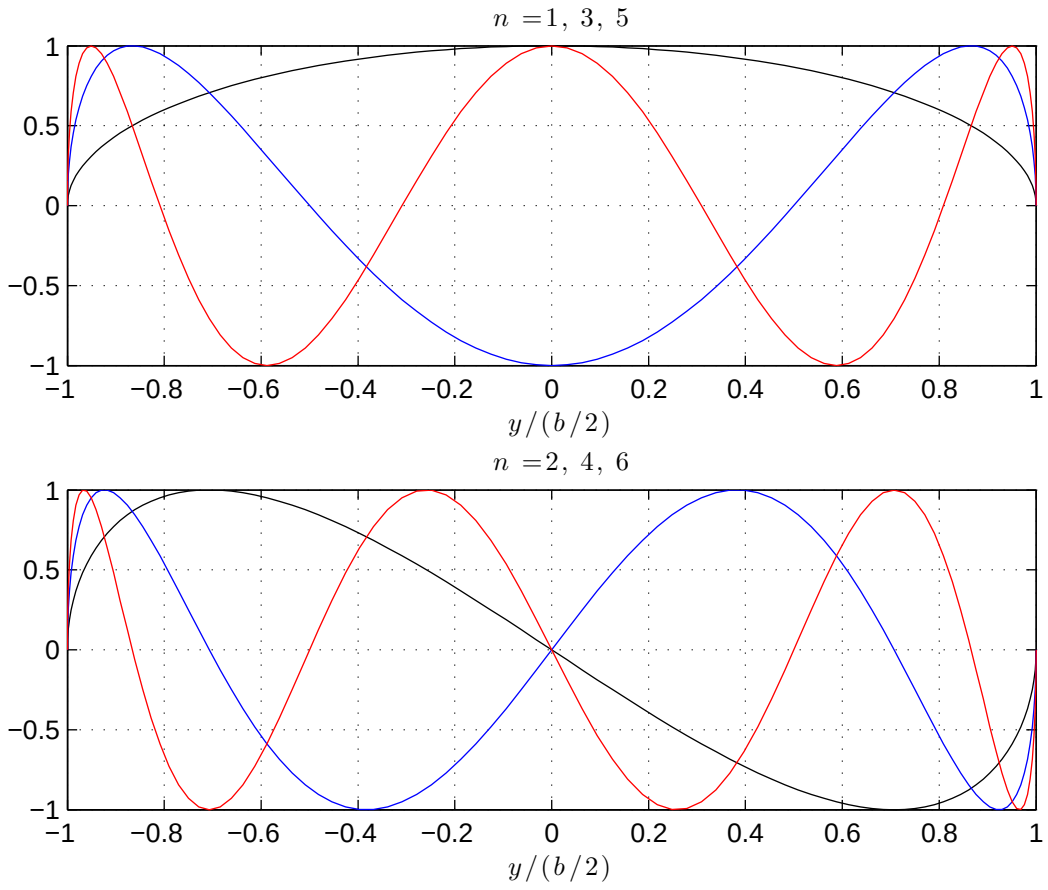


Figure 11.19: Plots of $\sin n\beta$ versus $y/(b/2) = -\cos\beta$.

- The $n = 1$ term ($\sin\beta$) corresponds to the elliptic lift distribution in Equation (11.50). Specif-

ically,

$$\Gamma = \Gamma_0\sqrt{1-\left(\frac{y}{b/2}\right)^2} \tag{11.87}$$

$$= \Gamma_0\sqrt{1-\cos^2\beta} \tag{11.88}$$

$$= \Gamma_0\sin\beta \tag{11.89}$$

- A Fourier series can be used to represent any (smooth) function. Thus, the use of a Fourier series to represent the circulation is not an assumption. Rather, it is just a re-statement of the problem where the unknowns are now the coefficients B_n.

11.4.10 Calculation of lift, induced drag, and span efficiency

11.7

Substituting the Fourier series into Equation (11.53),

$$L = \rho V_\infty \int_{-b/2}^{b/2} \Gamma(y)\mathrm{d}y \tag{11.90}$$

$$= \rho V_\infty^2 b^2 \sum_{n=1}^{\infty} B_n \int_0^\pi \sin n\beta \sin\beta \,\mathrm{d}\beta \tag{11.91}$$

$$\Rightarrow L = \frac{\pi}{2}\rho V_\infty^2 b^2 B_1 \tag{11.92}$$

where the last step of this derivation uses $\int_0^\pi \sin n\beta \sin\beta \,\mathrm{d}\beta = 0$ for $n > 1$ and equals $\pi/2$ for $n = 1$. Thus, the only term in the Fourier series that contributes to the lift is for $n = 1$. The lift coefficient then is,

$$C_L = \frac{L}{q_\infty S_{\text{ref}}} = \pi AR B_1 \tag{11.93}$$

The induced drag requires calculation of $w_i(y)$,

$$w_i(y) = \frac{1}{4\pi}\int_{-b/2}^{b/2} \frac{\gamma(y')\mathrm{d}y'}{y'-y} \tag{11.94}$$

First determining $\gamma(y')\mathrm{d}y'$,

$$\gamma\,\mathrm{d}y' = \frac{\mathrm{d}\Gamma}{\mathrm{d}y'}\mathrm{d}y' = \frac{\mathrm{d}\Gamma}{\mathrm{d}\beta'}\mathrm{d}\beta' = 2bV_\infty\sum_{n=1}^{\infty} nB_n\cos n\beta'\,\mathrm{d}\beta' \tag{11.95}$$

This gives,

$$w_i(\beta) = \frac{V_\infty}{\pi}\sum_{n=1}^{\infty}\left(nB_n\int_0^\pi \frac{\cos n\beta'\,\mathrm{d}\beta'}{\cos\beta-\cos\beta'}\right) \tag{11.96}$$

The value of the integral can be shown to be,

$$\int_0^\pi \frac{\cos n\beta'\,\mathrm{d}\beta'}{\cos\beta'-\cos\beta} = \pi\frac{\sin n\beta}{\sin\beta} \tag{11.97}$$

$$\Rightarrow w_i(\beta) = -V_\infty\sum_{n=1}^{\infty} nB_n\frac{\sin n\beta}{\sin\beta} \tag{11.98}$$

The induced drag can now be determined using Equation (11.60),

$$D_i = -\rho \int_{-b/2}^{b/2} w_{\mathrm{i}}(y)\Gamma(y)\mathrm{d}y \tag{11.99}$$

$$= \rho V_\infty^2 b^2 \int_0^\pi \left(\sum_{m=1}^{\infty} mB_m \sin m\beta\right)\left(\sum_{n=1}^{\infty} B_n \sin n\beta\right) \mathrm{d}\beta \tag{11.100}$$

$$\Rightarrow D_i = \frac{\pi}{2}\rho V_\infty^2 b^2 \sum_{n=1}^{\infty} nB_n^2 \tag{11.101}$$

We note that all of the terms in the induced drag are positive. Thus, $D_i > 0$ (technically, the induced drag could be zero but this is only for the trivial solution in which the circulation is zero everywhere on the wing).

A key result in the aerodynamic performance of wings can be now observed using the results for the lift in Equation (11.92) and induced drag in Equation (11.101). Specifically, while the lift only depends on B_1, all B_n produce positive contributions to the induced drag. Thus, for a specified amount of lift for a given wing (which sets B_1), the minimum induced drag occurs when $B_n = 0$ for $n > 1$. Therefore, as we previously stated in Section 11.4.6, the elliptic lift distribution produces the lowest amount of induced drag for a given wing and lift.

The induced drag coefficient is,

$$C_{D_i} \equiv \frac{D_i}{q_\infty S_{\mathrm{ref}}} = \pi AR \sum_{n=1}^{\infty} nB_n^2 \tag{11.102}$$

This can be written in a convenient form in terms of the lift coefficient using Equation (11.93),

$$C_{D_i} = \frac{C_L^2}{\pi AR e} \tag{11.103}$$

where e is called the *Oswald span efficiency factor* and using this lifting line model is given by,

$$e^{-1} = 1 + \sum_{n=2}^{\infty} n\left(\frac{B_n}{B_1}\right)^2 \tag{11.104}$$

This result shows that $e \leq 1$ and $e = 1$ only when $B_n = 0$ for $n > 1$ (i.e. when the lift distribution is elliptic).

11.4.11 Connecting circulation to wing geometry

11.7 11.8

We have used the lifting line model to derive many important results about the relationship between the lift distribution and induced drag. But, thus far, the properties of the airfoil sections have not entered the analysis. Thus, while we know that an elliptic lift distribution produces the lowest C_{D_i} for a given C_L and AR, we have no idea what the shape of the wing needs to be to achieve the elliptic lift distribution. Similarly, if we were given a particular wing shape (geometric twist and airfoil shapes), we would not know how to apply lifting line to estimate C_L and C_{D_i}. In this part of our lifting line presentation, we finally connect the wing shape to aerodynamic performance.

The classic approach utilized by Prandtl to connect the airfoil shape and geometric twist applies thin airfoil theory results to each section. In doing this, the angle of attack of each section is taken to be the effective angle of attack. Thus, each section's lift coefficient is given by,

$$c_l(y) = 2\pi\left[\alpha_{\mathrm{eff}}(y) - \alpha_{L=0}(y)\right] \tag{11.105}$$

Substituting in Equation (11.62) for α_{eff} gives,

$$c_l(y) = 2\pi \left[\alpha + \alpha_g(y) - \alpha_i(y) - \alpha_{L=0}(y)\right] \tag{11.106}$$

The sectional lift coefficient can also be related to the circulation distribution as follows,

$$\begin{aligned} c_l(y) &= \frac{L'_{\text{eff}}(y)}{q_\infty c(y)} && (11.107)\\ &= \frac{\rho V_\infty \Gamma(y)}{q_\infty c(y)} && (11.108)\\ &= 4\frac{b}{c(\beta)} \sum_{n=1}^{\infty} B_n \sin n\beta && (11.109) \end{aligned}$$

We note that when we write $c(\beta)$ we really should write $c(y(\beta))$ since c was described as a function of y. However, to keep the notation somewhat cleaner, we will use just $c(\beta)$ and similarly, $\alpha_g(\beta)$, $\alpha_{L=0}(\beta)$, and so on.

Substituting Equations (11.109), (11.63), and (11.98 into Equation (11.106) gives,

$$\frac{2}{\pi}\frac{b}{c(\beta)} \sum_{n=1}^{\infty} B_n \sin n\beta + \sum_{n=1}^{\infty} nB_n \frac{\sin n\beta}{\sin \beta} = \alpha + \alpha_g(\beta) - \alpha_{L=0}(\beta) \tag{11.110}$$

This equation has been written so that the Fourier coefficients B_n for the circulation distribution are all on the left-hand side. Suppose we wish to analyze a particular wing. In that case, b, $c(\beta)$, $\alpha_g(\beta)$, and $\alpha_{L=0}(\beta)$ will be given. The freestream angle of attack α will likely also be given though perhaps over a range of relevant values. Then, for a specific α, we would need to solve Equation (11.110) for all of the B_n. However, in practice, we do not solve for the infinitely many values of B_n. Instead, the approach taken is to approximate the solution with a chosen number of modes, and satisfy Equation (11.110) in some approximate manner. We will discuss how this can be done in Sample Problem 11.5.3.

In addition, we solve this equation to determine the shapes required to generate elliptic lift distributions in Sample Problems 11.5.1 and 11.5.2.

11.4.12 Assumptions of the lifting line model

11.7

The assumptions of the lifting line model have occurred throughout this entire section. The following is an explicit list of the assumptions we have utilized to derive the lifting line model:

- Incompressible, steady, inviscid, potential flow
- High aspect ratio, unswept wing without dihedral
- All of the assumptions required for thin airfoil theory
- Planar trailing vortex wake

edXproblem: 11.4.13 True and false for lifting line theory

11.8 11.3

Select all of the statements that are true according to the results of lifting line:

edXsolution

Video Link

11.5 Sample Problems

edXproblem: 11.5.1 Elliptic planform wings

11.8

Consider a wing that has no geometric twist with the same airfoil shape though the chord $c(y)$ can vary.

- Determine the chord distribution $c(y)$ which gives an elliptic lift distribution.
- Determine the $\frac{\mathrm{d}C_L}{\mathrm{d}\alpha}$. Use the planform area of the wing for S_{ref}.
- Determine the distribution of the sectional lift coefficient $c_l(y)$.

edXsolution

Video Link

edXproblem: 11.5.2 Achieving elliptic lift on a rectangular wing

11.8

The elliptic planform is somewhat difficult to manufacture. As an alternative to an elliptic planform, you wish to develop a rectangular wing that achieves an elliptic lift. Suppose that your target lift coefficient at the cruise condition is $C_L = 0.5$ and the aspect ratio of your rectangular wing is 10. Also, assume that a symmetric airfoil is used to further simplify the geometry. At cruise, the angle of attack is desired to be zero.

- What is the geometric twist distribution required to achieve an elliptic lift distribution at the cruise condition?
- Plot the geometric twist distribution (in degrees).
- Does the wing have washin or washout?
- Determine the distribution of the sectional lift coefficient $c_l(y)$.
- Does this wing produce an elliptic lift distribution at any C_L (not just $C_L = 0.5$)?

edXsolution

Video Link

edXproblem: 11.5.3 Approximate solutions to lifting line for a tapered wing

11.8

Consider a tapered, unswept wing that is untwisted ($\alpha_g = 0$) and has an aspect ratio of 10. The chord distribution is

$$\frac{c(y)}{c_r} = 1 - (1 - \lambda)\frac{|y|}{b/2} \tag{11.111}$$

with a taper ratio, $\lambda = 0.4$. The airfoil sections are cambered such that $\alpha_{L=0} = -2°$. For this analysis, let the angle of attack $\alpha = 3°$.

- Approximate B_1, B_3, and B_5 by satisfying Equation (11.110) at $\beta = \frac{\pi}{6}$, $\frac{\pi}{3}$, and $\frac{\pi}{2}$.
- Determine C_L, C_{D_i}, and e.
- Determine and plot $c_l(y)c(y)/c_r$ versus $y/(b/2)$ and $c_l(y)$ versus $y/(b/2)$.

edXsolution

Video Link

edXproblem: 11.5.4 Horseshoe vortex model with application to ground effect

11.3 11.7

In this problem, we develop a simple model of a lifting wing using a single horseshoe vortex. Then, we apply the model to estimate the impact that flying near the ground has on the lift and induced drag.

To begin, let's model a lifting wing with a single horseshoe vortex with strength Γ. However, instead of setting the span of the bound vortex to b, we will set the span to b_{eff} (see Figure 11.20) and determine b_{eff} such that the resulting model correctly predicts the induced drag for an elliptic lift distribution.

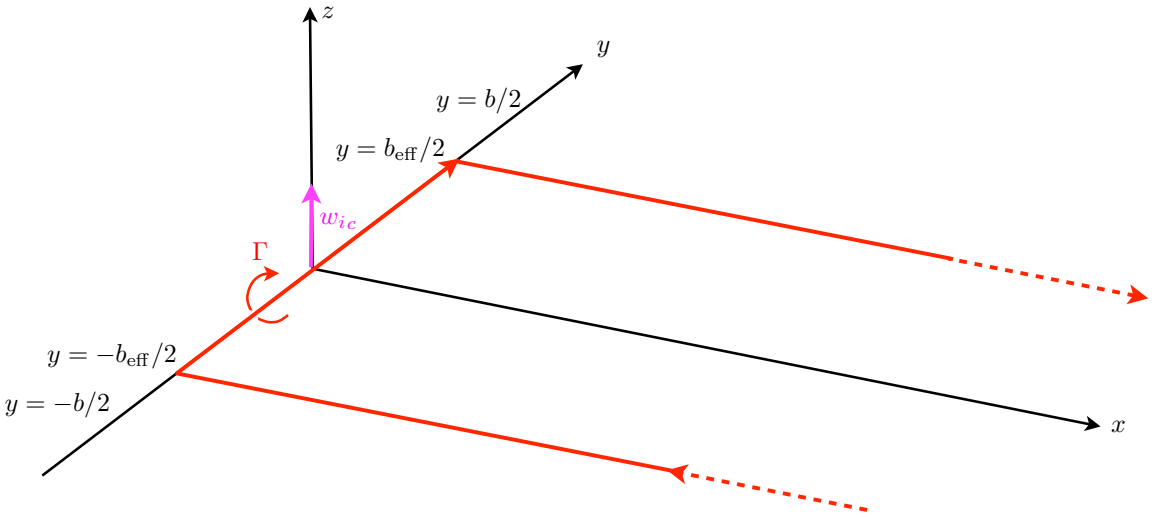


Figure 11.20: A horseshoe vortex model of a wing using an effective span b_{eff} which is different from the wing span b

The lift will be given by

$$L = \rho V_\infty \Gamma b_{\text{eff}} \tag{11.112}$$

We will estimate the drag using the downwash at the center of the bound vortex,

$$D_i = -\rho w_{ic} \Gamma b_{\text{eff}} \tag{11.113}$$

where w_{ic} is the velocity component in the z-direction induced by the trailing vortices at the center of the bound vortex.

Determine the b_{eff} so that the resulting induced drag and lift coefficients satisfy the elliptic lift result,

$$C_{Di} = \frac{C_L^2}{\pi AR} \tag{11.114}$$

Specifically, what is the value of $\frac{b_{\text{eff}}}{b}$? (Hint: it is a constant. Please enter the constant with at least three significant digits).

As the wing nears the ground, the flow can be modeled with a potential flow technique called the method of images. Suppose the wing were at a height $z = h$ above the ground as shown in Figure 11.21. A single horseshoe vortex would not satisfy flow tangency at the ground plane since the vortex would induce a non-zero normal velocity (that is $\mathbf{V} \cdot \hat{\mathbf{n}} = w(x, y, 0) \neq 0$). The method of images idea is to mirror the potential flow by placing another vortex filament below the ground at

$z = -h$. However, as shown in the figure, the circulation of the image vortex has the opposite sense from the vortex associated with the wing. By doing this, the potential flow model will now satisfy $\mathbf{V} \cdot \hat{\mathbf{n}} = w(x, y, 0) = 0$ because the normal velocity contributions from the image vortex exactly cancel the normal velocity contributions from the wing vortex at $z = 0$. Do not get confused with the idea of placing a filament below the ground. This is analogous to how a doublet is placed inside a cylinder or sphere even though the flow we are interested in analyzing is outside the body.

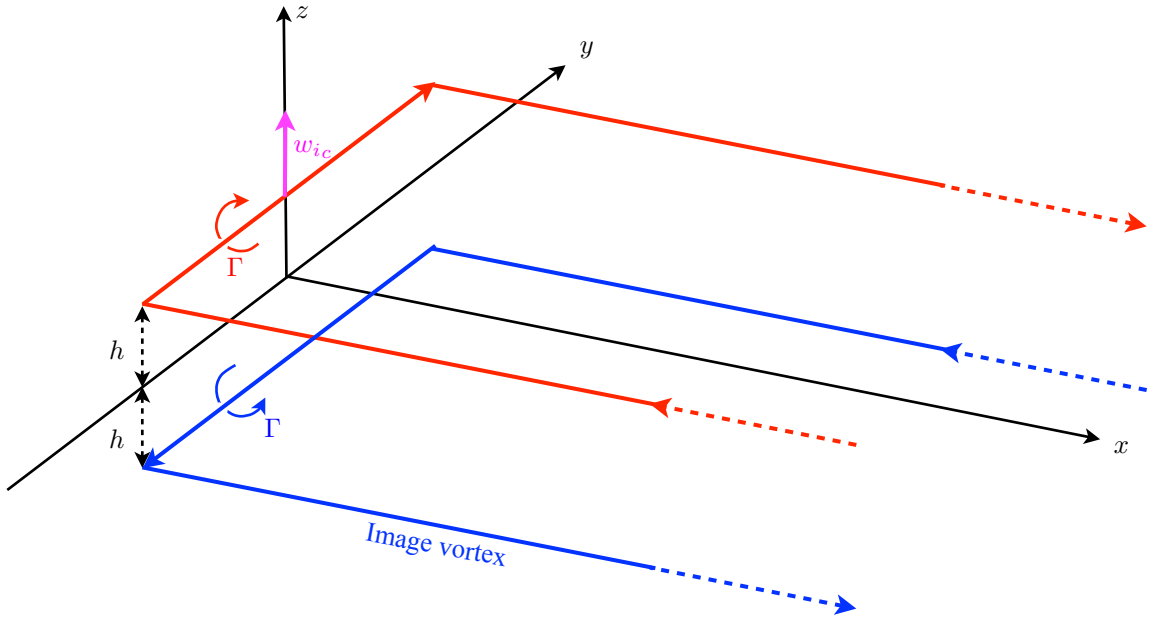


Figure 11.21: A horseshoe vortex model with an image vortex used to model a wing as its approaches the ground (at $z = 0$). The wing horseshoe vortex is located in the $z = h$ plane while the image is located in the $z = -h$ plane.

The downwash velocity w_{ic} at the center of the bound vortex on the wing will now include contributions from not only its own trailing filaments, but also the trailing filaments of the image vortex. Specifically, prove that w_{ic} can be written as,

$$w_{ic} = -\frac{\Gamma}{\pi b_{\text{eff}}}\left(1 - \frac{1}{f}\right) \tag{11.115}$$

where f is a function of the following form,

$$f = 1 + c_0\left(\frac{h}{b_{\text{eff}}}\right)^{c_1} \tag{11.116}$$

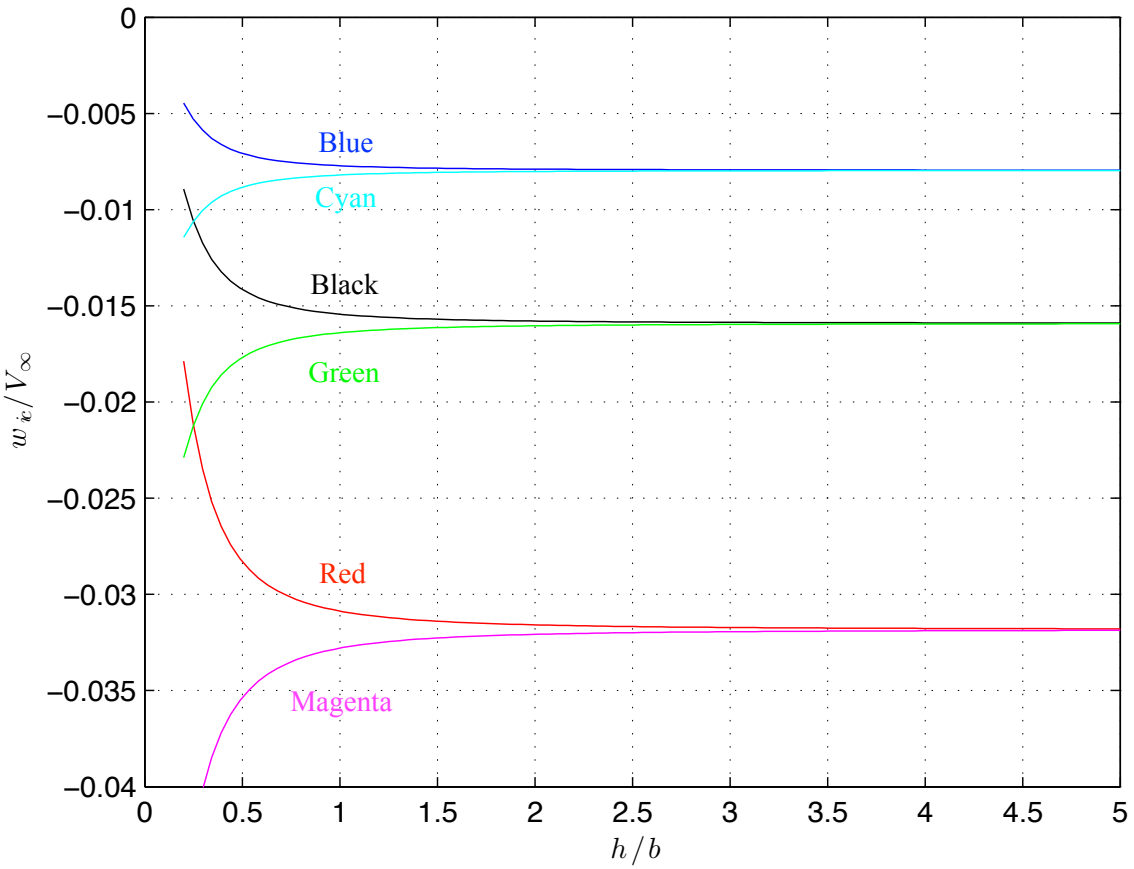
where c_0 and c_1 are constants.

What is the value of c_0?

What is the value of c_1?

Identify which of the curves in the figure above shows the variation of w_{ic} versus h/b for an $AR = 10$ wing producing a $C_L = 0.5$.

Identify which of the curves in the figure above shows the variation of C_{Di} versus h/b for an $AR = 10$ wing producing a $C_L = 0.5$.



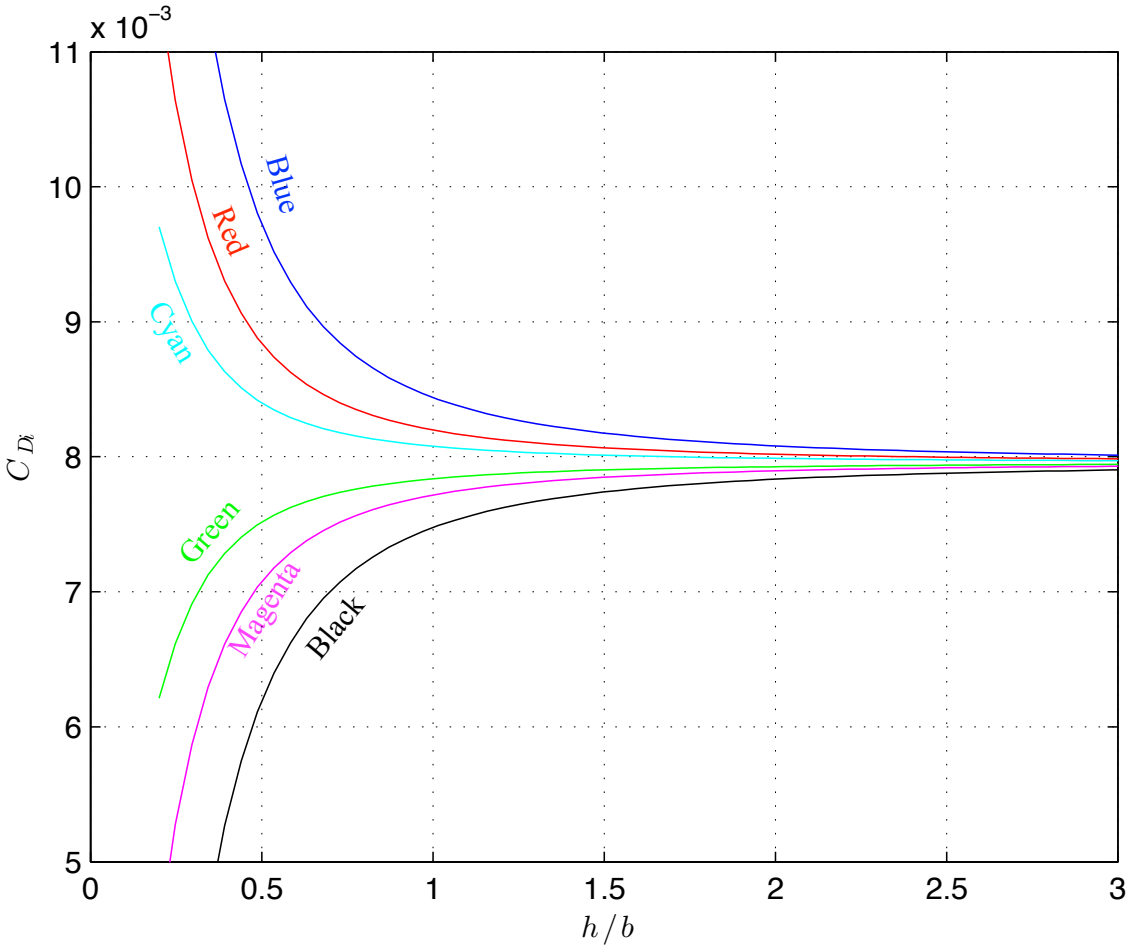
An airplane with an $AR = 6$ wing needs to generate a $C_L = 1$ as it lands. At an altitude of $h/b = 10$, the airplane produces a $C_L = 1$ at $\alpha = 5°$. At an altitude of $h/b = 0.25$, what will the angle of attack be to achieve $C_L = 1$? Assume the change in density is negligible. Provide your answer to the nearest 0.1 degrees.

edXsolution

This solution was quite long, so we divided the video solution into two parts.

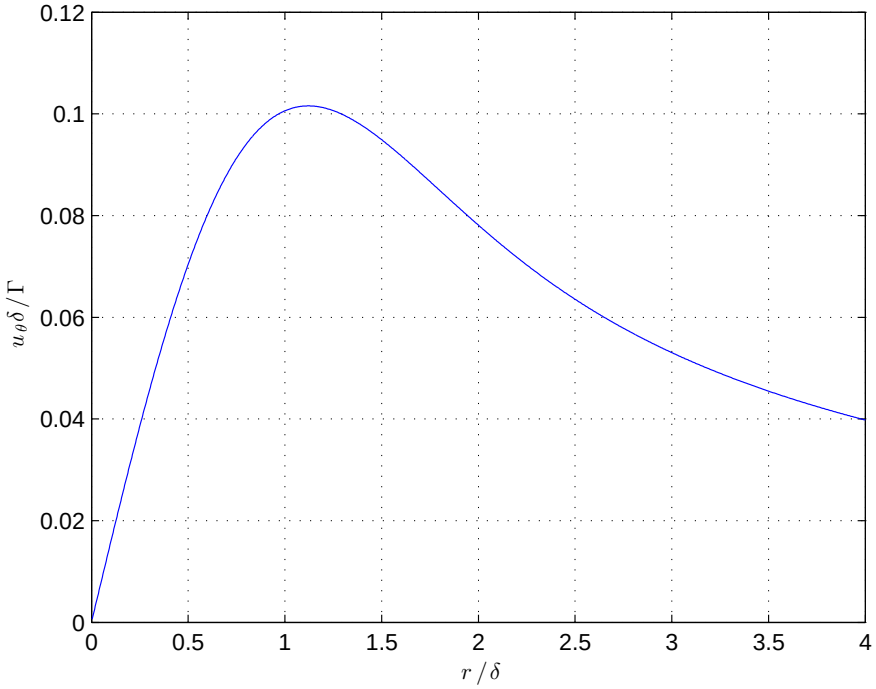
Video Link

Video Link


x 10^−3
11
10
9
8
7
6
5
0
0.5
1
1.5
2
2.5
3
C_Di
h / b
Blue
Red
Cyan
Green
Magenta
Black

edXproblem: 11.5.5 Wing tip vortex flows

6.1 | 7.1 | 8.2 | 11.8



A trailing vortex behind a high-aspect ratio wing has a crossflow velocity field far downstream of the wing (in the Trefftz plane) which is often well approximated by,

$$u_\theta(r) = \frac{\Gamma}{2\pi r}\left[1 - e^{-(r/\delta)^2}\right] \tag{11.117}$$

where the constants Γ and δ are the vortex circulation strength and vortex core size, respectively, and the radial velocity $u_r = 0$. As shown in the figure, the maximum value of u_θ occurs at $r/\delta = 1.12$. Note: we have chosen the (r, θ) coordinate system in the Trefftz plane as shown in the figure.

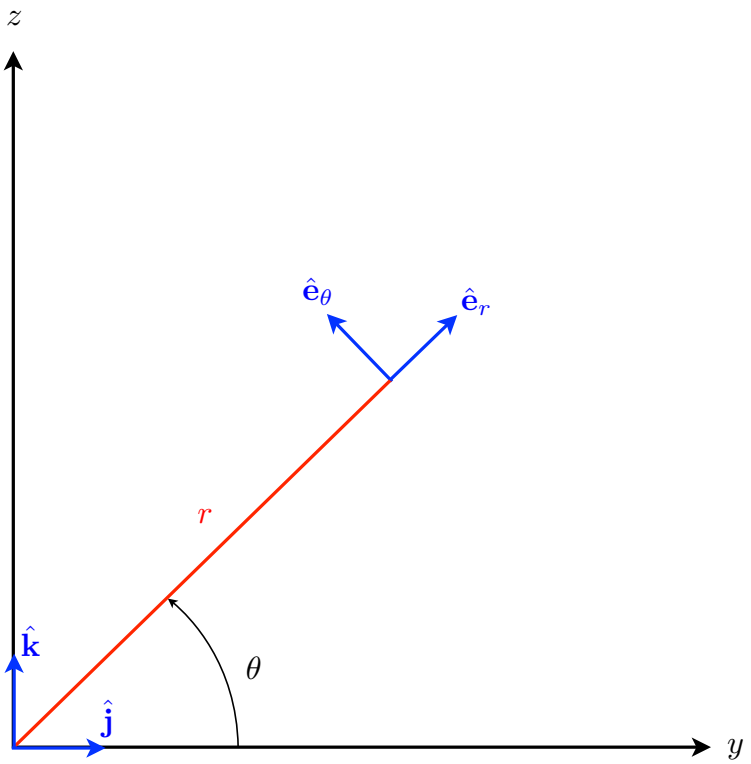
Assuming the flow does not vary in the x direction, then the only non-zero component of vorticity could be the x-component which is given by,

$$\nabla \times \mathbf{V} = \left[\frac{1}{r}\frac{\partial}{\partial r}(r u_\theta) - \frac{1}{r}\frac{\partial u_r}{\partial \theta}\right]\hat{\mathbf{i}} \tag{11.118}$$

Derive the formula for $(\nabla \times \mathbf{V}) \cdot \hat{\mathbf{i}}$ at $r = 0$. Enter your answers using G for Γ and d for δ.

Consider a large commercial airplane at take off. Assume that the lift distribution on the wing is approximately an elliptic distribution and use the following values,

- Take-off weight $= 4 \times 10^6$ Newtons
- $\rho = 1.20$ kg/m^3
- $V_\infty = 80$ m/s
- $b = 65$ m



- $\delta = b/15$

For this airplane, what is the maximum u_θ in the tip vortex? Enter your answer in m/s and use three significant digit in the form $X.YZeP$.

Far downstream of the wing, the net viscous stresses are neglible for the wing tip vortex flow. Which of the following best describes the variation of the pressure p as a function of r? Note that in the options below, the term *monotonically increasing* means that the pressure is a non-decreasing function of r (thus $dp/dr \geq 0$ everywhere). Similarly, *monotonically decreasing* means the pressure is a non-increasing function of r (thus $dp/dr \leq 0$ everywhere).

edXsolution

Video Link

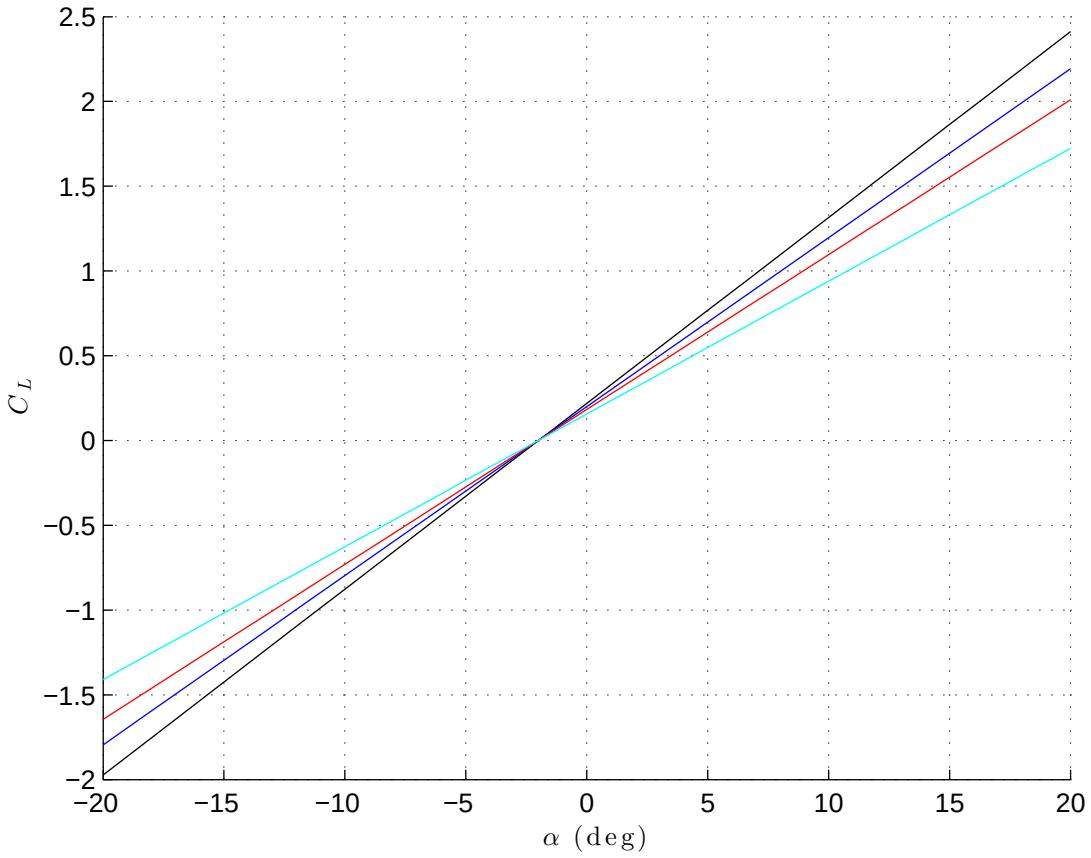
11.6 Homework Problems

edXproblem: 11.6.1 Aerodynamic trends for wings using lifting line

11.7 11.8

All of the results shown in the graphs for all questions in this problem were generated using a lifting line analysis with only two Fourier modes, specifically, B_1 and B_3. To determine B_1 and B_3, the fundamental lifting line equation (Equation 11.110) was satisfied at $\beta = \pi/4$ and $\pi/2$. One way to answer the questions would be to do the lifting line analysis yourself to determine the B_1 and B_3 values and construct the required plots. However, you can answer all of these questions (without solving the lifting line analysis explicitly) by applying an understanding of the lifting line model and the results of lifting line.

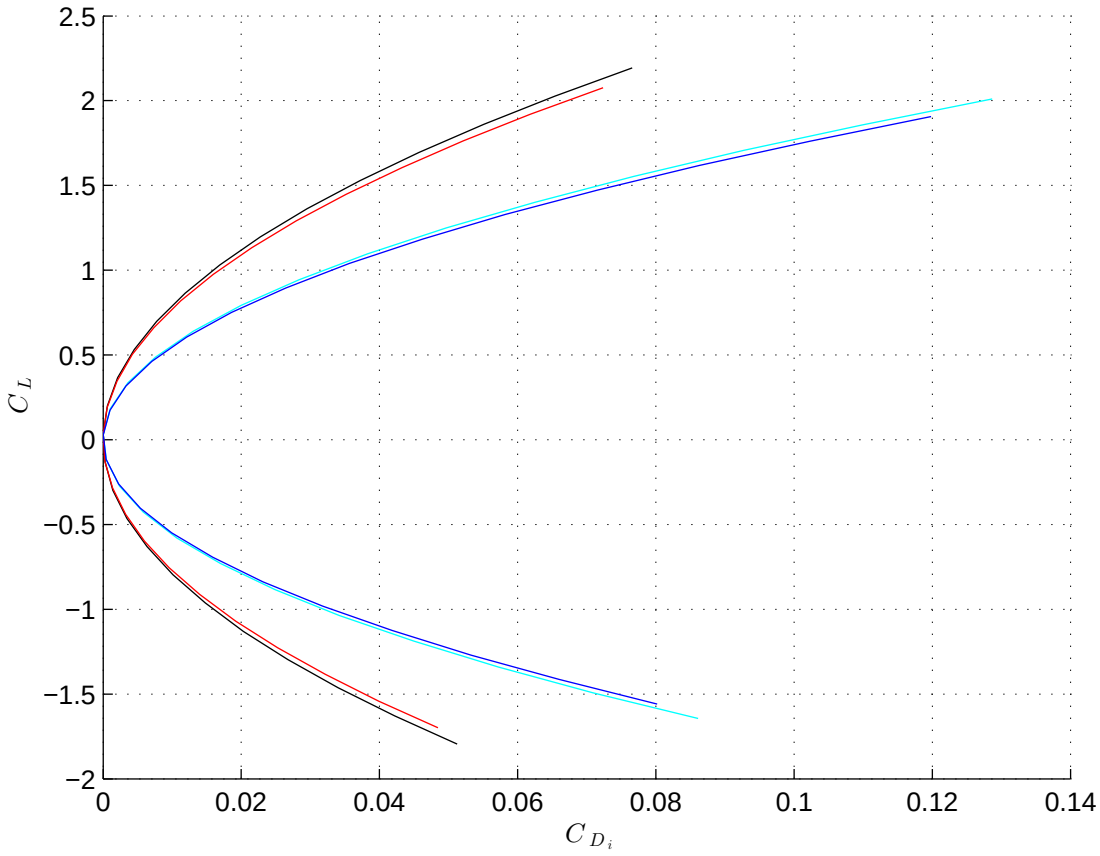
Also, one more clarification: in this problem, whenever we say a wing has no geometric twist, we mean that $\alpha_g(y) = 0$. Technically, a wing with $\alpha_g(y)$ constant is also a wing with no geometric twist, but just an offset from the reference line.



The results above are for four wings all with the same cambered airfoil and no geometric twist. Which wing is the red line?

These results are for four wings all with the same airfoil and no geometric twist. Which wing is the red line?

These results are for four wings all with the same cambered airfoil and no geometric twist. Which wing is the red line?

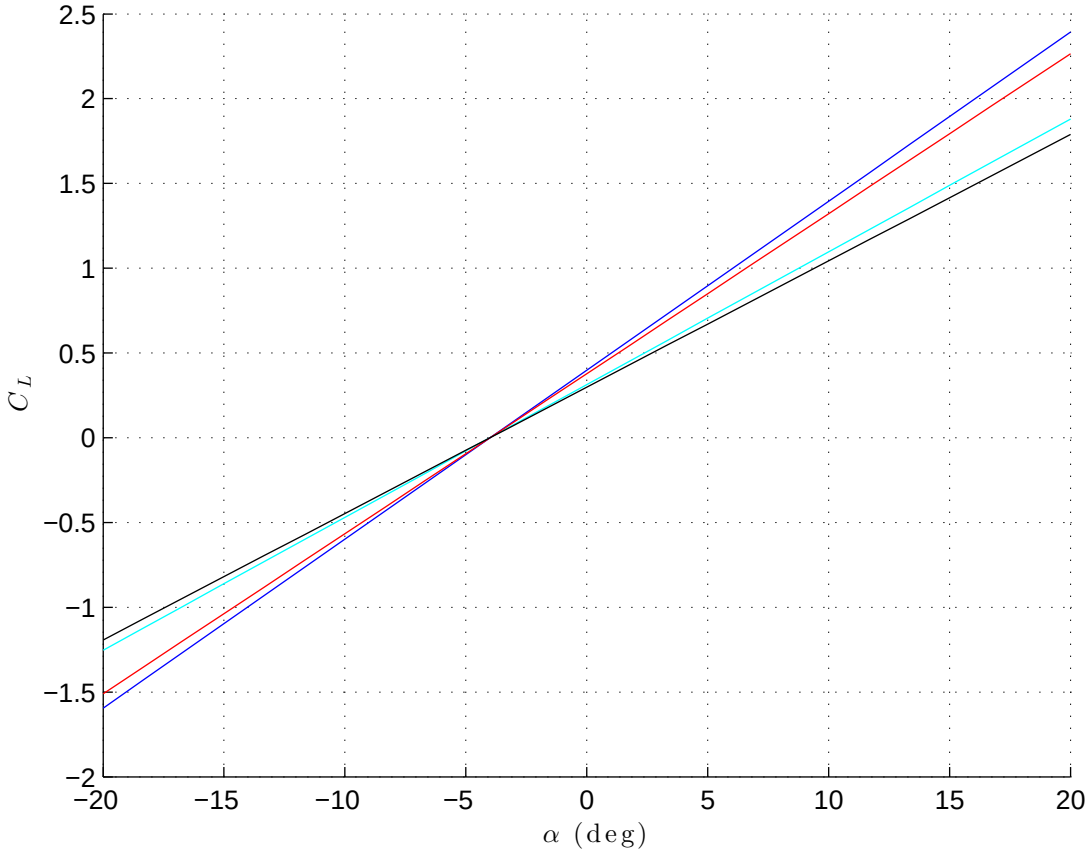


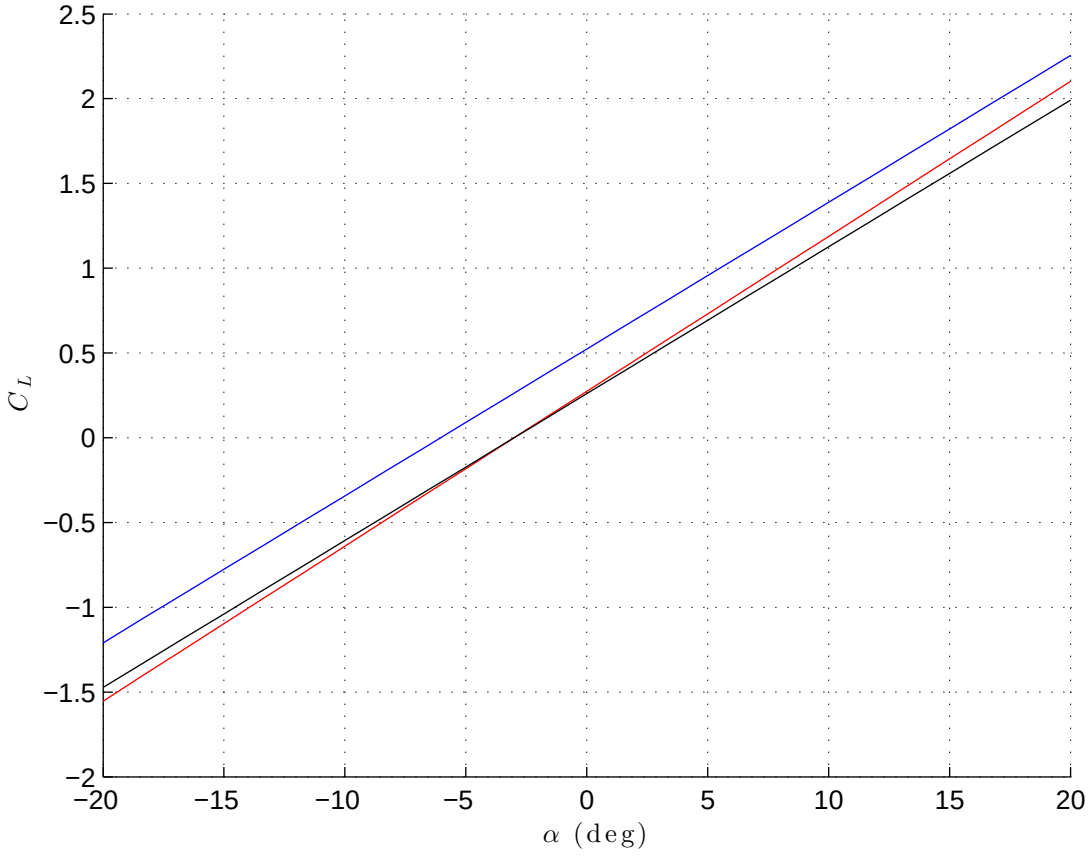
These results are for three wings all with the same airfoil and $AR = 10$. Which wing is the red line?

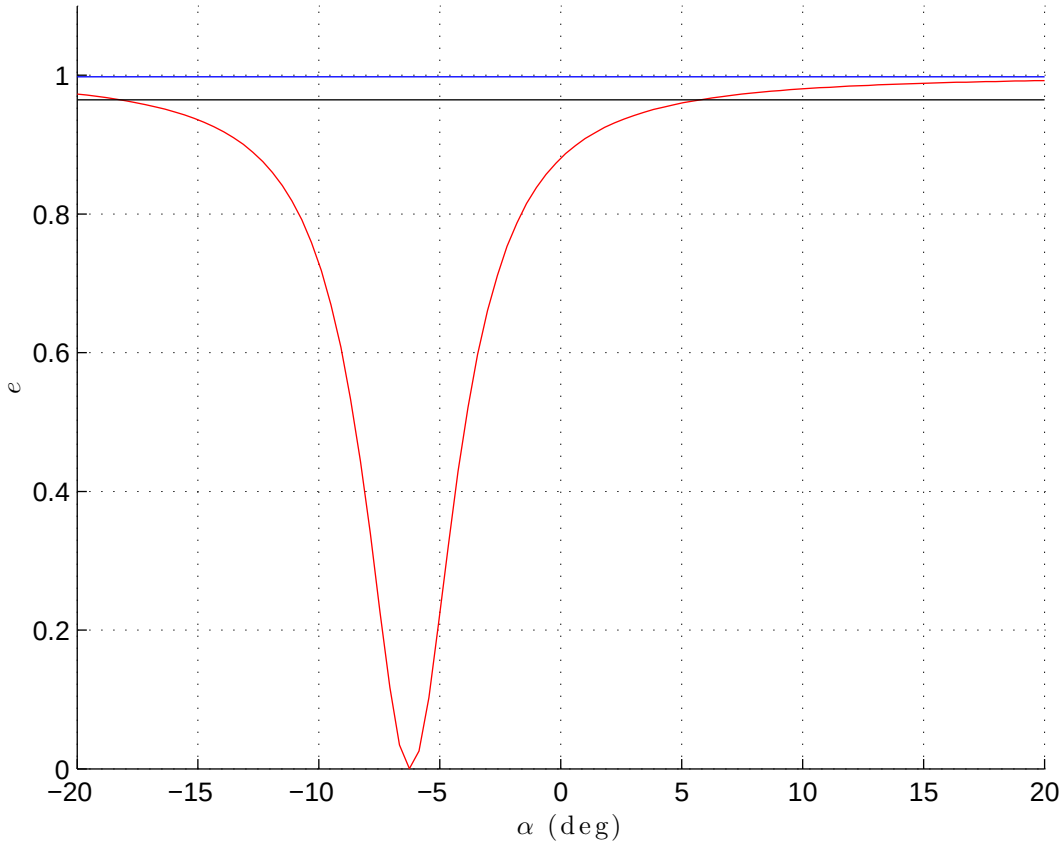
These results are for three wings all with the same airfoil and $AR = 10$. Which wing is the red line?

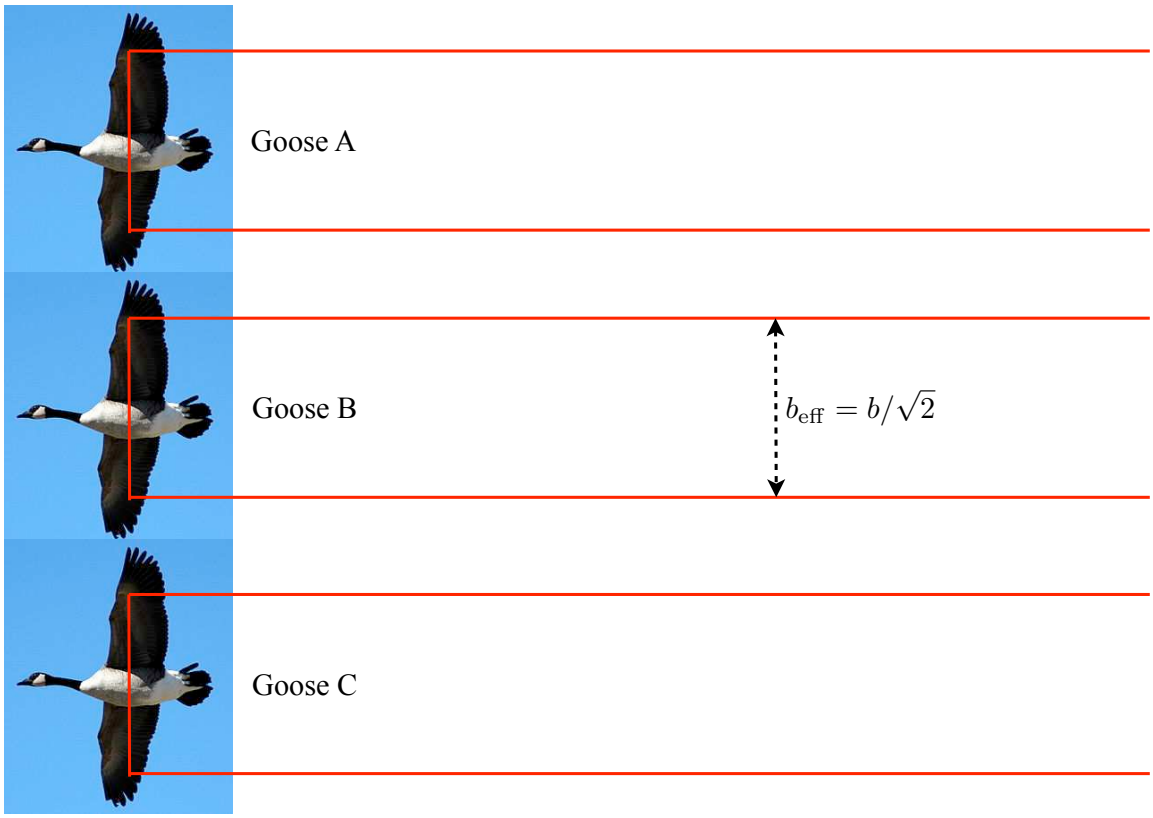
edXsolution

Video Link


2.5
2
1.5
1
0.5
0
−0.5
−1
−1.5
−2
−20
−15
−10
−5
0
5
10
15
20
C_L
α (deg)


2.5
2
1.5
1
0.5
0
−0.5
−1
−1.5
−2
−20
−15
−10
−5
0
5
10
15
20
C_L
α (deg)


1
0.8
0.6
0.4
0.2
0
e
−20
−15
−10
−5
0
5
10
15
20
α (deg)



edXproblem: 11.6.2 Modeling the impact of formation flight

11.3 11.8

In this problem, we will estimate the aerodynamic benefits of formation flight for geese. As shown in the above figure, consider three geese flying very close together, such that we will consider their wingtips to just touch. Assume that the wingspan for a goose is 1.5 m, the mass is 5 kg, and the flight speed is 80 kilometers per hour. Further, assume that the density of the air is 1.2 kg/m^3. In the following questions, use the single horseshoe vortex to model the bound and tip vortex system of a goose and let the effective span of the horseshoe vortex be equal to $b/\sqrt{2}$. Recall that the single horseshoe vortex model was used in Sample Problem 11.5.4.

1) When flying in isolation, what is the induced drag of a single goose? Enter your answer in Newtons with three digits of precision in the form X.YZeP.

2) When flying in isolation, what is the power required to overcome the induced drag for a single goose? Enter your answer in Watts with three digits of precision in the form X.YZeP.

3) When flying in formation, what is the induced drag of goose A? Enter your answer in Newtons with three digits of precision in the form X.YZeP.

4) When flying in formation, what is the power required to overcome the induced drag for goose A? Enter your answer in Watts with three digits of precision in the form X.YZeP.

5) When flying in formation, what is the induced drag of goose B? Enter your answer in Newtons with three digits of precision in the form X.YZeP.

6) When flying in formation, what is the power required to overcome the induced drag for goose B? Enter your answer in Watts with three digits of precision in the form X.YZeP.

7) When flying in formation, what is the induced drag of goose C? Enter your answer in Newtons with three digits of precision in the form X.YZeP.

8) When flying in formation, what is the power required to overcome the induced drag for goose C? Enter your answer in Watts with three digits of precision in the form X.YZeP.

edXsolution

Video Link

edXproblem: 11.6.3 Designing a wing for an RC aircraft

2.3 | 2.5 | 11.5 | 11.8

You are to design a candidate wing for a sport RC electric aircraft to the following requirements:

- density: $\rho = 1.2$ kg/m^3
- speed: $V = 6.0$ m/s
- lift: $L = 5.0$ N
- span: $b = 2.0$ m

Assume that the lift distribution is elliptic and that the lift coefficient for the wing's airfoils (i.e. in a 2D flow) is $c_l = 2\pi(\alpha - \alpha_{L'=0})$ where $\alpha_{L'=0} = -\pi/180$ rad.

Assume the wing planform is tapered with $\lambda = c_t/c_r = 0.4$, with

$$c(y) = c_r + (c_t - c_r)\,|2y/b| \tag{11.119}$$

Determine c_r and c_t such that $C_L = 0.8$.

What is c_r? Enter your answer in meters with two digits of precision in the form X.YeP.

What is c_t? Enter your answer in meters with two digits of precision in the form X.YeP.

What is the aspect ratio of the wing, AR? Enter your answer with three digits of precision in the form X.YZeP.

What is the induced drag of the wing? Enter your answer in Newtons with two digits of precision in the form X.YeP.

Determine $c_l(y)$. Specifically, find the maximum $c_l(y)$ and the spanwise location at which it occurs.

What is the maximum $c_l(y)$? Enter your answer with two digits of precision in the form X.YeP.

What is the value of $|2y/b|$ at which this maximum $c_l(y)$ occurs? Enter your answer with two digits of precision in the form X.YeP.

Assume that the aircraft will be designed to fly such that the angle of attack of the freestream relative to a chosen reference line is zero, that is $\alpha = 0$. Determine the distribution of the geometric twist angle, $\alpha_g(y)$, required to achieve the desired lift distribution.

What is α_g at the wing tips (i.e. at $|y| = b/2$)? Enter your answer in degrees with two digits of precision in the form X.YeP.

What is α_g at the wing root (i.e. at $y = 0$)? Enter your answer in degrees with two digits of precision in the form X.YeP.

What is largest value of α_g? Enter your answer in degrees with two digits of precision in the form X.YeP.

edXsolution

Video Link

edXproblem: 11.6.4 Bending moment and wing performance

11.5 11.8

In this problem, we will use the following two term symmetric circulation distribution,

$$\Gamma(\beta) = 2bV_\infty \left(B_1 \sin\beta + B_3 \sin 3\beta\right) \tag{11.120}$$

The bending moment at the wing root due to the lift generated on the $y > 0$ portion of the wing is,

$$M_{\text{bend}} = \int_0^{b/2} yL'(y)\mathrm{d}y \tag{11.121}$$

Determine M_{bend} in terms of B_1, B_3, V_∞, b and ρ. Two integrals which are helpful are,

$$\int_{\pi/2}^{\pi} \sin\beta \sin 2\beta \,\mathrm{d}\beta = -\frac{2}{3} \tag{11.122}$$

$$\int_{\pi/2}^{\pi} \sin 3\beta \sin 2\beta \,\mathrm{d}\beta = -\frac{2}{5} \tag{11.123}$$

Enter the resulting formula for M_{bend} using B1 for B_1, B3 for B_3, V for V_∞, b for b and r for ρ:

For a span efficiency factor of $e = 1$ and lift L, derive a formula for the bending moment in terms of L and b. Enter the resulting formula using L for L and b for b.

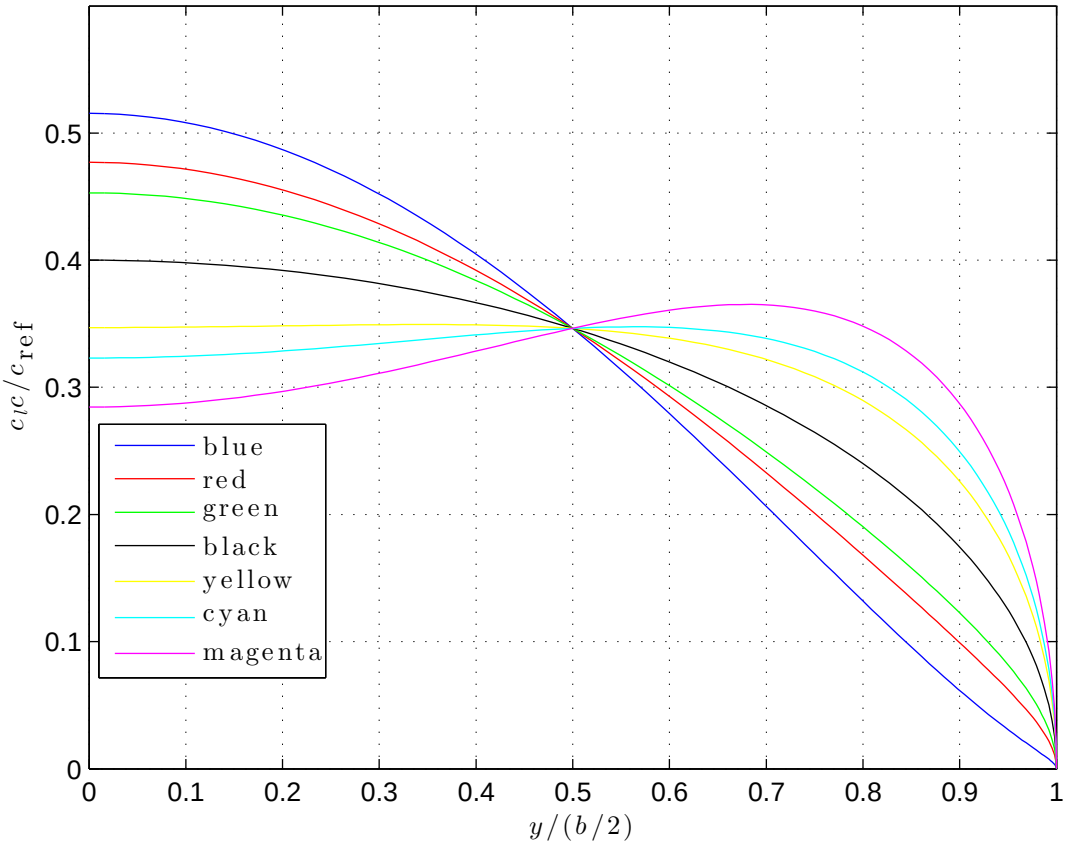
The line plots of $c_l c/c_{\text{ref}}$ are for wings having the same aspect ratio AR and producing the same C_L. The reference chord c_{ref} is chosen as,

$$c_{\text{ref}} \equiv \frac{S_{\text{ref}}}{b} \tag{11.124}$$

All plots were produced using a circulation distribution with only B_1 and B_3 being non-zero. Which line is the wing having the lowest bending moment with a span efficiency of $e = 0.9$ and only B_1 and B_3 non-zero?

edXsolution

Video Link


0.5
0.4
0.3
0.2
0.1
0
0
0.1
0.2
0.3
0.4
0.5
0.6
0.7
0.8
0.9
1
$c_l c / c_{\mathrm{ref}}$
$y/(b/2)$
blue
red
green
black
yellow
cyan
magenta

Module 12

Two-dimensional Inviscid Compressible Aerodynamic Models

12.1 Overview

12.1.1 Measurable outcomes

In this module, we will consider how compressibility effects the performance of airfoils in subsonic, transonic, and supersonic flows. In particular, we will see that even in inviscid two-dimensional flow models, the presence of a shock wave will lead to the creation of drag. However, for purely subsonic flows (without a shock wave), the incompressible flow theory we have studied previously (including thin airfoil theory and panel methods) remains largely unaltered.

Specifically, students successfully completing this module will be able to:

12.1. Derive the full potential equation for compressible flow.

12.2. Derive the linearized, two-dimensional compressible potential flow equation from the nonlinear full potential equation including derivation of the pressure coefficient.

12.3. Apply Prandtl-Glauert theory to estimate the pressure, lift, drag, and moments for subsonic flow over airfoils.

12.4. Relate the existence of wave drag to losses occurring across shock waves and describe typical trends in the lift, drag, and moment for airfoils in transonic flows.

12.5. Define the critical Mach number and estimate it for airfoils using Prandtl-Glauert theory.

12.6. Utilize supersonic linearized potential flow theory to estimate the lift, wave drag, and moments on airfoils.

12.1.2 Pre-requisite material

The material in this module requires the measurable outcomes from Modules 4, 6, 9, and 5.

12.2 Linearized Compressible Potential Equation

12.2.1 Assumptions and governing equations for full potential equation

12.1

This module removes the assumption of incompressibility in our study of potential flows. Specifically, in this module, we will assume that the flow is:

- Steady: the properties of the flow do not depend on time
- Inviscid: viscous stresses are assumed negligible
- Uniform freestream flow: the flow properties far upstream of the body are uniform
- Irrotational: the vorticity is zero essentially everywhere in the flow
- Isentropic: the entropy does not change and since the flow is uniform upstream, this implies the entropy is constant throughout the flow.
- Adiabatic: there is no heat added to the flow.
- Calorically perfect: thus, c_p, c_v and therefore γ are all constants.

This list of assumptions should be compared to those made previously in studying incompressible potential flows (see Section 8.3.1). We have replaced the incompressible assumption with isentropic and adiabatic flow assumptions. Note that we did not explicitly need to state the isentropic and adiabatic flow assumptions when studying the incompressible flow case. This is because the assumptions of inviscid and incompressible flow imply isentropic and adiabatic flow. In the compressible case, we now must explicitly state those assumptions.

Since the flow is irrotational, this implies that the velocity can be expressed as the gradient of a potential function,

$$\mathbf{V} = \nabla\phi \tag{12.1}$$

Thus, this is identical to the incompressible flow case. The difference though is that the conservation of mass must not account for varying density. Thus, the governing equation for the compressible potential flow is,

$$\nabla \cdot (\rho \nabla\phi) = 0 \tag{12.2}$$

We can express the density as a function of the potential using the various assumptions above. We begin with the relationship between the temperature and the stagnation temperature for a calorically perfect gas as defined in Equation (4.56),

$$T_o = T\left(1 + \frac{\gamma - 1}{2} M^2\right) \tag{12.3}$$

where T_0 is the stagnation temperature. Since the flow is adiabatic and the upstream is uniform, then T_0 is constant throughout the entire flow and may be evaluated using the freestream conditions,

$$T_o = T_\infty\left(1 + \frac{\gamma - 1}{2} M_\infty^2\right) \tag{12.4}$$

Combining Equation (12.3) and (12.4) we can then derive,

$$T\left(1+\frac{\gamma-1}{2}M^2\right) = T_\infty\left(1+\frac{\gamma-1}{2}M_\infty^2\right) \tag{12.5}$$

$$T+\frac{\gamma-1}{2}TM^2 = T_\infty+\frac{\gamma-1}{2}T_\infty M_\infty^2 \tag{12.6}$$

$$T = T_\infty+\frac{\gamma-1}{2}\left(T_\infty M_\infty^2-TM^2\right) \tag{12.7}$$

$$\frac{T}{T_\infty} = 1+\frac{\gamma-1}{2}M_\infty^2\left(1-\frac{TM^2}{T_\infty M_\infty^2}\right) \tag{12.8}$$

Since $M^2 = V^2/a^2 = V^2/(\gamma RT)$ then,

$$\frac{TM^2}{T_\infty M_\infty^2} = \frac{V^2}{V_\infty^2} \tag{12.9}$$

which gives,

$$\frac{T}{T_\infty} = 1+\frac{\gamma-1}{2}M_\infty^2\left(1-\frac{V^2}{V_\infty^2}\right) \tag{12.10}$$

In terms of the potential, $V^2 = \nabla\phi\cdot\nabla\phi$ thus,

$$\frac{T}{T_\infty} = 1+\frac{\gamma-1}{2}M_\infty^2\left(1-\frac{\nabla\phi\cdot\nabla\phi}{V_\infty^2}\right) \tag{12.11}$$

Finally, for isentropic variations of a calorically perfect gas, we can apply Equation (4.42) to find,

$$\frac{\rho}{\rho_\infty} = \left[1+\frac{\gamma-1}{2}M_\infty^2\left(1-\frac{\nabla\phi\cdot\nabla\phi}{V_\infty^2}\right)\right]^{1/(\gamma-1)} \tag{12.12}$$

Thus, the combination of this equation with Equation (12.2) is a nonlinear partial differential equation for ϕ and is often referred to as the *full potential equation*. With a bit of manipulation, we can make the substitution of Equation (12.12) into Equation (12.2) and arrive at the following form of the full potential equation for two-dimensional flows,

$$\left[1-\left(\frac{u}{a}\right)^2\right]\frac{\partial^2\phi}{\partial x^2}+\left[1-\left(\frac{w}{a}\right)^2\right]\frac{\partial^2\phi}{\partial z^2}-2\frac{uw}{a^2}\frac{\partial^2\phi}{\partial x\partial z} = 0 \tag{12.13}$$

where $u = \partial\phi/\partial x$, $w = \partial\phi/\partial z$, and the speed of sound can be written as,

$$\left(\frac{a}{a_\infty}\right)^2 = \frac{T}{T_\infty} = 1+\frac{\gamma-1}{2}M_\infty^2\left(1-\frac{\nabla\phi\cdot\nabla\phi}{V_\infty^2}\right) \tag{12.14}$$

12.2.2 Perturbation potential

12.2

In our analysis of compressible potential flow, we will consider flows which are small perturbations away from the freestream conditions. We will align the freestream along the x-direction and define the potential as a combination of a freestream potential ϕ_∞ and a perturbation potential $\tilde{\phi}$,

$$\phi = \phi_\infty+\tilde{\phi} \tag{12.15}$$

where

$$\phi_\infty = V_\infty x \tag{12.16}$$

Similarly, the velocity components can be defined in terms of a freestream and perturbation contribution giving,

$$u = V_\infty + \tilde{u} \tag{12.17}$$
$$w = \tilde{w} \tag{12.18}$$

where

$$\tilde{u} = \frac{\partial \tilde{\phi}}{\partial x} \tag{12.19}$$
$$\tilde{w} = \frac{\partial \tilde{\phi}}{\partial z} \tag{12.20}$$

Substitution of the perturbation potential and velocity components into Equation (12.13) gives,

$$\left[1 - \left(\frac{V_\infty + \tilde{u}}{a}\right)^2\right] \frac{\partial^2 \tilde{\phi}}{\partial x^2} + \left[1 - \left(\frac{\tilde{w}}{a}\right)^2\right] \frac{\partial^2 \tilde{\phi}}{\partial z^2} - 2\frac{(V_\infty + \tilde{u})\tilde{w}}{a^2} \frac{\partial^2 \tilde{\phi}}{\partial x \partial z} = 0 \tag{12.21}$$

We have not yet assumed small perturbations, so this equation is identical to Equation (12.13) (with the only assumption being that the freestream is in the x-direction).

12.2.3 Derivation of linearized compressible potential equation

12.2

We will now assume that the velocity perturbations are small,

$$\frac{|\tilde{u}|}{V_\infty} \ll 1 \text{ and } \frac{|\tilde{w}|}{V_\infty} \ll 1 \tag{12.22}$$

and derive a linearized form of the full potential equation. To begin, we derive the linearized form of the speed of sound relationship in Equation (12.14) by noting that,

$$\frac{\nabla\phi \cdot \nabla\phi}{V_\infty^2} = 1 + 2\frac{\tilde{u}}{V_\infty} + \frac{\tilde{u}^2}{V_\infty^2} + \frac{\tilde{w}^2}{V_\infty^2} \approx 1 + 2\frac{\tilde{u}}{V_\infty} \tag{12.23}$$

Thus, the speed of sound relationship when linearized gives,

$$\left(\frac{a}{a_\infty}\right)^2 \approx 1 - (\gamma - 1) M_\infty^2 \frac{\tilde{u}}{V_\infty} \tag{12.24}$$

Now, let's proceed to linearize each term of Equation (12.21) starting with,

$$\left[1 - \left(\frac{V_\infty + \tilde{u}}{a}\right)^2\right] \frac{\partial^2 \tilde{\phi}}{\partial x^2} = \left[1 - M_\infty^2 \left(\frac{V_\infty + \tilde{u}}{V_\infty}\right)^2 \left(\frac{a_\infty}{a}\right)^2\right] \frac{\partial^2 \tilde{\phi}}{\partial x^2} \tag{12.25}$$
$$\approx \left\{1 - M_\infty^2 \left[1 + 2\frac{\tilde{u}}{V_\infty}\right] \left[1 + (\gamma - 1) M_\infty^2 \frac{\tilde{u}}{V_\infty}\right]\right\} \frac{\partial^2 \tilde{\phi}}{\partial x^2} \tag{12.26}$$
$$\approx \left(1 - M_\infty^2\right) \frac{\partial^2 \tilde{\phi}}{\partial x^2} - M_\infty^2 \left[2 + (\gamma - 1) M_\infty^2\right] \frac{\tilde{u}}{V_\infty} \frac{\partial^2 \tilde{\phi}}{\partial x^2} \tag{12.27}$$

The second term on the right-hand side will be negligible compared to the first term because of its dependence on $\tilde{u}/V_\infty$ as long as M_∞ is not too close to 1. Thus, we will approximate,

$$\left[1 - \left(\frac{V_\infty + \tilde{u}}{a}\right)^2\right] \frac{\partial^2 \tilde{\phi}}{\partial x^2} \approx \left(1 - M_\infty^2\right) \frac{\partial^2 \tilde{\phi}}{\partial x^2} \tag{12.28}$$

under the additional requirement that M_∞ is not approaching sonic conditions (i.e. M_∞ is not too close to one). The precise definition of when this approximation will break down is a function of not only M_∞, but also will depend on the airfoil shape and angle of attack. But, generally, the theory we will develop will provide acceptable results when $M_\infty < 0.7$ and $M_\infty > 1.3$.

There is also an upper Mach number limit which will generally be a result of the shock strengths in the actual flow causing the isentropic assumption to break down. This break down of the isentropic assumption is also not solely a function of M_∞ but also will depend on the airfoil and angle of attack. However, the theory we will develop will generally provide acceptable results for $M_\infty < 3$.

The remaining two terms of Equation (12.21) give,

$$\left[1 - \left(\frac{\tilde{w}}{a}\right)^2\right] \frac{\partial^2 \tilde{\phi}}{\partial z^2} - 2\frac{(V_\infty + \tilde{u})\tilde{w}}{a^2} \frac{\partial^2 \tilde{\phi}}{\partial x \partial z} \approx \frac{\partial^2 \tilde{\phi}}{\partial z^2} \tag{12.29}$$

Finally, combining the results of Equations (12.28) and (12.29) gives the linearized compressible potential flow equation which will form the basis of our analysis of two-dimensional compressible flows around airfoils,

$$\left(1 - M_\infty^2\right) \frac{\partial^2 \tilde{\phi}}{\partial x^2} + \frac{\partial^2 \tilde{\phi}}{\partial z^2} = 0 \tag{12.30}$$

12.2.4 Pressure coefficient for linearized compressible potential flow

12.2

The pressure coefficient written in terms of the velocity perturbations for linearized compressible flow is identical to the incompressible result derived in Equation (12.31), specifically,

$$C_p \approx -2\frac{\tilde{u}}{V_\infty} \tag{12.31}$$

In the following video, we prove this result for linearized compressible flow.

Video Link

12.3 Subsonic Linearized Potential Flow

12.3.1 Prandtl-Glauert transformation

12.3

Equation (12.30) appears quite closely related to Laplaces equation which governs incompressible potential flow. In fact, by the Prandtl-Glauert transformation, it is possible to relate subsonic compressible flow to a corresponding incompressible flow. We begin by introducing the transformation. Note: the technique described in this section is not applicable to supersonic flow. We will discuss supersonic linearized potential flow in Section 12.5.

The transformation involves finding the potential in the (ξ, η) coordinate system which is related to (x, z) by,

$$\xi = x \tag{12.32}$$

$$\eta = \beta z \tag{12.33}$$

where the factor β is defined as,

$$\beta \equiv \sqrt{1 - M_\infty^2} \tag{12.34}$$

Clearly, in order for β to be a real number, the freestream must be subsonic.

We also define the potential $\hat{\phi}(\xi, \eta)$ as,

$$\hat{\phi}(\xi, \eta) = \beta \tilde{\phi}(x, z) \tag{12.35}$$

Now, we substitute Equation (12.35) into Equation (12.30),

$$\beta^2 \frac{\partial^2 \tilde{\phi}}{\partial x^2} + \frac{\partial^2 \tilde{\phi}}{\partial z^2} = 0 \tag{12.36}$$

$$\beta^2 \frac{\partial^2 \hat{\phi}}{\partial x^2} + \frac{\partial^2 \hat{\phi}}{\partial z^2} = 0 \tag{12.37}$$

Next, we relate derivatives with respect to (x, y) to derivatives with respect to (ξ, η).

$$\frac{\partial \hat{\phi}}{\partial x} = \frac{\partial \hat{\phi}}{\partial \xi}\frac{\partial \xi}{\partial x} + \frac{\partial \hat{\phi}}{\partial \eta}\frac{\partial \eta}{\partial x} \tag{12.38}$$

$$\frac{\partial \hat{\phi}}{\partial z} = \frac{\partial \hat{\phi}}{\partial \xi}\frac{\partial \xi}{\partial z} + \frac{\partial \hat{\phi}}{\partial \eta}\frac{\partial \eta}{\partial z} \tag{12.39}$$

Differentiation of Equations (12.32) and (12.33) gives,

$$\frac{\partial \xi}{\partial x} = 1 \qquad \frac{\partial \xi}{\partial z} = 0 \qquad \frac{\partial \eta}{\partial x} = 0 \qquad \frac{\partial \eta}{\partial z} = \beta \tag{12.40}$$

Thus,

$$\frac{\partial \hat{\phi}}{\partial x} = \frac{\partial \hat{\phi}}{\partial \xi} \tag{12.41}$$

$$\frac{\partial \hat{\phi}}{\partial z} = \beta \frac{\partial \hat{\phi}}{\partial \eta} \tag{12.42}$$

Similarly, the second derivatives are,

$$\frac{\partial^2 \hat{\phi}}{\partial x^2} = \frac{\partial^2 \hat{\phi}}{\partial \xi^2} \tag{12.43}$$

$$\frac{\partial^2 \hat{\phi}}{\partial z^2} = \beta^2 \frac{\partial^2 \hat{\phi}}{\partial \eta^2} \tag{12.44}$$

Substitution of these second derivative relations into Equation (12.37) gives,

$$\frac{\partial^2 \hat{\phi}}{\partial \xi^2} + \frac{\partial^2 \hat{\phi}}{\partial \eta^2} = 0 \tag{12.45}$$

Thus, $\hat{\phi}(\xi, \eta)$ satisfies Laplaces equation and thus can be interpreted as an incompressible flow.

The remaining step is to determine how the geometry for the actual compressible flow around the airfoil in (x, z) relates to the incompressible flow in (ξ, η). To do this, we must look at the flow tangency boundary condition. Since we have assumed small perturbations, we can use the same approach as in the thin airfoil theory derived in Section 9.4. Specifically, we will enforce flow tangency on the $z = 0$ axis from $x = 0$ to $x = c$. Flow tangency requires,

$$\left[(V_\infty + \tilde{u})\hat{\mathbf{i}} + \tilde{w}\hat{\mathbf{k}}\right] \cdot \hat{\mathbf{n}} = 0 \tag{12.46}$$

The normal $\hat{\mathbf{n}}$ incorporates both the angle due to the slope of the camberline as well as the angle of attack. Thus (assuming small angles),

$$\hat{\mathbf{n}} = \left(\alpha - \frac{\mathrm{d}z_c}{\mathrm{d}x}\right)\hat{\mathbf{i}} + \hat{\mathbf{k}} \tag{12.47}$$

Thus, the flow tangency condition becomes,

$$(V_\infty + \tilde{u})\left(\alpha - \frac{\mathrm{d}z_c}{\mathrm{d}x}\right) + \tilde{w} = 0 \tag{12.48}$$

This can be linearized (and re-arranged a little) to produce,

$$\frac{\tilde{w}(x, 0)}{V_\infty} = \frac{\mathrm{d}z_c}{\mathrm{d}x}(x) - \alpha \tag{12.49}$$

where we have included the location $(x, 0)$ where the condition is enforced (with $0 < x < c$). In terms of the perturbation potential, this flow tangency condition can be written,

$$\frac{1}{V_\infty}\frac{\partial \tilde{\phi}}{\partial z}(x, 0) = \frac{\mathrm{d}z_c}{\mathrm{d}x}(x) - \alpha \tag{12.50}$$

Using the transformation to (ξ, η) and $\hat{\phi}$, the flow tangency condition becomes,

$$\frac{1}{V_\infty}\frac{\partial \hat{\phi}}{\partial \eta}(\xi = x, 0) = \frac{\mathrm{d}z_c}{\mathrm{d}x}(x) - \alpha \tag{12.51}$$

Now, we can see that this equation is equivalent to the flow tangency condition that would be derived in the (ξ, η) coordinates if the same camberline and angle of attack occurred in these coordinates. Thus, we arrive at a key conclusion: *the perturbation potential $\tilde{\phi}(x, y)$ for the linearized compressible potential flow around an airfoil at an angle of attack and a subsonic Mach number M_∞ is equivalent to the perturbation potential $\hat{\phi}(\xi, \eta)$ for the linearized incompressible potential flow around the same airfoil at the same angle of attack.*

12.3.2 Prandtl-Glauert correction

12.3

The pressure coefficient for the subsonic flow can be determined using the Prandtl-Glauert transformation,

$$C_p = -2\frac{\tilde{u}}{V_\infty} \tag{12.52}$$

$$= -\frac{2}{V_\infty}\frac{\partial\tilde{\phi}}{\partial x} \tag{12.53}$$

$$= -\frac{2}{\beta}\frac{1}{V_\infty}\frac{\partial\hat{\phi}}{\partial\xi} \tag{12.54}$$

$$= -\frac{2}{\beta}\frac{\hat{u}}{V_\infty} \tag{12.55}$$

Since $-2\hat{u}/V_\infty$ is the C_p for the incompressible linearized flow around the same airfoil and same angle of attack, then,

$$C_p = \frac{C_{p,0}}{\beta} \tag{12.56}$$

where $C_{p,0}$ is the pressure coefficient for the incompressible linearized potential flow about the same airfoil at the same angle of attack.

This result can then be applied to determine the lift, drag, and moment coefficients for inviscid linearized subsonic flow,

$$c_l = \frac{c_{l,0}}{\beta} \tag{12.57}$$

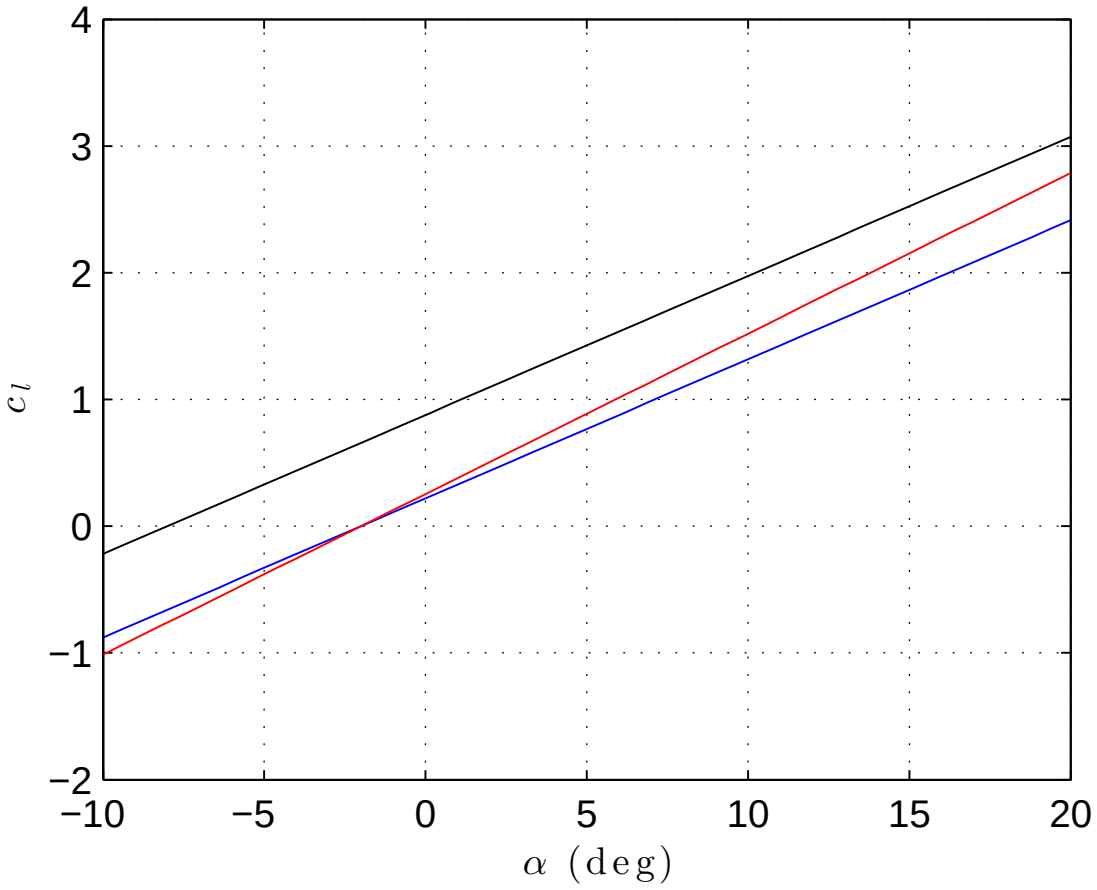
$$c_d = \frac{c_{d,0}}{\beta} \tag{12.58}$$

$$c_m = \frac{c_{m,0}}{\beta} \tag{12.59}$$

where $c_{l,0}$, $c_{d,0}$, and $c_{m,0}$ are the lift, drag, and moment coefficient for the incompressible linearized potential flow about the same airfoil at the same angle of attack.

edXproblem: 12.3.3 Coefficient of lift versus angle of attack using Prandtl-Glauert correction

12.3 9.4



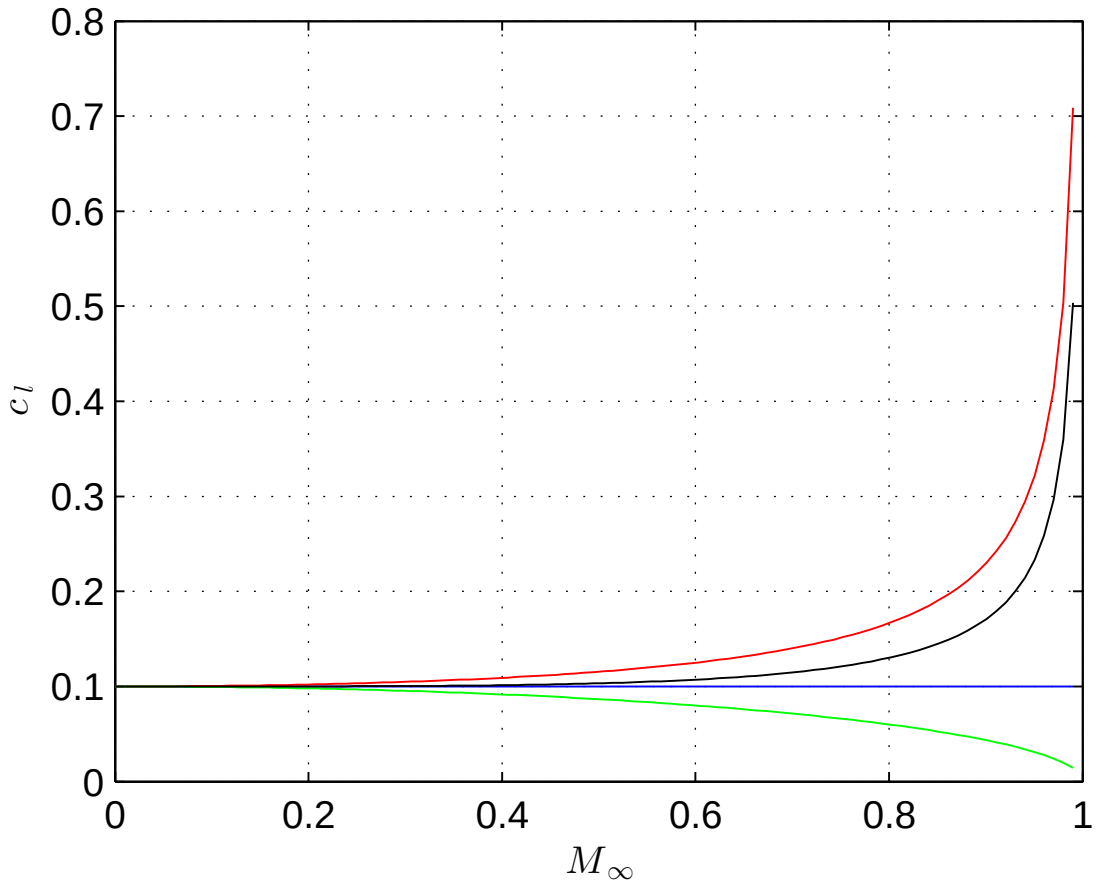
The three lines in the figure use Prandtl-Glauert theory to correct the results of incompressible thin airfoil theory. The airfoil analyzed is the same for all three lines except that one has a trailing edge flap deflection, while the other two do not have the flap deflected. Identify which airfoil corresponds to the red line.

edXsolution

Video Link

edXproblem: 12.3.4 Coefficient of lift versus Mach number using Prandtl-Glauert correction

12.3



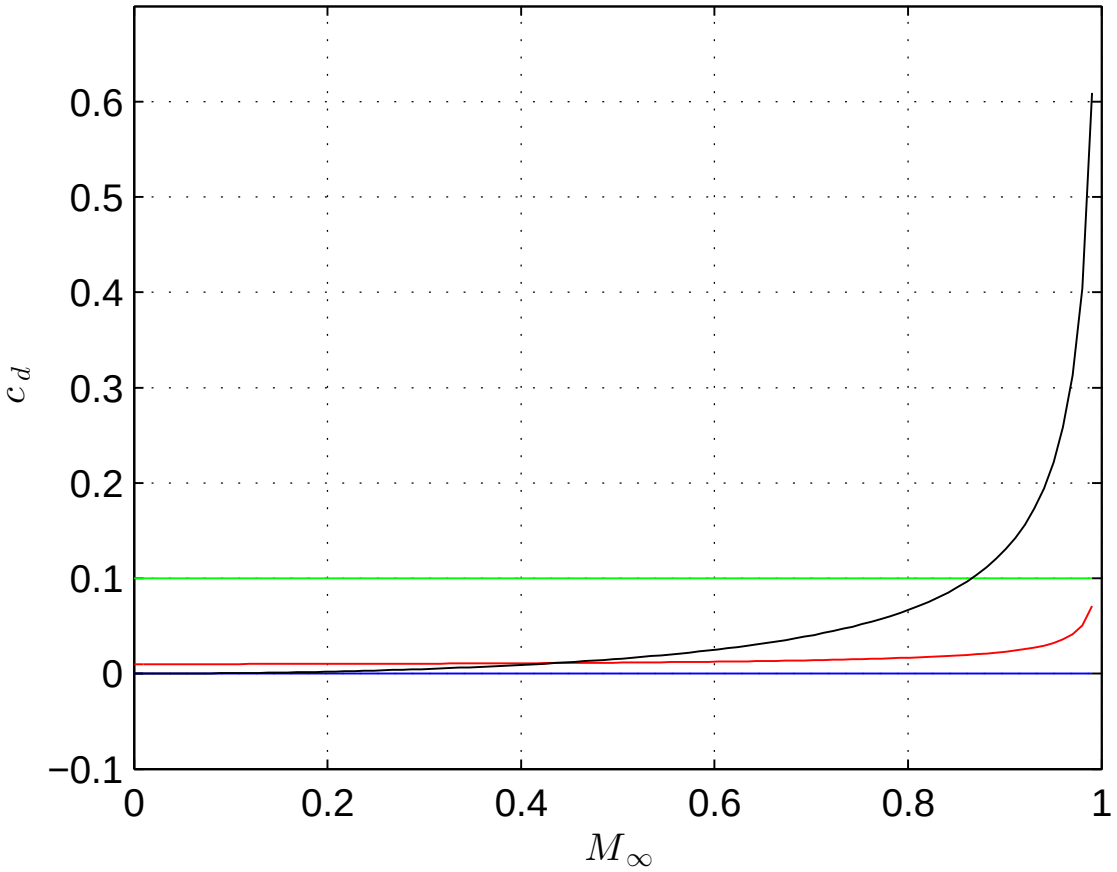
Identify which of the lines could possibly be the result of using Prandtl-Glauert theory to esimate c_l as a function of M_∞. Select all of the lines which are possibly from Prandtl-Glauert theory.

edXsolution

Video Link

edXproblem: 12.3.5 Coefficient of drag versus Mach number using Prandtl-Glauert correction

12.3 | 8.8



Identify which of the lines could possibly be the result of using Prandtl-Glauert theory to esimate c_d as a function of M_∞. Select all of the lines which are possibly from Prandtl-Glauert theory.

edXsolution

Video Link

12.4 Transonic Flow

12.4.1 Basic behavior of transonic flow

12.4 12.5

In this section, we discuss some aspects of transonic flow over airfoils and briefly on high-aspect ratio wings. It may be useful to revisit the brief description of transonic flows in Section 2.4.5.

To begin, we consider the flow over the RAE2822 airfoil for varying M_∞ with fixed Reynolds number and angle of attack. This airfoil has been widely studied in transonic aerodynamics both experimentally and computationally. In Figures 12.1-12.4, the surface C_p and contours of M around the airfoil are shown for increasing M_∞.

At $M_\infty = 0.5$, the flow appears similar to the incompressible and low M_∞ airfoil flows we have discussed previously.

For $M_\infty \geq 0.6$, the dotted line in the C_p plots corresponds to the C_p value at which the local flow would be sonic, that is $M = 1$, assuming isentropic behavior. We will denote this C_p value as $C_{p,\text{cr}}$ (meaning the critical C_p). We can calculate $C_{p,\text{cr}}$ using isentropic relationships. Specifically, assuming isentropic flow, the total pressure does not vary and we can therefore equate the total pressure in the freestream to the total pressure locally, to give,

$$p\left(1+\frac{\gamma-1}{2}M^2\right)^{\gamma/(\gamma-1)} = p_\infty\left(1+\frac{\gamma-1}{2}M_\infty^2\right)^{\gamma/(\gamma-1)} \tag{12.60}$$

Let p^* be the pressure when $M = 1$. Then, using the above relationship, we may find,

$$\frac{p^*}{p_\infty} = \left\{\frac{1+[(\gamma-1)/2]\,M_\infty^2}{1+(\gamma-1)/2}\right\}^{\gamma/(\gamma-1)} \tag{12.61}$$

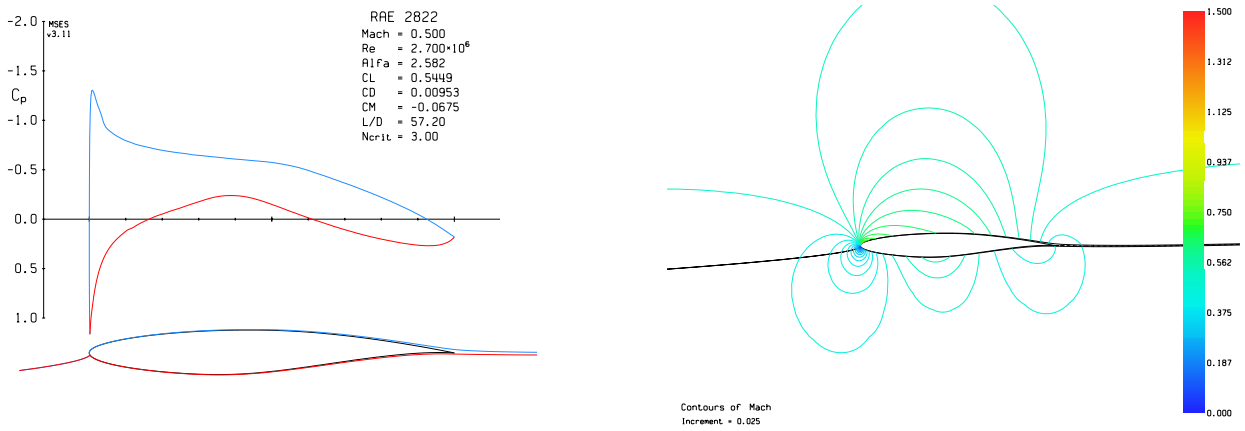
The critical C_p then is,

$$C_{p,\text{cr}} = \frac{p^*-p_\infty}{\frac{1}{2}\rho_\infty V_\infty^2} = \frac{2}{\gamma M_\infty^2}\left(\frac{p^*}{p_\infty}-1\right) = \frac{2}{\gamma M_\infty^2}\left[\left\{\frac{1+[(\gamma-1)/2]\,M_\infty^2}{1+(\gamma-1)/2}\right\}^{\gamma/(\gamma-1)}-1\right] \tag{12.62}$$

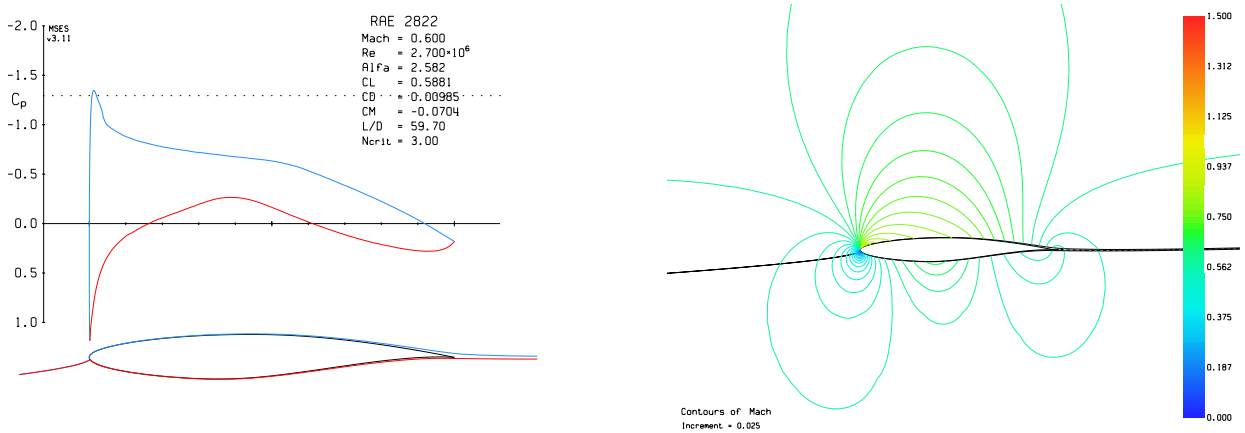
We note that $C_{p,\text{cr}} < 0$ since $M_\infty < 1$.

Looking at the surface C_p distributions, we see that for all $M_\infty \geq 0.6$, the surface $C_p \leq C_{p,\text{cr}}$ somewhere on the airfoil. Thus, the flow has local regions where $M > 1$. For the lower M_∞, this region of $M > 1$ occurs near the leading edge and grows in extent until at $M_\infty = 0.7$, the region where $M > 1$ extends from the leading edge until about $x/c = 0.5$.

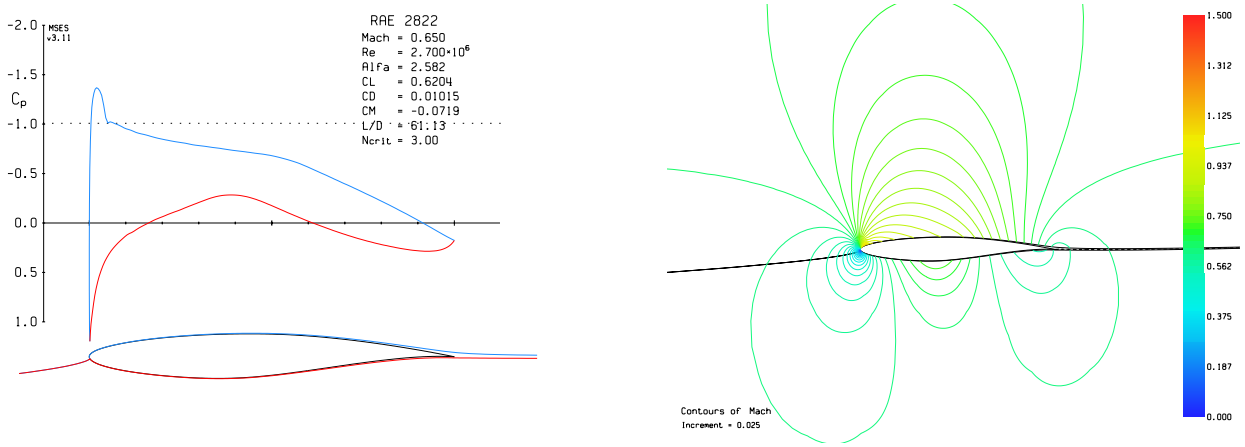
For $M_\infty = 0.712$, we see the presence of a shock wave around $x/c = 0.4$ in both the surface C_p and M contours. Then, as M_∞ is further increased, the shock moves further downstream reaching about $x/c = 0.6$ by $M_\infty = 0.75$. Above this Mach number, the boundary layer thickens substantially at the shock and shock no longer moves downstream with increasing M_∞. This situation in which the shock wave and boundary layer are strongly coupled is known as *shock-boundary layer interaction*. What this means is that while the shock wave is a cause of drag by itself (which we will consider more carefully in a moment), the interaction of the shock wave with the boundary layer can further increase the drag because of the thickening and possible separation of the boundary layer. Further, this thickening of the boundary layer also implies that the flow will not turn as effectively since the streamlines outside of the boundary layer do not follow the airfoil surface as effectively. Finally, we note that for $M_\infty \geq 0.8$, a shock wave also appears on the lower surface.



(a) $M_\infty = 0.5$



(b) $M_\infty = 0.6$



(c) $M_\infty = 0.65$

Figure 12.1: Surface C_p and Mach contours for RAE2822 at $Re_\infty = 2.7 \times 10^6$, $\alpha = 2.582°$, and $M_\infty = 0.5$, 0.6, and 0.65.

12.4.2 Behavior of lift, drag, and moments in transonic flow

12.4

The variation in the lift coefficient with Mach number is shown in Figure 12.5. We observe that c_l initially increases with M_∞ and that the behavior is well predicted by Prandtl-Glauert theory.

Note that the Prandtl-Glauert theory result uses the c_l at $M_\infty = 0.5$ to determine the incompressible c_l. Thus, the Prandtl-Glauert c_l curve uses the following relationship,

$$c_{l,\text{PG}}(M_\infty) = \frac{\beta(M_\infty = 0.5)}{\beta(M_\infty)} c_l(M_\infty = 0.5) \tag{12.63}$$

Above approximately $M_\infty = 0.75$, the actual c_l drops while the Prandtl-Glauert result continues to rise. For this airfoil, the reason for the c_l dropping is due to the shock-boundary layer interaction causing boundary layer thickening and eventual separation leading to a decrease in flow turning. However, even for flows without boundary layer separation, c_l will not increases indefinitely as $M_\infty \to 1$. The nonlinear effects which the Prandtl-Glauert theory ignores will dominate such that eventually the lift coefficient will reach a maximum with respect to M_∞.

The variation in the drag coefficient with Mach number is shown in Figure 12.6. Until approximately $M_\infty = 0.7$, the drag is relatively unaffected by changes in Mach number. For $M_\infty > 0.7$, the drag rapidly increases. Recall that it is just above $M_\infty = 0.7$ that the shock wave appears in the middle of the airfoil's upper surface. The drag is also separated into three parts in the figure, specifically, the drag due to friction, the form drag, and the drag due to the shock wave. We have not yet discussed the form drag but will as we discuss boundary layer flows in the upcoming modules. Briefly, form drag is a result of the surface pressure being modified (from what would occur if the flow were inviscid) due to the thickening and (eventual) separation of the boundary layer. Thus, while the form drag is due to pressure forces, the root cause is in fact the viscous effects in the boundary layer. The friction drag is relatively unaffected by the M_∞, even decreasing slightly (due to the thickening of the boundary layer after the shock waves).

Our focus in this module is the wave drag, which we consider in detail in the following video. Specifically, we show how the wave drag can be tied to the loss of total pressure that occurs at a shock wave. Thus, to design an efficient airfoil at transonic conditions, it is critical to keep the loss of total pressure at a shock as low as possible.

Video Link

Finally, the variation in the moment coefficient (at the quarter-chord) with Mach number is shown in Figure 12.7. At lower Mach numbers, the moment coefficient is approximately -0.07. Then, it rises rapidly as the shock waves appear becoming positive for $M_\infty \approx 0.84$. For aircraft which fly supersonically, this phenomenon in which the moment varies significantly and even switches signs is a major design challenge. Consider that as an aircraft attempts to accelerate through $M_\infty = 1$, this change in the moment will alter the stability of the aircraft.

12.4.3 Critical Mach number

12.3 12.5

Since the appearance of shock waves has such a significant effect on aerodynamic performance, an important consideration in the design of airfoils is determining at what M_∞ will shocks first appear. Since shocks waves require flow which is supersonic, a commonly used measure of the potential appearance of shock waves is the freestream Mach number at which the velocity becomes sonic (at any point in the flow). This freestream Mach number is called the *critical Mach number* and given the notation M_{cr}.

Prandtl-Glauert theory can be used to estimate M_{cr} using the C_p distribution from incompressible flow around an airfoil. Since Prandtl-Glauert theory simply scales the incompressible C_p by $1/\beta$, then the minimum C_p will not change location on the airfoil. Thus, the determination of M_{cr} using Prandtl-Glauert is,

- Determine $\min C_{p,0}$, the minimum surface pressure for the incompressible potential flow. We assume that the lowest pressures will occur on the airfoil surface.
- The minimum C_p for any subsonic M_∞ can be estimated from Prandtl-Glauert,

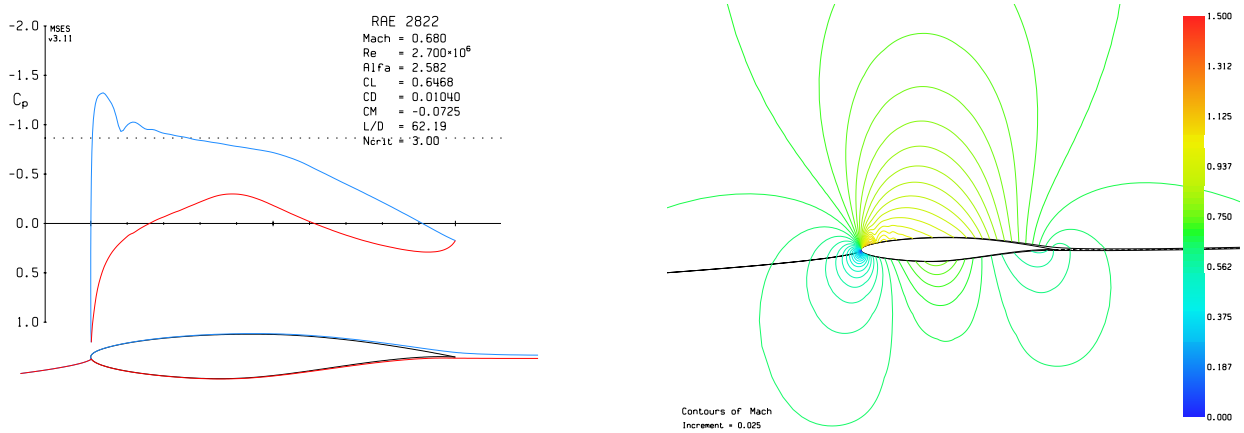
$$\min C_p(M_\infty) = \frac{\min C_{p,0}}{\sqrt{1 - M_\infty^2}} \tag{12.64}$$

- The critical C_p at which the local Mach number is 1 for any subsonic M_∞ can be determined with Equation (12.62),

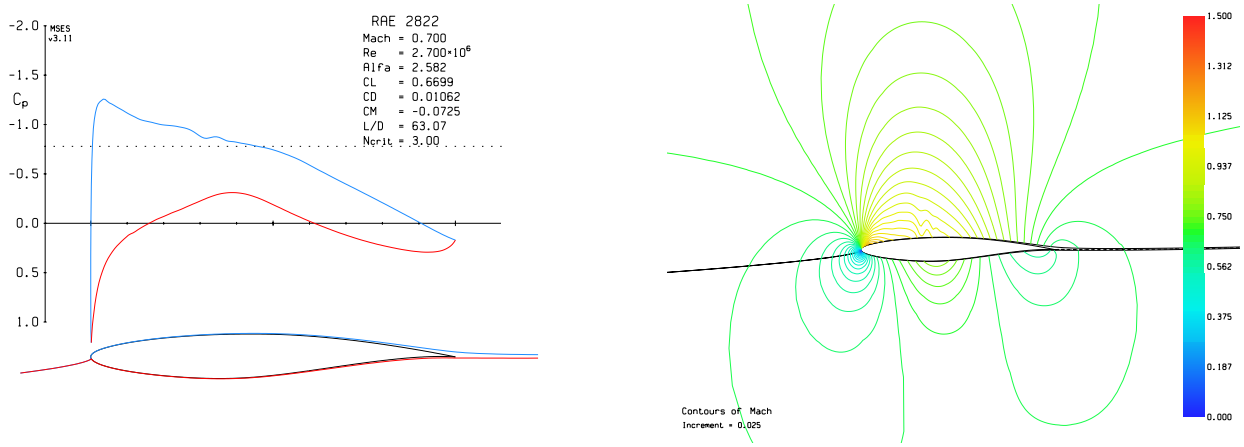
$$C_{p,\mathrm{cr}}(M_\infty) = \frac{2}{\gamma M_\infty^2}\left[\left\{\frac{1 + [(\gamma-1)/2]\, M_\infty^2}{1 + (\gamma-1)/2}\right\}^{\gamma/(\gamma-1)} - 1\right] \tag{12.65}$$

- Solve for M_{cr} such that $\min C_p(M_{\mathrm{cr}}) = C_{p,\mathrm{cr}}(M_{\mathrm{cr}})$.

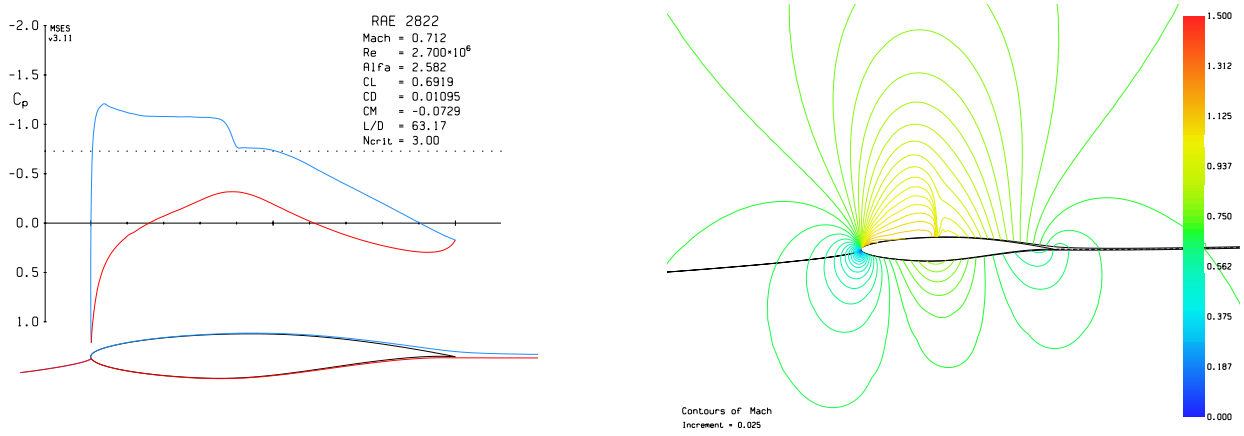
This process can be visualized graphically as determining the M_∞ when plots of $\min C_p(M_\infty)$ and $C_{p,\mathrm{cr}}(M_\infty)$ intersect. This M_∞ intersection point is M_{cr}. An example of this is shown in Figure 12.8 for a NACA 4412 airfoil at $\alpha = 1°$. For this angle of attack, $\min C_{p,0} = -0.9$ at $x/c = 0.25$ on the upper surface. The critical Mach number is found to be $M_{\mathrm{cr}} = 0.62$.



(a) $M_\infty = 0.68$

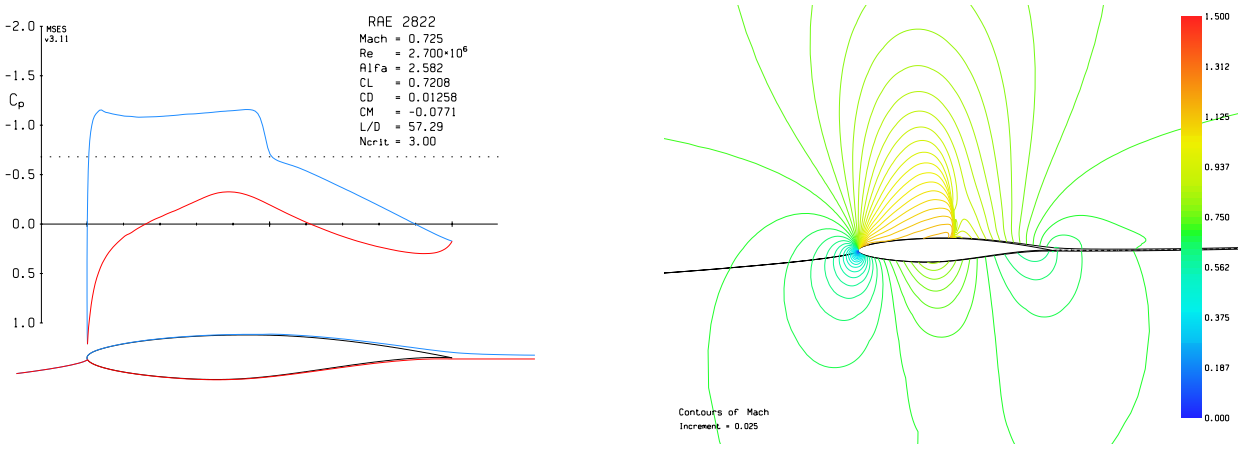


(b) $M_\infty = 0.7$

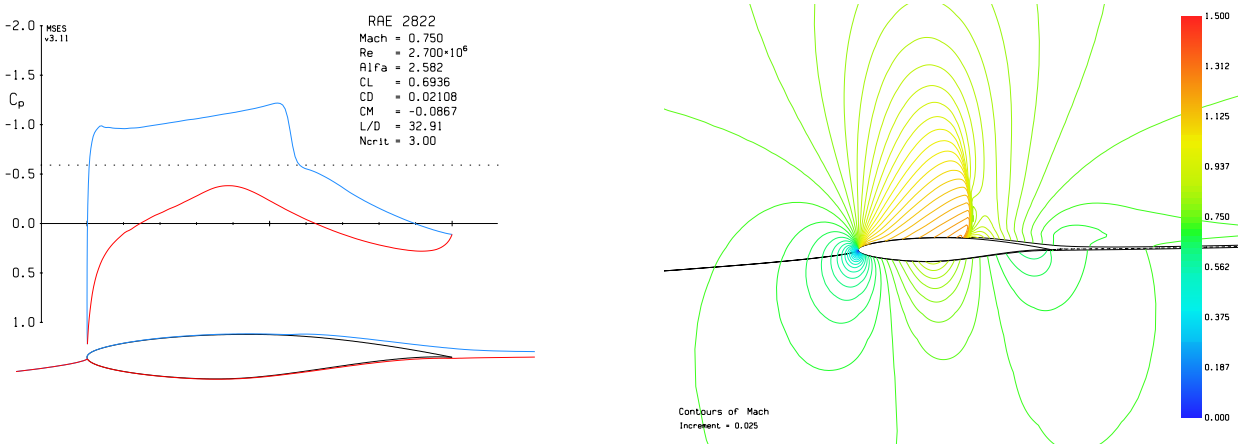


(c) $M_\infty = 0.712$

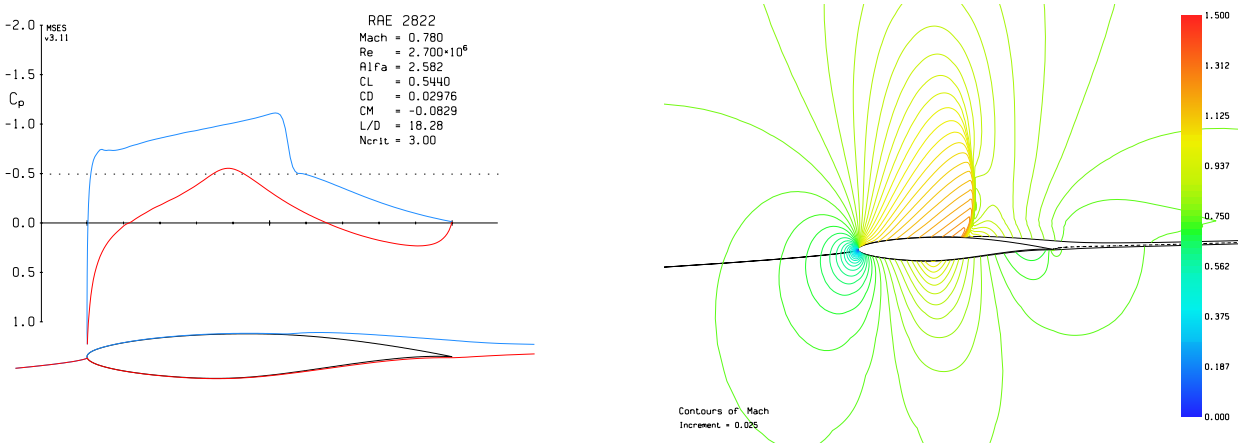
Figure 12.2: Surface C_p and Mach contours for RAE2822 at $Re_\infty = 2.7 \times 10^6$, $\alpha = 2.582°$, and $M_\infty = 0.68$, 0.7, and 0.712.



(a) $M_\infty = 0.725$

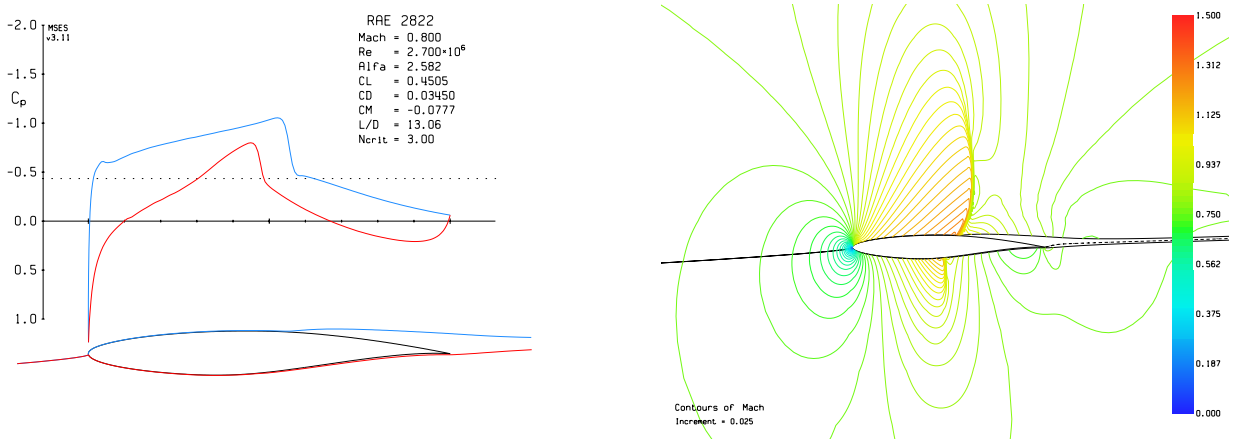


(b) $M_\infty = 0.75$

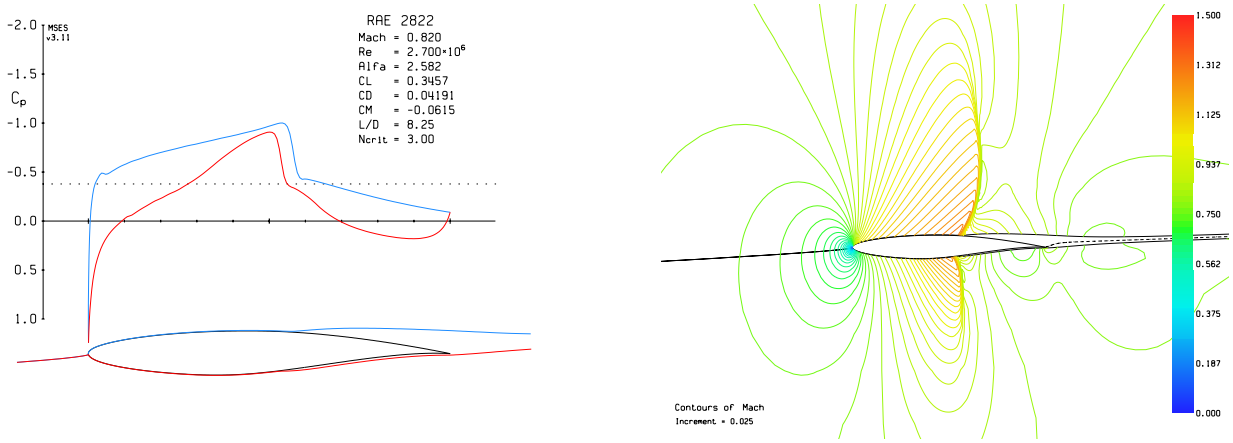


(c) $M_\infty = 0.78$

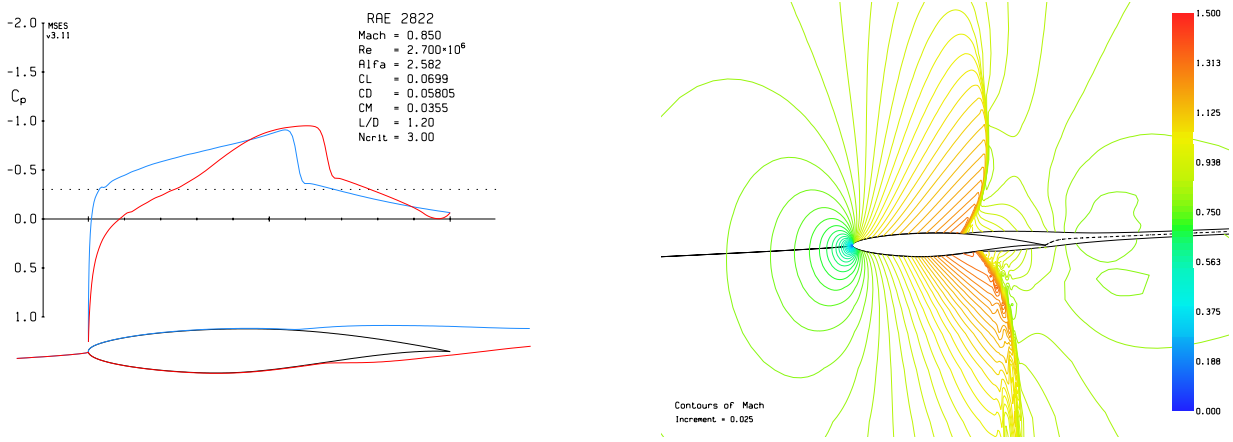
Figure 12.3: Surface C_p and Mach contours for RAE2822 at $Re_\infty = 2.7 \times 10^6$, $\alpha = 2.582°$, and $M_\infty = 0.725$, 0.75, and 0.78.



(a) $M_\infty = 0.8$



(b) $M_\infty = 0.82$



(c) $M_\infty = 0.85$

Figure 12.4: Surface C_p and Mach contours for RAE2822 at $Re_\infty = 2.7 \times 10^6$, $\alpha = 2.582°$, and $M_\infty = 0.8$, 0.82, and 0.85.

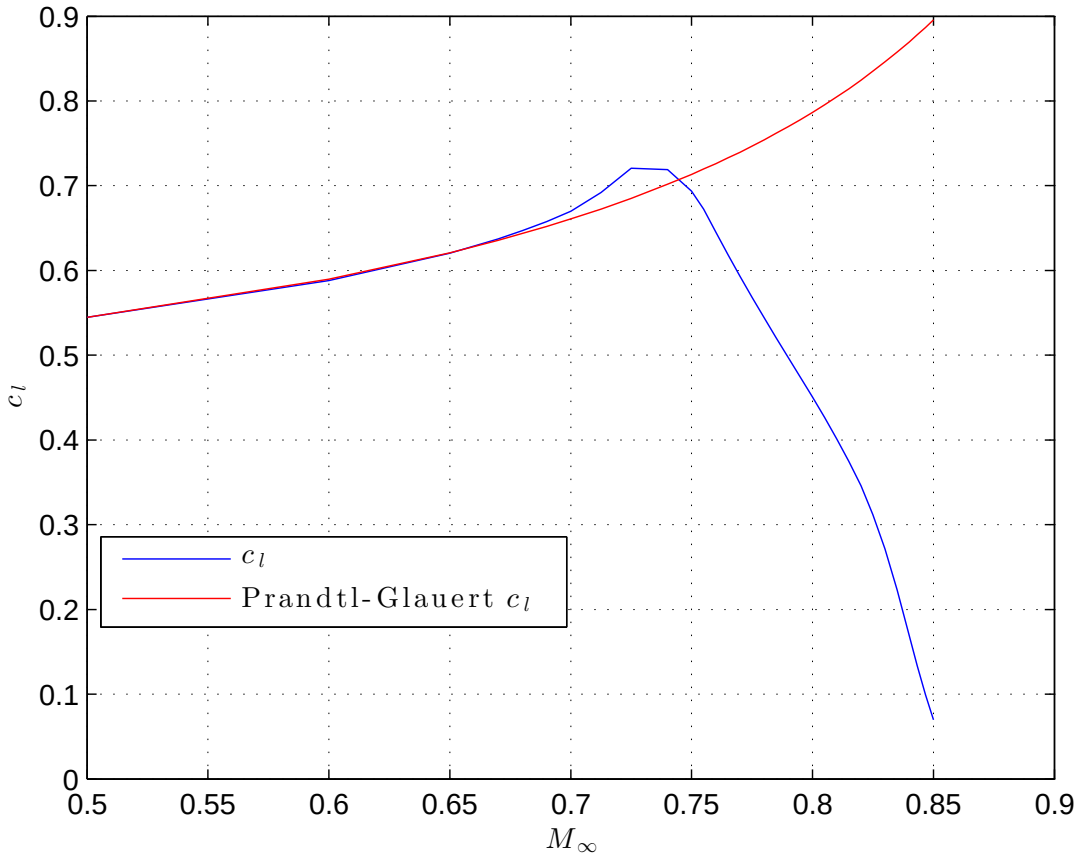


Figure 12.5: c_l versus M_∞ for RAE2822 at $Re_\infty = 2.7 \times 10^6$ and $\alpha = 2.582°$.

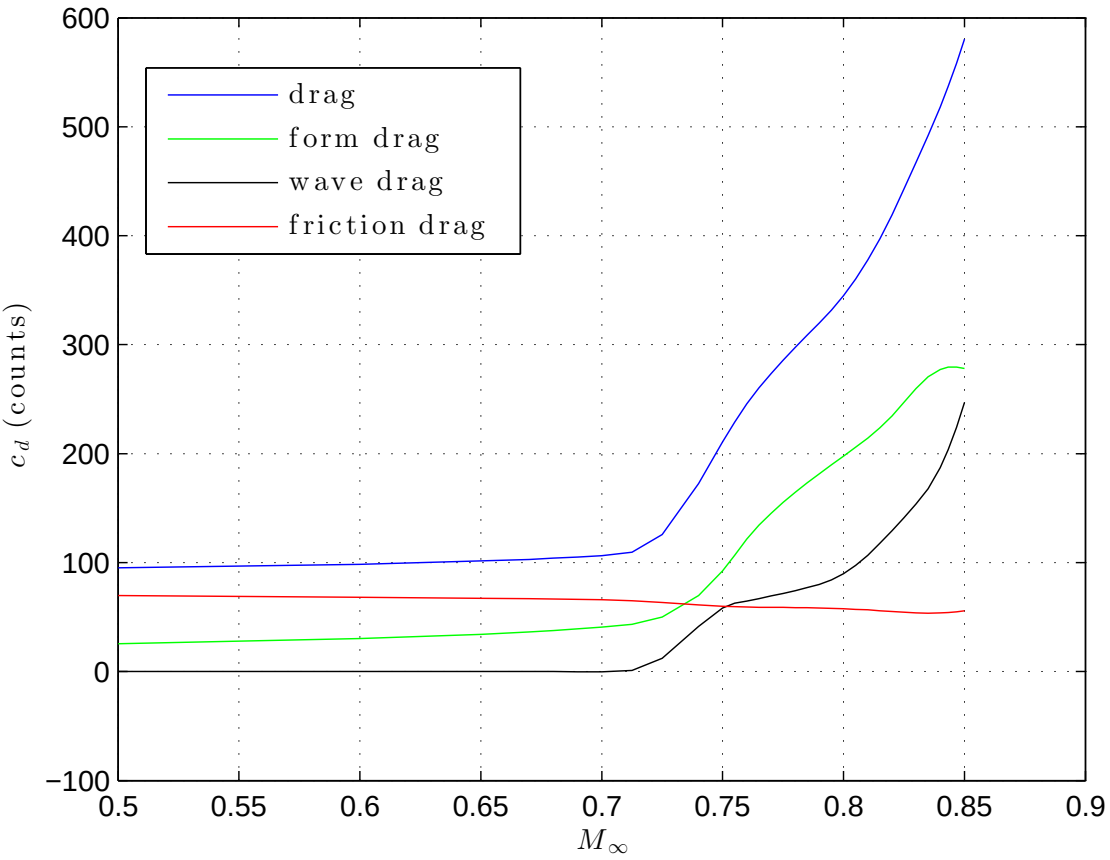


Figure 12.6: c_d (including breakdown into wave, form, and friction drag) versus M_∞ for RAE2822 at $Re_\infty = 2.7 \times 10^6$ and $\alpha = 2.582°$.

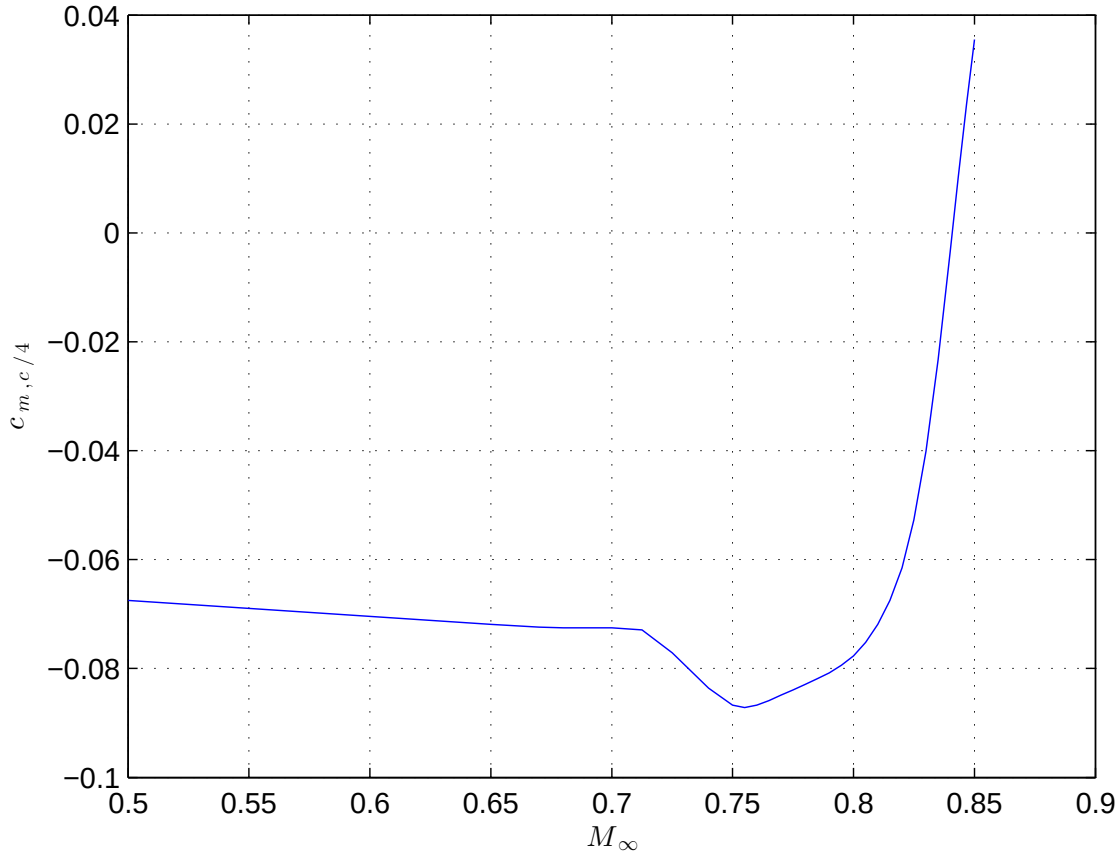


Figure 12.7: $c_{m,c/4}$ versus M_∞ for RAE2822 at $Re_\infty = 2.7 \times 10^6$ and $\alpha = 2.582°$.

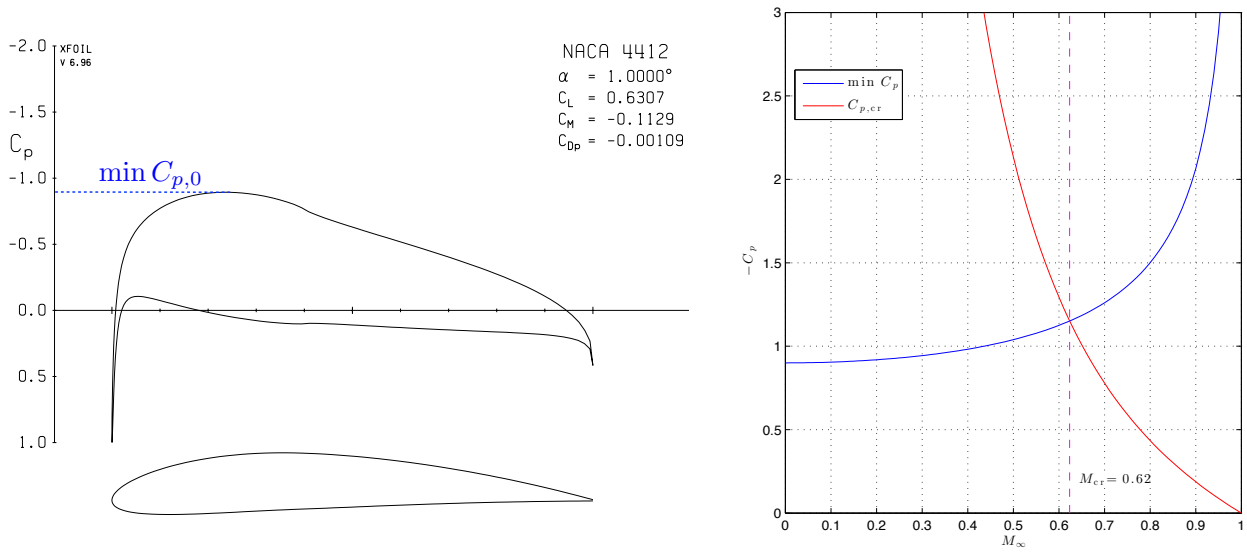


Figure 12.8: Determination of M_{cr} for NACA 4412 at $\alpha = 1°$

edXproblem: 12.4.4 Estimation of critical Mach number for a cylinder

12.3 12.5

Determine the critical Mach number for the flow over a cylinder. Enter your answer with two decimal places of precision (0.XY).

edXsolution

Video Link

12.5 Supersonic Linearized Potential Flow

12.5.1 Mach wave solutions

12.6

When $M_\infty > 1$, the character of the linearized potential equation changes significantly from the subsonic flow case. In particular, when $M_\infty > 1$ then the $1 - M_\infty^2 < 0$ and this sign change means that the governing equation for $\tilde{\phi}$ is no longer a transformed version of Laplaces equation, but instead is known mathematically as a wave equation. Specifically, for the $M_\infty > 1$ case, we re-arrange Equation (12.30) to emphasize this difference,

$$\left(M_\infty^2 - 1\right) \frac{\partial^2 \tilde{\phi}}{\partial x^2} - \frac{\partial^2 \tilde{\phi}}{\partial z^2} = 0 \tag{12.66}$$

This equation has a general solution of the following form,

$$\begin{aligned} \tilde{\phi}(x,z) &= \phi_p(\xi_p) + \phi_m(\xi_m) && (12.67)\\ \xi_p(x,z) &\equiv x + \lambda z && (12.68)\\ \xi_m(x,z) &\equiv x - \lambda z && (12.69)\\ \lambda &\equiv \sqrt{M_\infty^2 - 1} && (12.70) \end{aligned}$$

The solutions $\phi_p(\xi_p)$ and $\phi_m(\xi_m)$ are equivalent to the Mach waves which are described in Section 5.5.1. Recall that Mach waves are the result of infinitessimal sound waves which coalesce along the Mach angle $\mu = \arcsin(1/M)$. The variables ξ_p and ξ_m are constant along lines with slope of $-1/\lambda$ and $1/\lambda$, respectively. And, note that $\tan\mu = 1/\lambda$ confirming that the solution ϕ_p and ϕ_m are constant along the Mach angle of the freestream.

Next, we verify this is a solution to Equation (12.66) by substitution. To do this, we will need to take partial derivatives with respect to x and z,

$$\frac{\partial \xi_p}{\partial x} = 1 \qquad \frac{\partial \xi_p}{\partial z} = \lambda \tag{12.71}$$

$$\frac{\partial \xi_m}{\partial x} = 1 \qquad \frac{\partial \xi_m}{\partial z} = -\lambda \tag{12.72}$$

Then letting $\phi_p' \equiv \mathrm{d}\phi_p/\mathrm{d}\xi_p$ and $\phi_m' \equiv \mathrm{d}\phi_m/\mathrm{d}\xi_m$ gives,

$$\frac{\partial \phi_p}{\partial x} = \phi_p' \qquad \frac{\partial \phi_p}{\partial z} = \lambda\phi_p' \tag{12.73}$$

$$\frac{\partial \phi_m}{\partial x} = \phi_m' \qquad \frac{\partial \phi_m}{\partial z} = -\lambda\phi_m' \tag{12.74}$$

And similarly, the second derivatives are,

$$\frac{\partial^2 \phi_p}{\partial x^2} = \phi_p'' \qquad \frac{\partial^2 \phi_p}{\partial z^2} = \lambda^2\phi_p'' \tag{12.75}$$

$$\frac{\partial^2 \phi_m}{\partial x^2} = \phi_m'' \qquad \frac{\partial^2 \phi_m}{\partial z^2} = \lambda^2\phi_m'' \tag{12.76}$$

Finally, substitution into Equation (12.66) gives

$$\begin{aligned} \left(M_\infty^2 - 1\right) \frac{\partial^2 \tilde{\phi}}{\partial x^2} - \frac{\partial^2 \tilde{\phi}}{\partial z^2} &= \left(M_\infty^2 - 1\right)\left(\phi_p'' + \phi_m''\right) - \lambda^2(\phi_p'' + \phi_m'') && (12.77)\\ &= \left(M_\infty^2 - 1 - \lambda^2\right)\left(\phi_p'' + \phi_m''\right) && (12.78)\\ &= 0 && (12.79) \end{aligned}$$

12.5.2 Flow over a flat plate - revisited

12.6

In the following video, we will use the ϕ_p and ϕ_m solutions to solve for the flow over a flat plate at angle of attack α. Then, in Section 12.5.4, we will generalize the result to include airfoils with thickness and camber. For the flat plate, we will show the following key results,

$$c_l = \frac{4}{\sqrt{M_\infty^2 - 1}}\alpha \tag{12.80}$$

$$c_d = \frac{4}{\sqrt{M_\infty^2 - 1}}\alpha^2 \tag{12.81}$$

$$c_{m,c/2} = 0 \tag{12.82}$$

$$x_{cp} = x_{ac} = c/2 \tag{12.83}$$

Video Link

Before moving on to consider arbitrary flows, we recommend working on Sample Problem 12.6.1 in which we compare the flow modeled with linearized potential equations to the flow modeled using shock-expansion theory. This sample problem will help to better understand how the linearized potential solution behaves and how it compares to the nonlinear results found using shock-expansion theory.

edXproblem: 12.5.3 Sonic boom

12.6

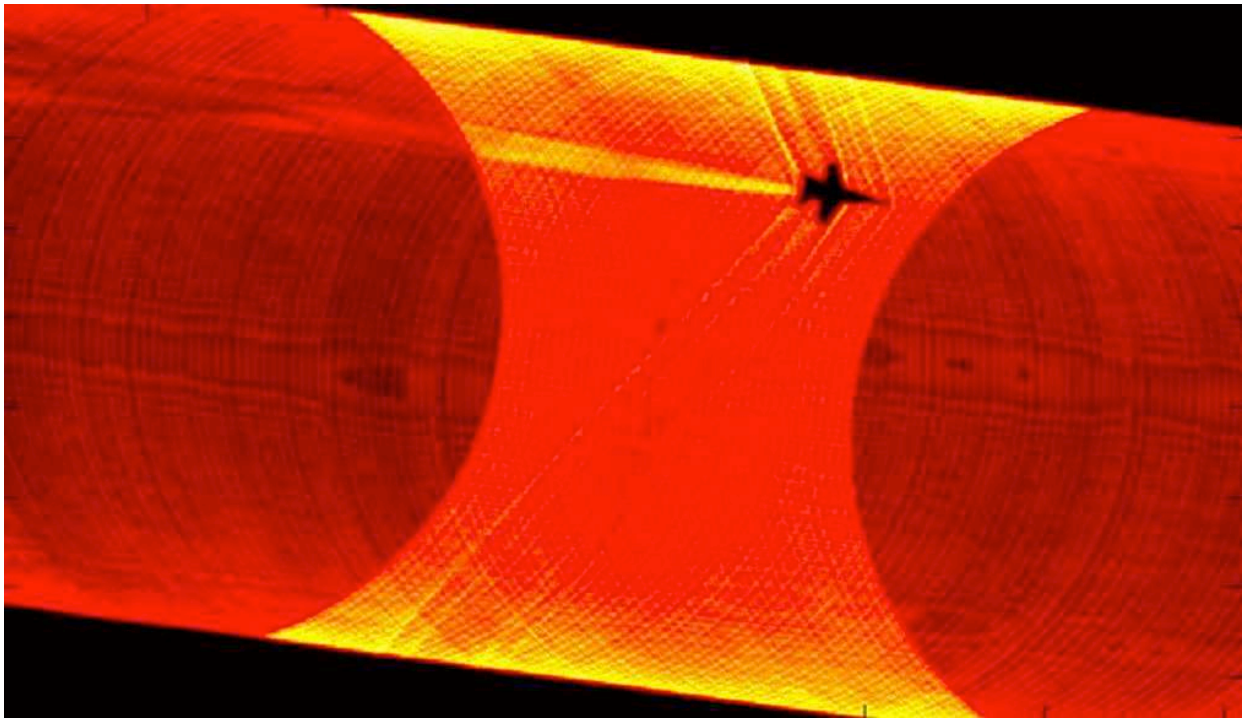


Figure 12.9: Shock wave structure on a F/A-18. Public domain image. Author: NASA/Leonard Weinstein.

Sonic booms are created by the compression waves generated by aircraft flying at supersonic speeds. These compression waves cause a rapid increase in the pressure, which generates the sound commonly refered to as a sonic boom. In this problem, we will assume that the compression waves are well modeled by linearized supersonic theory (which in fact they are once away from the immediate vicinity of the aircraft).

An airplane is flying over you at $M_\infty = 2$. You first hear the plane's sonic boom 10 seconds after the plane passed directly overhead. Another airplane, flying at the same altitude, passes directly overhead at $M_\infty = 4$. Approximately how many seconds will pass from the time when this $M_\infty = 4$ plane was directly overhead until you hear the plane's sonic boom? Assume that the variation of the speed of sound in the atmosphere for this problem is negligible. Enter your answer rounded to the nearest tenth of second (in the form XY.Z).

edXsolution

Video Link

12.5.4 Flow over an airfoil

12.6

We can apply the linearized supersonic potential flow theory to estimate the flow over an airfoil.

Assuming small thickness and camber, the upper and lower surface of the airfoil (not including angle of attack) is,

$$z_u(x) = z_c(x) + \frac{t(x)}{2} \tag{12.84}$$

$$z_l(x) = z_c(x) - \frac{t(x)}{2} \tag{12.85}$$

The outward-pointing upper and lower surface normals (including the angle of attack) are then,

$$\hat{\mathbf{n}}_u(x) = \left(-\frac{1}{2}\frac{\mathrm{d}t}{\mathrm{d}x} + \alpha - \frac{\mathrm{d}z_c}{\mathrm{d}x}\right)\hat{\mathbf{i}} + \hat{\mathbf{k}} \tag{12.86}$$

$$\hat{\mathbf{n}}_l(x) = \left(-\frac{1}{2}\frac{\mathrm{d}t}{\mathrm{d}x} - \alpha + \frac{\mathrm{d}z_c}{\mathrm{d}x}\right)\hat{\mathbf{i}} - \hat{\mathbf{k}} \tag{12.87}$$

Thus, the flow tangency condition on the upper surface and lower surfaces are,

$$\tilde{w}_u = V_\infty\left(\frac{\mathrm{d}z_c}{\mathrm{d}x} - \alpha + \frac{1}{2}\frac{\mathrm{d}t}{\mathrm{d}x}\right) \tag{12.88}$$

$$\tilde{w}_l = V_\infty\left(\frac{\mathrm{d}z_c}{\mathrm{d}x} - \alpha - \frac{1}{2}\frac{\mathrm{d}t}{\mathrm{d}x}\right) \tag{12.89}$$

Using the same derivation as in the video for the flat plate case (see Section 12.5.2), the pressure coefficients are,

$$C_{p,u} = \frac{2}{\lambda}\left(\frac{1}{2}\frac{\mathrm{d}t}{\mathrm{d}x} + \frac{\mathrm{d}z_c}{\mathrm{d}x} - \alpha\right) \tag{12.90}$$

$$C_{p,l} = \frac{2}{\lambda}\left(\frac{1}{2}\frac{\mathrm{d}t}{\mathrm{d}x} - \frac{\mathrm{d}z_c}{\mathrm{d}x} + \alpha\right) \tag{12.91}$$

The aerodynamic force applied to the airfoil is,

$$\mathbf{F}' = \int_0^c \left(-p_l\hat{\mathbf{n}}_l - p_u\hat{\mathbf{n}}_u\right)\,\mathrm{d}x \tag{12.92}$$

The lift is,

$$L' = \mathbf{F}'\cdot\hat{\mathbf{k}} \tag{12.93}$$

$$= \int_0^c \left(-p_l\hat{\mathbf{n}}_l - p_u\hat{\mathbf{n}}_u\right)\cdot\hat{\mathbf{k}}\,\mathrm{d}x \tag{12.94}$$

$$= \int_0^c (p_l - p_u)\,\mathrm{d}x \tag{12.95}$$

Then, non-dimensionalizing to give the lift coefficient,

$$c_l = \int_0^1 (C_{p,l} - C_{p,u})\,\mathrm{d}(x/c) \tag{12.96}$$

$$= \frac{4}{\lambda}\int_0^1 \left(\alpha - \frac{\mathrm{d}z_c}{\mathrm{d}x}\right)\,\mathrm{d}(x/c) \tag{12.97}$$

$$\Rightarrow c_l = \frac{4}{\lambda}\alpha \tag{12.98}$$

Thus, we see the surprising result that camber does not result in lift in a supersonic flow (unless nonlinear effects are included). Note: the camber contribution is zero because $z_c(0) = z_c(c) = 0$, so that the integral of $\mathrm{d}z_c/\mathrm{d}x$ will be zero.

The drag coefficient can be determined in the same manner by manipulating the $\mathbf{F}' \cdot \hat{\mathbf{i}}$. Admittedly, it is many more manipulations, but you might give it a try! The end result is,

$$c_d = \frac{4}{\lambda}\alpha^2 + \frac{4}{\lambda}\int_0^1 \left(\frac{\mathrm{d}z_c}{\mathrm{d}x}\right)^2 \mathrm{d}(x/c) + \frac{1}{\lambda}\int_0^1 \left(\frac{\mathrm{d}t}{\mathrm{d}x}\right)^2 \mathrm{d}(x/c) \tag{12.99}$$

Thus, we see that the angle of attack, camber, and thickness all contribute to the drag.

It is also possible to derive the following result for the moment coefficient about the mid-chord:

$$c_{m,c/2} = -\frac{4}{\lambda}\frac{\overline{z_c}}{c} \text{ where } \overline{z_c} \equiv \int_0^1 z_c \,\mathrm{d}(x/c) \tag{12.100}$$

Thus, the moment does not depend on the angle of attack and consequently the aerodynamic center is at $x_{ac} = c/2$ for any airfoil in supersonic (linearized) flow. Further, when the average camber $\overline{z_c}/c$ is positive, the moment at the mid-chord will be negative (nose down).

The drag coefficient (and lift and moment coefficients) are seen to become infinite as $M_\infty \to 1$. However, as discussed for transonic flow, this is not correct but rather is a result of the linear approximations which are not valid around sonic conditions. Though the drag coefficient does increase around $M_\infty = 1$, it remains finite.

edXproblem: 12.5.5 Minimum wave drag supersonic airfoil design

12.6

Using linearized supersonic potential flow, which of the following airfoils produces the smallest wave drag for a $c_l = 0.1$ and $M_\infty = 2.5$?

What is the drag coefficient for this minimum wave drag airfoil? Report your with two digits of precision of the form X.YeP.

edXsolution

Video Link

12.6 Sample Problems

edXproblem: 12.6.1 Comparison of linearized supersonic and shock-expansion theory

In Sample Problem 5.7.2, we applied shock-expansion theory to determine the lift and drag on a flat plate at $\alpha = 5^\circ$ with $M_\infty = 2$. Now, estimate the performance using linearized supersonic potential flow, in particular,

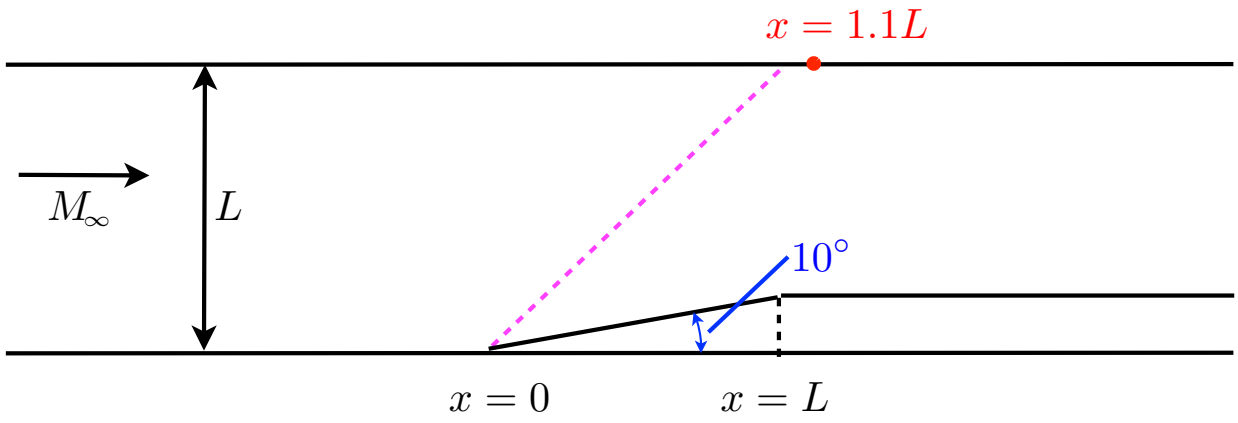
- Determine the C_p on the upper and lower surface of the plate
- Determine c_l and c_d
- Sketch streamlines

edXsolution

Video Link

edXproblem: 12.6.2 Supersonic flow in a duct

12.6



Apply linearized supersonic potential flow to analyze the duct shown.

- What is the value of M_∞ such that the Mach wave at the beginning of the ramp ($x = 0$) will hit the upper wall at exactly $x = L$?
- For this M_∞, what is the value of C_p on the upper wall at $x = 1.1L$?

edXsolution

Video Link

12.7 Homework Problems

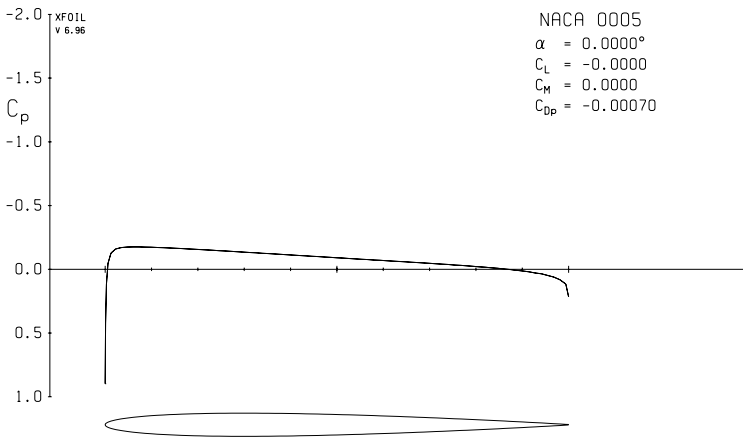
edXproblem: 12.7.1 Impact of thickness on critical Mach number

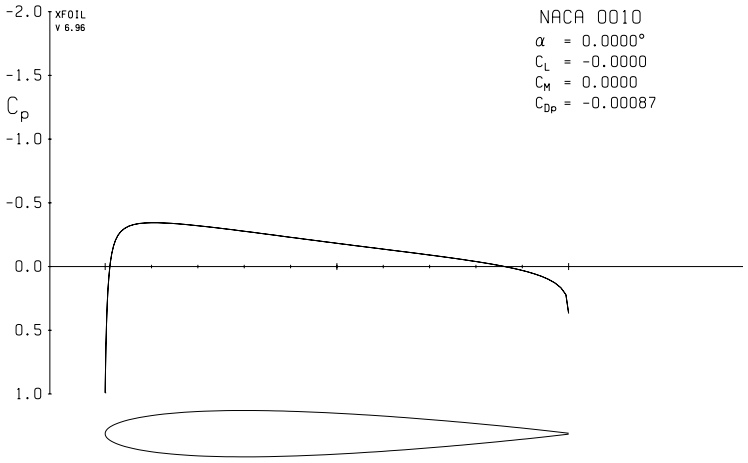
12.3 12.5

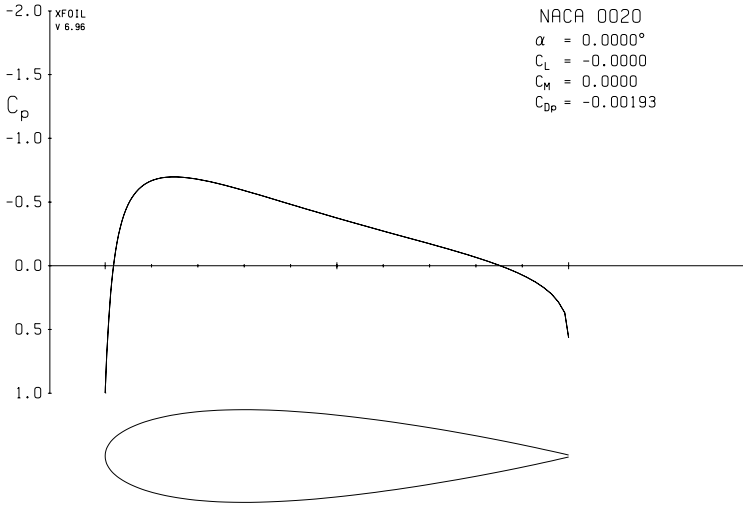
The plots above show the surface C_p for the incompressible flow around a NACA 0005, 0010, and 0020 at $\alpha = 0$. In the plot below, determine which line represents the dependence of the critical Mach number on the maximum thickness of these airfoils estimated using Prandtl-Glauert theory?

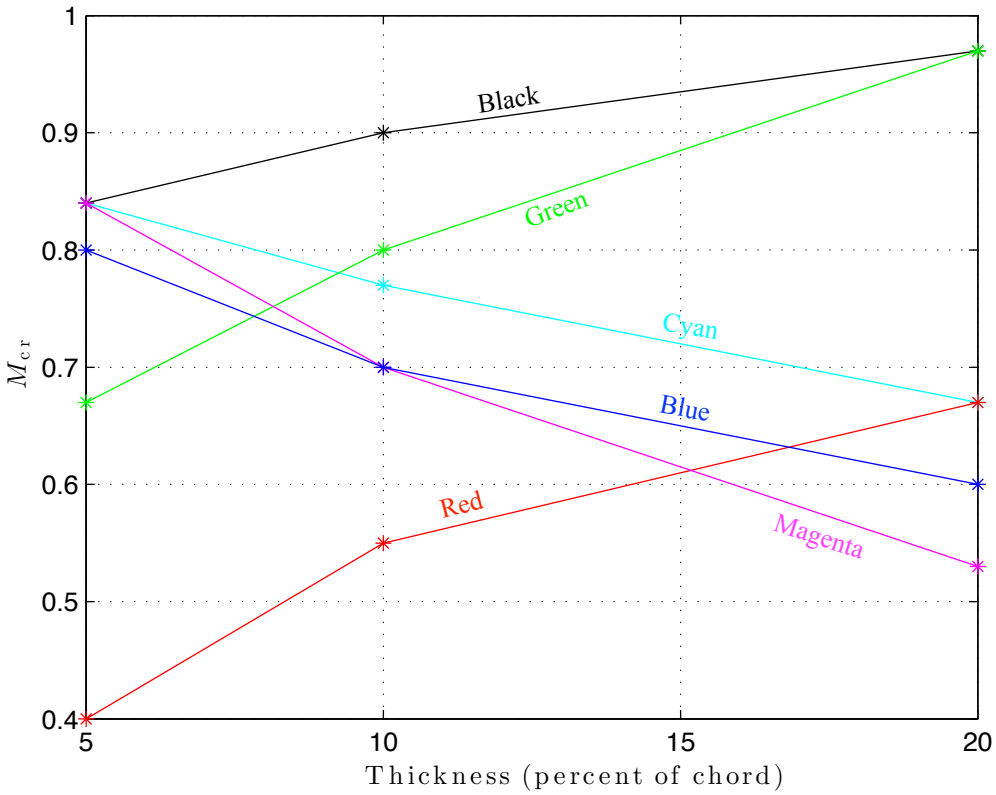
edXsolution

Video Link


XFOIL
v 6.96
NACA 0005
α = 0.0000°
CL = -0.0000
CM = 0.0000
CDp = -0.00070
-2.0
-1.5
Cp
-1.0
-0.5
0.0
0.5
1.0


XFOIL
v 6.96
NACA 0010
α = 0.0000°
CL = -0.0000
CM = 0.0000
CDp = -0.00087
-2.0
-1.5
Cp
-1.0
-0.5
0.0
0.5
1.0


XFOIL
v 6.96
NACA 0020
α = 0.0000°
CL = -0.0000
CM = 0.0000
CDp = -0.00193
-2.0
-1.5
Cp
-1.0
-0.5
0.0
0.5
1.0


1
0.9
0.8
0.7
0.6
0.5
0.4
M_{cr}
5
10
15
20
Thickness (percent of chord)
Black
Green
Cyan
Blue
Red
Magenta

edXproblem: 12.7.2 Impact of increased Mach number on lift in subsonic flow at constant altitude

2.2 | 2.5 | 9.4 | 12.3

- For all parts of this problem, use linearized two-dimensional subsonic potential flow theory.
- Consider an aircraft that is flying at a **constant** altitude.
- Assume that the wing is not twisted and has the same airfoil shape along the span.
- Assume that the sectional lift (L') on wing airfoil sections does not vary with M_∞ and at $M_\infty = 0.25$ the sectional lift coefficient is $c_l = 0.8$.
- Assume that the aspect ratio of the wing is sufficiently high so that three-dimensional effects such as the downwash, induced angle of attack, etc. can be ignored.

How much higher is the angle of attack α compared to the zero lift angle of attack $\alpha_{L=0}$ at $M_\infty = 0.25$. In other words, calculate $\alpha - \alpha_{L=0}$ at $M_\infty = 0.25$. Provide your answer in degrees with two digits of precision of the form $X.YeP$.

Determine the sectional lift coefficient c_l for $M_\infty = 0.5$. Provide your answer with two digits of precision of the form $X.YeP$.

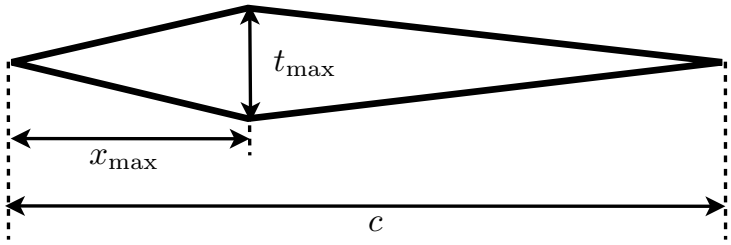
Calculate $\alpha - \alpha_{L=0}$ at $M_\infty = 0.5$. Provide your answer in degrees with two digits of precision of the form $X.YeP$.

edXsolution

Video Link

edXproblem: 12.7.3 Diamond airfoil performance

12.6



For all parts of this problem, use linearized supersonic potential flow theory.

Determine $x_{\max}/c$ for the diamond-type airfoil (shown in the figure) that produces the minimum drag coefficient. Enter your answer with two digits of precision (of the form 0.XY).

For $t_{\max}/c = 0.06$ and $M_\infty = 1.5$, what is the minimum drag coefficient due to just the thickness (do not include the drag contribution due to angle of attack). Use three digits of precision in the form X.YZeP

For the minimum drag diamond airfoil with $t_{\max}/c = 0.06$ and $M_\infty = 1.5$, and a lift coefficient of 0.2, what is the lift-to-drag ratio (L'/D')? Use three digits of precision (X.YZeP).

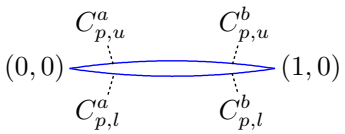
An aircraft is flying at a fixed altitude with the minimum drag diamond airfoil and $t_{\max}/c = 0.06$. Assume that the sectional lift (L') on the airfoil is fixed for any M_∞ and at $M_\infty = 1.5$ the sectional lift coefficient is 0.2. What is the lift-to-drag ratio when $M_\infty = 3$. Use three digits of precision (X.YZeP).

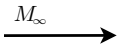
edXsolution

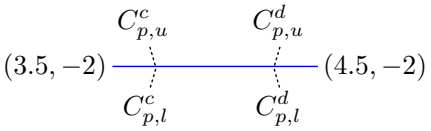
Video Link

edXproblem: 12.7.4 Interacting supersonic airfoils

12.6







For this problem, assume the following:

- The freestream Mach number is $M_\infty = \sqrt{5}$ and the flow is along the x-axis (i.e. $\alpha = 0$) as shown in the above figure.
- As shown in the figure, a symmetric airfoil (which we will call the *top airfoil*) has its leading edge at $(0,0)$ and trailing edge at $(1,0)$. The thickness distribution for this airfoil is,

$$t = 4t_{\max}\frac{x}{c}\left(1-\frac{x}{c}\right) \tag{12.101}$$

  with $t_{\max}/c = 0.075$.
- As shown in the figure, a flat plate airfoil (which we will call the *bottom airfoil*) has its leading edge at $(3.5,-2)$ and trailing edge at $(4.5,-2)$.
- Answer all of the questions in this problem using linearized supersonic potential flow theory.

Determine how the pressure coefficient behaves on the top airfoil at the locations shown. Specifically, $C^a_{p,l}$ and $C^b_{p,l}$ are the lower surface pressure coefficient values and $C^a_{p,u}$ and $C^b_{p,u}$ are the upper surface pressure coefficient values where $x_a = 0.25$ and $x_b = 0.75$. Select all of the correct answers.

Determine the drag coefficient for the top airfoil. Provide your answer with two digits of precision of the form $X.YeP$.

Determine the lift coefficient for the top airfoil. Provide your answer with two digits of precision of the form $X.YeP$.

Determine how the pressure coefficient behaves on the bottom airfoil at the locations shown. Specifically, $C^c_{p,l}$ and $C^d_{p,l}$ are the lower surface pressure coefficient values and $C^c_{p,u}$ and $C^d_{p,u}$ are the

upper surface pressure coefficient values where $x_c = 3.75$ and $x_d = 4.25$. Select all of the correct answers.

Determine the drag coefficient for the bottom airfoil. Provide your answer with two digits of precision of the form $X.YeP$.

Determine the lift coefficient for the bottom airfoil. Provide your answer with two digits of precision of the form $X.YeP$.

edXsolution

Video Link

Module 13

Incompressible Laminar Boundary Layers

13.1 Overview

13.1.1 Measurable outcomes

While we have discussed the importance of viscous effects in early modules, thus far we have not developed methods to analyze these effects either qualitatively or quantitatively. In this module, we now rectify that problem and consider viscous effects. Initially, we will focus on classical solutions to the Navier-Stokes equations which will form a foundation for the main event: boundary layers. In this module, we consider laminar boundary layers, and in the next module, we will extend these ideas to turbulent boundary layers.

Specifically, students successfully completing this module will be able to:

13.1. State the linear stress-strain rate relationship for a general compressible flow and its simplification for incompressible flow.

13.2. State the incompressible, constant viscosity form of the Navier-Stokes equations (including conservation of mass) and the no slip boundary condition at solid surfaces. Solve the incompressible Navier-Stokes equations for various classical (usually parallel) flows.

13.3. Explain the concept of a laminar boundary layer including the definition of the displacement thickness and the skin friction coefficient and the importance of the Reynolds number in determining the presence and behavior of a boundary layer.

13.4. Derive the laminar boundary layer equations by performing an order-of-magnitude scaling analysis on the incompressible Navier-Stokes equations.

13.5. Describe the balance of pressure force, viscous force, and momentum change that occurs in a laminar boundary layer. Apply the boundary layer equations to estimate the flow behavior in laminar boundary layers.

13.6. Apply the results of Blasius flat plate boundary layer theory to estimate the behavior of laminar boundary layers including the variation of the skin friction and boundary layer thickness with streamwise distance.

13.7. Explain how the boundary layer alters the streamlines of the outer inviscid flow and, using streamline curvature, describe the impact on the pressure distribution and drag (relative to purely inviscid flow).

13.8. Describe laminar boundary layer separation and the factors which contribute to it.

13.1.2 Pre-requisite material

The material in this module require the measurable outcomes from Modules 2.1 and 6.

13.2 The Navier-Stokes Equations

13.2.1 Stress tensor

13.1

In this section, we define the viscous stress tensor which is used to calculate the viscous stresses. Recall from Equation (6.59) that conservation of j-momentum is,

$$\rho \frac{\mathrm{D}u_j}{\mathrm{D}t} = -\frac{\partial p}{\partial x_j} + f_j^\tau \tag{13.1}$$

where f_j^τ is the net viscous force (in the j-direction) per unit volume acting on a fluid element and was defined in Equation (6.43) as,

$$\iiint_{\mathcal{V}} f_j^\tau \, \mathrm{d}\mathcal{V} = \iint_S \tau_j \, \mathrm{d}S \tag{13.2}$$

where $\mathcal{V}$ and S are the volume and surface of a fluid element.

Common practice in calculating f_j^τ is to use the viscous stress tensor, τ_{ij}. Figure 13.1 shows the convention used to define τ_{ij}. (Note that we will largely use only two dimensions in the figures and derivations for viscous flows. This is for simplicity, as the results all directly extend to three-dimensional flows.) Specifically, the definition of τ_{ij} is:

τ_{ij} is the viscous stress in the $\hat{e}_j$-direction acting on a surface with normal in the $\hat{e}_i$-direction.

Mathematically, we can write this definition of τ_{ij} as

$$\tau_{ij} \equiv \tau_j(\hat{e}_i) \tag{13.3}$$

As shown in the Figure 13.1, when the surface normal is in the positive i-direction, the stresses are defined by convention to be oriented in the positive j-directions. And, when the normal is in the negative i-direction, the stresses are in the negative j-directions. This switching of directions of τ_{ij} is required because the stress exerted on one face of a fluid element must be equal and opposite of the stress exerted on the fluid element sharing that face (applying Newton's Third Law).

Next, let's calculate the net viscous stress in the j-direction acting on the fluid element (again, only consider two-dimensional flows),

$$\begin{aligned}
\iint_S \tau_j \, \mathrm{d}S &= \mathrm{d}y \left[\tau_{1j}(x + \mathrm{d}x/2, y) - \tau_{1j}(x - \mathrm{d}x/2, y)\right] && (13.4)\\
&+ \mathrm{d}x \left[\tau_{2j}(x, y + \mathrm{d}y/2) - \tau_{2j}(x, y - \mathrm{d}y/2)\right] && (13.5)\\
&= \left(\frac{\partial \tau_{1j}}{\partial x} + \frac{\partial \tau_{2j}}{\partial y}\right) \mathrm{d}x \, \mathrm{d}y && (13.6)\\
\Rightarrow \lim_{\mathrm{d}x,\mathrm{d}y \to 0} \frac{1}{\mathrm{d}x\mathrm{d}y} \iint_S \tau_j \, \mathrm{d}S &= \frac{\partial \tau_{ij}}{\partial x_i} && (13.7)
\end{aligned}$$

where the derivation utilizes a Taylor series of τ_{ij} about (x, y). Then, substituting the result into Equation (13.2) gives,

$$f_j^\tau = \frac{\partial \tau_{ij}}{\partial x_i} \tag{13.8}$$

Finally, substitution into Equation (6.59) gives the conservation of j-momentum,

$$\rho \frac{\mathrm{D}u_j}{\mathrm{D}t} = -\frac{\partial p}{\partial x_j} + \frac{\partial \tau_{ij}}{\partial x_i} \tag{13.9}$$

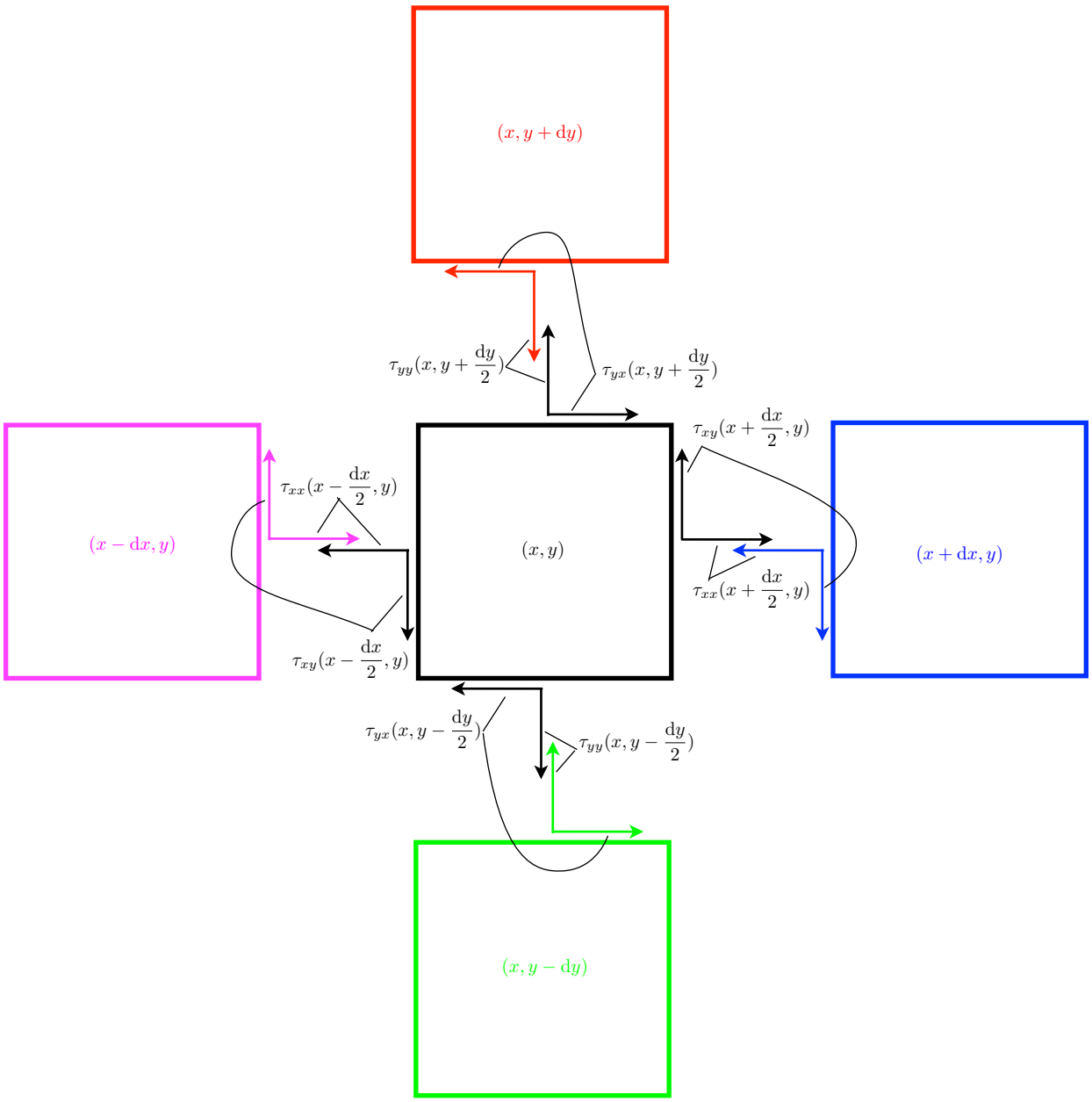


Figure 13.1: Viscous stress tensor τ_{ij} conventions

Another important fact about the viscous stress tensor is that it is symmetric, meaning that $\tau_{ij} = \tau_{ji}$. In the following video, we prove this relationship.

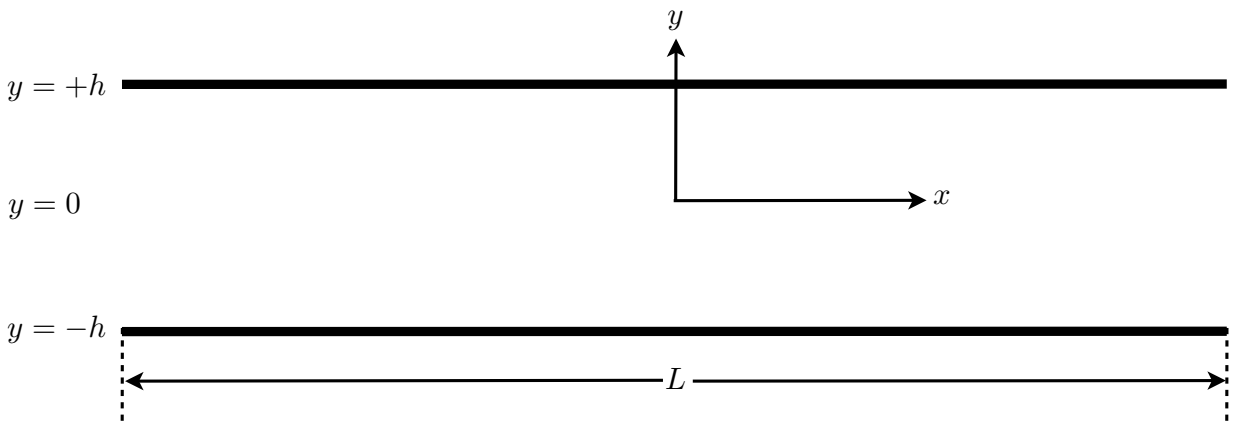
Video Link

As we close our introduction to the viscous stress tensor, we note that often the viscous stress must be calculated on a surface that does not align with the coordinate directions. Suppose the surface at a point had an outward pointing normal $\hat{n}$. Then, the viscous stress acting at that point is given by,

$$\tau_j(\hat{n}) = \tau_{ij}\hat{n}_i \tag{13.10}$$

edXproblem: 13.2.2 Stress acting on flow in channel

13.1



The two-dimensional flow in the channel shown above does not vary in x and has the following viscous stresses,

$$\tau_{xx} = 0 \qquad \tau_{xy} = \tau_{xy}(y) \qquad \tau_{yy} = 0 \tag{13.11}$$

Note: as we have in throughout the course, we will interchangeably use subscripts x, y, z and 1, 2, 3. So $\tau_{xy} = \tau_{12}$, etc.

What is the viscous force (per unit depth) in the x-direction acting on the wall? **Select all options that are correct.**

edXsolution

Video Link

13.2.3 Stress-strain rate relationship

13.1

The next step we take is to relate the stress tensor τ_{ij} to the strain rate tensor ϵ_{ij} for an incompressible flow. We begin by asking you to watch the following video in the NSF Fluid Mechanics Series. In this video, Professor Ascher Shapiro introduces the basic principles of viscosity and the relationship between stress and strain rate.

Video Link

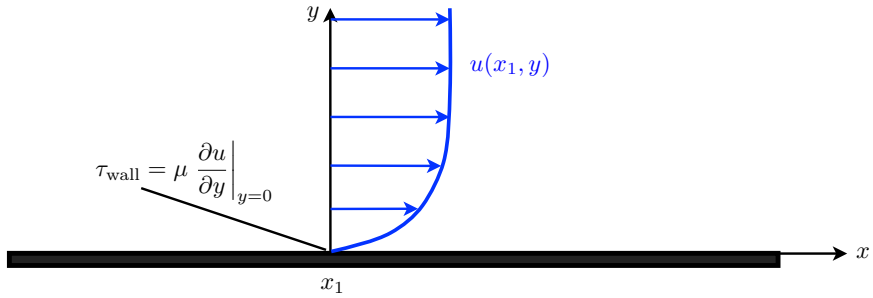


Figure 13.2: τ_{wall} for a straight wall

Now, let's start to get a little more specific. Consider the flow over a straight wall as shown in Figure 13.2. The stress acting on the wall due to the viscous stress in the flow is,

$$\tau_{\text{wall}} = \mu \left.\frac{\partial u}{\partial y}\right|_{y=0} \tag{13.12}$$

As derived in Equation (6.5), $\frac{\partial u}{\partial y}$ is the time rate of change of the shearing angle. Thus, as described by Professor Shapiro, the dynamic viscosity μ is the ratio of shear stress to the strain rate.

This result can be generalized to relate τ_{ij} to ϵ_{ij}. The key assumptions made in this generalization are that the fluid is isotropic. Isotropic behavior requires that the stress-strain rate relationship is unchanged by a rotation of the coordinate system. With this assumption (in addition to requiring the stress tensor to be dependent on linear combinations of the strain rate tensor), the following general form of the stress-strain rate relationship may be derived,

$$\tau_{ij} = 2\mu\epsilon_{ij} + \delta_{ij}\lambda\epsilon_{kk} \tag{13.13}$$

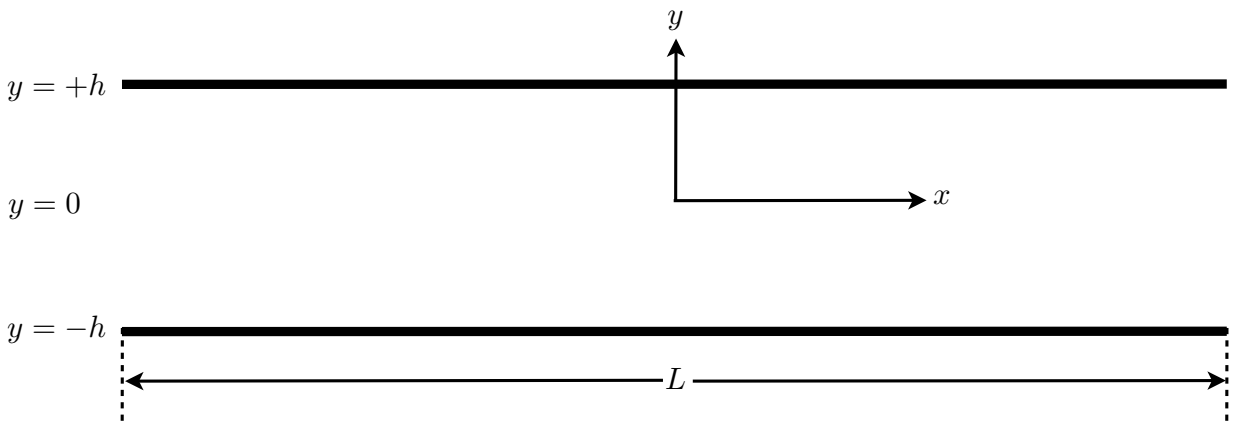
where δ_{ij} is the Kronecker delta which is equal to one when $i = j$ and equal to zero otherwise. λ is refered to as the bulk viscosity coefficient or the second coefficient of viscosity. This stress-strain rate model is known as a Newtonian fluid model and is a very accurate for air and gases in most conditions. Also, for liquids with simple molecular structures (like water), a Newtonian fluid model is very appropriate.

Noting that $\epsilon_{kk} = \partial u_k/\partial x_k = \nabla \cdot \mathbf{V}$, then we see that for an incompressible flow, the bulk viscosity term is zero (because of conservation of mass). Thus, for incompressible flow, the stress-strain rate relationship is,

$$\tau_{ij} = 2\mu\epsilon_{ij} \tag{13.14}$$

edXproblem: 13.2.4 Viscous stress and net viscous force for Couette and Poiseuille flow

13.1



In this problem, we revisit Couette and Poiseuille flows through channels with the walls located at $y = \pm h$. Both of these flows have velocity components in which $u = u(y)$ and $v = 0$. Specifically,

$$u_{\text{Couette}} = \frac{u_{\max}}{2}\left[1 + \frac{y}{h}\right] \tag{13.15}$$

$$u_{\text{Poiseuille}} = u_{\max}\left[1 - \left(\frac{y}{h}\right)^2\right] \tag{13.16}$$

We will define the Reynolds number for these flows as,

$$Re \equiv \frac{\rho u_{\max} h}{\mu} \tag{13.17}$$

where the flow is assumed incompressible with constant ρ and μ. Also, we will define a dynamic pressure based on the $u_{\max}$ as,

$$q_{\max} \equiv \frac{1}{2}\rho u_{\max}^2 \tag{13.18}$$

In the following problems, your answers can be expressed solely in terms of Re and y/h (not y or h independently, just the ratio y/h can appear). When entering your formula, please use R for Re and s for $s = y/h$. For example, if your answer was $Re/(y/h)^2$ you would enter R/s^2.

What is $\tau_{xy}/q_{\max}$ for Couette flow?

What is $f_x^\tau/(q_{\max}/h)$ for Couette flow?

What is $\tau_{xy}/q_{\max}$ for Poiseuille flow?

What is $f_x^\tau/(q_{\max}/h)$ for Poiseuille flow?

edXsolution

Video Link

13.2.5 Navier-Stokes equations for incompressible flow

13.1 13.2

For incompressible flows, we will also assume that the viscosity does not vary significantly. For gases and liquids, μ is largely a function of temperature, with little dependence on the pressure. Thus $\mu = \mu(T)$. We will assume that the variations in temperature result in small variations in μ. Including the temperature dependence of $\mu(T)$ does not change the qualitative behavior, but does significantly complicate the analysis. So, in this course, we will assume that μ is constant when analyzing viscous incompressible flows.

For the case of constant viscosity, the net viscous stress terms reduce significantly,

$$f_j^\tau = \frac{\partial \tau_{ij}}{\partial x_i} \tag{13.19}$$

$$= \mu \frac{\partial}{\partial x_i}\left(\frac{\partial u_j}{\partial x_i} + \frac{\partial u_i}{\partial x_j}\right) \tag{13.20}$$

$$= \mu \frac{\partial^2 u_j}{\partial x_i \partial x_i} + \mu \frac{\partial}{\partial x_i}\left(\frac{\partial u_i}{\partial x_j}\right) \tag{13.21}$$

$$= \mu \frac{\partial^2 u_j}{\partial x_i \partial x_i} + \mu \frac{\partial}{\partial x_j}\left(\frac{\partial u_i}{\partial x_i}\right) \tag{13.22}$$

$$= \mu \frac{\partial^2 u_j}{\partial x_i \partial x_i} \tag{13.23}$$

In the last step of this derivation, we use the fact that $\partial u_i / \partial x_i = 0$ for an incompressible flow. Thus, the momentum equation for incompressible, constant viscosity flow then becomes,

$$\rho \frac{\mathrm{D}u_j}{\mathrm{D}t} = -\frac{\partial p}{\partial x_j} + \mu \frac{\partial^2 u_j}{\partial x_i \partial x_i} \tag{13.24}$$

This is the incompressible form of the celebrated Navier-Stokes equation, named for Claude-Louis Navier and George Stokes. In addition, the incompressible form of the conservation of mass is also needed and, as we have seen many times now, is given by,

$$\frac{\partial u_i}{\partial x_i} = 0 \tag{13.25}$$

We could derive an energy equation for this incompressible, constant viscosity flow, however, it is not needed to solve for the velocity and pressure since the conservation of mass and momentum for this situation completely decouple from the internal energy. In other words, Equations (13.25) and (13.24) do not contain the internal energy (or related quantities such as the temperature). Said another way, for a d dimensional problem, we have $d+1$ unknown variables: the pressure and d velocity components. And, we have $d+1$ equations: the conservation of mass and d conservation of momentum components.

For viscous flows, we also modify the boundary condition at solid surfaces to require that the flow and the surface have the same velocity. This is known as the *no slip* condition. In other words, the flow velocity cannot *slip* relative to the surface. For a stationary surface, which is largely what we will focus on, the no slip condition reduces to all velocity components being zero. Thus, $\mathbf{V} = 0$ on stationary surfaces. Recall that we have discussed the molecular nature of this no-slip condition at the end of the video in Section 3.2.6 showing that for surfaces which are rough at a molecular scale, the random motion of gas molecules implies that the average velocity is zero in the vicinity of the surface.

13.2.6 Solution of two-dimensional Poisseuille flow

13.2

In the following video, we solve the incompressible Navier-Stokes equations for the parallel flow through a channel with walls at $y = \pm h$. We have already considered this flow several times throughout the course, however, in this video, we finally solve for the velocity field (as opposed to simply stating the result). I hope that you find it was worth the wait!

Video Link

13.3 Laminar Boundary Layers

13.3.1 Introduction to boundary layers

13.3 13.8

We will again return to the NSF Fluid Mechanics Series for an introduction to boundary layers. You'll find some nice flow visualization and a lot of useful terms (adverse and favorable pressure gradients, separation, laminar and turbulent boundary layers). The material on turbulent boundary layers we will not use until the next module.

Video Link

13.3.2 Order-of-magnitude scaling analysis: Introduction

13.3 13.4

We have seen in our study of potential flows that pressure distributions on airfoils and wings can often be reasonably predicted, even though viscous effects have been neglected. However, even when the pressure distributions are reasonably predicted from inviscid models, the viscous effects must be accounted for in estimating the drag. Further, viscous effects can, in fact, significantly modify pressure distributions from inviscid flow theory predictions. In particular, as boundary layers thicken and, in the extreme situation, when separation occurs, the pressure distributions observed on airfoils can deviate significantly from inviscid models.

In this section, we will begin our consideration of viscous effects in high Reynolds number flows. As previously described in Section 2.4.6, at high Reynolds numbers, boundary layers form near the surface of a body. In the boundary layer, the flow rapidly varies from near freestream velocities at the edge of the boundary layer to zero velocity at the wall. Fluid acceleration, pressure forces, and viscous forces play an equally important role in the evolution of the flow. To better understand how these three terms balance in the boundary layer, we will use a scaling analysis of the incompressible Navier-Stokes equations.

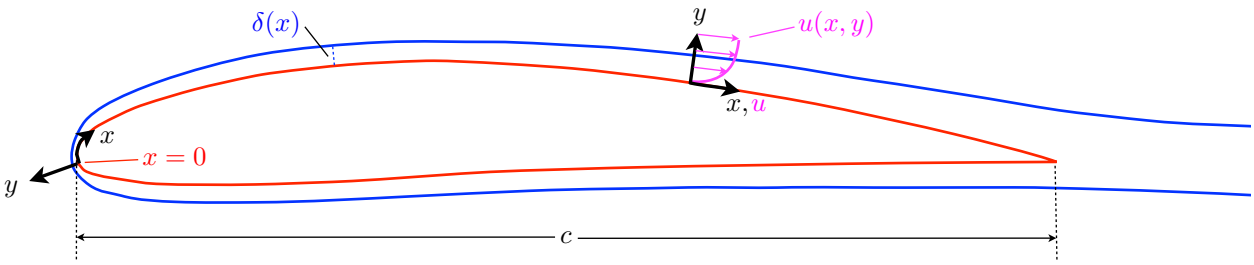


Figure 13.3: Boundary layer coordinate system

As shown in Figure 13.3, the (x, y) coordinate system for boundary layer analysis is wrapped around the surface with x being tangential to the surface and y being normal to the surface. Thus, the boundary layer coordinate system is curved. We place $x = 0$ at the location of the stagnation point at the leading edge. Further, we will assume that,

- $\delta/c \ll 1$ as $Re \to \infty$
- $\delta/R \ll 1$ as $Re \to \infty$

Though we do not prove this, the second assumption allows the governing equations in this curved coordinate system to be written unchanged from the usual equations for an (x, y) coordinate system

without curvature. Specifically, the governing equations for incompressible, steady, two-dimensional flow in this curved coordinate system are,

$$\frac{\partial u}{\partial x} + \frac{\partial v}{\partial y} = 0 \tag{13.26}$$

$$\rho u \frac{\partial u}{\partial x} + \rho v \frac{\partial u}{\partial y} = -\frac{\partial p}{\partial x} + \mu \frac{\partial^2 u}{\partial x^2} + \mu \frac{\partial^2 u}{\partial y^2} \tag{13.27}$$

$$\rho u \frac{\partial v}{\partial x} + \rho v \frac{\partial v}{\partial y} = -\frac{\partial p}{\partial y} + \mu \frac{\partial^2 v}{\partial x^2} + \mu \frac{\partial^2 v}{\partial y^2} \tag{13.28}$$

Note that if δ/R is not small, then the y-momentum equation must be modified to include the streamline curvature term $\rho V^2/R$.

Next, we non-dimensionalize these equations using the following non-dimensional variables,

$$x^* \equiv \frac{x}{c} \qquad y^* \equiv \frac{y}{c} \qquad u^* \equiv \frac{u}{V_\infty} \qquad v^* \equiv \frac{v}{V_\infty} \tag{13.29}$$

Substitution of these definitions into Equations (13.26)-(13.28) produces,

$$\frac{\partial u^*}{\partial x^*} + \frac{\partial v^*}{\partial y^*} = 0 \tag{13.30}$$

$$u^* \frac{\partial u^*}{\partial x^*} + v^* \frac{\partial u^*}{\partial y^*} = -\frac{1}{\rho V_\infty^2} \frac{\partial p}{\partial x^*} + \frac{1}{Re} \frac{\partial^2 u^*}{\partial x^{*2}} + \frac{1}{Re} \frac{\partial^2 u^*}{\partial y^{*2}} \tag{13.31}$$

$$u^* \frac{\partial v^*}{\partial x^*} + v^* \frac{\partial v^*}{\partial y^*} = -\frac{1}{\rho V_\infty^2} \frac{\partial p}{\partial y^*} + \frac{1}{Re} \frac{\partial^2 v^*}{\partial x^{*2}} + \frac{1}{Re} \frac{\partial^2 v^*}{\partial y^{*2}} \tag{13.32}$$

We see from these non-dimensional equations that by defining,

$$p^* \equiv \frac{p}{\rho V_\infty^2} \tag{13.33}$$

then the non-dimensional incompressible two-dimensional governing equations are,

$$\frac{\partial u^*}{\partial x^*} + \frac{\partial v^*}{\partial y^*} = 0 \tag{13.34}$$

$$u^* \frac{\partial u^*}{\partial x^*} + v^* \frac{\partial u^*}{\partial y^*} = -\frac{\partial p^*}{\partial x^*} + \frac{1}{Re} \frac{\partial^2 u^*}{\partial x^{*2}} + \frac{1}{Re} \frac{\partial^2 u^*}{\partial y^{*2}} \tag{13.35}$$

$$u^* \frac{\partial v^*}{\partial x^*} + v^* \frac{\partial v^*}{\partial y^*} = -\frac{\partial p^*}{\partial y^*} + \frac{1}{Re} \frac{\partial^2 v^*}{\partial x^{*2}} + \frac{1}{Re} \frac{\partial^2 v^*}{\partial y^{*2}} \tag{13.36}$$

A simplistic analysis of these equations would suggest that as $Re \to \infty$ then the viscous effects could be neglected. This leads to the inviscid equations and the potential flow models we have been studying. However, this conclusion neglects that fact that as Re increases, so does the magnitude of $\partial^2 u^*/\partial y^{*2}$ near the wall. As a result, the viscous terms cannot be entirely neglected in the high Reynolds number limit.

We now perform an order-of-magnitude scaling analysis on the incompressible Navier-Stokes equations. Our goal is to develop a model for the flow in the boundary layer which is less complex than the two-dimensional incompressible Navier-Stokes equations. And, by applying this model, we hope to gain insight into the fundamental physics at work in boundary layer flows.

We begin by considering the spatial length scales in the boundary layer flow shown in Figure 13.3. Two length scales are apparent:

- c, the chord of the airfoil

- $\delta(x)$, the thickness of the boundary layer

We expect that the airfoil chord will control the spatial variations in the x direction. In particular, we expect that the x-derivatives of the flow variables will scale with $1/c$. Mathematically, we write this as,

$$\frac{\partial}{\partial x} \sim \frac{1}{c} \tag{13.37}$$

Here is another way to think about this scaling idea. Consider the boundary layer problem with dimensional inputs, if we increase c by say a factor of two but keep everything else constant (ρ, μ, V_∞, airfoil shape), then our scaling assumption says that the x-derivatives in the flow will decrease by a factor of two.

In the y-direction, we expect the flow will vary over a distance of the boundary layer thickness, δ. For example, we know that at the wall that $\mathbf{V}(x, y = 0) = 0$ (no slip condition) but just outside of the boundary layer the velocity will be (approximately) $\mathbf{V}(x, \delta) \approx \mathbf{V}_\infty$. Thus,

$$\frac{\partial}{\partial y} \sim \frac{1}{\delta} \tag{13.38}$$

Similar to the length scales, we can set scales for other quantities. In particular, for the x-velocity, we will assume that the freestream velocity is an appropriate scale. Thus,

$$u \sim V_\infty \tag{13.39}$$

To make our scaling assumptions a bit more precise, we will introduce the following order-of-magnitude notation in the limit as $Re \to \infty$. Specifically, consider two functions, $f(Re)$ and $g(Re)$. These functions have the same order of magnitude,

$$f(Re) = O\left(g(Re)\right) \text{ as } Re \to \infty \tag{13.40}$$

if finite constants C and Re_0 exist such that,

$$|f(Re)| \leq C\,|g(Re)| \text{ for all } Re \geq Re_0 \tag{13.41}$$

Based on our previous scaling assumptions for x and u, we make the following order of magnitude assumption,

$$\frac{\partial(u/V_\infty)}{\partial(x/c)} = \frac{\partial u^*}{\partial x^*} = O(1) \tag{13.42}$$

Similarly, based on our previous scaling assumptions for y and u, we make the following order of magnitude assumption,

$$\frac{\partial(u/V_\infty)}{\partial(y/\delta)} = \frac{\delta}{c}\frac{\partial u^*}{\partial y^*} = O(1) \tag{13.43}$$

This last result can be re-arranged to show that,

$$\frac{\partial u^*}{\partial y^*} = O\left(\frac{c}{\delta}\right) \tag{13.44}$$

Thus, based on our assumptions, we see that as the boundary layer thickness decreases (relative to the chord), the magnitude of $\partial u^*/\partial y^*$ increases.

13.3.3 Order-of-magnitude scaling analysis: Conservation of mass

13.3 13.4

Next, we consider the order of magnitude of the terms in the conservation of mass. Clearly, the two terms in Equation (13.34) are the same order-of-magnitude since they sum to zero,

$$\Rightarrow \frac{\partial v^*}{\partial y^*} = O\left(\frac{\partial u^*}{\partial x^*}\right) = O(1) \tag{13.45}$$

We can then manipulate this result to determine the order-of-magnitude scaling for v^*:

$$\frac{\partial v^*}{\partial y^*} = \frac{c}{\delta}\frac{\partial v^*}{\partial (y/\delta)} \tag{13.46}$$

$$\frac{\partial v^*}{\partial (y/\delta)} = O\left(\frac{\delta}{c}\right) \tag{13.47}$$

$$\Rightarrow \frac{v}{V_\infty} = O\left(\frac{\delta}{c}\right) \tag{13.48}$$

The final result is true since at the wall, $v = 0$ and therefore a Taylor series analysis at the wall produces,

$$\frac{v}{V_\infty}\left(\frac{y}{\delta}\right) = O\left(\frac{y}{\delta}\frac{\delta}{c}\right) = O\left(\frac{\delta}{c}\right) \tag{13.49}$$

where the last step is true because in the boundary layer, $y/\delta = O(1)$. Thus, we see that the normal velocity is the same order as the boundary layer thickness (and therefore $v/V_\infty \ll 1$).

13.3.4 Order-of-magnitude scaling analysis: Conservation of x-momentum

13.3 13.4 13.5

Now we turn our attention to the x-momentum given by Equation (13.35). From our previous order-of-magnitude results, we see that,

$$u^*\frac{\partial u^*}{\partial x^*} = O(1) \text{ and } v^*\frac{\partial u^*}{\partial y^*} = O(1) \tag{13.50}$$

The pressure term, $\partial p^*/\partial x$, can also be assumed to be $O(1)$ since at the outer edge of the boundary layer, where viscous effects will be neglible, the pressure and acceleration terms must balance. This leaves the second-derivative terms arising from the viscous stress contributions. We will assume (x/c)-derivatives and (y/δ)-derivatives do not have any Reynolds number dependence, thus,

$$\frac{\partial^2 u^*}{\partial x^{*2}} = O(1) \text{ and } \frac{\partial^2 u^*}{\partial (y/\delta)^2} = O(1) \tag{13.51}$$

The (y/δ) derivative order-of-magnitude scaling can be re-arranged to give,

$$\frac{\partial^2 u^*}{\partial (y/\delta)^2} = \left(\frac{\delta}{c}\right)^2 \frac{\partial^2 u^*}{\partial y^{*2}} \tag{13.52}$$

$$\Rightarrow \frac{\partial^2 u^*}{\partial y^{*2}} = O\left((c/\delta)^2\right) \tag{13.53}$$

Thus, the two viscous terms have the following scaling,

$$\frac{1}{Re}\frac{\partial^2 u^*}{\partial x^{*2}} = O\left(Re^{-1}\right) \text{ and } \frac{1}{Re}\frac{\partial^2 u^*}{\partial y^{*2}} = O\left(Re^{-1}\,(c/\delta)^2\right) \tag{13.54}$$

This shows that, as $Re \to \infty$, the x-derivative term in the viscous stress is negligible compared to all of the other terms in the x-momentum equation. Further, since in the boundary layer we must have some viscous effect that is not negligible, we will require that y-derivative viscous stress term must have the same order as the other terms in the momentum equation. Since these other terms are $O(1)$, this means that,

$$Re^{-1} (c/\delta)^2 = O(1) \tag{13.55}$$

$$\Rightarrow \frac{\delta}{c} = O\left(\frac{1}{\sqrt{Re}}\right) \tag{13.56}$$

This is a classic result in laminar boundary layer theory. It is quite general and says that the thickness of a boundary layer relative to the chord is expected to scale with $Re^{-1/2}$ for increasing Reynolds number.

edXproblem: 13.3.5 Boundary layer thickness dependence on chord length

13.4

Consider two thin airfoils that have the same shape except that the chord of airfoil A is twice the chord of airfoil B, specifically, $c_A = 2c_B$. Let the boundary layer at the trailing edge of the airfoils be δ_A and δ_B. Assuming laminar incompressible flow, which is most likely true when the airfoils have the same freestream conditions?

edXsolution

Video Link

13.3.6 Order-of-magnitude scaling analysis: Conservation of y-momentum

13.3 13.4 13.5

Now we turn our attention to the y-momentum given by Equation (13.36). Recall from Equation (13.48) that $v^* = O(\delta/c)$. Then, using the result that $\delta/c = O(Re^{-1/2})$, gives

$$v^* = O\left(Re^{-\frac{1}{2}}\right) \tag{13.57}$$

Except for the pressure gradient, the terms of the y-momentum equation have the following order-of-magnitude,

$$u^*\frac{\partial v^*}{\partial x^*} = O\left(Re^{-\frac{1}{2}}\right) \qquad v^*\frac{\partial v^*}{\partial y^*} = O\left(Re^{-\frac{1}{2}}\right) \tag{13.58}$$

$$\frac{1}{Re}\frac{\partial^2 v^*}{\partial x^{*2}} = O\left(Re^{-\frac{3}{2}}\right) \qquad \frac{1}{Re}\frac{\partial^2 v^*}{\partial y^{*2}} = O\left(Re^{-\frac{1}{2}}\right) \tag{13.59}$$

Since all of these terms are negligible at $Re \to \infty$, this implies that the pressure gradient in y must also be negligible in the boundary layer.

$$\frac{\partial p^*}{\partial y^*} \approx 0 \tag{13.60}$$

As a result, the pressure in the boundary layer is only a function of x. Therefore, the pressure in boundary layer analysis is often refered to as the edge pressure and given the notation $p_e(x)$.

13.3.7 Boundary layer equations

13.3 13.4 13.5

In this section, we summarize the two-dimensional, incompressible laminar boundary layer equations. Specifically, the boundary layer equations are,

$$\frac{\partial u}{\partial x} + \frac{\partial v}{\partial y} = 0 \tag{13.61}$$

$$\rho u\frac{\partial u}{\partial x} + \rho v\frac{\partial u}{\partial y} = -\frac{\mathrm{d}p_e}{\mathrm{d}x} + \mu\frac{\partial^2 u}{\partial y^2} \tag{13.62}$$

$$p(x,y) = p_e(x) \tag{13.63}$$

Another manipulation that is frequently applied is to relate the edge pressure to the velocity at the edge of the boundary layer using Bernoulli equation. This is permissible because outside of the boundary layer, the flow is assumed to be inviscid. Thus, Bernoulli equation gives,

$$p_e + \frac{1}{2}\rho V_e^2 = \text{constant} \tag{13.64}$$

This can be simplified a bit further since the normal velocity $v/V_\infty = O(1/\sqrt{Re})$ is much smaller than the tangential velocity $u/V_\infty = O(1)$. Thus,

$$\lim_{Re\to\infty} V_e^2 = \lim_{Re\to\infty} u_e^2 + v_e^2 = u_e^2 \tag{13.65}$$

Thus, Bernoulli's equation applied at the edge of the boundary layer is,

$$p_e + \frac{1}{2}\rho u_e^2 = \text{constant} \tag{13.66}$$

Differentiating with respect to x gives,

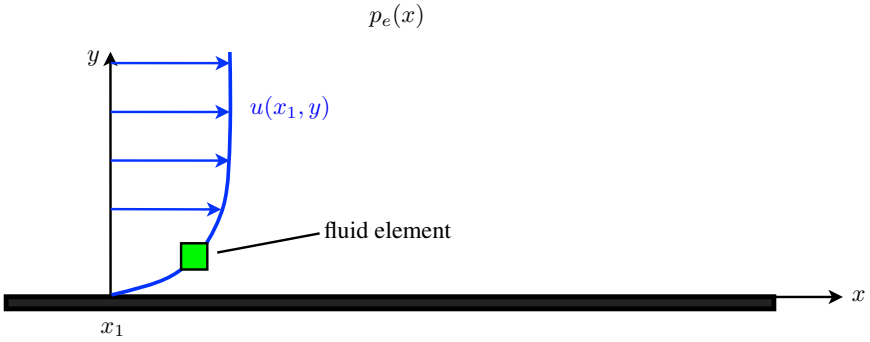
$$\frac{\mathrm{d}p_e}{\mathrm{d}x} = -\rho u_e \frac{\mathrm{d}u_e}{\mathrm{d}x} \tag{13.67}$$

Thus, an equivalent form of the boundary layer x-momentum equation is,

$$u\frac{\partial u}{\partial x} + v\frac{\partial u}{\partial y} = u_e \frac{\mathrm{d}u_e}{\mathrm{d}x} + \nu\frac{\partial^2 u}{\partial y^2} \tag{13.68}$$

edXproblem: 13.3.8 Forces on a fluid element in a boundary layer

13.5



Consider the fluid element and velocity distribution shown in the figure. Assume the flow is steady and well-modeled by the incompressible (and constant viscosity) boundary layer equations. In the following questions, you are asked to select **all of the options that are possible** for the x-velocity of the fluid element immediately after the instant shown.

If the edge pressure is constant with respect to x, it is possible for the x-velocity of the fluid element (immediately after the instant shown) to:

If the edge pressure is increasing with x, it is possible for the x-velocity of the fluid element (immediately after the instant shown) to:

If the edge pressure is decreasing with x, it is possible for the x-velocity of the fluid element (immediately after the instant shown) to:

edXsolution

Video Link

13.3.9 Blasius flat plate boundary layer solution

13.6 | 13.3 | 2.9

The boundary flow over a flat plate (at zero angle of attack) was theoretically studied by Blasius, a doctoral student of Prandtl, in 1908. For the flat plate analysis, we assume that the boundary layer is thin enough so that the edge pressure can be well-approximated as a constant. That is,

$$p_e(x) = p_\infty \tag{13.69}$$

The boundary layer equations for the flat plate case therefore have the following form,

$$\frac{\partial u}{\partial x} + \frac{\partial v}{\partial y} = 0 \tag{13.70}$$

$$u\frac{\partial u}{\partial x} + v\frac{\partial u}{\partial y} = \nu\frac{\partial^2 u}{\partial y^2} \tag{13.71}$$

where ν is the kinematic viscosity, $\nu = \mu/\rho$. These two equations can be reduced to a single equation by defining the velocity components as derivatives of a streamfunction ψ,

$$u = \frac{\partial \psi}{\partial y} \qquad v = -\frac{\partial \psi}{\partial x} \tag{13.72}$$

Substitution of Equation (13.72) into the conservation of mass shows that it is identically satisfied,

$$\frac{\partial u}{\partial x} + \frac{\partial v}{\partial y} = \frac{\partial}{\partial x}\left(\frac{\partial \psi}{\partial y}\right) + \frac{\partial}{\partial y}\left(-\frac{\partial \psi}{\partial x}\right) = 0 \tag{13.73}$$

And, the x-momentum equation is then given by,

$$\frac{\partial \psi}{\partial y}\frac{\partial^2 \psi}{\partial x \partial y} - \frac{\partial \psi}{\partial x}\frac{\partial^2 \psi}{\partial y^2} = \nu\frac{\partial^3 \psi}{\partial y^3} \tag{13.74}$$

Thus, we have reduced the boundary layer equations down to a single partial differential equation for ψ.

This equation can even be further reduced by transforming from (x, y) to (x, η) where,

$$\eta \equiv y\sqrt{\frac{V_\infty}{\nu x}} \tag{13.75}$$

and making the following substitution for ψ,

$$\psi = \sqrt{\nu x V_\infty} f(\eta) \tag{13.76}$$

where $f(\eta)$ is the unknown function, and is only a function of η. The velocity components are given by,

$$\frac{u}{V_\infty} = f' \tag{13.77}$$

$$\frac{v}{V_\infty} = \frac{1}{2}\sqrt{\frac{\nu}{V_\infty x}}\left(\eta f' - f\right) \tag{13.78}$$

where $()'$ denotes differentiation with respect to η. After a lot of algebra, Equation (13.74) can be reduced to,

$$2f''' + ff'' = 0 \tag{13.79}$$

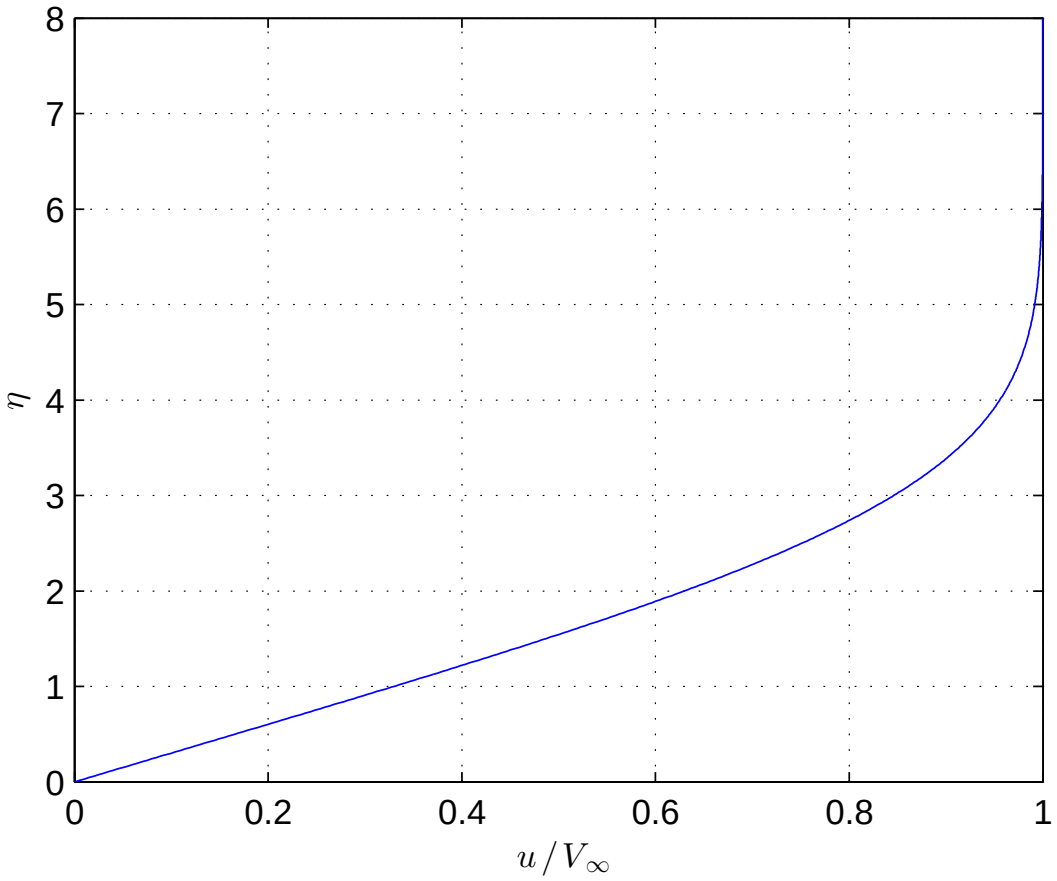


Figure 13.4: u/V_∞ distribution for Blasius flat plate laminar boundary solution

.

which is an ordinary though still nonlinear differential equation. Because of nonlinearity, the Blasius equation does not have a closed-form analytic solution and must be solved numerical. More importantly, we see that the u velocity profile will be solely a function of η. The profile is plotted in Figure 13.4.

A common measure of the thickness of the boundary layer is the y location at which the velocity in the boundary layer reach 99% of the freestream value. We will simply use the symbol δ for this 99% thickness. For the flat plate boundary layer, we can first find the value of η at which $u/V_\infty = 0.99$. This occurs at $\eta \approx 4.91$. Thus,

$$\delta\sqrt{\frac{V_\infty}{\nu x}} = 4.91 \tag{13.80}$$

$$\delta = 4.91\sqrt{\frac{\nu x}{V_\infty}} \tag{13.81}$$

A very common parameter used throughout boundary layer theory is the Reynolds number based on distance from the leading edge which is defined as,

$$Re_x \equiv \frac{V_\infty x}{\nu} \tag{13.82}$$

Using Re_x, the Blasius result for δ can be written,

$$\delta = 4.91\frac{x}{\sqrt{Re_x}} \tag{13.83}$$

Recall from Equation (2.32) that the wall stress τ_{wall} is typically reported in a non-dimensional form as the skin friction coefficient, C_{f} defined as,

$$C_{\text{f}} \equiv \frac{\tau_{\text{wall}}}{\frac{1}{2}\rho_\infty V_\infty^2} \tag{13.84}$$

For the specific case of the Blasius flat plate boundary layer, C_{f} is,

$$C_{\text{f}} = \frac{0.664}{\sqrt{Re_x}} \tag{13.85}$$

Finally, we consider the drag coefficient on a flat plate (at zero angle of attack) in an incompressible flow. The drag for the flat plate is can be found by integrating the wall stress,

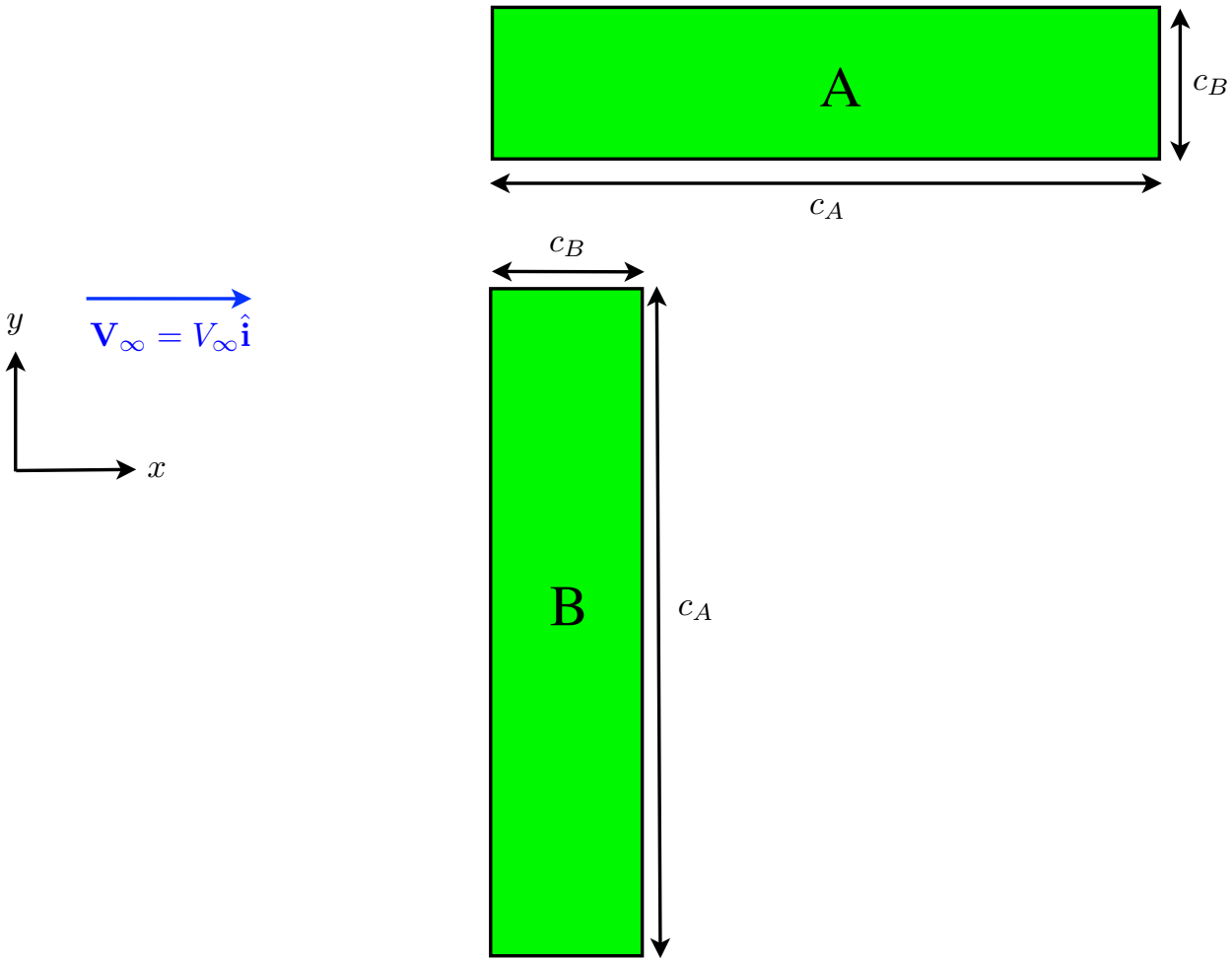
$$D' = 2\int_0^c \tau_{\text{wall}}\,\mathrm{d}x \tag{13.86}$$

where the factor of 2 is to account for both the upper and lower surfaces of the plate. The drag coefficient is then,

$$\begin{aligned}
c_d &= \frac{D'}{q_\infty c} && (13.87)\\
&= 2\int_0^1 C_{\text{f}}\,\mathrm{d}(x/c) && (13.88)\\
&= 1.328\int_0^1 \sqrt{\frac{\nu}{V_\infty x}}\,\mathrm{d}(x/c) && (13.89)\\
&= 1.328\int_0^1 \sqrt{\frac{\nu}{V_\infty c}}\sqrt{\frac{c}{x}}\,\mathrm{d}(x/c) && (13.90)\\
&= \frac{1.328}{\sqrt{Re}}\int_0^1 \sqrt{\frac{c}{x}}\,\mathrm{d}(x/c) && (13.91)\\
\Rightarrow c_d &= \frac{2.656}{\sqrt{Re}} && (13.92)
\end{aligned}$$

edXproblem: 13.3.10 Dependence of laminar flow drag on planform orientation

13.6



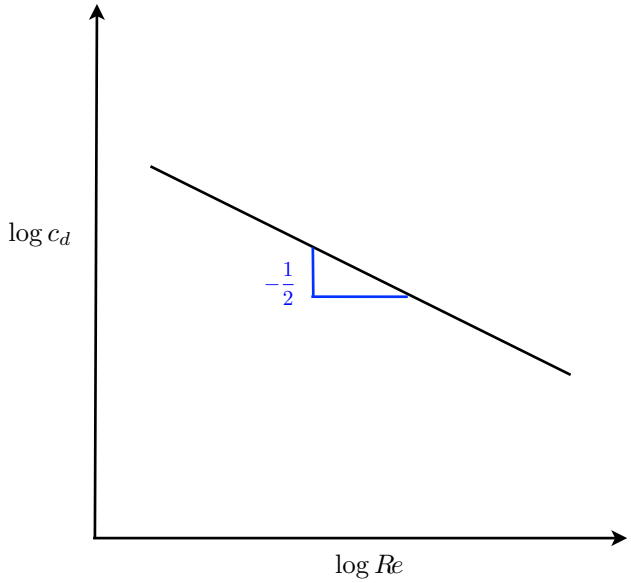
Consider a flat plate with dimensions $c_A \times c_B$ (with infinitesimal thickness in the z-direction). Assuming incompressible laminar boundary layer flow with density ρ_∞ and viscosity μ_∞, determine how the drag in the two planform orientations compare to each other. (Note: assume that the freestream velocity is non-zero, so D_A and D_B will be non-zero). **Select as many options as are possible.**

edXsolution

Video Link

edXproblem: 13.3.11 Dependence of laminar flow drag on velocity

13.6



An airfoil has the $c_d(Re)$ behavior shown above. Let D_1' be the drag on the airfoil in a freestream with velocity V_∞. Let D_2' be the drag on the airfoil in a freestream with velocity $2V_\infty$. Assume the density and the viscosity do not change with the freestream velocities. Which of the following is true:

edXsolution

Video Link

13.4 Form Drag and Separation

13.4.1 Displacement thickness and effective body

13.3 13.7

In our previous study of potential flows, we developed methods (panel methods and thin airfoil theory in particular) to estimate the pressure distributions around airfoils. Since these models are purely inviscid, they completely ignored the presence of the boundary layer. Although we can often model the flow outside of the boundary layer as being inviscid, this outer inviscid flow is in fact modified by the presence of the boundary layer. In particular, the boundary layer causes the streamlines to be displaced away from the body relative to a purely inviscid flow model.

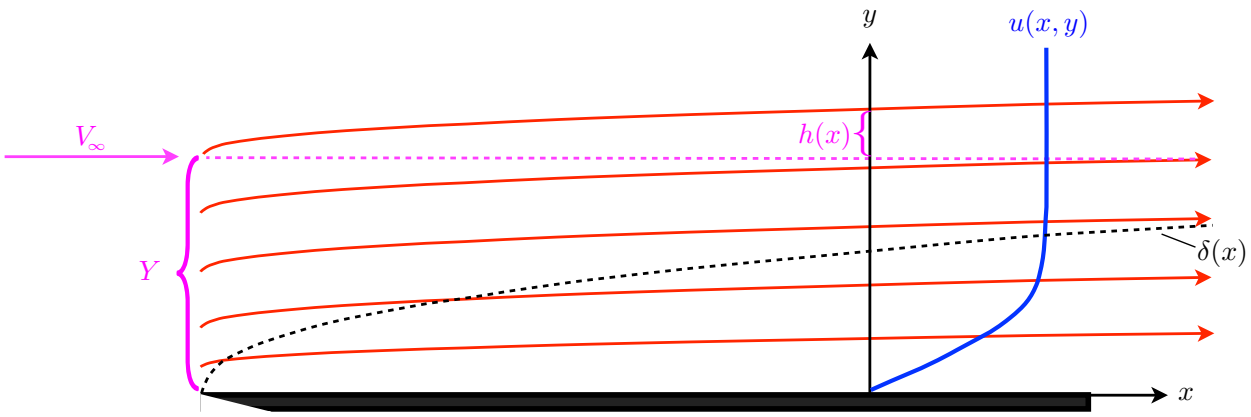


Figure 13.5: Streamlines for flat plate boundary flow showing the displacement $h(x)$ of a streamline that is a height Y above the plate at the leading edge.

Consider the boundary flow over a flat plate. The streamlines for this flow are sketched in Figure 13.5. As shown in the sketch, a streamline that is a height Y above the plate at the leading edge is displaced a distance $h(x)$ due to the growth of the boundary layer. A purely inviscid flow would remain a distance Y above the plate, since $\mathbf{V}(x, y) = V_\infty \hat{\mathbf{i}}$ everywhere.

The displacement of the streamlines due to the boundary layer could be modeled in an inviscid flow by determining an effective body shape that would produce the same streamlines as the viscous flow. This concept is illustrated in Figure 13.6. $\delta^*(x)$ is known as the *displacement thickness* and is the distance the actual body surface needs to be displaced so that the streamlines of the inviscid flow around this *effective body* are the same as the viscous flow around the actual body. To determine this displacement thickness, we apply conservation of mass so that the inviscid flow has the same amount of mass as the boundary layer flow. Specifically,

$$\rho u_e (Y - \delta^*) = \rho \int_0^Y u \, \mathrm{d}y \tag{13.93}$$

$$u_e \delta^* = \int_0^Y (u_e - u) \, \mathrm{d}y \tag{13.94}$$

$$\Rightarrow \delta^* = \int_0^Y \left(1 - \frac{u}{u_e}\right) \mathrm{d}y \tag{13.95}$$

The specific distance Y used in this definition does not need to be precisely defined as long as it is at least δ. Since for $y > \delta$, the velocity $u(x, y) \approx u_e(x)$ and therefore the contribution to the integral will negligible.

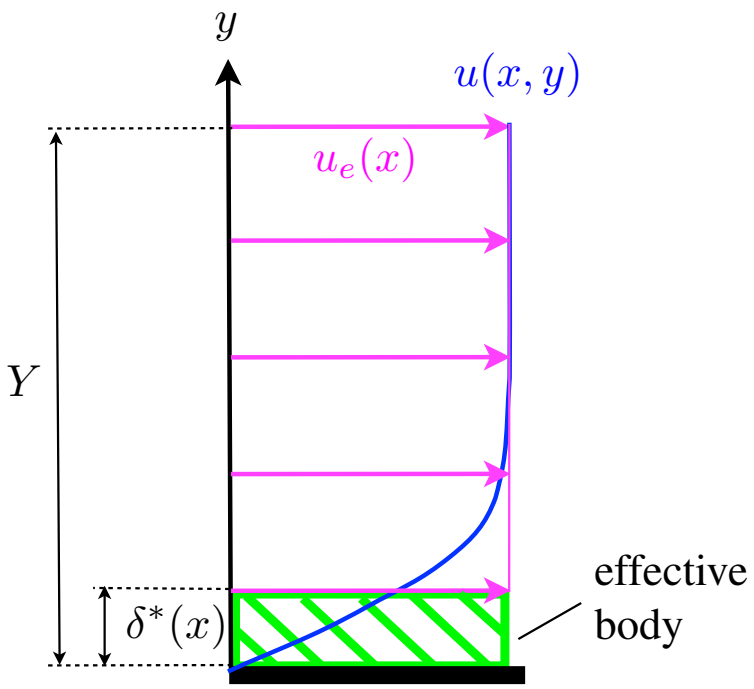


Figure 13.6: Displacement thickness and effective body

For the Blasius laminar flat plate, the displacement thickness is,

$$\delta^* = 1.72\frac{x}{\sqrt{Re_x}} \tag{13.96}$$

13.4.2 Form drag

13.3 13.7

The displacement effect of the boundary layer modifies the pressure from a purely inviscid flow around the (actual) body. As a result, the pressure forces acting on an airfoil will produce a finite drag. This source of drag is commonly refered to as *form drag*.

The form drag will generally be larger when δ^* is larger. Thus, from the Blasius result, we expect δ^* to be larger for lower Reynolds numbers since $\delta^* \propto 1/\sqrt{Re_x}$. The Table shows the drag coefficient data for NACA 0006 and NACA 0012 airfoils at $\alpha = 0$ and $Re = 10^3$ and 10^4. The Reynolds number trends clearly show that the form drag decreases with increasing Reynolds number. The friction drag data also shows the expected decrease with Reynolds number. In particular, the flat plate c_{df} values (taken from Equation 13.92) are shown to be good approximations to the c_{df} for the NACA airfoils. Note that there is no form drag for a flat plate since the surface of the flat plate only has normals in the y-direction and thus the pressure stresses only act in the y-direction.

Figure 13.7 shows the c_p distributions and the effective shape of the body. The effective shape (which is drawn as the airfoil shape with the displacement thickness δ^* added normal to the shape) is clearly seen to be closer to the actual shape for the higher Reynolds number. As a result, the c_p distributions for the viscous flow more closely approximates the inviscid flow c_p (shown in the dashed line of the plots) and, therefore, the form drag also decreases.

Though somewhat difficult to discern from Figure 13.7, note that the displacement thickness for the NACA 0012 airfoil is larger than that of the NACA 0006 airfoil on the downstream half ($0.5 < x/c < 1$) of the airfoils. This can be explained as follows. The NACA 0012 airfoil generates a lower

Airfoil	Re_∞	c_{df}	$c_{d\text{form}}$	c_d
flat plate	1×10^3	0.0840	0	0.0840
flat plate	1×10^4	0.0266	0	0.0266
NACA 0006	1×10^3	0.0892	0.0166	0.1058
NACA 0006	1×10^4	0.0257	0.0059	0.0316
NACA 0012	1×10^3	0.0833	0.0346	0.1179
NACA 0012	1×10^4	0.0232	0.0162	0.0395

Table 1: Drag coefficient due to friction (c_{df}), form drag ($c_{d\text{form}}$) and total drag (c_d) for flat plate (Blasius solution), NACA 0006, and NACA 0012 at $\alpha = 0$

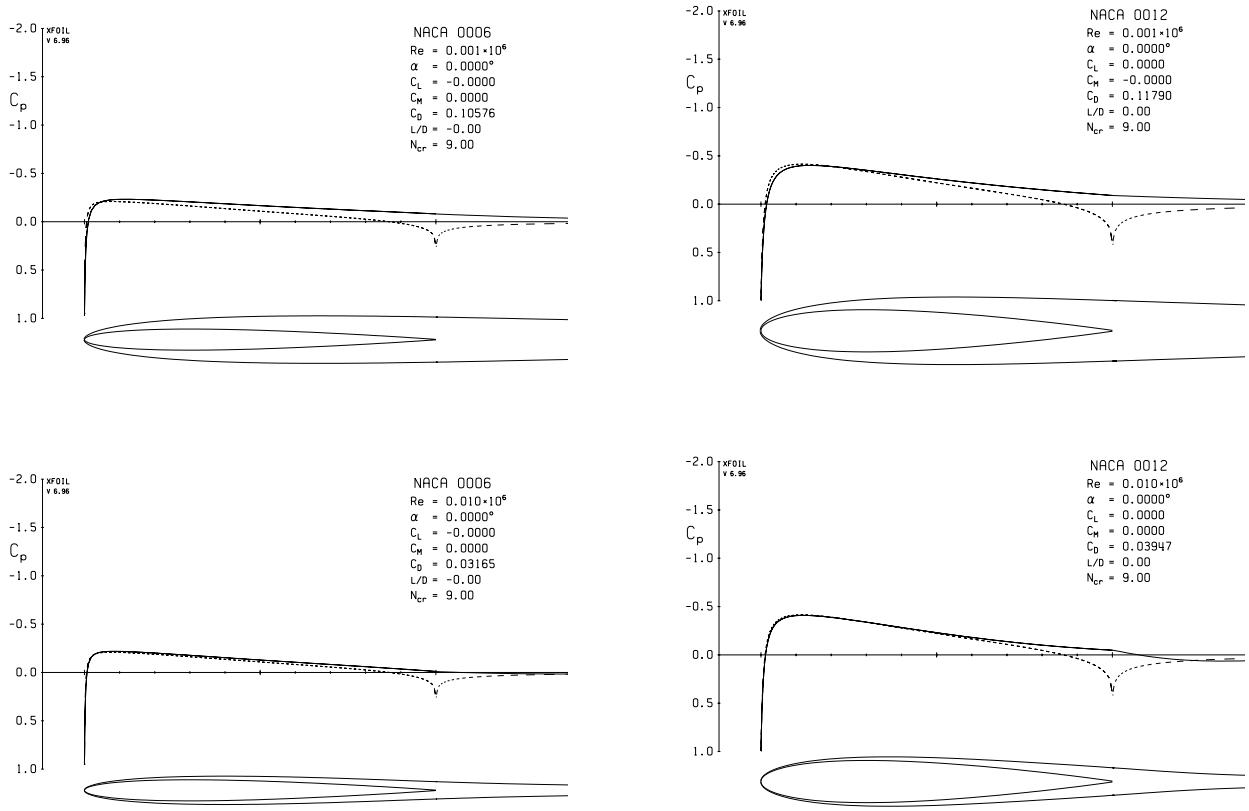


Figure 13.7: c_p and effective shape for NACA 0006 and NACA 0012 incompressible laminar flows at $\alpha = 0$ and $Re = 1,000$ and $10,000$. Note: c_p for purely inviscid flow is shown as dashed line in c_p plot.

minimum pressure (roughly at the location of maximum thickness) than the NACA 0006 because of the decreased radius of curvature for the thicker airfoils (see Section 7.3.3 for the streamline curvature discussion of the impact of thickness on c_p). As a result, the edge pressure gradient, $\mathrm{d}p_e/\mathrm{d}x$ will tend to be larger (more adverse) on the downstream half of the NACA 0012 than on the NACA 0006. Note that if the flow were inviscid, the velocity at the trailing edge for both of these airfoils would stagnate and the pressure at the trailing edge would therefore be the freestream stagnation pressure. Thus, a lower minimum pressure on the airfoil implies generally larger adverse pressure gradients would be observed downstream. The connection between the pressure gradient and the boundary layer thickness can be explained by considering the momentum equation along the streamwise direction in a boundary layer. This equation can be shown to be,

$$\rho u \frac{\partial u}{\partial s} = -\frac{\mathrm{d}p_e}{\mathrm{d}s} + \mu \frac{\partial^2 u}{\partial n^2} \tag{13.97}$$

Note, the essential differences between this equation and the boundary layer x-momentum equation (Equation 13.62) are that

- the derivatives are taken along a streamline direction (s) and normal to the streamline (n) as opposed to in x and y.
- the normal velocity term in the substantial derivative, $u_n \partial u/\partial n$ is zero since the velocity normal to a streamline is, by definition, zero (i.e. a streamline is tangent to the velocity).
- While the velocity in the substantial derivative terms of this equation should be V (the velocity magnitude), since v is neglible compared to u, then $V \approx u$ in the limit of high Re.

Dividing Equation (13.97) by ρu gives,

$$\frac{\partial u}{\partial s} = -\frac{1}{\rho u}\frac{\mathrm{d}p_e}{\mathrm{d}s} + \frac{\mu}{\rho u}\frac{\partial^2 u}{\partial n^2} \tag{13.98}$$

This equation shows that for regions of lower velocity, the pressure gradient will create a larger change in the velocity. In particular, for adverse pressure gradients, this leads to a feedback in which the adverse pressure gradient ($\mathrm{d}p_e/\mathrm{d}s > 0$) decelerates the velocity ($\partial u/\partial s < 0$) which then further amplifies the impact of an adverse pressure gradient. For favorable pressure gradients, the opposite happens in which the favorable pressure gradient accelerates the flow and lessens the impact of further favorable pressure gradients. As a result, while the decreased pressure due to increased thickness of an airfoil will tend to decrease δ^* on the upstream portion of the airfoil, the negative feedback will generally lead to larger δ^* on the downstream portion of the airfoil. This behavior of δ^* can be observed in Figure 13.8 which shows a plot of $\delta^*(x)$ for the two airfoils and the flat plate result (Equation 13.96) at $Re = 1,000$. In summary, increased airfoil thickness overall will tend to increase δ^* and lead to larger form drags.

Beyond increased airfoil thickness, any effect that results in larger adverse pressure gradients on the airfoil also increases the likelihood of larger δ^* and therefore increased form drag. In particular,

- Increasing c_l will require lower pressures on the upper surface which will lead to increased adverse pressure gradients as the pressure increases towards the rear of the airfoil.
- Suction peaks create very low pressures which will result in large adverse pressure gradients immediately downstream of the peak.

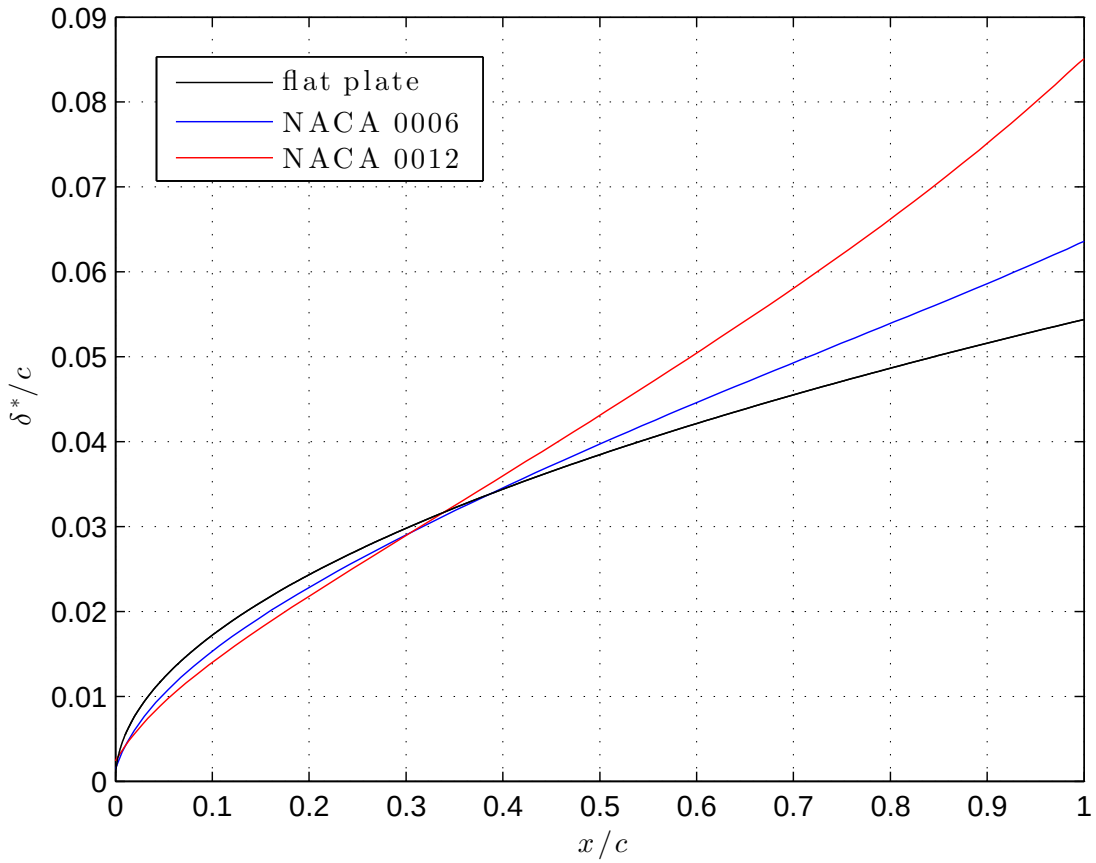
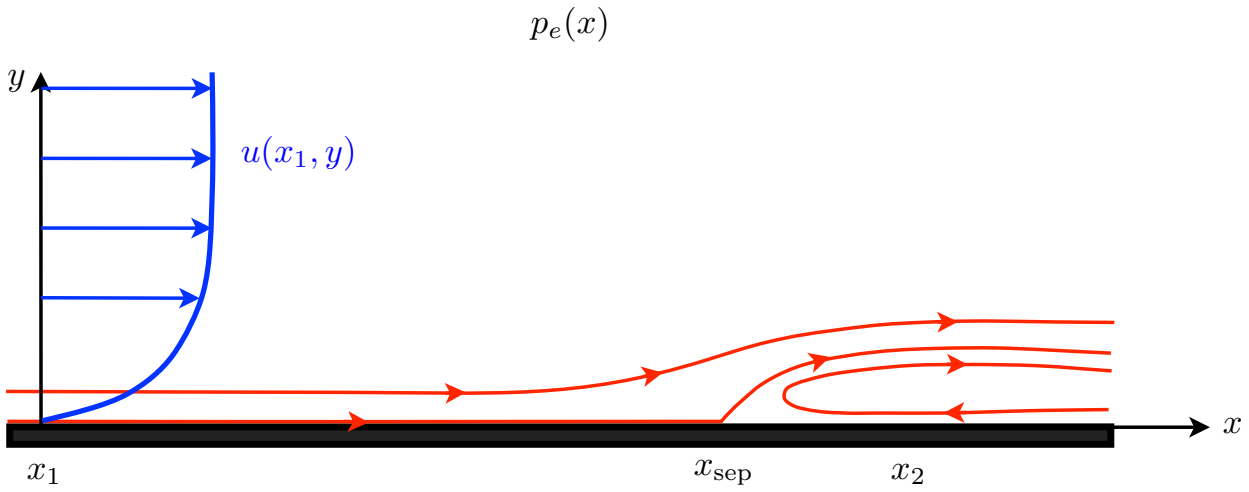


Figure 13.8: δ^*/c versus x/c for incompressible laminar flows at $\alpha = 0$ over a flat plate and NACA 0006 and NACA 0012 airfoils at $Re = 1,000$.

edXproblem: 13.4.3 Skin friction behavior in separation

13.8



The figure shows a typical streamline pattern around the location of flow separation x_{sep}. Immediately behind the separation location, the flow reverses direction. At x_2, the value of τ_{wall} is:

edXsolution

Video Link

13.4.4 Separation

13.8

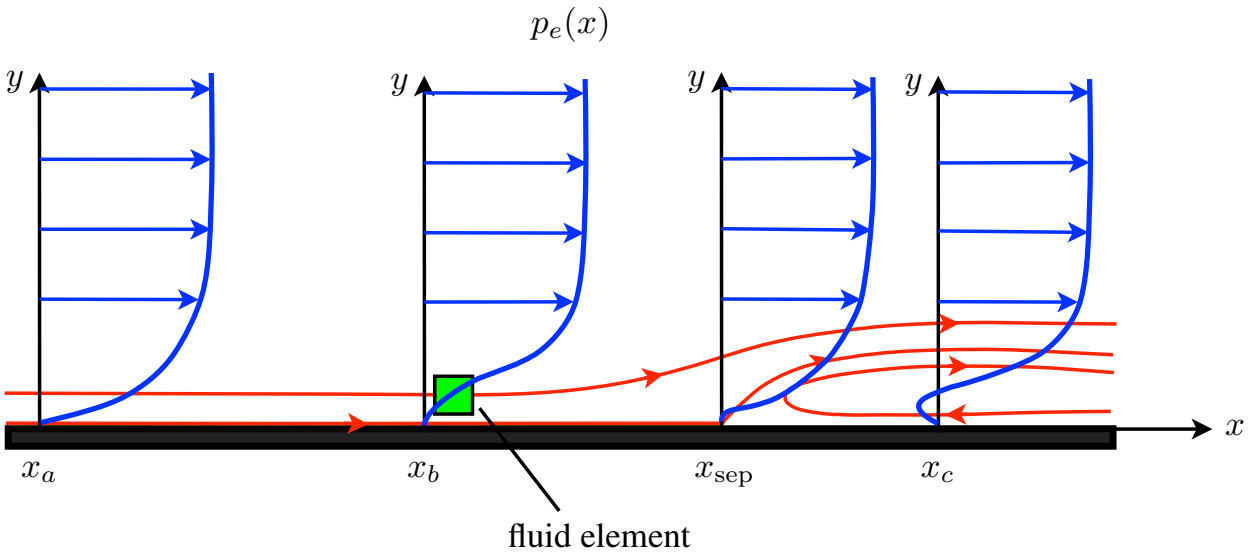


Figure 13.9: Velocity profiles and streamlines in the vicinity of flow separation.

As shown in Figure 13.9, the separation location x_{sep} is where the streamline infinitesimally above the surface no longer remains tangent to the surface (on the surface, the flow always has zero velocity and is always tangent). As discussed in Problem 13.4.3, the skin friction $\tau_{\text{wall}} = 0$ at this location. Thus, $C_{\text{f}} = \tau_{\text{wall}}/q_\infty = 0$ at separation.

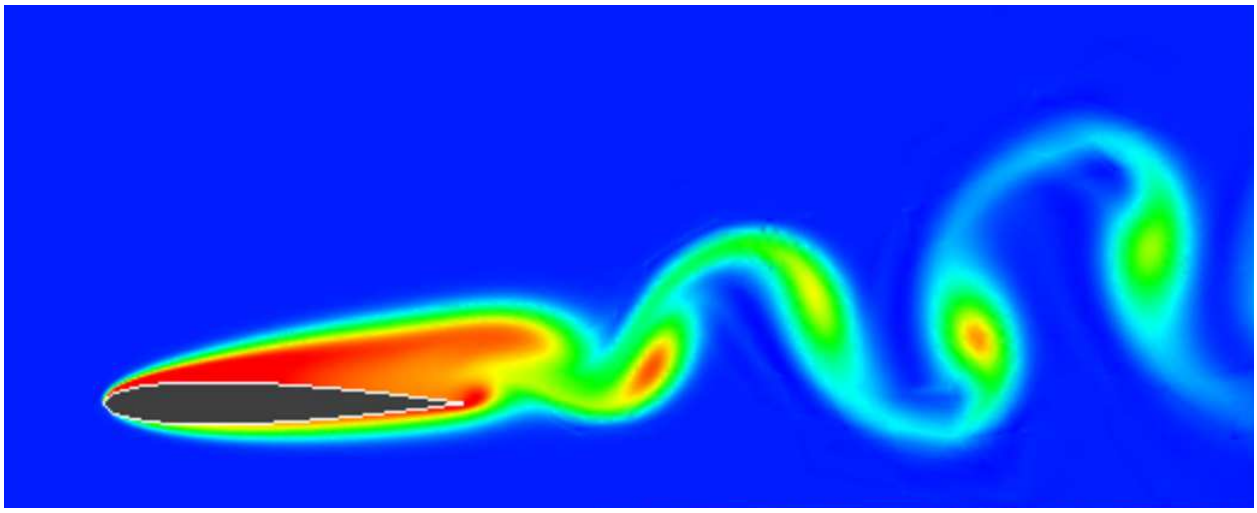


Figure 13.10: Instantaneous distribution of the entropy for large-scale separation of a NACA 0012 airfoil at $Re = 1,500$, $M_\infty = 0.5$, and $\alpha = 10^\circ$ (Results from Joshua Krakos, MIT PhD Thesis, 2012)

Depending on the specific situation, separation can range from a relatively small bubble near the leading-edge of an airfoil, to a larger separation region on the downstream portions of the airfoil, or even to massive separation occurring over essentially the entire airfoil (such as shown for laminar flow in Figure 13.10). An example of separation near the trailing edge is actually the NACA 0012 $\alpha = 0$, $Re = 10,000$ we discussed in Section 13.4.2. Viewing only the displacement thickness distribution for this flow in Figure 13.7, it is impossible (at least I think so) to tell separation has occurred. The velocity profiles, shown in Figure 13.11, do not help significantly either. However, if you look

closely enough, you might convince yourself that there is a region of reversed flow (only very near the surface) as the trailing edge is approached. More effective for identification of separation is the skin friction coefficient shown in Figure 13.12. The presence of $C_\mathrm{f} < 0$, and therefore separation, is clearly evident for approximately $x/c > 0.8$.

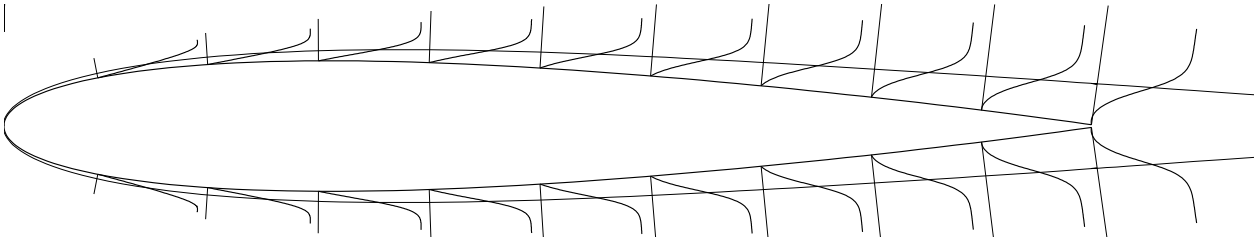


Figure 13.11: Boundary layer velocity profiles with the displacement thickness superimposed for incompressible laminar flows at $\alpha = 0$ over a NACA 0012 airfoil at $Re = 10,000$.

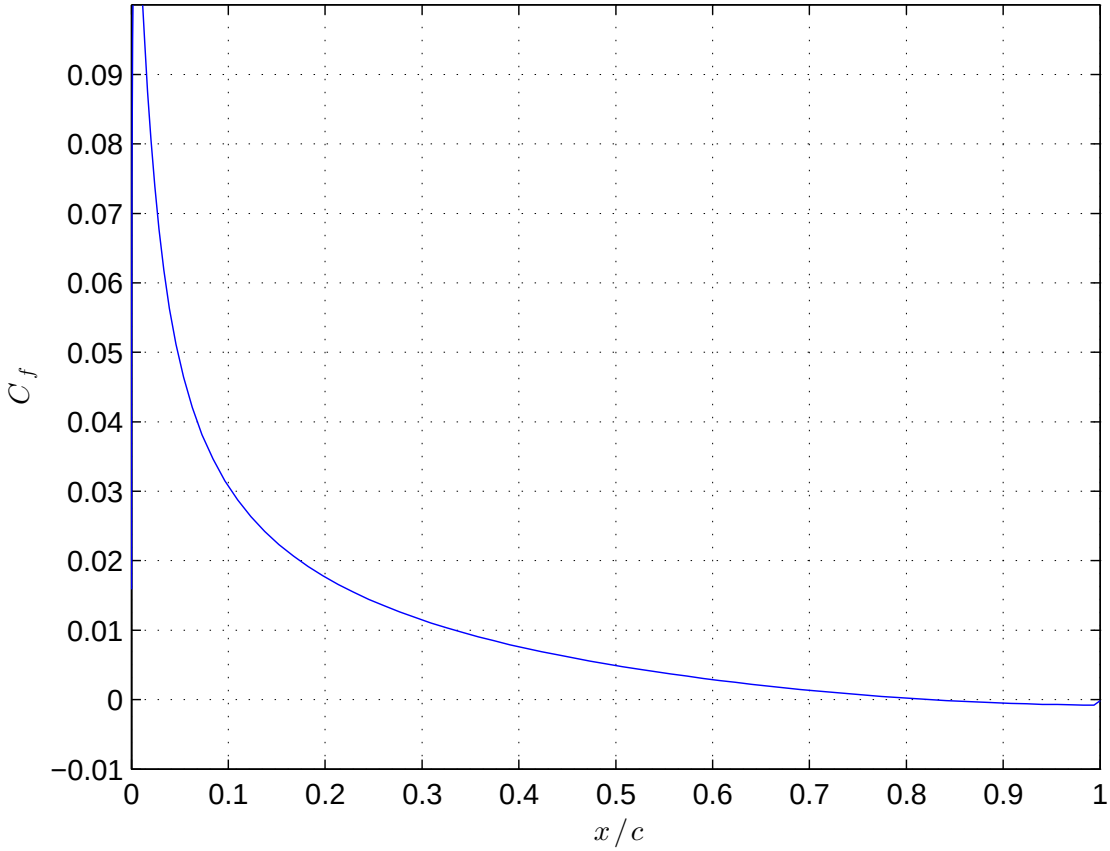


Figure 13.12: C_f distribution for incompressible laminar flows at $\alpha = 0$ over a NACA 0012 airfoil at $Re = 10,000$.

Exactly if separation occurs and the form it takes (leading bubble, moderate trailing edge separation, large-scale separation, etc) is dependent on many factors including the airfoil geometry, the angle of attack, the Reynolds number, the surface roughness, the level of turbulence in the freestream, and many other parameters. As a result, separation remains among the most significant challenges to predict using theoretical methods including computational simulation. Further, experiments are equally challenged because of the difficulty in achieving dynamic similarity for many

aeronautical applications. We will revisit separation in more detail in the following module on turbulent boundary layers.

However, one certain thing which can be said is that adverse pressure gradients play a critical role. As we discussed in Section 13.4.2, adverse pressure gradients cause the flow near the wall to decelerate more rapidly than the flow at the edge of the boundary layer. As a result, flow near the wall can reverse directions while the flow outside the boundary layer is still directed downstream.

Further, for the flow upstream of separation as shown in Figure 13.9, adverse pressure gradients must be present as viscous effects cannot, by themselves, cause flow reversal. To see this, consider the velocity profile at $x = x_b$ in the figure, which is the typical profile just before separation. For fluid elements near the wall, $\mathrm{d}^2u/\mathrm{d}y^2 > 0$. Thus, the viscous effects for fluid elements in this region will cause a positive net force in the x-direction. That is, the low speed flow near the wall is being *pulled* along by the fast flow above it. Without an adverse pressure gradient, the flow would not separate.

13.5 Sample Problems

edXproblem: 13.5.1 Pipe flow

13.2

Consider the incompressible flow through a pipe with a constant radius R. Assume that the flow is axisymmetric without any swirl. The governing equations for this type of flow are,

$$\frac{1}{r}\frac{\partial}{\partial r}(ru_r) + \frac{\partial u_z}{\partial z} = 0 \tag{13.99}$$

$$\rho\left(\frac{\partial u_r}{\partial t} + u_r\frac{\partial u_r}{\partial r} + u_z\frac{\partial u_r}{\partial z}\right) = -\frac{\partial p}{\partial r} + \mu\left[\frac{1}{r}\frac{\partial}{\partial r}\left(r\frac{\partial u_r}{\partial r}\right) + \frac{\partial^2 u_r}{\partial z^2} - \frac{u_r}{r^2}\right] \tag{13.100}$$

$$\rho\left(\frac{\partial u_z}{\partial t} + u_r\frac{\partial u_z}{\partial r} + u_z\frac{\partial u_z}{\partial z}\right) = -\frac{\partial p}{\partial z} + \mu\left[\frac{1}{r}\frac{\partial}{\partial r}\left(r\frac{\partial u_z}{\partial r}\right) + \frac{\partial^2 u_z}{\partial z^2}\right] \tag{13.101}$$

Assume that the flow is steady and that the velocity does not depend on z, that is $u_r = u_r(r)$ and $u_z = u_z(r)$.

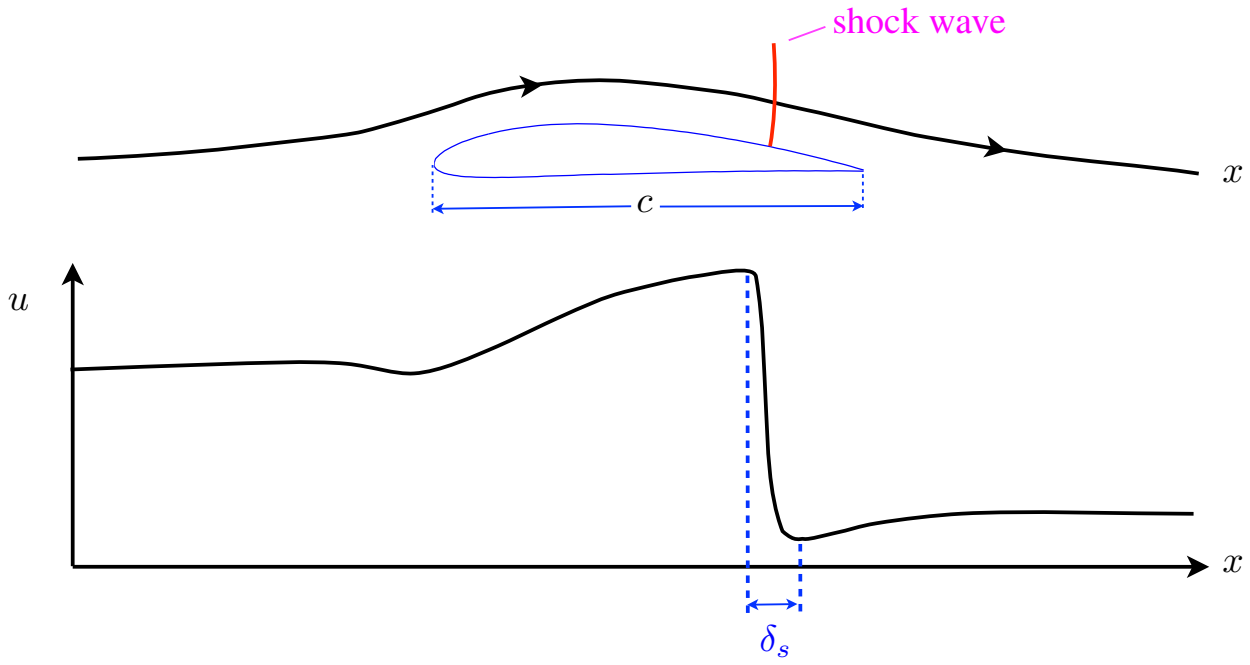
- Determine the solution for the axial velocity $u_z(r)$.
- Determine the maximum axial velocity.
- Determine the mass flow rate through the pipe, $\dot{m}$.
- The pumping power required (per unit length of pipe) is $-\dot{m}\mathrm{d}p/\mathrm{d}z$. For a fixed mass flow, how does the pumping power required depend on the radius of the pipe?

edXsolution

Video Link

edXproblem: 13.5.2 Shock thickness order-of-magnitude scaling analysis

13.4



Perform an order-of-magnitude scaling analysis to determine how the ration of the shock thickness-to-chord scales with the Reynolds number as $Re \to \infty$. Specifically, determine the coefficient a for,

$$\frac{\delta_s}{c} = O(Re^a) \tag{13.102}$$

The flow along a streamline passing through the shock can be modeled by the compressible one-dimensional momentum equation given by,

$$\rho u \frac{\partial u}{\partial x} = -\frac{\partial p}{\partial x} + \frac{\partial \tau_{xx}}{\partial x} \tag{13.103}$$

$$\tau_{xx} = (2\mu + \lambda)\epsilon_{xx} \tag{13.104}$$

And, you may assume that the second viscosity coefficient λ is well-modeled by Stokes hypothesis which states that $\lambda = -\frac{2}{3}\mu$.

At a Reynolds number of 10^6, would you expect a boundary layer or shock to have larger thickness?

edXsolution

Video Link

13.6 Homework Problems

edXproblem: 13.6.1 Method of assumed profiles with application to stagnation point boundary layers

13.3 | 13.5 | 13.6

A common technique to analyze boundary layer flows is to assume a velocity profile $u(x,y)$ and use that assumed profile to approximately solve the boundary layer equations. For example, consider the following velocity profile for $0 < y < \delta(x)$,

$$\frac{u(x,y)}{u_e(x)} = 2\tilde{y} - 2\tilde{y}^3 + \tilde{y}^4 + \frac{\Lambda}{6}\left[\tilde{y}(1-\tilde{y})^3\right] \text{ where } \tilde{y} = \frac{y}{\delta(x)} \tag{13.105}$$

with $\Lambda(x)$ being a parameter that is determined by approximately solving the boundary layer equations. For $\tilde{y} > 1$, $u(x,y) = u_e(x)$.

Applying the x-momentum equation at the wall (i.e. at $y = 0$), determine Λ. Specifically, show that Λ has the following form,

$$\Lambda = c_0 \delta^{c_1} \nu^{c_2} \left(\frac{\mathrm{d}u_e}{\mathrm{d}x}\right)^{c_3} \tag{13.106}$$

where the c_i are all real number constants.

What is the value of c_0?

What is the value of c_1?

What is the value of c_2?

What is the value of c_3?

Near the stagnation point at an airfoil's leading edge, the edge velocity can be approximated as,

$$u_e = 2V_\infty \frac{x}{R} \tag{13.107}$$

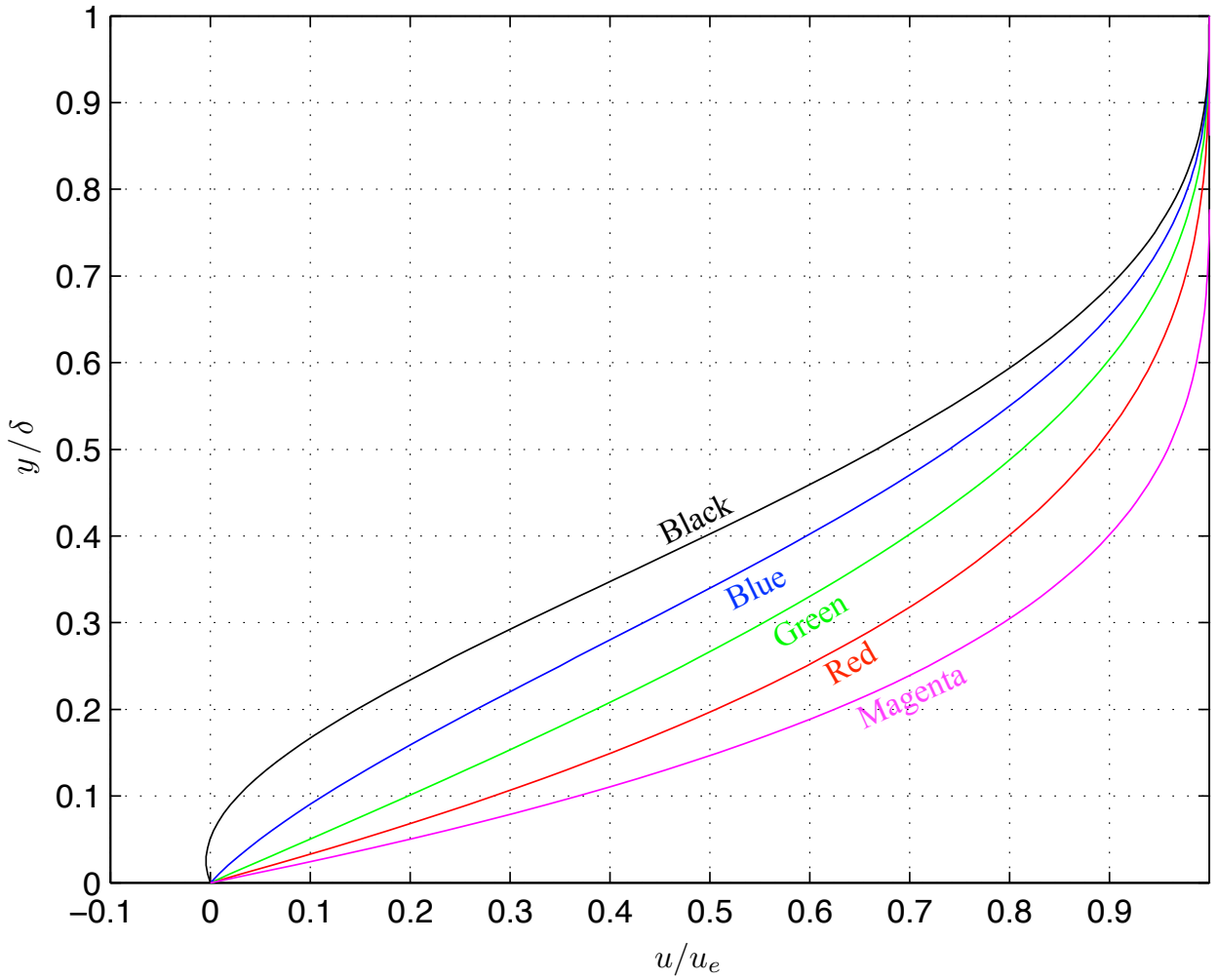
where R is the radius of curvature of the leading edge. For this flow, $\Lambda = 7.05$. In other words, Λ does not vary with x for the boundary layer in the vicinity of a stagnation point.

Based on this result, in the vicinity of a stagnation point, select all of the responses which are true,

Consider an airfoil for which $R/c = 0.05$.

What is δ/R at the leading-edge stagnation point of the airfoil when the Reynolds number (based on chord) is $Re = 10^4$? Provide your answers with two significant digits of precision (of the form $X.YeP$).

What is δ/R at the leading-edge stagnation point of the airfoil when the Reynolds number (based on chord) is $Re = 10^6$? Provide your answers with two significant digits of precision (of the form $X.YeP$).



The figure shows plots of the velocity profile given in Equation (13.105) for different values of Λ.

Which profile corresponds to the stagnation point boundary layer flow?

Which profile corresponds to the (zero pressure gradient) flat plate boundary layer flow?

edXsolution

Video Link

edXproblem: 13.6.2 Airfoil drag and skin friction comparisons

13.6

Consider two thin airfoils moving at constant velocities, zero angle of attack, and at the same altitude (thus the density and viscosity are the same). The first airfoil has a chord of $c_1 = 1$ meters and is moving at $V_{\infty 1} = 20$ m/sec. The second airfoil has a chord of $c_2 = 0.5$ meters and is moving at $V_{\infty 2} = 40$ m/sec. Assume that the boundary layers of these thin airfoils can be well-approximated using Blasius' flat plate boundary layer solution.

What is the ratio of the drag coefficients c_{d1}/c_{d2}?

What is the ratio of the drag D'_1/D'_2?

What is the ratio of the skin friction coefficient $C_{\mathrm{f}1}/C_{\mathrm{f}2}$ evaluated at the same x/c?

What is the ratio of the wall stress $\tau_{\mathrm{wall}1}/\tau_{\mathrm{wall}2}$ evaluated at the same x/c?

edXsolution

Video Link

edXproblem: 13.6.3 Low Drag Foils, Inc.

13.3 | 13.7 | 13.8

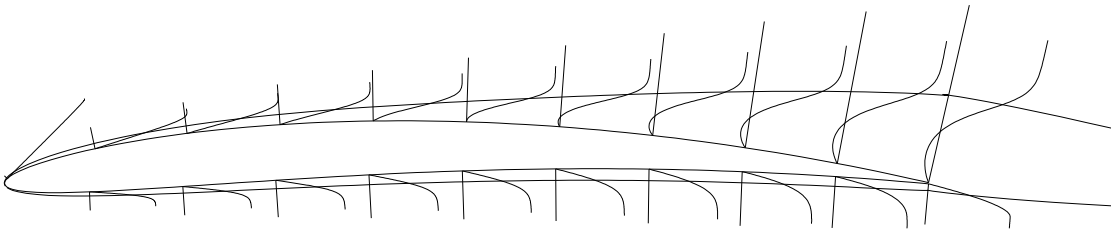
Having worked hard to earn your 16.101x certificate, you were promoted to Chief Aerodynamicist at Low Drag Foils Incorporated. The former Chief Aerodynamicist had conducted an aerodynamic analysis of a recently proposed laminar flow airfoil for $Re = 1 \times 10^4$ and 5×10^5 at lift coefficients of $c_l = 0.3$ and 0.6 (in other words, a total of four different operating conditions). Unfortunately, the former Chief Aerodynamicist departed the company hastily and the results of that study were left unorganized. All that remains of the study are the following pairs of drag coefficient and form drag coefficient and the plots of the boundary layer profiles with δ^* superimposed.

c_d	$c_{d\text{form}}$
0.0140	0.0108
0.0346	0.0315
0.0395	0.0140
0.0568	0.0336

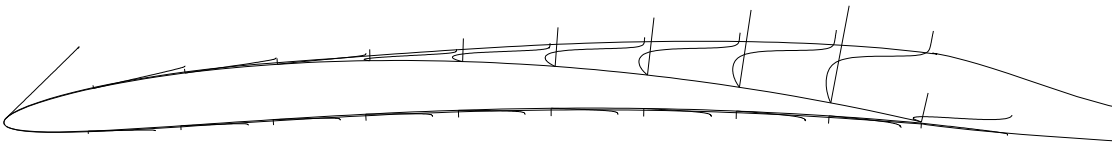
Plot A



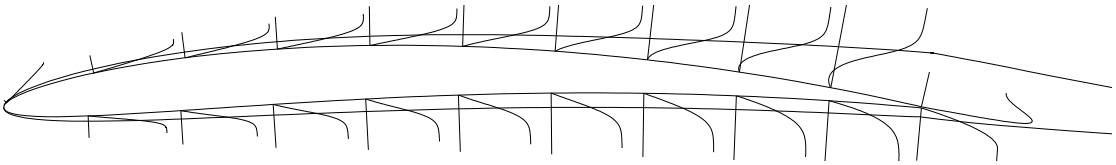
Plot B



Plot C



Plot D



Your task now is to determine which drag values and boundary layer profile plots correspond to which combination of Re and c_l. Specifically:

What values of Re, c_l, c_d, $c_{d\text{form}}$ correspond to plot A?

What values of Re, c_l, c_d, $c_{d\text{form}}$ correspond to plot B?

What values of Re, c_l, c_d, $c_{d\text{form}}$ correspond to plot C?

What values of Re, c_l, c_d, $c_{d\text{form}}$ correspond to plot D?

edXsolution

Video Link

Module 14

Boundary Layer Transition and Turbulence

14.1 Overview

14.1.1 Measurable outcomes

We have now made it to the final module! Congratulations! In this module, we discuss the onset and impact of turbulence in boundary layers. The boundary layers discussed in Module 13 were assumed to be steady flows and refered to as a *laminar boundary layer*. However, for many aeronautics applications, the flow inside the boundary layers is in fact not steady. The technical term for this unsteadiness is turbulence, and the boundary layer is refered to as a *turbulent boundary layer*. Turbulence makes dramatic changes in the boundary layer behavior and therefore is critical to account for in the design of most aeronautical vehicles.

Specifically, students successfully completing this module will be able to:

14.1. Explain transition, i.e. the onset of turbulence in a boundary layer and the use of linear stability analysis to predict transition, and describe the dependence of transition on Reynolds number and pressure gradient.

14.2. Explain the qualitative effects of turbulence on boundary layer evolution including the impact on velocity profile, skin friction coefficient, boundary layer thickness, and separation.

14.3. Estimate friction drag on 2-D and 3-D configurations by decomposing the geometry into patches and assuming appropriate skin friction behavior including the possibility of laminar or turbulent boundary layer conditions.

14.1.2 Pre-requisite material

The material in this module requires the measurable outcomes from Module 13.

14.2 Boundary Layer Transition

14.2.1 Introduction to flow instability

14.1

We return to the excellent NSF Fluid Mechanics Series to introduce the basic ideas of flow instability. While the video does not address instability in boundary layers (which is our application of interest), the basic concepts of flow instability are the same.

Video Link

The key concepts in this video which we will use in describing boundary layer transition are:

- From approximately 1:29 to 1:50 of the video, a smoke plume is shown rising. The plume starts out steady and laminar at its source and as it rises becomes unstable and, eventually, turbulent. Boundary layer behavior is very similar. Near the leading edge of a body, boundary layers can be stable. Due to a variety of effects (which we will consider shortly), the boundary layer can become unstable further downstream along the surface of the body, eventually leading to a transition to a turbulent boundary layer flow at some downstream location.
- From approximately 5:15 to 13:35, Prof. Erik Mollo-Christensen discusses instability of surface waves and shows several key concepts in flow instability. Specifically:
  - There are ranges of parameters in a flow problem under which small disturbances are amplified. For this surface wave demonstration, the wind speed is the parameter varied. More generally, this wind speed would be non-dimensionalized with combinations of other inputs in the problem to produce a non-dimensional parameter.
  - Even in parameter ranges where the flow is unstable, not all disturbances are amplified. That is, the flow acts as a selective amplifier. Specifically, only disturbances in a specific range of frequencies are amplified. Curves of constant amplication rate can be drawn as functions of the wind speed and frequency. Along the *neutral curve*, disturbances do not decay or amplify. Just to one side of the neutral curve, the combination of parameter value and frequency will be stable (i.e. the disturbance at the given wind speed and frequency will decay); while just to the other side of this neutral curve, the combination of parameter value and frequency will be unstable (i.e. the disturbance will amplify).
  - The critical parameter value is the lowest value of a parameter for which some frequency is amplified. Below this critical parameter value, small disturbances decay and the flow is stable (to small disturbances). Above this parameter value, a range of frequencies will be amplified.
- From approximately 23:50 to 25:10, the flow around a cylinder is shown to have a critical Reynolds number above which the wake is unsteady and forms a vortex sheet (known as a Karman vortex sheet). However, in an important demonstration, Prof. Mollo-Christensen shows that by introduction of a larger disturbance, it is possible to cause a vortex sheet even below the critical Reynolds number. This phenomenon of subcritical, or bypass, transition, occurs in many flows and in particular in boundary layers. This implies that transition will be a function of the amplitude of disturbances present in the flow field. That is, for infinitesimal disturbances, a flow may be stable, but with a sufficiently large disturbances, the flow may still transition to a different (frequently turbulent) state.

14.2.2 Types of boundary layer transition

14.1

Next in our consideration of boundary layer transition to turbulence, we recommend revisiting NSF Fluid Mechanics Series video on boundary layers. In particular, please focus on the discussion of boundary layer transition from 15:25 to 16:45.

Video Link

The transition process described in the video is commonly referred to as *natural transition* and is representative of boundary layer transition when the disturbances in the flow are very small.

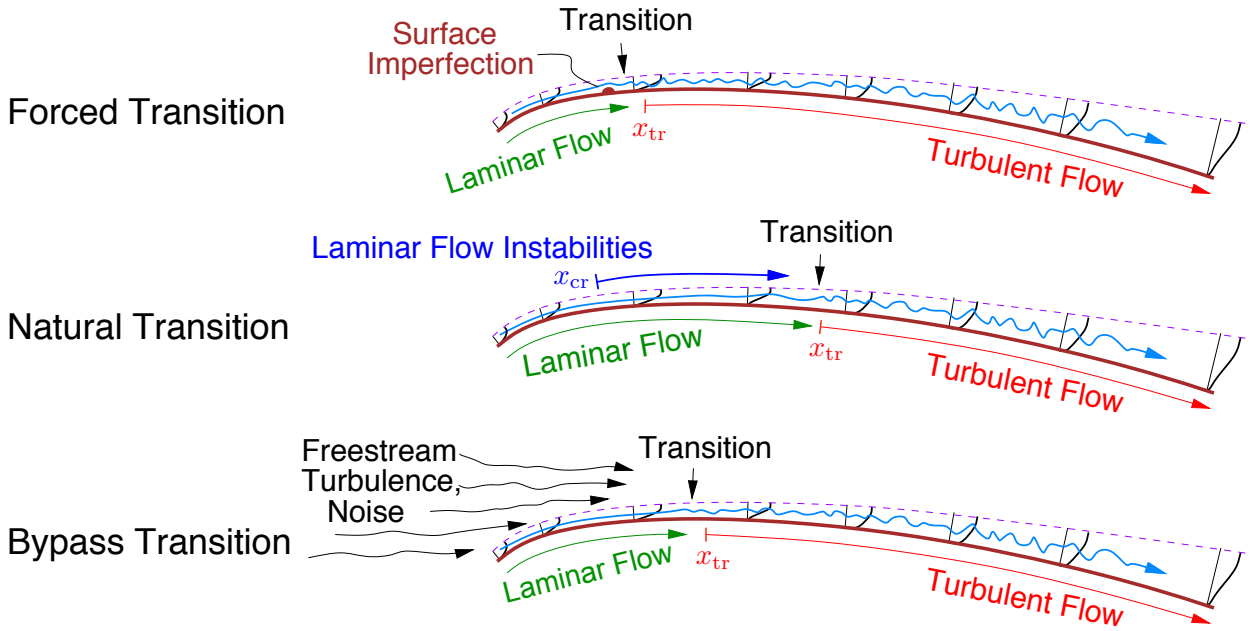


Figure 14.1: Types of boundary layer transition. (Adapted from Drela, *Flight Vehicle Aerodynamics*)

Figure 14.1 shows three types of boundary layer transition: forced transition, natural transition, and bypass transition. Note that the location at which the flow becomes turbulent is labeled x_{tr}. While this figure may imply that the location at which the flow is turbulent is precisely defined, in fact that is not true. This is really because the definition of turbulent flow is not precise.

- Forced transition occurs when a geometric perturbation causes the boundary layer to become turbulent. This geometric perturbation may be unintentional (e.g. due to surface roughness or icing) or may be intentional (e.g. trips strips placed with the intention of causing transition).
- Natural transition occurs when small disturbances are amplified in the boundary layer due to the instability of the laminar boundary layer flow. The point at which the boundary layer is unstable and some disturbances are amplified is called the critical location, x_{cr}. This initial growth of disturbances in natural transition is well described by linearized boundary layer theory. As the disturbances amplify, at some point they will become sufficiently large for nonlinear effects to be important and, eventually, the flow becomes turbulent at x_{tr}.
- Bypass transition occurs when the flow disturbances outside the boundary layer (due to freestream turbulence or noise sources) are sufficiently large that the linear behavior is never observed and the boundary layer immediately becomes turbulent.

14.2.3 Spatial stability of the Blasius flat plate boundary layer

14.1

The natural transition process begins with the amplification of infinitesimal waves once the boundary layer flow becomes unstable at x_{cr}. As described in Section 14.2.1, the boundary layer flow acts as a selective amplifier above a critical Reynolds number. The amplification of infinitesimal waves can be analyzed using linear stability theory. Linear stability theory consists of linearizing the Navier-Stokes equations about a steady laminar flow solution and determining if infinitesimal disturbances will be amplified (i.e. the flow is unstable) or will be damped (i.e. the flow is stable).

In particular, we will consider *spatial stability* of boundary layer flows. Spatial stability determines if infinitesimal disturbances with a temporal frequency f grow as they move downstream (that is as x increases). Specifically, we will consider infinitesimal perturbations (about a steady laminar flow) of the form,

$$\tilde{u}(t,x,y,z) = \exp(i2\pi ft)\,\hat{u}(x,y,z) \tag{14.1}$$
$$\tilde{v}(t,x,y,z) = \exp(i2\pi ft)\,\hat{v}(x,y,z) \tag{14.2}$$
$$\tilde{w}(t,x,y,z) = \exp(i2\pi ft)\,\hat{w}(x,y,z) \tag{14.3}$$
$$\tilde{p}(t,x,y,z) = \exp(i2\pi ft)\,\hat{p}(x,y,z) \tag{14.4}$$

So, a spatially stable boundary layer flow is one in which $\hat{u}$, $\hat{v}$, $\hat{w}$, and $\hat{p}$ all decrease in magnitude as $x \to \infty$. Applying spatial stability theory to Blasius flat plate boundary layer flow gives the neutral curve shown in Figure 14.2 plotted as a function of Re_{δ^*},

$$Re_{\delta^*} \equiv \frac{V_\infty \delta^*}{\nu_\infty} \tag{14.5}$$

The critical Reynolds number is,

$$Re_{\delta^*,\text{cr}} \approx 400 \tag{14.6}$$

Using Equation (13.96), the critical Reynolds number based on x can be determined,

$$Re_{x,\text{cr}} = Re_{\delta^*,\text{cr}} \left(\frac{x}{\delta^*}\right)_{\text{cr}} \tag{14.7}$$
$$= Re_{\delta^*,\text{cr}} \frac{\sqrt{Re_{x,\text{cr}}}}{1.72} \tag{14.8}$$
$$\Rightarrow Re_{x,\text{cr}} = \left(\frac{Re_{\delta^*,\text{cr}}}{1.72}\right)^2 \tag{14.9}$$
$$\Rightarrow Re_{x,\text{cr}} = 54,000 \tag{14.10}$$

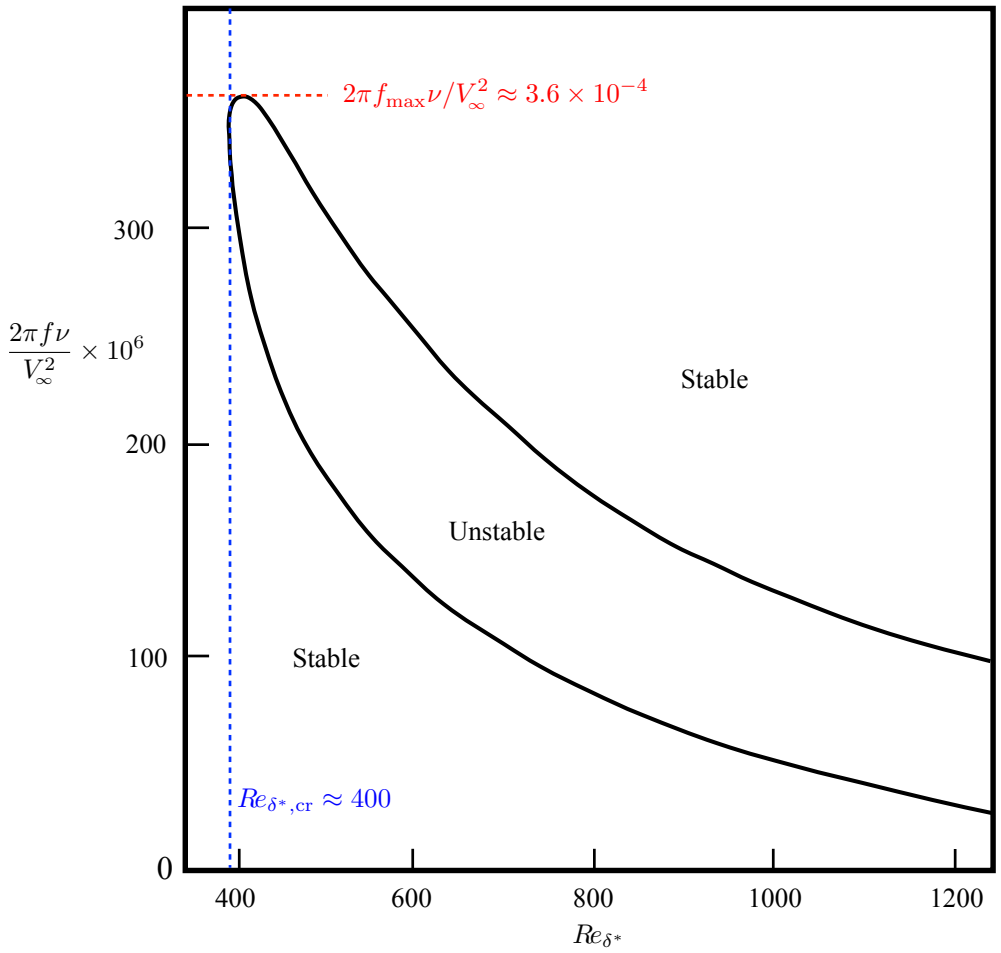


Figure 14.2: Neutral curve for Blasius boundary layer flow

edXproblem: 14.2.4 Critical condition for boundary layer instability on a sailplane

14.1

Consider a sailplane flying with speed $V_\infty = 100\,\text{km/hr}$ and at an altitude where the kinematic viscosity $\nu_\infty = 2.1 \times 10^{-5}\,\text{m}^2/\text{s}$. Assume that the behavior of the boundary layers before $Re_{x,\text{cr}}$ is well approximated by Blasius flat plate theory.

How far from the leading edge is the critical location at which infinitesimal disturbances are first amplified (i.e. determine x_{cr})? Provide your answer in meters with two digits of precision (of the form X.YeP).

What is the displacement thickness of the boundary layer at x_{cr}? Provide your answer in meters with two digits of precision (of the form X.YeP).

What is the frequency f of the disturbances that are amplified at x_{cr}? Provide your answer in cycles/sec with one digit of precision (of the form XeP).

edXsolution

Video Link

14.2.5 Transition prediction

14.1

Although small disturbances are amplified once the boundary layer is unstable, the flow does not immediately transition at x_{cr} as the disturbances must grow to sufficient amplitude for turbulence to occur. A common engineering approach for the prediction of transition is known as the e^N method and is based on the spatial stability theory discussed in Section 14.2.3. The idea is to estimate the amplification of disturbances as a function of downstream distance. Let the amplitude of a disturbance of frequency f be $a_f(x)$. The amplification (or growth) rate of this disturbance is defined as $\alpha_f(x)$ where,

$$\frac{\mathrm{d}a_f}{\mathrm{d}x} = \alpha_f a_f \tag{14.11}$$

Or, alternatively, this can be written as,

$$\frac{\mathrm{d}}{\mathrm{d}x}\left(\ln a_f\right) = \alpha_f \tag{14.12}$$

Note that the dependence of the growth rate on f and x can be observed in the flat plate boundary layer results in Figure 14.2. For low x values (i.e low Re_{δ^*} values), disturbances are damped and therefore $\alpha_f < 0$. Then, as x increases, for certain values of f, the flow is unstable and therefore $\alpha_f > 0$.

The e^N method considers the greatest amplification for all f by defining the overall amplitude A,

$$\frac{\mathrm{d}}{\mathrm{d}x}\left(\ln A\right) \equiv \max_f(\alpha_f, 0) \tag{14.13}$$

Let the initial amplitude of a disturbance as it enters the boundary layer be A_0. The e^N method claims that transition to turbulence occurs when A/A_0 reaches a critical value of $e^{N_{cr}}$. Or, taking the natural log, transition occurs when $\ln A/A_0 = N_{cr}$. We note that Equation (14.13) can be written equivalently as,

$$\frac{\mathrm{d}N}{\mathrm{d}x} = \max_f(\alpha_f, 0) \qquad \text{where } N \equiv \ln\left(A/A_0\right) \tag{14.14}$$

And then transition occurs when $N = N_{cr}$.

The value of N_{cr} is dependent on the disturbances which are present in the flow, including geometry perturbations or any other effect which can create flow disturbances. Some typical values of N_{cr} are:

- For very clean flow such as a sailplane in flight or a very clean wind tunnel $N_{cr} = 12$.
- For an average wind tunnel, $N_{cr} = 9$.
- For a fairly turbulent wind tunnel, $N_{cr} = 4$.

An example of the evolution of N for a NACA 0004 airfoil at $\alpha = 0°$ at $Re = 10^5$ and 2×10^6 is shown in Figure 14.3 (these results were generated using Xfoil). For the $Re = 1 \times 10^5$ flow, the value of $N = 0$ until approximately $x/c = 0.5$, at which point N increases indicating the boundary layer has become unstable. Since the airfoil is quite thin, we expect the behavior to be similar to a flat plate flow. Recalling that for flat plate flow $Re_{x,cr} = 54,000$, then we expect,

$$\frac{x_{cr}}{c} = \frac{Re_{x,cr}}{Re} = \frac{54,000}{Re} \tag{14.15}$$

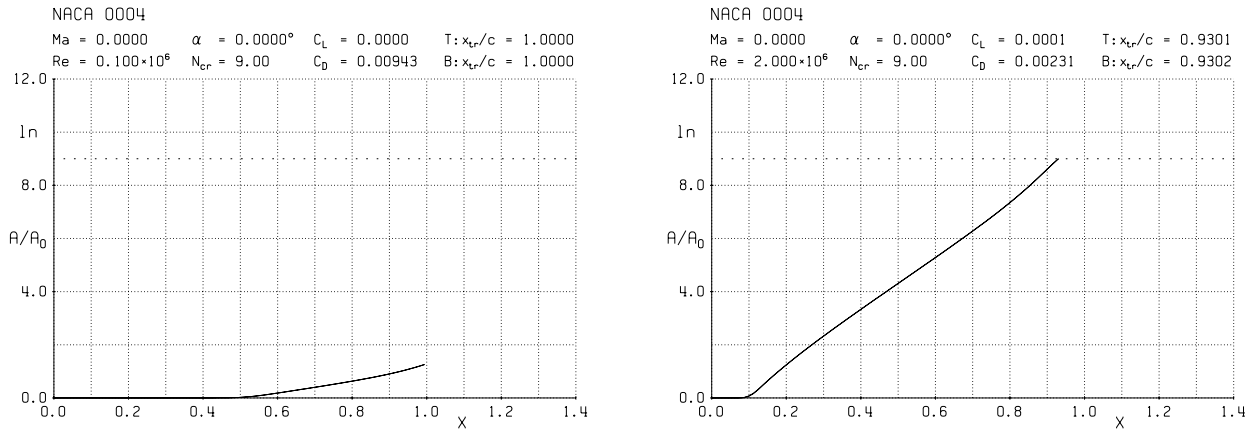


Figure 14.3: $N(x)$ variation for NACA 0004 incompressible flow at $\alpha = 0°$, and $Re = 1 \times 10^5$ and $Re = 2 \times 10^6$

Thus, for $Re = 10^5$, flat plate theory would predict $x_{\text{cr}}/c = 0.54$, which is in good agreement with the results of the figure. For $x/c > 0.5$, the results show that N increases to approximately a value of 1.5 at the trailing edge. Thus, transition does not occur at this condition (unless $N_{\text{cr}} \leq 1.5$ which is highlighly unlikely).

For the higher Reynolds number $Re = 2 \times 10^6$ flow, instability is observed in the Xfoil results at approximately $x/c = 0.1$. This is in reasonable agreement with the flat plate result which gives $x_{\text{cr}}/c = 0.03$. At this higher Reynolds number, $N(x)$ grows and reaches the critical value, which was chosen as $N_{\text{cr}} = 9$. Specifically, transition is predicted at $x_{\text{tr}}/c = 0.93$.

In general, boundary layers in regions with adverse pressure gradients are unstable and will amplify disturbances, and the greater the magnitude of the adverse pressure gradient the larger the amplification will tend to be. While favorable pressure gradients generally improve the stability of a boundary layer, the impact is not as significant as the destabilizing influence of an adverse pressure gradient. As a result, any effect that lowers the minimum surface pressure on the airfoil almost always will increase the likelihood of transition. This behavior is demonstrated in Figure 14.4 which shows $N(x)$ for a set of symmetric NACA airfoils at $Re = 10^5$ and $\alpha = 0°$. As the thickness increases, and therefore the minimum pressure drops, the boundary layer has large values of $N(x)$. Thus, the boundary layers transition sooner on the thicker airfoils.

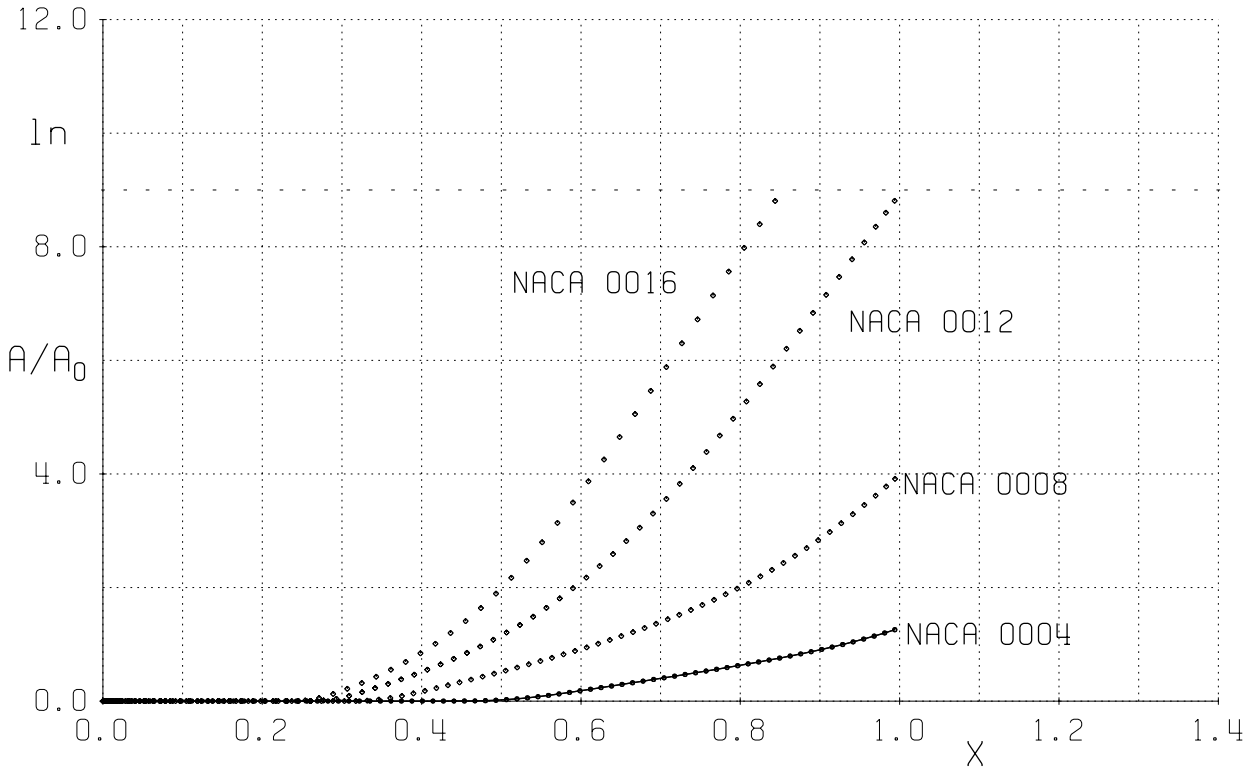


Figure 14.4: $N(x)$ variation for incompressible flow over NACA 00XX airfoils at $\alpha = 0°$ and $Re = 10^5$

edXproblem: 14.2.6 Improved flow quality in wind tunnel

14.1

A project was undertaken to improve the quality of the flow in a low speed wind tunnel. A series of tests were run on the NACA 0012 and NACA 0016 airfoils prior to the improvements and then after the improvements. The transition location relative to the chord (i.e. x_{tr}/c) for $Re = 10^5$ was observed to be:

Airfoil	Before improvements	After improvements
NACA 0012	0.80	0.95
NACA 0016	0.65	0.80

Based on the e^N results shown in Figure 14.4, what was an appropriate *integer* value of N_{cr} before the improvements to the wind tunnel?

Based on the e^N results shown in Figure 14.4, what is an appropriate *integer* value of N_{cr} after the improvements to the wind tunnel?

edXsolution

Video Link

14.3 Turbulent boundary layers

14.3.1 Introduction to turbulence

14.1 14.2

We once again return to the NSF Fluid Mechanics Series to introduce the basic ideas of turbulence.

Video Link

The key concepts in this video with respect to turbulent boundary layers are:

- The unsteadiness in a turbulent flow causes mixing that significantly changes the distribution of the mean velocity in a turbulent boundary layer from the steady flow in a laminar boundary layer. Specifically, the turbulent motion causes higher velocity fluid away from the wall to be mixed into the flow near the wall causing an increase in the mean velocity near the wall. Similarly, the low velocity fluid near the wall is mixed into the flow away from the wall causing the mean velocity away from the wall to decrease. As a result, the skin friction will generally be larger for a turbulent boundary layer compared to a laminar boundary layer (at similar Reynolds number) since the near-wall velocity and, therefore, the velocity gradient ($\partial u/\partial y$) will be larger in a turbulent flow. Further, because of these slower mean velocity away from the wall, a turbulent boundary layer will tend to be thicker than a laminar boundary layer (assuming the flow has not separated). This discussion of the impact of turbulent mixing on the velocity field is demonstrated in the discussion of the velocity distribution in pipe flow from 10:05 to 14:05. In particular, carefully study the motion of the colored dye flow to see how the fluid in the center of the pipe moves toward the wall, and similarly the fluid near the wall moves toward the center of the pipe.
- The large scale motion of a turbulent flow is not significantly affected by the Reynolds number. However, the Reynolds number does impact the fine scale motion. For turbulent flows, the length scales of the smallest eddies (relative to the largest length scales in the flow) will decrease as the Reynolds number increases. This Reynolds number effect is discussed from approximately 16:00 to 22:00.

edXproblem: 14.3.2 Comparison of laminar and turbulent velocity profiles

14.1

Consider a flat plate at zero angle of attack in which the freestream conditions are:

$$V_\infty = 100\,\text{m/s}, \quad p_\infty = 1.0 \times 10^5\,\text{N/m}^2, \quad \rho_\infty = 1.2\,\text{kg/m}^3, \quad \mu_\infty = 1.8 \times 10^{-5}\,\text{kg/(ms)} \tag{14.16}$$

If the boundary layer transitions at $Re_x = 500,000$, determine x_{tr}, the distance from the leading edge of the flat plate at which this occurs. Provide your answer in meters with two digits of precision (of the form X.YeP).

Assume that the boundary layer rapidly transitions from laminar to turbulent conditions such that we can effectively model the transition as occurring instantaneouly at x_{tr}. Using the Blasius flat plate result, determine the 99% boundary layer thickness for the laminar flow at x_{tr} (i.e. just before transition occurring). Provide your answer in meters with two digits of precision (of the form X.YeP).

A commonly-used result for the thickness of a turbulent boundary layer is,

$$\frac{\delta}{x} = 0.376 Re_x^{-0.2} \tag{14.17}$$

Using this result, estimate the 99% boundary layer thickness for the turbulent flow at x_{tr} (i.e. just after transition occurring). Provide your answer in meters with two digits of precision (of the form X.YeP).

For $y \leq \delta$, the velocity profile in a laminar flat plate boundary layer is well approximated by,

$$\frac{u}{V_\infty} = \sin\left(\frac{\pi}{2}\frac{y}{\delta}\right) \tag{14.18}$$

and a turbulent flat plate boundary layer is well approximated by,

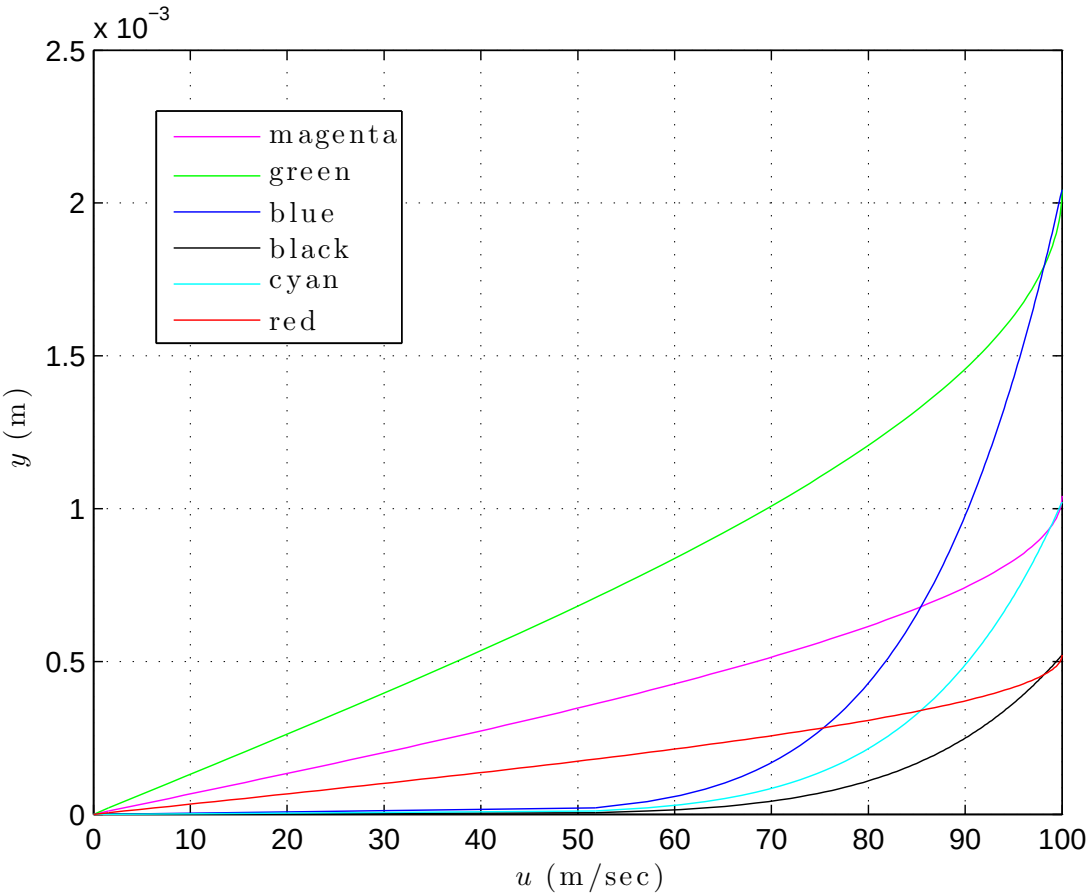
$$\frac{u}{V_\infty} = \left(\frac{y}{\delta}\right)^{1/7} \tag{14.19}$$

Which of the following line plots corresponds to the laminar velocity profile at x_{tr}?

Which of the following line plots corresponds to the turbulent velocity profile at x_{tr}?

edXsolution

Video Link



14.3.3 Turbulent flat plate flow

14.2 14.3

As described in the previous section, the skin friction in a turbulent boundary layer is generally higher than a laminar boundary layer at similar Reynolds numbers because of the fuller velocity profile. Figure 14.5 shows a comparison of laminar and turbulent skin friction coefficients C_f as a function of Re_x. The laminar result is taken from the Blasius flat plate boundary layer theory. The two turbulent results are based on experimental data and are frequently used when estimate skin friction drag of turbulent flows. The most accurate skin friction result is

$$C_f = 0.370\,(\log_{10} Re_x)^{-2.58} \tag{14.20}$$

which accurately represents the experimental behavior of turbulent flows over the entire range of Reynolds numbers shown. The other result is

$$C_f = 0.0576 Re_x^{-0.2} \tag{14.21}$$

While this approximation is frequently used because of its simplicity, it is only quantitatively accurate from approximately $10^5 \leq Re_{\leq} 10^6$ (though clearly the qualitative trends of $C_f(Re_x)$ are still well represented outside of this range).

Depending on the specific Reynolds number, we note that the skin friction in the turbulent regime can be 3-6 times larger than the skin friction in the laminar regime (at the same Reynolds number). Thus, this large difference in skin friction combined with the general uncertainty of where

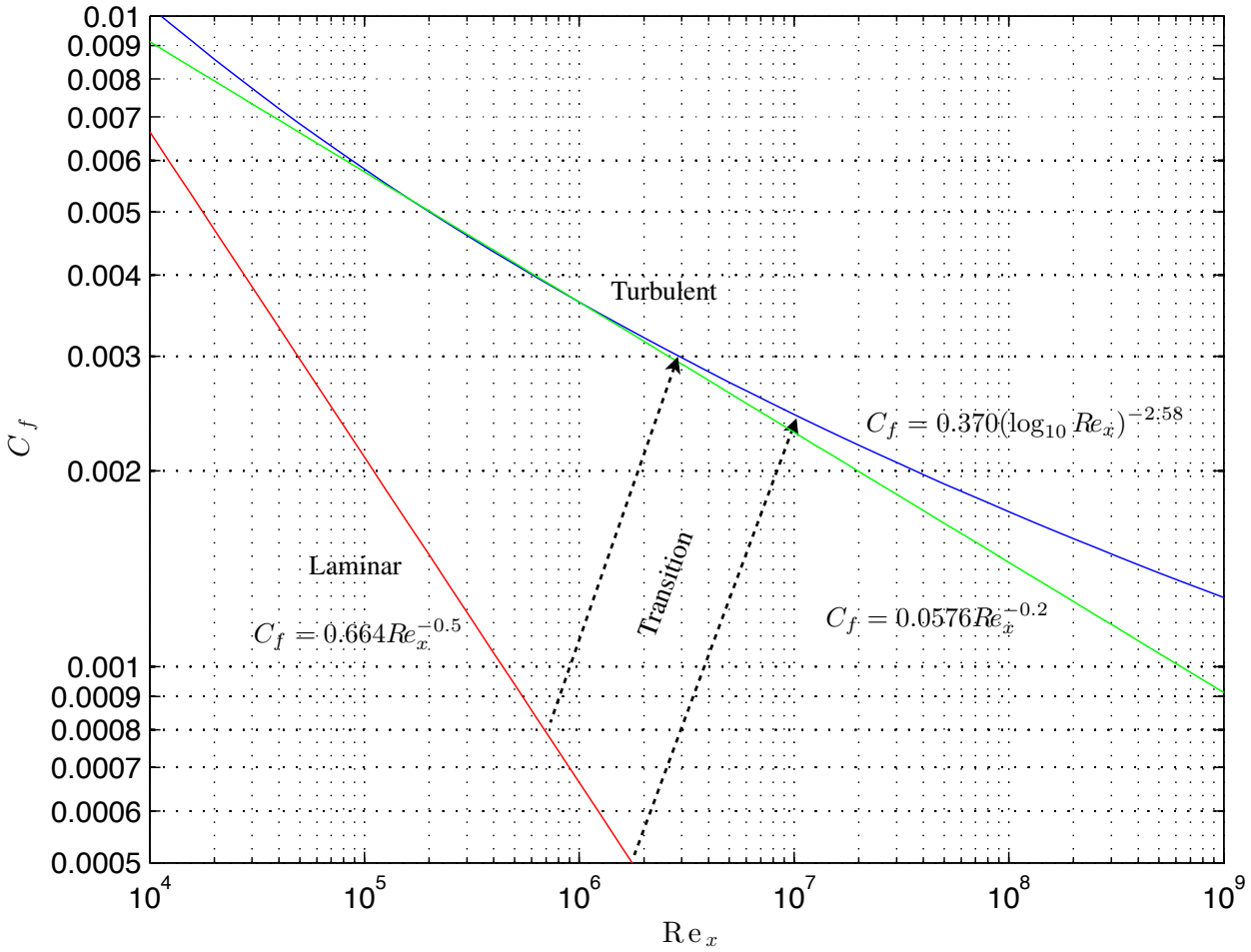
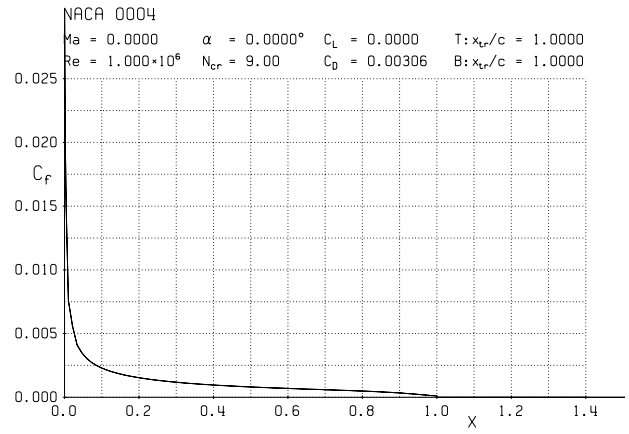
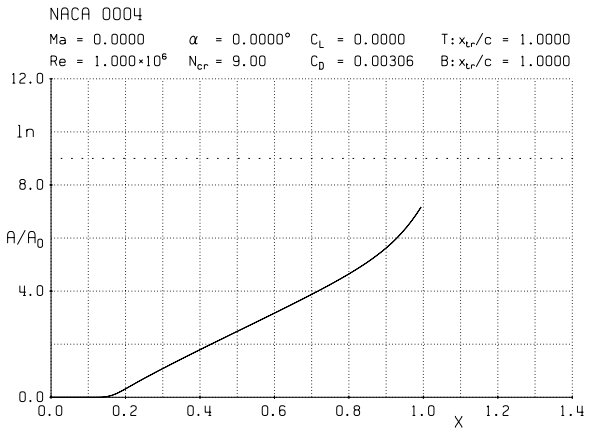


Figure 14.5: Comparison of skin friction on a flat plate for laminar and turbulent flow. Note that the $C_\mathrm{f} = 0.370(\log_{10} Re_x)^{-2.58}$ turbulent flow formula is accurate of the entire range of Reynolds numbers while the $C_\mathrm{f} = 0.0576 Re_x^{-0.2}$ is only accurate from approximately $10^5 < Re_x < 10^6$

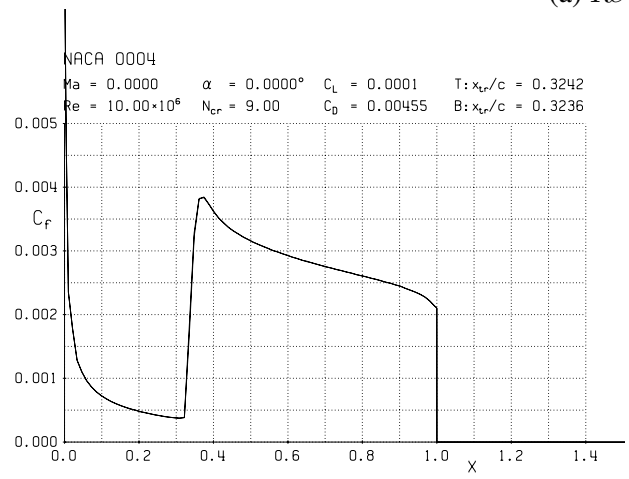
transition will occur on an airfoil makes the estimation of friction drag difficult for problems in which the chord Reynolds number is between approximately $10^4 < Re < 10^7$. For $Re < 10^4$, the flow generally does not transition unless separation is involved. And, for $Re > 10^7$, the flow transition typically occurs so close to the leading edge that we can effectively model the entire boundary layer as being turbulent with minimal errors.

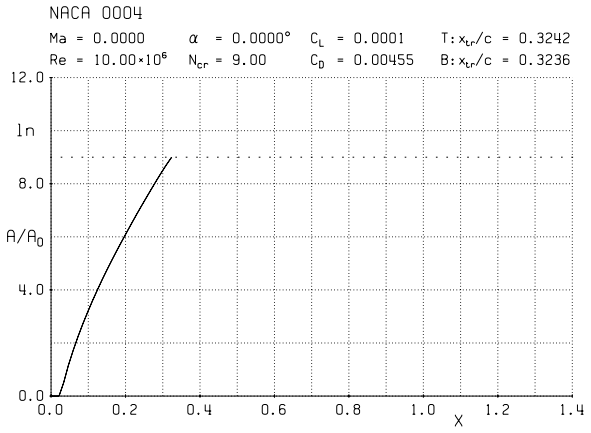
Figure 14.6 demonstrates how the C_f behavior is impacted by changes in Re, and in particular shows that when transition occurs the C_f increases rapidly. We note that for $Re = 10^6$, transition does not occur (using $N_\mathrm{cr} = 9$), while for $Re = 10^7$ the transition occurs at approximately 33% of the chord. And, for $Re = 10^8$, transition occurs within the first few percent of the chord. In both cases, note the rapid increase in C_f as a result of transition to turbulence.



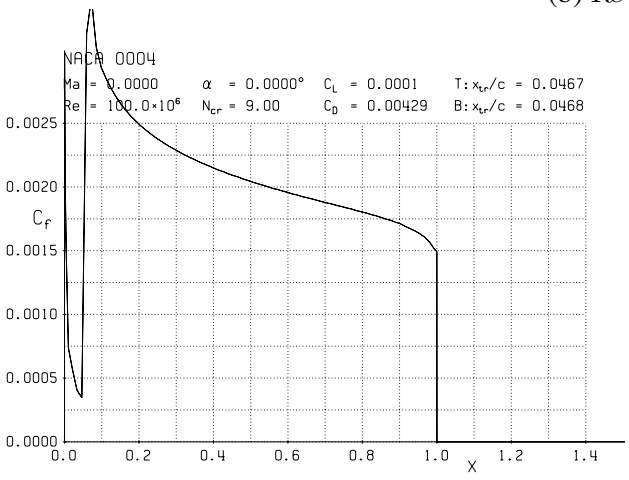


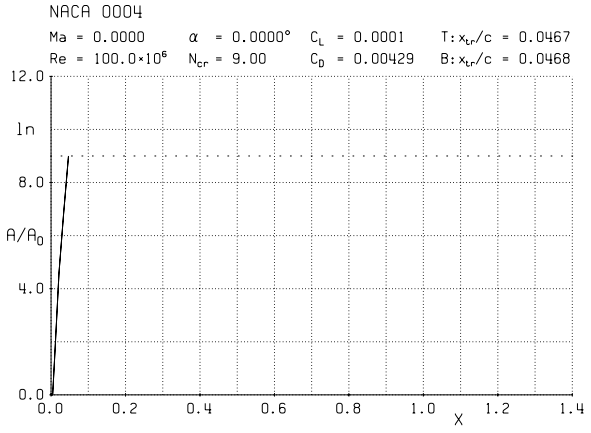
(a) $Re = 10^6$





(b) $Re = 10^7$



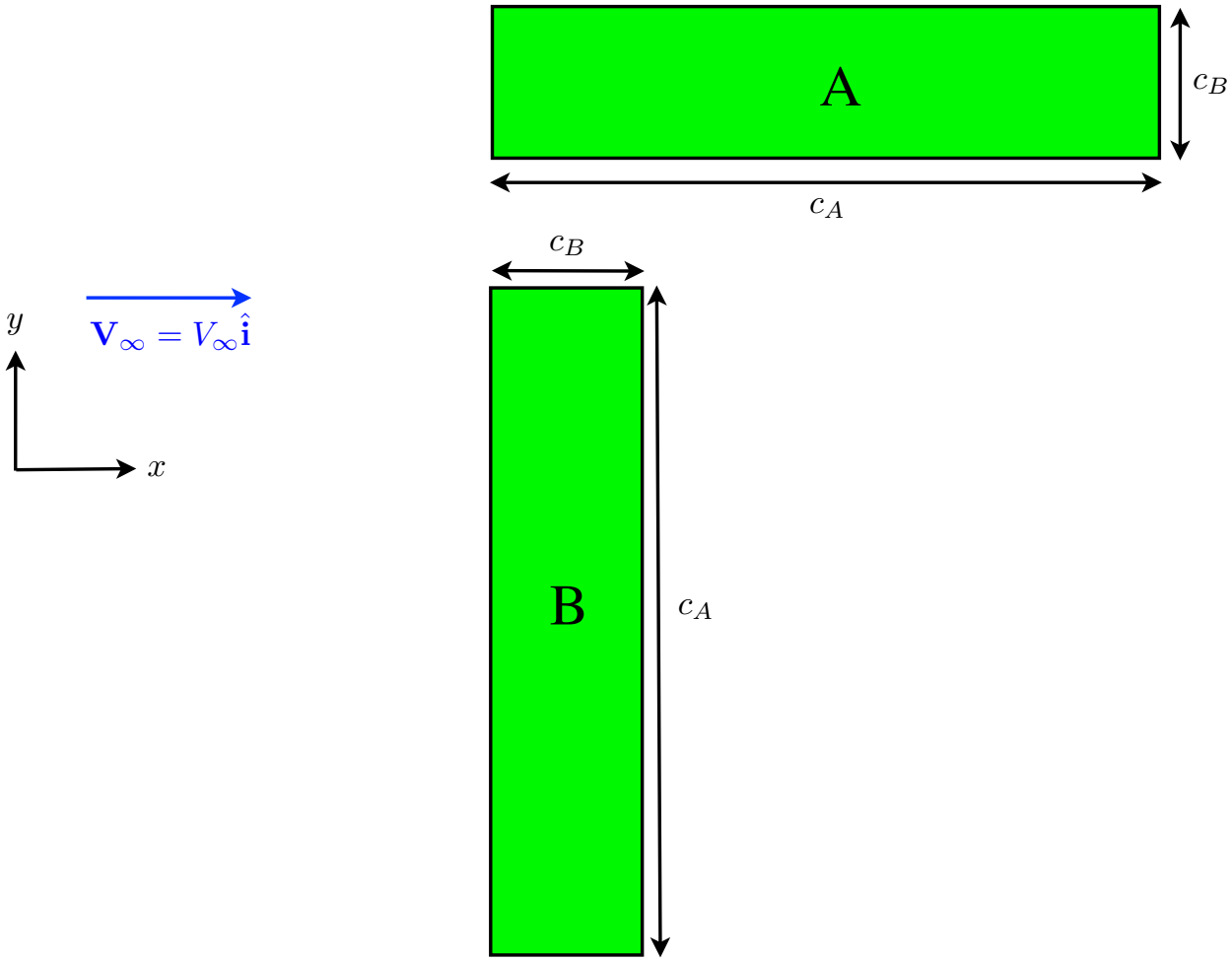


(c) $Re = 10^8$

Figure 14.6: Impact of Re on $C_{\mathrm{f}}(x/c)$ and $N(x/c)$ for NACA 0004 airfoil at $\alpha = 0$

edXproblem: 14.3.4 Dependence of skin friction drag on planform orientation including transition

14.1 | 14.2 | 14.3



Consider a flat plate with dimensions $c_A \times c_B$ (with infinitesimal thickness in the z-direction). Assuming incompressible boundary layer flow with density ρ_∞ and viscosity μ_∞, determine how the drag in the two planform orientations compare to each other. (Note: assume that the freestream velocity is non-zero, so D_A and D_B will be non-zero). You must account for the possibility of transition in your analysis. **Select as many options as are possible.**

edXsolution

Video Link

14.3.5 Turbulence and separation

14.2

While mixing in a turbulent boundary layer leads to an increase in skin friction, the mixing is actually beneficial in terms of separation. As we discussed in Section 13.4.4, separation is a result of adverse pressure gradients which decelerate the flow near the wall eventually leading to a reversal of the flow direction (relative to the flow outside of the boundary layer). However, since turbulent mixing continually brings higher velocity fluid towards the wall, then a turbulent boundary layer will be able to sustain larger increases in pressure before separation occurs (relative to laminar flow).

To demonstrate this behavior, we consider the flow over a NACA 5512 airfoil at $\alpha = 0.5°$. For $Re = 10^5$ with natural transition (see Figure 14.7), the flow separates from the upper surface at approximately $x/c = 0.53$ (this can be determined from where $c_f < 0$). The flow in this separation does transition to turbulence at $x/c = 0.83$, however, it remains separated. The associated table shows the drag and lift coefficient for this flow. The total drag $c_d = 0.02737$ is quite high with most of this drag due to the form drag $c_{d\text{form}} = 0.02030$. The lift is also low with $c_l = 0.4904$ compared to the inviscid (potential flow) value of $c_l = 0.7150$.

A common approach for flows in this Reynolds number regime is to cause turbulent mixing by tripping the flow prior to where separation would otherwise occur. This is shown in Figure 14.8 where the flow on the upper surface has been tripped at $x/c = 0.5$. As the results show, the flow no longer separates and the overall drag is significantly reduced to $c_d = 0.01507$. This reduction is due solely to the decreased form drag which is now $c_{d\text{form}} = 0.00545$; in fact, the skin friction drag has increased because the boundary layer remains attached. The lift, $c_l = 0.5804$, is also higher because of the flow remaining attached.

Finally, we consider natural transition again, but this time at a higher Reynolds number of $Re = 5 \times 10^6$. As shown in Figure 14.9, transition occurs at $x/c = 0.58$ on the upper surface and the flow remains attached without the need for forcing transition. Thus, higher Reynolds number flows will generally be more resistant to separation because of the greater likelihood of turbulence in the boundary layers. We also note for this high Reynolds number case that the lift $c_l = 0.7150$ is nearly the inviscid value.

Re	Transition	c_d	c_{df}	$c_{d\text{form}}$	c_l
10^5	natural	0.02737	0.00707	0.02030	0.4904
10^5	tripped	0.01507	0.00962	0.00545	0.5804
5×10^6	natural	0.00514	0.00429	0.00085	0.7150
Inviscid					0.7575

Table 1: Aerodynamic performance of NACA 5512 at $\alpha = 0.5°$

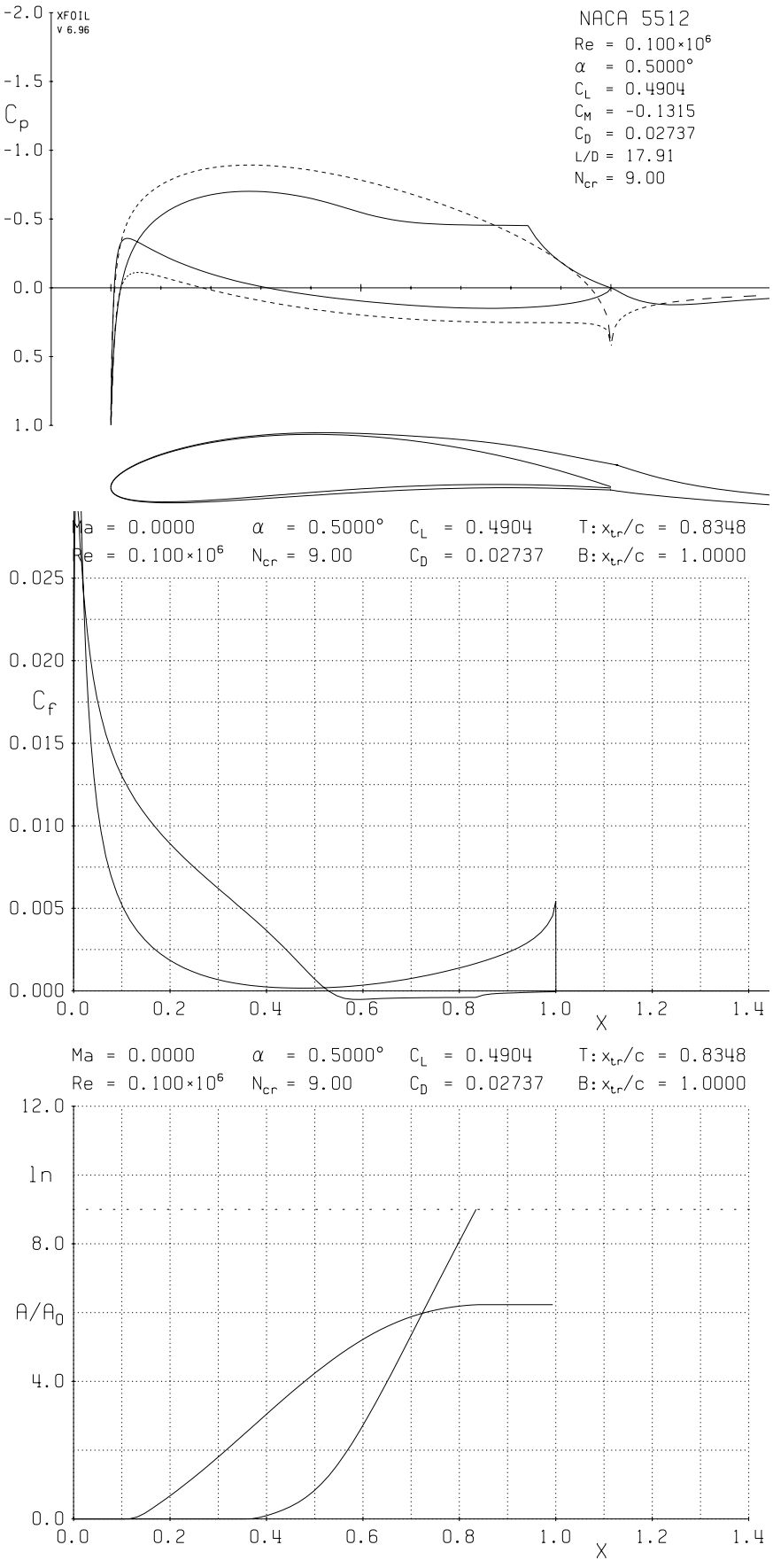


Figure 14.7: NACA 5512 at $\alpha = 0.5°$, $Re = 10^5$, natural transition with $N_{\rm cr} = 9$

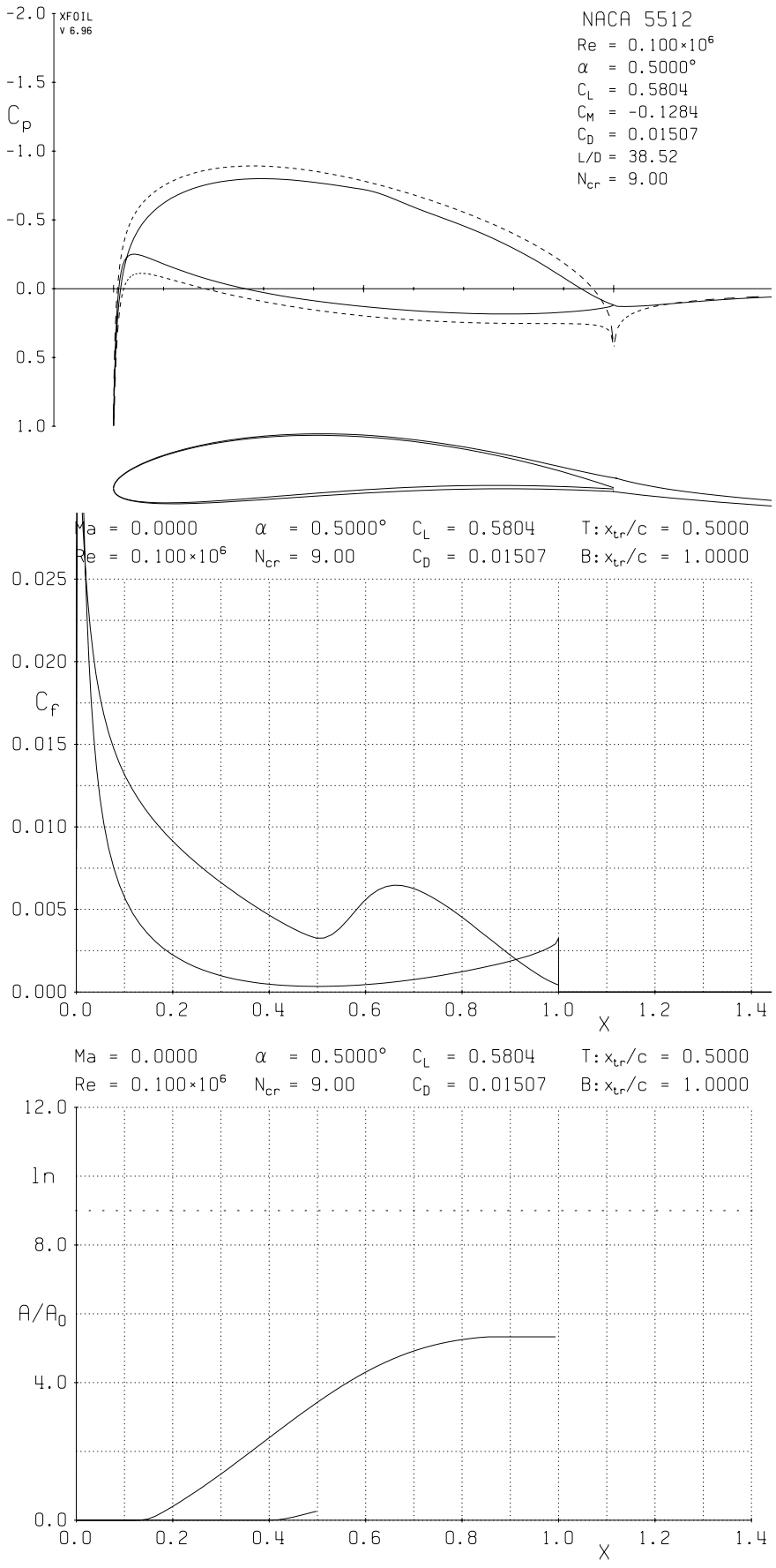


Figure 14.8: NACA 5512 at $\alpha = 0.5°$, $Re = 10^5$, tripped on upper surface at $x/c = 0.5$

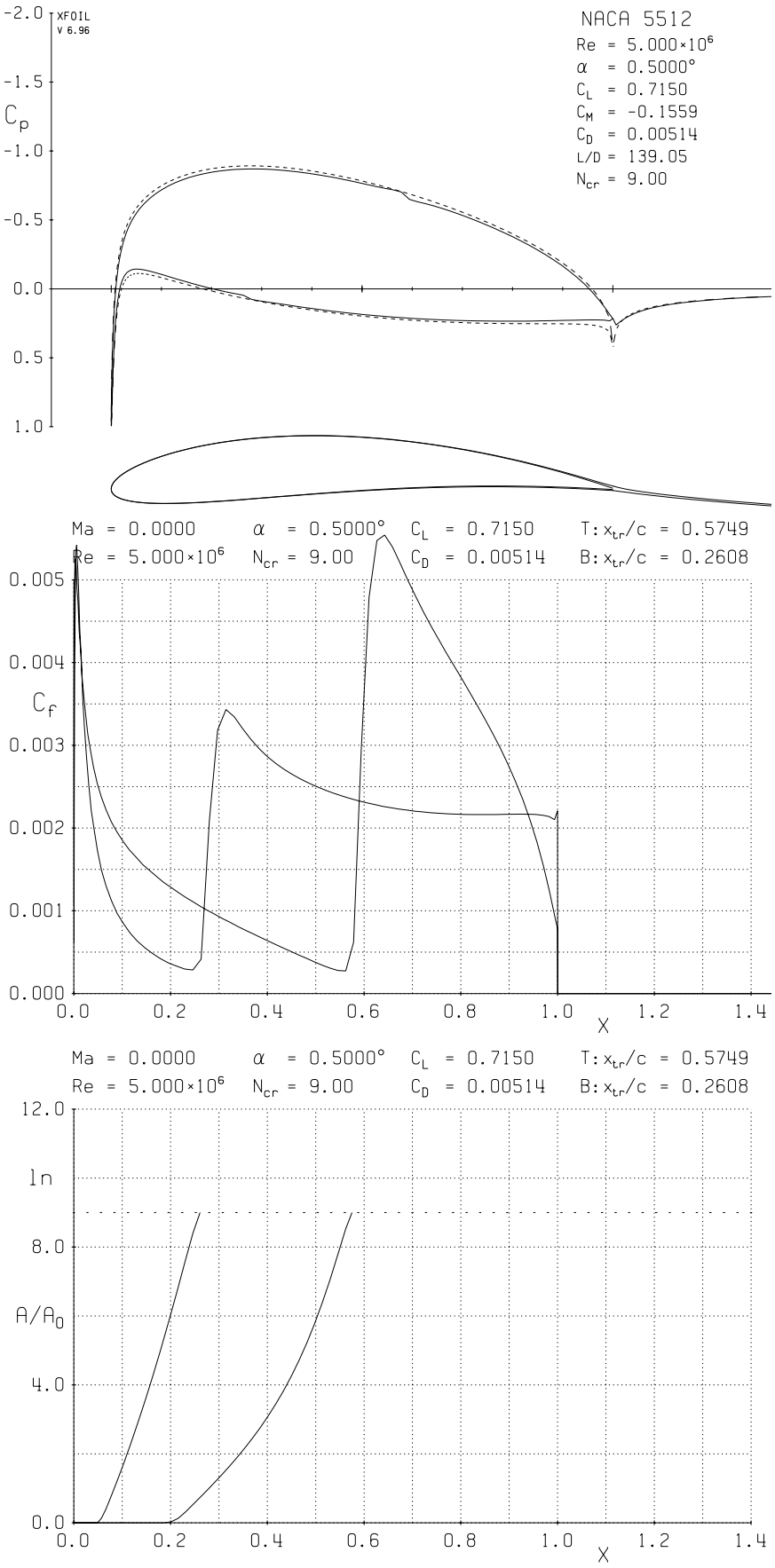


Figure 14.9: NACA 5512 at $\alpha = 0.5°$, $Re = 5 \times 10^6$, natural transition with $N_{\rm cr} = 9$

14.4 Sample Problems

edXproblem: 14.4.1 Wind tunnel testing for transitional airfoil flows

14.1 14.2 14.3

For dynamic similarity, wind tunnel testing requires matching of the Mach number and Reynolds number. However, at low Mach numbers, the effects of compressibility are usually minimal; thus, all that is typically required is to match Reynolds numbers. Even Reynolds number matching can be difficult to do for large aircraft. In this problem, we consider this issue of Reynolds number matching. To begin, let's develop a model for the friction drag in a transitional flow. In the laminar regime, we will use the Blasius flat plate C_f results. In the turbulent flow regime, use the turbulent flow C_f estimate given in Equation (14.21). Determine the friction drag coefficient as a function of Re and x_{tr}/c. Specifically, prove that the drag coefficient from this simple model is,

$$c_d = 2.656 Re^{-1/2} \left(\frac{x_{tr}}{c}\right)^{1/2} + 0.144 Re^{-1/5} \left[1 - \left(\frac{x_{tr}}{c}\right)^{4/5}\right] \tag{14.22}$$

Now, using this formula, calculate the drag coefficients for the following situations:

- The full-scale conditions at $Re = 10^7$. Assume that the flow naturally transitions at $Re_x = 2 \times 10^6$.
- The wind tunnel conditions at $Re = 10^6$. Assume that the flow naturally transitions at $Re_x = 2 \times 10^6$.
- The wind tunnel conditions at $Re = 10^6$. Place a trip on the airfoil surface at the x_{tr}/c location at which the full-scale airfoil transitions (such that the boundary layer now transitions at the correct x/c location).

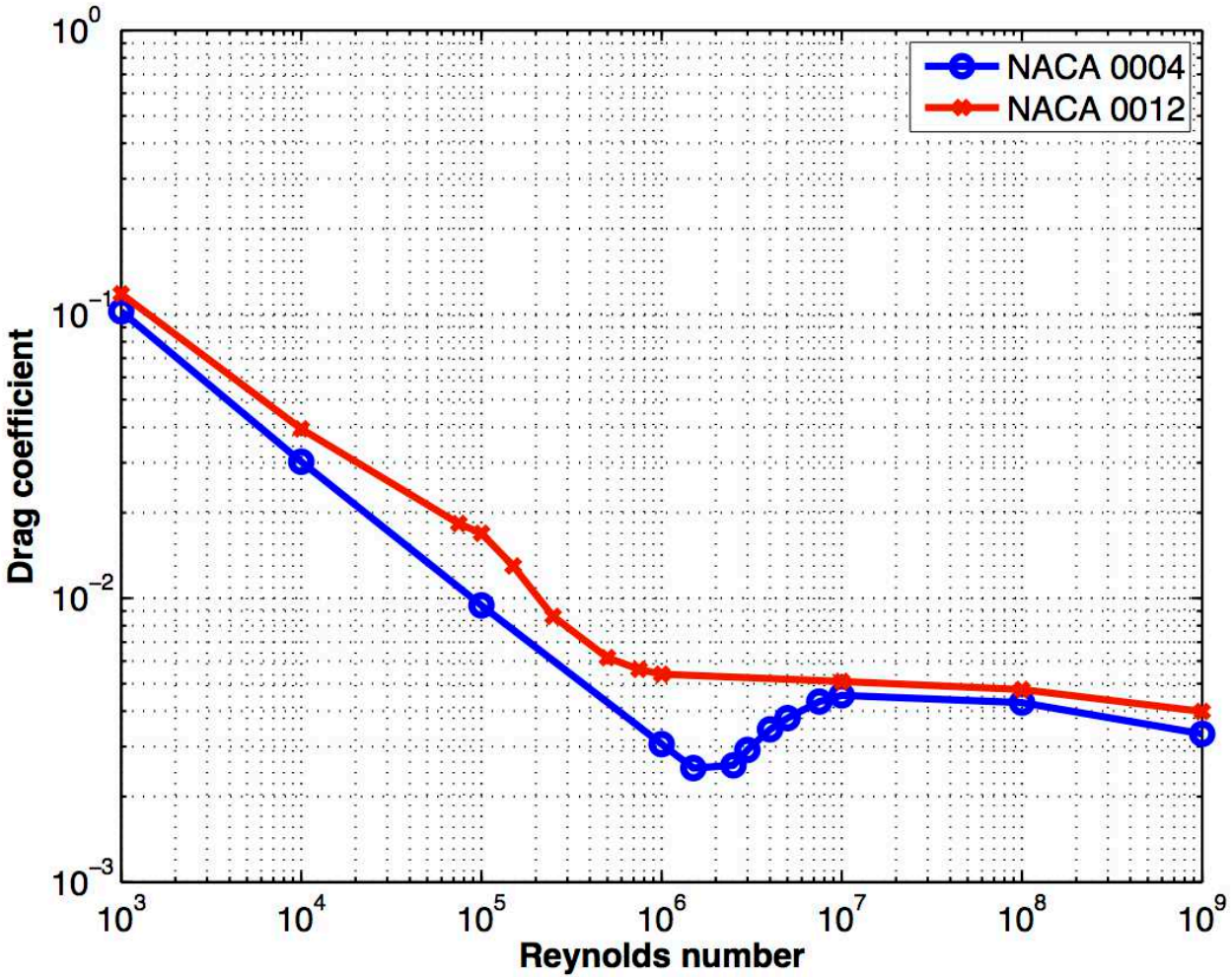
Also, draw a plot of $c_d(Re)$ for natural transition at $Re_x = 2 \times 10^6$ and for x_{tr}/c fixed at the natural transition location for $Re = 10^7$.

edXsolution

Video Link

edXproblem: 14.4.2 Drag versus Reynolds number behavior for thick and thin airfoils

14.1 14.2 14.3



The figure shows the variation of c_d with Re for the NACA 0004 and 0012 airfoils.

- For the NACA 0012 for $Re \leq 10^5$, the slope of c_d versus Re is not $-1/2$ as predicted from flat plate, laminar boundary layer theory. Explain why this is happening by inspecting the boundary layer behavior.
- For Re just greater than 10^5, the drag coefficient on the NACA 0012 drops rapidly. Explain why this is happening by inspecting the boundary layer behavior.
- For the NACA 0004, the drag coefficient changes behavior around $Re = 2 \times 10^6$. Explain why this is happening by inspecting the boundary layer behavior.

In the additional pages of this problem, you will find C_p, C_f, and N distributions versus x/c at the following conditions:

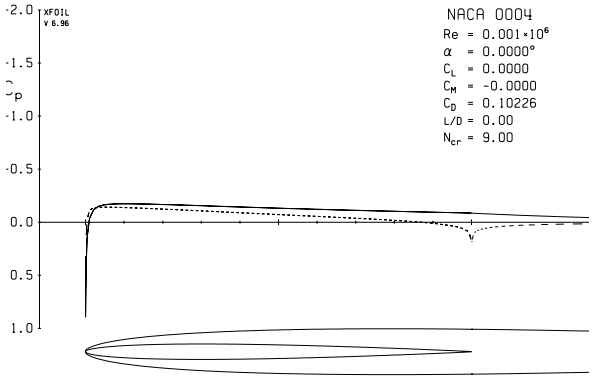
- NACA 0004: Re = 1e3, 1e4, 1e5, 1e6, 2e6, 5e6, 1e7, 1e9
- NACA 0012: Re = 1e3, 1e4, 1e5, 2e5, 5e5, 1e6, 1e7, 1e9

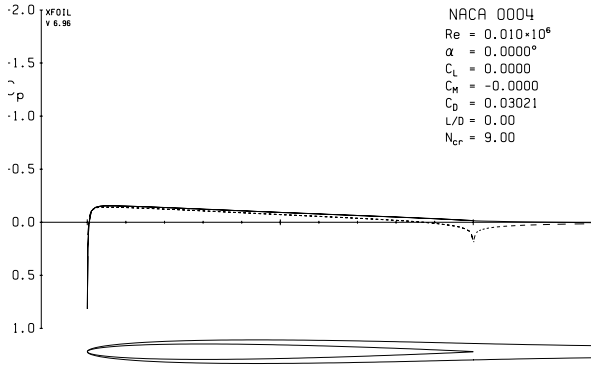
Use these plots to answer the questions above.

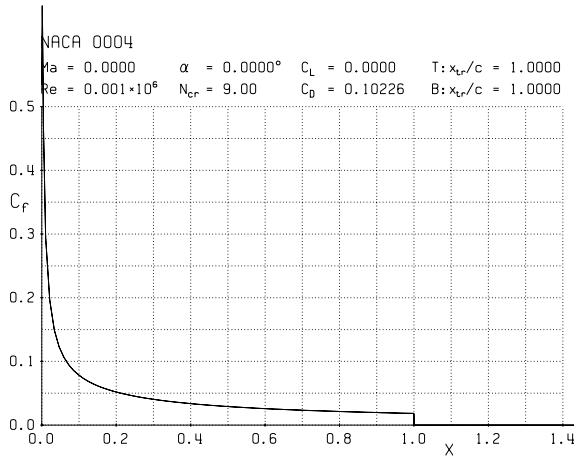
edXsolution

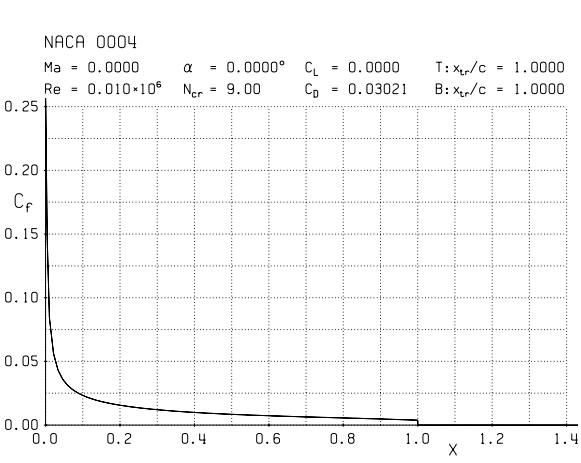
Video Link

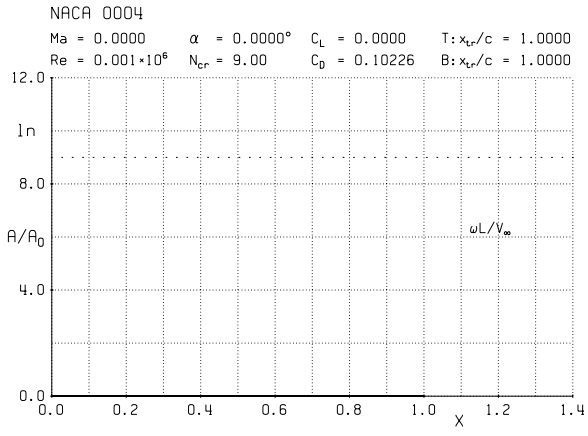
NACA 0004 plots

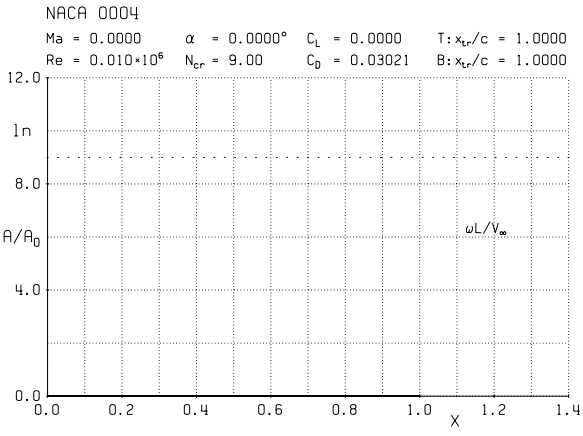


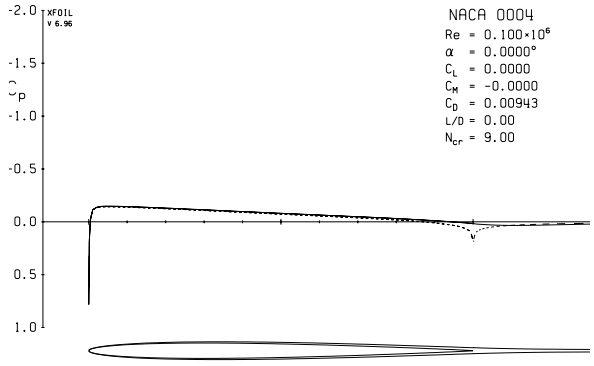


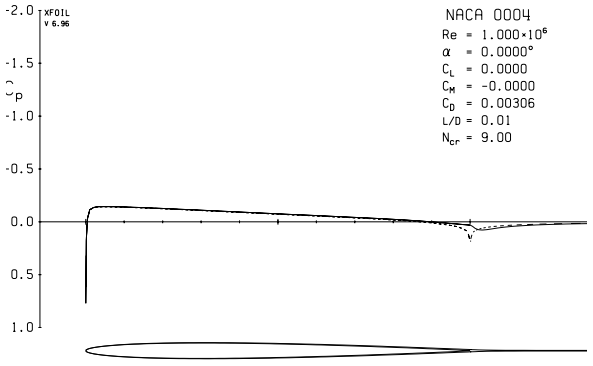


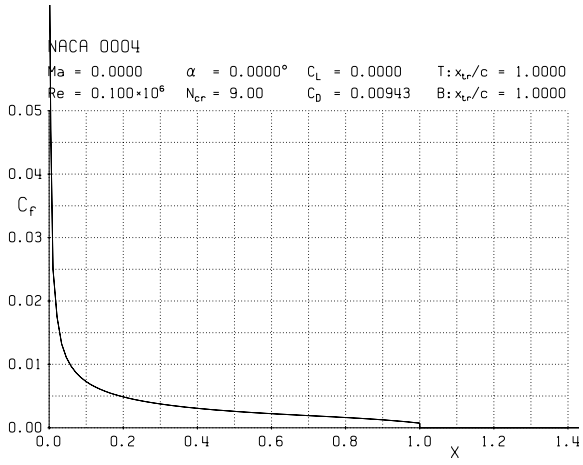


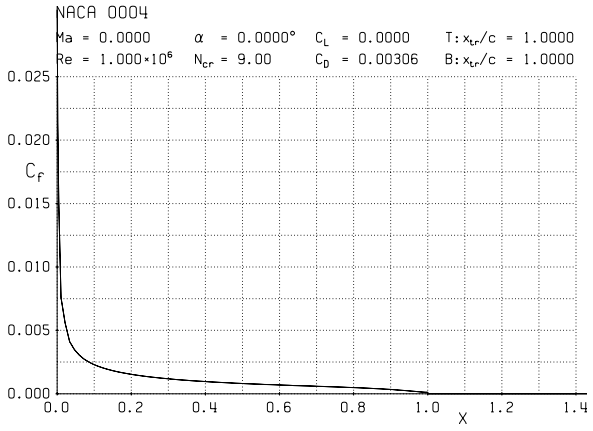


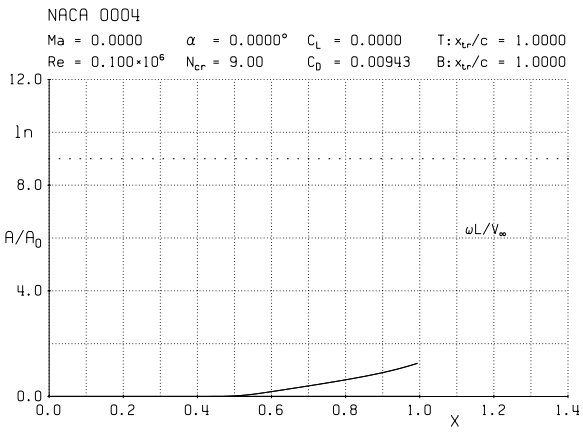


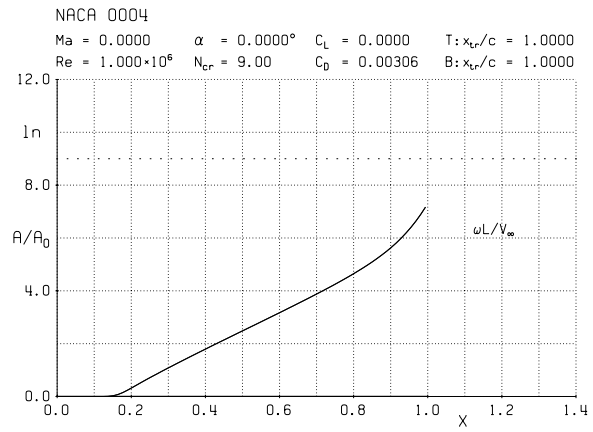

XFOIL
v 6.96
NACA 0004
Re = 0.100×10^6
α = 0.0000°
C_L = 0.0000
C_M = -0.0000
C_D = 0.00943
L/D = 0.00
N_cr = 9.00
-2.0
-1.5
-1.0
-0.5
0.0
0.5
1.0
C_p

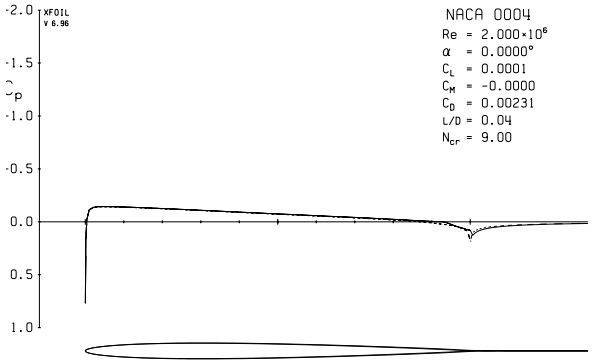

XFOIL
v 6.96
NACA 0004
Re = 1.000×10^6
α = 0.0000°
C_L = 0.0000
C_M = -0.0000
C_D = 0.00306
L/D = 0.01
N_cr = 9.00
-2.0
-1.5
-1.0
-0.5
0.0
0.5
1.0
C_p

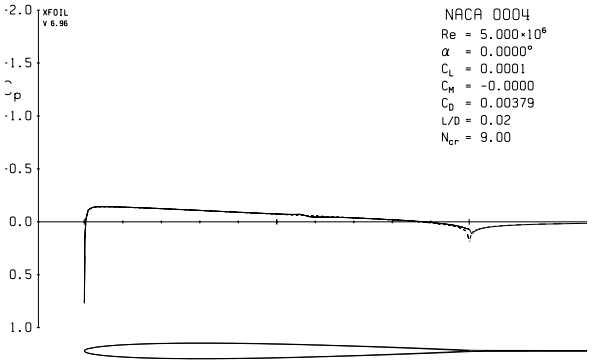

NACA 0004
Ma = 0.0000 α = 0.0000° C_L = 0.0000 T: x_tr/c = 1.0000
Re = 0.100×10^6 N_cr = 9.00 C_D = 0.00943 B: x_tr/c = 1.0000
C_f
X
0.00
0.01
0.02
0.03
0.04
0.05
0.0
0.2
0.4
0.6
0.8
1.0
1.2
1.4

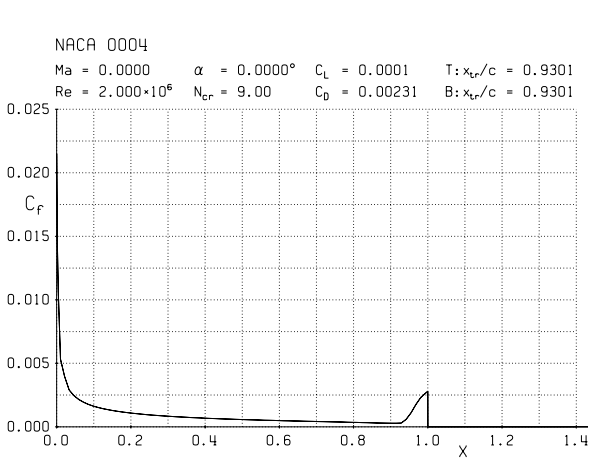

NACA 0004
Ma = 0.0000 α = 0.0000° C_L = 0.0000 T: x_tr/c = 1.0000
Re = 1.000×10^6 N_cr = 9.00 C_D = 0.00306 B: x_tr/c = 1.0000
C_f
X
0.000
0.005
0.010
0.015
0.020
0.025
0.0
0.2
0.4
0.6
0.8
1.0
1.2
1.4

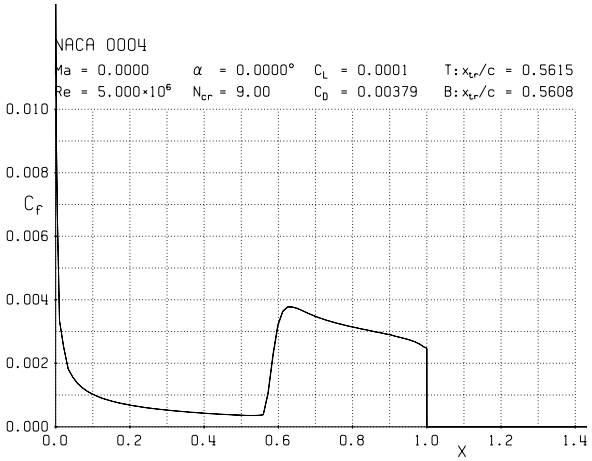

NACA 0004
Ma = 0.0000 α = 0.0000° C_L = 0.0000 T: x_tr/c = 1.0000
Re = 0.100×10^6 N_cr = 9.00 C_D = 0.00943 B: x_tr/c = 1.0000
ln A/A_0
ωL/V_∞
X
0.0
4.0
8.0
12.0
0.0
0.2
0.4
0.6
0.8
1.0
1.2
1.4

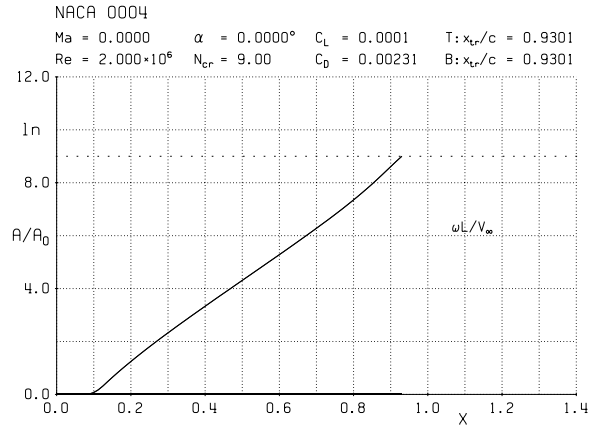

NACA 0004
Ma = 0.0000 α = 0.0000° C_L = 0.0000 T: x_tr/c = 1.0000
Re = 1.000×10^6 N_cr = 9.00 C_D = 0.00306 B: x_tr/c = 1.0000
ln A/A_0
ωL/V_∞
X
0.0
4.0
8.0
12.0
0.0
0.2
0.4
0.6
0.8
1.0
1.2
1.4

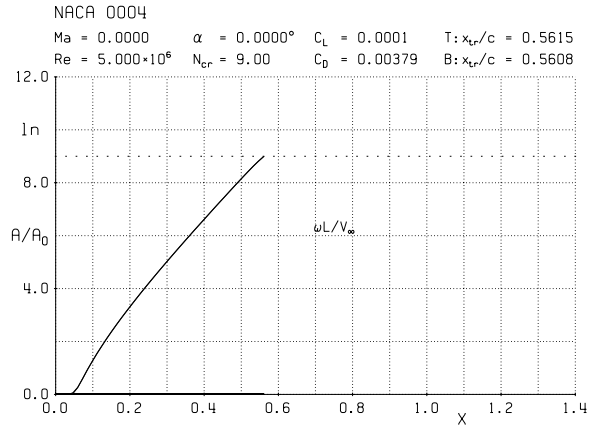

XFOIL
v 6.96
NACA 0004
Re = 2.000×10^6
α = 0.0000°
C_L = 0.0001
C_M = -0.0000
C_D = 0.00231
L/D = 0.04
N_cr = 9.00
-C_p

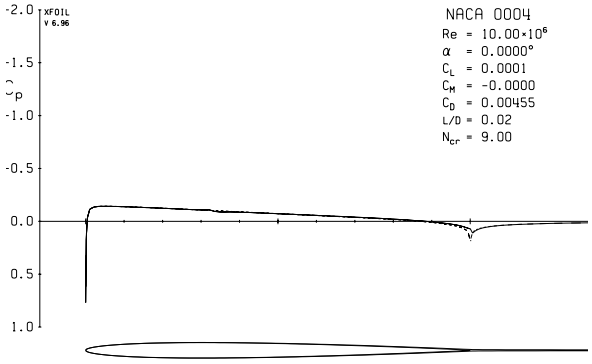

XFOIL
v 6.96
NACA 0004
Re = 5.000×10^6
α = 0.0000°
C_L = 0.0001
C_M = -0.0000
C_D = 0.00379
L/D = 0.02
N_cr = 9.00
-C_p

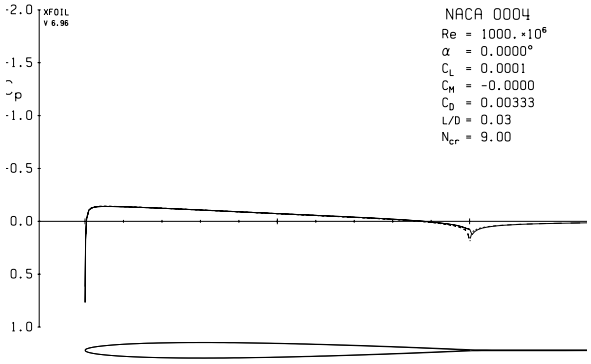

NACA 0004
Ma = 0.0000 α = 0.0000° C_L = 0.0001 T: x_tr/c = 0.9301
Re = 2.000×10^6 N_cr = 9.00 C_D = 0.00231 B: x_tr/c = 0.9301
C_f
X

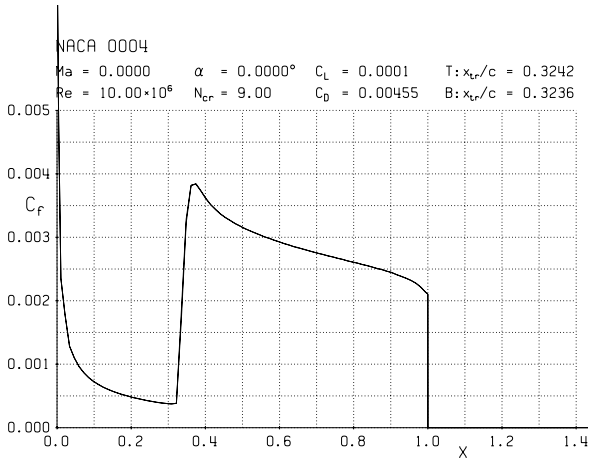

NACA 0004
Ma = 0.0000 α = 0.0000° C_L = 0.0001 T: x_tr/c = 0.5615
Re = 5.000×10^6 N_cr = 9.00 C_D = 0.00379 B: x_tr/c = 0.5608
C_f
X

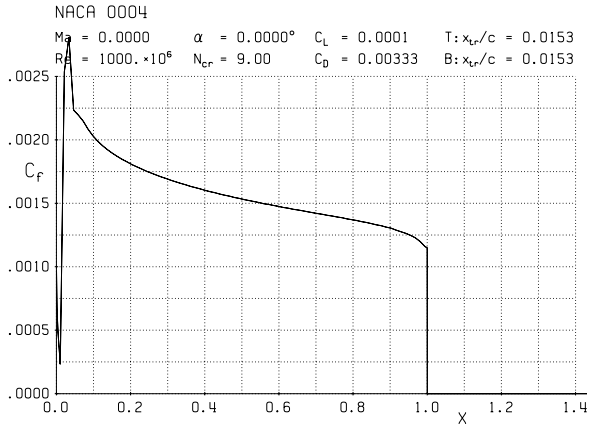

NACA 0004
Ma = 0.0000 α = 0.0000° C_L = 0.0001 T: x_tr/c = 0.9301
Re = 2.000×10^6 N_cr = 9.00 C_D = 0.00231 B: x_tr/c = 0.9301
ln
A/A_0
ωL/V_∞
X

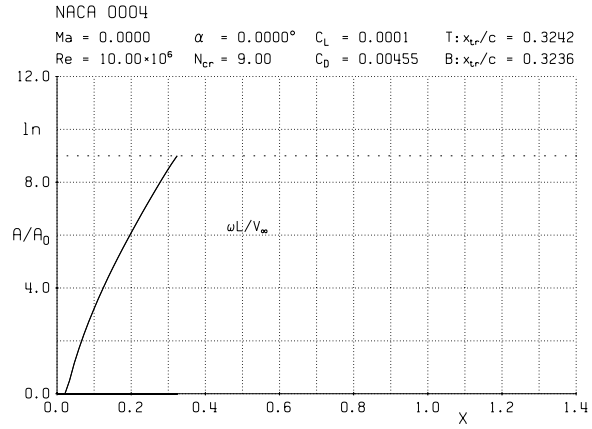

NACA 0004
Ma = 0.0000 α = 0.0000° C_L = 0.0001 T: x_tr/c = 0.5615
Re = 5.000×10^6 N_cr = 9.00 C_D = 0.00379 B: x_tr/c = 0.5608
ln
A/A_0
ωL/V_∞
X

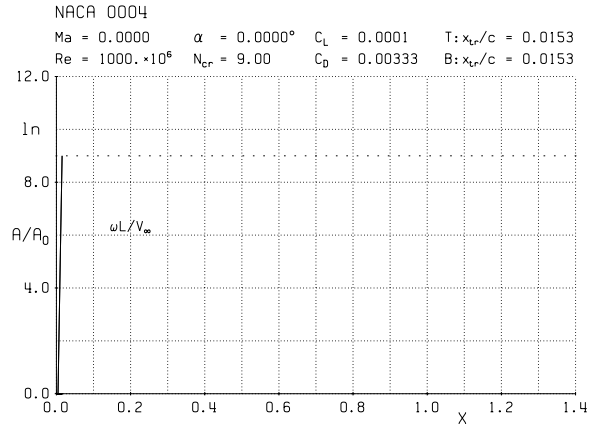

XFOIL
v 6.96
NACA 0004
Re = 10.00×10⁶
α = 0.0000°
C_L = 0.0001
C_M = -0.0000
C_D = 0.00455
L/D = 0.02
N_cr = 9.00
-2.0
-1.5
-1.0
-0.5
0.0
0.5
1.0
C_p


XFOIL
v 6.96
NACA 0004
Re = 1000.×10⁶
α = 0.0000°
C_L = 0.0001
C_M = -0.0000
C_D = 0.00333
L/D = 0.03
N_cr = 9.00
-2.0
-1.5
-1.0
-0.5
0.0
0.5
1.0
C_p

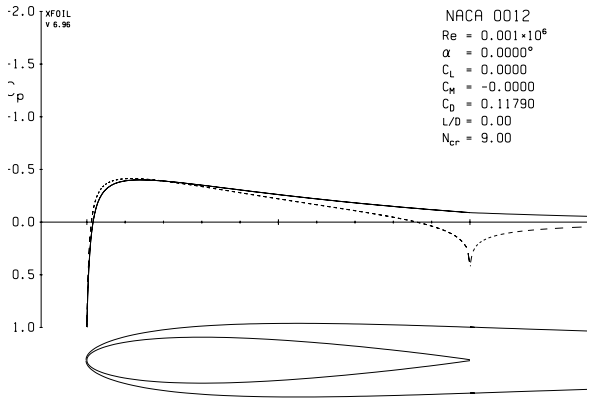

NACA 0004
Ma = 0.0000 α = 0.0000° C_L = 0.0001 T: x_tr/c = 0.3242
Re = 10.00×10⁶ N_cr = 9.00 C_D = 0.00455 B: x_tr/c = 0.3236
0.005
0.004
0.003
0.002
0.001
0.000
C_f
0.0
0.2
0.4
0.6
0.8
1.0
1.2
1.4
X

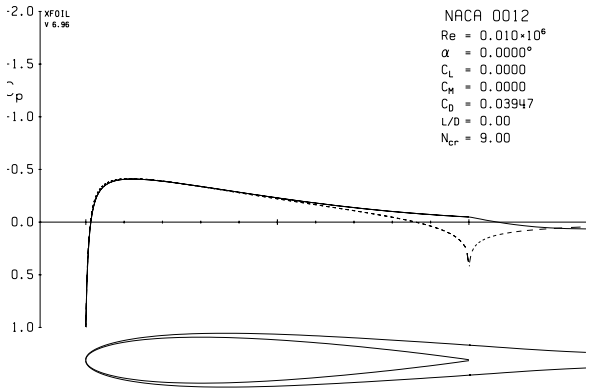

NACA 0004
Ma = 0.0000 α = 0.0000° C_L = 0.0001 T: x_tr/c = 0.0153
Re = 1000.×10⁶ N_cr = 9.00 C_D = 0.00333 B: x_tr/c = 0.0153
.0025
.0020
.0015
.0010
.0005
.0000
C_f
0.0
0.2
0.4
0.6
0.8
1.0
1.2
1.4
X

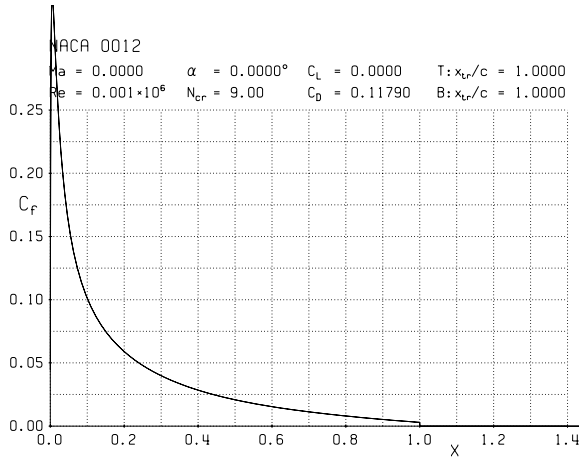

NACA 0004
Ma = 0.0000 α = 0.0000° C_L = 0.0001 T: x_tr/c = 0.3242
Re = 10.00×10⁶ N_cr = 9.00 C_D = 0.00455 B: x_tr/c = 0.3236
12.0
8.0
4.0
0.0
ln
A/A_0
ωL/V_∞
0.0
0.2
0.4
0.6
0.8
1.0
1.2
1.4
X

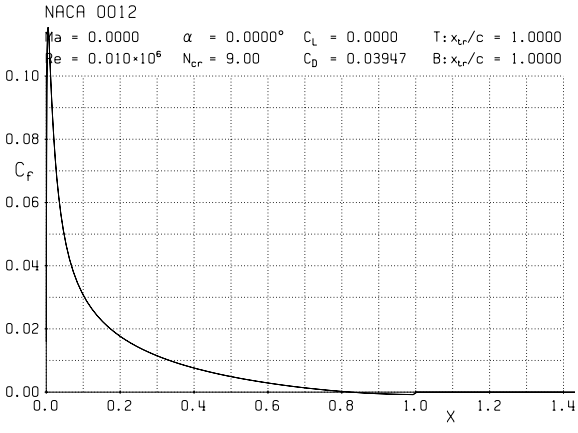

NACA 0004
Ma = 0.0000 α = 0.0000° C_L = 0.0001 T: x_tr/c = 0.0153
Re = 1000.×10⁶ N_cr = 9.00 C_D = 0.00333 B: x_tr/c = 0.0153
12.0
8.0
4.0
0.0
ln
A/A_0
ωL/V_∞
0.0
0.2
0.4
0.6
0.8
1.0
1.2
1.4
X

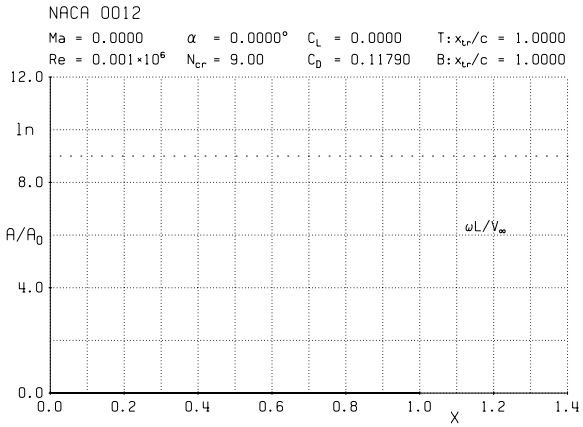
NACA 0012 plots

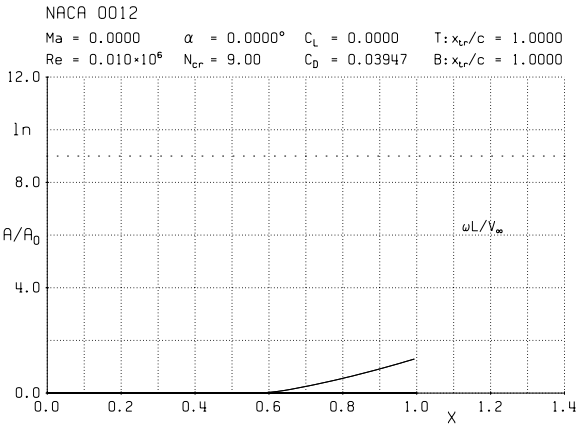


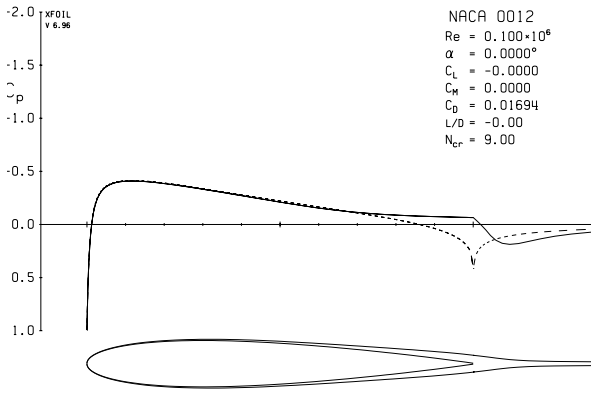


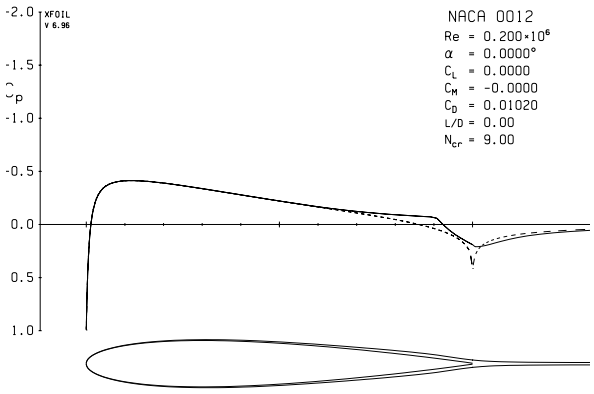


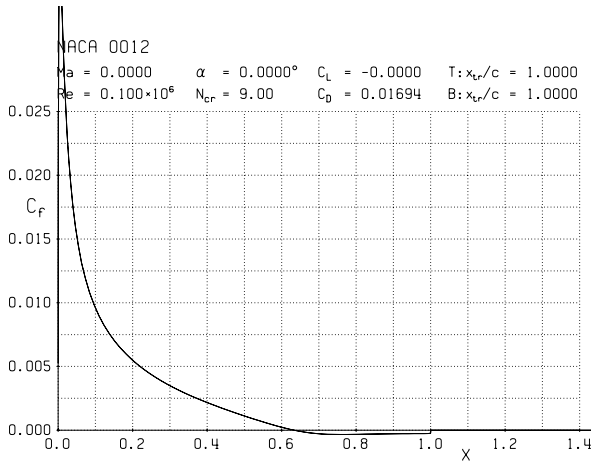


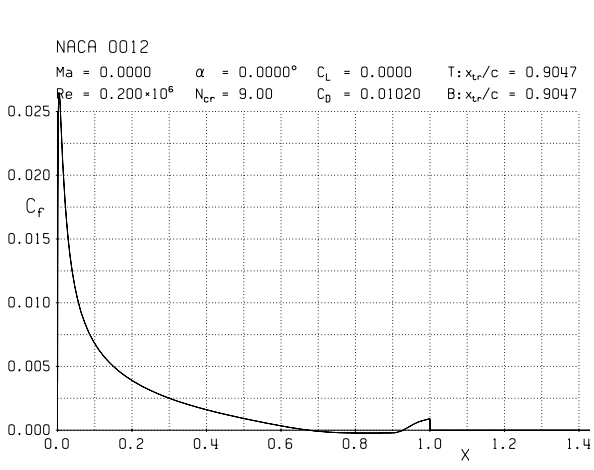


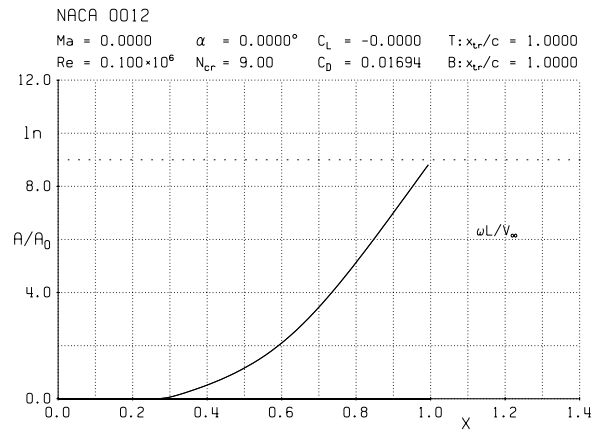


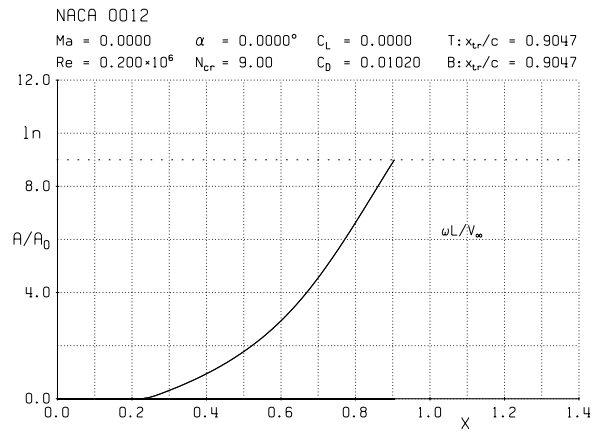

XFOIL
v 6.96
NACA 0012
Re = 0.100×10^6
α = 0.0000°
C_L = -0.0000
C_M = 0.0000
C_D = 0.01694
L/D = -0.00
N_cr = 9.00
C_p

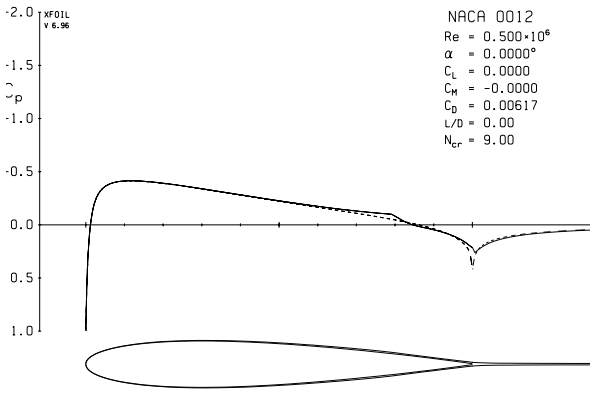

XFOIL
v 6.96
NACA 0012
Re = 0.200×10^6
α = 0.0000°
C_L = 0.0000
C_M = -0.0000
C_D = 0.01020
L/D = 0.00
N_cr = 9.00
C_p

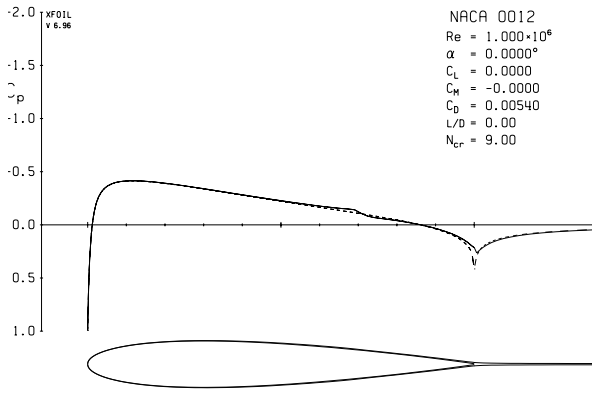

NACA 0012
Ma = 0.0000 α = 0.0000° C_L = -0.0000 T: x_tr/c = 1.0000
Re = 0.100×10^6 N_cr = 9.00 C_D = 0.01694 B: x_tr/c = 1.0000
C_f
X

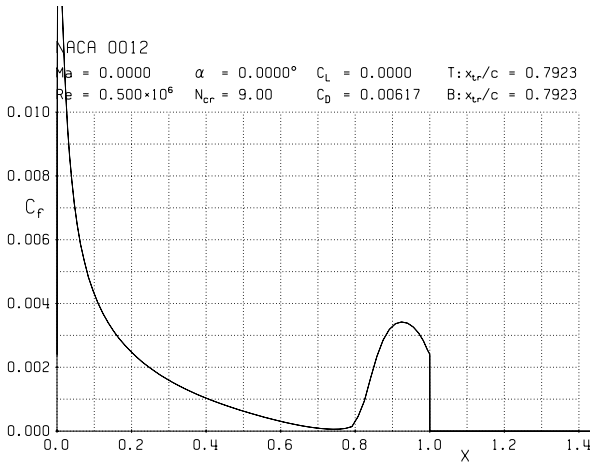

NACA 0012
Ma = 0.0000 α = 0.0000° C_L = 0.0000 T: x_tr/c = 0.9047
Re = 0.200×10^6 N_cr = 9.00 C_D = 0.01020 B: x_tr/c = 0.9047
C_f
X

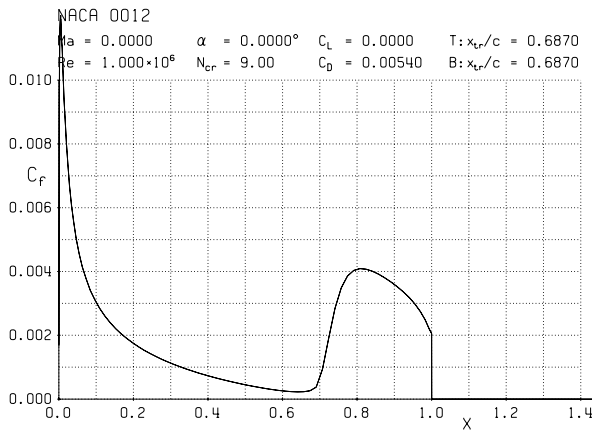

NACA 0012
Ma = 0.0000 α = 0.0000° C_L = -0.0000 T: x_tr/c = 1.0000
Re = 0.100×10^6 N_cr = 9.00 C_D = 0.01694 B: x_tr/c = 1.0000
ln
A/A_0
ωL/V_∞
X

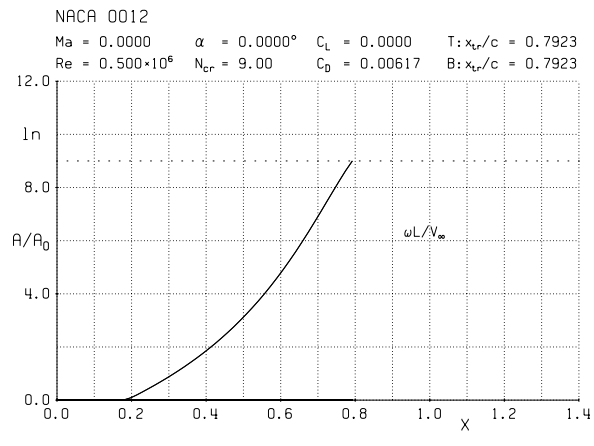

NACA 0012
Ma = 0.0000 α = 0.0000° C_L = 0.0000 T: x_tr/c = 0.9047
Re = 0.200×10^6 N_cr = 9.00 C_D = 0.01020 B: x_tr/c = 0.9047
ln
A/A_0
ωL/V_∞
X

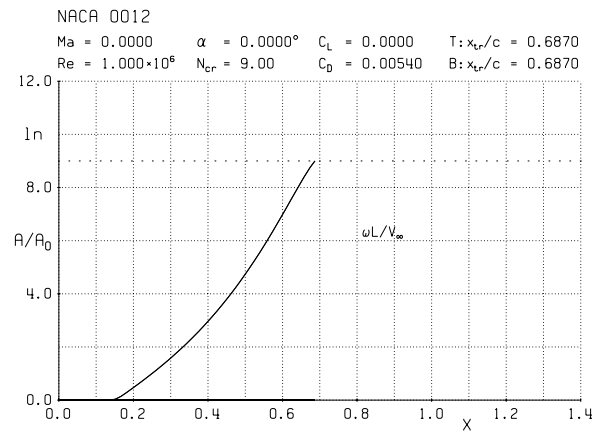

XFOIL
v 6.96
NACA 0012
Re = 0.500×10^6
α = 0.0000°
C_L = 0.0000
C_M = -0.0000
C_D = 0.00617
L/D = 0.00
N_cr = 9.00
-2.0
-1.5
-1.0
-0.5
0.0
0.5
1.0
C_p

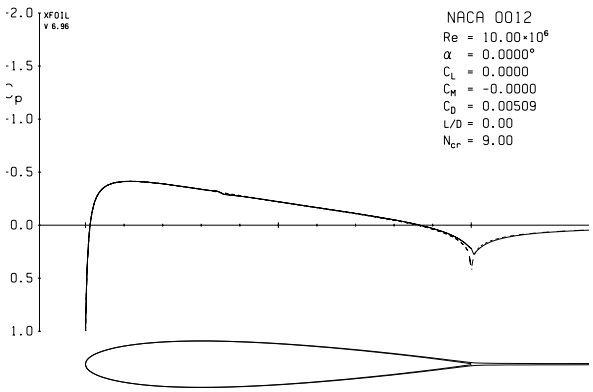

XFOIL
v 6.96
NACA 0012
Re = 1.000×10^6
α = 0.0000°
C_L = 0.0000
C_M = -0.0000
C_D = 0.00540
L/D = 0.00
N_cr = 9.00
-2.0
-1.5
-1.0
-0.5
0.0
0.5
1.0
C_p

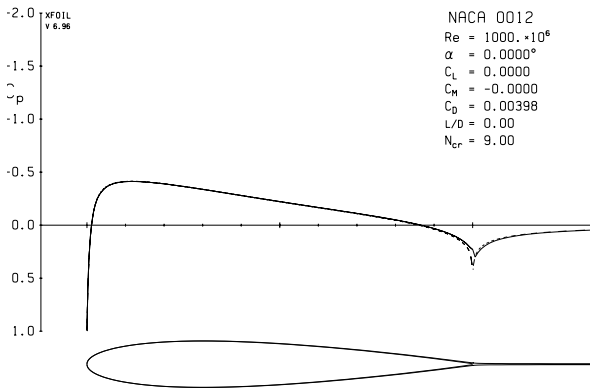

NACA 0012
Ma = 0.0000 α = 0.0000° C_L = 0.0000 T: x_tr/c = 0.7923
Re = 0.500×10^6 N_cr = 9.00 C_D = 0.00617 B: x_tr/c = 0.7923
0.010
0.008
C_f
0.006
0.004
0.002
0.000
0.0
0.2
0.4
0.6
0.8
1.0
1.2
1.4
X

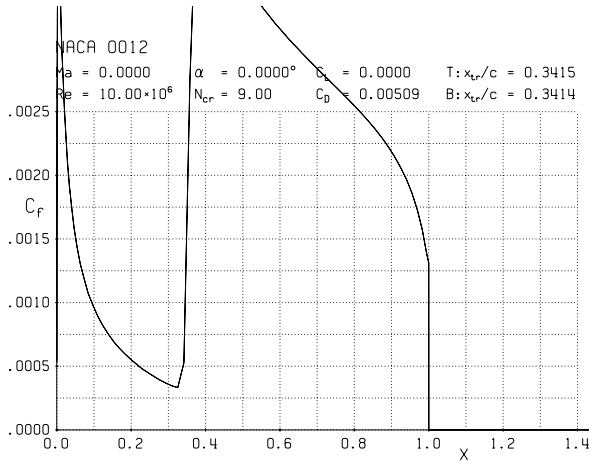

NACA 0012
Ma = 0.0000 α = 0.0000° C_L = 0.0000 T: x_tr/c = 0.6870
Re = 1.000×10^6 N_cr = 9.00 C_D = 0.00540 B: x_tr/c = 0.6870
0.010
0.008
C_f
0.006
0.004
0.002
0.000
0.0
0.2
0.4
0.6
0.8
1.0
1.2
1.4
X

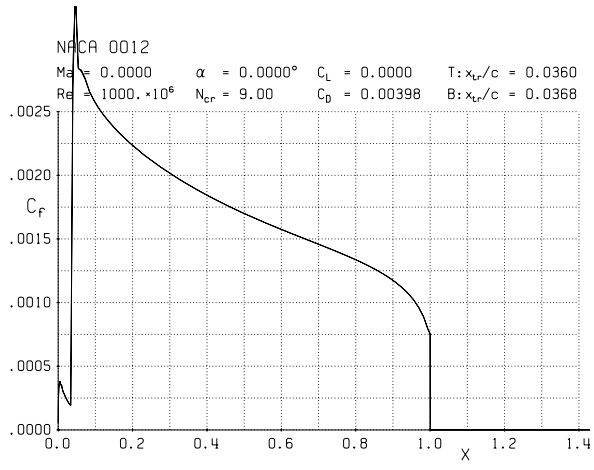

NACA 0012
Ma = 0.0000 α = 0.0000° C_L = 0.0000 T: x_tr/c = 0.7923
Re = 0.500×10^6 N_cr = 9.00 C_D = 0.00617 B: x_tr/c = 0.7923
12.0
ln
8.0
A/A_0
4.0
0.0
ωL/V_∞
0.0
0.2
0.4
0.6
0.8
1.0
1.2
1.4
X

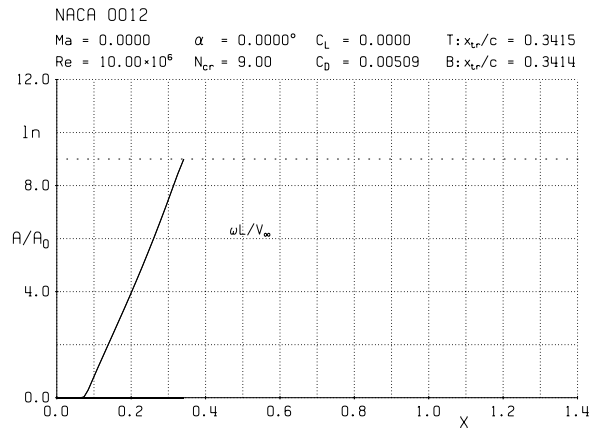

NACA 0012
Ma = 0.0000 α = 0.0000° C_L = 0.0000 T: x_tr/c = 0.6870
Re = 1.000×10^6 N_cr = 9.00 C_D = 0.00540 B: x_tr/c = 0.6870
12.0
ln
8.0
A/A_0
4.0
0.0
ωL/V_∞
0.0
0.2
0.4
0.6
0.8
1.0
1.2
1.4
X

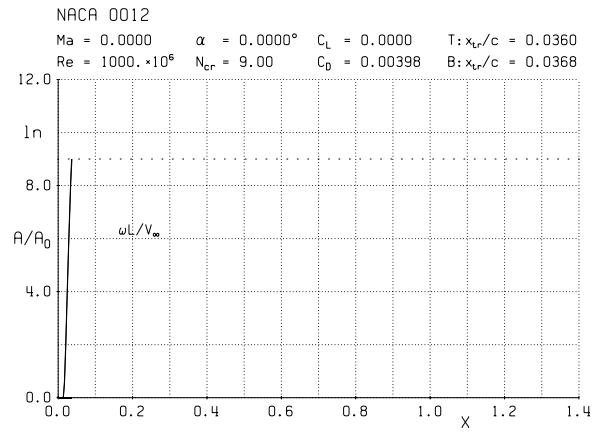

XFOIL
v 6.96
NACA 0012
Re = 10.00×10⁶
α = 0.0000°
C_L = 0.0000
C_M = -0.0000
C_D = 0.00509
L/D = 0.00
N_cr = 9.00
-2.0
-1.5
-1.0
-0.5
0.0
0.5
1.0
Cp


XFOIL
v 6.96
NACA 0012
Re = 1000.×10⁶
α = 0.0000°
C_L = 0.0000
C_M = -0.0000
C_D = 0.00398
L/D = 0.00
N_cr = 9.00
-2.0
-1.5
-1.0
-0.5
0.0
0.5
1.0
Cp


NACA 0012
Ma = 0.0000 α = 0.0000° C_L = 0.0000 T: x_tr/c = 0.3415
Re = 10.00×10⁶ N_cr = 9.00 C_D = 0.00509 B: x_tr/c = 0.3414
.0025
.0020
.0015
.0010
.0005
.0000
C_f
0.0
0.2
0.4
0.6
0.8
1.0
1.2
1.4
X


NACA 0012
Ma = 0.0000 α = 0.0000° C_L = 0.0000 T: x_tr/c = 0.0360
Re = 1000.×10⁶ N_cr = 9.00 C_D = 0.00398 B: x_tr/c = 0.0368
.0025
.0020
.0015
.0010
.0005
.0000
C_f
0.0
0.2
0.4
0.6
0.8
1.0
1.2
1.4
X


NACA 0012
Ma = 0.0000 α = 0.0000° C_L = 0.0000 T: x_tr/c = 0.3415
Re = 10.00×10⁶ N_cr = 9.00 C_D = 0.00509 B: x_tr/c = 0.3414
12.0
8.0
4.0
0.0
ln
A/A0
ωL/V∞
0.0
0.2
0.4
0.6
0.8
1.0
1.2
1.4
X

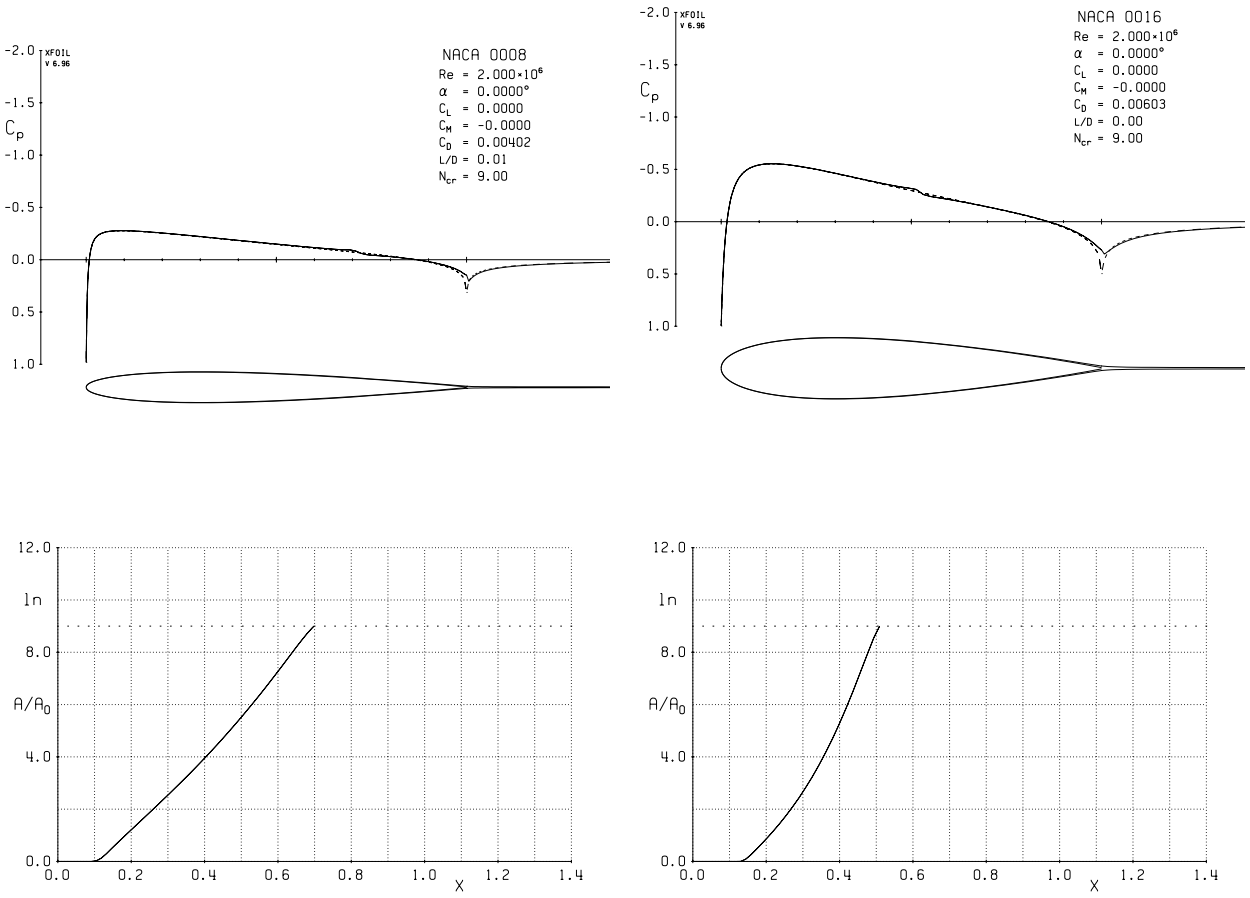

NACA 0012
Ma = 0.0000 α = 0.0000° C_L = 0.0000 T: x_tr/c = 0.0360
Re = 1000.×10⁶ N_cr = 9.00 C_D = 0.00398 B: x_tr/c = 0.0368
12.0
8.0
4.0
0.0
ln
A/A0
ωL/V∞
0.0
0.2
0.4
0.6
0.8
1.0
1.2
1.4
X

14.5 Homework Problems

edXproblem: 14.5.1 Comparison of transitional flow over NACA 0008 and 0016 airfoils

14.1 | 14.2 | 14.3

According to spatial stability analysis of a laminar flat plate flow in Section 14.2.3, what is the value of x/c for which instability would first appear on a flat plate with $Re = 2 \times 10^6$? Provide your answer with two digits of precision in the form X.YeP.



The above results show $C_p(x)$ and $N(x)$ for a NACA 0008 and NACA 0016 airfoil at $Re = 2 \times 10^6$ and zero angle of attack.

According to these results, what is the value of x/c for which instability first appears on the NACA 0008? Provide your answer with two digits of precision in the form X.YeP.

According to these results, what is the value of x/c for which instability first appears on the NACA 0016? Provide your answer with two digits of precision in the form X.YeP.

According to the previous plots, for a value of $N_{\text{cr}} = 9$, what is the value of x/c for which transition occurs on the NACA 0008? Provide your answer with one digit of precision in the form 0.X.

According to the previous plots, for a value of $N_{\text{cr}} = 9$, what is the value of x/c for which transition occurs on the NACA 0016? Provide your answer with one digit of precision in the form 0.X.

Using the drag estimate in Equation (14.22) and the transition locations determined above, estimate the friction drag coefficient for the NACA 0008 and NACA 0016 airfoils.

Enter your estimate for the friction drag coefficient for the NACA 0008. Provide your answer with two significant digits of precision in the form X.YeP.

Enter your estimate for the friction drag coefficient for the NACA 0016. Provide your answer with two significant digits of precision in the form X.YeP.

edXsolution

Video Link

edXproblem: 14.5.2 Airfoil flow classification

14.1 | 14.2 | 14.3

In this problem, you will identify various aspects of different airfoil flows based on plots of C_p, C_f, and N. The flow conditions are chosen among the following options:

- All of the flows are incompressible.
- The Reynolds number is one of the following three values: $Re = 10^4$, 10^6, or 10^8.
- Transition could occur naturally or transition could be forced by using a trip on the surface of the airfoil.
- The results are either from an atmospheric flight test in which the level of freestream turbulence is low (simulated using $N_{cr} = 9$), or from a wind tunnel test in which the level of freestream turbulence is high (simulated using $N_{cr} = 4$).

Flow 1

Select all of the options that apply:

Flow 2

Select all of the options that apply:

Flow 3

Select all of the options that apply:

Flow 4

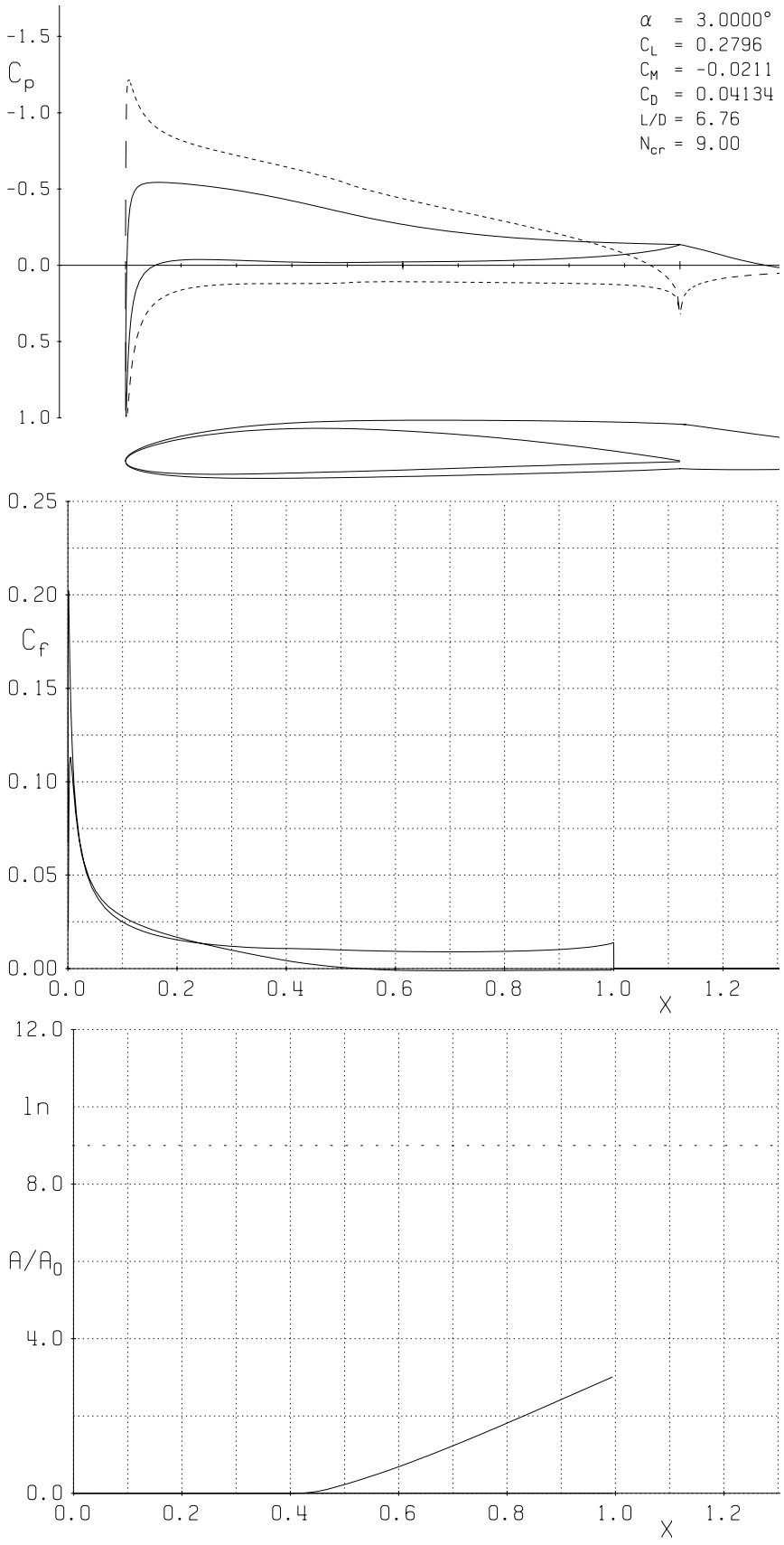
Select all of the options that apply:

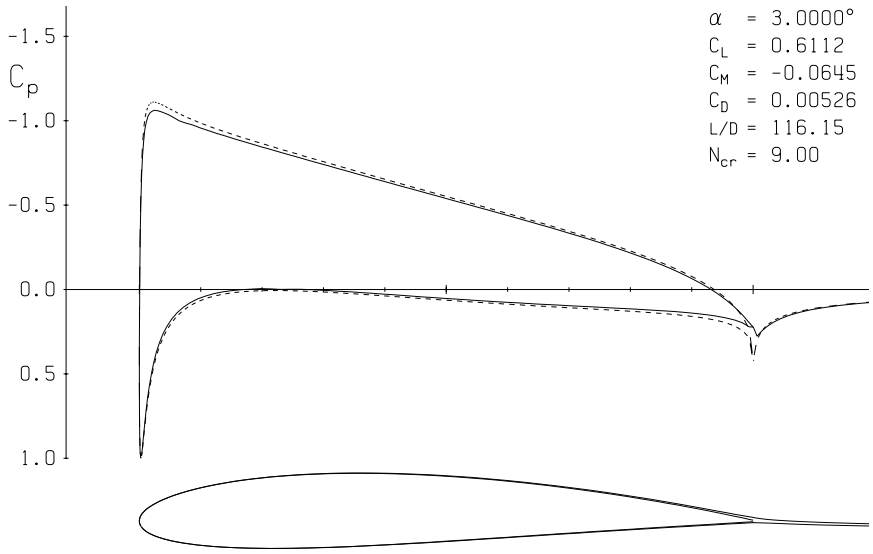
Flow 5

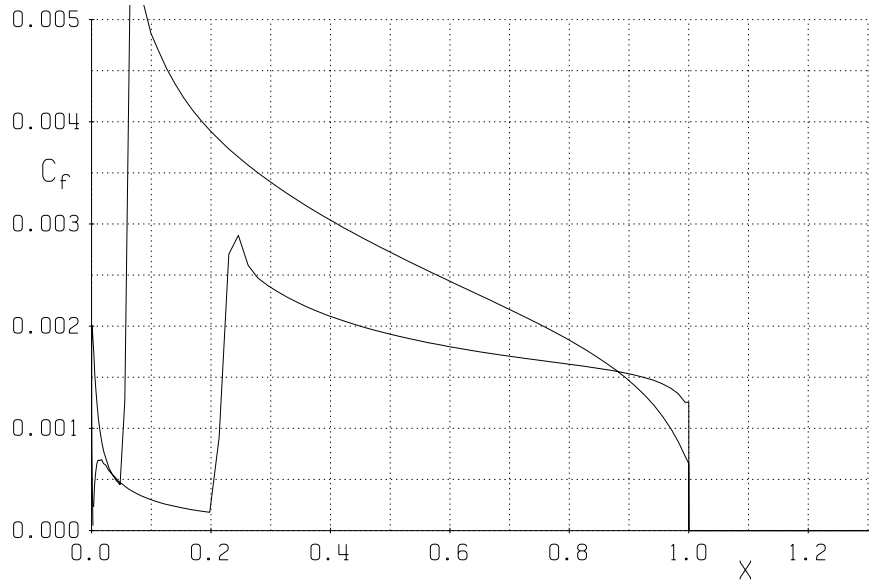
Select all of the options that apply:

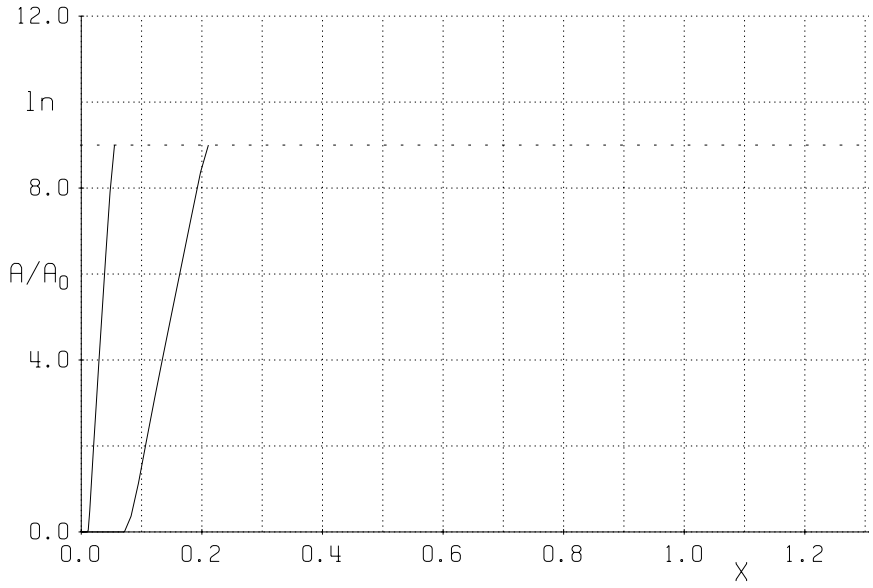
edXsolution

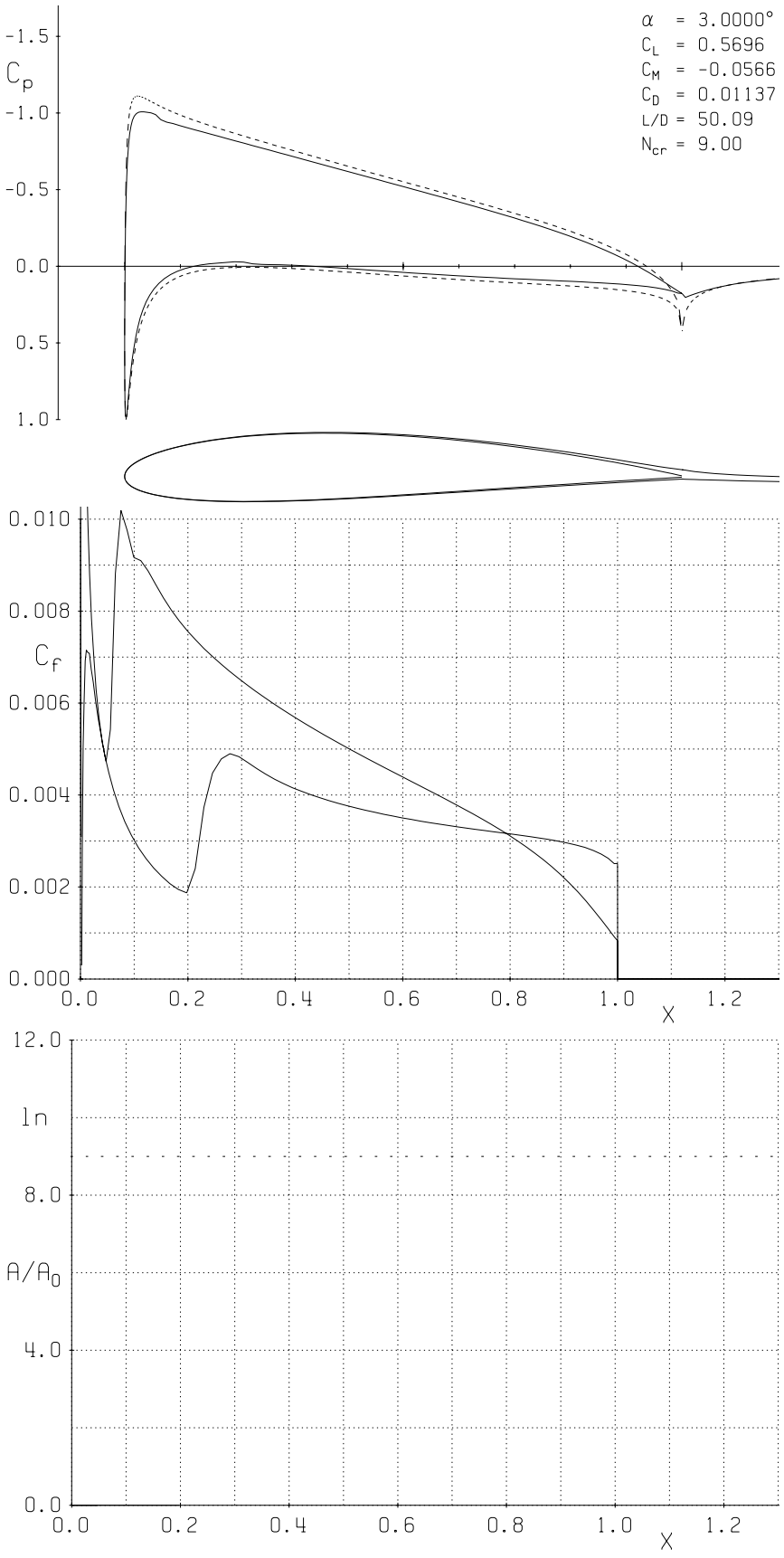
Video Link

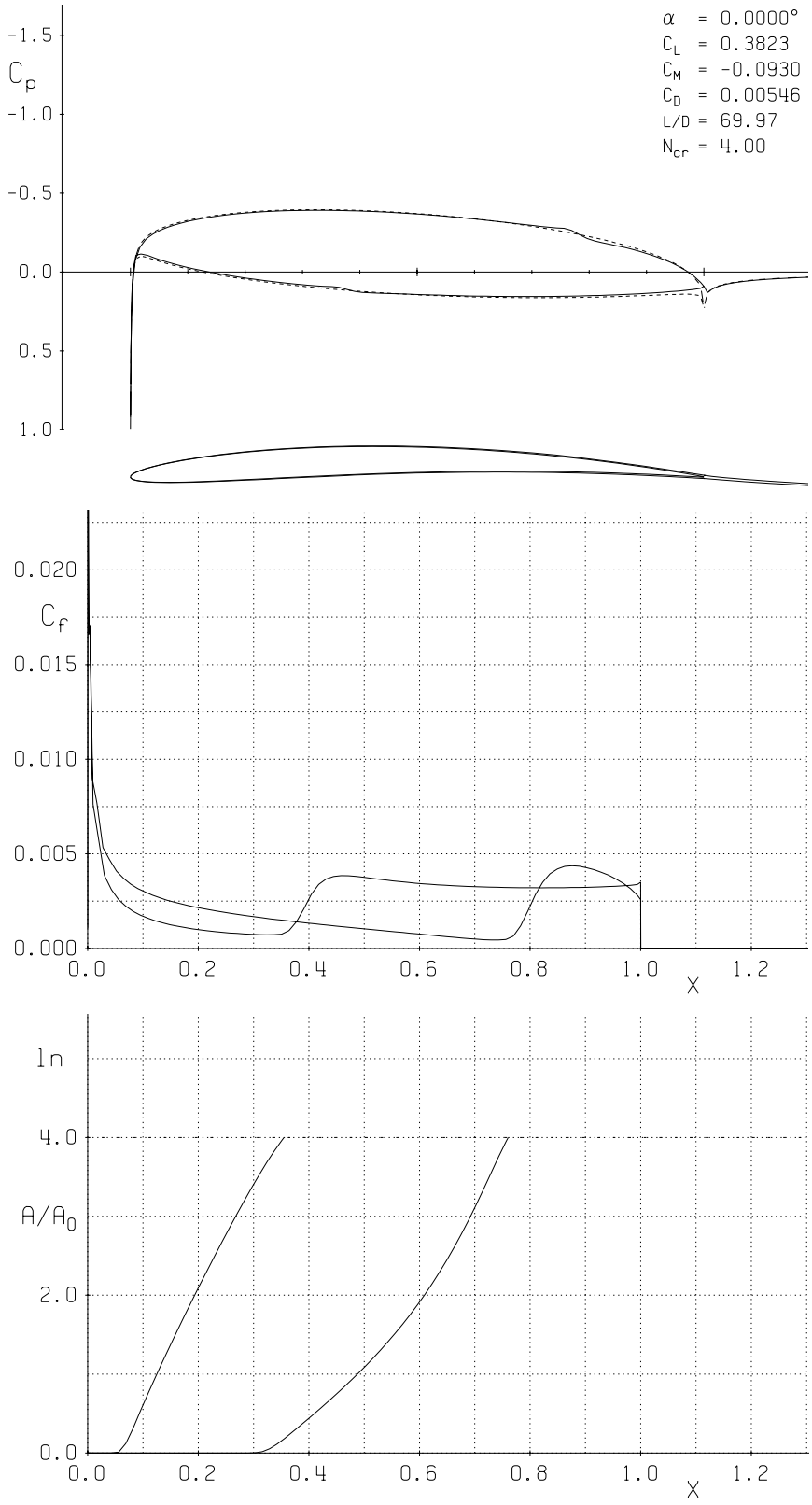

α = 3.0000°
C_L = 0.2796
C_M = -0.0211
C_D = 0.04134
L/D = 6.76
N_{cr} = 9.00
C_p
-1.5
-1.0
-0.5
0.0
0.5
1.0
C_f
0.25
0.20
0.15
0.10
0.05
0.00
0.0
0.2
0.4
0.6
0.8
1.0
1.2
X
ln
12.0
8.0
4.0
0.0
A/A_0

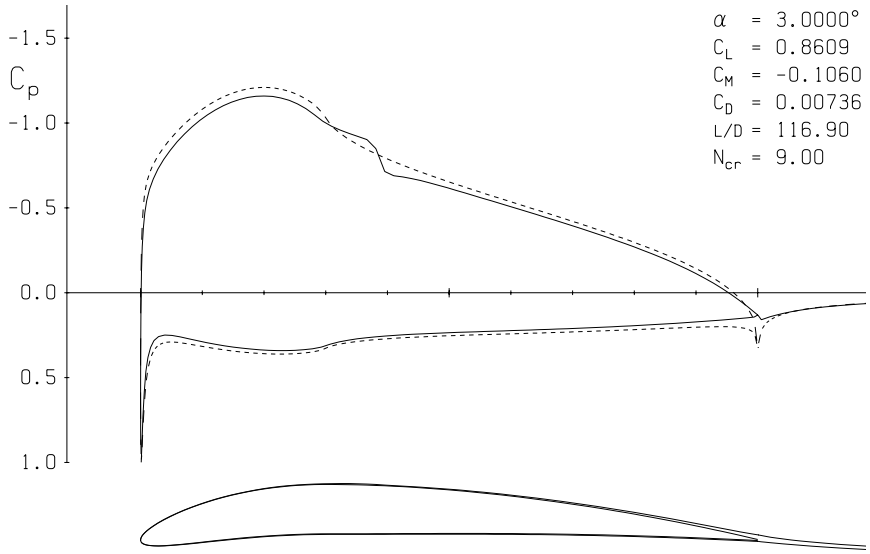

α = 3.0000°
C_L = 0.6112
C_M = -0.0645
C_D = 0.00526
L/D = 116.15
N_{cr} = 9.00
C_p
-1.5
-1.0
-0.5
0.0
0.5
1.0

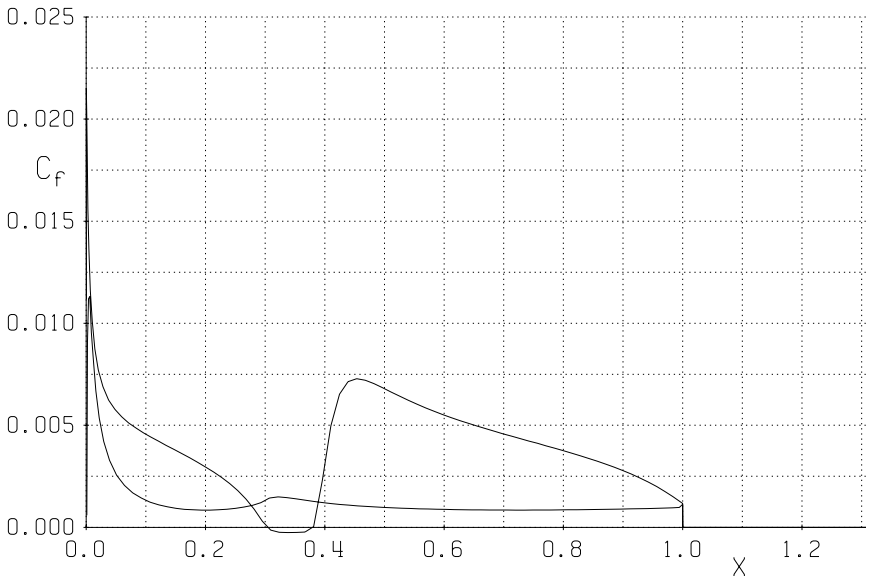

C_f
0.005
0.004
0.003
0.002
0.001
0.000
0.0
0.2
0.4
0.6
0.8
1.0
1.2
X

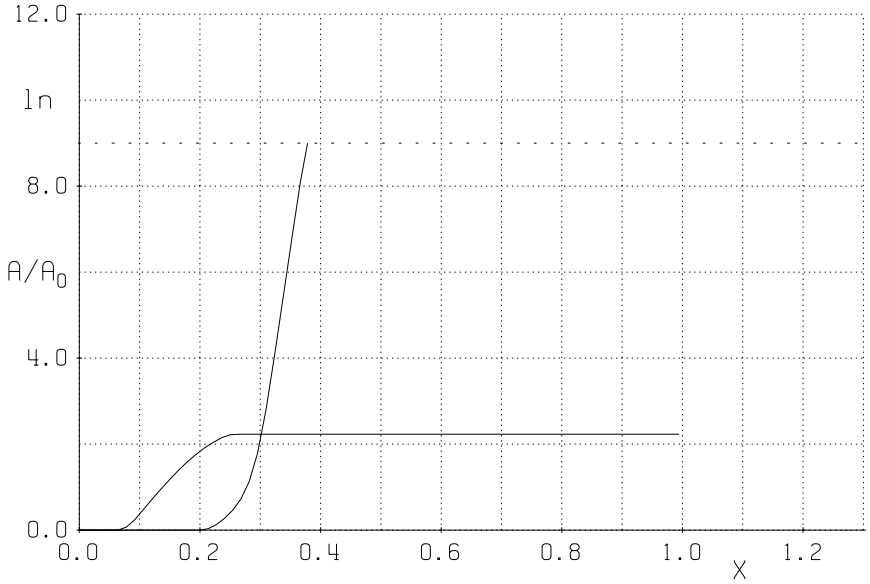

ln
A/A_0
12.0
8.0
4.0
0.0
0.0
0.2
0.4
0.6
0.8
1.0
1.2
X


α = 3.0000°
C_L = 0.5696
C_M = -0.0566
C_D = 0.01137
L/D = 50.09
N_{cr} = 9.00
C_p
-1.5
-1.0
-0.5
0.0
0.5
1.0
C_f
0.010
0.008
0.006
0.004
0.002
0.000
0.0
0.2
0.4
0.6
0.8
1.0
1.2
X
ln
A/A_0
12.0
8.0
4.0
0.0


α = 0.0000°
C_L = 0.3823
C_M = -0.0930
C_D = 0.00546
L/D = 69.97
N_{cr} = 4.00
C_p
-1.5
-1.0
-0.5
0.0
0.5
1.0
C_f
0.020
0.015
0.010
0.005
0.000
0.0
0.2
0.4
0.6
0.8
1.0
1.2
X
ln
A/A_0
4.0
2.0
0.0
0.0
0.2
0.4
0.6
0.8
1.0
1.2
X


α = 3.0000°
C_L = 0.8609
C_M = -0.1060
C_D = 0.00736
L/D = 116.90
N_{cr} = 9.00
C_p
-1.5
-1.0
-0.5
0.0
0.5
1.0


C_f
0.025
0.020
0.015
0.010
0.005
0.000
0.0
0.2
0.4
0.6
0.8
1.0
1.2
X


ln
A/A_0
12.0
8.0
4.0
0.0
0.0
0.2
0.4
0.6
0.8
1.0
1.2
X

edXproblem: 14.5.3 Another airfoil flow classification

14.1 14.2 14.3

In this problem, you will identify various aspects of different airfoil flows based on plots of C_p, C_f, and N. The flow conditions are chosen among the following options:

- All of the flows are incompressible.
- The Reynolds number is one of the following three values: $Re = 10^3$, 10^5, or 10^7.
- Transition could occur naturally or transition could be forced by using a trip on the surface of the airfoil.
- The results are either from an atmospheric flight test in which the level of freestream turbulence is low (simulated using $N_{cr} = 10$), or from a wind tunnel test in which the level of freestream turbulence is moderate (simulated using $N_{cr} = 6$).

Flow A

Select all of the options that apply:

Flow B

Select all of the options that apply:

Flow C

Select all of the options that apply:

Flow D

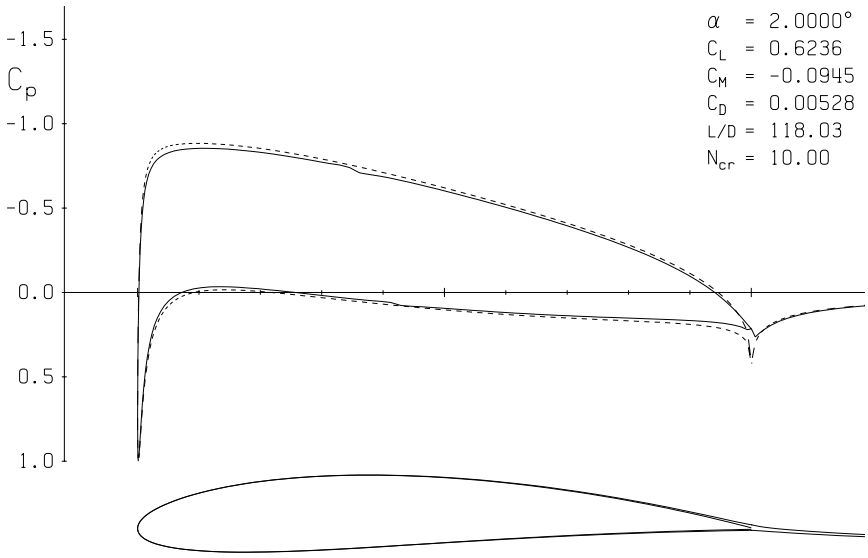
Select all of the options that apply:

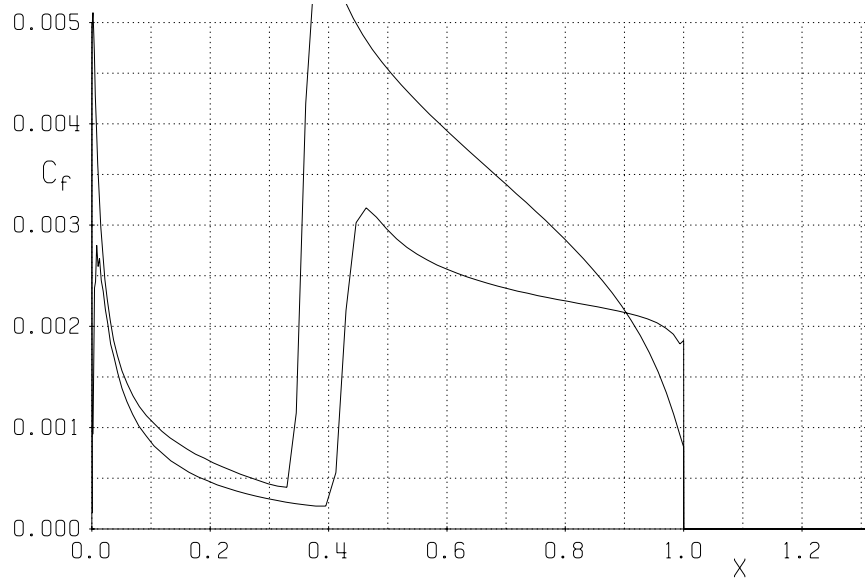
Flow E

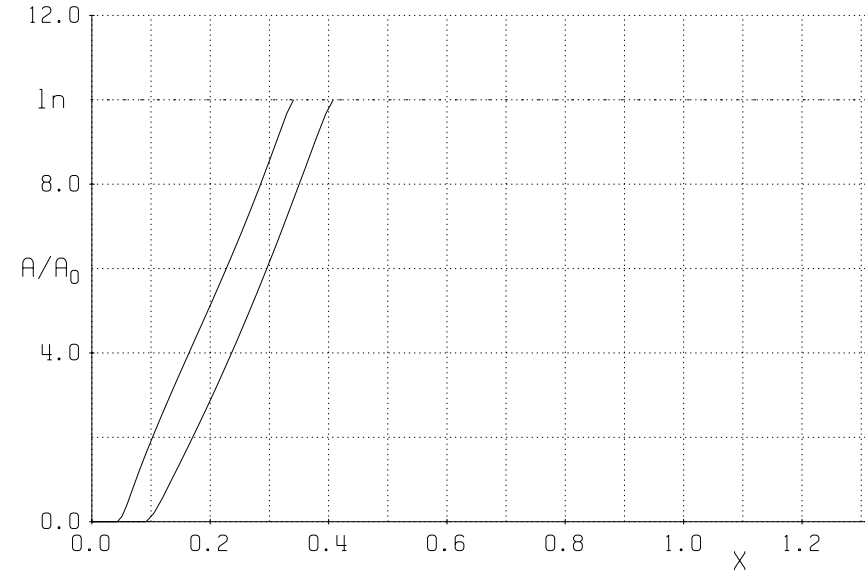
Select all of the options that apply:

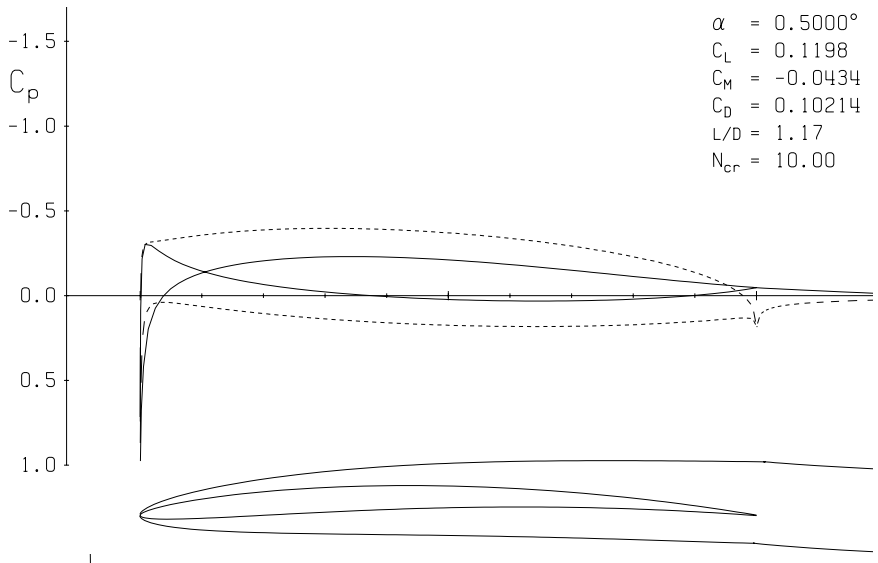
edXsolution

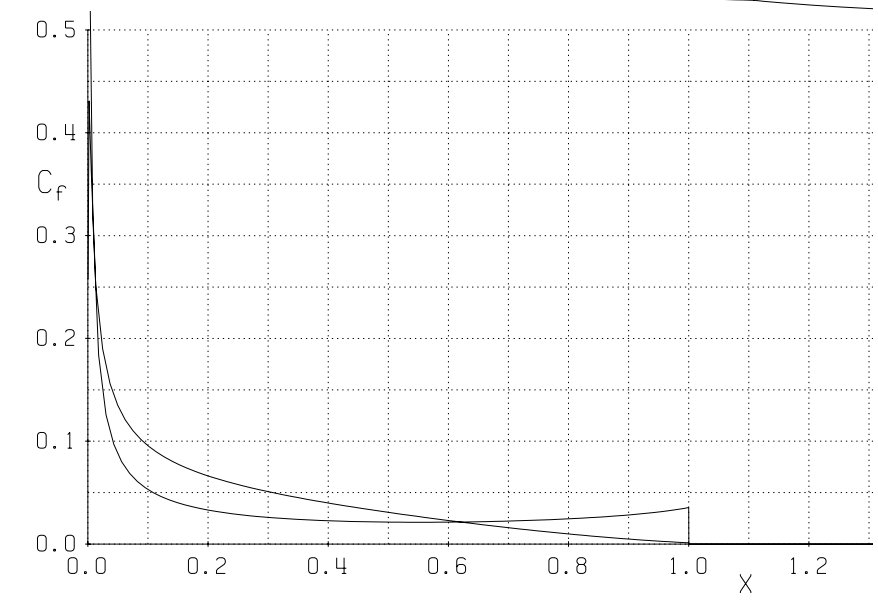
Video Link

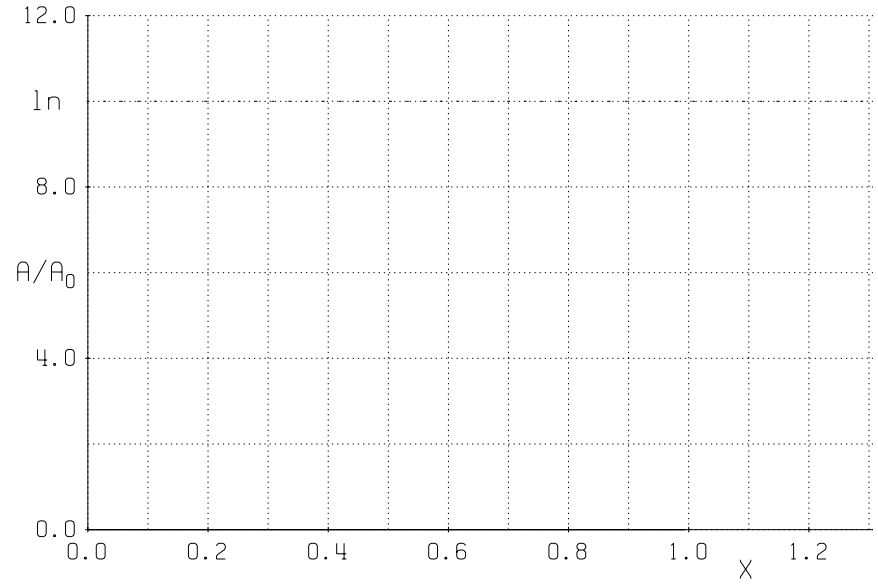

α = 2.0000°
C_L = 0.6236
C_M = -0.0945
C_D = 0.00528
L/D = 118.03
N_cr = 10.00
-1.5
C_p
-1.0
-0.5
0.0
0.5
1.0

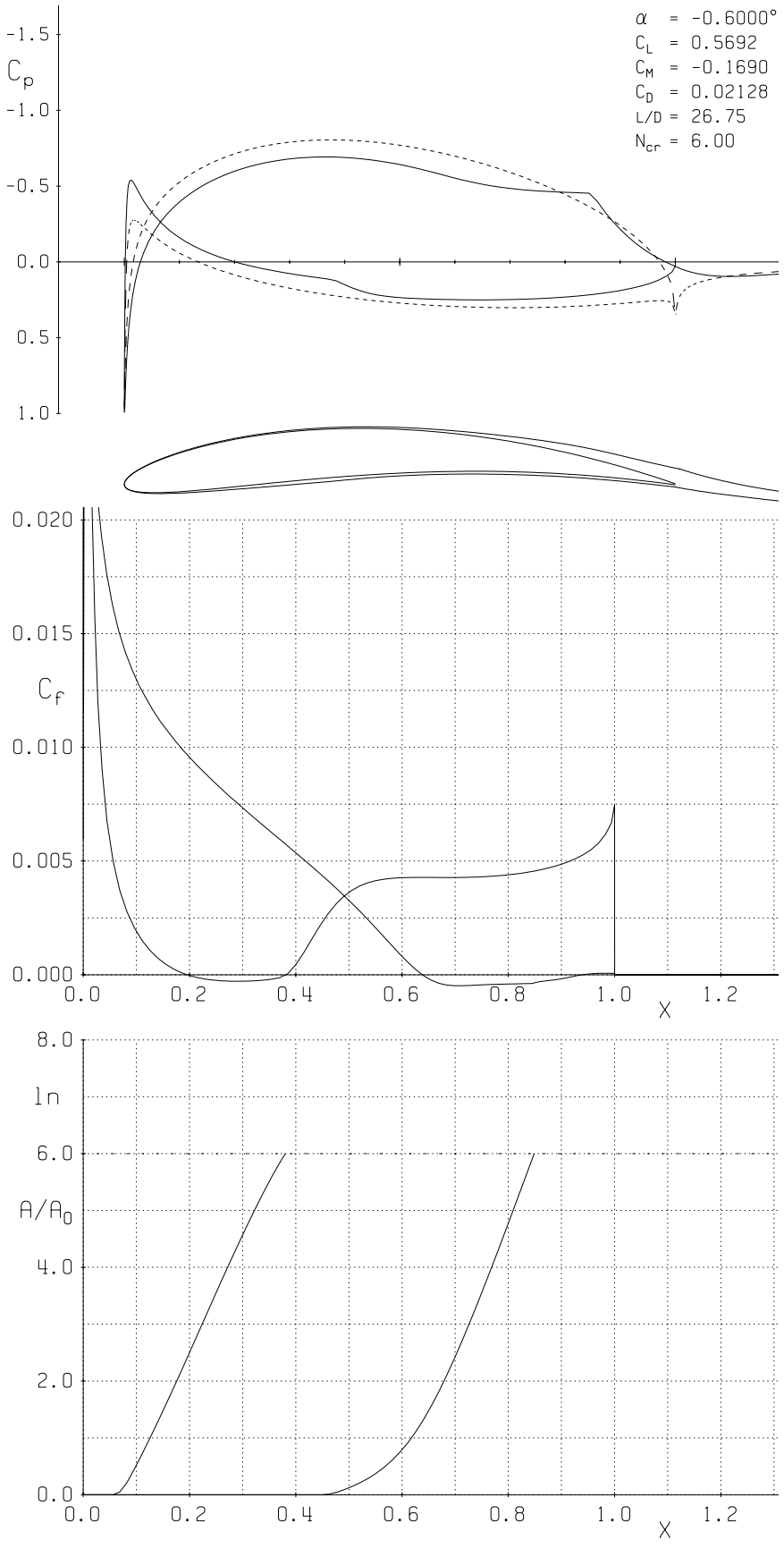

0.005
0.004
C_f
0.003
0.002
0.001
0.000
0.0
0.2
0.4
0.6
0.8
1.0
1.2
X

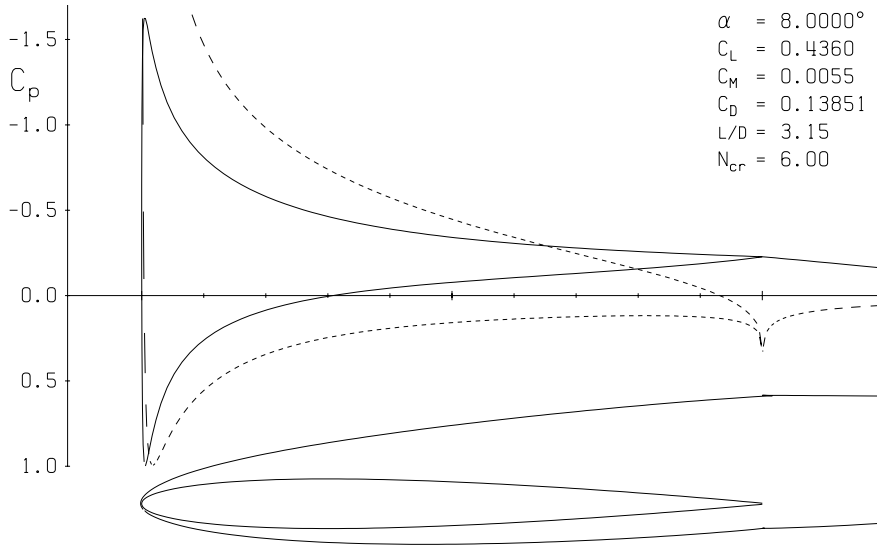

12.0
ln
8.0
A/A_0
4.0
0.0
0.0
0.2
0.4
0.6
0.8
1.0
1.2
X

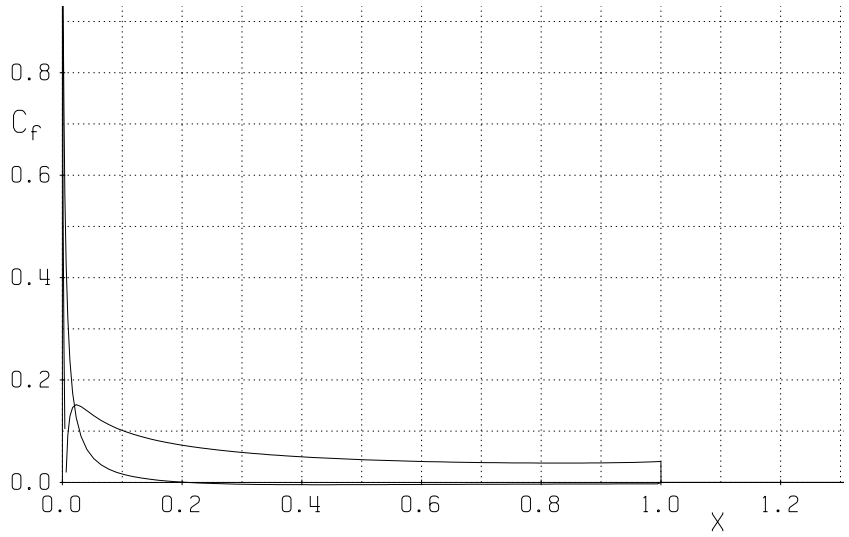

α = 0.5000°
C_L = 0.1198
C_M = -0.0434
C_D = 0.10214
L/D = 1.17
N_cr = 10.00
C_p
-1.5
-1.0
-0.5
0.0
0.5
1.0

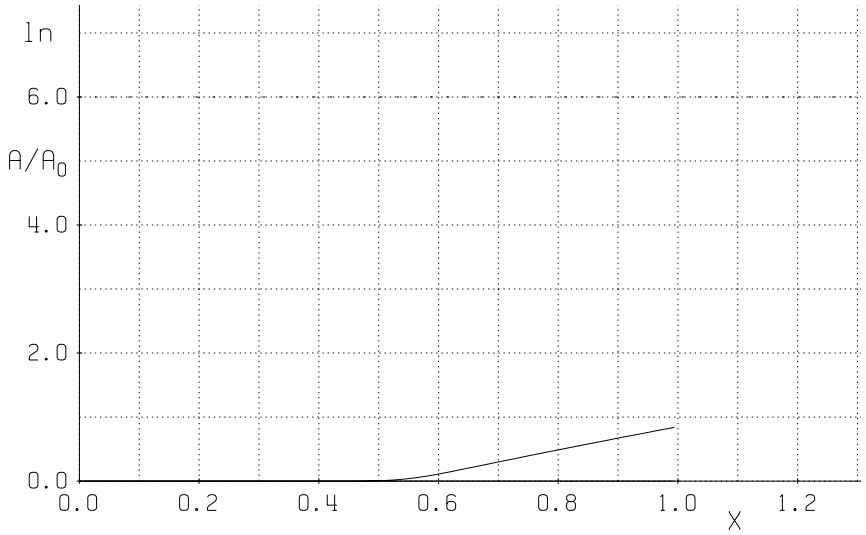

C_f
0.5
0.4
0.3
0.2
0.1
0.0
0.0
0.2
0.4
0.6
0.8
1.0
1.2
X

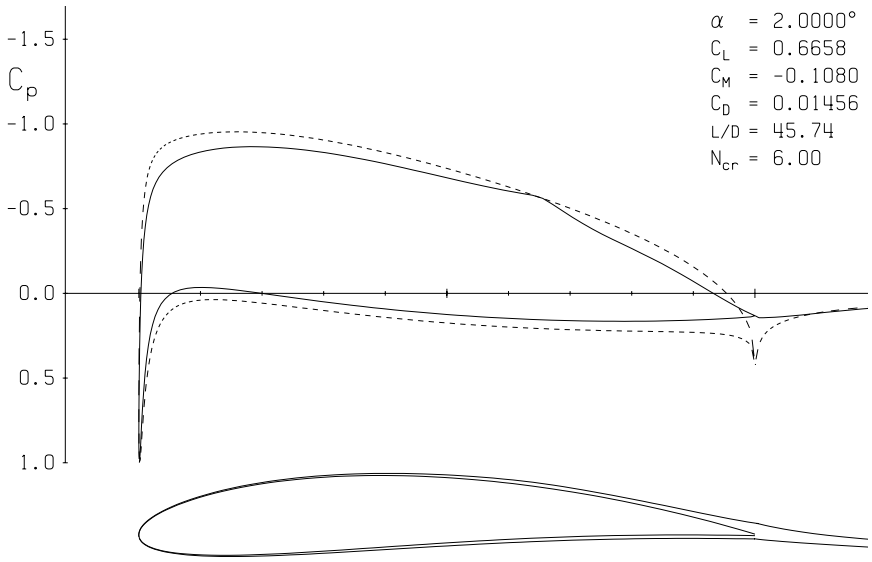

ln
A/A_0
12.0
8.0
4.0
0.0
0.0
0.2
0.4
0.6
0.8
1.0
1.2
X

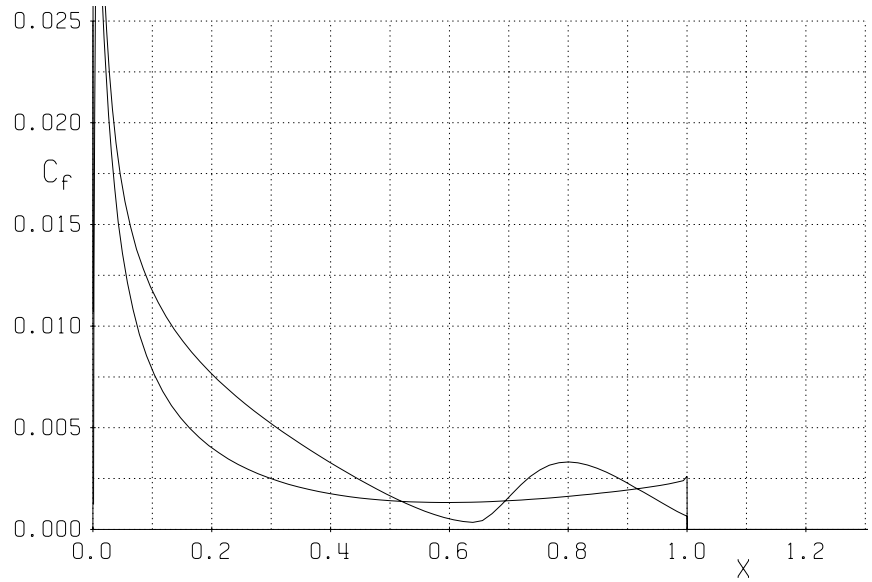

α = -0.6000°
C_L = 0.5692
C_M = -0.1690
C_D = 0.02128
L/D = 26.75
N_cr = 6.00
C_p
-1.5
-1.0
-0.5
0.0
0.5
1.0
C_f
0.020
0.015
0.010
0.005
0.000
0.0
0.2
0.4
0.6
0.8
1.0
1.2
X
ln
A/A_0
8.0
6.0
4.0
2.0
0.0

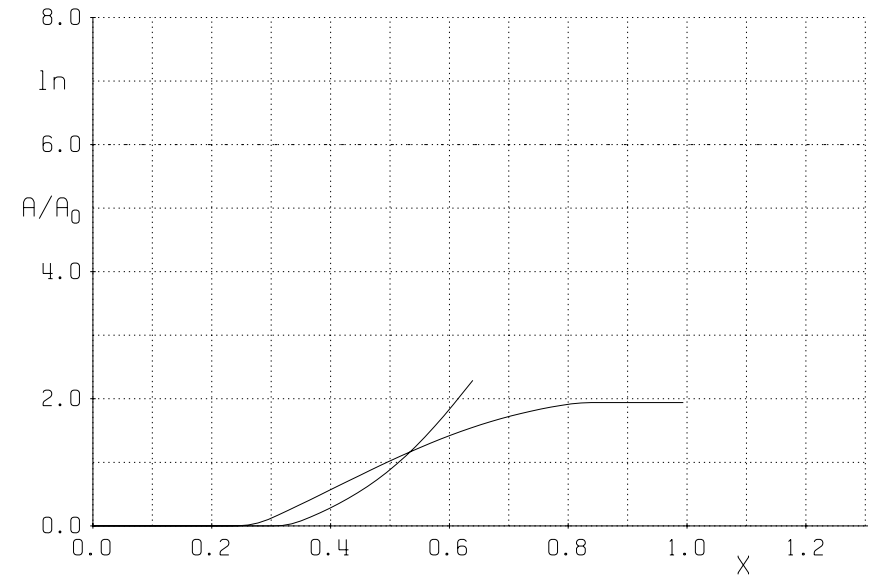

α = 8.0000°
C_L = 0.4360
C_M = 0.0055
C_D = 0.13851
L/D = 3.15
N_{cr} = 6.00
C_p
-1.5
-1.0
-0.5
0.0
0.5
1.0


C_f
0.8
0.6
0.4
0.2
0.0
0.0
0.2
0.4
0.6
0.8
1.0
1.2
X


ln
A/A_0
6.0
4.0
2.0
0.0
0.0
0.2
0.4
0.6
0.8
1.0
1.2
X


α = 2.0000°
C_L = 0.6658
C_M = -0.1080
C_D = 0.01456
L/D = 45.74
N_{cr} = 6.00
C_p
-1.5
-1.0
-0.5
0.0
0.5
1.0


C_f
0.025
0.020
0.015
0.010
0.005
0.000
0.0
0.2
0.4
0.6
0.8
1.0
1.2
X


ln
A/A_0
8.0
6.0
4.0
2.0
0.0
0.0
0.2
0.4
0.6
0.8
1.0
1.2
X

edXproblem: 14.5.4 Drag estimation and breakdown for an airplane

2.2 | 2.5 | 11.8 | 12.5 | 12.4 | 14.3

- An airplane flying at $M_\infty = 0.5$ has a lift coefficient of $C_L = 0.552$ and drag coefficient of $C_D = 0.02$.
- The wing has an aspect ratio of $AR = 10$ and span efficiency of $e = 0.97$.
- The wing planform area is used as the reference area for the lift and drag coefficients (i.e. $S_{\text{ref}} = S_{\text{plan}}$).
- The surface area of the entire airplane, S_{body}, includes all parts of the airplane which are in contact with the external air (see Equation 2.7 and Section 2.2.4 for more information). Thus, S_{body} includes not only the upper and lower surfaces of the wing, but also all other parts of the airplane that contact the air such as the fuselage, horizontal and vertical tails, etc. For this airplane, $S_{\text{body}} = 4S_{\text{plan}}$.
- Assume that the average skin friction acting on the body is $\overline{C_f} = 0.002$, where,

$$\overline{C_f} = \frac{1}{S_{\text{body}}} \int_{S_{\text{body}}} C_f \, dS \tag{14.23}$$

  Also, you may assume that the viscous stress acting on the airplane is largely in the freestream direction (because the body is relatively thin and aligned with the freestream over most of its surface).
- The critical Mach number for the aircraft at this orientation is $M_{\text{cr}} = 0.7$.

Determine the induced drag coefficient, C_{D_i}. Give your answer with two-digits of precision in the form X.YeP.

Estimate the friction drag coefficient. Give your answer with two-digits of precision in the form X.YeP.

Determine the wave drag coefficient. Give your answer with two-digits of precision in the form X.YeP.

Estimate the form drag coefficient. Give your answer with two-digits of precision in the form X.YeP.

edXsolution

Video Link

Module 15

Final Exam

15.1 Instructions

15.1.1 Instructions

The following instructions for the Final applied to the Fall 2015 offering of 16.101x. We have left these instructions for you to have a sense of what was required when 16.101x was last offered for certification. These instructions no longer apply and you can feel free to discuss all of these problems.

This is a reminder that Final exam begins on Monday, January 11th at 20:00 UTC. You have until Monday, January 18th at 20:00 UTC to complete the exam.

You must complete the exam on your own without help from others. If there is a question of clarification or if you have double checked your work and think there might be a bug in the system, please communicate that in the discussion forum. Please do NOT use the discussion forum (or any other means) to discuss the problems on the exam in any other way until after the exam deadline has passed. Such posts in our 16.101x forum will be immediately deleted. Also, in terms of the content, the focus of the Final Exam will be on the Measurable Outcomes from Part 2, however, since that material builds on Part 1, some parts of the Final Exam will be on the Measurable Outcomes from Part 1.

Good luck!

15.2 Final Exam Problems

edXproblem: 15.2.1 Final Problem One: 25 Points

11.5 11.8

Suppose that an airplane's sectional lift distribution in a cruise condition is,

$$L'(y) = L_0 \left[1 - \left(\frac{y}{b/2}\right)^2\right]$$

where L_0 is the sectional lift at $y = 0$. We will refer to this as a parabolic lift distribution.

1) For a parabolic lift distribution, find the lift L in terms of L_0 and b. Note: L is the total lift generated over the wing from $-b/2 \leq y \leq b/2$. Enter the resulting formula for L using L0 for L_0 and b for b.

2) The bending moment at the root due to the lift generated on the $y > 0$ portion of the wing is,

$$M_{\text{bend}} = \int_0^{b/2} yL'(y)\mathrm{d}y \tag{15.1}$$

For a parabolic lift distribution, find M_{bend} in terms of L_0 and b. Enter the resulting formula for M_{bend} using L0 for L_0 and b for b.

3) For the same total lift L, determine

$$\frac{M_{\text{bend, parabolic}}}{M_{\text{bend, elliptic}}} \tag{15.2}$$

i.e. the ratio of the bending moment for a parabolic lift distribution to the bending moment for an elliptic lift distribution.

4) Determine the span efficiency factor (e) for a parabolic lift distribution. In determining this, the following integrals might be useful:

$$\int_0^{\pi} \sin n\beta \sin m\beta \,\mathrm{d}\beta = \begin{cases} \frac{\pi}{2} & \text{if } m = n, \\ 0 & \text{if } m \neq n \end{cases} \tag{15.3}$$

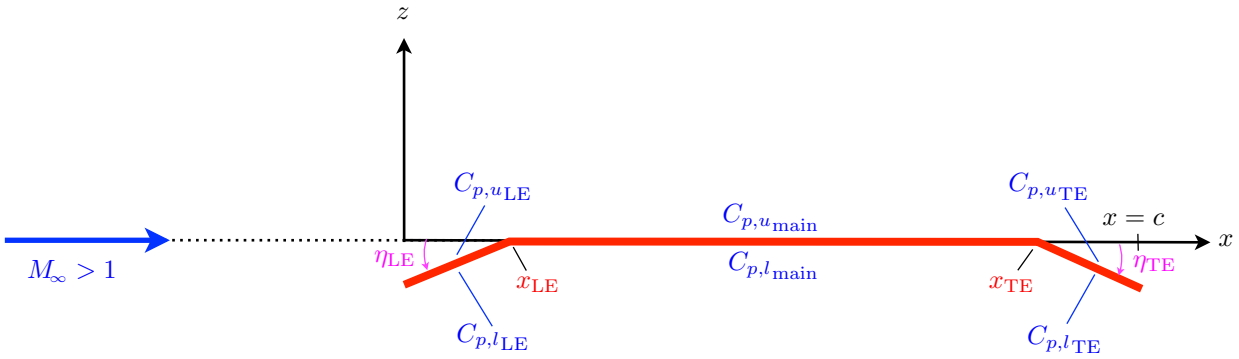
$$\int_0^{\pi} \sin^2 \beta \sin m\beta \,\mathrm{d}\beta = \begin{cases} \frac{-4}{m^3 - 4m} & \text{if } m \text{ is odd}, \\ 0 & \text{if } m \text{ is even} \end{cases} \tag{15.4}$$

edXsolution

Video Link

edXproblem: 15.2.2 Final Problem Two: 25 Points

12.6



In this problem, use linearized supersonic potential flow theory to analyze the flow around the flat plate airfoil shown in the figure. The upstream flow is aligned along the x-axis. The flap hinge locations are at $x_{\mathrm{LE}} = 0.1c$ and $x_{\mathrm{TE}} = 0.9c$.

1) First, consider the situation in which both the leading edge and trailing edge flaps are deflected downward ($\eta_{\mathrm{LE}} > 0$ and $\eta_{\mathrm{TE}} > 0$). Select all of the correct answers about the pressure coefficient behavior.

2) Now, consider the situation in which $M_\infty = \sqrt{5}$, $\eta_{\mathrm{LE}} = 0$ and $\eta_{\mathrm{TE}} = 3.6/\pi$ degrees. In other words, only the trailing edge flap is deflected.

2a) Determine the lift coefficient. Provide your answer with two digits of precision (X.YeP).

2b) Determine the drag coefficient. Provide your answer with two digits of precision (X.YeP).

3) Now, consider the situation in which $M_\infty = \sqrt{5}$, $\eta_{\mathrm{LE}} = 3.6/\pi$ degrees and $\eta_{\mathrm{TE}} = 0$. In other words, only the leading edge flap is deflected.

3a) Determine the lift coefficient. Provide your answer with two digits of precision (X.YeP).

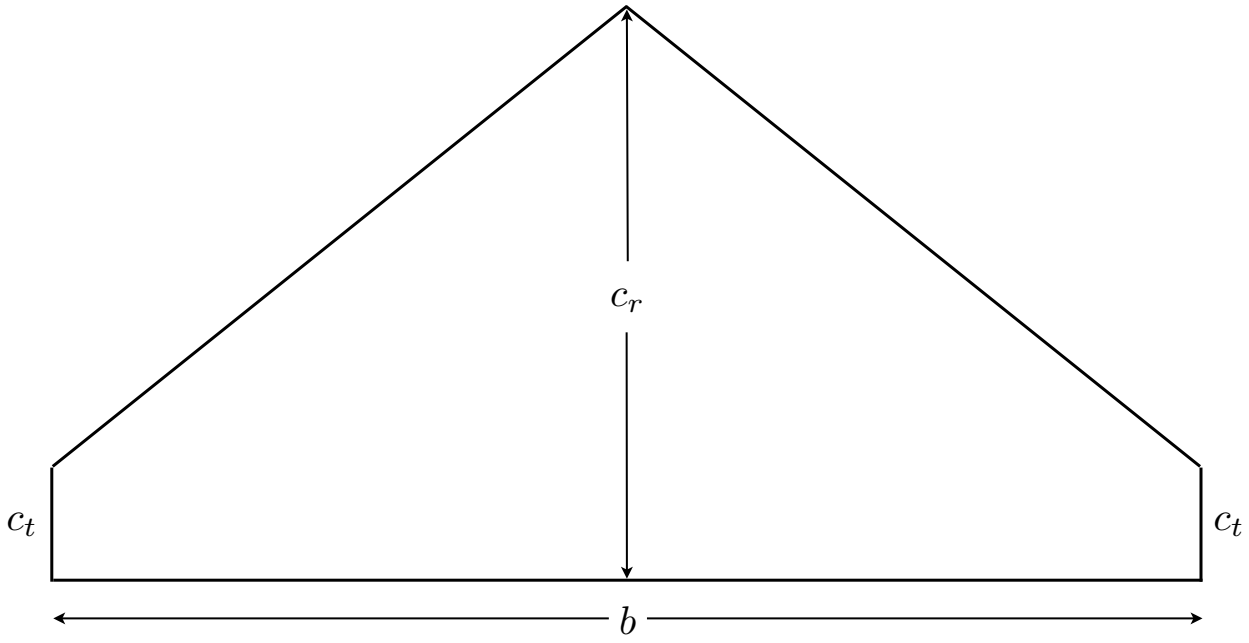
3b) Determine the drag coefficient. Provide your answer with two digits of precision (X.YeP).

edXsolution

Video Link

edXproblem: 15.2.3 Final Problem Three: 25 Points

14.1 14.3



The planform of the tapered wing shown above has $c_r = 5\,\text{m}$, $c_t = 1\,\text{m}$, and $b = 10\,\text{m}$. The flight conditions are $V_\infty = 100\,\text{m/s}$, $\rho_\infty = 1.2\,\text{kg/m}^3$, and $\mu_\infty = 1.8 \times 10^{-5}\,\text{Ns/m}^2$. The angle of attack is $\alpha_\infty = 0$.

The wing is flat and the skin friction drag at any spanwise cross-section will be modeled as the skin friction drag on a flat plate. In particular, at any airfoil spanwise location y, the sectional drag coefficient due to friction, $c_d(y)$, will be estimated using

$$c_d = 2.656 Re^{-1/2} \left(\frac{x_{\text{tr}}}{c}\right)^{1/2} + 0.144 Re^{-1/5} \left[1 - \left(\frac{x_{\text{tr}}}{c}\right)^{4/5}\right] \tag{15.5}$$

where Re is the Reynolds number based on the chord, $c(y)$, of the local section and x_{tr} is distance of the transition location **from the leading edge of that local section.** Note: Equation (15.5) was first derived in the solution video discussing Equation (14.22). Assume that natural transition occurs at $Re_x = 10^6$ (Re_x is the Reynolds number based on the distance from the leading edge of the local section).

1a) Determine the sectional drag coefficient due to friction at the wing root (i.e. $c = c_r$). Provide your answer with three digits of precision (X.YZeP).

1b) Determine the sectional drag coefficient due to friction at the wing tip (i.e. $c = c_t$). Provide your answer with three digits of precision (X.YZeP).

The surface area of the wing exposed to the air is often referred to as the wetted area. For this flat wing, $S_{\text{wet}} = 2S_{\text{plan}} = (c_t + c_r)b$. Let S_{lam} be the portion of the wetted area for which the flow is laminar (including the unstable flow prior to transition to turbulence) and S_{turb} be the portion of the wetted area for which the flow is turbulent. Note that $S_{\text{lam}} + S_{\text{turb}} = S_{\text{wet}}$.

1c) Determine $S_{\text{lam}}/S_{\text{wet}}$, the fraction of the wetted area for which the flow is laminar. Provide your answer with three digits of precision (X.YZeP).

Next, consider a $1/10^{\text{th}}$ scale model of this wing that will be placed in a wind tunnel. The wind tunnel conditions are $V_\infty = 40\,\text{m/s}$, $\rho_\infty = 2.0\,\text{kg/m}^3$, and $\mu_\infty = 2.4 \times 10^{-5}\,\text{Ns/m}^2$. The angle of attack is $\alpha_\infty = 0$.

2a) Determine the sectional drag coefficient due to friction at the wing root. Provide your answer with three digits of precision (X.YZeP).

2b) Determine the sectional drag coefficient due to friction at the wing tip. Provide your answer with three digits of precision (X.YZeP).

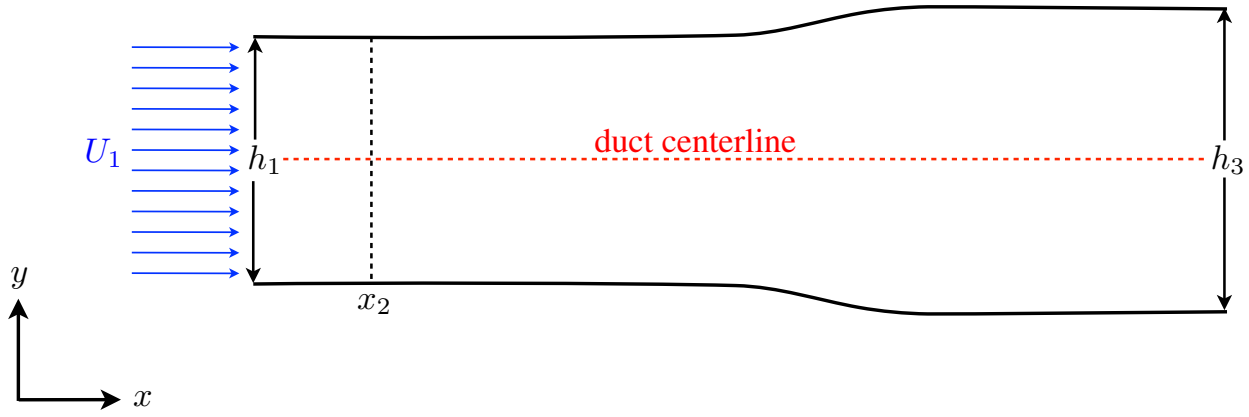
2c) Determine $S_{\text{lam}}/S_{\text{wet}}$. Provide your answer with three digits of precision (X.YZeP).

edXsolution

Video Link

edXproblem: 15.2.4 Final Problem Four: 25 Points

3.6 | 8.2 | 13.3 | 13.6



A diffuser duct is shown above. You may assume that the flow is two-dimensional and incompressible with density $\rho = 1\,\text{kg/m}^3$. The flow enters the diffuser with uniform velocity $U_1 = 10\,\text{m/s}$ and uniform pressure p_1. The inlet height is $h_1 = 1\,\text{m}$ and the outlet height is $h_3 = 1.25\,\text{m}$.

1) Consider first the case of inviscid flow and assume that the flow at the outlet has uniform velocity U_3. Determine U_3 in m/s. Provide your answer with three digits of precision (X.YZeP).

Now consider viscous flow in which the viscosity $\mu = 2 \times 10^{-5}\,\text{Ns/m}^2$ is constant.

2a) At a location which is $x_2 = h_1/2$ downstream of the inlet, the flow is still laminar. Use Blasius flat plate boundary layer theory to estimate the (99%) boundary layer thickness δ_2 at this location. Use units of m and provide your answer with three digits of precision (X.YZeP).

2b) At location x_2, the velocity U_2 outside of the boundary layer is uniform (i.e. it does not vary in y). Estimate the velocity difference $U_2 - U_1$ in m/s. Provide your answer with three digits of precision (X.YZeP).

2c) At the outlet x_3, the velocity inside the boundary layer is well-approximated by $u = U_3(y/\delta_3)^{1/5}$ while outside the boundary layer the velocity is uniform and equal to U_3. Determine the ratio δ_3^*/δ_3 where δ_3^* is the displacement thickness at the outlet. Provide your answer with three digits of precision (X.YZeP).

2d) Measurements taken at the outlet give that $U_3 = 9\,\text{m/s}$. Determine δ_3^*. Use units of m and provide your answer with three digits of precision (X.YZeP).

2e) Let p_1, p_2, and p_3 be the pressure along the centerline of the duct at the inlet, x_2, and outlet locations. And, let $p_{3,\text{inv}}$ be the pressure at the center of the duct at the outlet if the flow were assumed to be inviscid (i.e. as analyzed in part 1 of this problem). Select all of the correct answers.

edXsolution

Video Link